

Analysis of the PWV variations observed by a hyper-dense network of GNSS receivers prior to localized rainfall

IWAKI, Yuya¹ ; REALINI, Eugenio¹ ; TSUDA, Toshitaka^{1*} ; SATO, Kazutoshi¹ ; OIGAWA, Masanori¹

¹RISH, Kyoto University

Sudden and localized heavy rainfall events are posing increasing danger to urban areas, not only for the generation of floods, but also for the possibility to trigger landslides and damage crucial infrastructures. Numerical weather prediction models need to be supported by observations with sufficiently high spatial resolution, in order to be able to successfully forecast such localized precipitation events. To this aim, a crucial parameter to be monitored is the amount of precipitable water vapor (PWV), as well as its spatial distribution over the area of interest, and its variation over time. The Global Positioning System (GPS), which is one of the Global Navigation Satellite Systems (GNSS) currently available, has been increasingly used not only for positioning, but also for the remote sensing of physical parameters useful in Earth sciences. The PWV, or integrated amount of water vapor along the zenith direction, can be estimated by GPS (or GNSS) meteorology, which is a method that associates the amount of water vapor to the tropospheric delays which affect the signals of positioning satellites.

We deployed a dual-frequency (DF) GNSS network around Uji campus of Kyoto University, Japan, with inter-station distances of about 1-2 km. By using this network, we built a basic system to observe PWV fluctuations occurring within a small horizontal scale (less than 10 km), which are then analyzed to identify possible precursors of local torrential rain. Results from two observation campaigns (executed in the summer of 2011 and 2012) to retrieve and study GPS-derived PWV showed that its difference from other meteorological instruments was at most 2 mm in RMSE. We analyzed the variations of PWV detected when localized heavy rain was observed on July 9 and 25, 2012. Both the averaged value and the variance of PWV among GNSS stations increased before a nearby meteorological radar detected the rain clouds. In the latter case, the relative value of PWV among stations was larger than 5 mm.

For turning this system into practical use, e.g. for supporting a heavy rain early warning system, real-time satellite orbit and clock products are required. To estimate and correct the error of predicted satellite clock information, we used stations from the existing nation-wide GPS network in Japan (GEONET), with long baselines (~100 km). The difference between the real-time PWV and that obtained in post-processing by means of precise orbit and clock products was 1.5 mm in RMSE.

Furthermore, the cost-effective deployment of hyper-dense GNSS networks over urban areas would benefit from the usage of inexpensive single-frequency (SF) receivers. We implemented and tested a software application that estimates and interpolates the ionospheric delay from DF stations surrounding the hyper-dense network, in order to compensate SF observations for the effect of the ionosphere, according to a method called SEID (Satellite-specific Epoch-differenced Ionospheric Delay), which was originally developed at the GFZ in Potsdam, Germany. By applying SEID for SF PWV retrieval, the error in terms of PWV with respect to the DF solution was about 1.6 mm in RMSE. The PWV horizontal distribution obtained by SF analysis with this model could detect localized PWV inhomogeneity emerging prior to a rainfall which occurred within a small horizontal scale (less than 10 km).

Keywords: GNSS, GPS, PWV, precipitation, tropospheric delay, ionospheric delay

PWV retrieval by radiosondes and GPS receivers in Indonesia: spatial and time variations associated to rain events

REALINI, Eugenio¹ ; SATO, Kazutoshi² ; TSUDA, Toshitaka^{1*} ; SUSILO, .³ ; MANIK, Timbul⁴

¹RISH, Kyoto University, Japan, ²RISH, Kyoto University, Japan - now at JAXA, Japan, ³Indonesian Geospatial Information Agency (BIG), Indonesia, ⁴National Institute of Aeronautics and Space (LAPAN), Indonesia

Flooding due to local convective rain is a serious problem in the urban area of Jakarta, Indonesia. However, accurate prediction of local heavy rainfall events by means of current mesoscale numerical prediction models is difficult, partly because of lacking meteorological observations in Indonesia. Spatial and time variations of water vapor over a given area are expected to increase before precipitation occurs, due to the accumulation of water vapor in the lower troposphere, followed by convective instability. A means to reliably and continuously monitor Precipitable Water Vapor (PWV) is needed in order to detect such variations before the formation of rain clouds. GPS meteorology, i.e. the retrieval of PWV above a GPS station of known coordinates, is a useful technique to achieve this objective. The GPS signal delay induced by tropospheric refractivity is related to the amount of water vapor along the slant path between each satellite and the receiver antenna, therefore each fixed GPS station can be effectively employed as a sensor that continuously monitors the PWV with high temporal resolution (down to few seconds). By deploying multiple GPS stations that concurrently estimate the amount of PWV at different locations within an area of interest, one can evaluate the spatial and time fluctuations of the water vapor field, and investigate their relation to rain events.

We conducted a PWV observation campaign from 23 July to 5 August 2010 by using five GPS receivers installed at four different locations in Jakarta and Bogor, on Java island, Indonesia. Radiosondes were launched three to four times a day, from a site co-located with two of the receivers, in order to validate the GPS-derived PWV data. The validation resulted in a root mean square error of 2-3 mm. The influence of atmospheric pressure and temperature on GPS-derived PWV can be significant, therefore it was evaluated by referring to ground pressure and temperature measured by weather stations, and radiosonde temperature profiles. A regular semi-diurnal pressure oscillation was observed, showing an amplitude ranging from 3 to 5 hPa, which corresponds to 1.1-1.8 mm in PWV. A temperature inversion layer was observed in the radiosonde profiles during the night, which resulted in an error of about 0.5 mm in the retrieved PWV.

During the campaign, there was a passage of precipitation clouds over western Java, moving southwestward from the Equator towards the Indian Ocean, from 26 to 29 July. A second precipitation event, with localized rain clouds near Bogor, occurred on 2 August. Both events were observed also by a C-band Doppler Radar, operated in Serpong by the Japan Agency for Marine-Earth Science and Technology (JAMSTEC) as part of the HARIMAU project. The highest value of GPS-derived PWV (about 68 mm) was observed on 27 July, coinciding with the first rainfall event. Spatial and time variations in the estimated PWV between the four sites were enhanced before both the analyzed rainfall events, on 27 July and 2 August. We thus suggest the possibility that the spatial and time inhomogeneity of PWV detected by a network of GPS receivers could be used to support the prediction of rainfall events.

Keywords: PWV, GPS, precipitation, Indonesia

A Dense Observation of the Tokyo Metropolitan Area Convective Study for Extreme Weather Resilient Cities (TOMACS)

SHOJI, Yoshinori^{1*}

¹Meteorological Research Institute

It is recognized that large cities with populations of several million people are inherently vulnerable to severe weather, such as torrential rainfall, lightning, and tornados. An increase in the occurrence of torrential rainfall and strong typhoons, which can be caused by global warming, can cause extensive damage to large cities (Ishihara, 2013). The number of days with thunderstorms has been increasing in Tokyo in recent years, and the requirement of an advanced monitoring and forecasting system for extreme weather is becoming greater.

An unprecedented dense observation campaign and relevant modeling and societal studies have been conducted since April 2010 by the National Research Institute for Earth Science and Disaster Prevention (NIED), Meteorological Research Institute (MRI), and more than 25 national institutions and universities in Japan that target local high-impact weather (LHIW) in the Tokyo metropolitan area. The objectives of the project, the Tokyo Metropolitan Area Convection Study for Extreme Weather Resilient Cities (TOMACS), include the 1) elucidation of the mechanism of LHIW in urban areas (e.g., local torrential rain, flash flood, strong wind, lightening), 2) improvement of nowcasting and forecasting techniques of LHIW, and 3) the implementation of high resolution weather information to end-users through social experiments.

One of the unique features of TOMACS is the utilization of dense meteorological instruments in the Tokyo Metropolitan area, which is one of the most urbanized areas in the world. Their objectives are to target the tropospheric environment, boundary layer, initiation of convections and the lifecycles of thunderstorms. For the study of the mechanism of LHIW, data are used from the advanced observational instruments owned by participating organizations (including X-band and C-band polarimetric radars, a Ku-band fast scanning radar, Doppler lidars, microwave radiometers, a network of Global Positioning Systems (GPS), radiosondes and unmanned aerial vehicles), which are currently deployed in the Tokyo metropolitan area in addition to the operational observation networks of the Japan Meteorological Agency (JMA) and the Ministry of Land, Infrastructure, Transport and Tourism (MILT) of Japan. The intensive operational period (IOP) of the observations was set to the summers of 2011, 2012 and 2013.

During the IOP, several LHIW events occurred and have been energetically studied. In this topic, we briefly overview the necessity of this study, observation system, and results obtained so far.

Keywords: Mesoscale Meteorology, Dense Observation, Climate Change, Extreme Weather

A case study on the local front prior to the cumulonimbus cloud and the verification of JMA-NHM simulation

NAGUMO, Nobuhiro^{1*} ; YAMADA, Yoshinori¹ ; KAWABATA, Takuya¹ ; SATO, Eiichi¹

¹Meteorological Research Institute

The local fronts observed over the Kanto plain on July 23, 2013 have been analyzed that is the origin of the isolated cumulonimbus cloud in Tokyo metropolitan area and verified numerical simulation by JMA-NHM.

The local fronts and cumulonimbus cloud formation have been examined based on the data from dense observation network around Kanto plain including Doppler radar for Airport Weather (DRAW) at Haneda, Doppler lidar installed in Tokyo Institute of Technology (Ookayama Campus) and surface meteorological data by Japan Meteorological Agency (JMA). The verification of numerical simulation was based on the results of 500 m horizontal resolution of Japan Meteorological Agency Non-Hydrostatic Model (JMA-NHM). As the initial and boundary data, JMA Meso-analysis data of 15 UTC July 22, 2013 have been adopted. The first simulations have been done with 5 km resolution covering East Japan and then nesting of 1 km and 500 m resolution have been done covering a large part of Kanto Plain. The simulation of 500 m resolution has been analyzed for 10 hours from 02UTC July 22, 2013 and the boundary process is based on Deardorff (1980).

The formation of cumulonimbus clouds in Kanto plain is often explained by the convergence of southerly wind and easterly wind. The southerly warm moist wind flows from Sagami Bay and Tokyo Bay by high pressure system in the south of Japan or sea breeze. The easterly wind flows from Kashima Bay. However, in one case of on July 23, it was found that the trigger of cumulonimbus was convergence with two different directions of sea breeze fronts and in addition gust front also plays an important role. The daytime sea breeze front is formed along the Sagami and Tokyo Bay, has entered inland at 1 m/s approximately. Several isolated cumulonimbus clouds have been formed in the rear of sea breeze front and some of them have been lost later, to form a gust front. The spread speed of gust front was about 3 m/s. The sea breeze front that was located in front of the gust front turned the direction to northwest. This sea breeze front and original northeast direction of front from Tokyo Bay have formed the convergence over Tokyo metropolitan area.

On the other hand, numerical simulations have predicted the strong rainfall in the Kanto plain but not all precipitation have been expressed. Comparing JMA-NHM 500 m resolution simulation with DRAW at Haneda, the horizontal distribution of sea breeze front was close to the position of real position. The simulations also have expressed the isolated cumulonimbus rear of sea breeze front. But the gust front spreading was small to the real one.

Doppler lidar had identified the horizontal and vertical structure of these fronts. The simulated structure by JMA-NHM can be compared with Observation. The knowledge of the representation of simulation leads to improve forecast accuracy. We would like to go on to investigate the similarities or difference between simulation and observation of these front structures.

Keywords: convective cloud, local front, numerical simulation

Numerical simulations using WRF model for reproducing localized delay signals derived from InSAR

KINOSHITA, Youhei^{1*} ; FURUYA, Masato¹

¹Natural History Sciences, Hokkaido University

For elucidating the mechanism of meso-scale phenomena involving a phase change of water molecule, water vapor is one of the most important but poorly understood parameter in meteorology. Recently, the Global Navigation Satellite System (GNSS) are routinely used to provide near-real-time estimates of PWV (Foster et al., 2005) and to assimilate routine weather forecasts (e.g. Nakamura et al., 2004). However, the limitation using GNSS atmospheric delay for meteorology is its spatial resolution, for example about 20 km for the Japanese GNSS network (GEONET). Interferometric Synthetic Aperture Radar (InSAR) phase signals, which can detect surface deformations with high-spatial resolution, are affected by earth's atmosphere like GNSS. Therefore, InSAR can detect water vapor distribution with high spatial resolution without any surface deformation signals or other errors and thus is potentially useful for meteorological applications. In previous studies, Hanssen et al. (1999) showed the coincidence between water vapor signals detected by InSAR and spatial distributions of rainfall echo detected by a weather radar (WR), indicating the possibility of InSAR as a water vapor sensor. Kinoshita et al. (2013) showed the water vapor distribution during the heavy rain event using ALOS/PALSAR emergency observation data. They conducted the estimation of the three-dimensional (3D) water vapor distribution and performed numerical simulations by means of the Weather Research and Forecast (WRF) model, which could reproduce a convective system observed as a localized signal in the InSAR image. However, there were still few cases detecting localized water vapor signals with InSAR and few studies using InSAR for meteorological applications.

In our past presentations, we reported several case studies detecting localized water vapor signals associated with deep convective systems with InSAR derived from ALOS/PALSAR data (Kinoshita et al., JpGU 2013), some of which reached over 20 cm in the line-of-sight direction within 10 km square. Observed locations of these interferograms are at Niigata (two cases), Shizuoka, Kyoto, Saga and Miyazaki. These signals are equivalent to about 21 mm in the precipitable water vapor, and are higher than that around each signal. Each signal located at the very location of high rainfall intensity in the WR data, and is regarded as including few ionospheric effects because of the use of PALSAR data with descending orbit. Such localized signals strongly suggest the existence of developed convective systems at SAR observation time. However, it is difficult to elucidate mechanisms of phenomena that caused these localized signals.

In this study, we will perform numerical simulations using the WRF model for the purpose of investigate mechanisms of these phenomena and compare simulation results with derived InSAR data. At the presentation, we will show these results and discuss them.

Keywords: InSAR, Water vapor, WRF, Propagation delay, Numerical simulation

Development and Observation of the Phased Array Radar at X band

USHIO, Tomoo^{1*} ; SHIGEHARU, Shimamura¹ ; KIKUCHI, Hiroshi¹ ; WU, Ting¹ ; MEGA, Tomoaki¹ ; MIZUTANI, Fumihiko² ; WADA, Masakazu² ; SATOH, Shinsuke³ ; IGUCHI, Toshio³

¹Osaka University, ²Toshiba, ³NICT

A new Phased Array Radar (PAR) system for meteorological application has been developed by Toshiba Corporation and Osaka University under a grant of NICT, and installed in Osaka University, Japan last year. It is now well known that rapidly evolving severe weather phenomena (e.g., microbursts, severe thunderstorms, tornadoes) are a threat to our lives particularly in a densely populated area and the number of such phenomena tends to increase as a result of the global warming. Over the past decade, mechanically rotating radar systems at the C-band or S-band have been proved to be effective for weather surveillance especially in a wide area more than 100 km in range. However, rapidly evolving weather phenomena have temporal and spatial scales comparable to the resolution limit (-10 min. and -500m) of typical S-band or C-band radar systems, and cannot be fully resolved with these radar systems. In order to understand the fundamental process and dynamics of such fast changing weather phenomena, volumetric observations with both high temporal and spatial resolution are required. The phased array radar system developed has the unique capability of scanning the whole sky with 100m and 10 to 30 second resolution up to 60 km. The system adopts the digital beam forming technique for elevation scanning and mechanically rotates the array antenna in azimuth direction within 10 to 30 seconds. The radar transmits a broad beam of several degrees with 24 antenna elements and receives the back scattered signal with 128 elements digitizing at each elements. Then by digitally forming the beam in the signal processor, the fast scanning is realized. After the installation of the PAR system in Osaka University, the initial observation campaign was conducted in Osaka urban area with Ku-band Broad Band Radar (BBR) network, C-band weather radar, and lightning location system. The initial comparison with C band radar system shows that the developed PAR system can observe the behavior of the thunderstorm structure in much more detail than any other radar system. The observed high temporal resolution images of the severe thunderstorm are introduced, showing the potential capabilities of the PAR system. The correlation coefficient of the reflectivity in PAR with C band radar ranges from 0.6 to 0.9 as a function of the distance from the PAR.

Although the phased array radar system using the digital beam forming technique can estimate the 3 dimensional structure of the precipitation system within 10 to 30 seconds with 100 meter resolution, the observation results also shows the received signal was seriously contaminated by the relatively high received power from ground clutter and strong precipitation echoes through the side lobes of the transmitting beam. To avoid this problem, a beam forming technique using the MMSE (Minimum Mean Square Error) formulation was proposed and tested. This approach can adaptively mitigate the masking interference that results from the standard digital beam forming method in the vicinity of ground clutter and strong precipitation area. The proposed method is compared with the standard beam forming technique by applying to the huge raw IF signal data digitized at each 128 antenna elements. The results show that the proposed technique can correctly estimate the precipitation echo within a few dB even in the presence of a strong ground clutter that is more than 20 dB higher than the precipitation echo with 15 pulse repetition number. The MMSE based technique is shown to be superior to the standard DBF scenarios under the small number of pulse repetitions to achieve the rapid scanning.

Keywords: Phased Array Radar, Precipitation

Descending reflectivity core analysis by Ku-band radar

SATO, Eiichi^{1*} ; KUSUNOKI, Kenichi¹ ; FUJIWARA, Chusei¹ ; SAITO, Sadao¹ ; SHOJI, Yoshinori¹

¹Meteorological Research Institute

In order to observe extreme weather such as localized heavy rainfall, tornado etc., we installed a Ku-band radar in Musashino-shi, Tokyo in 2011. Since the radar can create a 3D volume scan per minute, we expect that the data observed by the radar will contribute to understanding mechanisms of such phenomena.

In our research, we defined a cell as an area whose reflectivity is $\geq 25\text{dBZ}$, and a core as a reflectivity peak in the cell. The procedures of the cell/core detection are as follows: 1) conversion from $r\theta$ data to xyz data, 2) cell detection by binarization and labeling, and 3) core detection by method of steepest descent(ascent).

In this presentation, results of an automatic cell/core detection algorithm will be shown.

Keywords: descending reflectivity core, Ku-band radar, fast scan radar, extreme weather

Influence of urban heat excess on heavy rain environment

SUGAWARA, Hirofumi^{1*} ; SEINO, Naoko² ; ODA, Ryoko³

¹National Defense Academy, ²Meteorological Research Institute, ³Chiba Institute of Technology

There are several observed fact that cities give influence on the precipitation, or cumulus generation. However the mechanism of urban influence on precipitation is not clarified. There would be three physical processes. Buildings could form updraft through a roughness effect. Much heat excess from cars, air conditioners and asphalt roads could also form updraft. Urban aerosol can be a condensation nuclei and gives chance to form cloud, however too much nuclei should suppress cloud droplets growing.

This study focuses on the heat effect. We measured surface sensible heat flux in urban, suburban and rural areas, and evaluated the urban heat excess quantitatively. The resulted heat excess amount was used to in calculation of atmospheric stability index.

In the heat flux measurement, the eddy correlation method which should be the most reliable way of heat flux measurement was used at the rural and suburban site. At urban site, we used the scintillation method which has a advantage of larger scale of measurement (km scale) than that of the eddy correlation method (100 m scale). The reason for taking scintillation method at urban site is severe heterogeneity in urban area. Urban area is mosaic of buildings, roads, parks, bare soil on the school ground field, and sometimes rivers or channels. Scintillation method enable us to measure the area-averaged heat flux in the urban heterogeneity. We used a modified scintillation method which takes into account of surface unevenness by the buildings. We operated measurement site for three years and analyzed a hourly composite of 50 fine days in July. As a result, urban heat flux is largest followed by suburban and rural. The difference between urban and rural was 140 Wm⁻² at noon time.

We evaluated CAPE index for each site. We used simple 1D model to calculate the change of temperature profile by the surface flux. The morning initial condition to calculate daytime growing of mixed layer was acquired from the sonde observation. We adopted same initial profile for urban, suburban and rural, and give observed surface heat flux for each. This way of analysis evaluates thermal influence of land-use on CAPE index. The CAPE at 1500 LST is largest in cities and the difference between rural and city is 15%.

Keywords: heat island, urban climate

OROGRAPHIC PRECIPITATION OBSERVATION IN JEJU ISLAND, KOREA (2012-2013)

LEE, Dong-in^{1*}

¹Department of Environmental Atmospheric Sciences, Pukyong National University

In summer monsoon season, a Korean Peninsula is influenced by several weather phenomena such as the Changma-front, typhoon, strong low pressure, and local heavy precipitation. Especially, the orography plays an important role in controlling the cloud formation, amount and precipitation distribution. To find out the precipitation development mechanism by orographic effect, we performed the intensive field observation around Mt. Halla in Jeju island (33.21 N and 126.32 E, width 78 km and length 35 km) which is located at the southern part of Korea with JNU (Jeju National University), KNU (Kyungpook National University), IJU (Inje University), KMA (Korea Meteorological Administration), and NIMR (National Institute of Meteorological Research). We installed and arranged the observational instruments such as, AWS, radiosonde (including mobile sonde and ship sonde), Parsivel, 2DVD, ultrasonic anemometer, and raingauge along the altitudes in Jeju island. Each disdrometer sites were located in straight line considering topography between two S-band Doppler radars. We analyzed synoptic condition by NCEP/NCAR reanalysis data and kinematic characteristics of precipitation by dual Doppler radar analysis using S-band radars in KMA.

In 2012 case, the Changma-front was located in the northern part of the Jeju island and the precipitation system passed from the southwest to the northeast. The accumulated precipitation (31.7 mm) was recorded at the site PR4 which was placed in the highest (H: 975 m). During the passage of precipitation, the south westerly wind ($>12 \text{ m s}^{-1}$) with warm and humid air and the cold (lower layer) and warm advection (upper layer) were observed. From the microphysical analyses, PR2 (windward side, H: 571 m) and PR6 (leeward side, H: 324 m) sites indicated high rain rate about 60 to 75 mm hr^{-1} by orographic effect.

In 2013 case, the Changma-front located in the center of Jeju island and precipitation system passed from the southwest to northeast. The warm advection in lower layer and cold advection in upper layer were observed by radiosonde analyses, relatively. Strong southwesterly winds were blown with moist environment in surface layer. By the wind field analysis, convergence in west and divergence in east were existed and updraft in Jeju island and downdraft in ocean area, relatively. High number concentration at PR4, 5 and PR8 were shown with small size raindrops (less than 2 mm), however large size raindrops (larger than 6 mm) were distributed at PR7(northeast in island) and PR9(southwest in island).

Keywords: Orographic precipitation, intensive field observation, Jeju island

Characteristics of distribution and preceding surface conditions of cumulonimbus clouds appeared on Kofu Basin on a calm

SANO, Tetsuya^{1*} ; SUETSUGI, Tadashi¹ ; OISHI, Satoru²

¹International Reserch Center for River Basin Environment, University of Yamanashi, ²Research Center for Urban Safety and Security, Kobe University

On a calm summer day, cumulonimbus clouds often appear on complex terrains with the thermal induced local circulations. The appearance of such cumulonimbus clouds on a basin is not so frequent ordinarily. Once a cumulonimbus cloud appears on a basin, it often brings much rainfall in a short time, which becomes triggers of weather related disaster in urban city on a basin. However, the characteristics of the generation of cumulonimbus clouds on a basin and the conditions in a basin preceding the generation of them have not been known enough. In this study, for the example of above situation, we analyze the distribution of the appearance of cumulonimbus clouds on Kofu Basin and the conditions in Kofu Basin preceding the appearance of them.

The days of the appearances of cumulonimbus clouds on Kofu basin in a calm day confirmed by the observation of X-MP radar of University of Yamanashi (UYR) were 8 days out of 1 July to 30 September on 2012. Although the number of the events was limited, they brought large rainfall amount of 20 to 30 mm in an hour. The positions of the appearance concentrated from center to eastern side on Kofu Basin.

Before the appearance, south-southwesterly (SSW-ly) and southeasterly (SE-ly) surface wind was measured on western and eastern sides on Kofu Basin, respectively. When SSW-ly or SE-ly wind expanded to reach Kofu city that locates center of Kofu Basin, surface equivalent potential temperature (θ_e) increased. From The meso-scale objective analyzed data of Japan Meteorology Agency (JMA-MANAL) shows strong south-component wind with high- θ_e toward Kofu Basin from Suruga Bay through a valley connecting Suruga Bay to Kofu basin at the level of about 900 hPa. At the eastern side of Kofu Basin, strong east-component wind with high- θ_e crossing the mountains on the eastern side was appeared. Then, the south-component wind and the east-component wind formed horizontal convergence on Kofu basin. So, we consider that, the winds entering from the outer side of Kofu Basin, conditional instability intensified and horizontal convergence formed in Kofu Basin, which played a role as trigger of precipitating cell on Kofu Basin.

Keywords: Cumulonimbus cloud, Kofu Basin, Conditions preceding the appearance of a cumulonimbus cloud

Transition to resilience to extreme weather ,high-resolution monitoring and international synergies

SCHERTZER, Daniel^{1*} ; MAKI, Masayuki² ; TCHIGUIRINSKAIA, Ioulia¹

¹Ecole des Ponts ParisTech, U. Paris Est, ²Research and Education Center for Natural Hazards, Kagoshima U.

Transition from high vulnerability to extreme weather to resilience is a major challenge for megacities in response to two main drivers: urban sprawling and climate change. The functioning of cities, particularly the large ones, should be observed, understood, simulated and monitored on much larger ranges of scales than usually done. This requires at first observations of many geophysical fields with an unprecedented resolution to achieve high-resolution monitoring. However, this also require an advanced understanding/modeling of the nonlocal interactions between large and small scales, e.g. between weather and climate scales.

Finally, this pleads in favor of methodological approaches across scales, rather than over very limited ranges of scales. Such methodologies aim in fact to quotient out non trivial symmetries and therefore should enable us to dig out the relevant information from otherwise under-exploited big data.

Such approaches have been often invoked, but barely achieved because they correspond to formidable tasks that require an unprecedented development of international cooperation on both advanced technologies and methodologies. We will illustrate these questions with examples of research and innovation programs on flood resilience which seem rather complementary across national boundaries but require nevertheless much stronger international synergies.

Keywords: extreme weather, cities, resilience, high-resolution, synergies, international

The effect of scaling anisotropy on weather extremes

FITTON, George^{1*} ; TCHIGUIRINSKAIA, Ioulia¹ ; SCHERTZER, Daniel¹

¹Universite Paris Est, Ecole des Ponts ParisTech, LEESU, 6-8 avenue B. Pascal, Cite Descartes, 7745

Predicting extreme weather events in and around cities is far from straight forward. Even in a stable and unbounded atmosphere, crude numerical approximations of the Navier-Stokes equations are required for reasonable computation times. Hence, numerical simulations of the weather in and around cities become even more complex, and therefore require much coarser space and time scales to model both the macro weather and the complex boundary conditions created by buildings and other urban structures. Such models will severely underestimate extremes due to the necessary truncation of scales to deal with these additional complexities.

While progress in numerical simulation depends on the next fastest processor, measurement techniques on the other hand are becoming rapidly more and sophisticated. There appears however to be a gap forming in the ability to utilise the enormous datasets produced from new measurement techniques. This seems mainly due to outdated statistical methods that are used to make sense of these overwhelming databases.

In this study we propose a method, based on the structure function, that allows one to easily estimate the Levy index α of the wind. We show that due to the complex nature of a three-dimensional wind a rotated frame of reference is necessary in order to obtain a universal multifractal structure function exponent. We show that the angular dependency of the scaling exponent results in either an increase or decrease in dimension. This increase or decrease in dimension causes a first or second-order phase transition respectively. The kind of phase-transition that occurs is directly related to the generation of extremes of the wind.

The combination of this kind of analysis with the advancements in measurement techniques that are coming to light should allow for the better prediction of extreme weather events in and around cities.

Keywords: Extremes, Weather, Universal Multifractals, Wind, Anisotropy, Scaling

The Impacts of extreme weather on urban water bodies

MEZEMATE, Yacine^{1*} ; FITTON, George¹ ; TCHIGUIRINSKAIA, Ioulia¹ ; SCHERTZER, Daniel¹ ; BONHOMME, Celine¹ ; SOULIGNAC, Frederic¹ ; LEMAIRE, Bruno¹ ; VINCON LEITE, Brigitte¹

¹Universite Paris Est, Ecole des Ponts ParisTech, LEESU, Marne La Vallee, France

In the event of heavy rainfall, large amounts of storm water will carry roof runoff pollutants into urban lakes. This kind of discharge not only changes the dynamics of the lake (i.e. the mixing processes that occur) but also complicates ones ability to predict pollutant concentrations. Being able to quantify these changes in pollutant during and after extreme weather events is important for water quality management.

In the interest of understanding the impact of extreme weather events on water bodies, we set-up an Acoustic Doppler Current Profiler (ADCP) next to a storm water discharge point at the bottom of a shallow urban lake in Creteil, a region in Paris.

The ADCP is particularly useful for analysing the turbulent boundary-layer (TBL) during these extreme weather events as it is able to measure the 3D velocity, in 127 vertical cells, over 3 meters. This is a unique situation compared to the atmospheric boundary-layer where profilers are typically coarsely spaced in the vertical.

To analyse the TBL dynamics we look only at the scaling properties of the velocity field. If the velocity is scaling the log-log plot of the energy spectra will be linear in wavenumber (or frequency). The slope of the log-log plot of the spectra gives the spectral scaling exponent. Performing the analysis we find a spectral exponent close to -1. Dimensional arguments suggest that this exponent occurs when the energy flux becomes dependent on the friction velocity instead of the length scale; likely a result of the strong inflow during extreme rainfall events. The ADCP data allows us to observe a smooth transition from a free stream turbulent regime (-5/3) to a bounded-turbulent exponent (-1) through depth.

This kind of analysis suggests the possibility for a general scaling model of the TBL that can be used to predict the mixing of pollutants during and after extreme weather events.

Keywords: Urban Lake, Turbulence, Extreme Weather, Boundary-Layer

Statistical Analysis of Large Drop Occurrence and Its Effect on Drop Size Distribution

JUNG, Sung-a^{1*} ; MAKI, Masayuki² ; LEE, Dong-in¹ ; KIM, Ji-hyeon³ ; TSUCHIYA, Shyuichi⁴

¹Pukyong National University, Korea, ²Kagoshima University, Japan, ³Weather Radar Center, Korea, ⁴National Institute for Land and Infrastructure Management, Japan

A large data set of raindrop size distribution (DSD) measured by 2-Dimensional Video Distrometer (2DVD) on 12 locations in Japan is analyzed using the truncated modified gamma DSD model and the normalized gamma DSD model. The present study seeks to: 1) explore the general properties of DSD observed at Kanto, Hokuriku, Nagoya, Kinki and Kyushu in Japan; 2) find the governing parameters of DSD models in different geographical and seasonal regime; 3) statistics of big drops occurrence and intrinsic shape of the DSD with extremely large drops; 4) find relationships between DSD parameters such as the shape and slope parameters, the generalized intercept parameter and volume-weighted mean diameter, and etc. The present study on statistical analysis of DSD provide us information which is necessary to understand big drop microphysics and precipitation.

Keywords: large drop, DSD, 2DVD

A Social Experiments on Disaster Prevention by Using of the Advanced Weather Information

NAKATANI, Tsuyoshi^{1*} ; SHOJI, Yoshinori² ; MISUMI, Ryohei¹ ; NAKAMURA, Isao³ ; MAKI, Masayuki⁴

¹National Research Institute for Earth Science and Disaster Prevention, ²Dept. of Meteorological Satellite and Observation System Research, Meteorological Research Institute, ³Toyo Univ., Faculty of Sociology, ⁴ERCPD, Kagoshima Univ.

The National Research Institute for Earth Science and Disaster Prevention has been carried out the research project on Tokyo Metropolitan Area Convection Sturdy for Extreme Weather Resilient Cities(TOMACS) in cooperation with 25 research agencies, researchers of more than 100 people and disaster management personnel of local governments. In this project we have been working on the following three research subjects.

- (1) Studies on extreme weather with dense meteorological observations
- (2) Development of the extreme weather early detection and prediction system
- (3) Social experiments on extreme weather resilient cities

The study fields by the social experiment are Rescue Services (Tokyo Fire Department), Risk management(Edogawa ward, Yokohama city, Fujisawa city, Minamiashigara city), Infrastructure(JR East, JR Central, Obayashi) and Education and life(Toyo univ., The Certified and Accredited Meteorologists of Japan). In the social experiments, the each participated institutions have studied on the effective use of advanced weather information into disaster prevention according to their purposes.

The objective of social experiments are to enable the continuous use of advanced weather information through the fixing of the monitoring and prediction system of extreme weather.

And also to discuss the problems and issues revealed in the course of social experiment, and to summarize as creating resilient city in extreme weather towards relevant government ministries and agencies, local government, the general population.

In this paper, overview of the social experiments is briefly explained and issues for continue use of advanced weather information are reported through the reference to the case of Edogawa-Ward where the X-band MP radar rainfall information is providing to residents. Finally this project is supported by the Japan Science and Technology Agency and Ministry of Education, Culture, Sports, Science and Technology.

Keywords: Extreme weather, Disaster prevention, Social experiment

Analysis of meso-gamma-scale convection in tropical regions using GPS meteorology

MATSUDA, Takafumi^{1*}

¹Graduate School of Science, Kyoto University

In tropical regions such as Indonesia, strong wind with severe shower called squall occurs frequently, and has a large impact on residents in a rainy season. To predict accurately local heavy rain (occurring in a short time and in the range of a few km) is difficult today. Therefore, it is important to understand generation and development mechanism of the meso- γ -scale convection that leads to locally heavy rain.

"GPS meteorology" is a method to obtain the "atmospheric information" such as water vapor from atmospheric delay of radio waves based on a satellite "positioning error". We can estimate precipitable water vapor (PWV: integrated amount of water vapor along the zenith direction) with a high time resolution by using this method. Occurrence of rainfall associated with the meso- γ -scale convection has good correlation with the spatial non-uniformity and temporal variation of PWV estimated by the GPS meteorology technique (GPS-PWV).

The purpose of this study is to find out the generation mechanism of meso- γ -scale convection in the tropics by focusing on the GPS-PWV.

We analyzed GPS-PWV, radiosonde and rainfall data obtained from the campaign which was conducted during the rainy season of 2013 in Bandung, Indonesia.

We carried out accuracy validation of GPS-PWV by analyzing the radiosonde data. As a result, the rainfall data showed that precipitation occurred often in the late afternoon together with an increase of PWV. Furthermore, we found the daily cycle of PWV showing minimum and maximum values in the morning and late afternoon, respectively. In addition, there is a difference in an altitude of more than 1000 m in each observation point. The difference has a severe influence on GPS-PWV. Therefore, it is need to correct altitude difference effect.

Keywords: GPS meteorology, local heavy rain, meso-gamma-scale convection, tropical regions, Indonesia

Development of high resolution spatio-temporal precipitation data using a network of polarimetric X-band radars in Japan

KIM, Yu-ra^{1*} ; LEE, Dong-in¹ ; JEONG, Jong-hoon¹ ; MAKI, Masayuki²

¹Department of Environmental Atmospheric Sciences, Pukyong National University, ²Department of Research and Education Center for Natural Hazards, Kagoshima University

Localized convective precipitation develops rapidly in a very short time and is conducive to extreme local rainfall amount. The X-band polarimetric radar is useful to analyze the convective precipitation because it can provide us polarimetric radar parameters which are useful to understand microphysical process in the precipitation. However, the radar observation has some limitations in detecting initial stage of rapidly developing convective cell; the radar volume scan strategy adopted in operational radar is 5 minute interval which is not enough for measuring rapidly developing convective precipitation. To detect the early stage of convective cell, we developed the algorithm which is based on the interpolation method both in space and time. The algorithm reproduces higher resolution spatio-temporal volumetric data using the operational network of four X-band polarimetric radars. The mosaic of multiple radars could be benefit for increased sampling into a certain volume. In addition, different scan strategy at each radar also improve spatio-temporal resolution. The algorithm is applied to radar data of convective precipitations observed in Kanto area in 2012. The new volumetric data can recognize more detail about echo which developed rapidly and detect the first appearance of convective echo at upper layer. Early detection of convective precipitation at upper layer can be useful for nowcasting or very short-term forecasting.

Keywords: convective cell, X-band polarimetric radar, high resolution precipitation data

An Ensemble Nowcasting of Rainfall over the Kanto Region, Japan

P.C., Shakti^{1*} ; MISUMI, Ryohei¹ ; NAKATANI, Tsuyoshi¹ ; MAKI, Masayuki² ; SEED, Alan³

¹National Research Institute for Earth Science and Disaster Prevention(NIED), Tsukuba, Japan, ²Kagoshima University, Kagoshima, Japan, ³Bureau of Meteorology, Melbourne, Australia

Every year weather-related disasters: extreme rainfall, landslides and flooding destroy livelihoods and damage economics somewhere on the planet. Recently, number of flash flooding is believed to be increasing specially in urban areas. It has being a great challenge to forecast flood warning and urban drainage management. Nowcasting of rainfall (very short-range forecasting) is an important tool to minimize or manage all these weather-related disasters since precipitation is the main input. Common practice to forecast heavy precipitation for hydrological application varies from 0-6 hr and there are different kinds of nowcasting based on different method.

Nowcasting of rainfall comprises the detailed description of the current weather along with forecasts obtained by extrapolation for a different time period ahead. In this study, we focus on ensemble nowcasting of rainfall. It refers to the fact that many forecasts are produced, with the rainfall areas moving at slightly different speeds, and with the small rainfall features represented by slightly different random statistics. By comparing these different nowcasting of rainfall, the forecaster can decide how likely a particular weather event will be. It gives a much better idea of what weather events may occur at a particular time. Short Term Ensemble Prediction System (STEPS), one of the most advanced Quantitative Precipitation Forecast (QPF) systems currently available is considered for nowcasting of rainfall. Japan Meteorological Agency (JMA) and X-band multi-parameter (MP) radar data were considered to produce an ensemble nowcasting of rainfall. First, JMA radar rainfall data of Kanto region was fixed to check the performance of STEPS. Skill scores showed that STEPS can give a good forecast for less than one hour. However, more uncertainties can be seen during the starting and ending of rain event. High resolution of data (MP data) also used in the STEPS under the default condition. Overall, an ensemble nowcasting of rainfall seems close with real time data, which could be interesting to use them in hydrological model.

Keywords: nowcasting, ensemble, weather radar, extreme rainfall, STEPS, hydrological model

X-band polarimetric radar and C-band conventional radar composite rainfall map with high spatio-temporal resolution

MAKI, Masayuki^{1*} ; HIRANO, Kohin² ; P.C., Shakti² ; SCHERTZER, Daniel³

¹Kagoshima University, ²NIED, ³Ecole des Ponts ParisTech, U. Paris-Est

Radar with shorter wavelength such as the X-band (3-cm) wavelength has several advantages compared to C- and S-band radar. First, X-band wavelength radar has high sensitivity of the specific differential phase of the rain rate. Second, it is possible to achieve finer spatial resolution more economically; for example, X-band wavelength radar can achieve a 1 degree beam width with a 2 m diameter parabolic antenna, while S-band needs a 7 m diameter antenna to achieve the same beam width. Third, due to advantage number two, X-band radar is easier to setup in mountainous areas, and at lower cost compared to S- and C-band wavelength radar. In Japan, success in the detection of torrential rainfall that occurred in Tokyo in 2008 triggered the deployment of 35 operational X-band polarimetric radars in major urban cities by MLIT. This radar network named XRAIN provides rainfall information with high spatio-temporal resolution. In US, the X-band polarimetric radar network is constructed in Dallas Fort Worth, which is a research and innovation network linking academic researchers, local stakeholders, and industry to address water issues as they relate to urban sustainability. In Europe, The project named RAINGAIN is ongoing to improve fine-scale measurement and prediction of rainfall and to enhance urban pluvial flood prediction. Activities include the implementation and use of advanced radar technologies (X Band) in Leuven, London, Paris, and Rotterdam. Although X-band polarimetric radar has the advantages mentioned above and used in hydrological applications, there are essential disadvantages. First, the maximum range is shorter than that of C-band and S-band radar; maximum ranges of 200km or 300km are easily obtained in case of C- and S- band radar, while that of X-band radar is limited to 30km-60km. Second, signal extinction area which is defined as the area where the received signal is below the receiver noise level occurs behind heavy rainfall areas. These disadvantages will be a fatal flaw when extremely heavy rainfalls occur. Authors have experience that the maximum observation range of X-band radar was shorter than 3km when heavy rainfall passed over the radar site. The present paper aims to develop an algorithm to overcome these disadvantages. The method is based on the C-band and X-band radar composite map which attains the 1 minute time resolution and 250m spatial resolution by the interpolation method. The algorithm is applied to the heavy rainfall case observed on 12-14 July, 2012 in northern Kyusyu, Japan. The algorithm is validated with surface raingauge network: the composite radar rainfall estimation agreed well with raingauge data.

Keywords: polarimetric radar, X-band, precipitation, high resolution, MP radar

Entropic Balance Theory and Variational Field Lagrangian Formalism

SASAKI, Yoshi kazu^{1*}

¹University of Oklahoma

The entropic balance theory has been applied with outstanding results to explain many important aspects of tornadic phenomena. The entropic balance theory was originally developed in variational formalism with Lagrangian appropriate for supercell storm and tornadic phenomena. The entropic balance theory shares the same foundation as, symbolically called with keywords, "variational field Lagrangian formalism" in short "variational formalism". It is broadly used in modern physics, not only in classical mechanics, with Lagrangian density and action designed for each physical problem properly. The Clebsch transformation (equation) was developed in the classical variational formalism, but has not been used because of the unobservable and non-meteorological Lagrange multiplier.

The Lagrange multipliers appeared in the Clebsch transformation are analogous to the mathematical vector potential (and gauge field) of the theoretically found Aharonov-Bohm effect. Its experimental verification has been difficult and has not been made until two decades later. The Lagrange multipliers in the Clebsch transformation seem similar to the vector potential and gauge of electromagnetic field and in advanced physics disciplines.

The entropic balance condition is thus developed from the Clebsch transformation, changing the unobservable non-meteorological Lagrange multiplier to observable meteorological rotational flow velocity with entropy and making it applicable to tornadic phenomena.

Deterministic predictability of the most probable state and reformulation of variational data assimilation

TSUYUKI, Tadashi^{1*}

¹Meteorological Research Institute

Four-dimensional variational data assimilation (4DVar) and ensemble Kalman filter (EnKF) have been widely used for data assimilation in meteorology and oceanography. Since prior probability density functions (PDFs) used in 4DVar and EnKF are usually assumed to be Gaussian, those two methods may not work well for a strongly nonlinear system. Thus data assimilation with nonlinear systems or non-Gaussian PDFs is a challenge in geophysics. Theoretical study of the two methods for nonlinear systems may be expected to provide insight for further advancement of data assimilation. The present study addresses this issue by reformulating variational data assimilation.

A necessary condition for deterministic predictability may be that the forecast state starting from the most probable state at an initial time remains close to the most probable state at a forecast time. It is found from the Liouville equation that if the trace of the Jacobian matrix of a deterministic nonlinear system does not depend on the state variables (hereafter referred to as the trace condition), the mode of a PDF of the state variables evolves according to the governing equations of the system. A condition for the forecast state to be close to the mode of the PDF is derived under an assumption of small prediction error for general deterministic nonlinear systems. This condition depends on the sensitivity of the trace to an initial condition, the size of initial condition error, and the length of forecast lead time.

Since the dynamical cores of numerical models of the atmosphere and the ocean are based on fluid dynamics, it is interesting to examine whether the governing equations of fluid dynamics satisfy the trace condition. The trace of the Jacobian matrix is calculated for finite-dimensional analogs of several Eulerian equations of ideal fluids. It is readily found that the trace condition generally holds for unbounded fluids under periodic boundary conditions. It is shown that the trace condition also holds for the quasigeostrophic equations with rigid boundaries, the Boussinesq approximation with rigid boundaries, and the shallow water equations on a sphere, by expanding the state variables in eigenfunctions of the Laplacian operator or the curl operator. The shallow water equations in a channel and compressible fluid with top and bottom boundaries do not satisfy the trace condition due to divergence at the boundaries.

A new formulation of variational data assimilation is presented for deterministic nonlinear systems that satisfy the trace condition. Though the cost function in the new formulation takes the same form as the conventional one, it makes clear an advantage of 4DVar over EnKF. If the trace condition holds, the forecast state starting from the mode of the posterior PDF at the last analysis time is the mode of the prior PDF. In the new formulation, the logarithm of the prior PDF is expanded around the forecast state, and covariance globalization is introduced to take into account the global distribution of the prior PDF that may be non-Gaussian. A feasible method for the covariance globalization may be to replace the local covariance matrix at the mode with a forecast error covariance matrix taken from EnKF. It is proved that a non-Gaussian prior PDF that evolves according to the Liouville equation is implicitly used for assimilating observational data in 4DVar. Results from an assimilation experiment with a toy model suggest that 4DVar thus formulated outperforms EnKF if the global minimum of the cost function is found.

Finally, it is pointed out that enough observational data are necessary for variational data assimilation to work well for a deterministic nonlinear system that does not satisfy the trace condition. Otherwise, EnKF and ensemble prediction may be a better choice for data assimilation and prediction of the system.

Keywords: variational data assimilation, deterministic predictability, non-Gaussianity

Modal analysis of near-bank velocity profiles in a tidal river.

WELLS, John^{1*} ; PHAN, Tuy¹ ; NGUYEN, Linh V.¹ ; SUSUKI, Yoshihiko² ; BONNER, James³ ; ISLAM, Mohammad S.³ ; KIRKEY, William D.³

¹Ritsumeikan University, ²Kyoto University, ³Clarkson University

We apply two decompositions to long-beam velocities of a 600 kHz 3-beam Horizontal Acoustic Doppler Current Profiler (HADCP) at West Point on the Hudson River Estuary, so as to efficiently characterize the spatiotemporal variation of near-bank velocity. One main motivation is to test statistical tools with which to benchmark computations. The HADCP is deployed next to the USGS gauging station at West Point, some 100 km upriver from Manhattan, on the inner bank downstream of a sharp bend and its associated 40 m deep trough. We analyzed a time series of 1-minute averages from October 2011, out to 80 meters from the bank with 1 m bins.

The first decomposition we apply is Principal Component Analysis. The PCA generates an optimally convergent set of spatial eigenfunctions or "principal components" (PC), with which are associated temporally-varying amplitudes called "temporal coefficients". The first principal component captures more than 96.3% of the variance in velocity measured along the three HADCP beams, while the second PC captures about 2%. There appears an asymmetry between ebb and flood, as seen clearly from a phase plot of the temporal coefficient of the first PC versus that of the second.

The second is Fourier-based Koopman Mode Decomposition, i.e. decomposition into harmonic averages of the measurement vector. KMD associates a spatial structure with each of a series of temporal frequencies. For Oct 2011, the semidiurnal mode captured 74.33% of the variance. KMD also quantifies the phase lags at different distances from the river bank (and between normal and tangential velocity). Phase lags of tangential velocity between 10 and 80 m from the bank were about 1 hour for the semidiurnal mode, and 2 hours for the first (with a period of about 6 hours.), and this difference grew to a factor of four when considering flow within 10 m.

Keywords: principal component analysis, Koopman mode decomposition, ebb-flood asymmetry

Pathways of the North Pacific Intermediate Water identified through the tangent linear and adjoint codes of an OGCM

FUJII, Yosuke^{1*} ; NAKANO, Toshiya² ; USUI, Norihisa¹ ; MATSUMOTO, Satoshi² ; TSUJINO, Hiroyuki¹ ; KAMACHI, Masafumi¹

¹Meteorological Research Institute, ²Japan Meteorological Agency

We develop a strategy of tracing a target water mass, and apply it for analyzing the pathway of the North Pacific Intermediate Water (NPIW) from the subarctic gyre to the northwestern part of the subtropical gyre south of Japan in a simulation of an ocean general circulation model. This strategy estimates the pathway of the water mass that travels from an origin to a destination area during a specific period using a conservation property concerning tangent linear and adjoint models. In our analysis, a large fraction of the low salinity origin water mass of NPIW initially comes from the Okhotsk and Bering Seas, meets at the southeastern side of the Kuril Islands, and is advected to the Mixed Water Region (MWR) by the Oyashio current. It then enters into the Kuroshio Extension (KE) around the first KE ridge, and is advected eastward by the KE current. It, however, deviates southward from the KE axis around 158E over the Shatsky Rise, or around 170E on the western side of the Emperor Seamount Chain, and enters into the subtropical gyre. It is finally transported westward by the recirculation flow. This pathway corresponds well to the shortcut route of NPIW from MWR to the region south of Japan inferred from the analysis of the long-term freshening trend of NPIW observation.

Keywords: Adjoint, Sensitivity analysis, North Pacific Intermediate Water, Kuroshio Extension, Oyashio

Optimization of nested ocean circulation model by four dimensional variational data assimilation system

WAKAMATSU, Tsuyoshi^{1*} ; ISHIKAWA, Yoichi¹

¹Japan Agency for Marine-Earth Science and Technology

Optimization of a regional ocean circulation model by a data assimilation system is achieved by estimating optimal initial condition and external forcing terms which include boundary values. In a nested regional data assimilation system, extracting maximum information from optimized outer model through these control variables is crucial to obtain optimal performance of the nested regional data assimilation system and many schemes were proposed in the atmospheric and oceanic data assimilation studies. In this presentation, the optimization schemes of a nested atmosphere and ocean circulation model by four dimensional variation data assimilation system are summarized in a unified framework. Their performance will be analyzed using observability matrix of a variational data assimilation system constructed on regional ocean circulation model surrounding Japan islands.

Keywords: data assimilation, regional ocean circulation model

Estimated State of Ocean for Climate Research by Using a 4 Dimensional Variational approach

MASUDA, Shuhei^{1*} ; DOI, Toshimasa¹ ; OSAFUNE, Satoshi¹ ; SUGIURA, Nozomi¹ ; ISHIKAWA, Yoichi¹ ; FUKUDA, Kazuyo¹

¹JAMSTEC

A 4-dimensional variational data assimilation system has been used to better define the 50-year global ocean state estimation for climate research. The synthesis of available observations and general circulation model with a pelagic ecosystem model based on nitrogen cycle yields a dynamically self-consistent dataset. Obtained ocean state estimation possibly has greater information than do models or data alone. In our 4D-VAR approach, optimized 4-dimensional analysis fields are sought by minimizing a cost function on the basis of adjoint method for physical parameters and Green's function approach for biogeochemical ones. The assimilated elements are temperature and salinity based on EN3 dataset provided by Met Office Hadley Centre, sea surface height anomaly from AVISO, nitrate from WOA05, and chlorophyll-a from WOA98 and SeaWiFS. We here present the properties of the analysis fields and some results of climate study by using this state estimation named ESTOC. This report implies that our synthesis scheme as a dynamical interpolation for sparse observations including bio-geochemical parameters is possibly promising and useful for " Integrated Earth System Analyses " .

Keywords: data assimilation, ocean, climate change

Data assimilation for ocean and climate study

ISHIKAWA, Yoichi^{1*} ; NISIKAWA, Shiro¹ ; MASUDA, Shuhei¹ ; TOYODA, Takahiro² ; SUGIURA, Nozomi¹ ; WAKAMATSU, Tsuyohi¹ ; NISIKAWA, Haruka¹ ; SASAKI, Yuji¹ ; IGARASHI, Hiromichi¹ ; TANAKA, Yusuke¹ ; AWAJI, Toshiyuki³

¹JAPAN Agency for Marine-Earth Science and Technology, ²Meteorological Research Institute, ³Kyoto University

The data assimilation systems have been developed for the initialization of the numerical weather forecasting, and applied for other fields in recent studies. In the area of ocean and climate research, there are several interesting studies to utilize the advantage of the many aspects of the data assimilation, in addition to the "ocean weather forecasting".

The atmosphere-ocean coupled data assimilation system using variational adjoint method is one of the unique systems, which is developed in JAMSTEC. The target of this system is the variability of seasonal to inter-annual scale so that the integrated dataset of the observation both in atmosphere and ocean are derived using variational adjoint method. The remarkable feature of the system is that the bulk coefficients are estimated as well as the initial condition of the oceanic fields since the lower boundary condition of the atmospheric model are very important for seasonal to inter-annual time scale. Recently, the marine ecosystem model are embedded into this system and seasonal forecasting not only for physical fields but also for biogeochemical fields are carried out.

For oceanic long-term reanalysis dataset, the interesting data assimilation systems are developed using variational adjoint method (Masuda et al., 2010). In this data assimilation system, strong constraint conditions are applied for entire assimilation period over 50 years, so that the derived dataset are consistent with the dynamics in ocean general circulation model. This means that the derived dataset satisfies the conservation rules and suitable for the 4-dimensional analysis of the heat and water fluxes. This advantage is also suitable for the analysis of the oceanic tracers and useful for the biogeochemical studies.

The data assimilation system for the marine ecosystem model is also notable issues. Since it is difficult to identify the optimal parameters in the marine ecosystem model, the parameter estimation studies are widely used. The realistic fields of the biogeochemical variables are successfully obtained by parameter estimation (Toyoda et al., 2013).

Development of an ensemble-based data assimilation system with a coupled atmosphere-ocean GCM

KOMORI, Nobumasa^{1*} ; ENOMOTO, Takeshi² ; MIYOSHI, Takemasa³ ; YAMAZAKI, Akira¹ ; TAGUCHI, Bunmei¹

¹Earth Simulator Center, JAMSTEC, ²Disaster Prevention Research Institute, Kyoto University, ³RIKEN Advanced Institute for Computational Science

To enhance the capability of the local ensemble transform Kalman filter (LETKF) with the Atmospheric general circulation model (GCM) for the Earth Simulator (AFES), a new system has been developed by replacing AFES with the Coupled atmosphere-ocean GCM for the Earth Simulator (CFES). An initial test of the prototype of the CFES-LETKF system has been completed successfully, assimilating atmospheric observational data (NCEP PREPBUFR archived at UCAR) every 6 hours to update the atmospheric variables, whereas the oceanic variables are kept unchanged throughout the assimilation procedure.

An experimental retrospective analysis-forecast cycle with the coupled system (CLERA-A) starts on August 1, 2008, and the atmospheric initial conditions (63 members) are taken from the second generation of AFES-LETKF experimental ensemble re-analysis (ALERA2). The ALERA2 analyses are also used as forcing of stand-alone 63-member ensemble simulations with the Ocean GCM for the Earth Simulator (EnOFES), from which the oceanic initial conditions for the CLERA-A are taken.

The ensemble spread of SST is larger in CLERA-A than in EnOFES, suggesting positive feedback between the ocean and the atmosphere. Although SST in CLERA-A suffers from the common biases among many coupled GCMs, the ensemble spreads of air temperature and specific humidity in the lower troposphere are larger in CLERA-A than in ALERA2. Thus replacement of AFES with CFES successfully contributes to mitigate an underestimation of the ensemble spread near the surface resulting from the single boundary condition for all ensemble members and the lack of atmosphere-ocean interaction.

In addition, the basin-scale structure of surface and subsurface ocean temperature in the tropical Pacific is well reconstructed from the ensemble correlation in CLERA-A but not in EnOFES. This suggests that use of a coupled GCM rather than an oceanic GCM could be important even for oceanic analysis with an ensemble-based data assimilation system.

Data assimilation experiment of water vapor data derived from a hyper-dense GNSS network using a nested LETKF system

OIGAWA, Masanori^{1*} ; TSUDA, Toshitaka¹ ; REALINI, Eugenio¹ ; IWAKI, Yuya¹ ; SEKO, Hiromu² ; SHOJI, Yoshinori² ; SATO, Kazutoshi³

¹Research Institute for Sustainable Humanosphere (RISH), Kyoto University, ²Meteorological Research Institute (MRI), Japan Meteorological Agency (JMA), ³Japan Aerospace Exploration Agency (JAXA)

Data assimilation of observation data with high spatial and temporal resolutions within a numerical weather prediction model is important, in order to provide it with accurate and detailed initial conditions, which generally result in improved forecast accuracy for localized heavy rainfall. Assimilation of water vapor data is especially important because water vapor has a powerful effect on the initiation and development of cumulonimbus clouds. Many assimilation studies reported on the significant and positive impact of assimilating GNSS (Global Navigation Satellite System) derived PWV (Precipitable Water Vapor) data, i.e. the vertically integrated water vapor amount, on the modification of the initial distributions of water vapor, as well as on the forecast accuracy of localized heavy rainfall. The Japan Meteorological Agency (JMA) routinely assimilates PWV data derived from the nationwide GNSS observation network (GEONET) operated by the Geospatial Information Authority of Japan (GSI), which has a horizontal resolution of about 20 km. It is expected, however, that the assimilation of PWV data with higher spatial resolution will be needed as the horizontal resolution of numerical models becomes higher. Therefore, we investigated the assimilation impact of high resolution PWV observations derived from a hyper-dense GNSS network with a horizontal resolution of about 1 km, which we installed near Uji campus of Kyoto University (Sato et al., 2013).

The data assimilation carried out in this report is based on a two-way nested Local Ensemble Transform Kalman Filter (LETKF) system (Seko et al., 2013). Experiments were performed involving a heavy rainfall event that occurred on 14 August 2012, which brought about 260 mm of accumulated rain amount in 6 hours. First, GEONET-derived PWV data were assimilated into an outer model, with horizontal resolution of 15 km. The analysis window and assimilation interval of this first experiment were 6 hours and 1 hour, respectively. Next, PWV data derived from the hyper-dense GNSS network were assimilated into an inner model, with horizontal resolution of 1.875 km. The analysis window and assimilation interval of this second experiment were 1 hour and 10 minutes, respectively. Surface observations and upper atmospheric sounding data used in operational analyses by JMA were also assimilated in both the experiments.

In an experiment without assimilation of any PWV data, the location of the reproduced rainfall region was shifted, and the precipitation intensity was lower, compared with the observation result. When GEONET-derived PWV were assimilated into the outer model and no PWV data were assimilated into the inner model, the location of the simulated rainfall system was improved, although there was no modification in precipitation intensity. When PWV derived from the hyper-dense GNSS network was assimilated into the inner model together with the assimilation of GEONET-derived PWV into the outer model, the precipitation intensity was also modified in addition to the modification of rainfall system location.

These results suggest the usefulness of assimilating high spatial resolution PWV data for heavy rainfall forecast. In the future, we are planning to investigate how the assimilation impact of high resolution PWV data will change depending on the number of observation points of the hyper-dense GNSS network. In this talk, assimilation results of slant water vapor data will also be reported, which is the accumulated water vapor amount along ray paths of radio signals from a receiver to GNSS satellites.

Keywords: Data assimilation, local heavy rainfall, Hyper-dense GNSS observation, nested LETKF

Data assimilation experiments of tropical cyclones with the NHM-LETKF

KUNII, Masaru^{1*}

¹Meteorological Research Institute

Intensity forecast of tropical cyclones (TCs) has still been a challenging task whereas TC track forecasts have constantly improved over the past several decades owing to advances in numerical weather prediction models as well as observational capabilities. This is partly due to the difficulties in TC initialization because TCs occur and remain almost throughout their existence over the ocean, where observational data have generally been scarce. In this study, TC vital observations are assimilated with an ensemble Kalman filtering, and their impacts are estimated by comparing with the conventional bogus assimilation scheme.

Keywords: data assimilation, ensemble Kalman filter, tropical cyclone

Tropical cyclone forecast using a hybrid EnKF-4DVar system

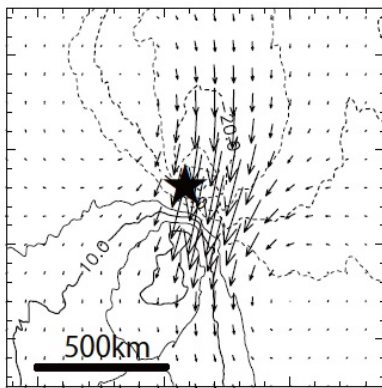
ITO, Kosuke^{1*} ; KUNII, Masaru² ; KAWABATA, Takuya² ; SAITO, Kazuo² ; HONDA, Yuki³

¹JAMSTEC, ²MRI, ³JMA

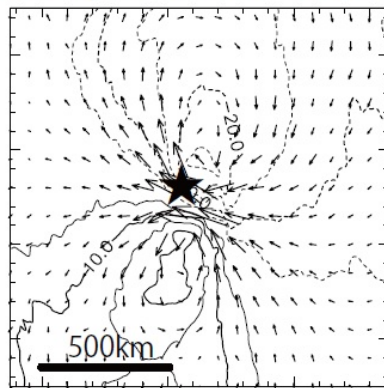
Analysis increment is dependent on the prescribed background error covariance \mathbf{B} in addition to innovation and model dynamics that describes the development of perturbations. Traditionally, \mathbf{B} is assumed to be static in time according to so-called NMC method. Following this method, the differences between pairs of forecasts valid at the same time, but having different lead times, are taken to represent the background error. While \mathbf{B} in NMC method approximates the climatological background error covariance, recent studies have shown that the forecast skill of 4DVar is further enhanced by making flow-dependent \mathbf{B} out of the perturbations in the ensemble-Kalman filter (EnKF) (Buehner et al. 2010). This system is referred to as Hybrid EnKF-4DVar. We have developed the meso Hybrid-4DVar system based on the meso 4DVar system (JNoVA) in the Japan Meteorological Agency since the improvements is thought to be more pronounced for severe impact weather such as tropical cyclones and heavy rainfall. In this presentation, we present a preliminary result for a forecast of tropical cyclone Talas (2011). Figure 1 shows the analysis increment of horizontal wind in the conventional 4DVar and hybrid EnKF-4DVar. The first guess of the zonal wind is overplotted. It shows a pseudo observation of wind field near the center of the tropical cyclone yields the analysis increment of a pair of cyclonic and anti-cyclonic circulations. It corresponds to a vortex displacement in the hybrid EnKF-4DVar system. In contrast, the analysis increment does not fit the structure of the tropical cyclone when using \mathbf{B} based on the NMC method. It suggests that the hybrid EnKF-4DVar system reproduces the reasonable analysis increment with a little information.

Keywords: data assimilation, tropical cyclone, 4DVar, ensemble Kalman filter

(a) conventional 4DVar



(b) Hybrid EnKF-4DVar



Dual-Scale Neighboring Ensemble Variational Assimilation for a Cloud-Resolving Model

AONASHI, Kazumasa^{1*}

¹Meteorological Research Institute, Japan Meteorological Agency

1. Introduction

The purpose of the present study is to develop an Ensemble-based Variational Assimilation (EnVA) scheme with sampling error damping method for the Cloud-Resolving Model (CRM). This is because, in ensemble-based assimilation schemes for CRMs, sampling error is serious, in particular, for precipitation-related variables (precipitation rate, vertical wind speed) because they are confined in rainy areas.

2. Dual-Scale Neighboring Ensemble Variational Assimilation method

Based on the CRM ensemble forecast error analyses for various precipitation cases, we developed the sampling error damping method that consisted of a Neighboring Ensemble (NE) method and a dual scale separation of NE. The NE method approximated the forecast error correlation using NE members within a reduced-grid box (5 x 5 grids in the present study) based on the spectral localization assumption. In the dual scale separation, we divided the NE forecast error into large-scale portions (13 x 13 grid averages in the present study) and small-scale deviations so as to reflect the horizontal scale differences in forecast error between precipitation-related variables and others.

In order to introduce the sampling error damping method to the three-dimensional EnVA, we assumed that the EnVA analysis increments were subject to the dual scale NE forecast error subspace. In addition, we introduced a vertical reduce approximation using the primary Singular Value Decomposition (SVD) modes of the vertical cross correlation of the dual scale NE forecast error. Since the SVD modes were mutually independent, the three-dimensional cost function of EnVA resulted in that for the horizontal component of the analysis increment of the each SVD mode. Then, we horizontally diagonalized the background term of the cost function using the horizontal correlation of the NE forecast error. We used the conjugate gradient scheme to solve the nonlinear minimization of the cost function, and obtained the optimal analysis increment for the ensemble mean. Then, we calculated the analysis increments for ensemble members with the analysis error covariance at the reduced grids.

3. Results of OSSEs

In order to examine the EnVA scheme, we performed OSSEs for several meteorological disturbance cases. The results show that the NE method was successful in producing plausible analyses of precipitation-related variables from the simulated surface precipitation even for grid points where less than 20 % of the ensemble members forecasted precipitation, and that the dual scale separation of NE made spatial scale changes in analysis increments in correspondence with precipitation rates. The EnVA scheme was also successful in retrieving precipitation flags and precipitation profiles from the simulated multi-channel microwave brightness temperatures that were non-linear functions of various precipitation-related variables.

Keywords: Ensemble-based variational data assimilation, Neighboring ensemble, Dual-scale separation, GPM, GCOM, microwave imager

Decadal climate prediction using 4D-VAR data assimilation approach

MOCHIZUKI, Takashi^{1*} ; ISHIKAWA, Yoichi¹ ; MASUDA, Shuhei¹ ; AWAJI, Toshiyuki²

¹JAMSTEC, ²Kyoto University

It is very recently that decadal climate prediction experiments have been carried out with initialization. As a first step in decadal prediction, simple initialization approaches have usually been used so far, particularly focusing on ocean states. An advanced initialization technique is a pressing concern toward further enhancing the decadal predictability by obtaining suitable atmospheric and oceanic initial conditions that are compatible with both the model and observations. Here, by employing a 4D-VAR data assimilation approach to initialize the atmosphere-ocean coupled climate model, we attempt to perform ensembles of decadal hindcast experiments in line with the CMIP5 protocol. We perform full-field initialization rather than anomaly initialization and assimilate the atmospheric states together with the ocean states. We can validate the predictive skills in the atmosphere and ocean temperature hindcasts in some areas and, roughly speaking, the spatial patterns of the hindcast skills are similar to those of the multi-model ensembles of the CMIP5 decadal hindcasts. While our assimilation system has been developed originally for the purpose of seasonal-to-interannual climate simulations and we use 9-month assimilation window in these experiments, the hindcast results suggest that the atmosphere and ocean states associated with low-frequency variations beyond annual timescales can also be effectively initialized through the iterations of the forward and backward runs of the 4D-VAR data assimilation.

Keywords: decadal prediction, climate prediction, global warming, data assimilation, 4D-VAR

Assimilation of TRMM-PR bright band heights

ENOMOTO, Takeshi^{1*} ; YAMAMOTO, Munehisa²

¹Disaster Prevention Research Institute, Kyoto University, ²Graduate School of Science, Kyoto University

Bright band heights in TRMM PR 2A23 are assimilated as temperature observations. Bright bands are strong radio echo from the melting layer. Bright band heights are located several hundred m below the 0C isotherms (Harris et al. 2000). In the TRMM PR algorithms (Awaka et al 2009), bright band heights are computed as the nadir projection of the distance between the satellite and the Earth ellipsoid minus the distance between the bright band peaks. Although the 0C isotherms from reanalysis or operational analysis are required in detection of bright bands, bright band heights are direct observations. Because bright band heights are valuable information to complement sparse direct measurements over ocean, the analysis can be improve when assimilated. Satellite radiances are mainly used in cloud-free area and assimilation of water substances are not straightforward. By contrast, because bright bands are associated with stratiform clouds, bright band heights are easily assimilated as conventional data over cloudy regions.

The data assimilation system ALEDAS2 (Enomoto et al. 2013) used in this study is composed of the atmospheric general circulation model for the Earth Simulator (AFES) and the local ensemble transform Kalman filter (LETKF). The resolution of the model is T119L48 (1 degree horizontally and 48 levels vertically) and the ensemble size is 63. ALERA2 produced with this system is regarded as the control. Bright band observations are processed as follows. First, each record is regarded as a 0C temperature observation at 500 m above the bright band height. Second, in order to avoid excessive horizontal correlations and computational load, super-observations are produced by the average of observations within 0.5 degree radius linearly weighted with the distance and converted to the LETKF input format in the 1 h window.

The number of the original bright band heights in January 2010 is 2572986 and that of the super-observations is 61905. The super-observations are widely distributed in the tropics and subtropics between 35S and 35N. In the Northern Hemisphere bright bands are clustered along the 30N over ocean, indicating bright bands due to stratiform associated with cyclones along the storm track (Yamamoto et al. 2006). A few bright bands are detected in the horse latitudes between the equator and 25N. In the Southern Hemisphere bright bands are distributed in the tropical and subtropical convergence zones. ALEDAS2 uses the 7 h data window for each analysis time every 6 h. The number of temperature observations increases by a few percent in synoptic hours of 0 and 12 UTC, but by a factor of 1.5 or 2 at 6 and 18 UTC.

In a preliminary experiment from 0 UTC 3 January for 4 d, the analysis ensemble spread, a measure of the analysis error, is reduced by 0.51 Pa and 0.94 Pa over the globe and in the Souther Hemisphere (35S-0), respectively at 0 UTC 7 January. The root mean square of the analysis increment increases by 2.4 % and 5.9 % in the global domain and in the Souther Hemisphere (35S-0).

Keywords: melting layer, satellite data assimilation in cloudy area, observing-system experiment

A Study on the Structure of Instability in the Mesosphere Using a High Resolution General Circulation Model

SATO, Kaoru¹ ; MASUDA, Akihiro^{1*} ; OKAMOTO, Kota¹

¹Dept Earth & Planetary Sci., The University of Tokyo

It is well known that in the winter mesosphere, a necessary condition of barotropic and/or baroclinic instability, i.e., negative latitudinal gradient of potential vorticity (PV), is frequently satisfied. This study examines dynamical mechanism of the formation of such instability condition in boreal winter using high-resolution general circulation model data. This model does not include gravity wave (GW) parameterizations and hence all GWs are resolved, allowing us to analyze GWs directly. This is a strong advantage of our study because GWs are quite important for the momentum budget in the mesosphere. First, the 2-d TEM analysis was made. It is shown that the negative PV gradient is regarded as an enhanced PV maximum. This maximum is due to the poleward shift of the westerly jet in associated with strong EP-flux divergence caused by planetary waves from the troposphere. Strong GW drag slightly above the westerly jet shifts poleward as well, which can be understood by a selective GW-filtering mechanism. It seems that this GW-drag shift induces strong upwelling in the middle latitudes and adiabatically cools the middle mesosphere. Resultant enhanced static stability is the main cause of the PV maximum in the upper mesosphere. Because of the dominance of planetary waves during this event, this process may not be zonally uniform. Thus, the 3-d analysis was made using recent theoretical formula by Kinoshita and Sato (2013). As expected, the GW drag is distributed depending on the longitude. The zonal structure of PV maximum is consistent with the GW drag distribution. An interesting fact is that the spatial distribution of GW drag is not largely correlated with that of the zonal wind at the same level but highly correlated with that in the stratosphere. This result indicates that the mesosphere reflects the zonal structure of the stratosphere via the selective GW filtering.

Dynamical mechanism of multiple tropopause structure observed over Syowa Station

SHIBUYA, Ryosuke^{1*}; SATO, Kaoru¹

¹Department of Earth and Planetary Science, Graduate School of Science, The University of Tokyo

Multiple tropopauses which are determined following the definition by the World Meteorological Organization (WMO) were detected in winter at Syowa Station (69.0S, 39.6E). It is shown that the multiple tropopause structures were observed along with a descent of the first (i.e., lowest) tropopause five times in the autumn period from 1 April and 16 May 2013. A detailed analysis using data from the PANSY radar and radiosonde observations was performed for a typical case in 8-11.

The mechanism of the multiple tropopause structure was analyzed using the PANSY radar and radiosonde observations. It is shown that the multiple tropopause structure was regarded as strong temperature fluctuations with a vertical length of about 3 km. Moreover, it is seen that the temperature fluctuations were out of phase with vertical wind fluctuations observed by the PANSY radar by 90°. This feature is consistent with the linear inertia-gravity wave theory. Thus, it is likely that the multiple tropopause structure above the first tropopause was due to the temperature fluctuations associated with an inertia-gravity waves (IGW) having a vertical length of about 3 km. The hodograph analysis also indicates that the multiple tropopause structure above the first tropopause is due to a monochromatic IGW.

To examine the dynamical mechanism and three-dimensional structure of this phenomenon, a numerical simulation was performed by NICAM without using any gravity wave parameterization. The model simulation period is from 0000 UTC 7 April 2013 to 0000 UTC 12 April 2013.

A close look at the time-height cross section of the zonal wind velocity and the static stability over Syowa Station indicates that the multiple tropopause structures together with the descent of the first tropopauses and associated wind disturbances were successfully simulated. A polar front jet strongly meanders in the time period from 8 April to 10 April and a tropopause folding structure is developed near Syowa Station. This means that the descent of the first tropopause was likely caused by the passage of a developing tropopause folding over Syowa Station. The IGW parameters were also consistent with those estimated by the hodograph analysis using the PANSY radar data.

Next, possible sources of the IGWs observed over Syowa Station were examined using data from the NICAM simulation. As a result, it was shown that wave packets observed over Syowa Station include gravity waves both excited by the steep topographic effect and the spontaneous adjustment process.

This mechanism is quite different from mechanisms which previous studies examined in the monsoon region or midlatitude, which is closely related to stratosphere-troposphere exchange (e.g. Randel et al. 2007). It is suggested this enable us to interpret a part of a significant seasonal sensitivity in the poles discussed by Anel et al. (2008). The static stability in the winter lower stratosphere in the Antarctic is particularly weaker than in other latitudes (Gettleman et al., 2011). It is likely because ozone heating is absent due to polar night. Based on the radiosonde observations, Tomikawa et al. (2009) also shows that the static stability in the lower stratosphere over Syowa Station is minimized in April through July. Temperature fluctuations associated with gravity waves are observed as fluctuations of the static stability. Thus, when the background static stability is sufficiently weak such as in the polar lower stratosphere, the temperature fluctuations associated with gravity waves can make local minima of the static stability which are detected as thermal tropopauses. Therefore, it is likely that multiple tropopause events due to IGWs are considered to occur frequently in the Arctic / Antarctic region in winter.

Keywords: Tropopause, Multiple tropopause, Gravity wave

Tropical non-migrating tides appearing in a high vertical resolution GCM

SAKAZAKI, Takatoshi^{1*} ; SATO, Kaoru² ; KAWATANI, Yoshio³ ; WATANABE, Shingo³

¹Research Institute for Sustainable Humanosphere, Kyoto University, ²Graduate School of Science, The University of Tokyo, ³JAMSTEC

Atmospheric tides are global scale waves with periods that are harmonics of a solar day. They are primarily excited in the troposphere and the stratosphere, and then, propagate upward. Tides are generally classified into two components: migrating (Sun-synchronous) and non-migrating (non-Sun-synchronous) tides. Although migrating tides were examined by many previous studies, a much fewer studies considered non-migrating tides particularly in the troposphere and the stratosphere. The purpose of this study is to reveal the horizontal and vertical structure of non-migrating tides and its seasonal variations in the region from the troposphere to the mesosphere, as well as to clarify the underlying physical processes.

In this study, data from a high-resolution (T213L256) global spectral climate model (Watanabe et al., 2008) are analyzed. This model covers quite a wide height range from the ground surface to the upper mesosphere (80 km in altitude), enabling us to investigate the full tidal coupling between the lower and upper atmosphere. Also, the vertical resolution is ~300 m in the vertical, which is almost sufficient to simulate realistic propagation and momentum deposition of gravity waves including tides. We compared the model data with data from COSMIC GPS-RO measurements and TIMED/SABER satellite measurements, and confirmed that the model captures the observed characteristics at least qualitatively.

In the model data, we clearly see that non-migrating tides are mainly excited over the two large continents: over Africa and South America. The excited tides are propagating three-dimensionally like internal inertia-gravity waves. During the propagation, tides with small wavenumbers are filtered out by background zonal wind (e.g., stratospheric semiannual oscillation (SAO)). Thus, both excitation and filtering processes are important for understanding the tidal variability.

Keywords: nonmigrating tides, KANTO, SABER, COSMIC

Stratospheric Geoengineering

WATANABE, Shingo^{1*}

¹Japan Agency for Marine-Earth Science and Technology

Overview of stratospheric geoengineering simulations proposed by GeoMIP (Geoengineering Model Intercomparison Project) will be presented with emphasis on impact of anthropogenic stratospheric aerosols on stratospheric ozone and surface UV.

Keywords: geoengineering, stratosphere, aerosol

Influence of topography onto the temperature variation around the tropical tropopause layer

KUBOKAWA, Hiroyasu^{1*} ; FUJIWARA, Masatomo² ; NASUNO, Tomoe³ ; MIURA, Hiroaki⁴ ; YAMAMOTO, Masayuki⁵ ; SATOH, Masaki¹

¹Atmosphere Ocean Research Institute, The University of Tokyo, ²Faculty of Environmental Earth Science, Hokkaido University, ³Japan Agency for Marine-Earth Science and Technology, ⁴Department of Earth and Planetary Science, Graduate School of Science, The University of Tokyo, ⁵Research Institute for Sustainable Humanosphere, Kyoto University

The tropical tropopause layer (TTL) is a region where the tropospheric air passes through before entering the stratosphere. Since this region is very cold, the air from the troposphere is dehydrated around here. It is known the Kelvin wave around the TTL affects the big temperature variation and strong dehydration. We investigated the temperature variations around the TTL using the Nonhydrostatic Icosahedral Atmospheric Model (NICAM) on December 2006 (Miura et al. 2007). We found that the temperature variations associated with Kelvin waves are very large over the mountain regions. The amplitude is about 2-times larger than that over the ocean even on the same latitude. We think this result would be a new scientific discovery from simulations or finding of unknown biases of simulations. In this study, we investigate the influence of the topography on the temperature variations around the TTL using the NICAM, re-analysis, satellite, and radiosonde data. We used the Constellation Observing System for Meteorology, Ionosphere, and Climate (COSMIC) data as a satellite data in December, January and February from 2006 to 2010 in order to investigate the temperature variations. The large temperature variations (standard deviation) were found over the mountain regions. This result satisfies the 90% statistical significance level, but the number of data samples is a few. We investigated some reanalysis data having different horizontal resolutions. The standard deviations of the TTL temperature near mountains became large as the horizontal resolution of the model became high. We checked a reanalysis data of the Year of Tropical Convection (YOTC) data from ECMWF with a horizontal resolution of 0.125 degree. When Kelvin waves passed through over the Western Pacific, the amplitude of temperature was large about 2 K over the mountain regions. The power spectrum in the mountains between 7 days and 12 days was actually larger comparing with the ocean. We compared the two local radiosonde data in Jambi and Kototabang (near mountains region). We found that there was no clear difference of temperature variation. Although the temperature variations at Kototabang were slightly large, it is associated with local diurnal variations but not the wave activities. In this study, we found large temperature variation over the mountain in the observational data and numerical models. We would discuss present results and the possibility of this work.

Constructing the Middle-Atmosphere Version of Non-hydrostatic Global Atmospheric Model NICAM

KODAMA, Chihiro^{1*} ; NASUNO, Tomoe¹ ; WATANABE, Shingo¹ ; KUBOKAWA, Hiroyasu² ; SATOH, Masaki²

¹Japan Agency for Marine-Earth Science and Technology, ²University of Tokyo

Atmospheric gravity wave, which is generated by topography, convective activity, frontal system, jet, and/or so on, affects the formation of the basic state in the troposphere and middle atmosphere through wave convergence. It is difficult for a GCM (general circulation model) to explicitly simulate processes of generation, propagation and convergence of the gravity wave, and gravity wave drag scheme is often used in such a model. Watanabe et al. [2008] successfully simulated realistic gravity wave and basic state of the middle atmosphere using high resolution GCM (60 km in horizon and 300 m in vertical) without gravity wave drag scheme. However, propagation characteristics of the gravity wave cannot be appropriately simulated by the GCM based on the hydrostatic system, since dispersion relationship of the gravity wave is different between the hydrostatic and non-hydrostatic system. In addition, GCM cannot explicitly simulate convection, which is one of the source of the gravity wave.

We are constructing the middle-atmosphere version of the non-hydrostatic global atmospheric model, NICAM (Non-hydrostatic Icosahedral Atmospheric Model). Horizontal resolution of the NICAM is 220 km, 56 km, or 14 km. We adopt hybrid-z*system as a vertical coordinate, in which the horizontal surface is almost flat in the middle atmosphere. Vertical level is located up to 80 km with the uniform interval in the middle atmosphere; the vertical interval is 2 km (61 layers), 1 km (91 layers), 500 m (162 layers), or 300 m (261 layers). We do not use gravity wave drag scheme and cumulus convection scheme. Other configurations are almost same as those in the standard NICAM, which is mainly used for the tropospheric research.

In this presentation, we will show initial results of the performance in the reproducibility of the basic state. Overall, zonal mean structure of the temperature and zonal wind are well simulated in both the troposphere and the middle atmosphere. Though axis of the polar night jet is biased poleward, it is somewhat improved as the vertical resolution is increased. Higher vertical resolution also brings better performance in the strength of the easterly jet in the summer hemisphere and in the QBO-like structure in the tropical lower stratosphere. In the winter hemisphere, cold bias is found around the pole in the upper stratosphere and the mesosphere, and too strong polar night jet is found. At present, the simulation tends to be numerically more unstable as the horizontal and/or vertical resolutions are increased. We will show the above points and wake up debate about the potential of the non-hydrostatic atmospheric model for future research of the whole atmosphere.

Keywords: nonhydrostatic global atmospheric model, atmospheric gravity wave, middle atmosphere, tropical convection

Physical interpretation on the mechanisms of spontaneous gravity wave radiation using the renormalization group method

YASUDA, Yuki^{1*} ; SATO, Kaoru¹ ; SUGIMOTO, Norihiko²

¹Department of Earth and Planetary Science, Graduate School of Science, The University of Tokyo, ²Department of Physics, Keio University

Gravity waves (GWs) are categorized into orographic ones and non-orographic ones. The mechanisms for non-orographic GW radiation are not clear, because the dynamics is quite nonlinear and complicated unlike orographic GWs. Recently it has been revealed that GWs are spontaneously radiated from an approximately-balanced flow, especially in the jet/front systems (e.g., O'Sullivan and Dunkerton 1995). The balanced adjustment theory proposed by Plougonven and Zhang (2007) is considered to be the most likely to describe the spontaneous radiation. However, their theory does not give physical interpretations on GW sources and radiation mechanisms. In this study, we derived a new theory and made physical interpretations.

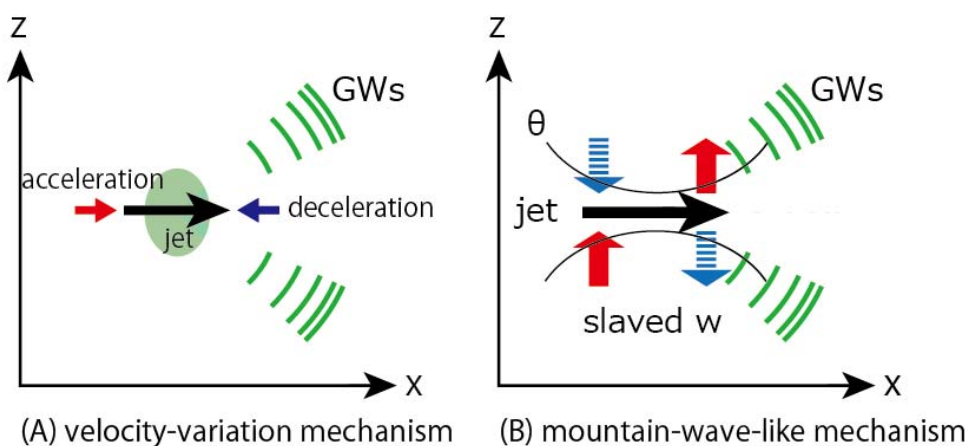
Using the renormalization group (RG) method (Chen et al. 1996), which is a singular perturbation method, the interaction between the vortical flow and the Doppler-shifted GWs which both have slow time-scales is formulated for the hydrostatic Boussinesq equations on the f plane. In general, the RG method enables us to extract slowly-varying components systematically and naturally from the system containing multiple timescale motions. The derived time evolution equations (RG equations, referred to as RGEs) describe the spontaneous radiation of GWs from the components slaved to the vortical flow through a quasi-resonance together with the GW radiation reaction on the large-scale vortical flow. The quasi-resonance occurs when the space and time scales of slaved components are comparable to those of GWs (quasi-resonance condition).

The RGEs are validated using numerical simulations of the vortex dipole by Japan Meteorological Agency Nonhydrostatic Model. The flow near the dipole center is quite strong due to the confluence, which is similar to a localized jet stream in the atmosphere. GW distribution obtained by the RGE integration accords well with the numerical simulation. This result supports the validity of our theory.

The main GW sources in the vortex dipole can be classified into two groups by using the RGEs. The GW sources in the first group are the slaved components produced by the horizontal divergence of acceleration of the vortical flow near the dipole center (Fig. A). The acceleration can be regarded as the sum of Coriolis and pressure gradient forces. This fact indicates that the GW sources express the horizontal compression of fluid. The horizontal compression can produce vertical motion, which radiates GWs when its space and time scales satisfy the quasi-resonance condition. This radiation mechanism corresponds to the velocity-variation mechanism proposed by Viúdez (2007).

The slaved component in the other group is mainly produced by the vortical flow over the deformed potential temperature surfaces (Fig. B). The deformation of potential temperature surfaces can be attributed to the Bernoulli effect due to the strong vortical flow near the dipole center. The vortical flow over the deformed potential surfaces can produce vertical motion, which radiates GWs when its space and time scales satisfy the quasi-resonance condition. In other words, the deformed potential temperature surfaces act like a mountain as in the radiation process of orographic GWs. This radiation mechanism corresponds to the mountain-wave-like mechanism proposed by McIntyre (2009).

Keywords: gravity wave, jet stream, spontaneous radiation, renormalization, wave, singular perturbation method



QBO-like oscillation in a radiative-convective equilibrium state obtained with a two-dimensional moist convection model

YODEN, Shigeo^{1*} ; BUI, Hoang-hai² ; NISHIMOTO, Eriko¹

¹Division of Earth and Planetary Sciences, Graduate School of Science, Kyoto University, ²Hanoi University of Science

Quasi-Biennial Oscillation (QBO) is a prominent internal variations in the equatorial stratosphere due to the interactions between a mean zonal wind and waves that propagate upward in the stratosphere. Over two decades ago, Held et al. (1993) investigated radiative-convective equilibrium states with a two-dimensional explicit moist convection model and obtained a QBO-like oscillation. Their model contains the fundamental dynamical processes of the QBO, though it is a highly-idealized two-dimensional model for a periodic domain without Coriolis effects. In this study, we re-examine the QBO-like oscillation found by H93 with a long enough integration period over two years, by using Advanced Research WRF Modeling System. We also investigate the sensitivity of the QBO-like oscillation in regards of different factors such as domain size, resolution and boundary conditions (e.g., prescribed zonal wind at the top and sea surface temperature).

The control experiment has a similar configuration to that of Held et al.; 640km domain width with a resolution of 5km, 130 vertical levels up to 26km. Convective parameterization is turned off in all simulations and only a cloud microphysics scheme is used. Other physics options are standard ones for short- and long-wave radiations, surface fluxes, planetary boundary layer, turbulence and diffusion, and Rayleigh damping near the top boundary. After spin up, the mean zonal wind shows a clear QBO-like oscillation with a period of 120.6 days. Unlike the observed QBO, the oscillation has a clear signal in the troposphere, in which moist convections dominate and gravity waves are generated. Such convectively generated gravity waves propagate into the stratosphere to produce the QBO-like oscillation in the stratosphere. On the other hand, intensity and propagation of organized convective systems, including zonal mean precipitation, are modulated in accordance with the oscillation of mean zonal wind in the troposphere.

Keywords: QBO, radiative-convective equilibrium, wave-mean flow interaction, two-dimensional moist convection model, stratosphere-troposphere dynamical coupling

Interannual changes of the semiannual oscillation induced by stratospheric sudden warming events

OHATA, Tsuyoshi^{1*} ; IIDA, Chihiro¹ ; HIROOKA, Toshihiko³ ; EGUCHI, Nawo²

¹Graduate School of Science, Kyushu University, ²Research Institute for Applied Mechanics, Kyushu University, ³Faculty of Science, Kyushu University

The semiannual oscillation (SAO) is observed in circulation changes in the equatorial middle atmosphere, which consist of two separate maxima centered near the stratopause (SSAO) and the upper mesosphere (MSAO) with an approximate out-of-phase relationship between the two [e.g., Andrews et al., 1987]. The SSAO has easterly and westerly maxima at solstices and equinoxes, respectively, while the MSAO shows an out-of-phase change with the SSAO. It is known that somewhat different consideration must be made between the SSAO and the MSAO for their forcing mechanisms, and it seems to be also true of their interannual changes. In this study, we make global gridpoint data for geopotential and temperature fields up to the mesopause level derived from Aura MLS data, to make dynamical analyses for equatorial zonal wind and temperature changes since August 2004 to present. It is found that the strength of both the SSAO and MSAO might be modulated by stratospheric sudden warming (SSW) events in boreal winter solstices. In the equatorial regions, enhanced poleward flows of the residual meridional circulation associated with SSW events lead to temperature perturbations consisting of a cooling in the stratosphere and a warming in the mesosphere. Such temperature perturbations may bring about opposite changes in the SSAO and the MSAO through the thermal wind balance at the equator, leading to their amplifications.

Keywords: semiannual oscillation, stratospheric sudden warming, MLS data

Recent variability and zonal asymmetry in upper troposphere and lower stratosphere observed with GPS radio occultation m

MEHTA, Sanjay^{1*} ; TSUDA, Toshitaka¹ ; FUJIWARA, Masatomo² ; SCHMIDT, Torsten³ ; VERNIER, Jean-paul⁴

¹Research Institute for Sustainable Humanosphere (RISH), Kyoto University, Japan, ²Faculty of Environmental Earth Science, Hokkaido University, Japan, ³GFZ German Research Centre for Geosciences, Potsdam, Germany, ⁴NASA Langley Research Center, Hampton, VA 23666, USA.

Tropical upper troposphere and lower stratosphere (UTLS) variability and zonal asymmetry are explored using global positioning system radio occultation (GPS-RO) measurements. GPS-RO offers global monitoring of fine structures of the UTLS temperature variability. GPS-RO continuous measurements from CHAMP (2001-2006) and COSMIC (2006-2013) for about 13 years allows us to study the interannual variability, trends (over the last decade) and its fine zonal structures. The warming of UTLS temperatures between 100 and 50 hPa, warming of tropopause and decrease in its height have been observed over the last decade. The possible reasons for such changes linking to the recent moderate volcanic eruptions and dynamical changes involving changes in sea surface temperature and Brewer Dobson circulation will be discussed. The variability and structure observed in GPS-RO will be compared with existing conventional radiosonde and reanalysis datasets.

Keywords: UTLS Temperature, Zonal Assymetry, GPS Radio Occultation, Moderate Volcanic Eruptions, Dynamical Changes

The role of the mid-latitude oceanic front in the ozone-induced climate change in the Southern Hemisphere

OGAWA, Fumiaki¹ ; OMRANI, Nour-eddine² ; NISHII, Kazuaki^{1*} ; NAKAMURA, Hisashi¹ ; KEENLYSIDE, Noel³

¹RCAST, University of Tokyo, ²GEOMAR, University of Kiel, ³Geophysical Institute, University of Bergen

The Southern Hemisphere Annular Mode (SAM) is the dominant mode of low-frequency atmospheric variability in the extratropical Southern Hemisphere, exerting substantial impacts on regional distributions of temperature and precipitation. Its multi-decadal trend in the troposphere observed in late 20th century has been related to the lower-stratospheric changes induced by the ozone depletion. Known as a manifestation of meridional shift of the eddy-driven polar-front jet (PFJ), which is collocated with the storm-track, the SAM variability may be sensitive to the near-surface baroclinicity associated with the midlatitude oceanic frontal zone.

In the present study, aqua-planet atmospheric general circulation model experiments are conducted with two different zonally symmetric profiles of sea-surface temperature (SST) whose frontal gradient in midlatitudes is retained or eliminated. A comparison of the tropospheric response to the assigned stratospheric ozone depletion between the two SST profiles reveals critical importance of the frontal SST gradient for the intensified stratospheric polar vortex, which is due to the ozone depletion, in triggering and keeping positive phase of the tropospheric SAM in late spring through summer.

We also reveal that the SAM trend in late 20th century simulated in CMIP3/5 models is sensitive to the position and intensity of the mid-latitude oceanic frontal zone. Specifically, a model that simulates the zonal-mean frontal zone at higher latitude tends to simulate the maximum positive trends in the zonal-mean westerlies and midlatitude precipitation also at higher latitudes than another model with the oceanic frontal zone at lower latitude. This relationship is more obvious in a subset of the models with the relatively strong oceanic fronts.

Keywords: Ozone hole, Annular mode, Oceanic front

Global response to the major volcanic eruptions in 9 reanalysis datasets

FUJIWARA, Masatomo^{1*} ; HIBINO, Takashi¹ ; MEHTA, Sanjay² ; GRAY, Lesley³ ; MITCHELL, Daniel³ ; ANSTEY, James³

¹EES, Hokkaido Univ., ²RISH, Kyoto Univ., ³Oxford Univ.

The global climate response to the eruptions of Mount Agung in 1963, El Chichón in 1982 and Mount Pinatubo in 1991 is investigated using 9 reanalysis datasets (ERA-40, ERA-Interim, JRA-25/JCDAS, JRA-55, MERRA, NCEP/NCAR, NCEP/DOE, NCEP-CFSR, and 20CR). Multiple linear regression is applied to the zonal and monthly mean time series of key dynamical variables by considering the components of linear trends, seasonal variations, the Quasi-Biennial Oscillation (QBO), solar cycle, and El Niño Southern Oscillation (ENSO). The residuals are used to define the volcanic signals. Latitude-altitude distributions of the volcanic signals and of the regression coefficients are compared and discussed among the different reanalyses. In response to the Mount Pinatubo eruption most reanalyses show statistically significant negative and positive temperature anomalies in the tropical troposphere and in the tropical lower stratosphere, respectively. The signals are similar for the El Chichón eruption, with a statistically insignificant tropospheric response. The response to the Mount Agung eruption is asymmetric about the equator with significant warming in the Southern Hemisphere midlatitude upper troposphere to lower stratosphere. This work is a contribution to the SPARC Reanalysis Intercomparison Project (S-RIP).

Keywords: volcanic eruption, climate, reanalysis, stratosphere, troposphere

Simulation of stratospheric aerosol changes after the Pinatubo eruption

SEKIYA, Takashi^{1*} ; SUDO, Kengo¹

¹Graduate School of Environmental Studies, Nagoya University

An explosive volcanic eruption can inject a large amount of SO₂ into the stratosphere, which is oxidized to form sulfate aerosol. Such aerosol has an impact on the Earth's radiative budget by enhancing back-scattering of the solar radiation, and causes stratospheric ozone depletion through heterogeneous chemical reactions. This study investigates spatiotemporal changes in the volcanic aerosol after the 1991 Pinatubo eruption. We particularly focus on impacts of (1) heating due to volcanic ash, (2) injection height, and (3) temporal evolution of the aerosol radius, on transport and distribution of the volcanic aerosol. We conducted a control simulation and three sensitivity simulations using the MIROC-ESM-CHEM chemistry — climate model. In the control simulation, 20 Mt of the SO₂ and 30 Mt of the ash were injected into the altitudes between 16 km and 18 km over the Mt. Pinatubo on June 15th 1991. The radius of stratospheric sulfate aerosol is prescribed by the data estimated from SAGE II in the control simulation. The first sensitivity simulation injected only the SO₂ into the altitudes between 16 km and 18 km. The second sensitivity simulation injected the SO₂ into the altitudes between 17 km and 26 km. In the third sensitivity simulation, the radius of the sulfate aerosol was fixed to 0.08 μm. The control simulation reproduced a general feature of the observed aerosol optical depth (AOD) derived from SAGE II and AVHRR, although the simulated residence time of the aerosol is longer than the observed one. The sensitivity simulations show the following: (1) heating due to the ash causes an anomalous upward and equatorward transport of the volcanic aerosol during 4 — 5 days after the eruption, (2) the SO₂ injection into the altitudes of 17 — 26 km does not represent the anomalous transport due to the heating which is caused by long-wave absorption of the ash, (3) the temporal evolution of the aerosol radius slightly facilitates the removal of the aerosol from the stratosphere.

Keywords: stratospheric aerosol, volcanic eruption, chemistry-climate model

Recent Results for Middle Atmospheric Sciences using Data from SMILES

SHIOTANI, Masato^{1*}

¹Research Institute for Sustainable Humanosphere, Kyoto University

The Superconducting Submillimeter-Wave Limb-Emission Sounder (SMILES) aboard the Japanese Experiment Module (JEM) of the International Space Station (ISS) made atmospheric measurements of minor species in the stratosphere and mesosphere for about six months from October 2009 to April 2010. Data for scientific community are now provided from DARTS (Data ARchives and Transmission System) of ISAS/JAXA (<http://darts.isas.jaxa.jp/iss/smiles/>). In this talk, we will present recent results from the SMILES measurements in association with middle atmospheric chemistry and dynamics. The main topics to be highlighted are as follows.

[Diurnal ozone variations in the stratosphere] The SMILES observations have revealed the global pattern of diurnal ozone variations throughout the stratosphere. The peak-to-peak difference in the stratospheric ozone mixing ratio reaches 8% over the course of a day, suggesting careful consideration when merging ozone data from different satellite measurements (Sakazaki et al., 2013).

[Ozonesonde bias suggested from comparisons with SMILES] The SMILES ozone data have been extensively compared with other satellite data sources (Imai et al., 2013a). Further comparisons of SMILES ozone profiles with those from ozonesondes show that the agreement was generally good, but at low latitudes the SMILES ozone data showed larger values than those at middle and high latitudes. To explain this bias, we examined an issue of the ozonesonde's response time, and found a negative bias in ozonesonde measurements more than 7% at 20 km in the equatorial latitude (Imai et al., 2013b).

[Mesospheric ozone variations during the solar eclipse] During the annular solar eclipse on 15 January 2010, SMILES successfully captured temporal changes in ozone concentration. We found that in the lower mesosphere ozone amounts get closer to the normal nighttime average, and the mechanism is detailed with use of an atmospheric chemistry box model (Imai et al., 2014).

Keywords: Middle Atmosphere, Ozone, Satellite Observation

Stratospheric ClO observation by JEM/SMILES

SUZUKI, Makoto^{1*}; MANAGO, Naohiro²; MITSUDA, Chihiro³; IMAI, Koji¹; OZEKI, Hiroyuki⁴; SAKAZAKI, Takatoshi⁵; SHIOTANI, Masato⁵

¹JAXA/ISAS, ²Chiba U./CEReS, ³Fujitsu FIP.Corporation, ⁴Faculty of Science, Toho University, ⁵Kyoto U./RISH

SMILES operated on the ISS from Oct. 12, 2009 to Apr. 21, 2010. Since the detector (Superconductor-Insulator-Superconductor: SIS mixer) was cooled down to 4K, SMILES showed system noise figure, $T_{sys} \sim 250K$, or spectral noise floor $\sim 0.4K$, which gave one order better signal to noise ratio compared to previous sub-mm observations from space (Aura/MLS and Odin/SMR).

Aura/MLS have been measuring ClO with a 0.1 ppbv precision at 25-50km altitude. Theoretical precision of SMILES has been reported to be about 0.01 pptv at 30 km. This value can be verified from bin-width of histogram of nighttime ClO, which should be almost zero below 35km at the background atmosphere. We obtained actual bin-width, or ClO random error, to be 0.015 pptv, which is slightly larger than the theoretical value. It has been estimated that

the additional random error might come from IFOV pointing error, a priori pressure error, or baseline fitting error.

In tropical region (N10-S10), difference between day and night profiles was 792 pptv at 25km. This result agreed quite well with reproductive calculated value (nearby 80 pptv) by using Chemical Transport Model (SD-WACCM). On the other hand, in middle latitude (N30-50) during Mar. 13-25, 2010, SMILES value were 712 pptv at 22km, and 352 pptv at 19 km. These value were significantly larger than reported as 10 pptv by airplane and balloon observation in 1986. SMILES mid-latitude value is about 3-7 times higher than the past observation, however, agrees with reproductive calculated value like as tropical region. These discrepancy in the mid-latitude between SMILES and past observation can be explained partly by the historical increase of total Clx from 2.4 pptv in 1968 to the present value, ~ 3.0 ppbv.

Keywords: Chlorine monoxide, Stratosphere, International Space Station, submm, ozone, SMILES

Correlation between O₃ and HCl in the lower stratosphere as observed by SMILES

SUGITA, Takafumi^{1*}; KASAI, Yasuko²; TERAO, Yukio¹; HAYASHIDA, Sachiko³; SAGAWA, Hideo²; SUZUKI, Makoto⁴; SHIOTANI, Masato⁵

¹NIES, ²NICT, ³Nara Women's Univ., ⁴JAXA, ⁵Kyoto Univ.

Ozone (O₃) in the upper troposphere (UT) has an effect on radiative forcing. One of poorly constrained source of tropospheric O₃ is the stratosphere. Marcy et al. (Science, 2004) have suggested that measurements of HCl in the UT can be used to calculate how much O₃ was transported from the lower stratosphere (LS). Using the correlation between O₃ and HCl in the LS, a fraction of the source of the stratosphere has been quantified from measurements in the UT. To perform such a study, it is important to establish the O₃/HCl correlations in the LS. Here, we will present the O₃/HCl correlations as observed by the Superconducting Submillimeter-Wave Limb-Emission Sounder (SMILES) on board the International Space Station (ISS) (Kikuchi et al., JGR, 2010). We first focus on latitudes between 30°S and 66°S in periods of November 2009, February 2010, and April 2010, when SMILES mainly covered the Southern Hemisphere (S.H.). Both the slope and intercept of the O₃/HCl correlation in the S.H. Feb. are larger than those in Nov. (outside the Antarctic vortex). This is probably due to mixing of air inside and outside the Antarctic vortex, where the enhanced HCl values were observed only inside the vortex (The break-up of the vortex occurred in Dec. 2009 in the LS). Then, hemispheric contrasts in spring and fall will also be presented. In the S.H. Nov. (late spring), the slope is larger than that in the N.H. Apr. (30-66°N). Also, in the S.H. Apr. (fall), the slope is larger than that in the N.H. Oct. (30-66°N). Although, the reason for these larger slopes in the S.H. is not known, the O₃/HCl correlations obtained from SMILES give recent references for the mid to high latitude LS in both the hemispheres.

Keywords: SMILES, ISS, ozone, chlorine

Reincrease of total columns of HCl and HF observed with FTIR at Tsukuba

MURATA, Isao^{1*} ; NAKAJIMA, Hideaki² ; MORINO, Isamu² ; AKIYOSHI, Hideharu²

¹Graduate School of Environmental Studies, Tohoku University, ²National Institute for Environmental Studies

The vertical column densities of HCl and HF have been observed with high-resolution Fourier transform spectrometer at Tsukuba, Japan since 1998. SFIT1 spectral fitting program was used to derive the vertical column densities.

HCl and HF are the reservoir species of Chlorine and Fluorine, respectively. Chlorofluorocarbons are the main sources of both of them.

Daily averaged HCl column increased from 1999 to 2001, decreased from 2003 to 2006 and again increased after 2007. Daily averaged HF column increased from 1999 to 2002, level off from 2003 to 2006 and again increased after 2007. The trend fitting shows -1.8%/yr (2001-2006) and +1.0%/yr (2007-2013) for HCl, and +0.3%/yr (2001-2006) and +2.5%/yr (2007-2013) for HF.

The reason why HCl and HF increase again has not been investigated yet but this increase may lead to the delay of ozone recovery. One possible reason is the change of atmospheric circulation. Simulation result of chemical transport model with observed meteorological data (ERA-interim) shows stop of decrease of HCl at around 2008 while the result without observed meteorological data shows continuous decrease. Another possible reason is the increase in emissions of HCFCs and HFCs which increased the input of Cl and F to the stratosphere but there is no observational evidence.

Keywords: FTIR, Trace Species, CFCs

The impact of altitude mis-estimation caused by Vaisala RS80 pressure bias on ozone and temperature profile data

INAI, Yoichi^{1*} ; SHIOTANI, Masato¹ ; FUJIWARA, Masatomo² ; HASEBE, Fumio²

¹RISH, Kyoto Univ., ²EES, Hokkaido Univ.

Non-biased meteorological data are necessary for studies for detecting long-term climate change. Vaisala RS80 radiosonde is widely used for operational and scientific observations. It has been known, however, that the RS80 has pressure bias. The pressure bias affects height information of the profile in a traditional way where the geometric height (or geopotential height in some cases) is calculated from the hydrostatics equation. In addition, the pressure measurements affect the mixing ratio values of any chemical species because the calculation needs air pressure value. The RS80 pressure bias is estimated to be -0.3 ± 0.2 hPa, -0.4 ± 0.1 hPa, and -0.4 ± 0.1 hPa (1σ) at 20 km, 25 km, and 30 km, respectively from the observations using RS80 together with global positioning system (GPS) sensor in the Soundings of Ozone and Water in the Equatorial Region (SOWER) project during from December 2004 to January 2010. Since ozone mixing ratio and temperature are also measured simultaneously, the impact of the mis-estimated altitude on observed profiles of ozone and temperature was evaluated. The net biases of $-1.3 \pm 1.4\%$, $-0.5 \pm 0.7\%$, and $3.1 \pm 1.9\%$ (1σ) at 20 km, 25 km, and 30 km, respectively for ozone mixing ratio and that of -0.1 ± 0.2 K, -0.2 ± 0.3 K, and -0.4 ± 0.7 K (1σ) at 20 km, 25 km, and 30 km, respectively for temperature are estimated as impacts from RS80 pressure bias. Those ozone and temperature biases can result in artificial variation in the long-term meteorological records when there is a radiosonde change from or to RS80. Especially, sign-reversed biases of ozone and temperature appear as artificial variations when the instrument is changed from RS80 to non-pressure-biased radiosonde (for example GPS sonde).

Keywords: sonde observation, observational bias, stratospheric ozone, stratospheric temperature, stratospheric long-term variation

Total ozone reduction over Rio Gallegos (Argentina) in November 2009 simulated by MIROC3.2 Chemical Transport Model

AKIYOSHI, Hideharu^{1*} ; KADOWAKI, Masanao¹ ; NAKAMURA, Haruna² ; SUGITA, Takafumi¹ ; NAKAMURA, Tetsu³ ; MIZUNO, Akira⁴

¹NIES, ²Fujitsu FIP, ³Arctic Environment Research Center, NIPR, ⁴STEL, Nagoya University

de Laat et al. (Geophys. Res. Lett., 2010) reported three weeks of reduced total ozone columns over the southern tip of South America in November 2009. The duration of the low total ozone was unusual for the regions. Ozone vertical profile measurements at Rio Gallegos, Argentina (51S, 69W) by ozone LIDAR suggest that the isentropic surfaces of 675K and 475K over Rio Gallegos was inside the Antarctic polar vortex around 13-14 November and 22-23 November respectively thus the low total ozone lasted for three weeks (Wolfram et al, 5th SPARC General Assembly, Queenstown, New Zealand, 2014). MIROC 3.2 Chemical Transport Model with a horizontal resolution of T42 (corresponding to 2.8 degree by 2.8 degree in grids) simulates this long term reduced total ozone over Rio Gallegos. The dynamical and chemical fields around the Antarctica in November 2009 are analyzed. Investigations of these fields for the other past years and comparisons with those in 2009 will be performed.

Keywords: Argentina, ozone hole, CTM, polar vortex, SATREPS, November 2009

Relationship between total ozone and wave activities in Antarctic region

KADOWAKI, Masanao^{1*} ; AKIYOSHI, Hideharu¹ ; YAMASHITA, Yousuke¹ ; NAKAMURA, Tetsu²

¹National Institute for Environmental Studies, ²Arctic Environment Research Center, National Institute of Polar Research

It is well known that the formation, development and inter-annual variation of the ozone hole are related to the dynamics in winter polar stratosphere. Stratospheric sudden warming was detected in the Southern Hemisphere in 2002 for the first time and then the ozone hole area (defined by the area inside 220DU) was reduced to less than 5 million square kilometers. A similar reduction of ozone hole was also simulated by CCSR/NIES CCM with CCMVal-REF2 scenario, in which the wave number 2 was unusually developed.

These suggest a possibility that ozone hole may suddenly be reduced in a specific year by the dynamics in the future, apart from the effect of the decrease in chlorine and bromine concentration in the atmosphere due to the halogen regulation. Thus, in order to speculate ozone hole trend and the variability in the course of the long-term climate change of the future, it is needed to clarify the relationship between wave activity and ozone hole in the past. Relationships among the ozone hole indices (maximum ozone hole area and minimum total ozone), wave activity and temperature in the Southern Hemisphere were investigated using observation data and chemical transport model output.

Keywords: stratospheric ozone, dynamics, chemical transport model

Interannual and intraseasonal variability of gravity waves revealed from high resolution AIRS observations

TSUCHIYA, Chikara¹ ; SATO, Kaoru^{1*} ; ALEXANDER, M. Joan² ; HOFFMANN, Lars³

¹University of Tokyo, ²NorthWest Research Associates, ³Forschungszentrum Juelich

An analysis was made of high-resolution temperature data from satellite onboard Atmospheric Infrared Sounder (AIRS) over eight years from 2003/2004 to 2010/2011 to examine gravity wave (GW) characteristics around an altitude of 40 km in terms of the interannual and intraseasonal variability in austral summer (DJF). AIRS is a nadir-view instrument and sensitive to the temperature fluctuations with vertical wavelengths greater than 15 km. The S-transform was applied to the data series in both cross-track or along-track directions to estimate GW characteristics. First, the DJF-mean time series of GW amplitudes and precipitation were regressed to the sea surface temperature time series in NINO.3 region. It is shown that both GW amplitudes and precipitation are large to the northeast (southwest) of the South Pacific convergence zone (SPCZ) in the El Nino (La Nina) phase. Second, the intraseasonal variation of GWs were examined in terms of the Madden-Julian Oscillation (MJO). Ten-day-mean time series was examined as a function of the longitude for GW amplitudes and precipitation that were averaged over the latitudes of 0-20S. Large GW amplitudes are observed in association with the eastward migrating precipitation of MJO, which is more clearly described by a regression to the Real-time Multivariate MJO Index. Another interesting finding is that the GW amplitudes are significantly weak when the zonal wind at 100 hPa is eastward regardless of the precipitation amount. These results suggest that the interannual and intraseasonal variations of GWs in the subtropical middle stratosphere are modified largely by ENSO and MJO through the precipitation as GW sources and the zonal wind around the tropopause regulating GW vertical propagation.

Keywords: gravity waves, ENSO, MJO, QBO

Balloon-borne observations of lower stratospheric water vapor at the Antarctic Syowa Station

TOMIKAWA, Yoshihiro^{1*} ; SATO, Kaoru² ; TSUTSUMI, Masaki¹ ; NAKAMURA, Takuji¹ ; HIRASAWA, Naohiko¹

¹National Institute of Polar Research, ²The University of Tokyo

A variation of water vapor in the lower stratosphere has a large radiative forcing. It is considered that increase and decrease of lower stratospheric water vapor before and after 2000, respectively, altered the surface temperature trend by up to 30% in each period. However, since the water vapor content abruptly changes with height around the tropopause, it is hard to capture its variation exactly by satellite observations with a low vertical resolution. Many in-situ (i.e., balloon-borne and aircraft) observations with a high vertical resolution have been performed in low and middle latitudes, but few in the polar region. At the Antarctic Syowa Station (69.0S, 39.6E), three balloon-borne cryogenic frost-point hygrometer observations were performed in 2013 by the 54th Japanese Antarctic Research Expedition (JARE54), so that high precision and high vertical resolution data up to about a 25km altitude were obtained successfully. In this paper, a preliminary result of these observations is presented, and it will be discussed how important it is to continue the water vapor observation at Syowa Station.

Keywords: water vapor, sonde, Antarctic, lower stratosphere

Three dimensional structure of planetary wave activity from tropical to extratropical regions in ENSO

KINOSHITA, Takenari^{1*} ; SATO, Kaoru² ; HITCHMAN, Matthew, H.³

¹Natl. Inst. of Information Comm. Tech., Japan, ²Graduate School of Science, The University of Tokyo, ³University of Wisconsin, Madison

It is known that the distribution of extratropical column ozone is modulated with El Niño Southern Oscillation (ENSO) (Hitchman and Rogal 2010a, b). This modulation is recognized as the 10 ~20 day-scale responses including "Tropical convective outflow into the upper troposphere and lower stratosphere", "amplification of subtropical anticyclone associated with transport of low potential vorticity" and "modulated synoptic scale disturbances in extratropical regions". On the other hand, it is suggested that planetary scale disturbances influence the distribution of extratropical column ozone. However, this is yet to be identified. The present study examines the modulation of planetary wave activity associated with ENSO from upper troposphere to stratosphere using the formulae describing wave-mean interaction in three dimensions and analytical techniques derived by Kinoshita and Sato (2013a, 2013b), Sato et al. (2013).

First, we use the ERA-Interim reanalysis data and focus from August to October. Based on the Ocean Niño Index by NOAA, 1991, 1997, 2002, 2004, 2006, 2009 are selected as El Niño seasons and 1998, 1999, 2000, 2007 are selected as La Niña seasons. The Planetary scale disturbances are defined as the waves with zonal wavenumbers 1 ~3 and periods more than 30 days.

We calculated the three dimensional wave activity flux and its divergences associated with the planetary scale disturbances. The results show that the planetary wave activity is amplified around Asian monsoon regions in La Niña seasons and the planetary wave propagates from tropical upper troposphere to polar stratosphere. The planetary wave activity in El Niño seasons is weak in this region. On the other hand, in the eastern Pacific regions, the planetary wave activity in El Niño seasons is amplified and the planetary wave propagates from tropical upper troposphere to polar stratosphere, while the activity in La Niña seasons is weak. It is suggested that the source of tropospheric planetary waves is different between tropical and polar regions in both seasons. We plan to calculate the three dimensional material transport associated with the planetary waves and compare the transport and that associated with the mechanism shown by Hitchman and Rogal (2010a, b).

Keywords: middle atmosphere, planetary wave, wave activity flux, residual mean circulation

A study of Antarctic ozone variation by using FORMOSAT-3/COSMIC observation

HSIAO, Chun-chieh¹ ; LIU, Jann-yenq^{1*} ; YU, Shiann-jeng¹

¹National Space Organization

The Formosa Satellite 3, also named as the Constellation Observing System for Meteorology, Ionosphere, and Climate (abbreviated as FORMOSAT-3/COSMIC, F3/C), is a constellation of six micro-satellites, designed to monitor weather and space weather. The constellation was launched into an initial circular low-Earth orbit at an altitude of 512 km on 15 April 2006. The six micro-satellites have deployed to six mission orbits at around 800 km altitude with 30-degrees separation in longitude for evenly distributed global coverage. The major payload onboard F3/C, GPS occultation experiment (GOX) instrument daily provides more than 2000 soundings of atmospheric vertical temperature profile. By binning radio occultation observations, the three-dimensional temperature structure can be obtained to monitor Antarctic temperature variation. Real-time measurements of vertical temperature structures over the Antarctic region are important for monitoring the formation of polar stratospheric clouds (PSCs) which is a critical factor in the ozone variation. On the other hand, the Ozone Monitoring Instrument (OMI) in the Aura mission observes for total ozone and other atmospheric parameters related to ozone chemistry and climate. The instrument observes Earth's backscattered radiation with a wide-field telescope feeding two imaging grating spectrometers. In this work, more than 5 years observation will be used to make a quantitative comparison of ozone and atmospheric temperature variation in Antarctic.

Keywords: FORMOSAT 3/COSMIC, ozone, Antarctic

Interannual variations of stratospheric water vapor in microwave limb sounding observations and climate model simulation

KAWATANI, Yoshio^{1*} ; JAE, Lee³ ; HAMILTON, Kevin²

¹JAMSTEC, ²University of Maryland, ³IPRC, Univ. Hawaii

Using the almost decade-long record of water vapor (H₂O) measurements now available from the Microwave Limb Sounder (MLS) instrument on the NASA AURA satellite, the time-height structure of interannual variations in H₂O content are investigated. The interannual anomalies display upward propagation below about 10 hPa in a manner analogous to the seasonal tape recorder, but at higher levels the anomalies in H₂O appear to propagate downward. An explanation for this effect is sought by examining stratospheric water vapor in simulations of a fine horizontal and vertical resolution (T106L72) version of the MIROC-AGCM. This model is notable for its rather realistic simulation of the quasi-biennial oscillation (QBO) in the tropical stratosphere. The interannual anomalies in simulated stratospheric H₂O display a similar propagation as seen in the MLS data. Further analysis shows that the upward propagation in the lower stratosphere is related to the mean advection of interannual water content anomalies induced by the QBO at the tropopause, while the downward propagation is due to the advection of the mean vertical gradient of water content by QBO's interannual fluctuations in the vertical wind. This conclusion is supported by additional experiments run with a modified MIROC that had a significantly different the mean vertical H₂O gradient in the middle and upper stratosphere. Also analyzed are global warming simulations in both the MIROC model and in several other global models included in the recent Coupled Model Intercomparison Project 5 (CMIP5). The upward propagating interannual H₂O variations are projected to become weaker in all these models because of a weakened QBO amplitude in the lowermost stratosphere.

Keywords: quasi-biennial oscillation

Basic characteristics of forecast skill variations in JMA 1-month hindcast experiments

TAGUCHI, Masakazu^{1*}

¹Aichi University of Education

This study investigates basic characteristics of stratospheric predictability in the Northern Hemisphere using 1-month hindcast (HC) experiment data of the Japan Meteorological Agency for 1979-2009. We describe characteristics of forecast properties of spread, error (root mean square error), and anomaly correlation, contrasting the stratosphere and troposphere for different seasons, as well as explore the so-called spread-skill relationship for the winter stratosphere. We also examine the role of stratospheric sudden warmings (SSWs) in variations in the forecast skills. Our results show that for lead times shorter than about 10 to 15 days, the forecast skills of the HC data are higher on average and more variable in the stratosphere than in the troposphere especially for Northern winter. This is reflected in larger average and variability in predictable time limit, or characteristic time scale of useful predictions, for the winter stratosphere. We also reveal that the spread-skill relationship for the Northern winter stratosphere is characterized by the existence of notable outliers from their expected linear distribution; the outliers have markedly large errors, or low skills, for given spreads. Most of the outliers are contributed by HC sets initialized before observed major SSWs. Such HC data fail to reproduce the strength and/or shape of the stratospheric polar vortex including both onset and recovery phases of SSWs. The HC data tend to yield too strong vortex and shorter-than-average predictable limit.

Impacts of the Arctic ozone depletion on Japan observed with FTIR

HASHIMOTO, Yuki¹ ; MURATA, Isao^{1*} ; NAKAJIMA, Hideaki² ; NAGAHAMA, Yoshihiro² ; MORINO, Isamu² ; NAGAHAMA, Tomoo³

¹Graduate School of Environmental Studies, Tohoku University, ²National Institute for Environmental Studies, ³Solar Terrestrial Environment Laboratory, Nagoya University

The ozone depletion occurs not only in the Antarctic but also in the Arctic. A record Arctic ozone depletion which was comparable to the Antarctic ozone depletion occurred in 2011. The ozone depletion itself occurs inside the polar vortex. But the air mass from the inside of the polar vortex is spread to mid-latitude in spring after its breakup. The purpose of this study is to quantify the impact of Arctic ozone depletion on mid-latitude by comparing the amounts of ozone in mid-latitude air masses before and after the breakup of the polar vortex.

Vertical profiles of O₃, HF and N₂O have been retrieved from infrared spectra observed with Fourier transform infrared spectrometers (FTIR) at Tsukuba and Rikubetsu using the SFIT2 spectral fitting program. Spectra observed from 2006 to 2013 for Tsukuba and from 1997 to 2008 for Rikubetsu were used in this analysis.

HF and N₂O can be used as a tracer of the transport, because they are chemically stable species in the lower stratosphere. O₃ and HF (or N₂O) usually show a high correlation in the lower stratosphere because both species are stable. But the correlation will be changed when ozone is chemically perturbed. Therefore, we examined the correlations of mixing ratios between O₃ and HF (or N₂O) in the mid-latitude air masses before and after the breakup and determined the chemical loss amount of ozone at the observational sites.

Some chemical ozone losses were found at the altitudes of 19 km and 21 km from O₃-HF correlation. Chemical losses in total ozone were also found from O₃-HF correlation and O₃-N₂O correlation. Then, these observed chemical loss amounts of ozone were compared with the total chemical loss amounts of ozone in the Arctic derived from Japanese Meteorological Agency [2012], Pommereau et al. [2013] and Rex et al. [2013].

Positive correlations were found between the observed chemical loss amounts of ozone at the altitude of 21 km for Tsukuba and at the altitude of 19 km for Rikubetsu and the total chemical loss amounts of ozone in the Arctic. Observed chemical losses in total ozone for both Tsukuba and Rikubetsu also showed positive correlation with the total chemical loss amounts of ozone in the Arctic.

The half-maximum total ozone loss amounts of 15 DU for Tsukuba and 20 DU for Rikubetsu were estimated from the correlations, which result in the increases of 6 % and 7% of UV radiation, respectively.

Keywords: FTIR, Arctic ozone depletion, mid-latitude

The first observation of ozone enhancement in the lowermost atmosphere over China from a spaceborne ultraviolet spectrom

HAYASHIDA, Sachiko^{1*} ; YURIKO, Keyamura¹

¹Faculty of Science, Nara Women's University

This is the first report of observation from space using ultraviolet radiance for significant enhancement of ozone in the lowermost altitudes (0 to about 3000 m) over East and Central China. The recent retrieval products of the Ozone Monitoring Instrument (OMI) onboard EOS/Aura satellite revealed the spatiotemporal variation of the ozone distribution in the lowermost troposphere [Liu et al., ACP, 2010]. The ozone enhancement over East and Central China was clear in June and July every year, associated with enhancement of CO observed from Measurements Of Pollution In The Troposphere (MOPITT) and hotspots taken from MODerate resolution Imaging Spectroradiometer (MODIS). It suggests that considerable part of the enhancement can be attributed to the emissions of ozone precursors from residue burning after harvesting winter wheat in this area. Ozone enhancement was also observed in autumn and early winter over East and Central China every year, sometimes not accompanied by signals of burning, It implies that CO emissions from industrial activity, automobiles and coal burning for heating would affect on ozone production rather than biomass burning in winter.

Acknowledgments

This is a joint study with Dr. Xiong Liu and Dr. Kelly Chance at Harvard-Smithsonian Center for Astrophysics. This study was supported by GRENE-ei program.

Keywords: tropospheric ozone, satellite observation, ultraviolet radiation, atmospheric pollution

The validity of the estimation of ozone origin by sectoral air mass classification verified with tracer-tagging simulation

NAGASHIMA, Tatsuya^{1*} ; IKEDA, Ayaka² ; SUDO, Kengo³ ; HAYASHIDA, Sachiko²

¹National Institute for Environmental Studies, ²Nara Women's University, ³Nagoya University

The air quality in East Asia has changed rapidly in recent years, especially region-wide transboundary air pollution is the main issue in the atmospheric environment in this region. Therefore, the solution to this issue is of great importance today in East Asia, and the scientific understanding of the structure about this region-wide scale air pollution is necessary. The sectoral air mass classification method has been used to estimate the origin of air pollutants in East Asia, and demonstrated the characteristics of air mass with different origins and extended the understanding of the structure of air pollution. However, this method has a problem to erroneously estimate the origin of air pollutant due to the simpleness of the method. Here, we validate of the estimation of ozone origin by sectoral air mass classification by using the tracer-tagging simulation done by a global chemical transport model (CTM). The analysis suggested that the origin of ozone estimated by these two different methods (sectoral air mass classification and tracer-tagging) generally agreed with each other in the warm season, but the two differ significantly in the cold season. The results suggested that the sectoral air mass classification method should consider the different threshold of residence time to separate the air mass into different origins.

Long-term MAX-DOAS network observations of NO₂ in Russia and Asia: comparisons with OMI satellite observations

KANAYA, Yugo^{1*} ; IRIE, Hitoshi² ; TAKASHIMA, Hisahiro³ ; IWABUCHI, Hironobu⁴ ; AKIMOTO, Hajime⁵ ; SUDO, Kengo⁶ ; GU, Myojeong⁷ ; CHONG, Jihyo⁷ ; KIM, Young-joon⁷ ; LEE, Hanlim⁷ ; LI, Ang⁸ ; SI, Fuqi⁸ ; XU, Jin⁸ ; XIE, Pinhua⁸ ; LIU, Wenqing⁸ ; DZHOLA, Anatoly⁹ ; POSTYLYAKOV, Oleg⁹ ; IVANOV, Victor¹⁰ ; GRECHKO, Evgeny⁹ ; TERPUGOVA, Svetlana¹¹ ; PANCHENKO, Mikhail¹¹

¹JAMSTEC, ²Chiba University, ³Fukuoka University, ⁴Tohoku University, ⁵Asia Center for Air Pollution Research, ⁶Nagoya University, ⁷Gwangju Institute of Science and Technology (GIST), ⁸Anhui Institute of Optics and Fine Mechanics, Chinese Academy of Sciences, ⁹A. M. Obukhov Institute of Atmospheric Physics, Russian Academy of Sciences, ¹⁰Belarusian State University, ¹¹V. E. Zuev Institute of Atmospheric Optics, Siberian Branch of the Russian Academy of Sciences

We conducted long-term network observations using standardized Multi-Axis Differential optical absorption spectroscopy (MAX-DOAS) instruments in Russia and ASia (MADRAS) from 2007 onwards. At seven locations (Cape Hedo, Fukue, and Yokosuka in Japan, Hefei in China, Gwangju in Korea, and Tomsk and Zvenigorod in Russia) with different levels of pollution, we obtained 80,927 retrievals of tropospheric NO₂ vertical column density (TropoNO₂VCD) and aerosol optical depth (AOD). This large data set was used to analyze NO₂ climatology systematically, including temporal variations from the seasonal to the diurnal scale. The results were compared with Ozone Monitoring Instrument (OMI) satellite observations and global model simulations. Two NO₂ retrievals of OMI satellite data (NASA ver. 2.1 and Dutch OMI NO₂ (DOMINO) ver. 2.0) generally showed close correlations with those derived from MAX-DOAS observations, but had low biases of ~50%. The bias was distinct when NO₂ was abundantly present near the surface and when the AOD was high, suggesting that the aerosol shielding effect could be important, especially for clean sites where the difference could not be attributed to the spatial inhomogeneity. Except for constant biases, the satellite observations showed nearly perfect seasonal agreement with MAX-DOAS observations, suggesting that the analysis of seasonal features of the satellite data were robust. A global chemical transport model, MIROC-ESM-CHEM, was validated for the first time with respect to background NO₂ column densities during summer at Cape Hedo and Fukue in the clean marine atmosphere.

Keywords: Nitrogen dioxide, MAX-DOAS, Satellite data validation, temporal variation

Temporal variations of aerosol, glyoxal, and formaldehyde retrieved by MAX-DOAS based on detailed error analysis

IRIE, Hitoshi^{1*} ; CHIN, Sei¹ ; NI, Wentao¹ ; NAKAYAMA, Tomoki² ; YAMAZAKI, Akihiro³ ; TAMIO, Takamura¹ ; KHATRI, Pradeep¹

¹Chiba University, ²Nagoya University, ³Meteorological Research Institute

The degradation of volatile organic compounds (VOCs) results in the formation of ozone (O₃) and secondary organic aerosols (SOA) in the troposphere. This process consists of the oxidation of VOCs by hydroxyl radical (OH), O₃, and nitrate radical (NO₃). Detailed understanding of the VOC degradation mechanism is challenged by the co-existence of vast variety of VOC species in the atmosphere. However, investigations on ubiquitous oxidation intermediates, e.g., formaldehyde (HCHO) and glyoxal (CHOCHO), can help us to test and improve the current knowledge of the VOC sources and degradation pathways.

We installed one ground-based Multi-Axis Differential Optical Absorption Spectroscopy (MAX-DOAS) system in Meteorological Research Institute (MRI) located at Tsukuba, Japan (36.06N, 130.13E) in June 2010. In addition, two more systems were installed in Chiba University at Chiba, Japan (35.63N, 140.10E) in June and December 2012, respectively. Since then, we have retrieved lower-tropospheric vertical profile information for eight components; aerosol extinction coefficients at two wavelengths, 357 and 476 nm, and NO₂, HCHO, CHOCHO, H₂O, SO₂, and O₃ concentrations. For a detailed evaluation for the aerosol retrieval, which is a key step in the MAX-DOAS eight-component retrieval, simultaneous aerosol observations with the Cavity Ring-Down Spectroscopy (CRDS) and the sky radiometer were conducted at Tsukuba on October 5-18, 2010 and September 7-18, 2012. At Chiba, in addition to the comparison with sky radiometer data, a self-consistency test was performed by comparing results obtained from two MAX-DOAS systems operated at the same place. Through these detailed evaluations, our retrieval method was improved significantly, attaining excellent agreement with CRDS and sky radiometer data. On the basis of these efforts, seasonal and diurnal temporal variations in HCHO and CHOCHO concentrations retrieved from our MAX-DOAS system are discussed in this talk.

Keywords: CHOCHO, HCHO, MAX-DOAS, CRDS, sky radiometer

Development of an angle-resolved polar nephelometer and its application to non-spherical particles

NAKAGAWA, Maho^{1*} ; SASAGO, Hiroshi¹ ; NAKAYAMA, Tomoki¹ ; MATSUMI, Yutaka¹ ; UEDA, Sayako¹

¹Solar-Terrestrial Environment Laboratory, Nagoya University

Angular distribution of scattering is one of the important optical properties contributing to the radiation balance in the Earth's atmosphere. Therefore, accurate description of the single-scattering properties of aerosol particles is required. In addition, the angular distribution of scattering of individual aerosol particle provides useful information to determine its size, shape, and refractive index of particles.

We are developing a new polar nephelometer, which can measure angular distribution of the optical light scattered by an individual particle. Laser light at 532 nm from a 300 mW YAG laser was used as light source. The laser beam intersects with a stream of aerosol particles introduced with a sheath flow using a double pipe. There are 21 photodiode detectors arrayed in each plane, totaling 42. Detector apertures were placed to limit sensing angles and minimize background light scattered from walls.

In this system, angular distributions of scattering for an incident light polarized parallel and perpendicular to the scattering plane were measured simultaneously. In the experiments, particles were atomized using a nebulizer and dried using a diffusion dryer. Then, size of particle was selected using a Differential Mobility Analyzer (DMA) and Aerosol Particle Mass Analyzer (APM) and introduced into the polar nephelometer.

The performance of the system was tested by measuring angular distributions of scattering by gaseous molecules (HFC-134 and CO₂) and spherical particles. Polystyrene latex sphere is non-light absorbing spherical particle, while nigrosine are light-absorbing spherical particle. The measured scattering angular distribution was compared with the simulation result calculated from the Mie scattering theory considering detection efficiency and of scattering angle range of each detector.

As a result, the scattering angular distributions could be reproduced by the simulation results for PSL particles with diameters between 150 and 900 nm. The scattering angular distributions for nigrosine particles, were in good agreement with the theoretical curve calculated using a literature refractive index value, $n = 1.63 + 0.24 i$. This result suggests that light absorbing particles is distinguishable by the scattering angle distribution measurement.

In order to examine the influence of the difference of the shape, we also performed measurements of the scattering angle distributions of non-spherical particles such as sodium chloride and soot particles. In the presentation, capabilities of the system to determine the shape and refractive index of particle will also be discussed.

Lidar With Multiple Field-Of-View Receiver To Determine Aerosol Size-Distribution

LIU, Yutong^{1*} ; YABUKI, Masanori¹ ; TSUDA, Toshitaka¹

¹Research Institute for Sustainable Humanosphere, Kyoto University

Knowledge of aerosol size distribution is essential for human health studies, because small particles are able to penetrate lung tissues, thus increasing the risk of bronchitis or of lung diseases. Optical remote sensing techniques such as lidar are effective for monitoring aerosols with high temporal and spatial variations. Aerosol instruments that use light with UV, VIS, and near-IR wavelengths have been used to effectively detect particles with diameters comparable to the wavelength. However, to quantitatively estimate the shape of the particle number-size distribution, more information is required with respect to small particles in the size range of sub-micrometer and below.

Conventional lidar employs very small field-of-view (FOV) for profiling aerosol distribution, and thus simply detects single scatter in the direction opposite to that of incident light. Multiple scattered signals are influenced not only by aerosol distribution along the laser path, but also by the size of aerosols. In this study, depolarization UV lidar with a multiple FOV receiver was used for detecting such multiple scattering effects in order to obtain more quantitative information concerning particle-size distribution. Considering the advantage of high scattering cross section for small particles, we employ a UV laser of 266 nm or 355 nm. A program-controlled mechanical FOV selector is used for a receiver system that can change the FOV from 0.1 mrad to 12.4 mrad. In the presentation, we introduce a retrieval method for aerosol size distribution using this feature and show preliminary results from field measurements by the multiple FOV lidar.

Keywords: Lidar, Aerosol

Retrieval of decadal record on the deposition of particulate refractory carbon urban and remote sites in Japan

KANEYASU, Naoki^{1*} ; MATSUMOTO, Kiyoshi² ; YAMAGUCHI, Takashi³ ; AKIYAMA, Masayuki³ ; NOGUCHI, Izumi³ ; MURAO, Naoto⁴ ; NISHIMOTO, Shunya⁴ ; FUNAKI, Daisuke⁵ ; TAKAKI, Satoshi⁵

¹National Institute of Advanced Industrial Science and Technology, ²University of Yamanashi, ³Hokkaido Research Organization, ⁴Graduate School of Engineering, Hokkaido University, ⁵Shimane Prefectural Institute of Public Health and Environment Science

The atmospheric concentration of refractory carbonaceous aerosol (black carbon, or elemental carbon) concentration are used for the evaluation of their direct radiative forcing. In addition, the deposition of such light absorbing substances on the snow or ice surface will result in the increase of the positive radiative forcing at the surface level. Long-term record of deposition for such relative inert substances is expected to reflect the change in the regional emission strength.

However, the reported measurements of deposition to the ground surface are scarce. We thus have conducted the retrieval of decadal record on the deposition of refractory carbon at two sites in the northern Japan (Rishiri Island: a remote site, and Sapporo City: an urban site). At these sites, the environmental monitoring division of local government have been measuring the total deposition of water-soluble aerosol components in the collected water by use of deposition gauges. To remove insoluble particles from the collected water placed beneath the funnel, a membrane pre-filter is placed at the bottom of the funnel of these deposition gauges. Such pre-filters were stored for more than 18 years for Sapporo site. These can be regarded as the long-term record of the deposited water-insoluble aerosol components in the past, as those in ice-core samples collected in glaciers.

We re-suspend these water-insoluble components into the aqueous phase by dissolving the membrane filter (mixed cellulose acetate) by an organic solvent and re-filter the suspended particles through quartz fiber filters for the analysis of TOT refractory carbon. Before dissolved into organic solvent, carbonate in soil dust particles were removed by the 2N HCl with heat. Collection efficacy of quartz fiber filters were corrected by the amount of retained particulate carbon on the first and second filters placed in series.

The deposition flux of TOT-EC is larger in Sapporo, while that in Rishiri showed a large seasonal variation, in general. In Sapporo, the flux decreased greatly in 2010s compared to those in 1990s, probably due to the introduction of regulations for diesel exhaust emission in 2000s. In addition, the deposition sample has been collected in Oki Island since 2013 spring. The preliminary result for this site will also be shown in the presentation.

Keywords: black carbon, deposition flux, decadal record, forest fire, long-range transport, diesel-powered vehicle exhaust

The main controlling factor of black carbon mass concentration in rainwater during 2010-2013 summer in East Asia

MORI, Tatsuhiro^{1*} ; OHATA, Sho¹ ; KONDO, Yutaka¹ ; MOTEKI, Nobuhiro¹ ; MATSUI, Hitoshi² ; IWASAKI, Aya³ ; TOMOYOSE, Nobutaka³ ; KADENA, Hisashi³

¹Department of Earth and Planetary Science, Graduate School of Science, University of Tokyo, Japan, ²Japan Agency for Marine-Earth Science and Technology, Tokyo, Japan, ³Okinawa Prefectural Institute of Health and Environment

Black carbon (BC) particles are emitted into the atmosphere by incomplete combustion processes, and removed by precipitation. The measurements of BC mass concentration in rainwater improve the quantitative understanding of BC loss because wet deposition is the major sink of BC. We measured BC mass concentration in the air (M_{BC}) and in rainwater (C_{BC}) simultaneously at Cape Hedo on Okinawa Island, Japan, in the East China Sea, from April 2010 to March 2013 in order to understand C_{BC} in each rain event during 2010-2013 summer. The rainwater is collected by an automated wet-only sampler during a 24 period. Photo-absorption photometer with heated inlet (COSMOS) is used to measure M_{BC} . C_{BC} was measured by a system consisting of an ultrasonic nebulizer and a Single Soot Photometer (SP2).

It is often heavy rain by cumulonimbus cloud during summer in East Asia, so that M_{BC} an hour before raining is expected to be related to C_{BC} . However, the correlation between M_{BC} and C_{BC} in all rain events during 2010-2013 summer is not agreed ($r^2 = 0.12$). Then, we extracted the heavy rain events, which had positive convective available potential energy (CAPE). These extraction was performed with the National Centers for Environmental Prediction (NCEP) Final (FNL) Operational Global Analysis data every 6 hours. This result was that C_{BC} was correlated with M_{BC} ($r^2 = 0.47$).

In order to investigate if C_{BC} (Estimated C_{BC}) is explained with M_{BC} and the liquid water content, Estimated C_{BC} is verified by comparing the observed C_{BC} . The liquid water content is maximum at the equilibrium level (EL) by the condensation process theoretically if the total water mixing ratio is conserved in the air parcel. If BC in the parcel is active as cloud condensation nuclei (CCN) at lifted condensation level and removed by precipitation at EL, the equation of Estimated C_{BC} at EL is represented as Estimated $C_{BC} = M_{BC} / (m_v * WCR)$. m_v is the water vapor content an hour before raining at the ground level. Water condensation ratio (WCR) is the mass ratio of liquid water content to water vapor content, which is calculated with the NCEP reanalysis data. Compared with the observed C_{BC} , Estimated C_{BC} is correlated with the observed C_{BC} well ($r^2 = 0.68$). It suggests that Estimated C_{BC} is correctly represented as C_{BC} with M_{BC} and the most liquid water content at EL. The observed C_{BC} is three times higher than Estimated C_{BC} because the cloud droplets including BC particles might be collected during falling down.

Keywords: Black Carbon, wet deposition

Number size distribution of ambient aerosols at Cape Hedo, Okinawa and Fukue Island, Nagasaki

MIYOSHI, Takao^{1*} ; TAKAMI, Akinori¹ ; IREI, Satoshi¹

¹NIES

[Introduction]

Recent drastic economical growth in the East Asian region has caused large emission of anthropogenic pollutants to the atmosphere. Some aerosols act as cloud condensation nuclei (CCN) and influence the global climate. There was a report that the higher ratio of inorganic aerosol to the sum of inorganic and organic aerosol and the larger particle size resulted in the higher ratio of CCN to condensation nuclei at the same water vapor supersaturation.

We have conducted field studies for chemical compositions of ambient aerosols at some locations in the East Asian region. In this work, measurement results of number size distribution of aerosols, which potentially influences cloud formation, are presented. Obtained data at two locations were analyzed for better understanding the spatial distribution of aerosol size in the region.

[Observation]

The number concentration was measured at Cape Hedo, Okinawa (lat 26.9°N, long 128.3°E) from 15 to 22 February 2012 and at Fukue Island, Nagasaki (lat 32.8°N, long 128.7°E) from 15 to 28 February 2013 using a Wide-Range Particle Spectrometer (WPS, MSP Corp.), which has a capability to measure a wide particle size range. The WPS consists of two main parts: a combination of a Differential Mobility Analyzer (DMA) and a Condensation Particle Counter (CPC) for particle measurement from 5 to 350 nm (or from 10 to 500 nm) and a Laser Particle Spectrometer (LPS) for measurement from 350 to 10000 nm.

Simultaneously, chemical compositions of ambient aerosols (ammonium, nitrate, sulfate, chloride and organics) were measured by a Quadrupole Aerosol Mass Spectrometers (Q-AMS, Aerodyne Research, Inc.) at Cape Hedo and an Aerosol Chemical Speciation Monitor (ACSM, Aerodyne Research, Inc.) at Fukue Island. At Fukue Island only, sulfur dioxide concentrations were also measured by an SO₂ analyzer (Model 43i, Nippon Thermo Co., Ltd.). Sulfur dioxide concentrations at Cape Hedo were monitored at Hedo Acid Deposition Monitoring Station (Ministry of the Environment).

[Results and Discussion]

The size distributions at Cape Hedo consistently had two peaks at 50 nm and 200 nm. On the other hand, those at Fukue Island varied. There were two peaks at 50 nm and 150 nm after 0:00 a.m. JST on 23 February 2013. Ambient aerosols at 150 nm were largest among the particles which were measured at Fukue Island. There was one peak at 15-25 nm after 12:00 p.m. JST on 24 February 2013 when the number concentration was over 100000 #/cm³. The concentration was also high on 16 and 25 February 2013. The growth of nucleation mode particles was observed from noon to night of each day. We believed that these cases were new particle formation (NPF) events. Such a case was not observed at Cape Hedo.

The molar ratio of sulfur dioxide to the sum of sulfur dioxide and sulfate was studied at both monitoring sites during the observation period by a WPS. When NPF events occurred at Fukue Island, the ratio increased over 80%. On the other hand, the ratio at Cape Hedo was at most 60% even on 17 February 2012 when the transport time of air masses from China according to back trajectory analyses (NOAA HYSPLIT) was approximately one day. The transport time was as long as that to Fukue Island. It was inferred that enough gases such as sulfur dioxide to cause NPF were around Fukue Island and semi-volatile vapors which were newly generated by photochemical reactions condensed on pre-existing particles because the concentrations of gases were low and those of aerosols such as sulfate were high around Cape Hedo.

Keywords: Number size distribution, East Asia, Wide-range particle spectrometer (WPS), New particle formation

Continuous measurement of organic nitrates at Suzu, the Noto peninsula

SADANAGA, Yasuhiro^{1*}; TAKAJI, Ryo¹; ISHIYAMA, Ayana¹; MATSUKI, Atsushi²; SATO, Keiichi³; OSADA, Kazuo⁴; BANDOW, Hiroshi¹

¹Osaka Prefecture University, ²Kanazawa University, ³Asia Center for Air Pollution Research, ⁴Nagoya University

Peroxyacyl nitrates (PANs) and alkyl nitrates (ANs) act as one of the reservoirs of nitrogen oxides (NO_x) in the atmosphere. Since their lifetime is longer than that of NO_x , they can be transported over a long-distance and would be important as trans-boundary pollutants. In this research, continuous measurement system of total PANs and ANs in the troposphere has been developed by using a thermal dissociation / cavity attenuated phase shift spectroscopy (TD/CAPS) method. Both PANs and ANs are thermally decomposed to produce NO_2 and then NO_2 is measured by CAPS method. This system can observe PANs and ANs with high time resolution while this system cannot separate constituents of PANs and ANs. Total PANs and ANs can be measured separately by setting up decomposition lines at different temperatures.

Continuous field observations of PANs and ANs concentrations have been being carried out at NOTOGRO (NOTO Ground-based Research Observatory) supersite in Suzu, Noto Peninsula, since November 2012. NO_x , NO_y , total inorganic nitrate (T.NO_3), O_3 and CO concentrations have also been being observed at NOTOGRO.

NO_y concentrations were in agreement with the sum of observed NO_y components ($= \text{NO}_x + \text{T.NO}_3 + \text{PANs} + \text{ANs}$) regardless of seasons. NO_x fractions were the highest in NO_y constituents. T.NO_3 fractions were small in winter and increased in spring. Opposite tendencies were observed for PANs fractions. These reflect that wet deposition of T.NO_3 is promoted in winter and temperature increasing accelerates decomposition of PANs.

Seasonal variations of both PANs and ANs concentrations showed spring maximum and summer minimum. From winter to spring, both PANs and ANs concentrations from Korea-China air mass origin were higher than those from the other air mass origins. On the other hand, both PANs and ANs concentrations were independent of air mass origins from spring to summer. These indicate that PANs and ANs concentrations in winter and spring are governed by long-range transport and local photochemical productions of PANs and ANs are relatively important from spring to summer. In addition, PANs and ANs diurnal variations being high and low in the daytime and nighttime, respectively, in spring and summer also imply the local photochemical productions of PANs and ANs.

Keywords: Organic nitrates, Total odd nitrogen species, Long-range transport

Light absorption and morphological properties of soot-containing particle mixed with sulfate observed at Noto Peninsula

UEDA, Sayako^{1*} ; NAKAYAMA, Tomoki¹ ; MATSUMI, Yutaka¹ ; TAKETANI, Fumikazu² ; ADACHI, Kouji³ ; MATSUKI, Atsushi⁴ ; IWAMOTO, Yoko⁴ ; SADANAGA, Yasuhiro⁵

¹STEL, Nagoya University, ²JAMSTEC, ³Meteorological Research Institute, ⁴Kanazawa University, ⁵Osaka Prefecture University

Black carbon (BC) in atmospheric soot particle is known as strongly absorber of visible spectrum solar radiation in the atmosphere. The coating materials on soot particle can enhance the magnitude of light absorption by the soot-containing particles, according to the coating conditions including composition, amount and morphology. Several studies have indicated that the estimation by assuming core-shell shaped particle and simple composition tends to estimate larger than that for the real soot-containing particles (Adachi et al., 2010; Lack and Cappa, 2010; Cappa et al., 2012). To elucidate the enhancement of light absorption of aged soot-containing particles and their relation with the individual particle condition, we made an observation for continental outflow at Noto Peninsula, Kanazawa, Japan, in spring 2013.

Atmospheric observations were conducted at NOTO Ground-base Research Observatory (NOTOGRO) in Suzu City, Kanazawa, Japan from April 17 to May 14 in 2014. Absorption and scattering coefficients at 405, 532, and 781 nm, and soot mass concentrations of PM1 particles were measured using the photoacoustic soot photometer (DMT, PASS-3) and a single-particle soot photometer (DMT, SP2), after passing through diffusion dryers and one of the heaters controlled at 25, 300, and 400 deg C every 10 min. Aerosol samples were collected using two-stage cascade impactors (50% cutoff diameters of the two stages were 1.5 μ m and 0.3 μ m) on carbon-coated nitrocellulose (collodion) films for individual analysis using a transmission electron microscope (TEM). Elemental compositions of individual particles were analysed for particles on second stage using an energy-dispersive X-ray spectrometer (EDS) used along with the TEM. Mixing states between non-volatile chain-like soot and volatile materials to high-density electron beam were identified by comparing photograph before and after EDS analysis.

Increase in BC light absorption due to coating was estimated by comparing absorption coefficients at 781 nm with and without heating (300 deg C). The increase in BC light absorption on average was $23 \pm 25\%$. The maximum values of the increase in BC light absorption ($>40\%$) were observed in air mass condition that derived from around Shanghai across the East China Sea, based on backward air mass trajectory analysis. In the TEM sample obtained at the air mass, most of soot were found as internally-mixed particles, which were well-embedded into round-shaped sulphate. On the other hand, increase in light absorption estimated at 405 nm was usually less than that at 781 nm over the entire observation period. Particularly the increase in light absorption at 405 nm tended to be negative under air mass derived from around Japan or the Korean Peninsula. Because absorption at 405 nm is more affected from OC, the negative values might to be attributed to formation of brown carbon in thermo denuder. In TEM sample obtained when the increase in light absorption were negative at 405 nm and $<25\%$ at 781 nm, most of soot were also internally-mixed particles with sulphate. The differences with sample of air mass from Shanghai were that many soot-containing particles were irregular shape, and that carbonaceous residues other than soot were found in particles after irradiation of high electron beam. Our results suggest that the variation of increase in BC light absorption were attributed to morphology and mixing state with OC of internally mixed soot-containing particles.

Adachi, K. et al., *J. Geophys. Res.*, 115, D15206 (2010)

Lack, D. A. and Cappa, C. D., *Atmos. Chem. Phys.*, 10, 4207-4220 (2010)

Cappa, C. D. et al., *Science*, 337, 1078-1081 (2012)

Keywords: Aerosol optical properties, Ambient measurement, Black carbon, electron microscope, Lensing effect

Mixing states of summer time aerosol particles in Noto peninsula

YAMADA, Reina^{1*}; KAMIGUCHI, Yusuke¹; KINOUCHI, Kento²; IWAMOTO, Yoko³; UEDA, Sayako⁴; ADACHI, Kouji⁵; MATSUKI, Atsushi³

¹College of Science and Engineering, Kanazawa University, ²Graduate School of Natural Science and Technology, Kanazawa University, ³Institute of Nature and Environmental Technology, Kanazawa University, ⁴Solar-Terrestrial Environment Laboratory, Nagoya University, ⁵Meteorological Research Institute

Mixing state is one of the factors that determine the characteristic of aerosol particles, and it is important for evaluating their climatic impact. Until recently, summer time aerosol particles in the remote region of central Japan didn't attract much attention since human influence was considered minimal during the season. However, our measurement in the last few years showed that particle number concentrations in summer time were the highest in all seasons. In order to understand the characteristics of the summer time aerosols, we analyzed composition and mixing state of individual particles using transmission electron microscopy (TEM) coupled to energy dispersive W-ray spectrometer (EDX). We conducted quasi-daily sampling at research facility NOTOGRO (NOTO Ground-based Research Observatory) situated at tip of the Noto peninsula from 9th, Jun to 23rd, August. Samples collected during episodes of high aerosol loadings were selected and analyzed. Winds tend to transport air-mass from the Pacific Ocean to the sampling site in summer. However, we found that there were some other flow patterns including flow from the continent of Asia, associated with the high aerosol concentrations. Major composition of particles differed depending on the flow patterns. In addition, many particles were internally mixed, and organics were predominant in smaller diameter range, while sulfates were predominant in larger diameter range. Above results showed that, depending e.g. on the difference of the flow patterns, mixing state of aerosols observed in high concentrations in summer exhibit high temporal variability, and such mixing state are often unevenly distributed among different particle sizes.

Keywords: atmospheric aerosols, mixing state, organic aerosol particles, sulfate aerosol particles

Observation of new particle formation event at Noto peninsula

KAGAMI, Sara^{1*} ; MATSUKI, Atsushi² ; IWAMOTO, Yoko² ; KINOUCHI, Kento³

¹College of Science and Engineering, Kanazawa University, ²Institute of Nature and Environmental Technology, Kanazawa University, ³Graduate School of Natural Science and Technology, Kanazawa University

New Particle Formation (NPF) of atmospheric aerosol particle is an important production process which increases the number concentration of the aerosol particles that would act as Cloud Condensation Nuclei and potentially affect the global climate. The measurement of number size distribution of atmospheric aerosol particles was conducted at the atmospheric observation site, NOTOGRO in Noto peninsula, from October 2012 to September 2013. We identified NPF events throughout the measurement period and this is the first year-round observation reported on the NPF events from coastal region of the Sea of Japan. NPF events tended to occur when Condensation Sink (CS) was relatively low. CS is a measure of the amount of preexisting particle concentration and depends on the particle size distribution. Comparing with meteorological parameters, NPF events were concentrated in daytime, which suggests interaction with solar radiation. However, precipitation preceding the event tended to trigger NPF events by lowering CS (i.e. preexisting particle concentration) especially in winter and summer. On the other hand, NPF events observed in autumn and spring tended to concentrate on days with particularly low relative humidity. Above results suggested that, the conditions favorable for the NPF event is closely related to the seasonal climatic features of the measurement region, that is, the winter monsoon in winter, the rainy season and typhoon in summer and anticyclones in autumn and spring.

Keywords: atmospheric aerosol, new particle formation, condensation sink, precipitation, seasonal variation

Origin of atmospheric gaseous mercury using the Hg/CO ratio in pollution plume observed at Mt. Fuji Weather Station

NAGAFUCHI, Osamu^{1*} ; YOKOTA, Kuriko² ; KATO, Syungo³ ; OSAKA, Ken'ichi¹ ; NAKAZAWA, Koyomi¹ ; KOGA, Masaru¹ ; HISHIDA, Naoko¹ ; NISHIDA, Yuki¹

¹the University of Shiga Prefecture, ²Toyohashi university of technology, ³Tokyo Metropolitan University

Mercury (Hg) is a global pollutant, which is dispersed worldwide mainly in gaseous elemental form via long-range atmospheric transport. Due to the increasing fossil fuel consumptions and industrial emissions, Asia now contributes more than 50% of the global anthropogenic Hg emission with China being the largest atmospheric Hg emitter. Previous studies have demonstrated that the trans-Pacific Asian Hg export could impact North America. Therefore, we would like to study its transport mechanism in the free troposphere by monitoring atmospheric Hg concentrations at high elevation site in Japan. The sampling site is at the summit of Mt. Fuji Weather Station, which is 3,777 m above sea level.

Gaseous mercury and particulate mercury in the atmosphere were separately collected by using a mercury sampler developed by Kagaya et. al., (2007). A quartz filter (Palflex2000, Tokyo Dylec) was attached at the tip of a mercury absorbing tube in which amalgamated gold was impregnated, and the air was aspirated by an air pump through the filter and the mercury absorbing tube at a rate of 0.5L/min. Particulate mercury was filtered by the quartz filter and gaseous mercury was absorbed by the amalgamated gold in the tube. Both particulate and gaseous mercury were analyzed by an atomic absorbance spectrophotometer (Nippon Instruments, MA-2000) after vaporization by heating.

The mercury sampler was set in a place 5m or more away from the building at summit of Mt. Fuji (N35.21'.38", E138.43'39"). The sampling was performed from 11 to 18 August, 2008. The filter and the absorbing tube were changed with 12-24 hour-intervals.

Atmospheric mercury concentrations observed at summit of Mt. Fuji and Japan. High concentrations of both gaseous and particulate mercuries were observed at the summit of Mt. Fuji. Swartzendruber et al. reported the gaseous and particulate mercury concentrations in the free troposphere at the Mt. Bachelor as 1.54 and 0.0043 ng/m³, respectively. Hans R. Friedli et al reported that gaseous elemental mercury were found in industrial plumes exiting China, Korea, and Japan ~6.3ng/ m³, ~3ng/ m³ and ~3ng/ m³, respectively. The higher atmospheric mercury concentrations at the summit of Mt. Fuji may imply that there is a specific pollution source in the East Asia. Because from the result of the back trajectory calculation, the air mass came from the China during this observation periods.

Clarification of lead (Pb) species and its formation mechanisms in coarse and fine aerosol particles using X-ray absorpt

SAKATA, Kohei^{1*} ; SAKAGUCHI, Aya¹ ; TANIMIZU, Masaharu² ; TAKAHASHI, Yoshio¹

¹Graduate school of Science, Hiroshima University, ²JAMSTEC

There are very few studies on chemical speciation and atmospheric chemistry of trace elements. Among the trace elements in the aerosol particles, lead(Pb) has long been measured due to the toxicity of this element. The measurement of Pb isotope ratios in aerosol particles has also been employed as a powerful tracer for air-mass transportation because Pb isotope ratios differ significantly depending on the emission area/source. However the speciation of Pb has not been clarified, although their solubility is important to estimate the health effects for human/animal body. Furthermore, Pb in the aerosol particle is the dominant source of Pb, which is used as oceanic circulation tracer, in the surface seawater. Thus, the speciation of Pb in the aerosol particle is one of the important issue. In this study, we attempted to determine the Pb species in aerosol samples using X-ray absorption fine structure (XAFS) analysis.

Size-fractionated aerosol particles were collected by a high-volume aerosol sampler with cascade impactor at Higashi-Hiroshima. Lead LIII-edge (absorption edge: 13.04 keV) X-ray absorption near-edge structure (XANES) spectra were recorded on SPring-8 on BL01B1 and at KEK PF-AR on NW10A to identify the Pb species. The analyzed sample-sets of size-fractionated aerosol particles are follows: Spring (Asian dust event), summer (two sample sets), fall, and winter (transboundary pollution event).

Lead species in size-fractionated aerosol particles are different between fine and coarse aerosol particles. In the fine aerosol particles, the dominant Pb species were two or three components, PbSO_4 , $\text{Pb}(\text{NO}_3)_2$ and PbC_2O_4 , in all seasons. That is, the seasonal variation of Pb species in the fine aerosol was not found. It is because the Pb species in the fine aerosol particles are formed by uniform chemical reaction with H_2SO_4 , HNO_3 and oxalic acid in droplet through a year. Pb species in the coarse aerosol particles, except for on Asian dust event, were $2\text{PbCO}_3\text{-Pb}(\text{OH})_2$, $\text{Pb}(\text{NO}_3)_2$ and PbC_2O_4 . These $2\text{PbCO}_3\text{-Pb}(\text{OH})_2$ and partial PbC_2O_4 were derived from road dust, and $\text{Pb}(\text{NO}_3)_2$ in coarse aerosol particles was formed by chemical reactions with HNO_3 on the surface of the particle. In Asian dust event, the coarse aerosol particles showed PbSiO_3 as major Pb species, although other species, $2\text{PbCO}_3\text{-Pb}(\text{OH})_2$ and PbC_2O_4 , were also obtained. Thus we could found the clear seasonal variation in the coarse aerosol particles. These results will be able to estimate the accurate estimation of Pb solubility to the surface seawater.

Methyl chloride in the upper troposphere observed by CARIBIC: large-scale distributions and Asian summer monsoon outflow

UMEZAWA, Taku^{1*} ; K. BAKER, Angela¹ ; ORAM, David² ; SAUVAGE, Carina¹ ; O'SULLIVAN, Debbie² ; RAUTHE-SCHOECH, Armin¹ ; A. MONTZKA, Stephen³ ; ZAHN, Andreas⁴ ; A.M. BRENNINKMEIJER, Carl¹

¹Max Planck Institute for Chemistry, ²National Centre for Atmospheric Science, School of Environmental Sciences, University of East Anglia, ³Earth System Research Laboratory, NOAA, ⁴Institute for Meteorology and Climate Research, Karlsruhe Institute of Technology

CARIBIC is a flying observatory onboard a Lufthansa A340-600 aircraft that observes various atmospheric compounds at almost monthly intervals. In this study, we present spatial and temporal variations of methyl chloride (CH₃Cl) in the upper troposphere (UT) observed mainly by CARIBIC for the years 2005-2011. The CH₃Cl mixing ratio in the UT over Europe was higher than that observed at a European surface baseline station throughout the year, indicative of a persistent positive vertical gradient at NH mid latitudes. A series of flights over Africa and South Asia show that CH₃Cl mixing ratios increase toward tropical latitudes, and the observed UT CH₃Cl level over these two regions and the Atlantic was higher than that measured at remote surface sites. Strong emissions of CH₃Cl in the tropics combined with meridional air transport through the UT may explain such vertical and latitudinal gradients. Comparisons with carbon monoxide (CO) data indicate that non-combustion sources in the tropics dominantly contribute to forming the latitudinal gradient of CH₃Cl in the UT. We also observed elevated mixing ratios of CH₃Cl and CO in air influenced by biomass burning in South America and Africa, and the emission ratios derived for CH₃Cl to CO in those regions agree with previous observations. In contrast, correlations indicate a high CH₃Cl to CO ratio of 2.9 ± 0.5 ppt ppb⁻¹ in the Asian summer monsoon anticyclone and domestic biofuel emissions in South Asia are inferred to be responsible. We estimated the CH₃Cl emission in South Asia to be 134 ± 23 Gg Cl yr⁻¹, which is higher than a previous estimate due to the higher CH₃Cl to CO ratio observed in this study.

Keywords: CARIBIC, aircraft observation, methyl chloride, upper troposphere

Flattening of the equatorial bulge of annual mean APO observed in the Western Pacific during the 09/10 El Nino event

TOHJIMA, Yasunori^{1*} ; MUKAI, Hitoshi¹ ; MACHIDA, Toshinobu¹ ; TERAOKA, Yukio¹ ; NOJIRI, Yukihiro¹

¹National Institute for Environmental Studies

A tracer known as atmospheric potential oxygen ($APO=O_2+1.1\times CO_2$) has been proved to be useful to study air-sea gas exchange. Although both atmospheric CO_2 and O_2 concentrations are affected from the air-sea and air-land gas exchanges, APO mainly reflect the air-sea gas exchange because APO is invariant with respect to the land biotic gas exchanges (-1.1 in the definition represents the molar land biotic $-O_2:C$ exchange ratio). To investigate the spatio-temporal variations in the APO over the Pacific region, we have been observing the atmospheric CO_2 and O_2 concentrations onboard commercial cargo ships sailing between Japan and US/Canada and Australia/New Zealand since December 2001. Our previous studies based on the shipboard flask measurements for 7-year period (2002-2008) revealed that the average latitudinal distribution of the annual-mean APO in the Western Pacific (from 40 deg. S to 50 deg. N) show a maximum near the equator and decreasing trends toward the mid-latitude in both hemisphere (Tohjima et al, 2012). This latitudinal distribution of the annual-mean APO is mainly attributed to the latitudinal differences in the air-sea gas exchange: outgassing fluxes around the equator and ingassing fluxes in the mid and high latitude. In the previous study, the equatorial bulge was robust and always observed during the 7-year period. However, the equatorial bulge disappeared and the latitudinal distribution was flattened especially in the Southern Hemisphere during the period from July 2009 to June 2010, when the most recent El Nino event occurred. Simulated APO based on an atmospheric transport model (NIES99) driven by a set of climatological oceanic O_2 and CO_2 fluxes also shows suppression of the equatorial bulge during El Nino periods, indicating that the atmospheric transport substantially contributes to the inter-annual change in the latitudinal distribution of the annual-mean APO. The simulated APO, however, cannot fully reconstruct the flattening of APO in the Southern Hemisphere. Thus, the suppression of the Eastern Pacific upwelling during the El Nino period might reduce O_2 and/or CO_2 outgassing around the equatorial ocean.

Keywords: atmospheric potential oxygen, APO, air-sea gas exchange, El Nino, Tropical western Pacific ocean

Separation of gross primary production and ecosystem respiration of a Japanese forest using atmospheric O₂/N₂ ratio

ISHIDOYA, Shigeyuki^{1*} ; MURAYAMA, Shohei¹ ; KONDO, Hiroaki¹ ; SAIGUSA, Nobuko² ; KISHIMOTO, Ayaka³ ; YAMAMOTO, Susumu¹

¹National Institute of Advanced Industrial Science and Technology (AIST), ²National Institute for Environmental Studies, ³National Institute for Agro-Environmental Sciences (NIAES)

The atmospheric O₂/N₂ ratio ($\delta(O_2/N_2)$) has been observed globally since the early 1990s to elucidate the global CO₂ budget (e.g. Manning and Keeling, 2006). To apply this method, the global average terrestrial biospheric O₂:CO₂ molar exchange ratio is needed. Keeling (1988) estimated the O₂:CO₂ exchange ratio (hereafter referred to as ER) of 1.05 by surveying the results from various elemental abundance studies. Severinghaus (1995) revised the ER to be 1.10 ± 0.05 , which has been used for the global average terrestrial biospheric ER in recent studies. However, Seibt et al. (2004) and Ishidoya et al. (2013) observed the ER values associated with respiration and photosynthesis in forests and reported that the ER for net turbulent O₂ and CO₂ fluxes between the forest ecosystem and the atmosphere above the canopy (hereafter referred to as ER_F) could be different from 1.1 significantly, based on one-box canopy O₂/CO₂ budget model analyses. Moreover, the ER_F reported by Seibt et al. (2004) is quite different from that by Ishidoya et al. (2013); the former is larger than 1.1 and the latter is smaller than 1.0 under the condition of uptake of CO₂ from the atmosphere to a forest. Therefore, direct observation of the ER_F at various forests is expected to validate the global average terrestrial biospheric ER. In addition, such the observation of the ER_F will lead to estimate the gross primary production (GPP) and the ecosystem respiration (RE) of the forest separately.

In this study, we present the average daily mean ER_F at Takayama deciduous broadleaf forest site in central Japan (36°09' N, 137°25' E, 1420 m a.s.l.; designated as TKY in the Asia Flux site code database) for the period May 24 – August 28, 2013, observed firstly based on an aerodynamic method (Yamamoto et al., 1999). The observed average daily mean ER_F is 0.79 ± 0.08 , which is not only smaller than 1.0 as predicted by Ishidoya et al. (2013) but also significantly smaller than the assumed global average terrestrial biospheric ER (1.10 ± 0.05). We also separate the average daily mean NEP for the corresponding period observed by the eddy covariance method (Saigusa et al., 2005) into average daily mean GPP and RE, by using the observed average daily mean ER_F in this study as well as the ER_A (the ER for GPP) and ER_R (the ER for RE) at TKY reported by Ishidoya et al. (2013). Then, the separated average daily mean RE is compared with that estimated from an empirical function of air temperature (Saigusa et al., 2005) and the soil CO₂ efflux observed using soil chamber experiments (Mo et al., 2005), to discuss the validity of the observed ER_F and its implication to the forest and global carbon cycle (Ishidoya et al., in manuscript in prep.).

Reference

Ishidoya, S., Murayama, S., Takamura, C., Kondo, H., Saigusa, N., Goto, D., Morimoto, S., Aoki, N., Aoki, S., Nakazawa, T. (2013) O₂:CO₂ exchange ratios in a cool temperate deciduous forest ecosystem of central Japan. *Tellus* 65B, 21120, <http://dx.doi.org/10.3402/tellusb.v65i0.21120>.

Keywords: atmospheric O₂/N₂ ratio, O₂:CO₂ exchange ratio between a forest and the atmosphere, gross primary production, ecosystem respiration, forest carbon cycle

Seasonal changes of greenhouse gases in the upper troposphere/lower stratosphere observed by commercial airliner

SAWA, Yousuke^{1*} ; MACHIDA, Toshinobu² ; MATSUEDA, Hidekazu¹ ; NIWA, Yosuke¹ ; TSUBOI, Kazuhiro¹ ; MURAYAMA, Shohei³ ; MORIMOTO, Shinji⁴ ; AOKI, Shuji⁴

¹Meteorological Research Institute, ²National Institute for Environmental Studies, ³National Institute of Advanced Industrial Science and Technology, ⁴Tohoku University

Atmospheric mixing ratios of greenhouse gases at about 11 km altitude were analyzed from monthly air sampling aboard commercial airliner during the flights between Europe and Japan from April 2012 to August 2013. Compared to the subtropic, higher CH₄ and SF₆ mixing ratios, similar values of N₂O, and larger seasonal changes of CO₂ were found in the upper troposphere. CH₄, N₂O and SF₆ in the lower stratosphere, above the tropopause up to 30 K in potential temperature, showed simultaneous increases from June to October, and faster decreases at higher altitudes from January to March. Mean age of the air in the lower stratosphere was estimated based on SF₆ mixing ratios to be about 2 years in late spring and 1 year in autumn, suggesting stronger influences on the mixing ratios in the stratosphere from troposphere in summer.

Keywords: Atmospheric Chemistry, Greenhouse Gas, Upper Troposphere/Lower Stratosphere

Long-term changes of CH₄ concentration and its carbon isotopic ratio in the lower stratosphere over Japan

SUGAWARA, Satoshi^{1*}; MORIMOTO, Shinji²; UMEZAWA, Taku³; AOKI, Shuji²; NAKAZAWA, Takakiyo²; ISHIDOYA, Shigeyuki⁴; TOYODA, Sakae⁵; HONDA, Hideyuki⁶

¹Miyagi Univ. of Education, ²CAOS, Tohoku Univ., ³Max Planck Institute for Chemistry, ⁴AIST, ⁵Tokyo Institute of Technology, ⁶ISAS/JAXA

It is expected that $\delta^{13}\text{C}$ of CH₄ provides us with useful information not only about CH₄ emissions from biogenic and abio-genic sources but also about its oxidation process in the atmosphere. Therefore, measurements of $\delta^{13}\text{C}$ have been carried out for the major CH₄ sources as well as for the background atmosphere. However, the measurements are still insufficient for elucidating the CH₄ cycle on the earth's surface. In the stratosphere, CH₄ is destroyed by reactions with OH, O(1D) and Cl atom. These destruction processes play an important role in the stratospheric chemistry, but the respective contributions to the CH₄ loss and their temporal changes have not been yet well understood quantitatively. Measurements of the isotopic ratios of the stratospheric CH₄ are one of the most promising methods to detect possible change of the CH₄ destruction processes in the stratosphere on the basis of the different isotopic fractionations occurring in the different reactions. However, only a few measurements have been made so far, due mainly to difficulty of collecting air samples in the stratosphere. Systematic collections of stratospheric air samples have been carried out over Japan since 1985 using a balloon-borne cryogenic sampler. We analyzed the air samples collected in the period of 1994-2010 for concentrations of CH₄, N₂O, CO₂ and SF₆, and $\delta^{13}\text{C}$ of CH₄. In this study, we report the preliminary results of the long-term change of $\delta^{13}\text{C}$ of CH₄ in the stratosphere. Almost linear and compact relationships between CH₄ and N₂O concentrations were found for the all observations in the different years. CH₄ concentration and $\delta^{13}\text{C}$ also showed compact relationships in the lower stratosphere, although those in the mid-stratosphere were less correlated. The tight correlations between CH₄ and N₂O in spite of the different destruction processes suggest that the ratio of both destruction rates has been kept as almost constant during the transport process in the stratosphere. It is well known that tropospheric CH₄ and N₂O have been secularly increasing in the recent decades. Such increasing trends should have been propagated into the stratosphere, and the compact relationships between the stratospheric CH₄ and N₂O would change depending on their increase rates. To elucidate an inter-annual changes of the stratospheric CH₄ and its $\delta^{13}\text{C}$, we employed N₂O-loss, instead of the N₂O concentration, as an indicator of how the chemical reactions have proceeded during the stratospheric transport. The N₂O-loss was calculated as a concentration difference between the tropical troposphere and the stratosphere by considering the mean age of air estimated from CO₂ and SF₆ concentrations. This procedure eliminates the effect of the secular N₂O increase from the relationships between CH₄ and N₂O, and enables us to detect possible change in the stratospheric CH₄. As a result, we found that the CH₄ concentration increased at a rate of 4.5 ± 0.9 ppbv/year in the lower stratosphere during 16 years. This increase rate is consistent with those observed in the troposphere. The same technique was applied to the correlations between CH₄ concentration and $\delta^{13}\text{C}$, and we found no significant changes of $\delta^{13}\text{C}$ in the lower stratosphere. Considering the fact that $\delta^{13}\text{C}$ in the troposphere also does not show a clear trend in a recent decade, our result implies that the relative contributions of the CH₄ destruction processes have been unchanged in the lower stratosphere over the observed period.

Keywords: stratospheric methane, carbon isotopic ratio

Laboratory biomass burning experiments to investigate the dependence of emissions of volatile organic compounds on burni

INOMATA, Satoshi^{1*}; TANIMOTO, Hiroshi¹; PAN, Xiaole²; TAKETANI, Fumikazu²; KOMAZAKI, Yuichi²; MIYAKAWA, Takuma²; KANAYA, Yugo²

¹NIES, ²JAMSTEC

Biomass burning is one of major sources of primary fine carbonaceous aerosols and organic compounds.¹ A field observation campaign in a rural area of the Yangtze River Delta, China, was carried out during the harvest season in June of 2010 and air masses of open crop residue burning were frequently observed. It was found that the emission ratios of elemental carbon (EC) and organic carbon (OC) to CO were enhanced during the biomass burning episodes compared with those in urban pollution.² In addition, oxygenated volatile organic compounds were predominantly emitted during the biomass burning.³ To investigate the emission properties of aerosols and organic compounds under controlled conditions, we carried out biomass burning experiments in the laboratory. Two types of crop residues, wheat straws and oilseed rapes, which were actually burned during the campaign, were used as the sample. We will mainly show the dependence of the emission ratios of volatile organic compounds to CO on burning conditions and compare with the field observation.

References

- 1) Akagi et al., Atmos. Chem. Phys. 11, 4039-4072, 2011.
- 2) Pan et al., J. Geophys. Res. 117, D22304, 2012.
- 3) Kudo et al., submitted to J. Geophys. Res., 2013.

Keywords: Biomass burning, Volatile organic compounds, Crop residue, Combustion efficiency, PTR-MS, SP2

Impact of VOC emission from gasoline cars on ozone formation

HIROYUKI, Yamada^{1*} ; INOMATA, Satoshi² ; TANIMOTO, Hiroshi²

¹National Traffic Safety and Environment Laboratory, ²National Institute for Environmental Studies

Ozone has been known that it was produced by the atmospheric reactions of volatile organic compounds (VOC) and NO_x. The impact of VOC on ozone formation varies species by species. Thus, to evaluate the ozone formation in atmosphere, discussion based of ozone formation potential (OFP) is important.

This study discussed VOC emission from gasoline vehicle with OFP. Usually it is thought that main source of VOC from vehicles were tailpipe emissions, however our former study suggested that main source from gasoline cars is not tailpipe emissions but evaporative emissions. So in this study, addition to tailpipe emissions, OFP of evaporative emissions were measured.

Keywords: ozone, ozone formation potential, evaporative emissions, gasoline cars, tailpipe emissions

Improvement of measurement system for organic nitrates produced in the mixture of VOC, NO_x and O₃

MATSUMOTO, Jun^{1*}

¹Faculty of Human Sciences, Waseda University

Organic nitrates, ONs, are important as an intermediate of secondary organic aerosols (SOAs). Additionally, the branching ratio between ONs and NO₂ formation after the reactions of NO with peroxy radicals (RO₂) are critical for tropospheric ozone formation. In this study, laboratory experiments were conducted for the reaction of VOCs/O₃/NO mixture. After the reactor, total ONs were monitored by the thermal-desorption laser-induced fluorescence (TD-LIF) technique. At this time, an improved glass double-tube flow reactor was constructed. The inner tube (Pyrex, O.D. 10 mm, I.D. 8 mm) was for the O₃ flow, and the outer (Pyrex, O.D. 150 mm, I.D. 143 mm, length 500 mm) was for the additional flow (VOC sample and NO) to reduce the wall loss of ozone at the edges of reactor. As a result, after the improvement of the reactor and its conditions, the sensitivity of formed ONs was three times as large as the previous system. The sensitivity was defined as the slope of the regression line between VOC concentration and ONs increment. Observed sensitivities for isoprene and limonene were 0.00085 and 0.013 ppbv/ppbv, respectively. Sensitivity for limonene was 15 times as large as that for isoprene. Meanwhile, the reaction rate constant of limonene with ozone is 16 times larger than that of isoprene with ozone. It was experimentally indicated that the initial reaction of VOCs with ozone be critical for production of organic nitrates. It was also confirmed that measurements of ONs produced in the mixture of VOC, NO_x and O₃ was promising. As a next step, RO₂ productivity of initial reactions (VOC+O₃) and branching ratio between ONs and NO₂ formation will be explored to clarify characteristics of ONs production in detail.

Acknowledgements: This work has been supported financially by a Grant-in-Aid for Scientific Research (No. 24651014), from the Ministry of Education, Culture, Sports, Science and Technology (MEXT) of the Japanese Government.

Keywords: Nitrogen oxides, Volatile organic compounds, Tropospheric ozone, Organic nitrates, Laboratory experiments, Gas phase reactions

Humidity dependence of extinction coefficients of secondary organic aerosols and its relation with chemical properties

NAKAYAMA, Tomoki^{1*} ; MATSUMI, Yutaka¹ ; SATO, Kei² ; IMAMURA, Takashi²

¹Solar-Terrestrial Environment Laboratory, Nagoya University, ²National Institute for Environmental Studies

Atmospheric aerosols scatter and absorb solar radiation, thereby influencing the Earth's radiation balance. Light extinction is the sum of scattering and absorption. The aerosol extinction coefficient depends on chemical composition, particle size, shape and mixing state in addition to wavelength of light. The uptake of water by aerosol particles can change extinction coefficients by changing size and refractive index of particles. Therefore, the detailed understanding of the relative humidity (RH) dependence of the extinction coefficients is important to estimate the impact of aerosols on radiation balance. However, the RH dependence of optical properties for secondary organic aerosol (SOA) has not been studied in detail.

In this work, we have determined the RH dependence of extinction coefficients of the SOAs generated during (1) the photooxidation of toluene in the presence of NO_x and (2) the ozonolysis of α -pinene. The SOAs were generated in a 6 m³ teflon coated stainless-steel chamber in the absence of seed particles. The RH dependence of aerosol extinction coefficients at 532 nm was measured using a custom-made cavity ring-down spectrometer (CRDS). The CRDS has two measurement cells, in which the RH were controlled at <10% and 80%, respectively. The size distributions and chemical compositions of the SOAs were also measured using a scanning mobility particle sizer (SMPS, TSI) and a time of flight aerosol mass spectrometer (ToF-AMS, Aerodyne), respectively.

The ratio of extinction coefficients measured under high RH condition (RH=80%) to those measured under dry condition, $F(\text{RH})$, were compared with the relative abundance of the ion signal $m/z=44$ measured by the ToF-AMS to total organic signal, f_{44} . The f_{44} factor is known as a marker of oxygenated species such as organic di-acids, poly-acids, oxo-acids, hydroxy-acids, and acyl peroxides. Small RH dependence of extinction coefficients was found for the α -pinene-SOA with $F(\text{RH})$ of about 1.05, but the $F(\text{RH})$ values for the toluene-SOA were increase up to 1.4-1.6 with increasing the f_{44} . Interestingly, the relationship between $F(\text{RH})$ and f_{44} for the toluene-SOAs did not depend on the initial NO_x concentrations. Our results suggest that the increase in hygroscopicity due to oxidation of the SOAs mainly contributes to the observed RH dependence of extinction coefficients for the toluene-SOA.

Keywords: Secondary organic aerosol (SOA), Optical property, Humidity dependence, Chemical property, Climate change

Insoluble metal-oxalate complexes in the atmosphere: its stability and global cooling effect

YAMAKAWA, Yoshiaki^{1*} ; SAKATA, Kohei¹ ; MIYAHARA, Aya¹ ; MIYAMOTO, Chihiro² ; SAKAGUCHI, Aya¹ ; TAKAHASHI, Yoshio¹

¹Department of Earth and Planetary Systems Science, Graduate School of Science, Hiroshima University, ²Department of Science, Hiroshima University

Aerosols have cooling effect on the earth, which is divided into direct and indirect effects. The direct effect is reflection of sunlight directly by aerosols, whereas the indirect effect is the reflection by clouds formed by the aid of aerosols working as cloud condensation nuclei (CCN). Oxalic acid is a main component of secondary organic aerosols and abundant in the atmosphere, which is formed by degradation of organic matters with longer carbon chain such as cyclic olefin. Oxalic acid is hygroscopic, which can work as CCN with indirect cooling effect. It has been estimated that the degree of cooling effect by the aerosols are equal to that of the warming effect of carbon dioxide (CO₂). However, there is large uncertainty in the estimation. In addition, it is suggested that oxalic acid may form insoluble metal-oxalate complexes and does not have the indirect cooling effect. Therefore, it is important to re-evaluate the cooling effect of aerosols for precise prediction of global warming. Although dicarboxylic acid including oxalic acid is decomposed into CO₂ by photolysis, oxalic acid is more abundant than the other dicarboxylic acids. It is possible that oxalic acid can be stabilized by forming metal-oxalate complexes. This study was aimed (i) to measure the concentration of metal-oxalate complexes in the atmosphere to contribute to precise prediction of global warming and (ii) to measure the half-life time to evaluate the stability of metal-oxalate complexes during photoreaction.

Size-fractionated aerosol samples were collected at Higashi-Hiroshima in winter (Dec., 2012-Jan., 2013), spring (April, 2013), and summer (July-Aug., 2013). The ratio of oxalic acid and total metal-oxalate complexes was estimated based on the X-ray absorption fine structure (XAFS) spectroscopy for zinc (Zn), lead (Pb), and calcium (Ca). Photolysis experiments were conducted by ultraviolet ray for oxalic acid, Zn complex, and magnesium (Mg) complex, while absorption spectra were measured to evaluate photoreactivity.

As a result, metal-oxalate complexes were found in finer particles. There was a positive correlation between the ratio of oxalate/nitrate and ratio of metal-oxalate complexes/total oxalate species. Therefore, it is considered that metal-oxalate complexes are formed by relative increase of oxalate for nitrate. Although concentration of total oxalate species was largest, the ratio of metal-oxalate complexes/total oxalate species was smallest in summer. Concentration of total oxalate species was higher than that of metal ions (Zn²⁺, Pb²⁺, and Ca²⁺). Therefore, it is considered that the ratio of metal-oxalate complexes is smallest in summer.

This ratio was about 30% to 50% for each sample through the year. This result showed that the cooling effect of oxalic acid may be smaller than previous estimation.

As a result of photolysis experiments, half-life time of oxalic acid, Mg complex, and Zn complex is 19 min, 71 min, and 172 min, respectively. This result showed that photoreactivity of oxalic acid was decreased by forming metal-oxalate complexes. Compared to absorption spectra between oxalic acid and metal-oxalate complexes, absorbance was decreased by forming metal-oxalate complexes. Therefore, it is considered that the increase of half-life time may be caused by the decrease of absorbance by forming metal-oxalate complexes.

Keywords: Aerosol, Metal-Oxalate Complex, Global Cooling Effect, Photoreactivity, X-ray Absorption Fine Structure Spectroscopy

Volatility basis-set approach simulation of organic aerosol formation in East Asia

MATSUI, Hitoshi^{1*}; KOIKE, Makoto²; KONDO, Yutaka²; TAKAMI, Akinori³; KANAYA, Yugo¹; TAKIGAWA, Masayuki¹

¹Japan Agency for Marine-Earth Science and Technology, ²University of Tokyo, ³National Institute for Environmental Studies

Organic aerosol (OA) accounts for a significant mass fraction of the submicron aerosols in the atmosphere, and it influences the Earth's climate either directly (by scattering/absorbing of solar radiation) or indirectly (by modifying cloud microphysical properties). Recent studies show that secondary OA accounts for a large fraction of OA globally. However, as secondary OA formation processes are very complicated, estimates of the secondary OA burden in the atmosphere and its impact on climate and human health remain highly uncertain compared with those of other aerosols such as inorganic species.

In this study, OA simulations using the volatility basis-set approach were made for East Asia and its outflow region. Model simulations were evaluated through comparisons with OA measured by aerosol mass spectrometers in and around Tokyo (at Komaba and Kisai in summer 2003 and 2004) and over the outflow region in East Asia (at Fukue and Hedo in spring 2009). The simulations with aging processes of organic vapors reasonably well reproduced mass concentrations, temporal variations, and formation efficiency of observed OA at all sites. As OA mass was severely underestimated in the simulations without the aging processes, the oxidations of organic vapors are essential for reasonable OA simulations over East Asia. By considering the aging processes, simulated OA concentrations considerably increased from 0.24 to 1.28 $\mu\text{g}/\text{m}^3$ in the boundary layer over the whole of East Asia. OA formed from the interaction of anthropogenic and biogenic sources was also enhanced by the aging processes. The fraction of controllable OA was estimated to be 87 % of total OA over the whole of East Asia, showing that most of the OA in our simulations formed anthropogenically (controllable). A large portion of biogenic secondary OA (78 % of biogenic secondary OA) formed through the influence of anthropogenic sources. The high fraction of controllable OA in our simulations is likely because anthropogenic emissions are dominant over East Asia and OA formation is enhanced by anthropogenic sources and their aging processes. Both the amounts (from 0.18 to 1.12 $\mu\text{g}/\text{m}^3$) and the fraction (from 75 % to 87 %) of controllable OA were increased by aging processes of organic vapors over East Asia.

Keywords: aerosol, organic aerosol, regional three-dimensional model, anthropogenic-biogenic interaction, East Asia, volatility basis-set

Impacts of BVOCs changes on global atmospheric chemistry: off-line coupling of CHASER and VISIT

SUDO, Kengo^{1*} ; ITO, Akihiko²

¹Graduate School of Environmental Studies, Nagoya University, ²National Institute of Environmental Studies

Biogenic volatile organic compound (BVOC) is one of important factors to control global atmospheric environment and climate change, affecting tropospheric chemistry which involves ozone production/loss, OH radical abundance (atmospheric oxidizing power), and global production of secondary organic aerosols (SOA). Emissions of BVOCs are basically determined by land ecosystem processes, but also tightly linked to climate factors (such as temperature and precipitation), atmospheric CO₂ concentration, and deposition of nitrogen species. Therefore, a modelling framework to couple atmospheric chemistry with land ecosystem is needed for considering BVOCs changes and associated impacts. In this study, coupled simulation of global atmospheric chemistry and terrestrial ecosystem has been developed by combining atmospheric chemistry model CHASER (Sudo et al., 2002, 2007) and land ecosystem/trace gas emission model VISIT (Ito et al., 2008). The CHASER model, also developed in the framework of the MIROC earth system model (MIROC-ESM-CHEM), simulates detailed chemistry in the troposphere and stratosphere with an on-line aerosol simulation including SOA production. The VISIT model calculates terrestrial emissions of CO₂, CH₄, N₂O, and BVOCs. This paper focuses on isoprene as a proxy of BVOCs, and discusses the impacts of the past isoprene emission changes on global atmospheric chemistry using the CHASER model constrained with off-line input from the VISIT simulation. VISIT calculates an increase in global isoprene emissions from 420 to 520 TgC a⁻¹ (24%) from the first half of the 20th century to 2011. As a response to this emission change, CHASER simulated a ~2% increase in global ozone production causing ~4% increases in ozone concentration in the tropical middle-upper troposphere. The model also showed that OH decreases by 5-10% in the most of NH due to the isoprene emission change, resulting in 2-4% decreases of CO in NH. Also, SOA is largely increased by more than 30% in the major part of the troposphere (especially in the tropics).

Keywords: biogenic VOCs, chemistry climate model, land ecosystem model, secondary organic aerosol, atmosphere-land interaction

Emission of iodine molecule and iodine monoxide from frozen solutions containing iodide ion

OKUMURA, Masanori¹ ; YABUSHITA, Akihiro^{1*}

¹Kyoto University

Iodine oxides are receiving increasing attention in atmospheric chemistry, because it may contribute to ozone depletion and atmospheric particle formation in polar region. Iodine monoxide(IO) generates from the reaction of iodine atom with ozone. Iodine atoms may be formed by photolysis of iodine(I₂) or volatile iodocarbons, the main source of which is oceanic biogenic production. Emission processes from inorganic source are also being proposed, but they are so far unexplained. Iodine compounds were found above, below and within the sea ice of the Weddell Sea, and these measurements show the Weddell Sea as an iodine hotspot. But, the calculated fluxes from biological production of iodocarbons are too small to explain the observed atmospheric IO, and the modelled I₂ is also smaller than the observed I₂. This observation suggests there is an unidentified iodine source. One of the candidates is presumably an inorganic source. In this work, we studied the surface reaction between gaseous ozone and a frozen sodium iodide solution by using cavity ring-down spectroscopy to detect gaseous products, iodine, I₂(g) and an iodine monoxide radical, IO(g).

The I₂(g) and IO(g) emissions were observed during ozonolysis of liquid and frozen NaI aqueous solutions. The concentrations of NaI were typically 1 and 5 mM. The concentrations of flowing O₃(g) were (0.5-4.2)×10¹⁵ molecules cm⁻³. The observed products concentrations were ~10¹¹ molecules cm⁻³ for IO(g) and ~10¹⁴ molecules cm⁻³ for I₂(g). The peak of I₂(g) emission was markedly enhanced on a frozen NaI aqueous solution more than that on a liquid at pH 2. The peak of IO(g) emission was also enhanced on a frozen solution under the same condition. The physical structures of the ice substrates supposedly play an important role in this enhancement. Iodide anions are expected to be excluded from ice matrix during freezing. This exclusion process leads to the formation of concentrated iodide anions at the air-ice interface. In fact, sea ice contains brine microchannels that permit transport of reactants over large distances. It was found that the amounts of I₂(g) and IO(g) produced depend on [NaI], I₂(g) production is markedly enhanced at pH <4, and I₂(g) emission is decreased with decreasing temperature of a frozen NaI solution. Acidification of the brine by atmospheric trace acids could potentially lead to low pH. These results imply that a surface reaction between gaseous ozone and frozen iodide could be responsible for the inorganic source of iodine.

Keywords: iodine, iodine monoxide, ice, ozone, heterogeneous reaction, cavity ring-down spectroscopy

Speciation of S and Ca species in aerosols with its relations to global cooling effects and processes of chemical reacti

MIYAMOTO, Chihiro^{1*}; YAMAKAWA, Yoshiaki²; SAKATA, Kohei²; MIYAHARA, Aya²; SAKAGUCHI, Aya²; SUGA, Hiroki²; TAKEICHI, Yasuo³; ONO, Kanta³; TAKAHASHI, Yoshio²

¹Faculty of Science, Hiroshima University, ²Graduate School of Science, Hiroshima University, ³Photon Factory, KEK

Speciation of particles in aerosols is necessary to interpret what effects each species in the aerosols can have on environment. For example, global cooling effect by aerosols influences earth's climatic change (IPCC, 2007). In particular, sulfate aerosols are known to cool the earth by forming cloud condensation nuclei (CCN) because of their high hygroscopicity, which induces indirect cooling effect. Because the hygroscopicity differs depending on the species, sulfate speciation in aerosols is important for the determination of the magnitude of the indirect cooling effect.

In this study, major ion concentrations in aerosol samples were measured by ion-chromatography. In addition, chemical species of calcium and sulfur in the each aerosol sample were determined using X-ray absorption near-edge structure (XANES) measured at BL-9A in Photon Factory, KEK. The speciation analyses can have some implications on the influence on the environment and the processes of chemical reaction of aerosols collected during several periods, such as (a) dust (Kosa) period (March 4-9, 2013), (b) the period with high PM_{2.5} concentration (Jan. 31-Feb. 1, 2013), and (c) the periods before and after (a) and (b).

Major ion concentration data showed that Ca²⁺, which is originated from soil, and NO₃⁻ and SO₄²⁻, which were from human activities, increased in the period (a) compared with those in the periods before and after the period (a). On the other hand, SO₄²⁻ and NH₄⁺, which were emitted from human activities, increased in the period (b). In the period (a), it is considered that species originated from acids such as sulfate and nitrate which were incorporated into the particles increased in the samples whose aerodynamic diameter is over 1.0 μm, because they have reacted with CaCO₃ which was increased by Kosa event. In addition, from the fitting of XANES spectra, it was found that gypsum with low hygroscopicity were the main sulfur species in the period (a), whereas NH₄HSO₄, (NH₄)₂SO₄, and hydrated sulfate with high hygroscopicity were main sulfur species in the period (b). Therefore, it is considered that when the concentration of PM_{2.5} increases, the indirect cooling effect can be large due to the large fraction of NH₄HSO₄, (NH₄)₂SO₄, and hydrated sulfat. On the other hand, the indirect cooling effect by sulfate aerosols can be smaller during the dust period due to the formation of non-hygroscopic gypsum by high amount of calcite in the atmosphere.

Using the results of calcium and sulfur speciation both in the bulk and at the surface by fluorescence and conversion-electron yield detection, respectively, in the XANES analyses, we can discuss how chemical reactions occur at the surface of aerosol particles in each period. The abundance ratios of gypsum, CaCO₃, and Ca(NO₃)₂ were different at the surface and the bulk. As a result, it was concluded that calcium species changes from gypsum, Ca(NO₃)₂, to CaCO₃ from the surface to the core of the calcite particle. This results showed that (i) sulfuric acid from the atmosphere forms insoluble gypsum at the surface of calcite, (ii) Ca(NO₃)₂, formed as a result of the reaction of nitric acid and calcite, exists in the middle part, and (iii) unreacted CaCO₃ remains in the core of the particle.

Keywords: aerosol, XANES, sulfate, grobal cooling effect

Properties of Fe-containing particles and structure of mineral particles in the mountain, urban, and marine atmosphere

MIKI, Yusuke^{1*} ; UEDA, Sayako² ; MIURA, Kazuhiko¹ ; KATO, Hiroki¹ ; FURUTANI, Hiroshi³ ; UEMATSU, Mitsuo³

¹Tokyo University of Science, ²Nagoya University, ³University of Tokyo

Atmospheric aerosol particles play an important role in global material cycles and global climate by acting as an agent which transports materials over long distances. Iron (Fe) is an essential element for marine phytoplankton growth especially in high nutrient and low chlorophyll (HNLC) area. Long-range transportation of atmospheric aerosols from the continent and subsequent deposition is an important process to supply Fe to the ocean. The dry and wet depositions of aerosol particles depend on the particle size and the mixing states with water-soluble materials. In order to study the properties of Fe-containing particles and modification of individual particles, we collected aerosol particles at the top of Mt. Fuji, at Kagurazaka, Tokyo, and on the ship over the mid-latitude western North Pacific Ocean during the KH-12-1 (EqPOS) Leg 2 cruise of the R/V Hakuho Maru. We collected aerosol particles with a low pressure impactor. Collected particles were analyzed using a transmission electron microscopy (TEM) with a water dialysis method and an energy-dispersive X-ray (EDX) analysis. We chose the samples which were collected in the long-range transportation events from the continent on the basis of 5-day backward air trajectory analysis, number size distribution of aerosols measured by an optical particle counter (OPC), and the results of the TEM-EDX analysis.

Water-insoluble materials such as mineral dusts and industrial anthropogenic metals are main sources of Fe. This study focused on water-insoluble materials and performed the EDX analysis. In each sample, most of water-insoluble materials were internally mixed with water-soluble materials (internal mixed particles). The volume percent of the water-soluble materials in the mixed particles on a marine sample was higher than that of other samples, indicating that water-insoluble materials as well as Fe-containing particles were mixed with water-soluble materials during transportation.

Structures of some mineral particles were verified using the focused-ion-beam (FIB) technique. Particles larger than 5 μm collected on the Ti-plate were sliced into 200 nm in thickness. We performed selected-area electron diffraction (SAED) on the cross section of the sliced particles. On the basis of the diffraction patterns and EDX results, structures of the mineral particles were verified. CaCl_2 was found on the surface of the particle and bounded on CaCO_3 , suggesting that CO_3^{2-} was replaced by Cl^- ($\text{CaCO}_3 + 2\text{HCl} \rightarrow \text{CaCl}_2 + \text{CO}_2 + \text{H}_2\text{O}$). Fe was included in the particle. There is a possibility that changing insoluble CaCO_3 to soluble CaCl_2 changes the ability of cloud nuclei and/or ice nuclei and the solubility of Fe.

Keywords: aerosol, Fe, water-soluble materials, water-insoluble materials, long-range transportation

Source of atmospheric lead in Omura City, west Japan, tied to the source of mineral particles

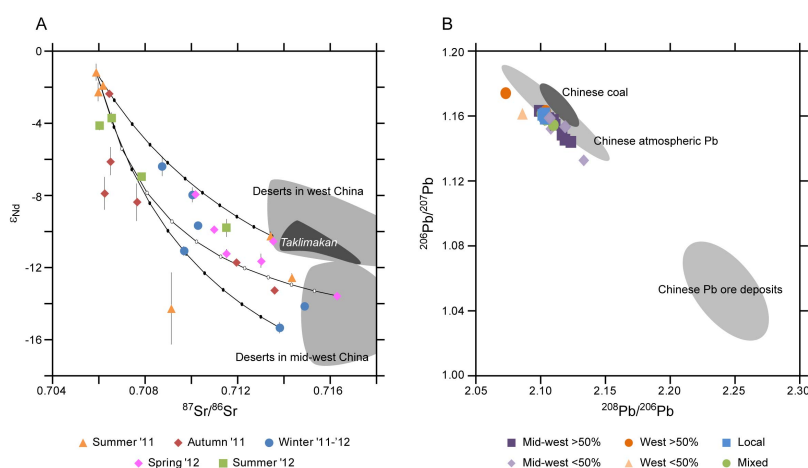
SAITOH, Yu^{1*} ; UMEZAWA, Yu² ; KAWAMOTO, Kazuaki² ; TANIMIZU, Masaharu³ ; ISHIKAWA, Tsuyoshi³

¹Center for Advanced Marine Core Research, Kochi University, ²Graduate School of Fisheries Science and Environmental Studies, Nagasaki University, ³Kochi Institute for Core Sample Research, JAMSTEC

Lead is one of the major environmental pollutants, which seriously harms human body. Atmospheric lead concentration has been suppressed in Japan after the forbiddance of leaded gasoline in 1970s. However, the cross-border air pollution is getting unable to disregard with industrial development in neighboring countries. Identifying the source of aerosol particles is essential in painting a precise picture of the cross-border air pollution. The northern part of the Kyushu Island is the most affected area of the cross-border pollution in Japan due to closeness to the continent. We conducted isotopic analysis of aerosol particle samples corrected with high temporal resolution, once per a few days, from June 2011 to August 2012 in Omura City in the north Kyushu. Pb isotope ratios of 1M-HCl soluble component ("leachate") of the corrected particles indicate the direct source of anthropogenic lead, while Sr-Nd isotope ratios of the residual mineral component digested by concentrated HF-HNO₃ ("silicate") indicate the source area of the mineral particles. High resolution sampling allowed us to distinguish the sources much more sensitively than commonly adopted monthly order sampling.

Sr-Nd isotope ratios of silicates indicate that the main source area of mineral particles changes seasonally. They have local origin in summer, while they are derived from deserts in mid-west China in fall and winter, and those in west China in spring (Figure A). Pb isotope ratios of leachates are distinct when the source of mineral particles is the mid-west China (Figure B). The values suggest the influence of the Chinese lead ore deposits. On the other hand, Pb isotope ratios of leachates are indistinguishable between samples of local origin and those originated from west China. An additional character of samples of west China origin is high amount of Pb in leachate relative to that of mineral component. Anthropogenic lead may be easier to be entrained to wind when the mineral particles comes from mid-west China because the wind trajectory should be much lower in altitude than when particles come from further distant west China. Cross-border atmospheric Pb pollution is suggested more serious in fall and winter when wind trajectory is low than in spring when the westerly transports vast amount of mineral particles known as "Kosa" from the deserts in west China.

Keywords: dust, anthropogenic lead, PM10, Sr isotope ratio, Nd isotope ratio, Pb isotope ratio



Difference of composition and mixed state of dust particles by height

KAMIGUCHI, Yusuke^{1*} ; IWAMOTO, Yoko² ; IWATA, Ayumi³ ; HARA, Kazutaka² ; KINOUCI, Kento³ ; MAKI, Teruya¹ ; KOBAYASHI, Fumihisa¹ ; KAKIKAWA, Makiko² ; MATSUKI, Atsusi²

¹College of Science and Engineering, Kanazawa University, ²Institute of Nature and Environmental Technology, Kanazawa University, ³Graduate School of Natural Science and Technology, Kanazawa University

Continental Asia has been recognized as one of the most important sources of atmospheric dust particles. Many investigators have pointed out the importance of the atmospheric processing of dust particles in the course of long-range transport. Such processing can potentially change their radiative properties and their ability to act as cloud condensation nuclei. Three major factors that govern the processing of dust particles are dust mineral composition, relative humidity and concentration of acidic gas species. These factors are considered to be closely related with the height at which dust particles are transported. However, there has been no report so far on the direct comparison of the morphology and chemical composition of individual dust particles in the free troposphere and in the planetary boundary layer in the event of a same dust outbreak.

The helicopter was employed as the airborne platform in this study. Aerosol particles were directly collected by aerosol impactor over Hakui city, Isikawa, Japan (36.9 N, 136.7 E) on March 19, 2013. Then, Dust event was observed western Japan by Japan Meteorological Agency. Morphology and elemental composition of the collected particles were later examined on individual basis under SEM-EDX (Scanning Electron Microscope equipped with Energy Dispersive X-ray spectrometry).

Atmospherically processed dust particles (with apparent morphological modification) were hardly found in the free troposphere. On the other hand, large fraction of dust particles was found modified in the planetary boundary layer, showing spherical outline. High proportion of Calcium and Magnesium were detected from the modified particles. Also, dust particles collected in the planetary boundary layer contained Sulfur in higher abundance.

It is suggested that the atmospheric conditions in the free troposphere are less favorable for the dust particles to be modified than in the planetary boundary layer, because the vertical supply of acidic gases and water vapor into free troposphere is generally limited by the temperature inversion layer.

Keywords: mineral dust, free troposphere, planetary boundary layer, SEM-EDX

Demonstration test of atmosphere sampling system using combination of solar and fuel battery at Western part of Yakushim

NAGAFUCHI, Osamu^{1*} ; YOKOTA, Kuriko² ; OSAKA, Kenichi¹ ; NAKAZAWA, Koyomi¹ ; TEZUKA, Kenshi³

¹the University of Shiga prefecture, ²Toyohashi University of Technology, ³YOCA

We have measured PM 2.5 using solar panel and fuel cell system at Southern area of Yakushima island Japan.

In order to clarify the long-range transport of atmospheric pollutants in the East Asian regions, we have challenged the continuous observation at a mountainous area without the commercial power. Although, we are considered to be better the system with a solar battery, the pump was sometimes stopped for the brownout cause by the lack of insolation. Thereupon, we make an attempt the continuous observation of atmospheric pollutants using the combination of the solar and fuel battery. And thus we achieve the continuous observation of the atmospheric pollutants. Consequently, we will report new monitoring system.

Development of a method to measure the hygroscopicity of black carbon-containing particles

OHATA, Sho^{1*} ; MOTEKI, Nobuhiro¹ ; SCHWARZ, Joshua P.² ; KONDO, Yutaka¹

¹Department of Earth and Planetary Science, Graduate School of Science, The University of Tokyo, ²Earth System Research Laboratory, National Oceanic and Atmospheric Administration

Black carbon (BC) aerosols are generated by the combustion of fossil fuels and biomass. During transport in the atmosphere, BC particles acquire "coating materials" through the condensation of semi-volatile gaseous components, and coagulation with the other aerosols. Freshly emitted BC particles are generally hydrophobic, so the hygroscopicity of BC-containing particles is largely controlled by the composition and amount of coating materials. Although measurement of the hygroscopicity of ambient BC-containing particles is important to understand their cloud condensation nuclei activity and optical properties, measurement data are still quite limited (McMeeking et al, 2011; Liu et al. 2013). In this study, we present a modified single particle soot photometer (SP2) as a humidified-SP2 (hSP2), which quantifies the BC mass and the amount of coating material within individual aerosol particles, under controlled relative humidity (RH), by detecting both the laser-induced incandescence emitted and laser light scattered from each BC-containing particle. High time-resolved measurements of growth factor (GF: the ratio of wet particle diameter to dry diameter) and hygroscopicity parameter κ for BC-containing particles can be achieved by combining an aerosol particle mass analyzer (APM) or a standard SP2 with the newly developed hSP2.

We have tested the hSP2 in the laboratory using both homogeneous ammonium sulfate, and internally mixed particles of BC (fullerene soot) and ammonium sulfate. These particles were dried and classified by an APM and subsequently measured by the hSP2 between 60% and 90% RH. We assumed a core-shell geometry for the BC-containing particles, and took account of the reduction in refractive index of the coating materials due to their hygroscopic growth. Measured GFs of the laboratory-generated BC-containing particles agreed with GFs predicted by κ -Köhler theory to within measurement uncertainty, demonstrating the applicability of the hSP2 for ambient measurements.

Keywords: black carbon, hygroscopicity

An Empirical Correction Factor for Filter-based Photo-absorption Black Carbon Measurements

IRWIN, Martin^{1*} ; KONDO, Yutaka¹ ; MOTEKI, Nobuhiro¹

¹The University of Tokyo

Long-term observations of black carbon (BC) aerosol provide important information regarding seasonal variations, emission source attribution, and regional distribution & transport. Filter-based BC measurement techniques such as the Continuous Soot Monitoring System (COSMOS) are particularly well suited to this application, due to their relative robustness and reliability. However, caution is required when determining the threshold transmittance, Tr_{thresh} (proportional to the time interval between filter changes), in order to ensure that acceptable measurement accuracy is maintained throughout the sampling period. We present a new, empirically derived transmittance-dependent correction factor used to interpret the response characteristics of filter-based aerosol absorption measurements performed by COSMOS. Simultaneous measurements of ambient BC aerosol mass (M_{BC}) were conducted in Tokyo, Japan, using two identical COSMOS instruments operated with different threshold transmittance, Tr_{thresh} , values, of 0.95 and 0.6. The derived values for M_{BC} were consistently underestimated by the COSMOS operating at lower Tr_{thresh} , as a function of decreasing filter transmittance. The 1-hour averaged values of M_{BC} were underestimated by around 10 %, incorporating measurements across the entire range of filter transmittance (1 - 0.6), with a maximum underestimation at around 17 % immediately preceding filter advancement (i.e. $Tr = \sim 0.60$), and a minimum of ~ 1 % immediately following filter advancement (i.e. $Tr = \sim 1$). An empirical second-order correction factor was derived from these ambient measurements, and was applied to M_{BC} as a function of filter transmittance, resolving the instruments to within 2 %.

Furthermore, the operational performance of COSMOS was tested for a new quartz fibre filter (HEPA). A comparison of different filter types demonstrated a systematic overestimation of M_{BC} of around 6 - 8 % when using HEPA filters. A sensitivity study of a radiative transfer model indicated that this enhanced absorption was primarily a result of the increased thickness of the HEPA filter.

Keywords: aerosol, black carbon, filter-based measurements, absorption

Ship-borne measurements of black carbon aerosols over northwestern Pacific and Bering Sea

MIYAKAWA, Takuma^{1*} ; KANAYA, Yugo¹ ; TAKETANI, Fumikazu¹ ; PAN, Xiaole¹ ; KOMAZAKI, Yuichi¹

¹Japan Agency Marine-Earth Science and Technology

Black carbon (BC) aerosol can strongly absorb the solar radiation and act as cloud condensation nuclei depending on the mixing state. Therefore, BC abundance and mixing state are key physicochemical properties to estimate the radiative impacts of BC aerosols [1]. Measurements of BC aerosols over the area where BC concentrations are very low are still limited because of the lack of high-sensitivity analytical methods. Single Particles Soot Photometer (SP2), which has been developed by Droplet Measurement, Inc., allows us to quantify the BC mass of single BC-containing particle and measure the BC number/mass concentration even in ultra-clean air [2]. Here we report the concentrations and mixing state of BC-containing particles observed using a SP2 on the research vessel *Mirai* during the research cruise over the northwestern Pacific and Bering Sea (MR13-05 cruise, 8/12-26, 2013).

BC mass concentrations over the sea near Japan (<145°E) were elevated to $\sim 200 \text{ ng m}^{-3}$, whereas they were less than $\sim 40 \text{ ng m}^{-3}$ over the northwestern Pacific and Bering Sea. Mixing states as a function of BC-containing particles deduced from SP2 raw data were categorized into three types; bare/thinly coated (type1), thickly coated (type2), and non-core-shell (type3) BC. Over the northwestern Pacific and Bering Sea, the number fractions of type1-BC were ~ 0.13 , whereas those of type2-BC were as high as 0.8. We also found the minor but significant presence of type3-BC ($\sim 4\%$) over the remote ocean.

References

- [1] Bond et al., J. Geophys. Res., 118, 5380-5552, doi:10.1002/jgrd.50171, 2013.
- [2] Schwarz et al., Geophys. Res. Lett., 37, L18812, doi:10.1029/2010GL044372, 2010.

Keywords: Black carbon, Mixing state, Laser Induced Incandescence, Ship-borne measurement, Marine atmosphere

High- m/z ion signal to total mass signal ratios measured for secondary organic aerosol using aerosol mass spectrometer

SATO, Kei^{1*} ; FUJITANI, Yuji¹ ; TANABE, Kiyoshi¹ ; MORINO, Yu¹ ; FUSHIMI, Akihiro¹ ; TAKAMI, Akinori¹ ; IMA-MURA, Takashi¹ ; HIKIDA, Toshihide² ; SHIMONO, Akio²

¹NIES, ²Shoreline Science Inc.

A volatility basis-set (VBS) model in which oligomerizations are taken into account has recently been tested for further improvements of conventional VBS models.¹⁾ In order to study the oligomerization rates during secondary organic aerosol (SOA) formation and the ratio of high- m/z ion to total SOA mass spectrum ion signal, SOA particles produced during laboratory chamber experiments were analyzed by using an Aerodyne aerosol mass spectrometer (AMS). Photooxidation of α -pinene, isoprene, toluene, and 1,3,5-trimethylbenzene (TMB) was investigated in the presence of NO_x . Ozonolysis of α -pinene and isoprene was also studied. A stainless steel tube was used as a collection tube for AMS. A mass spectrum measured for organic aerosol (OA) in the region $m/z = 10 - 675$ was divided into seven mass regions; the total signal of each mass region was studied as a function of time. Increase in the signal intensity was observed with increasing of the OA level in a region $m/z < 500$. The oligomer signals increased up to substantial levels within one hour after nucleation. After substantial amounts of oligomers were produced, the ratio of the total signal of each mass region to total OA signal was constant. Next, the ratio of total mass signal in the region $m/z > m_1$ to total OA mass signal, ϕ , was determined:

$$\phi = \text{OA} (m/z > m_1) / \text{OA}(\text{total}),$$
$$m_1 = n m_C (\text{OM}/\text{OC}),$$

where n is the number of carbon atoms in SOA precursor, m_C is the carbon atomic mass, and OM/OC is organic matter to organic carbon mass ratio measured by AMS. The m_1 values of α -pinene, isoprene, toluene, and TMB were determined to be 217, 147, 180, and 204, respectively. We assumed that a contribution from monomer signals is low in a region $m/z > m_1$. Signals measured by electron ionization of AMS contain both the fragment and parent ions of organic compounds. Note that the value, ϕ , is an index of oligomer to total SOA ratio, but does not represent an absolute value of that ratio. The ϕ value of SOA from the same precursor decreased with increasing of SOA mass loading (Fig. 1), showing that oligomer formation is suppressed under high mass loading conditions. In a region $10 - 100 \mu\text{g m}^{-3}$, the ϕ value of toluene SOA was the highest, whereas that of α -pinene SOA was the lowest. No apparent effect of oxidation method (photooxidation or ozonolysis) was observed.

Acknowledgements: This work was supported by Grant-in-Aid for Scientific Research of Japan Society for the Promotion of Science (No. 25340021, FY2013 - 2015) and Cross-Center Collaborative Research Fund of NIES (No. 1214AO001, FY2012 - 2014).

References: ¹⁾ Trump and Donahue, Oligomer formation within secondary organic aerosol: equilibrium and dynamic considerations. *Atmos. Chem. Phys. Discuss.*, **13**, 24605 - 24634 (2013).

Keywords: secondary organic aerosol, oligomerizations, aerosol mass spectrometer, aerosol mass loading, chemical structure

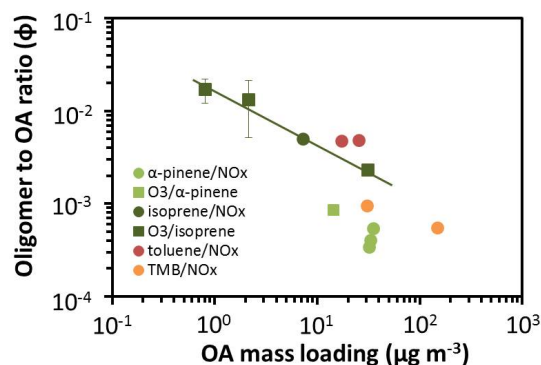


Fig. 1. Effects of OA mass loading on the oligomer to OA signal ratio (ϕ).

Controlling factors of aerosol size distribution over East Asia

HASHIOKA, Hideaki^{1*}; SHIBANO, Yuki¹; MOTEGI, Nobuhiro¹; KITA, Kazuyuki²; MATSUI, Hitoshi³; KOIKE, Makoto¹; KONDO, Yutaka¹

¹Department of Earth and Planetary Science, Graduate School of Science, University of Tokyo, Japan, ²Faculty of Science, Ibaraki University, Mito, Japan, ³Japan Agency for Marine-Earth Science and Technology, Tokyo, Japan

Aerosol is known for its direct and indirect effects on climate, with both effects having a larger uncertainty than other radiative forcing elements, such as carbon dioxide. Investigating ambient aerosol size distributions is an important factor in estimating radiative forcing effects, as aerosol size is a major contributing factor to both the aerosol direct and indirect effects.

Ambient aerosol size and spatial distributions are controlled by various processes; e.g. new particle formation, coagulation, transportation, and wet deposition. For this reason, in situ measurements and analyses based on such processes are essential. However, results from measurements with high time resolution and low detection limits (e.g. of aerosol diameter) are rare. In this research, we introduce measurements of the aerosol size distribution over East Asia using the ultra high sensitivity aerosol spectrometer (UHSAS), and have tried to analyze the results based on wet removal processes.

The UHSAS is an optical particle counter. With its 2 types of photon diode and its efficiency in collecting scattering light, the UHSAS can obtain measurements of aerosol diameter in a wide range (about 70 to 1500 nm). We improved the hardware and software of the UHSAS specifically for use in aircraft measurements, to improve time resolution data and the instrumental precision of measurements of aerosol number concentration and size distribution (assuming spherical particles with refractive index 1.52). In addition, we have installed a robust mass-flow controlling system to deal with the significant changes in pressure associated with aircraft measurements. Scattering light signals obtained from photon diodes are saved to an external storage medium, which aids us in distinguishing signal from noise. We also present results showing the successful estimation of the optics inside UHSAS, in order to obtain highly precise diameter information using known standard particles.

The aerosol radiative forcing in East Asia (A-Force 2013W) aircraft campaign was conducted from late February to early March. We obtained air samples in real time from a forward facing inlet outside of the aircraft, Air was sampled by a variety of instruments including the UHSAS in real-time from a forward facing inlet outside of the aircraft. Data from the UHSAS showed good consistency with other instruments. During the campaign, the mean size distribution shifted to smaller diameters with increasing altitude. The transport efficiency (TE) of BC, which describes the degree of the wet removal of BC (calculated from the carbon monoxide mixing ratio and BC mass concentration), also decreased with increasing altitude (i.e. strong wet removal tendency for higher altitude). As the TE became smaller, the mean size distribution also shifted to smaller diameters, independent of altitude. This shows that the TE is the dominant factor controlling the aerosol size distribution, rather than absolute altitude. When the TE is smaller, the size distribution shifted to smaller diameters; this is the first observation of the size-dependent wet removal of general aerosols based on Köhler theory. This dynamic state of aerosol size distribution observed by the UHSAS surely contributes to quantitative understanding of aerosol direct and indirect effects on climate.

Keywords: aerosol, size distribution, wet removal process, black carbon, transport efficiency, UHSAS

Vertical profiles of aerosol size distribution in small forest within a western suburb of Tokyo

YABUKI, Masanori^{1*} ; TAKAHASHI, Kenshi¹ ; TSUDA, Toshitaka¹ ; MATSUDA, Kazuhide²

¹Research Institute for Sustainable Humanosphere, Kyoto University, ²Tokyo University of Agriculture and Technology

Forests interact in a complex manner with the atmosphere by acting as sinks for many atmospheric pollutants and trace gases, and by emitting biogenic volatile organic compounds into the air. These constituents influence the atmospheric chemistry and composition, including aerosols related to cloud condensation nuclei (CCN). Aerosol chemical and physical properties vary both temporally and spatially owing to various atmospheric processes (e.g., scavenging, nucleation, evaporation, and condensation) during the dispersion and transportation of air mass within and above forest canopies.

In this paper, we report on the field observations conducted from a 30-m-high tower in a small forest at the Field Museum Tama Hills, an experimental forest of the Tokyo University of Agriculture and Technology, located in a western suburb of Tokyo, between July 27 and August 3, 2013. At this site, atmospheric aerosols were expected to include the particles both from natural and anthropogenic sources. Using five sampling inlets placed at altitudes ranging from 8 m to 30 m, we conducted altitude-resolved measurements of particle number size distributions in the size range of 10-5000 nm. Herein, we present an outline of the observation systems, as well as the preliminary results of variability of sub-micrometer and nano particles within and above the forest canopy.

Keywords: Aerosol, Size distribution, Vertical distribution, Forest canopy

Measurement of fluorescent particles over the western Pacific

TAKETANI, Fumikazu^{1*} ; PAN, Xiaole¹ ; MIYAKAWA, Takuma¹ ; KOMAZAKI, Yuichi¹ ; KANAYA, Yugo¹ ; MATSUMOTO, Kazuhiko¹ ; HONDA, Makio¹

¹JAMSTEC

Recently, fluorescence from suspended single particles has been employed to identify and classify the certain types of organic/biological particles. Bioaerosols, including bacteria and other particles derived from living organisms, may explain large unidentified fraction of organic aerosols and play important roles in the cloud formation. In this study, we employed a single-particle fluorescence sensor, WIBS-4, to understand the abundance of bioaerosol particles over the western Pacific.

We conducted ambient air measurements over the western Pacific at July 2011, 2012, and 2013 by R/V MIRAI cruise. In order to avoid analyzing the particles emitted by ship's funnel, we eliminated the data by the wind direction. In the cruises, the bioaerosol particles based on fluorescent pattern were in the range of 0.1-2 particles/cc over the western Pacific. In the presentation, we will compare ocean surface chlorophyll data with detected fluorescence particles.

Keywords: aerosol particles, fluorescence

Impact of the Kuroshio warm SST on low altitude clouds: Numerical model simulation with smoothed SST

ASANO, Naruhiko^{1*} ; KOIKE, Makoto¹ ; MATSUI, Hitoshi² ; NAKAMURA, Hisashi³

¹University of Tokyo, ²Japan Agency for Marine-Earth Science and Technology, ³RCAST, University of Tokyo

Along the Kuroshio ocean current, high sea surface temperature (SST) is maintained even in winter and a steep SST gradient is formed across the current. In winter and spring, cold northwesterly air often flows from the Asia continent into the East China Sea. Once this cold air reaches the Kuroshio warm current, a large temperature contrast between sea surface and surface air (SAT) causes the marine boundary layer unstable and affect low altitude cloud formation. The northwesterly wind also transports a large amount of anthropogenic aerosols to East China Sea. These aerosols work as cloud condensation nuclei (CCN) and they affect microphysical properties of clouds. Because the marine boundary layer stability affects aerosol activation to form cloud particles, the large contrast between SST and SAT over the Kuroshio can also affect the aerosol-cloud interaction as proposed by Koike et al. [2012].

In order to assess the impact of Kuroshio warm SST on low clouds, we made WRF model calculations for a period between 21 Mar and 30 Apr 2009. In addition to the control calculation, we made sensitivity calculations, in which artificially smoothed SST was given for a lower boundary condition. In this smoothed SST, the SST gradually decreases toward higher latitudes and the maximum along the Kuroshio current no longer exists.

In the control calculation, the monthly mean cloud fraction (frequency of cloud occurrence in April 2009) was high in the south of Kuroshio and had a steep north-south gradient, corresponding to the SST steep gradient. A monthly mean liquid water path (LWP) was large along Kuroshio and small in East China Sea, although it enhanced when cyclones passed. As compared with the control calculation, both the cloud fraction and LWP decreased over the Kuroshio in smoothed-SST calculations, and their north-south gradients became gentler.

LWP differences between control and sensitivity calculations varied depending on the wind direction. In northerly wind conditions, the LWP decreased in warmer flank (downwind) of a SST front. Under calm and horizontally homogeneous wind conditions, water vapor transport convergence was relatively small over the Kuroshio and column-integrated water vapor increased mainly by evaporation from the sea surface. In such case, LWP decreased on the Kuroshio in sensitivity calculation. This suggests that warm SST associated with Kuroshio enhances the evaporation and contributes to increase LWP of low clouds.

Keywords: low clouds, Kuroshio

Measurement of the hygroscopic growth factor distributions of aerosol particles and the mass spectra of single particles

KAWANA, Kaori^{1*} ; NAKAYAMA, Tomoki² ; MOCHIDA, Michihiro¹

¹Graduate School of Environmental Studies, Nagoya University, ²Solar-Terrestrial Environmental Laboratory, Nagoya University

Hygroscopicity is a property that relates to the lifetime, chemical reactivity and cloud condensation nucleus activity of atmospheric aerosol particles. The amount of water retained by the particles as a function of relative humidity (RH) is governed by the phase state and chemical composition. In this study, hygroscopic growth factor distributions of atmospheric aerosol particles and mass spectra of single particles selected by the growth factors were measured using a combination of hygroscopicity tandem differential mobility analyzer (HTDMA) and a high resolution time-of-flight aerosol mass spectrometer (AMS) in Nagoya.

The observation of urban aerosols was performed on Higashiyama campus of Nagoya University in June and July, 2013. After aerosols were passed through PM1 cyclone and dried in diffusion driers, 300 nm particles were selected in the first DMA of the HTDMA. The growth factor distributions of the particles were measured under humidified conditions (setting RH: 37%, 65%, and 87%). The measurements were performed in both humidification and dehumidification modes. The mass spectra of single particles with specific hygroscopic growth factors g (1.0 at setting RH of 37%; 1.0, 1.1, and 1.25 at setting RH of 65%; 1.0 and 1.5 at setting RH of 87%) were measured using the AMS. The size distributions of aerosol particles were measured separately. The concentrations of organic carbon and elemental carbon in parts of the study period were also obtained.

In the humidification mode, the averages of the growth factor distributions at setting RH of 37% and 65% did not show substantial hygroscopic growth in terms of mean g (1.00 and 1.02, respectively), and those at setting RH of 87% showed large mean g (1.48). In the dehumidification mode, mean g of the averages of the growth factor distributions at setting RH of 37% and 65% (1.07 and 1.18, respectively) were substantially larger than those in the humidification mode, suggesting the presence of metastable-state aqueous solutions in the particles. At setting RH of 87%, the mean g in the dehumidification mode was large (1.44) as in the case of the humidification mode. The mass spectra of single particles with specific g were extracted from the obtained data; the number of these spectra was 349.

Keywords: hygroscopicity, single particle

CCN activity of aerosol and its relation to air mass origins: an analysis based on year-round observation at Noto, Japan

IWAMOTO, Yoko^{1*} ; KINOUCHI, Kento² ; MATSUKI, Atsushi¹

¹Institute of Nature and Environmental Technology, Kanazawa University, ²Graduate School of Natural Science and Technology, Kanazawa University

Atmospheric aerosols play an important role in controlling the earth's radiation balance and/or the hydrological system by acting as cloud condensation nuclei (CCN). For a quantitative evaluation of CCN characteristics in the East Asia, CCN activity of atmospheric aerosols in submicrometer size range were measured at Noto Ground-based Research Observatory (NOTOGRO), located at the tip of Noto peninsula, facing the Sea of Japan. The observation was conducted from October 2012 to September 2013, to investigate the seasonal variability in CCN activity of the atmospheric aerosols.

CCN efficiency spectra, where CCN number fraction is plotted against the diameter of aerosols, were obtained at four different supersaturation (SS) conditions (0.1%, 0.2%, 0.5% and 0.8%) by using a scanning mobility CCN analysis (SMCA) system (Moore et al., 2010). Hygroscopicity parameters kappa (Petters and Kreidenweis, 2007), which depends on the chemical composition of aerosols, were estimated through analyses of the CCN spectra. The bulk chemical composition of non-refractory submicrometer-sized aerosols was also measured by an aerosol chemical speciation monitor (ACSM). Seven-days backward trajectories at the height of 500 m above the sea level were calculated by using NOAA/HYSPLIT4 model.

The CCN activation diameters of the atmospheric aerosols were clearly larger than those of pure ammonium sulfate throughout the year. The mean kappa values ranged between those of pure ammonium sulfate (0.61) and several pure organic compounds (0 to 0.25). These evidences suggest that the atmospheric aerosols were mixture of ammonium sulfate and organics. The bulk chemical composition derived by ACSM also showed that organics, sulfate and ammonium were three major components throughout the observation period. The contribution of organics to the CCN activity of the atmospheric aerosols observed in this study was more apparent than those obtained in the previous studies in the East Asia. As most of the previous CCN studies in East Asia were conducted in the season significantly affected by Asian outflow of pollutants, current numerical models might overestimate CCN concentrations in the East Asia.

The mean kappa values were 0.30, 0.26, and 0.18 during the spring, autumn and summer, respectively. The difference in kappa values among the seasons might be caused by difference in air mass origin. Air masses to the NOTOGRO site came mainly from NW across the Sea of Japan during the autumn and spring, whereas air masses of Pacific origin, those passed over the Japan islands, prevailed in the summer. Relatively high kappa values were observed under the influence of continental polluted air masses with high sulfate concentration. On the other hand, organic aerosols derived by photochemical oxidation were dominant in summer, resulted in low kappa values. The variation in kappa values of organics with air mass origins will also be discussed.

References

- Petters and Kreidenweis (2007), *Atmos. Chem. Phys.*, 7, 1961-1971.
Moore et al. (2010), *Aerosol Sci. Tech.*, 44, 861-871.

Keywords: atmospheric aerosol, cloud condensation nuclei, organic aerosol, hygroscopicity parameter, East Asia

Long-term observation of initial droplet growth of activated CCN at Noto peninsula, Japan

KINOUCHI, Kento^{1*} ; IWAMOTO, Yoko² ; KAGAMI, Sara³ ; MATSUKI, Atsushi²

¹Graduate School of Natural Science & Technology, Kanazawa university, ²Institute of Nature and Environmental Technology, Kanazawa university, ³College of Science and Engineering, Kanazawa university

Atmospheric aerosols affect the climate indirectly by changing optical property and lifetime of clouds through their ability to act as cloud condensation nuclei (CCN). Size of cloud droplets is an important factor to consider in the climate predictions because it can influence cloud albedo and frequency of precipitation. Important factors controlling the growth of cloud droplets are; 1. water vapor supersaturation (SS), 2. CCN size and 3. CCN chemical composition. Chemical composition of aerosols is a very important factor controlling the initial droplets growth. Recent studies indicate that there is high mass fraction of organics in the CCN relevant particles, and the droplet growth kinetics following the activation of such organic containing CCN is not fully understood.

East Asia is regarded as one of the most aerosol (hence CCN) dense regions in the world, but long-term monitoring of CCN properties in this region is relatively scarce. In this study, we conducted in-site and year-round measurement of CCN activity of submicron aerosols and related cloud droplet growth kinetics at NOTOGRO (acronym for NOTO Ground-based Research Observatory) located Suzu city, Noto Peninsula. A CCN counter (CCNC, CCN-100, DMT) was operated at four different supersaturation conditions (SS=0.1%, 0.2%, 0.5%, 0.8%). The diameters of cloud droplets activated from ambient aerosols ($D_{ambient}$) were compared to those activated from ammonium sulfate (D_{AS}) which is regarded as representative inorganic CCN. In order to identify factors that can potentially influence the initial cloud droplet growth, simultaneously measured chemical composition of aerosols with an Aerosol Chemical Speciation Monitor (ACSM, Aerodyne Inc.).

The measurement result showed that $D_{ambient}$ was not significantly difference from D_{AS} under higher SS conditions (i.e. SS=0.5% and 0.8%) throughout all seasons. However, there are periods that droplet growth was inhibited under lower SS conditions (i.e. SS=0.1% and 0.2%) especially during spring and autumn. Therefore, it was suggested that droplet growth under lower SS condition was more sensitive to other factors (other than SS). Based on the ACSM results, chemical composition of CCN was mainly contributed by various organics, ammonium and sulfate during the entire measurement period. The periods with limited droplet growth coincided with the periods with high organic mass fraction, and the negative correlation was found between the cloud droplets' diameters and organic mass fraction within atmospheric aerosols in CCN relevant sizes. On the other hand, we did not observe significant fluctuation in the cloud droplet diameters in winter. The measurement site is under the strong influence of winter monsoon especially during winter and the chemical species comprising CCN that are carried to the site may be considerably different from other seasons.

Keywords: cloud condensation nuclei, cloud droplet, chemical composition

Seasonal variations of peroxyacyl nitrates and alkyl nitrates concentration at Suzu, the Noto Peninsula

ISHIYAMA, Ayana^{1*} ; TAKAJI, Ryo¹ ; SADANAGA, Yasuhiro¹ ; MATSUKI, Atsushi² ; SATO, Keiichi³ ; OSADA, Kazuo⁴ ; BANDOW, Hiroshi¹

¹Osaka Prefecture University, ²Kanazawa University, ³Asia Center for Air Pollution Research, ⁴Nagoya University

NO_x emissions have been increasing in East Asia with recent remarkable economic progress. NO_x has relatively short lifetime and NO_x concentrations are governed by local NO_x emissions. On the other hand, descendant photochemical products of NO_x such as T.NO_3 (the sum of gaseous nitric acid and particulate nitrates), PANs (peroxyacyl nitrates) and ANs (alkyl nitrates) have longer lifetime than NO_x , so that they can be transported over a long-distance. In order to understand influences of the cross-border pollution, it is important to clarify the long-range transport of T.NO_3 , PANs, and ANs.

We have been continuously observing several pollutants at NOTOGRO (Noto Ground-based Research Observatory) super-site in Suzu, the Noto Peninsula. NOTOGRO is located at 37.45N and 137.36E. NO_x were determined by an LED photolytic converter / NO-O_3 chemiluminescence method. NO_y and T.NO_3 were observed by a scrubber difference / NO-O_3 chemiluminescence method. CO was monitored by a non-dispersive infrared photometer. PANs and ANs were measured by a thermal dissociation / cavity attenuated phase shift spectroscopy method.

In this presentation, observational results and discussion from December, 2012 to July, 2013 are described, focusing on seasonal variations of PANs and ANs. The air mass origins arriving at Suzu were classified into the following four groups, Russia and North China (RC), Korea and Middle China (KC) and Japan (JP) and Sea (S) using backward trajectory analyses. From winter to spring, both PANs and ANs concentrations from KC were higher than those from the other air mass origins. From spring to summer, their concentrations were independent of air mass origins.

From winter to spring, the lifetimes of PANs and ANs are long because of low temperature and weak solar radiation. In addition, their in-situ photochemical generation rates are low, so that PANs and ANs concentrations in this season are governed by long-range transport. From spring to summer, the lifetimes of PANs and ANs become shorter and their photochemical production rates become higher, that is, local photochemical productions of PANs and ANs are relatively important. Diurnal variations of PANs and ANs also support these concentration variation factors. From winter to spring, no diurnal variations were observed. Meanwhile, PANs and ANs concentrations began to be higher and lower in the daytime and nighttime, respectively, from spring to summer.

Keywords: peroxyacyl nitrates and alkyl nitrates, long-range transport, seasonal variation

Development of a continuous measurement system of PANs and alkyl nitrates in the atmosphere and observations at Suzu, th

TAKAJI, Ryo^{1*} ; ISHIYAMA, Ayana¹ ; SADANAGA, Yasuhiro¹ ; MATSUKI, Atsushi² ; SATO, Keiichi³ ; OSADA, Kazuo⁴ ; BANDOW, Hiroshi¹

¹Osaka Prefecture University, ²Kanazawa University, ³Asia Center for Air Pollution Research, ⁴Nagoya University

Peroxyacyl nitrates (PANs) and alkyl nitrates (ANs) are generated in the atmosphere by oxidation of NO_x in the presence of solar ultraviolet. They have a comparatively long lifetime, and are important as transboundary air pollutants. On the other hand, PANs and ANs act as the reservoirs of NO_x . In order to clarify transboundary pollution of nitrogen oxides, comprehensive measurements of total odd nitrogen species (NO_y), including PANs and ANs, are required. In this research, a continuous measurement system of total PANs and ANs has been developed by a thermal dissociation / cavity attenuated phase shift spectroscopy (TD/CAPS) method.

This instrument consists of heated quartz tubes to decompose PANs and ANs into NO_2 , and a CAPS- NO_2 analyzer. This system has three intake lines; NO_2 , PANs and ANs lines. The NO_2 line equip of a quartz tube without heating. The PANs and ANs line equip quartz tubes heated at 433 K and 633 K, respectively for thermally decomposing them into NO_2 . Concentrations of NO_2 , $\text{NO}_2 + \text{PANs}$ and $\text{NO}_2 + \text{PANs} + \text{ANs}$ can be obtained from the NO_2 , PANs and ANs lines, respectively. These concentrations are sequentially measured by switching solenoid valves and then NO_2 , PANs and ANs concentrations are obtained. Since a part of HNO_3 is pyrolyzed in the ANs line, annular denuder coated with NaCl to remove HNO_3 is set before the heated quartz tube in the ANs line. The decomposition efficiencies of PANs and ANs were calibrated to be 100 and 95%, respectively, for all kinds of PANs and ANs examined.

Continuous field observations of PANs and ANs have been being performed at NOTOGRO (Noto ground-based Research observatory) supersite in Suzu, the Noto Peninsula, since November 2012. Continuous measurements of NO_x , NO_y , T. NO_3 (the sum of gaseous nitric acid and particulate nitrate) O_3 , and CO have also been being conducted. NO_y concentrations were in agreement with the sum of observed NO_y components (= $\text{NO}_x + \text{T.NO}_3 + \text{PANs} + \text{ANs}$) regardless of seasons. NO_x fractions were the highest in NO_y constituents. Fractions of T. NO_3 in January and February were lower than those in other months. This reflects that wet deposition of T. NO_3 would be accelerated in winter due to snowfall. On the other hand, PANs fractions in spring and summer were smaller than those in winter. This suggests that temperature increasing promotes decomposition of PANs.

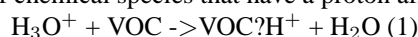
Keywords: peroxyacyl nitrates (PANs), alkyl nitrates, total odd nitrogen species, cavity attenuated phase shift spectroscopy

On-line measurements of multiple alkanes by chemical ionization mass spectrometry using NO^+ as the reagent ion

INOMATA, Satoshi^{1*} ; TANIMOTO, Hiroshi¹ ; YAMADA, Hiroyuki²

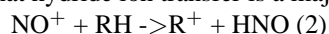
¹NIES, ²NTSEL

Proton transfer reaction mass spectrometry (PTR-MS) is a technique that allows for fast and sensitive measurement of volatile organic compounds (VOCs) at trace levels in air. Proton transfer is an example of chemical ionization: it enables soft ionization of chemical species that have a proton affinity (PA) higher than that of the reagent species (i.e., water):



Unlike gas chromatography, PTR-MS does not require any sample treatment such as drying and/or preconcentration, which makes possible quantitative measurement of alkenes (except ethylene), aromatics, and even oxygenated VOCs. However, the proton transfer in reaction (1) does not occur for alkanes because they have lower PAs than water. Very recently, a method to measure C_{12} - C_{18} alkanes using PTR-MS was demonstrated. They were, however, detected by a series of fragment ions with formula $\text{C}_n\text{H}_{2n+1}$ and were detected not individually, but as an ensemble.

Reactions of alkanes with NO^+ have been investigated by selected ion flow tube mass spectrometry (SIFT-MS). It was reported that hydride ion transfer is a major channel in the reaction of alkanes (RH) with NO^+ .



Recently, the PTR-MS instrument has been combined with switchable reagent ion capability, which allows for easy and fast switching between H_3O^+ and NO^+ (proton-transfer-reaction *plus* switchable reagent ion mass spectrometry (PTR + SRI-MS)).

In the present study, the detection properties of alkanes by PTR + SRI-MS are investigated. We confirmed that alkanes (RH) were usually detected as R^+ by PTR + SRI-MS using NO^+ as the reagent ion and detection sensitivities were comparable to those of aromatics observed by H_3O^+ ionization. We also demonstrated time-resolved measurements of C_4 - C_{16} alkanes in automotive exhaust during the Japanese JC08 transient cycle. It can be concluded that sensitive on-line measurement of multiple alkanes is possible by PTR + SRI-MS using NO^+ as the reagent ion.

Keywords: PTR-MS, alkane, NO^+ chemical ionization, Gasoline vehicle, Diesel vehicle, Exhaust gas

Observation of formaldehyde and glyoxal variations by MAX-DOAS in Chiba and Tsukuba in 2013

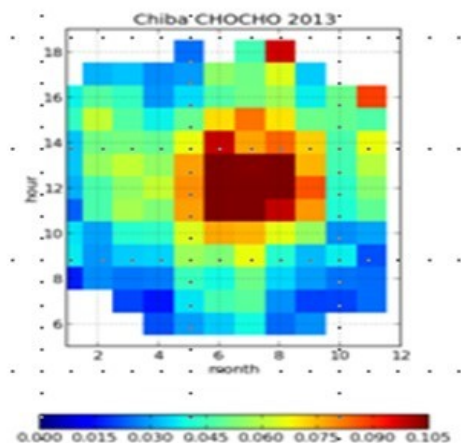
CHIN, Sei^{1*} ; NI, Wentao¹ ; IRIE, Hitoshi¹

¹Chiba university

BVOCs (Biogenic Volatile Organic Compounds) are plant-released organic chemicals that are volatile in air at normal ambient temperature and pressure. Reactions of BVOC in the atmosphere have a great influence on the OH abundance in the atmosphere. In addition, the reactions lead to the formation of ozone, which is not only adversely affecting plants and human health but also acting as a greenhouse gas. Furthermore, part of the products from the oxidation reaction of BVOCs forms aerosols, which play a critical role in cloud formation processes and radiation balance. Thus, BVOCs are deeply related with climate and air quality surrounding us. Recently, formaldehyde and glyoxal are recognized as important indicators of oxidations of BVOCs. However, their observations have been limited. In this study, we use the data got from MAX-DOAS to analysis the diurnal variation, seasonal variation of formaldehyde and glyoxal for the first time. And then we try to find the reason or the factors which makes the variations.

Figure1 shows the data of glyoxal concentration observed in Chiba during 2013. To know the diurnal and seasonal variation, we calculated the average value of every hour in each month. We found the clearly pattern that the concentration of glyoxal is high during the day and summer. At noon of the summer, the concentration of glyoxal was increased to more than 0.105ppbv. We also found the same pattern in Tsukuba. In this study, we observed glyoxal and formaldehyde in the same time, and organize the data of Chiba and Tsukuba in 2013 and try to find the reason of the variation.

Keywords: Formaldehyde, Glyoxal, MAX-DOAS, diurnal variation, seasonal variation



Development of a direct measurement system of photochemical ozone production rate in the troposphere

KAWASAKI, Shio^{1*} ; SADANAGA, Yasuhiro¹ ; TANAKA, Yuki¹ ; KAJII, Yoshizumi² ; BANDOW, Hiroshi¹

¹Osaka Prefecture University, ²Kyoto University

Recently, ozone concentrations in the troposphere have been rising in spite of a steady decrease in concentrations of ozone precursors such as NO_x and volatile organic compounds. Photochemical production processes of ozone are non-linear to concentrations of ozone precursors. In addition, ozone concentration variations are influenced by meteorological factors such as transport and deposition processes as well as photochemistry. It is useful that the meteorological and photochemical factors could be divided to discuss ozone concentration variations. In order to discuss only "photochemical" factors for ozone production, a direct measurement system of photochemical ozone production rate has been developed.

Ambient air is introduced into "reaction" and "reference" chambers. The reaction and reference chambers (171-mm inner diameter and 500-mm length) are made of quartz and Pyrex, respectively. Inner walls of both the chambers are coated with Teflon to avoid wall loss of ozone. An outer wall of the reference chamber is coated with a UV-cut film (50%-cutoff wavelength of 405 nm). In the reaction chamber, photochemical reactions proceed to generate ozone. On the other hand, ozone is not produced photochemically in the reference chamber. Air passed from the reaction and reference chambers is introduced into "NO-reaction" tubes to convert O₃ to NO₂ in the presence of a high concentration of NO, and then the air is introduced into an NO₂ measurement system by a laser-induced fluorescence technique. Increment of ozone (ΔO_3) is defined by the difference of NO₂ concentrations derived from the reaction chamber and those from reference chamber. The ozone production rate is obtained by dividing ΔO_3 by a mean residence time of air in the reaction chamber (τ). In this system, O₃ concentrations are not directly measured but NO₂ concentrations converted by the reaction of O₃ with excess NO are observed. This is because the photostationary states between NO_x and O₃ are different between in the reaction and reference chambers, and ozone concentrations vary apparently. The sum of ozone and NO₂ concentrations (abbreviated as PO) are kept in the different photostationary states, so that this instrument measures production rates of PO instead of those of ozone practically.

Important parameters in this system are (1) ultraviolet transmittance of the reaction and reference chambers, (2) τ , and (3) conversion efficiency of O₃ to NO₂ in the NO-reaction tube. For (1), we measured solar spectra at inside and outside of the chambers using a spectroradiometer. Almost a hundred % of solar UV was transmitted into the reaction chamber. A wall of the reference chamber cut off solar UV adequately. For (2), about 10 ppmv of pulsed NO₂ was added into the reaction chamber and temporal variations of LIF signals were measured. τ was calculated to be 22.1 ± 0.5 min using the temporal variation the signals. For (3), quantitative conversions of O₃ up to 160 ppbv by NO in the NO-reaction tube were confirmed under the excess NO condition 0.97 ppmv.

Keywords: photochemical ozone, direct measurement of ozone production rate, laser-induced fluorescence

Transboundary ozone pollution from China to Japan; a case study

YURIKO, Keyamura^{1*}; HAYASHIDA, Sachiko¹

¹Faculty of Science, Nara Woman's University

These days, high concentrations of atmospheric ozone are often observed at the ground and/or in the lower troposphere over Japan, and transboundary ozone pollution from China would be one the possibility.

In this study we sampled highly concentrated ozone events observed at the ground and in the lower troposphere, and calculated backward trajectories hourly from the observation sites and compared the trajectories with the ozone map obtained by satellite measurement. The ozone lidar used here is the MRL (Meteorological Research Laboratory) ozone lidar [Nakazato et al., Applied Optics, 2007], which has short wavelengths in UV and thus continuous day-and-night measurements are possible. We also utilized the surface ozone monitoring network organized by Ministry of Environment.

The ozone distribution maps at the lower troposphere were obtained by OMI ozone product provided by Liu et al. [ACP, 2010]. They retrieved ozone profiles from the ground up to about 60 km into 24 layers among which 3 layers are in the troposphere. The lowermost layer (24th layer) is corresponding to 0 ~ about 3 km.

From analysis mentioned above, we found some cases indicating clear evidence of transboundary pollution from China to Korea and Japan.

This study was supported by a Grant-in-Aid from the Green Network of Excellence, Environmental Information (GRENE-i) program. And OMI data were provided by Dr. X.Liu and Dr. K.Chance, and Ozone lidar data were provided by Dr. M.Nakazato.

Keywords: troposphere, ozone, trajectory, transport, China

Validation observation for the derivation of lower tropospheric ozone by remote sensing

YANAKA, Fumiya^{1*}; KITA, Kazuyuki²; YAMAGUCHI, Yuuki¹; FUKUJU, Tabito¹; ITABASHI, Ryohei¹; KINASE, Takeshi¹; IRIE, Hitoshi³; NOGUCHI, Katsuyuki⁴; NAKAYAMA, Tomoki⁵; MATSUMI, Yutaka⁵; NAGAI, Tomohiro⁶; SAKAI, Tetsu⁶; ZAIZEN, Yuji⁶; MORINO, Isamu⁷; UCINO, Osamu⁷; INOUE, Makoto⁷; TANAKA, Tomoaki⁸

¹Graduate School of Science and Engineering, Ibaraki University, ²College of Science, Ibaraki University, ³Center for Environmental Remote Sensing, Chiba University, ⁴Faculty of Science, Nara Women's University, ⁵Solar-Terrestrial Environment Laboratory, Nagoya University, ⁶Meteorological Research Institute, ⁷National Institute for Environmental Studies, ⁸NASA Ames Research Center

The lower tropospheric ozone is a major component of photochemical oxidant which causes photochemical smog, adversely affecting human health and vegetation when it comes to high concentration. Therefore knowing their behavior as air pollution is an important. In recent years, contrary to the reduction of lower tropospheric ozone precursor gases, their amount is increasing. It has been suggested that the long-range transport of the lower tropospheric ozone from Asian Continent affects air quality in Japan and other wide areas. Remote sensing from a satellite is effective to observe such extensive/transboundary air pollution. However it has been quite difficult to measure the lower tropospheric ozone from satellite.

We have proposed that it can be evaluated with simultaneous measurement of solar backscattering spectra in the ultraviolet(UV) and visible(Vis) regions. Because the atmospheric Rayleigh scattering cross-section is much larger in UV than that in Vis, lower tropospheric light path length of the solar scattered radiation observed from space is significantly different in these two wavelength regions. This difference of light path enables us to detect the lower tropospheric ozone by the simultaneous measurement of UV and Vis solar backscattered spectra from space.

For the validation of this technique, we carried out aircraft experiments to validate this method over Tsukuba on 10th and 13rd September 2012. UV and Vis backscatter spectra were measured with two spectrometers (Maya2000pro, Ocean Optics, USA) at two altitudes 2500 ft (760 m) and 25000 ft (7600 m). Simultaneously, ozone profile was measured with ozone monitors on-board the aircraft, with ozonesonde launched near Tsukuba, and the tropospheric ozone lidar. Because aerosol scattering may significantly affect the evaluation of the lower tropospheric ozone amount, in situ aerosol observation with the CRDS, PSAP, and PASS instruments and the lidar observation were carried out in the Meteorological Research Institute. From the aircraft, we observed solar scattered radiation from zenith, nadir and 20 degree oblique directions in ultraviolet(300 - 380nm wavelength) and visible(400 - 700nm wavelength) spectral range. Because the surface reflected light greatly contribute to the scattered light from nadir, especially in the visible spectral range, for accurately estimation of the ozone amount, it is particularly important to understand the surface reflection spectrum. In this experiment, ground reflection spectra at different surface conditions such as rice paddy, forest, urban, farm areas and so on were measured at a low altitude of 2500ft (760m). It is necessary to consider the effect of scattering near the aircraft to estimate the surface reflected light. We estimated it with SCIATRAN (Rozanov et al., 2005). Results of these observations will be presented at this session.

Keywords: Remote Sensing, Lower tropospheric ozone

The Relationship between CO Concentration and Biomass Burning over the North China Plain

KAYABA, Satoko^{1*} ; HAYASHIDA, Sachiko¹ ; ONO, Akiko¹

¹Faculty of Science, Nara Women's University

Carbon monoxide (CO) controls the greenhouse gasses (e.g., CH₄, O₃) indirectly through a chemical reactions. Therefore, CO is regarded as an indirect-greenhouse gas and thus it is important to understand its spatiotemporal variation.

Wang et al.,[JGR, 2002] suggested that the open crop residue burning in June over the North China Plain affects on CO concentration, and it was confirmed by field campaign at Mt.Tai and investigated by model simulations [Kanaya et al.,2013 and reference therein]. Besides, the recent rapid industrialization in China brought significant increase in emission of CO [Ohara et al., ACP, 2007].

In this study, we analyzed the relationship between fire outbreak and CO concentration over the North China Plain by using satellite data. The CO data are taken from Measurement Of Pollution In The Troposphere (MOPITT). We used the Version 5 product. The fires detected by satellite observations are expressed as the hotspot numbers that are derived from the MODIS thermal anomaly product [Takeuchi and Yasuoka, 2006], using the algorithm by [Giglio et al.RSE,2003]. Here we used the hotspot numbers as proxy of the fire detection index.

CO concentration in June increases accompanied by a large number of the hotspot counts, which is consistent as previous studies. On the other hand, CO concentration gradually increases in fall and winter with only few hotspot numbers. It implies that CO emissions are possibly from industrial activity, automobiles and coal burning for heating rather than biomass burning in fall and winter. In addition, the year-to-year variability of CO concentration in June and in fall and winter was different.

This study was supported by a Grant-in-Aid from the Green Network of Excellence, Environmental Information (GRENE-ei) program.

Development of Atmospheric Environmental Risk Management System in Chile and Argentina

MIZUNO, Akira^{1*} ; SUGIMOTO, Nobuo² ; NAGAHAMA, Tomoo¹ ; OHYAMA, Hirofumi¹ ; NAKAJIMA, Tac¹ ; SUGITA, Takafumi² ; AKIYOSHI, Hideharu² ; NAKANE, Hideaki³ ; YAMAGISHI, Hisao⁴ ; OGAWA, Hideo⁵

¹Solar-Terrestrial Environment Laboratory, Nagoya University, ²National Institute for Environmental Studies, ³Kochi University of Technology, ⁴National Institute of Polar Research, ⁵Osaka Prefecture University

We started an international collaboration project on research of ozone/UV and aerosol in South America since 2013. This project is supported by Japan Science and Technology Agency (JST) and Japan International Cooperation Agency (JICA) under SATREPS program. The counterpart institutions are CEILAP (Laser Application Research Center) in Argentina and Magellan University in Chile. The major aims of this project are (1) to construct new aerosol lidar network in Chile and Argentina, (2) to consolidate the ozone monitoring capability at the South Patagonian Atmospheric Observatory (OAPA, 52S, 69W) in Rio Gallegos at the southern end of the South American continent. The new aerosol lidar network consists of 9 lidars. Six of them are Raman lidars and the other 3 are high-resolution lidars with an iodine filter. Eight lidars are distributed over Argentine territory to observe volcanic ashes from volcanos in Andes, Patagonian dust, and black carbon from Bolivia and Brazil. From the observatory in Rio Gallegos, we will make comprehensive observations of ozone by using a Differential Absorption Lidar (DIAL), millimeter-wave spectral radiometer, brewer spectrometer, and so on. In addition to the consolidation of observing network, we will develop data analysis and data distribution system to deliver the data to the relevant organizations in the both countries.

In the presentation, we will introduce the overview of this project and present a progress report after the first year.

Keywords: Aerosol, Ozonehole, Lidar, Millimeter-wave spectroscopy, International cooperation, Contribution to society

Observations of horizontal distributions of air pollutants by MAX-DOAS

NI, Wentao^{1*} ; IRIE, Hitoshi¹ ; CHEN, Cheng¹ ; TAKAMURA, Tamio¹ ; KHATRI, Pradeep¹

¹Chiba University

In June 2012 we set up a MAX-DOAS device in Chiba University and continuous observations have been conducted since then. The MAX-DOAS method measures the spectra of scattered sunlight in ultraviolet and visible regions at various elevation angles. By analyzing the measured spectra with a radiative transfer model and an inversion method, vertical distributions of aerosol and gas and their column amounts can be retrieved (Irie et al., 2008,2009, Vlemmix, 2010). In this study, firstly, we compared the aerosol optical depth measured by the MAX-DOAS to that measured by the sky radiometer. We found the consistency of differences between MAX-DOAS and sky radiometer AOD values are within 30%. Secondly, we set up two MAX-DOAS devices (machine No.1 and No.2) for simultaneous observations at the same place. For both devices, the wavelength regions of 460-490nm and 338-370nm were analyzed with the DOAS method to derive the differential slant column densities (DSCDs) of O₄. In order to quantify the effect of the systematic offset of the elevation angle in O₄ DSCDs, we have biased the offset of elevation angles by $\pm 0.5, \pm 1.0$ degrees. Comparisons such as correlation analysis etc. show that the effect is insignificant as there is only 20% differences found in the O₄ DSCD comparisons between two devices. Based on such a detailed error evaluation, since December 2013, we have directed the machine No.1 to north and No.2 to west to perform quantitative observations of horizontal-distribution of aerosols. Results will be discussed in this work.

Keywords: MAX-DOAS, Elevation angle offset, vertical profile, tropospheric column amount, differential slant column density

Validation of GOSAT SWIR xCH₄ using TCCON and Airborne Measurements

IWASAKI, Chisa^{1*} ; HAYASHIDA, Sachiko¹ ; ONO, Akiko¹ ; MACHIDA, Toshinobu²

¹Faculty of Science, Nara Women's University, ²NIES

As methane (CH₄) is one of the most important Short-Lived Climate Pollutants (SLCPs), global monitoring of atmospheric CH₄ with enough accuracy is expected to estimate its sources and sinks. For measurements of global distribution of CO₂ and CH₄ concentration from space, the Greenhouse gases Observing SATellite (GOSAT) was launched in 2009, and has continued measurements up to the present. However, cloud interferes satellite observation. To understand CH₄ emission from a cloudy region, the selection of an adequate criterion of cloud screening, and validation of data quality are necessary.

In this study, we validate the GOSAT CH₄ products of the column-averaged dry-air mole fractions (xCH₄) derived from Short-Wavelength InfraRed (SWIR) radiation by comparing them with data of Total Carbon Column Observing Network (TCCON). Yoshida et al. (AMT, 2013) had already carried out the validation for the NIES product, but we extended the period and involved more TCCON sites; Yoshida et al. (2013) used data observed at the 13 TCCON sites from June, 2009 to December, 2012 and we used data at the 17 TCCON sites from June, 2009 to August, 2013. We found that the average difference between TCCON and GOSAT for the whole period is -6.0 ± 16.1 ppbv.

We also examined the appropriate cloud screening for xCH₄ product from RemoTeC-MACC. The product was obtained by using the "proxy method" by which we can obtain more data under cloudy conditions. In this study, we also tried to compare GOSAT data with aircraft measurements over Siberia and other areas.

Acknowledgements

This research was supported by the Environment Research and Technology Development Fund of the Ministry of the Environment, Japan (A1202). The RemoTeC-MACC product was provided by Dr. Andre Butz (IMK-ASF, Karlsruhe Institute of Technology; KIT).

Keywords: GOSAT, validation, methane, cloud screening, aircraft

Variations of tropospheric methane over Japan during 1988-2010

UMEZAWA, Taku^{1*} ; GOTO, Daisuke¹ ; AOKI, Shuji¹ ; ISHIJIMA, Kentaro² ; PATRA, Prabir² ; SUGAWARA, Satoshi³ ; MORIMOTO, Shinji¹ ; NAKAZAWA, Takakiyo¹

¹Center for Atmospheric and Oceanic Studies, Graduate School of Science, Tohoku University, ²Research Institute for Global Change, JAMSTEC, Yokohama, Japan, ³Miyaigi University of Education, Sendai, Japan

Mixing ratios of greenhouse gases and related trace gases have been measured using chartered and commercial aircraft in the lower to upper troposphere (LT and UT) over Japan by Tohoku University. We present variations of CH₄ during 1988-2010. The analysis is aided by simulation results using an atmospheric chemistry transport model (i.e. ACTM). Tropospheric CH₄ over Japan shows altitude-dependent interannual and seasonal variations, reflecting differences in air mass origins at different altitudes. The long-term trend and interannual variation of CH₄ in the LT are consistent with previous reports of measurements at surface baseline stations in the northern hemisphere. However, those in the UT show excursions from those in the LT. In the UT, CH₄ mixing ratios show seasonal maximum in August due to efficient transport of air masses influenced by continental CH₄ sources, while LT CH₄ reaches its seasonal minimum during summer due to seasonally maximum chemical loss. Vertical profiles of the CH₄ mixing ratios also vary with season, reflecting the altitude-dependent seasonal cycles. In summer, transport of CH₄-rich air from Asian regions elevates UT CH₄ levels, forming the uniform vertical profile above the mid troposphere. On the other hand, CH₄ decreases nearly monotonically with altitude in winter-spring. The ACTM simulations with different emission scenarios reproduce general features of the tropospheric CH₄ variations over Japan. Tagged tracer simulations using the ACTM indicate substantial contributions of CH₄ sources in South Asia and East Asia to the summertime high CH₄ values observed in the UT. This suggests that our observation data over Japan are highly valuable for capturing CH₄ emission signals, particularly from the Asian continent.

Keywords: aircraft observation, methane, troposphere, over Japan

Measurement of CO₂ stable isotope ratio by mid-inferred laser absorption spectrometry; analysis of CO₂ cycle in urban

YUBA, Akie^{1*} ; TAKAHASHI, Kenshi² ; NAKAYAMA, Tomoki¹ ; MATSUMI, Yutaka¹

¹Solar-terrestrial environment laboratory, Nagoya university, ²Research Institute for Sustainable Humanosphere, Kyoto University

CO₂ concentration has been increasing from the range of 275 ppmv (parts per million by volume) to 285 ppmv in the previous industrial period to about 400 ppmv in 2013. IPCC reported that CO₂ has the most effective on the positive radiative force. The insight of CO₂ emission and absorption flux helps us to estimate the variation of radiative forcing and atmospheric environment. CO₂ concentration changed with the anthropogenic and biogenic emission and absorption. The stable isotope ratio of CO₂ ($\delta^{13}\text{C}$ and $\delta^{18}\text{O}$) is associated with the CO₂ source such as combustion and biogenic respiration. The contribution of each CO₂ source in the urban area was estimated by using the stable isotope ratio of CO₂.

We conducted the continuous measurement for CO₂ concentration and stable isotope ratio of CO₂ using the mid-inferred absorption spectrometry which can obtain CO₂ concentration and its isotope ratio with high time resolution. The water vapor and stable isotope ratios of water vapor (δD and $\delta^{18}\text{O}\text{-H}_2\text{O}$) were measured to show the relationship between H₂O and CO₂ due to the isotopic exchange reaction. CO and NO_x concentrations were obtained as a tracer of anthropogenic emission. The measurement was conducted for two weeks in summer and winter. The seasonal variation of CO₂ source was shown according to the comparison of CO₂ concentration and stable isotope ratio. Especially, we focused on the contribution of biogenic process to CO₂ concentration variation in the urban area.

CO₂ concentration and stable isotope ratio of CO₂ in the summer showed the diurnal variation. On the other hand, those in the winter had no diurnal variation. CO₂ concentration variation in the winter was correlated with CO concentration variation. These results suppose that CO₂ concentration variation in the winter was mainly dominated by the anthropogenic emission and that in the summer was related with biogenic process as well as anthropogenic emission. We will discuss the relationship between stable isotope ratio and meteorological condition or water vapor isotope ratio to identify the detail of CO₂ source.

Keywords: CO₂ stable isotope ratio, Urban area, CO₂ cycle, mid-inferred laser absorption spectrometry

Temporal and spatial variations of Radon-222 in the western North Pacific

TSUBOI, Kazuhiro^{1*} ; MATSUEDA, Hidekazu¹ ; SAWA, Yousuke¹ ; NIWA, Yosuke¹ ; MURAYAMA, Shohei²

¹Meteorological Research Institute, ²National Institute of Advanced Industrial Science and Technology

A new compact radon measuring system has been developed for high-resolution observation of low-level radon-222 (Rn) for the remote sites, in collaboration with the MRI and AIST. The Rn measuring system was installed at 4 stations of Minamitorishima (MNM), Yonagunijima (YON), Chichijima (CCJ) and Ryori (RYO) operated by Japan Meteorological Agency (JMA) since 2007. The Rn measurements clearly show that distinct seasonal variations as well as frequent episodic events with Rn enhancement peaks on a synoptic scale are successfully captured at all 4 stations. Although the seasonal cycles depended on the stations, significant correlations between the Rn and other trace gases were found for the most of the synoptic-scale events, indicating a large impact of widespread pollutions from the East-Asian countries on the regional air quality over the western North Pacific.

Keywords: Radon

Estimation of Several Kilometer Scale PWV Distribution using GNSS Slant Path Delay for Monitoring of Cumulus Convection

SHOJI, Yoshinori^{1*}

¹Meteorological Research Institute

A procedure for estimating precipitable water vapor (PWV) distribution around each ground-based station of the global navigation satellite system (GNSS) on a scale of several kilometers is presented. This procedure utilizes the difference between zenith total delay above a GNSS station and zenith mapped slant path delay (SPD). By assuming an exponential distribution for the horizontal water vapor gradient, this difference can be used to estimate the PWV gradient in each SPD direction. Shoji (2013) proposed the WVI index, which is defined as the standard deviation of the PWV_{SPD} . The retrieved PWV gradient in this study can be regarded as another utilization of PWV_{SPD} . In the WVI index, ray path direction data is not utilized. The PWV gradient proposed in this paper utilizes both the deviation of PWV_{SPD} and information on its direction.

The procedure was tested for an estimation of the PWV variation associated with the parent storm of an F3 Fujita scale tornado that occurred in Ibaraki prefecture on May 6, 2012. Differential reflectivity observed by a dual-polarimetric radar showed the existence of a developed parent cloud approximately 1 h before the tornado occurred. A high-resolution numerical weather model simulation showed the existence of a strong PWV gradient around the parent cloud, made evident by the co-existence of a strong updraft and downdraft within an approximately 5-km radius. The PWV gradient calculated using the GNSS observation network with an average spacing of approximately 17 km could not detect such a small-scale, strong PWV gradient. The PWV gradient estimated using the proposed procedure revealed a strong PWV gradient and its enhancement. In this case, higher order inhomogeneity component of each SPD played a critical role.

However, the gradient was weaker than the NWP simulation. This might be partly because of the insufficient observation density. Horizontal scale of the higher order inhomogeneity component of each SPD is about several kilometers and we adopt distance cutoff of 5 km. In order to analyze several kilometer scale PWV distribution, we need denser GNSS network with at least 10 km horizontal spacing. Another possible reason for the weaker gradient may be insufficient and inhomogeneous coverage of GPS satellites. As of 2012, carrier waves transmitted from six to twelve GPS satellites could be observed simultaneously at each GNSS site in Japan. This might be insufficient for estimating the water vapor gradient in all directions. Also, we need to carefully check the quality of each SPD. In this study, following Shoji (2013), the effects of the satellite clock error and multi-path (reflected wave) are tried to eliminate. However it is difficult to distinguish atmospheric signal with those noises, especially under local severe weather.

The number of GNSSs has been increasing. As of December 2013, 24 satellites of the Russian GLONASS are in operation. The European Union's GNSS (Galileo) is in the experimental phase and China is also developing an independent GNSS system named COMPASS. Furthermore, a number of space-based augmentation systems (e.g., Japan's QZSS) and regional navigation satellite systems (e.g. the Indian Regional Navigation Satellite System, or IRNSS) will contribute further satellites and signals to the multi-constellation GNSS. In the next step of this study, we will assess the impact of the increased number of SPDs on multi-GNSS.

Keywords: Mesoscale meteorology, Watervapor, Global Navigation Satellite System

Numerical Simulation on Retrieval of Meso-gamma Scale PWV Distribution with the Quasi-Zenith Satellite System (QZSS)

OIGAWA, Masanori^{1*} ; REALINI, Eugenio¹ ; SEKO, Hiromu² ; TSUDA, Toshitaka¹

¹Research Institute for Sustainable Humanosphere (RISH), Kyoto University, ²Meteorological Research Institute (MRI), Japan Meteorological Agency (JMA)

A simulation study was conducted to investigate the retrieval of meso-gamma scale Precipitable Water Vapor (PWV) distribution with QZSS, using the output of a non-hydrostatic numerical weather prediction model. The evaluation was performed on PWV values obtained by simulating three different methods: using all GPS satellites above an elevation angle higher than 10 degree (PWVG) (conventional GPS meteorology method), using only the QZSS satellite at highest elevation (PWVQ) and using only the GPS satellite at highest elevation (PWVHG).

The RMSEs of PWVG, PWVQ and PWVHG were compared, assuming the vertically integrated water vapor amount of the model as true PWV. As a result, the RMSEs of PWVG, PWVQ and PWVHG were 2.78, 0.13 and 0.59 mm, respectively, 5 minutes before the rainfall. The PWVHG time series had a large discontinuity (~2 mm) when the GPS satellite at the highest elevation changed, whereas that of the PWVQ time series was small, because the elevation angle at which the replacement of the highest elevation QZSS satellite occurs is much higher. The standard deviation of PWVQ was smaller than those of PWVG and PWVHG, which vary largely depending on the GPS satellites geometry.

When the spatial distributions of PWVG and PWVQ were compared to the meso-gamma scale distribution of the reference PWV, PWVG smoothed out the PWV fluctuations whereas PWVQ captured them well, due to the higher spatial resolution achievable by using only high-elevation slant paths. These results suggest that meso-gamma scale water vapor fluctuations associated with a thunderstorm can be retrieved by using a dense GNSS receiver network and analyzing PWV derived from a single high elevation GNSS satellite. In this paper we focus on QZSS, as this constellation is especially promising in this context since it is going to provide nearly continuous PWV observations also as its highest satellite changes, contrary to using highest satellites from multiple GNSS constellations.

Keywords: precipitable water vapor, Quasi-Zenith Satellite System, thunderstorm, non-hydrostatic model

Data assimilation experiments of refractivity distribution observed by an operational Doppler Radar of JMA

SEKO, Hiromu^{1*} ; SATO, Eiichi² ; SAKANASHI, Takanori³

¹Meteorological Research Institute, JAMSTEC, ²Meteorological Research Institute, ³Japan Meteorological Agency

Because low-level convergence of water vapor generates the convections, accuracy of local heavy rainfall forecasts is expected to be improved when horizontal distribution of low-level water vapor is observed. We focused on radio waves of Doppler Radars that are returned from fixed structures. Because the radio waves are delayed by water vapor while passing atmosphere, we can estimate refractivity, which is a function of temperature and water vapor, from the delay of radio waves. If radio waves of many Doppler Radars that have been deployed in Japan are used in producing initial conditions of numerical forecasts, the forecast accuracy of thunderstorms is expected to be improved through improvement of water vapor fields by using this technique.

In this presentation, temporal variations of refractivity observed by Tokyo Radar and the impacts of refractivity on the rainfall forecasts will be presented.

Acknowledgements:

This study was supported by "Grants-in-Aid for Scientific Research: Establishment of estimation methods of water vapor from Radar phase data reflected from fixed structures" and "Projection of Planet Earth Variations for Mitigating Natural Disasters (Field 3)" in "Strategic Programs for Innovative Research (SPIRE)".

Keywords: Doppler Radar, Refractivity, Water vapor, Data assimilation

Overview and future strategy of docomo Environmental Sensor Network(ESN)

TSUBOYA, Hisakazu^{1*} ; HIGASHI, Kuniaki² ; FURUMOTO, Jun-ichi²

¹Division of life support business promotion, NTT DOCOMO Corporation, ²Research Institute for Sustainable Humanosphere, Kyoto University

NTT docomo had launched a nation-wide and hyper-dense network for the measurement of both weather and environmental element since 2008 and provide them as new information contents to the markets. Its realtime data could be applied to various industrial issues, namely hazard prediction, agriculture, and medical&healthcare. docomo make the new network infrastructure more sophisticated and is planning to expand its sensor stations, which has been set only to its radio base stations up to now, to any customers who need to measure their own environment.

High Dense Ground Observation Network "POTEKA" in Gunma, Japan

MAEDA, Ryota^{1*}; YOSHIKURA, Tomomi¹; KURE, Hiroataka¹; YADA, Takuya¹; MORITA, Toshiaki¹; IWASAKI, Hiroyuki²

¹Meisei Electric co., Ltd., ²Faculty of Education, Gunma University

Meisei developed compact weather sensor (POTEKA Sta.) and cloud data-transfer system (POTEKA Lab.) to achieve high dense observation network. "POTEKA" stands for "Point Tenki Kansoku". POTEKA project has been demonstrated the validity for the use of disaster prevention, health and medical care, teaching material, agriculture and energy management, and comfortable living environment in cooperation with local companies and education board since August 2013.

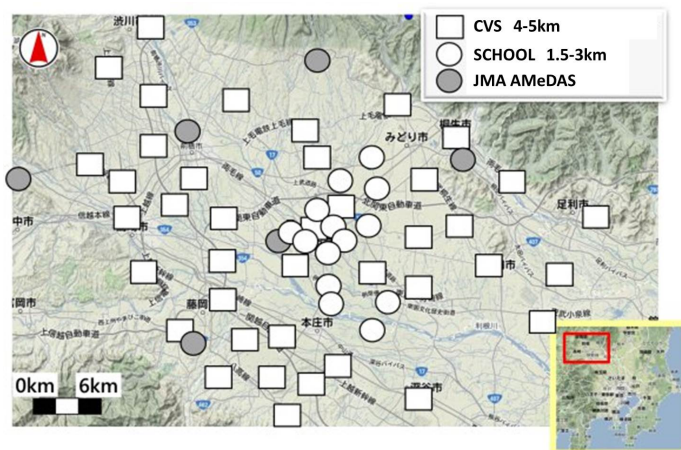
POTEKA Sta. measures wide range of meteorological and environmental variables such as temperature, relative humidity, pressure, sunlight, and rain detection with a one minute resolution. This low-cost weather sensor enables us to achieve finer-meshed or higher density weather observation system economically. Finer-meshed and more extensive data collected are easily accessible through ordinal Web sites (PC, Tablets, etc.) without any special software.

Spatio-temporal high dense observation network (total 55 stations, 1.5~4km-mesh) was installed in Isesaki city, Gunma, Japan. Observation with elementary/junior high school and convenience store (SAVE ON) are performed at 14 stations and 41 stations, respectively, which spatially captured local surface weather phenomenon (fig. 1).

This paper presents some examples including 1. local distribution of surface temperature around Isesaki, 2. preventing heat stroke at school, and 3. school education for class and research.

Acknowledgments: The authors would like to thank SANDEN Corporation, SAVE ON, and Board of Education of Isesaki city for support POTEKA project.

Keywords: dense, big data, instrument, network, observation



Observation of downburst in Takasaki and Maebashi city, Gunma on 11 August 2013

NOROSE, Keiko^{1*} ; KOBAYASHI, Fumiaki¹ ; KURE, Hirotaka² ; MORITA, Toshiaki²

¹National Defense Academy, ²Meisei Electric

On the evening of 11 August 2013, a severe thunderstorm passed over the Takasaki and Maebashi city, Gunma prefecture, and produced gusty wind damages. The change of surface weather elements was recorded by dense observation network POTEKA when gust occurred. In this study, we follow the development and propagation of gust-front and downburst through the analysis of features of the pressure field observed by POTEKA. The result of this analysis reveals that the reason of gust caused damages in Maebashi city is downburst.

Helicopter-borne thermocamera measurements of surface temperatures in downtown Tokyo -Comparison of 2013 with 2007-

TSUNEMATSU, Nobumitsu^{1*} ; YOKOYAMA, Hitoshi¹ ; HONJO, Tsuyoshi³ ; ICHIHASHI, Arata¹ ; ANDO, Haruo¹ ; MATSUMOTO, Futoshi¹ ; SETO, Yoshihito²

¹Tokyo Metropolitan Research Institute for Environmental Protection, ²Chiba University, ³Tokyo Metropolitan Research Institute for Environmental Protection/Tokyo Metropolitan University

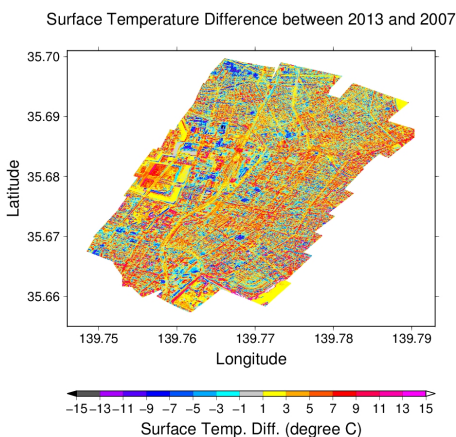
Annual mean air temperatures in downtown Tokyo have increased about 3 degrees Celsius in the past 100 years due to global warming and urban heat island. The frequency of heat stroke outbreaks in Tokyo tends to increase in recent years. The Tokyo metropolitan research institute for Environmental Protection has therefore investigated the current situation of the temperature rises in Tokyo through the monitoring of urban heat island. This can contribute to verification of measure effects on urban heat island.

As part of the investigations, we performed helicopter-borne infrared thermocamera measurements of surface temperatures in downtown Tokyo (mainly an Otemachi-Marunouchi-Yurakucho area) on two different extremely hot days, Aug. 19, 2013 (hereafter, HTM13) and Aug. 7, 2007 (HTM07). The measurements were carried out in the daytime (12-13 local time) and the nighttime (20-22 local time), using a Robinson R22 helicopter with a longwave (8-14um) infrared thermocamera (TS7302) developed at NEC Avio Infrared Technologies Co., Ltd. An altitude of the helicopter flight was 610 m. The daytime air temperatures on those days reached 32-33 degrees Celsius although southerly sea breezes prevailed in the area. Compared with the HTM07 case, a higher air temperature condition was predominant prior to HTM13.

Results of analyses of data from the thermocamera-derived images (a 2 m ground resolution) show that surface temperatures obtained from HTM13 are relatively large in the greater part of the area, compared with HTM07 (refer to a figure shown below), whereas, smaller surface temperatures can be recognized in redevelopment areas where new buildings have been constructed after 2007. (Note that the emissivity of each surface material can influence it.) Also, the thermocamera-derived images projected on Google Earth show higher surface temperatures on intersections.

In addition, we would like to show geographical distributions of the observed surface temperatures in the nighttime, differences between the daytime and nighttime surface temperatures, and a relationship between surface temperatures and sky view factors.

Keywords: Helicopter-borne measurements, thermocamera, surface temperature, downtown Tokyo, verification of measure effects on urban heat island, extremely hot days



How Does A Typhoon Affect The Local Downslope Wind Hirodo-Kaze In Japan?

FUDEYASU, Hironori^{1*} ; KIYOHARA, Yasutomo² ; OHASHI, Yukitaka³ ; KUWAGATA, Tsuneo⁴ ; MORIYAMA, Fumiaki¹

¹Yokohama National University, ²The Certified and Accredited Meteorologists of Japan, Japan, ³Okayama University of Science, Japan, ⁴National Institute for Agro-Environmental Sciences, Japan

The Hirodo-kaze is one of the well-known strong local winds in Japan. Hirodo-kaze occurs at the southern base of Mt. Nagi (1240 m) in the northeastern Okayama Prefecture, when the lower-troposphere synoptic wind is strong northerly in association with a typhoon. Previous studies have described the mechanisms that force downslope winds and large-amplitude mountain waves. However, descriptions of the effect of temporal changes in the large-scale environment on the severe downslope wind are not enough. The purpose of present study is to examine the forcing mechanisms during a Hirodo-kaze and the effects of typhoons on the occurrence of a Hirodo-kaze.

The Hirodo-kaze that occurred in association with Typhoon Pabuk was investigated as a case study. At 06 UTC on 21 August 2001, when Pabuk was located over the sea about 80 km southwest of the Kii peninsula, strong surface winds related to the cyclonic circulation of Pabuk were observed in Shikoku and Kinki districts. Relatively weak northerlies prevailed in Chugoku district far from Pabuk, but a strong northerly was observed at the station located in the lee of Mt. Nagi, about 5 km south of the crest of Mt. Nagi, namely Hirodo-kaze.

The mesoscale model, MM5, successfully reproduces the major features of the observed Hirodo-kaze and Typhoon Pabuk. During the Hirodo-kaze, the severe downslope winds in the transitional flow develop in the lower troposphere below the mean-state critical layer. The Hirodo-kaze is closely linked to the strong wind region accompanying the severe downslope winds. After the cessation of the Hirodo-kaze, distinct mountain waves dominate in the lower troposphere where the Scorer parameter decreases with height. The region of strong wind retreat windward as the Hirodo-kaze ceases. Temporal changes in the characteristics of mountain waves in the lee of Mt. Nagi are primarily attributed to the changes in the large-scale environmental winds due to the movement of Typhoon Pabuk.

The effects of intense typhoons on the occurrence of the Hirodo-kaze were also investigated statistically using data using European Center for Medium Range Weather Forecast 40-year reanalysis data (ERA-40). According to the several reports of Okayama meteorological station, twelve Hirodo-kaze events occurred between 1989 and 2001. During these events, strong lower-tropospheric northerlies were overlain by middle-tropospheric southerlies. These favorable conditions occur only as an intense typhoon moves over the sea southwest of Kii peninsula. Thus, the intense typhoon that moves over the sea southwest of the Kii peninsula creates favorable environmental conditions that support the occurrence of the Hirodo-kaze.

Keywords: typhoon, local downslope wind, MM5

Observation and application of the Phased Array Radar

USHIO, Tomoo^{1*} ; WU, Ting¹ ; KIKUCHI, Hiroshi¹ ; SHIMAMURA, Shigeharu¹ ; MEGA, Tomoaki¹ ; MIZUTANI, Fumihiko² ; WADA, Masakazu² ; IGUCHI, Toshio³ ; SATOH, Shinsuke³ ; TAKAHASHI, Nobuhiro³

¹Osaka University, ²Toshiba, ³NICT

The phased array radar system which was installed in 2012 in Osaka University has the unique capability of scanning the whole sky with 100m and 10 to 30 second resolution up to 60 km. The system adopts the digital beam forming technique for elevation scanning and mechanically rotates the array antenna in azimuth direction within 10 to 30 seconds. The radar transmits a broad beam of several degrees with 24 antenna elements and receives the back scattered signal with 128 elements digitizing at each elements. Then by digitally forming the beam in the signal processor, the fast scanning is realized. After the installation of the PAR system in Osaka University, the continuous operation has been done and succeeded in getting several hazardous rain fall events with lightning locations. The data for these events captured by the Phased Array Radar shows the unique capability of the high resolution weather radar. In this presentation, over view of the Phased Array Radar is firstly given, and after that observation results and future direction of the Phased Array Radar Network with polarimetric capability is shown.

Keywords: Radar, Phased Array, Precipitation

Statistical analyses on the characteristics of heavy rainfall events

TSUGUTI, Hiroshige^{1*} ; KATO, Teruyuki¹

¹Meteorological Research Institute

In this study, to clarify general characteristics of heavy rainfall events in Japan, we have conducted various statistical analyses on them.

For the warm seasons (April - November) from 1995 to 2009, we objectively extracted heavy rainfall events occurring in Japan by using Radar-Raingauge analyzed rainfall dataset produced by the Japan Meteorological Agency. As a result, 386 events were extracted. Over 75 % of all events occurred during three months of July, August, and September, and many events were distributed around the coastal areas of the Pacific Ocean in Kyushu, Shikoku, Kinki, and Tokai regions. Synoptic weather conditions causing the heavy rainfall events were clarified, and consequently the pattern associated with typhoons or tropical cyclones was the most predominant, which accounted for 32.4 % of all events. Then, stationary fronts, remote precipitation of typhoons or tropical cyclones, and low depressions accounted for 21.2 %, 17.9 %, and 14.2 %, respectively. The classification for the shape of the precipitation systems causing the heavy rainfall events showed that the most predominant system was "band-shaped", which accounted for 43.5 % of all events.

The environmental fields of heavy rainfall events (>130 mm/3hr) were statistically analyzed using the Japanese 55-year reanalysis data (JRA-55). Characteristics of them were elucidated by comparing the environmental fields of moderate rainfall events (10-30 mm/3hr). In July (the late Baiu season) in Kyushu region, the low-level equivalent potential temperature and water vapor flux in the vicinity of Kyushu Island were significantly larger in heavy rainfall events than in moderate ones, and the atmospheric stability became more unstable in heavy rainfall events. Furthermore, to distinguish heavy rainfall events from moderate ones, the combination of two elements of low-level water vapor flux and atmospheric stability was more effective than the unique usage of each element.

Keywords: heavy rainfall, statistical analysis

MRI Rapid-Scan and Super-Resolution Observations in severe storms: Recent Progress and Future Plans

KENICHI, Kusunoki^{1*} ; INOUE, Hanako¹ ; YOSHIDA, Satoru¹ ; KATO, Rhohei² ; FUJIWARA, Chusei³

¹Meteorological Research Institute, ²Alpha-denshi Co., Ltd., ³East Japan Railway Company

In this presentation, we will introduce the recent progress, present examples, and future plans of rapid-scan and super-resolution observations in severe storms of the Meteorological Research Institute (MRI).

1. A linear array of pressure and wind sensors for high resolution in situ measurements in winter tornadoes

In order to improve our understanding of near-surface tornadic features, we developed a linear array of wind and pressure sensors (LAWPS) for high resolution in situ measurements in winter tornado cores. The pressure and wind sensors were deployed along a 1.2km-long linear array that is located parallel to and about 100m from the shoreline. Wind data are obtained using 12 two-dimensional fast-response ultrasonic anemometers placed at a height of 5 m at intervals of 100 m. Pressure data are obtained using 25 barometers placed at a height of 50cm at intervals of 50m. The pressure ports are designed and loaded to the barometers to reduce the dynamic pressure associated with wind and turbulence. In this presentation, the system overview and the measurement technique will be described, as well as some examples of actual winter tornado observations of the system and X-band Doppler radar simultaneously.

2. An X-band phased array Doppler radar for the research of severe storms

Many severe storms evolve on time scales shorter than that resolved by conventional mechanically scanning radar systems. MRI has a new project of development of severe storm observations and detections from a phased array radar. The azimuth scan is similar to the conventional scan with a mechanically rotating antenna and at a variable rate between 1- 6 rpm. 128 slotted waveguide array elements fixed above the antenna panel produce transmit beam and an electronic elevation scanning will be performed. With the electronic elevation and mechanical azimuth scanning, the radar can observe the entire sky in less than a minute. Such high temporal resolution sampling will be expected to provide a realistic structure of rapidly evolving storm. In this presentation, some basic characteristics of the radar and a brief description of future tasks for detection and prediction of severe storms will be presented.

Keywords: tornado, rapid-scan and super-resolution observations, phased array radar

Fine radar echo structure revealed by a high scanning and high-range-resolution X-band marine radar

FUJIYOSHI, Yasushi^{1*}

¹Inst. Low Temp. Sci., Hokkaido Univ.

We used an X-band (9410 MHz) marine radar (KODEN Co., Ltd.), which is not powerful and not very sensitive (its peak transmitted power is 25 kW and minimum detection power is -90 dbm); however, the radar has a high range resolution (15 m). Although its antenna usually rotates horizontally to detect ships, we changed the rotation direction of the slot antenna (2 m in length) from horizontal to vertical (Range Elevation Indicator-scan), and recorded every 2 s. We deployed this radar at various places. We will report very interesting phenomena that are firstly detected by this high-scanning and high-resolution radar.

Keywords: marine radar, fine structure of radar echo, precipitating cloud, angel echo, gravity current head

Applications of weather radar network in private companies

TESHIBA, Michihiro^{1*}

¹Weathernews Inc.

Recently, various weather radars have been developed not only with novel functions of observation, but with low cost. As a result, each private companies can deploy their own weather radars and make a radar network. In the US, for example, local TV stations have their weather radars and the current situation is analyzed through their radars' data. However, in Japan weather radars have not been deployed yet. In this paper I would like to introduce the Weathernews (WNI)'s weather radar network in Japan and we would discuss future work in order to expand this type of network in Japan.

Keywords: weather radar, radar network, private company

Temporal Variation of Close-Proximity Soundings within a Significant Tornadoic Supercell Environment

ARAKI, Kentaro^{1*} ; ISHIMOTO, Hiroshi¹ ; MURAKAMI, Masataka¹ ; TAJIRI, Takuya¹

¹Meteorological Research Institute

We examined proximity soundings at intervals of a few minutes and at distances of less than 20 km from a significant tornadoic (SIGTOR) supercell that occurred on 6 May 2012 in Japan. We used a 1-dimensional variational (1DVAR) technique that combined the observations of a ground-based microwave radiometer with outputs from a numerical model. Based on the results of the 1DVAR, several supercell and tornado forecast parameters were calculated and compared with values typical of SIGTOR supercell environments in the United States. One and a half hours before the occurrence of the tornado, the value of convective available potential energy increased significantly to about 1000 J kg^{-1} , a value that is smaller than the typical value in the United States. Low-level vertical wind shear and some composite parameters attained maximum values at the time when the distance to the supercell was the smallest. The vertical wind shear parameters and some composite parameters indicated that the environment fell into the SIGTOR supercell category. This result shows that the thermodynamic environments became unstable before the approach of the supercell, and the low-level vertical wind shear changed locally near the supercell.

Keywords: tornado, supercell, microwave radiometer, 1DVAR

Data Assimilation experiment of Tsukuba tornado on May 6, 2012 using MRI Doppler Radar data

YOKOTA, Sho^{1*} ; KUNII, Masaru¹ ; SEKO, Hiromu²

¹Meteorological Research Institute, ²Meteorological Research Institute/JAMSTEC

A strong tornado with F3 scale caused serious damage in Tsukuba city on May 6, 2012. This tornado was generated at the southern tip of a precipitation area, which was moving northeastward over the Kanto Plain. Besides the Tsukuba tornado, two tornadoes were observed a few ten kilometers north of the Tsukuba tornado. The lower vortex associated with the Tsukuba tornado, as well as its precipitation area, was well captured by the Doppler Radar of the Meteorological Research Institute (MRI), because the Tsukuba tornado passed 15 km north of the MRI. However, data assimilation experiments using the high-resolution data, such as Radar data, have not been performed yet. In this study, Doppler wind data observed by the MRI-Radar were assimilated with an ensemble Kalman filter so as to evaluate the impact of the assimilation of Doppler wind.

In this experiment, a Nested Local Ensemble Transform Kalman Filter (Nested- LETKF) system, with 12 ensemble members, was used. In Outer-LETKF (horizontal grid interval: 15 km), hourly operational observation data used in the Japan Meteorological Agency (JMA) operational model were assimilated with 6 hour intervals. In Inner-LETKF (horizontal grid interval: 1.875 km), data obtained every 10 minutes was assimilated with 1 hour intervals. To assess the impact of the Doppler wind observations, we basically performed two experiments. The "CTL" experiment used conventional observations, that is, the original settings of the Nested-LETKF. The other "VR" experiment assimilated the Doppler wind data observed by MRI-Radar additionally in Inner-LETKF, while all other settings were the same as CTL. After the data assimilation experiments, downscaling ensemble experiments (horizontal grid interval: 350m) were carried out by using the analyses and 12 perturbations of each CTL and VR at 10:00 JST on May 6, 2012 as initial conditions.

In the downscaling ensemble experiments, two vortices were formed although three vortices were actually observed. The southern vortex in VR was stronger and passed about 2 km closer to the observed tornado than that in CTL. To clarify those differences, we focused on Storm Relative Helicity (SReH) and low level humidity (Low-Qv) at 10:00 JST. The SReH and Low-Qv were compared to the maximum velocity of the Tsukuba tornado vortex (Vmax) and to the latitude where the vortex existed when it passed 140E (L140), using the analyses and 12 perturbations of VR. As a result, Vmax had a positive correlation to SReH in and south of the precipitation area. It also had a positive correlation to the Low-Qv in the south of the precipitation area, and in the south of the genesis point of the vortices. In fact, Low-Qv in the south of the genesis point of vortices in VR was increased by the assimilation of Doppler wind. On the other hand, L140 had a negative correlation with Low-Qv in the south of the precipitation area. It shows that the precipitation area was elongated in the meridian directions and that the vortex was generated further to the south if humidity was higher in the south of the precipitation area.

The wind speed and location of the vortex had correlations with SReH in and south of the precipitation area. They also had correlations with Low-Qv in the south of the precipitation area and in the south of the genesis point of vortices. Therefore, proper correction of these values by data assimilation is important to better reproduce the vortex.

Acknowledgements:

The authors thank the members of the second Laboratory, Meteorological Satellite and Observation System Research Department, MRI for providing the Doppler radar data. This study was supported by "Projection of Planet Earth Variations for Mitigating Natural Disasters (Field 3)" in "Strategic Programs for Innovative Research (SPIRE)" and "Tokyo Metropolitan Area Convection Study for Extreme Weather Resilient Cities (TOMACS)".

Keywords: data assimilation, tornado, Doppler Radar

Development of Phased Array Weather Radar and Doppler Lidar Network Fusion Data System

SATOH, Shinsuke^{1*}; YASUI, Motoaki¹; MAENO, Hideo¹; HANADO, Hiroshi¹; TAKAHASHI, Nobuhiro¹; IWAI, Hironori¹; KAWAMURA, Seiji¹; KOJIMA, Shoichiro¹; AMAGAI, Jun¹; TANAKA, Kenji¹; OCHIAI, Satoshi¹; KUBOTA, Minoru¹; IGUCHI, Toshio¹

¹National Institute of Information and Communications Technology

At National Institute of Information and Communications Technology (NICT), we promote advanced research and development of remote sensing technology, to reduce the damage of severe weather disasters caused by localized heavy rainfalls or tornadoes. An industry-academia-government team consisting of Toshiba, Osaka University, and NICT developed one-dimensional phased array weather radar (PAWR) that it is possible to seamless 3D observation in 10 ? 30 seconds. In May 2012, we installed PAWR at Osaka University Suita Campus, and started test observation. From the observation, a first echo appeared in an isolated cumulonimbus cloud was falling to the ground for about 10 minutes. In order to predict the generation point of the cumulonimbus cloud, we need other data which includes wind fields before cloud generation, distributions of water vapor and aerosol, and so on. For that reason, we develop a sensor fusion system with PAWR, Doppler lidar, and others. We install the systems to both NICT Advanced ICT Research Institute (Iwaoka, Nishi-ku, Kobe, Hyogo) and NICT Okinawa Electromagnetic Technology Center (Onna, Kunigami, Okinawa), and install the network data system to NICT headquarters (Koganei, Tokyo).

The sensor fusion system consists of the PAWR antenna in a radome installed on the roof of a 20 m tower, Doppler lidar (Leosphere 400s) on the deck at the height of 15 m of the tower, microwave radiometer to measure water vapor, and sky-radiometer to measure aerosol. Also, temperature, humidity, wind speed components (u, v, w), pressure, rainfall amount, radiation budget, and cloud images (4 directions and whole sky) are measured. All sensors are connected by network for remote operation and automatic data acquisition. The observation data are transferred in real-time through the fast network lines (JGN-X) from Kobe and Okinawa to Koganei for data processing to make a composite map, and so on. The processing data are displayed on a big 4K display TV, and are published using a web server.

We will start test observation after the system completion in March, 2014. At NICT, we also promote research and development of network data system using advanced ICT for big-data processing, transfer, visualization. We give this system a nickname of PANDA: **P**hased **A**rray weather radar and **D**oppler lidar **N**etwork fusion **D**Ata system, and will publish the data from <http://panda.nict.go.jp/>.

Keywords: phased array weather radar, Doppler lidar, network data system, remote sensing, localized heavy rainfall

Campaign Observation at Keihanshin Area for Detecting Convection Genesis

YAMAGUCHI, Kosei^{1*}; NAKAKITA, Eiichi¹

¹Disaster Prevention Research Institute

In 2008, around 50 people who enjoyed sunny days along the riverside were flushed away by a sudden flash flood in a small river channel (Toga River) in Kobe urban area of Japan. This extreme event was a combinational result of steep basin slope, paved urban area, and severely localized heavy rainfall, which is more frequent happening in the recent summer of Japan. There are many short and steep rivers passing through urban areas in Japan, and the most of riverside along these rivers are used as a public open place. Because of the steep basin slope and the paved urban area, only short time of the localized heavy rainfall, such as 30 minutes of rainfall with 50mm/hr of intensity, can cause very dangerous situation in urban areas as in the Toga River case.

In order to prevent such flash flood damages, it is very necessary to detect the rain-cells, which may develop to severe storm, as soon as possible and to alert people to evacuate from riverfront before the severe events occur. In this study, we develop a detection technique for the early stage of rain-cell as the first cell aloft (hereafter, baby-cell) in the middle atmospheric layers before it generates heavy rainfall on the ground. The early detection technique is utilizing the 3-D volume scanning data from X-band Multi Parameter radars (X-MP radars), which are equipped near to the most urban area in Japan recently. In our recent study using the 3-D volume scanning information from the X-MP radars, we have successfully developed an algorithm (1) to detect newly generated baby-cells, (2) to identify dangerous level of the baby-cells, and (3) to trace the movement of the baby-cells.

In the developed algorithm, firstly, the detection of newly generated baby-cells is based on the information of 3-D volume scanning data with very fine resolution of the X-MP radars. Secondly, the identification of the dangerous level, whether the detected baby-cells will grow up to heavy rainfall on the ground, is evaluated with the information of vorticity of the baby-cells based on the Doppler velocity information from the radars. Finally, the tracking of the baby-cells is based on the conventional cell tracking scheme. The preliminary test of the algorithm shows that especially, the identification of the developing baby-cells with the vorticity information is very powerful, and most of baby-cells in the early stage of heavy rainfall events were successfully identified. In detail, all the 19 developing baby-cells under our surveillance were successfully detected, and there was only one false alarm (forecasted as a heavy rainfall event, but it was not).

In our presentation, upgraded performance index of our proposed algorithm will be introduced based on various rainfall events happened in Kyoto and Osaka area, Japan. In addition to improving this practical early detection algorithm for localized heavy rainfall events in urban area, we are conducting newly designed observation combination in Kansai area with numerous sensors and equipments as shown in figure to identify the mechanism of the localized heavy rainfall events in urban area, such as Osaka, Kobe and Kyoto. It is definitely our mission to realize a next-generation operational observation network with different types of sensors for earlier detection and/or prediction of generating storm from the stage of air plume and/or cloud. Presentation partly includes current situation and future plan of a plot type field experiment with X-band- polarimetric radar, Ku-band cloud radar, Lidar, and X-band phased array radar.

Keywords: Radar, Lidar, Videosonde, Urban Meteorology



Analysis of fine-scale airflows over complex topography by super-high-resolution numerical model

TAKEMI, Tetsuya^{1*}

¹Disaster Prevention Research Institute, Kyoto University

With the increase in computational resources, mesoscale meteorological simulations with the grid spacing on the order of 100 m have been conducted not only in idealized studies but also in studies that deal with real cases. In real cases, the benefits from such high-resolution simulations are considered to be better representations of surface topography such as complex terrains and complex distribution of man-made structures. In this presentation, we will demonstrate how fine-scale airflows over complex topography such as terrains and urban districts are represented in numerical simulations of local-scale wind fields under real meteorological settings. Some of the case studies of high wind events are described. For the numerical simulations of specific weather events, we use the Weather Research and Forecasting (WRF) model by downscaling from kilometer-scales to 100-meter-scales with the use of nesting capability. Further downscaling from 100-meter-scales down to 10-meters or higher requires the explicit representation of not only complex terrains but also buildings and structures. For this purpose, we developed an approach to couple a mesoscale meteorological model (i.e., the WRF model) and a computational fluid dynamics (CFD) model (Nakayama et al. 2012). A large-eddy simulation model for airflows over urban geometries (Nakayama et al. 2011) is employed as a CFD model. A unique feature of the present coupling approach, an improved version of the perturbation recycling method of Mayor et al. (2002), is to generate turbulence due to urban-like roughness obstacles with the meteorological effects produced by the mesoscale model being retained. The basic idea of this coupling approach and a case study for a high wind event in the downtown district of Tokyo are demonstrated. Furthermore, some other applications of the present approach for airflow simulations over complex topography including airflows over complex terrain of Fukushima during March 2011 will be briefly introduced.

Keywords: High-resolution numerical model, airflows over complex topography, mesoscale meteorological model, large-eddy simulation

A study on an atmospheric propagation delay estimation method using a fixed radio source

INAKA, Shigeru^{1*}; FURUMOTO, Jun-ichi¹; SEKO, Hiromu²; TSUDA, Toshitaka¹; HASHIGUCHI, Hiroyuki¹; ISHIHARA, Masahito³

¹Research Institute of Sustainable Humanosphere, Kyoto University, ²Meteorological Research Institute, ³Education unit for Adaptation to Extreme Weather Conditions and Resilient Society, Kyoto University

This study aims to develop a new method to observe water vapor horizontal distribution using a side-lobe emission of the 1.3 GHz-band wind profiling radar (WPR). The phase delay of the received side-lobe emission is mainly due to the refractive index fluctuation along the propagation path. In the atmospheric boundary layer, the temporal and spatial non-uniformity of water vapor determines the refractive index fluctuation. Main scope of the study is to extract humidity information from the atmospheric phase delay of side-lobe emission from a WPR. Horizontal humidity distribution can be derived by the data assimilation into numerical prediction model.

The receiver system and data analysis algorithm were developed. A software radio, USRP N200 with an RX daughter board was employed to detect side-lobe emission received by an antenna. A Rubidium frequency standard and a 1 pps signal source of GPS receiver were used for accurate estimation of phase delay variation. The frequency stability of a crystal oscillator, which is generally employed for a reference frequency source of WPR, is insufficient for the accurate estimation. We proposed a new method to compensate the frequency uncertainty of WPR by using data of the additional receiver nearby the WPR site.

IQ data detected by USRP B210 which is controlled by GNURadio, an open source software. By using GNURadio the system will be low cost. The program written in IDL language extracts the temporal variation of the phase delay from the received IQ signal. In order to achieve good performance even in low SNR conditions, we developed an algorithm using STFT (Short-term Fourier transformation) aiming to remove noise in undesired frequency range.

The developed system is promising to derive humidity information from side-lobe emission from various WPRs such as the operational WPR network in Japan (WINDAS (WInd profiler Network and Data Acquisition System)).

Keywords: Wind Profiling Radar, estimation of horizontal humidity distribution, non-hydrostatic forecast model, software radio, side-lobe, propagation delay

Development of a 266 nm Raman lidar for profiling atmospheric water vapor

UESUGI, Takuma^{1*} ; YABUKI, Masanori¹ ; LIU, Yutong¹ ; TSUDA, Toshitaka¹

¹Research Institute for Sustainable Humanosphere

It is projected that localized extreme weather events could increase due to the effects of global warming, resulting in severe weather disasters, such as a torrential rain, floods, and so on. Understanding water vapor's behavior in the atmosphere is essential to understand a fundamental mechanism of these weather events. Therefore, continuous monitoring system to measure the atmospheric water vapor with good spatio-temporal resolution is required. We have developed several water vapor Raman lidar systems employing the laser wavelengths of 355 and 532 nm. However, the signal-to-noise ratio of the Raman lidar strongly depends on the sky background because of the detection of the weak inelastic scattering of light by molecules. Therefore, these systems were mainly used during nighttime.

Hence, we have newly developed a water vapor Raman lidar using a quadrupled Nd:YAG laser at a wavelength of 266 nm. This wavelength is in the ultraviolet (UV) range below 300 nm known as the "solar-blind" region, because practically all radiation at these wavelengths is absorbed by the ozone layer in the stratosphere. It has the advantage of having no daytime solar background radiation in the system. The lidar is equipped with a 25 cm receiving telescope and is used for measuring the light separated into an elastic backscatter signal and vibrational Raman signals of nitrogen and water vapor at wavelengths of 266.1, 283.6, and 294.6 nm, respectively. This system can be used for continuous water vapor measurements in the lower troposphere. This study introduces the design of the UV lidar system and shows the preliminary results of water vapor profiles.

About the approach and the progress of the DoCoMo environmental sensor network

KANO, Kayo^{1*} ; MIYAJIMA, Akiko¹ ; KIKKAWA, Yoshiaki¹ ; TSUBOYA, Hisakazu¹ ; HIGASHI, Kuniaki² ; FURUMOTO, Jun-ichi²

¹Division of life support business promotion, NTT DOCOMO Corporation, ²Research Institute for Sustainable Humanosphere, Kyoto University

Since 2008, the automated meteorological observation network has been developed by NTT DOCOMO corporation and a total of 4,000 stations are operating now.

The hyper-dense wind measurement network was constructed through the industrial-academical corporation between NTT DOCOMO and Kyoto University, which enables us to elucidate the detailed characteristics of strong downslope windstorm, Hira Oroshi, blowing down in the West coast of the Lake Biwa.

This paper discussed the outline of our activities and fruitful results will be discussed in detail.

Keywords: Environmental Sensor Network

Surface Pressure Distributions of Downburst and Tornado captured by High Dense Ground Observation Network "POTEKA"

SATO, Kae^{1*} ; KURE, Hirotaka¹ ; YADA, Takuya¹ ; MAEDA, Ryota¹ ; KOJIMA, Shinya¹ ; MORITA, Toshiaki¹ ; IWASAKI, Hiroyuki²

¹Meisei Electric Co. Ltd., ²Faculty of Education, Gunma University

Meisei developed low-cost compact weather sensor (POTEKA Sta., hereinafter referred to as the POTEKA), which can measure temperature, relative humidity, pressure, sunlight, and rain detection per one minute and achieve higher density weather observation system economically. We installed economical and high dense ground observation network (total 55 stations, 1.5~4 km-mesh) in Gunma, Japan. This paper presents observation of wind gust phenomena around Takasaki city and Maebashi city on 11 August 2013 and tornado in Midori city on 16 September 2013.

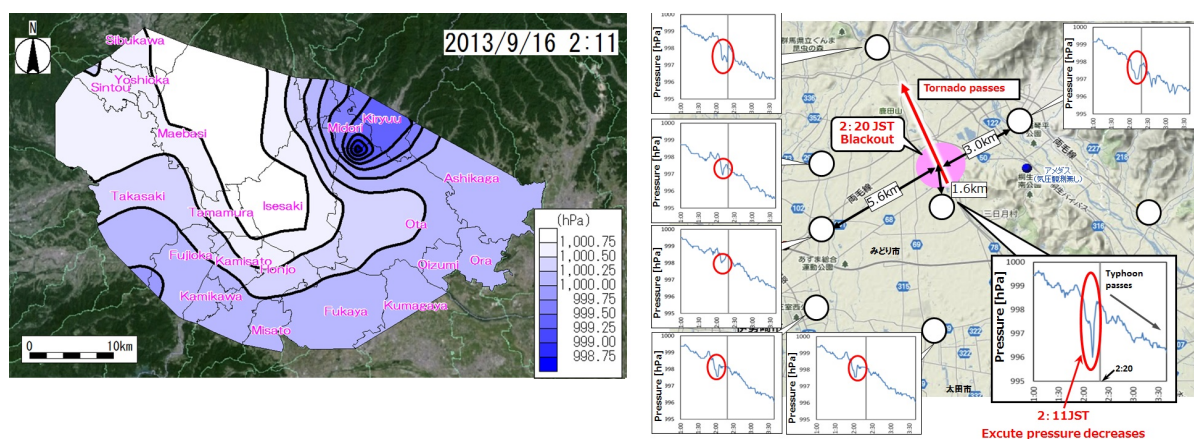
Pressure jumps of 1-2 hPa were recorded at POTEKA with one minute resolution, indicating that the temporal high pressure was caused by downburst downflow. Beside, two pressure jump can be found at some stations. The first and second jumps are coincided with gust fronts and down flow of downburst, respectively (Discrimination between downburst and gust-front by the surface dense observation network POTEKA).

In the September 16, tornado occurred in Typhoon passes, and blackout occurred at 2:20(JST). At the point from 1.2km away, surface pressure was decreasing 3hPa in 3 minutes at 1.6km blackout area away (Fig.)

Local weather observation network consisting of POTEKA succeeded in capturing the change of surface pressure caused by gust wind phenomena with unprecedented spatio-temporal resolution, which enables us not only to distinguish between gust fronts and downbursts but also to detect such wind phenomena earlier. The observation network is going to continue in the future to data accumulation.

Acknowledgments: The authors would like to thank SANDEN Corporation, SAVE ON, and Board of Education of Isesaki city for support POTEKA project.

Keywords: High Dence observation network, Downburst, Tornado



A sensibility study on the role of the urban land surface scheme for a regional climate model, NHRCM

SHIDO, Fumitake^{1*} ; AOYAGI, Toshinori¹ ; SEINO, Naoko¹ ; SASAKI, Hidetaka¹

¹Meteorological Research Institute, Japan Meteorological Agency

The conditions of land surfaces give large impacts on surface air temperature, via the dynamical and thermal energy exchanging. In order to forecast the physical quantities, such as momentum, heat, and vapor fluxes from the land surface, we have selected a sophisticated vegetation scheme of the SiB (Simple Biosphere) as the land surface scheme of the MRI's NHRCM (Non-Hydrostatic Regional Climate Model). Recently, as model-resolution became higher up to several kilo-meter, non-vegetation but urbanized grids had appeared, and these grids were treated as dried bare ground on the SiB to express the so-called urban deserts. But, in these grids, reproducibility of the climatology seemed to be insufficient. Therefore, we need to apply the new scheme to improve the representation of radiation and heat budgets in such urban area. For that purpose, we developed a new scheme for urban land surface to applied to a regional climate model. This new scheme is called SPUC (Square Prism Urban Canopy, Aoyagi and Seino 2011).

In this study, we applied SiB and SPUC scheme to the 4km-resolution NHRCM, executed present climate simulations, and compared outputs with observational data of JMA(Japan Meteorological Agency). The target area was Kanto-Koshin region including Tokyo metropolitan area. As initial and boundary condition, we used the JMA's RANAL (Regional analysis) dataset (20km resolution), which was downscaled once by NHRCM10km with SiB scheme for all grid. The 10km resolution dataset was also downscaled by NHRCM4km. We executed the 4km experiments, using SiB scheme for all land grids (NHRCM-SiB), and using both SiB for natural surface grids and SPUC for urban surface grids (NHRCM-SPUC).Time integration was continuously executed for about 5 years from August 1st, 2001 to September 1st, 2006.

The result of the experiment using SiB scheme had negative bias(about -1.3 °C) in the surface temperature in the Tokyo metropolitan area. By using SPUC scheme, this negative bias changed to positive(+1.55 °C). Although the bias remains, the correlation factor between the simulation and observation was improved from 0.73 (NHRCM-SiB) to 0.86 (NHRCM-SPUC). This improvement implies that NHRCM-SPUC had the better reproducibility on horizontal distribution of air temperature. On the other hand, the difference was hardly seen in total amount of precipitation in five years.

This research is supported by SOUSEI program of MEXT, Japan.

Keywords: regional climate, land surface, downscaling, urban canopy

Temporal and spatial characteristics of gust ratio in the

SAKAMOTO, Hiroto^{1*} ; HIGASHI, Kuniaki¹ ; MATSUI, Kazuyuki² ; KANO, Kayo³ ; TSUBOYA, Hisakazu³ ; FURUMOTO, Jun-ichi¹ ; HASHIGUCHI, Hiroyuki¹

¹Research Institute for Sustainable Humanosphere, ²Environmental Education Working Group in Biwako Region, ³NTT DO-COMO Corporation

Localized downslope wind often causes severe disasters, although the dynamics of these severe phenomena has not fully elucidated due to their small temporal and spatial scale. The damage by downslope wind is strongly determined by the instantaneous maximum wind speed. Since the numerical model can derive averaged wind speed along time and space determined by the model resolution. The classical analogous theory points out that the gust ratio, which is defined as the ratio of maximum wind velocity to the averaged wind velocity, becomes a constant value (1.5-2.0), depends only on the roughness length of surface condition.

In the actual atmosphere with the horizontal inhomogeneity, the gust ratio may varies with time even at the same location. The sophisticated modeling of gust ratio beyond the simple constant model is very important for the forecasting of gust damage. The detailed characteristics of gust ratio was investigated by the data of hyper-dense surface observation network in the Hira Oroshi region. The temporal and spatial characteristics of gust ratio and future prospective to install our algorithm into the numerical prediction models are discussed in the presentation.

An trial of direct monitoring of turbulence intensity by using the balloon-borne high-resolution temperature sensor

FURUMOTO, Jun-ichi^{1*} ; SHIMIZU, Kensaku² ; KAI, Kohei² ; HIGASHI, Kuniaki¹ ; HASHIGUCHI, Hiroyuki¹

¹Research Institute for Sustainable Humanosphere, ²Meisei Electric Corporation

The fine tungsten wire (10 um diameter) temperature sensor, whose response time is 5/1000sec on surface and 40/1000sec at around 30km altitude, were employed to detect turbulence intensities. For the temperture data at the sampling frequency of 16Hz were used for the tuebulence detection. The comtamination of the wake of the ballon should be carefully removed from the original data before the analysis of turbulence.

We are developing the new method to extract temperature purtarvation by turbulence at the vertical wavelength shorter than the effects of pendular movement of radiosondes.

The preliminary results show very promissing to detect turbulence intensities to compare with echo intensity of atmosphere radar.

The detailed scheme and first results are discussed in the presentation.

High resolution numerical study of migrating strong downslope wind "Hira-Oroshi" in Japan

HIGASHI, Kuniaki^{1*} ; FURUMOTO, Jun-ichi¹ ; HASHIGUCHI, Hiroyuki¹

¹Research Institute for Sustainable Humanosphere Kyoto University

This paper studied the generation mechanism of a unique downslope wind in the west coast of Lake Biwa, Shiga, Japan. This strong downslope wind, feared as "Hira-Oroshi" for millennial years shows the narrow gust of a few kilometers in the various location within 10 km width area. This feature cannot be explained by the conventional mechanism of previous studies: the location of downslope wind is strongly restricted by the location of valley in mountain range. Due to such distinct characteristic, the numerical prediction of this gust wind is too inaccurate to use operationally.

Considering strong demands to the prediction of this gust wind, this study aims to elucidate the mechanism via very fine numerical forecast model with the horizontal resolution of 50 m. The results successfully represented the narrow gust wind structure in the edge of the mountain range. The spots of gust wind due to complicated topographical structure is also seen in the simulation results, although the gust wind speed changes with the larger scale wind direction and speed. Because the stagnant region due to the breaking of the mountain wave is widely extended in the leeward of the mountain range in the free atmosphere (~1 km), the location of the gust wind looks to be determined by the detailed topographic structure of the mountain range and the a kilometer-scale eddies over the Lake Biwa.

The simulation results suggested these synergy effects determined the gust generation and its location. The unveiled behavior of the gust wind is also beneficial to the improvement of the gust prediction.

Keywords: High resolution numerical simulation, Downslope wind, Local wind

Modeling of marine biogeochemical and ecosystem in Japan: future perspective and review during the last 20 years

YAMANAKA, Yasuhiro^{1*}

¹Faculty of Earth Environmental Science, Hokkaido University

The first global 3-D marine biogeochemical modeling was developed by Bacastow and Maier-Reimer(1990), and marine ecosystem model was developed by Fasham(1993) as pioneer works, such as Yamanaka and Tajika (1996) and Kawamiya et al.(2000) in Japan. Around 2000, most of marine biogeochemical models have the explicit ecosystem components as well as ecosystem model with focusing short-termed changes in nutrient concentration and pCO₂ associated with spring bloom in sub-arctic regions. And representation of iron cycle was an important issue for both modeling, and trial of coupling between climate and carbon cycles was also started.

Everybody wish to develop the ultimate model explicitly and detailed representing hundreds, thousands, millions of plankton and nekton groups. As the first step, Plankton Functional Types (PFTs) models dealing with relatively small number of plankton and nutrient were introduced (e.g., Le Quere, 2005; Kishi et al., 2007). We have two directions as future model developments for marine biological cycles and marine ecosystem. Former focuses on grouping of phytoplankton having large energy (material) flow, and latter focuses on grouping of zooplankton having the linkage to higher trophic levels such as fish as wood web. If both two directions were covered by the almighty model, we would need unlimited number of prognostic values as plankton number multiplied by elemental components (and grazing-grazed relations proportional to square of plankton numbers). Therefore, model developing along two directions are separated necessarily. We are easily focusing on number of prognostic values as a discussion of model complexity (e.g., Friedrichs et al., 2007). But, we do not forget important improvements led by studying individual process and trade-off problem between parameters. For example, recent studies discussed formulation using affinity instead of half saturation constant as classical Michaelis-Menten formula, unrestricted nutrient uptake optimized by the parameter of restricted nutrient, and different impacts by the global warming between these formulations (Smith and Yamanaka, 2007; Smith et al., 2009). Many people are interesting in another type of models relevant to biodiversity are recently developed (Follows, 2007)

I would like to mention another view such as developing researcher community developing biogeochemical cycles and ecosystem model. Pioneers for marine biogeochemical modeling launched Ocean Carbon cycle Model Intercomparison Project (OCMIP). Studies are led by the pioneers at earlier periods but by young researchers relevant to OCMIP around the end of Phase 2. It goes without say that they are the present world-leading scientists in this academic field (such as Le Quere, Follows, Gruber etc.). MARine Ecosystem Model Intercomparison Project (MAREMIP) as going project is designed based on OCMIP experiences, and next generations figure just in this field. I should mention other groups. I think developing NEMURO, a marine ecosystem model, in North Pacific marine Science Organization (PICES) as another good international collaboration. As for formulating specific processes such as trade-off problem, North Germany group are leading. Finally, I would like to express my wish that next generation in Japan friendly and positively get chance to lead international research projects one of world-leading scientists with their beautiful lives. This is based on my cancelled invited talk in the last year.

Keywords: marine biogeochemical cycles, marine ecosystem, modeling, international research project, OCMIP, MAREMIP

Modeling fish production in the ocean: impacts on biogeochemical cycles and ecosystem service evaluation

ITOH, Sachihiko^{1*} ; ITO, Shin-ichi²

¹Atmosphere and Ocean Research Institute, The University of Tokyo, ²Tohoku National Fisheries Research Institute, Fisheries Research Agency

Marine organisms play fundamental roles in biogeochemical cycles in the ocean. Ecosystem models formulating chemical and biological processes relevant to these organisms and materials have been developed in the past few decades, enabling quantitative evaluation of biological production, carbon and nutrient cycles, and their impact on the climate system. However, many of these models consider trophic levels up to zooplankton. Although much of storage and flux of carbon and nutrients are observed in the lower trophic levels, which is a good reason to focus on this level, importance of higher trophic levels has been increasingly recognized. Here, we review modeling studies incorporating higher trophic levels than zooplankton, especially focusing on fish production models. There are two major motivations developing the fish production model. The first one is that lower trophic level models with zooplankton as the highest trophic level are sometimes controlled too strongly by parameterized zooplankton mortality terms. Although parameterization of mortality terms is needed unless the model contains the apex predator (trophic closure), inclusion of planktivorous fish components does decrease the arbitrariness of the biogeochemical cycle in the model. The second reason to develop fish production models, the more classical reason than the first one, is based on the fact that fish stocks themselves have been major food resources for human societies. In this context, some recent models do not only include commercially important large piscivorous fishes but also consider fishing fleets. Increasing concern for the conservations of marine mammals and sea birds also enhances the model development. There are two different streams of the fish modeling at present: size-based and species-based approaches. We review their advantages and limitations and discuss future improvements of preferable frameworks of the higher trophic models.

Keywords: fish production model, trophic closure, fisheries resources

The iron budget in ocean surface waters in the 20th and 21st centuries: projections by the Community Earth System Model

MISUMI, Kazuhiro^{1*} ; LINDSAY, Keith² ; MOORE, Keith³ ; DONEY, Scott⁴ ; BRYAN, Frank² ; TSUMUNE, Daisuke¹ ; YOSHIDA, Yoshikatsu¹

¹Central Research Institute of Electric Power Industry, ²National Center for Atmospheric Research, ³University of California at Irvine, ⁴Woods Hole Oceanographic Institution

We investigated the simulated iron budget in ocean surface waters in the 1990s and 2090s using the Community Earth System Model version 1 and the Representative Concentration Pathway 8.5 future CO₂ emission scenario. We assumed that exogenous iron inputs did not change during the whole simulation period; thus, iron budget changes were attributed solely to changes in ocean circulation and mixing in response to projected global warming, and the resulting impacts on marine biogeochemistry. The model simulated the major features of ocean circulation and dissolved iron distribution for the present climate. Detailed iron budget analysis revealed that roughly 70 % of the iron supplied to surface waters in high-nutrient, low-chlorophyll (HNLC) regions is contributed by ocean circulation and mixing processes, but the dominant supply mechanism differed by region: upwelling in the eastern equatorial Pacific and vertical mixing in the Southern Ocean. For the 2090s, our model projected an increased iron supply to HNLC waters, even though enhanced stratification was predicted to reduce iron entrainment from deeper waters. This unexpected result is attributed largely to changes in gyre-scale circulations that intensified the advective supply of iron to HNLC waters. The simulated primary and export production in the 2090s decreased globally by 6 and 13 %, respectively, whereas in the HNLC regions, they increased by 11 and 6 %, respectively. Roughly half of the elevated production could be attributed to the intensified iron supply. The projected ocean circulation and mixing changes are consistent with recent observations of responses to the warming climate and with other Coupled Model Intercomparison Project model projections. We conclude that future ocean circulation has the potential to increase iron supply to HNLC waters and will potentially buffer future reductions in ocean productivity.

Response of phytoplankton community structure to global warming

HASHIOKA, Taketo^{1*} ; HIRATA, Takafumi² ; CHIBA, Sanae¹ ; YAMANAKA, Yasuhiro²

¹JAMSTEC, ²Hokkaido Univ.

In recent studies using high-performance liquid chromatography (HPLC) pigment data, empirical relationships between total chl-a concentration and a phytoplankton size/PFT fraction on a global scale are shown. For example, a fraction of diatoms increases with total chl-a concentration. The same tendencies can be seen in the most of the hindcast experiments by current PFT models of MARine Ecosystem Model Intercomparison Project (MAREMIP) and Coupled Model Intercomparison Project Phase5 (CMIP5) although the reproduced absolute values of a phytoplankton fraction still has large uncertainties. Then, two different mechanisms can be expected as potential responses of phytoplankton community to global warming. One is a possibility that the phytoplankton community structure (i.e., relationships between a phytoplankton fraction and total chl-a concentration) can be significantly changed by changes in ecosystem dynamics under global warming condition (e.g., changes in grazing pass/strength, decomposition/mortality/respiration rate and phytoplankton stoichiometry). Another possibility is that the plankton community shifts to the other stable states associated with changes in total chl-a concentration (e.g., by decrease/increase in nutrient supply to the surface ocean by changes in stratification) while maintaining the current relationship between a phytoplankton fraction and total chl-a concentration. To clarify impacts of both effects, we analyzed model results of future simulation, which was conducted by CMIP5 and MAREMIP under the RCP8.5 emission scenario. PFT model more than half showed that relationships between phytoplankton composition and total chl-a concentration are stable against environmental changes associated with global warming. In these model results, changes in phytoplankton composition are mainly caused by plankton community shifts associated with changes in total chl-a concentration. This result suggests the possibility that current empirical relationships obtained by HPLC would be maintained in a future environment. Based on this hypothesis, we project a potential future community structure of phytoplankton using a multi-model ensemble mean of future changes in total chl-a concentration with the empirical relationship of HPLC. Some other models projected large changes in the community structure in specific regions and seasons. These results also suggest potentially important mechanisms, regions and seasons.

Keywords: Phytoplankton, Community structure, Global warming

Introduction to our on-going development of an adaptive model for plankton communities in the North Pacific

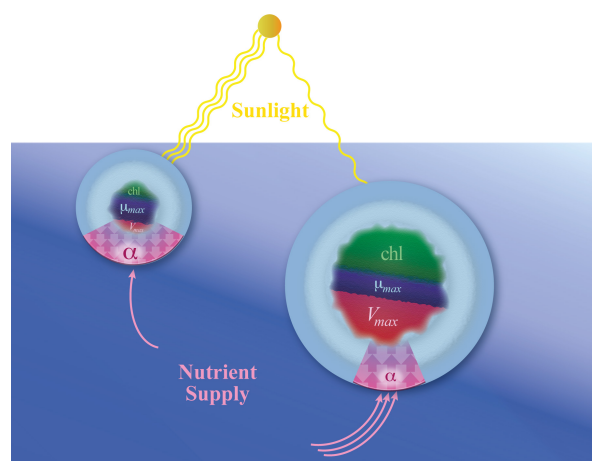
SMITH, S. Ian^{1*} ; YOSHIKAWA, Chisato¹ ; SASAI, Yoshikazu¹

¹RIGC, JAMSTEC, ²CREST, JST

This presentation will introduce our on-going efforts, as part of a CREST project funded by JST, to develop a new prototype model to represent the biodiversity and adaptive capacity of lower-trophic ecosystems in the North Pacific. The ultimate goal is to develop a computationally efficient representation of the community-level interactions of the producers (phytoplankton) and consumers (zooplankton) with each other and with the marine environment. This of course includes the adaptive response of plankton communities to changing environmental conditions, and later potential feedbacks, including for example the impact of plankton communities on controlling nutrient concentrations. We will present the size-based model of phytoplankton communities that is already under development and one scientific result already obtained, regarding the size-scaling of growth parameters, as commonly applied in large-scale models, in terms of the more commonly measured parameters for nutrient uptake kinetics. This scaling relationship provides a basis for consistently incorporating observed allometries into models based on Monod growth kinetics. This new simplified model of phytoplankton communities accounts for biodiversity via size-scaling of phytoplankton traits and for flexibility of the C:N ratio of biomass.

Fig. 1. Traits, which define how organisms respond to environmental conditions, have evolved subject to inescapable biophysical constraints. Thus have arisen trade-offs in competitive ability under different conditions, here illustrated for typical small phytoplankton adapted to low-nutrient, high-light conditions, which have high affinity (α), low maximum uptake rates (V_{max}) and relatively less allocation to chlorophyll/light harvesting ability, vs. large phytoplankton adapted to high-nutrient, low-light conditions, which have low α , high V_{max} , and relatively more allocation to chlorophyll/light harvesting ability. Maximum growth rate (μ_{max}) is constrained by the opportunity cost of allocating resources to the various processes necessary to support growth.

Keywords: plankton, ecosystem, model, traits, trade-offs, adaptive



Exploring mechanisms of phytoplankton coexistence using a marine ecosystem model with eddy-resolving resolution

MASUDA, Yoshio^{1*} ; YAMANAKA, Yasuhiro¹ ; NAKANO, Hideyuki²

¹Hokkaido University, ²Meteorological Research Institute, Japan

Observational studies estimate that there are over 70,000 phytoplankton species. Various mechanisms which enable phytoplankton coexistence are proposed. Niche segregation are inspected under pelagic environment, using a numerical model. Since we considered that variation of pelagic environment resulted in mesoscale eddies plays an important role on phytoplankton diversity, an eddy-resolving model is employed. Based on NEMUEO and MEM, we developed a marine ecosystem model which can express a few hundred phytoplankton species and combined it to a physical oceanic model, MRI.com. The physical field represents idealized subpolar and subtropical gyres in a rectangular model domain of 30 by 30 degrees. To explore niche segregation, we seeded 240 phytoplankton species which have different trait for temperature, light and nutrient. After 10 years integration, 31 species are survived. In the subpolar (subtropical) region, species favorable high (low) nutrient condition are survived. Segregation with temperature is also confirmed.

Keywords: Phytoplankton diversity, Marine ecosystem model, Mesoscale eddy

Numerical analysis of the influences of the meso-zooplankton mortality

YOSHIE, Naoki^{1*} ; TOMITA, Kazuyuki¹ ; OKUNISHI, Takeshi² ; ITO, Shin-ichi²

¹Center for Marine Environmental Studies, Ehime University, ²Tohoku National Fisheries Research Institute, Fisheries Research Agency

In recent years, marine lower-trophic level ecosystem consisting of phytoplankton and zooplankton has been seriously affected by the various environmental changes due to the climate changes and the human activities. The quantitative assessment of the lower-trophic level ecosystem changes with the environmental changes is important for the human beings in the world. This is because the lower-trophic level ecosystem changes closely links to the fisheries resources and the global carbon cycles. For example, copepod which is one of the meso-zooplankton in the lower-trophic level ecosystem is main food for the fishes of good-catch such as Japanese saury and anchovy. Copepod also exports a huge amount of organic carbon from the surface water to the deep water in the ocean by the seasonal vertical migration to around 1000m depth and the rapid sinking fecal pellet. We have been developing a plankton functional types (PFTs) model which explicitly calculates each functional group of organisms such as copepod above. In particular, we developed a PFTs model eNEMURO (4-Nutrient, 4-Phytoplankton, 4-Zooplankton, 4-Detritous), which was an extend version of NEMURO [a standard lower-trophic-level marine ecosystem model of PICES (The North Pacific Science Organization)] by introducing the microbial food web and the phosphorous cycles and dividing diatoms to two compartments according to temperature dependency. eNEMURO successfully reproduced the spatio-temporal variations in the lower-trophic level ecosystem around Japan. In this study, we investigated the influences of the meso-zooplankton mortality which was little known from the filed observations and the laboratory experiments on the lower-trophic level ecosystem. We conducted the sensitivity analysis of two parameters of the meso-zooplankton mortality in eNEMURO in five regions with different types of the lower-trophic level ecosystem around Japan. Model result shows that the increase of the meso-zooplankton mortality associated with water temperature rising has large impacts on the nutrients concentrations, the biomasses of phytoplankton and zooplankton, especially in the regions with the high temperature. We also introduce results from the biological parameters optimization of eNEMURO using the genetic algorithm method.

A benthic-pelagic coupled ecosystem model to clarify nutrient cycles in coastal areas

TATENO, Satoshi^{1*} ; HATA, Kyoko¹ ; NAGAO, Kentaro¹

¹IDEA Consultans, Inc.

In many enclosed coastal seas in Japan, coastal environments have changed due to an increase in nutrient loading and land development after the 1960s. This caused a loss of material cycle balance, generation of red tides, anoxic conditions, and hydrogen sulfide. Water quality has been gradually improved because of some policies such as water quality standards and water pollution control laws, but the loss of balance remains in many areas. It is because various factors such as the benthic system, fishery industry, and the open sea of the areas affect it.

We developed a benthic-pelagic coupled ecosystem model to clarify the role and the contribution of them. The model also included important factors for the coastal environment as dissolved oxygen, oyster, and eelgrass.

It was developed for Mitsu Bay area in the western part of Seto Inland Sea. In this area, oyster culture is distributed widely. Model results indicated that the most important factor for the material cycles was advection from outside the area. Nutrient load had a lower impact than advection and oyster. Anoxic water did not appear, but the oyster culture caused accumulation of organic matter on the sediment under oyster rafts and hydrogen sulfide production. It was suggested that control of it is important to improve the material circulation and keep it in balance.

Keywords: Marine Ecosystem Model, Marine Material Cycles

A challenge to investigate environmental factors which determine spawning migration variability of small pelagic.

ITO, Shin-ichi^{1*} ; OHNO, Sohsuke¹ ; OKUNISHI, Takeshi¹ ; SUYAMA, Satoshi¹ ; NAKAGAMI, Masayasu¹ ; AMBE, Daisuke¹ ; KAMEDA, Takahiko¹ ; KAKEHI, Shigeo¹

¹Fisheries Research Agency

In recent years, lower trophic ecosystem models, which represent phyto and zoo-plankton, have been coupled to fish growth-migration models. These coupled models enable to elucidate fish response to climate variability. However, mechanisms of fish migration has not been well clarified. Especially the mechanisms of spawning migration, by which spawner fish can home on to their spawning grounds, are one of the most difficult behavior to represent by a numerical model. Using realistic initial and boundary condition, an Euler-type model of Pacific saury was applied to investigate environmental factors which determine spawning migration variability. The initial distribution of Pacific saury was defined by synoptic surface trawl surveys and satellite derived environmental conditions were used as forcing; sea surface temperature (SST), prey density estimated from surface chl-a concentration and surface current speed. Growth of Pacific saury was calculated by a fish bioenergetics model (NEMURO.FISH). A fitness algorithm was applied for feeding migration in which the fish are assumed to be moving towards a place with optimal growth condition. A larvae fitness algorithm was applied for spawning migration in which the spawning fish moves to a place of the optimal growth of larvae. For spawning migration, westward migration was added to reproduce realistic spawning grounds around Japan Islands. Strength of the westward migration was adjusted to realize observed variability of saury migration to fishing grounds. The adjusted westward migration variability showed high correlation with basin wide SST in the North Pacific. This result suggested a strong influence of climate to fish spawning migration.

Keywords: ecosystem model, fish growth-migration model, Pacific saury, ocean environment

Impacts of global warming on fisheries estimated from climate models: An application to Japanese scallops in Hokkaido

SHIBANO, Ryota^{1*} ; FUJII, Masahiko¹ ; YAMANAKA, Yasuhiro¹ ; YAMANO, Hiroya² ; TAKAO, Shintaro¹

¹Faculty of Env. Earth Sci., Hokkaido Univ., ²NIES

Climate change such as global warming is considered to affect marine ecosystem. For example, rise in seawater temperature in future may change distributions of marine species. We estimated the impacts of global warming on Japanese scallop, *Mizuhopecten yessoensis*, in Hokkaido. Japanese scallops are important target species for Japanese fisheries resources. Combining sea surface temperature output obtained from climate models and simplified indices that express distribution of Japanese scallops, we estimated suitable domains for Japanese scallop fisheries. We found rise in water temperature from 1990 to 2100 has an impact to aquaculture industries of Japanese scallops across Hokkaido. This study suggests a simplified method to estimate distributions of coastal marine species and the importance of observed data in the future projection.

Keywords: Global warming, Fisheries resources, Japanese scallop, CMIP5

Interannual variations and its control factors of evapotranspiration in a temperate Japanese cypress forest

TSURUTA, Kenji^{1*} ; KOSUGI, Yoshiko¹ ; TAKANASHI, Satoru² ; TANI, Makoto¹

¹Graduate School of Agriculture, Kyoto University, ²Forestry and Forest Products Research Institute

1.Introduction

Evapotranspiration from forests is a major factor affecting water yield and therefore water resources. Understanding the long-term impacts of variations of meteorological factors on variability of evapotranspiration is important, especially in the context of current and future climate change. Long-term continuous measurements of evapotranspiration using the eddy covariance method provide an opportunity to examine the response of forest ecosystem processes to climate change. We quantified the interannual variations of evapotranspiration, and examined its control factors using the multi layer model.

2.Material and methods

Observations were made in the Kiryu Experimental Watershed in the south of Shiga Prefecture, central Japan. The forest around the watershed comprises mainly 50-year-old Japanese cypress forest. A meteorological observation tower is located in the watershed. The fluxes of momentum, sensible heat, latent heat, and CO₂ were measured using eddy covariance methods at a tower height of 28.5 m. Precipitation was observed at the open site.

We used the multi layer model to clarify the control factors of interannual variations of evapotranspiration. The model contained sub-models that calculated the gas exchange processes, including H₂O and CO₂ exchanges of leaves and the ground surface. This multi layer model simulates the above-canopy fluxes based on vertical profiles of meteorological factors. This model requires the above-canopy environmental variables as the input data. The parameters representing leaf gas exchange characteristics are determined by leaf gas exchange measurements. We used 7 years of eddy covariance data (from January 2001 to December 2007) in this study.

3.Results and discussion

Annual evapotranspiration for the seven years ranged between 715 (2001) and 780 mm (2004) with the average of 743 mm. Maximum interannual fluctuation in evapotranspiration was 75 mm.

Diurnal, seasonal, and interannual variations of evapotranspiration for the seven years were reproduced by a model simulation. This indicates that the model structure and parameterization are validated.

We calculated the components of evapotranspiration such as transpiration, evaporation, and soil evaporation. Each component shows interannual variations relating to meteorological factors. Wet years such as 2001 and 2002 had small annual evaporation and large annual transpiration. Dry years such as 2003 and 2006 had large annual evaporation and small annual transpiration. Both annual evaporation and transpiration were relatively large in 2004. Annual soil evaporation was slightly smaller than evaporation and transpiration. Interannual fluctuations in soil evaporation were also small compared with evaporation and transpiration.

We examined seasonal variations of evapotranspiration for the contrasting two years; 2004 and 2003 with maximum and minimum annual evapotranspiration simulated, respectively. The deviations of evapotranspiration for the two years were large in summer from June to August. Transpiration increased with vapor pressure deficit and solar radiation. Transpiration was relatively small in 2003, which had low vapor pressure deficit and solar radiation in the summer. Transpiration was relatively large in 2004, which had high vapor pressure deficit and solar radiation in the summer. Soil evaporation for the two years showed the similar seasonal variations with transpiration. Seasonal variations of evaporation were the similar to those of precipitation.

Each component of evapotranspiration showed different responses to the meteorological factors seasonally and annually. Interannual variations of evapotranspiration were almost explained by those of meteorological factors.

Keywords: Evapotranspiration, Interannual variation, Eddy covariance, Multi layer model, Japanese cypress forest

Evapotranspiration and water use efficiency on a coniferous planted forest watershed in south western Japan

SHIMIZU, Takanori^{1*}; TAMAI, Koji¹; KUMAGAI, Tomo'omi²; ISHIZUKA, Shigehiro³; OHTANI, Yoshikazu¹; SHIMIZU, Akira³

¹Forestry and Forest Products Research Institute, ²Hydrospheric Atmospheric Research Center, Nagoya University, ³Kyushu Research Center, Forestry and Forest Products Research Institute

Japanese cedar (*Cryptomeria japonica* D. Don) and Japanese cypress (*Chamaecyparis obtusa* Endl.) are the most popular planted species in Japan. These species cover about 20% of the land surface of the country. On a mountainous topography which is common in Japan, Japanese cedar was usually planted from valleys to lower hillsides with relatively wet and fertile soils, while Japanese cypress was planted on the drier and more nutrient poor ridge areas. Accordingly, evapotranspiration (*ET*) and carbon assimilation may be variable in the two species.

We applied multiple methods to estimate *ET* from a planted forest watershed located in Kyushu Island, south western part of Japan. The watershed existed on mountainous terrain, and the right bank was mainly covered with well-grown Japanese cedar while the larger part of the left bank was covered with relatively less-grown Japanese cypress. We applied the eddy covariance method, using an observation tower built in the center of the watershed. The eddy covariance data were experimentally divided to two sectors by wind direction, right bank side and left bank side of the watershed, and the lack of data for each wind sector were interpolated by the mutual imputation method. The analysis period in this study is 2007-2008. Within the period, the rainfall interception loss (I_c) and sap-flux density were also measured in Japanese cedar plots, and the lower canopy *ET* was estimated by a model. From the eddy covariance result, *ET* from the left bank side was estimated as 85% of that from the right bank side in the period. Compared the right bank side *ET* with the combination of I_c , upper- and lower-canopy *ET*, the difference in annual total *ET* was about 1% when global solar radiation (S_d) was greater than 0, which assured the accuracy of the eddy covariance method even over the complex terrain.

As for carbon assimilation, we simultaneously measured CO₂ flux and CO₂ concentration profile by using the observation tower. Based on the measurements, we can estimate the CO₂ exchange between the forest and atmosphere through the similar procedure to *ET*. Thus in this study, we will estimate the carbon budget and calculate the water use efficiency of the whole ecosystem of the watershed and of the both bank sides. From the tentative result obtained at present, the average NEE of the left bank side was 87% to that of the right bank side, in the daytime ($S_d > 0$) in 2007-2008. From the value and the aforementioned *ET* ratio (0.85), the water use efficiency of the both bank sides were might be almost the same as each other. In the presentation, we will discuss about the detail, considering the respired CO₂ in the nighttime and the rainfall interception in the Japanese cypress plot.

Keywords: Planted coniferous forest stand, Growth difference, Water vapor flux, Carbon dioxide flux, Water use efficiency

Water budget and the consequent canopy duration period in a teak plantation in a dry tropical region

TANAKA, Katsunori^{1*}

¹Japan Agency for Marine-Earth Science and Technology

A soil-plant-air continuum multilayer model was used to numerically simulate canopy net assimilation (A_n), evapotranspiration (ET), and soil moisture in a deciduous teak plantation in a dry tropical climate of northern Thailand to examine the influence of soil drought on A_n . The timings of leaf flush and the end of the canopy duration period (CDP) were also investigated from the perspective of the temporal positive carbon gain. Two numerical experiments with different seasonal patterns of leaf area index (LAI) were carried out using above-canopy hydrometeorological data as input data. The first experiment involved seasonally varying LAI estimated based on time-series of radiative transmittance through the canopy, and the second experiment applied an annually constant LAI. The first simulation captured the measured seasonal changes in soil surface moisture; the simulated transpiration agreed with seasonal changes in heat pulse velocity, corresponding to the water use of individual trees, and the simulated A_n became slightly negative. However, in the second simulation, A_n became negative in the dry season because the decline in stomatal conductance due to severe soil drought limited the assimilation, and the simultaneous increase in leaf temperature increased dark respiration. Thus, these experiments revealed that the leaflessness in the dry season is reasonable for carbon gain and emphasized the unfavorable soil water status for carbon gain in the dry season. Examining the duration of positive A_n (DPA) in the second simulation showed that the start of the longest DPA (LDPA) in a year approached the timing of leaf flush in the teak plantation after the spring equinox. On the other hand, the end appeared earlier than that of all CDPs. This result is consistent with the sap flow stopping earlier than the complete leaf fall, implying that the carbon assimilation period ends before the completion of defoliation. The model sensitivity analysis in the second simulation suggests that a smaller LAI and slower maximum rate of carboxylation likely extend the LDPA because soil water from the surface to rooting depth is maintained longer at levels adequate for carbon gain by decreased canopy transpiration. The experiments also suggest that lower soil hydraulic conductivity and deeper rooting depth can postpone the end of the LDPA by increasing soil water retention and the soil water capacity, respectively. These hypotheses will be verified based on observations.

Keywords: canopy duration period, carbon gain, dry tropical region, soil-plant-air continuum system, teak plantation, water budget

Influence of canopy interception on the recovery in water balance after clear-cutting at a small headwater catchment

ODA, Tomoki^{1*} ; EGUSA, Tomohiro¹ ; OHTE, Nobuhito¹ ; HOTTA, Norifumi² ; TANAKA, Nobuaki³ ; GREEN, Mark⁴ ; SUZUKI, Masakazu¹

¹Graduate School of Agricultural and Life Sciences, The University of Tokyo, ²Faculty of Life and Environmental Sciences, University of Tsukuba, ³Ecohydrology Research Institute, The University of Tokyo Forests, Graduate School of Agricultural and, ⁴Center for the Environment, Plymouth State University

The impact of forest disturbance on stream runoff has been well studied using the paired catchment approach, usually finding increased stream runoff following forest disturbance due to the decline of transpiration and canopy interception. However the recovery processes of transpiration and interception have rarely been directly observed under a recovering forest, therefore mechanisms behind recovery time of stream runoff following forest cutting is still not well understood. The objective of this study is to evaluate the contribution of interception to the change of stream runoff after forest cutting. This study was conducted in a pair of small headwater catchments, where one catchment was clear-cut in 1999 and planted with the same species in 2000. Annual runoff increased 200 to 300 mm/yr after forest cutting and the higher runoff remains 12 years after cutting. Interception ratio in the clear-cut catchment were lower than 10 % of precipitation in 2007, 2011 and 2012, and those in the control catchment were 20 to 24 % of precipitation. The mean annual interception was still around 300 mm/yr smaller in the young forest compared to the mature forest, although canopy cover and LAI were similar. These results suggested that the recovery of interception rate is an important controlling factor for the recovery of stream runoff after forest cutting, and not only canopy structure, but also the microclimate condition above the canopy of young forest could be also important factors affecting interception.

Keywords: forest cutting, water balance, canopy interception, headwater catchment

Changes in interannual variability of runoff in a conifer and deciduous hardwood mixed forested watershed

NOGUCHI, Shoji^{1*} ; MURAKAMI, Wataru¹ ; TANI, Makoto²

¹Forestry and Forest Product Research Institute, ²Graduate School of Agriculture, Kyoto University

The National Forest Management conducts forest management in National Forests for the fulfillment of multi functional roles of forest including long-term wood production management. On the other hand, there are few studies that evaluated the runoff characteristics including a state of the forest for a long term. This study was conducted within the Kamabuchi No1 experimental watershed (3.06ha) in North part of Japan. Hydrological observation has been continued in cold snowy region since 1939. It is the longest record in this region in Japan. The site is covered with Natural hardwood forest (ex. *Fagus crenata*, *Quercus mongolica* var. *grosseserrata* and *Quercus serrata*) and coniferous plantation forest (*Cryptomeria japonica* and *Chamaecyparis obtuse*) which planted around 1912 to 1916. Surficial geology is tuff and shaletic tuff of the Tertiary period and soils are clay loam. Meteorological observation was conducted Yamagata experimental forests located to 800m from the watershed to the northeast. A 71-year record (1939-2010) of the precipitation and runoff was used for an analysis of the flow-duration curve. Tree (DBH \geq 6cm) census in the watershed was also conducted at 5 times (1942, 1950, 1957, 1979, 2008). The tree volume of *Chamaecyparis obtuse* is a regular tendency and the tree volume of *Cryptomeria japonica* linearly increased. Stem volume of oak trees has increased remarkably from 1942 to 1979 but there was a close tendency of an increase in 2008 because mortality of oak trees occurred in the watershed. Based on 5 times tree census, positive linear relationship was found between tree volume and age of stand. While the proportion of plentiful runoff has shown a tendency to decrease over long term, those of ordinary, low and scanty runoffs have tended to increase with increasing the tree volume.

Keywords: duration curve, cold snowy region, long term hydrological observation, runoff characteristics

Is there any general rainfall-runoff response function in mountainous catchments?

UCHIDA, Taro^{1*} ; ASANO, Yuko² ; KANBARA, Jun'ichi¹ ; TOMOMURA, Mitsuhidde³

¹National Institute for Land and Infrastructure Management, ²University of Tokyo, ³Meteorological Engineering Center

Clarifying rainfall-runoff response function in mountainous catchments is one of key issues for flood and sediment disaster prediction, management of aquatic environment, water supply and so on. So, rainfall-runoff response function in mountainous catchments has been debated in more than several decades. A variety of studies, observation, modeling, theoretical studies etc., has been conducted. Many noble efforts have been conducted for clarifying complex systems in catchment hydrology through intensive observations. These observations were effective for documentation of the idiosyncrasies of each catchment environments. However, it has been difficult to derive general rainfall-runoff response function from these basin-centric approaches. So, several researchers emphasized the importance of intercomparison so as to better see first order controls of hydrologic responses. Except for several exceptions, intercomparisons for rainfall-runoff responses in many catchments are still limited. Thus, still it is very hard to predict rainfall-runoff response function at ungauged basin.

Thus, we compiled rainfall and stream flow data for around 150 catchments in Japan. We focused relatively small catchment (<100 km²) and a variety of geological, topographical and climatic conditions. We removed catchments where strongly affected human activities, such as urbanized catchment etc., from our intercomparison.

In this study, we randomly sampled 10 storms, i.e., total rainfall amounts were large than 50 mm, for each catchment and calculated three indices, peak specific discharge, peak lag time and direct runoff ratio, to characterize rainfall-runoff response. Also, we defined rainfall-runoff responses using three reservoirs model. We parameterized all of catchments using four storms data using SCE-UA method and validated these parameters using other four storms data. Then, we tested the roles of rainfall condition, climate, geology and topography on rainfall-runoff responses. We used multiple regression analysis to define first order controls of rainfall-runoff responses.

We found large variability in rainfall-runoff responses and it is hard to define general response patterns. While, through multiple regression analysis, we found several interesting results, as follow;

-Climatic conditions affected peak specific discharge and direct runoff ratio, suggesting that climate might give impacts on hydrological characteristics soil and bedrock.

-Geology, such as type of rocks and geological age, gave impacts on rainfall-runoff responses, but effects of geology were not so large, although many study focused on rock-controls on hydrology.

-Flowpath length, calculated by DEM, was one of important topographic parameters for describing rainfall-runoff responses.

Keywords: headwater catchment, rainfall-runoff response, database, multiple regression analysis

A method of generating virtual drainage-basin by introducing models of slope/stream evolution

NAKAKITA, Eiichi^{1*}

¹Eiichi Nakakita

A method of generating virtual drainage basin to understand relationship among characteristics of geomorphic distribution, rainfall distribution, and runoff distribution was developed. Here the concept of generating virtual drainage-basin is that the drainage-basins are generated at random under some physically based conditions on the basin form. The method is an improvement of Nakakita and Matsuda (2007). They proposed the method of generating virtual drainage-basin based on erosional developing model of channel network by Horton (1945). For the improvement, mathematical models of evolution of slopes and streams were introduced into the methodology. As a result, we achieved to introduce the concept of time into the generating virtual drainage-basin model.

Keywords: drainage basin, landform evolution, channel network, slope evolution, longitudinal profile

Rock control, denuded hillslope and discharge system in warm humid regions

IIDA, Tomoyuki^{1*}

¹Center for Research in Isotopes and Environmental Dynamics, University of Tsukuba

Under humid and warm regions as Japan, a stable discharge system of seepage water in hillslope is maintained by not only geophysical structures(soil and weathered layer) but also biological system such as forest. From long term point of view, topography, soil, ecosystem and water discharge system play hydro-geomorphological interactions directly or indirectly to one another. In the discharge system, both macro and micro pores of soil layer or weathered bedrock play especially important roll, which controls the permeability and storage capacity under the ground. Among them, natural pipes consisting of continuous macro pores play a roll in the water discharge during a heavy rainfall event. The capillary water stored in micro pore can be used by trees in dry season. These macro pores and micro pores are made by physical and chemical weathering processes. However, biological weathering is the most important for the development of these pores in soil. Forest ecosystems can evolve a matured soil system from soil particles in order to adjust a suitable environment for their own lives. Because the tree root system needs not only water but also enough air, an efficient discharge system may be created as one of the most important environment. This discharge system changes as follows according to the rainfall conditions.

1) In the case of usual storms: The discharge system is stable and it can discharge successfully the seepage water.

2) In the case of unusual heavy storms: The slope failure may occurs due to increasing of water pressure when the water table of throughflow, rises or the pipe-discharge system becomes plugged and partially destroyed. However, this system is recovered with the recovery of forest and soil. This can be called a healthy feedback. The humid and warm climate suitable for forest contributes much to these recovery. Therefore, this feedback can control the expansion of a denuded area made by a slope failure and a wide denuded area may not be naturally developed.

3) In the case of unusual heavy storms in bare lands created by severe human activities: In this case, especially in granite area or the Tertiary area, an unhealthy feedback acts because the critical threshold of healthy feedback is exceeded. Then, the bare land expands rapidly throughout a mountain area. It is almost impossible for forest and soil to be recovered naturally. Human afforestation work is necessary. Such hillslopes were founded in the wide area of Japan till the second half of 20th century. There is no stable discharge system in such bare hillslopes. Consequently, frequent occurrence of overland flow surface flows caused severe floods and soil hazard.

The discharge system seems to be made as a part of hillslope development. The geological character of the bedrock and the climate (rainfall and temperature) play an important roll in making of the discharge system. This system can be considered as one of the effects of rock control.

Keywords: hillslope hydrogy, discharge system, rock control, bare land, ground structure, hydro-geomorphological interaction

The making method of two dimensional distribution map of the collapse prevention force with tree survey

ATSUJI, Makoto^{1*} ; KITAHARA, Hikaru² ; ONO, Hiroshi²

¹Graduate School of Agriculture, Shinshu University, ²Faculty of Agriculture, Shinshu University

The collapse prevention force of the forest root system is a grand total of the pulling out resistance of each root per vertical cross section (1m^2) of soil layer. The pulling out resistance of root (T, N) shows a following equation using root diameter (D, mm), $T=aD^{1.6}$, varies in the coefficient by a tree class. The quantity of root system is distributed concentrically from the tree center and decreases for distance from tree exponentially.

Here I propose the two dimensional distribution map of the collapse prevention force with only the ground information of tree survey, breast height diameters and distribution of trees.

I performed an investigation that each in 3 Hinoki artificial plantation stand and 1 natural broadleaf forest, and made a two dimensional distribution map of the collapse prevention based on the tree positioning and the diameter of trees at breast-height. And I compared which I got by investigating every tree and compared the outcome of maps and the actual measurement that I dug a trench. As a result, the estimated values and the actual values did not exactly match, however a very meaningful relation was seen in both value within 1% of the risk ratio.

Furthermore, I applied this method and estimated a chronological order change of the collapse prevention force. Because the data required for estimating the ability of collapse prevention are only positioning of the trees and diameter measurement at trees breast-height, I can even estimate a change in the result after thinning, by using it in conjunction with the growth prediction by the density management curve.

Keywords: root system, collapse prevention force, artificial plantation, natural forest, two dimensional distribution map

The growth-collapse simulation method of soil depth in which the effect of vegetation was taken into consideration

KUROKAWA, Ushio^{1*}

¹Kyushu Research Center, FFPRI

The impact accompanying the transition of the watershed conditions in a forest appears under the structurally development process of a triplex in which time scales differ; geographical feature is formed by a tubercle and erosion of a mountain, the soil which supports and grows up in the root system of a vegetation repeats a collapse and a renature, the forest grows and withers. Without understanding this process, the runoff impact evaluation of watershed conditions cannot occur. We paid our attention to the collapse process in which a soil grows up again, after the soil was supported by the root of the forest, grew up and collapsed with progress of a temporal. And the development method of the longterm soil growth simulation was considered.

This method is computed for every mesh. The following routines perform the compute process of geomorphic development. First, the amount of growths of the soil stratum in the fixed period in each mesh is computed. The amount of developments of the soil depth used the equation of the following which Heimsath et al. (1999) proposed.

Soil Production(m/million year)= $77 \times \exp(-0.024 \times \text{Soil Depth})$

The soil depth after a fixed period is computed by applying to the initial soil depth of each mesh the value calculated by the equation. Slope stability is computed using the soil depth set up newly. It is considered by the equation that the mesh by which the safety factor was computed or less with one is that to which the collapse occurred. After setting the value of the soil depth in the mesh to 0, the altitude data after a collapse and a soil depth are re-calculated. A prolonged soil development simulation is computed by repeating the predetermined number of these processes. The simulation was computed at the place which many shallow landslides caused by heavy rainfall. The initial soil depth in the mesh which the collapse caused by the heavy rain was set to 0, and the mesh which has not collapsed was set to 1 m. And, the soil layer assumed the condition of being completely saturated by the heavy rain. In addition, the effective soil internal angle was 32 degrees, effective soil cohesion was 0.01 kPa, unit weight of the moist soil was 17.64 kN/m^3 , and unit weight of water was 9.8 kN/m^3 . The effect of the vegetation was included in the simulation as the cohesion.

As results of the simulation, It was confirmed that the soil layer which collapsed with progress of the temporal is recovered. Moreover, when a vegetation does not exist, the probability that a soil layer will repeat a collapse becomes high, but when a vegetation exists, a soil layer does not collapse but is recovered early.

Keywords: soil depth, geographical feature, vegetation, simulation method

Limits of Soil Production and the Couplings with Hillslope Hydrology

HEIMSATH, Arjun^{1*}

¹School of Earth and Space Exploration, Arizona State University

Rocky mountain ranges are broken down to sediment that is ultimately removed to the sea. Tectonic forces continually push mountains up, while physical and chemical processes continually transform bedrock to sediment and move it down. This simple sounding cycle is thought to regulate global climate over long timescales, while also responding to climate forcing itself, although the causal direction remain a mystery despite decades of sleuthing. Similarly mysterious are the connections between mechanisms of sediment production and the responses of watersheds to changes driven by humans, climate, or tectonics.

To address some of the potential connections between sediment production and hillslope hydrology, I focus here on soil mantled and steeply sloped landscapes from around the world, some thought to be at a critical threshold of soil cover. Observations reveal that even in the most rapidly eroding landscape there are significant areas mantled with soil that fit the conceptual framework of a physically mobile layer derived from the underlying parent material with some locally-derived organic content. The extent and persistence of such soils depends on the long-term balance between soil production and erosion despite the perceived discrepancy between high erosion and low soil production rates. I present cosmogenic Be-10-derived soil production and erosion rates that show that soil production increases with catchment-averaged erosion, suggesting a feedback that enhances soil-cover persistence, even in threshold landscapes. I also show that a process transition to landslide-dominated erosion results in thinner, patchier soils and rockier topography, but find that there is no sudden transition to bedrock landscapes. The landslide modeling is combined with a detailed quantification of bedrock exposure for these steep, mountainous landscapes.

To conclude, I draw an important conclusion connecting the physical processes producing and transporting soil and the chemical processes weathering the parent material by measuring parent material strength across three different field settings. Parent material strength is observed to increase with overlying soil thickness and, therefore, the weathered extent of the saprolite. Soil production rates, thus, decrease with increasing parent material competence. These observation highlight the importance of quantifying hillslope hydrologic processes where such multi-facted measurements are made.

Keywords: Soil erosion, Soil production, Critical Zone, Weathering, Hillslope hydrology, Saprolite

Soil production functions and soil layer mobility in Japanese mountainous catchments underlain by granitoid rocks

MATSUSHI, Yuki^{1*} ; MATSUZAKI, Hiroyuki²

¹DPRI, Kyoto University, ²MALT, The University of Tokyo

Soil-mantled hillslopes cover a major area of mountainous catchments in humid temperate regions. The soil layer on hillslopes is maintained by a balance between soil production and transport especially at hill noses, while the soil accumulated in hollows is eventually removed by a rainfall-induced shallow landslide. The rates of soil production and soil creep pace the growth of soil thickness at a hollow and thus determine the return period of landsliding. The soil layer buffers rainfall infiltration into hillslopes and hence controls subsurface runoff system in a catchment. Hydro-geomorphological evolution of a catchment results from the interaction between long-term soil layer development and short-term rainfall runoff processes. The quantification of soil dynamics on hillslopes is thus critical in understanding present-day hydrological condition of a catchment and for geomorphological landslide hazard mitigation.

The uppermost part of decomposed bedrock (saprolite) gradually disintegrates to form the mobile soil layer, which achieves to a steady-state thickness reflecting sediment budget at a soil column. The saprolite-to-soil conversion rate beneath a soil column decreases with increasing thickness of the soil layer, which is called as soil production function (SPF). Soil particles apart from the saprolite move downslope by soil creep at a rate controlled by slope gradient, biological activity and soil thickness. Evaluation of SPF as well as the soil layer mobility is essential when we simulate soil dynamics on a hillslope. SPF can be determined from concentration of terrestrial cosmogenic nuclides at uppermost part of saprolite, while soil layer mobility can be estimated by soil thickness survey by digging pits on a nose-hollow pair of hillslopes. We present examples of SPFs in Japanese mountainous catchment underlain by granitic rocks, and demonstrate results of simulation of soil development to map potential sites of shallow landslide and to assess volume of sediment that may yield at a catastrophic landslide event by heavy rainfall.

Keywords: soil production function, terrestrial cosmogenic nuclides, sediment transport, shallow landslide, landscape evolution

Interrelation between hillslope soil moisture and stream flow in a Paleozoic sedimentary rock watershed

HOSODA, Ikuhiro^{1*}

¹Kansai Research Center, FFPRI

It is well known that geology is one of influential factors on river regime. In the Paleozoic sedimentary rocks area in Japan, hydrographs are characterized by low base flow and spiky peak flow. To clarify the reasons of such characteristics occur, observation focused on hillslope soil moisture condition was conducted in the gauged Tatsunokuchi-yama Minami-tani watershed (34° 42' N, 133° 58' E, 50-257 m, 23 ha) underlain by Paleozoic sedimentary rocks. The watershed is covered with primarily *Quercus serrata* dominant mixed forest, and partly *Chamaecyparis obtusa* stands planted in 1970s. Annual precipitation is about 1200 mm with little snowfall.

Ground water levels (GWL) and soil moisture were continuously measured in and around boreholes in a concave slope in the middle reach. Deeper than 0.3 m from ground surface, a thick fractured and weathered bed rock layer extends down to about 10 m at upper slope, and about 16 m at mid-slope. Below the weathered bed rock layer, boring core was relatively unweathered. But conspicuous cracks were obviously seemed to perform as water flow pathway because the surface of crack was dyed. Low coefficients of permeability which ranged from 2^{-8} to 1^{-6} m/s were measured by in situ test in the boreholes.

In the mid-slope, GWL appeared about 15 to 17.5 m in depth from ground surface when surface soil layer was more than field moisture capacity. Although GWL greatly respond to about over 40 mm rainfall events, direct flow rate did not simply increased. In a little antecedent rainfall condition, GWL rising was detected only at the lower slope. Depending on increase of antecedent rainfall, fluctuations of GWL at the mid-slope and the upper slope became obvious, and also direct flow rate went up. The greater amount of rainfall including antecedent rainfall was brought, the more GWL rising belated to stream flow peak observed. The greater intensity of rainfall leads quick rising of stream flow, but it was not effective for GWL rising. According to the stream water quality, rain water component increased when intense rain was brought, subsequently ground water component increased for the duration of rainfall event.

It is realized that water movement is having macroscopic interrelation in the space from upper slope to stream channel. Its complexity would be derived from large soil moisture change by rainfall amount and vegetation activity in the thick weathered bed rock layer in the hillslope as water flow pathways. And it is considered that since the permeability of subsoil is low, stream flow respond by spiky peak against intense rainfall.

Keywords: permeability, soil water pF, ground water, Seto inland sea climate, Tatsunokuchi-yama

Variability of the chemistry of streamwater and bedrock groundwater at a weathered granite mountain, Japan

FUJIMOTO, Masamitsu^{1*} ; KOSUGI, Ken'ichirou² ; MASAOKA, Naoya² ; BANBA, Naoki¹ ; UEDA, Ryuya¹ ; SAKAI, Yasuhiro¹ ; FUKAGAWA, Ryouichi² ; TANI, Makoto¹

¹Ritsumeikan University, ²Kyoto University

Introduction

Previous studies have noted that bedrock groundwater is one of the important factors influencing stream discharge and streamwater chemistry. However, most previous studies were conducted not by direct measurement of bedrock groundwater but by using indirect methods, such as solute tracers and water budget analysis. Thus, the movement and chemical characteristics of bedrock groundwater remain incompletely understood based on direct measurements of bedrock groundwater. To better understand the dynamics of bedrock groundwater, we investigated groundwater table movement and water chemistry of bedrock groundwater using dense borehole wells at a small catchment in a mountainous area.

Methods

The study was performed at the Fudoji Experimental Watershed located in the Tanakami Mountains in the southeastern part of Shiga Prefecture, central Japan. Precipitation was monitored using tipping-bucket rain gauges, and discharges were observed at eight small catchments, ranging in area from 0.1 to 2.3 ha. Seven small catchments (subcatchments) were included in the largest catchment (2.3 ha), within which we installed 61 borehole wells. The water table of bedrock groundwater was then observed at these borehole wells. Rainwater, streamwater from the small catchments and bedrock groundwater from the borehole wells were sampled, and the concentrations of major ions and SiO₂ as well as the water stable-isotope ratios δ¹⁸O and δD were measured in the Graduate School of Agriculture, Kyoto University.

Results and Discussion

The results of the analysis of the groundwater table of bedrock groundwater indicated that there were several fluctuating characteristics and that these characteristics of groundwater table change had locality. At the area having higher altitude in the ridge, the bedrock groundwater-table changes were gradual but the ranges of fluctuation were larger than those of the lower wells. At the lower-altitude points, although the bedrock groundwater table responded rapidly, the ranges of fluctuation of the groundwater table were small relative to those of the higher points. Some areas responded only to peak rainfall over a short time. Based on the groundwater flux analysis, bedrock groundwater moves across the surface divide. A catchment inflowed by a neighboring catchment showed a high specific discharge. Additionally, the direction of groundwater movement changed during rainfall events, and such changes were similar for rainfall events of the same size.

The relationships among chemistries derived from the chemical weathering of bedrock indicated that although the weathering processes were similar in the catchment, the weathering level varied among the borehole wells. The chemistries of bedrock groundwater at each catchment and of streamwater at each catchment showed large variability. The concentrations of Na⁺ and Ca²⁺ had local characteristics, but no clear characteristics were observed among other bedrock groundwater components. The chemical concentrations of bedrock groundwater were higher than those of streamwater. We chose borehole wells that may contribute directly to the stream based on the direction of groundwater movement by an analysis of groundwater flux and distance from the borehole wells, and noticed that there were also large gaps between the chemistries of streamwater and bedrock groundwater. These results indicate that complex processes of chemical dynamics occur in the weathered bedrock and from the weathered bedrock to the stream.

Keywords: weathered bedrock, densely bore holes, chemical variability, bedrock groundwater

Mean residence time and hydrochemistry of bedrock groundwater aquifer in a Granite mountain

KATSUYAMA, Masanori^{1*} ; KOSUGI, Ken'ichiro² ; TANI, Makoto²

¹Center for the Promotion of Interdisciplinary Education and Research, Kyoto University, ²Graduate School of Agriculture, Kyoto University

Bedrock groundwater dynamics is one of the latest frontier of hillslope- and catchment hydrology. Although it relate to water resources as well as sediment disasters, only few studies have accessed directly with boreholes to bedrock groundwater aquifer because of, for example, high costs. In this context, tracer approach is effective to clarify the bedrock groundwater dynamics and water pathways within deeper layers of mountains. We have been keeping on monitoring of the chemical and isotopic compositions of bedrock groundwater and streamwater in Kiryu Experimental Watershed (KEW), Japan since 2003. We set up a nested observation system; a hillslope plot (AP, 0.024ha), a subcatchment (A catchment, 0.086ha), and whole of KEW (K catchment, 5.99ha), and monthly sampled the streamwater of K and A, the outflow from AP, which occurs as saturated throughflow on the soil-bedrock interface during rainstorms, and groundwater in the soil sediment. Moreover, we excavated the bedrock and installed some tension lysimeters at 0.1, 0.2, 0.4, and 0.8 m deep and boreholes at 12, 15, and 20 m deep below bedrock surface, and sampled them. The stream flow from K and A were perennial. The SiO₂ and Na⁺ concentrations increased along with the infiltration process. On the other hand, the NO₃⁻ concentration was highest at the surface soil water, and removed along with the infiltration process. The concentrations of both solutes in the streamwater from A and K were intermediate between the concentrations in the surface soil water and bedrock groundwater. These facts mean that the streamwater is the mixture of shallow soil water and deep groundwater. The mean residence times calculated by delta 18O variations were about 4 or 5 months in the groundwater in the soil sediment and in the shallow (<0.8m) bedrock groundwaters, about 50 months in 12- and 15 m deep, and about 120 months in 20 m deep, respectively. That in the streamwater in A was estimated as about 30 months. Thus, the MRT in 20 m deep groundwater is quite different from the others. The relationship between the MRTs and the solute concentrations were different in each solute; for SiO₂, the concentration increased as a saturation curve, and it increased as linearly for Na⁺. It exponentially decreased for NO₃⁻. The streamwater chemistries in A were on these curves. Therefore, the solute concentrations can be described as functions of MRTs. These results suggest that a part of the bedrock groundwater can contribute to the stream from the shallower layers. The fact that the stream flow is perennial in this subcatchment A means that plentiful supply of groundwater from the relatively shallow bedrock layers exist. On the other hand, other part of the bedrock groundwater infiltrate deeply and less contribute to the stream in this small subcatchment; we have to consider whether the deeply infiltrated groundwater may contribute at the outlet of K catchment. Moreover, as the deeper bedrock groundwater have especially long residence time, we have to keep long-term monitoring to understand the dynamics and roles of this groundwater to hydrological and hydrochemical processes, because it will be a key of spatio-temporal scaling of these processes, as well as the water yield function of forests.

Keywords: Bedrock groundwater, Tracer, Mean residence time, granite catchment

Hydrological change at the catchment scale: The need to address both velocity and celerity

MCDONNELL, Jeffrey^{1*}

¹Global Institute for Water Security, University of Saskatchewan CANADA

Water quantity and quality response to climate- and land use change are difficult to predict. Much of this relates to the complexities of water flow paths and our inability to relate measureable catchment properties to measureable hydrologic response metrics. To date, most work has focused on rainfall-runoff response — that is, the celerity component of change. Here I present new work from 15 headwater catchments, (0.1 to 100 km²) in the Oregon Cascades and Oregon Coast Range in the USA, aimed at quantifying both celerity and flow velocities (i.e. particle transport through the system). I illustrate this velocity component through stable isotope analysis of runoff components and the mean transit time and residence time analysis of surface water and groundwater, respectively. Results show that despite very similar rainfall-runoff determined celerities, these systems have distinctly different tracer velocities, where transit time of headwater streamflow is 1-3 years in the catchments draining the Western Cascade mountains and 3-11 years in the streams draining the Coast Range mountains. More importantly, the scaling of surface water mean residence time in the Cascades is linked to internal topographic structure of individual sub-catchments whereas Coast Range sites show no evidence of this; and streamwater residence times scale linearly with catchment area. I discuss the implications of these celerity-velocity differences for catchment-scale climate- and landuse change effects in the USA Pacific Northwest and for more general efforts like the IAHS Panta Rhei initiative.

Keywords: Hillslope, Rainfall-runoff, Stable isotope, Climate change, Landuse, Groundwater

Toward understanding causal interrelationships between stormflow and erosion processes in a steep zero-order basin

TANI, Makoto^{1*}

¹Graduate School of Agriculture, Kyoto University

Stormflow generation and soil-erosion process on a steep zero-order basin have close interdependencies though their timescales are far different. This study pays attention to a difference in interdependences of stormflow and erosion processes between a near-ridge nose and a concave hollow within a zero-order basin.

Due to strong erosional forces in an active tectonic region, soil moves down by the gravity force throughout the basin. In a convex nose near the ridgeline, soil moves gradually by diffusive processes, and the curvature of bedrock surface controls the soil depth (Heimsath, *Geomorphology* 27, 1999). On the other hand, in a concave hollow, soil layer suddenly collapses as a landslide and a long-term soil-layer evolution at a timescale of 10^2 - 10^4 years continues unless a landslide occurs (Tsukamoto et al., *IAHS Publ.* 137, 1982). In the nose, the soil layer may move downslope with vegetation on it without disturbances. The recovery of soil layer after a landslide occurrence in a hollow is supported by the soil supply from the nose by the diffusive movement. The diffusive process near nose and the recovery process near hollow are closely related each other.

In order to ensure these processes, saturation excess overland flow should be suppressed both in a nose and a hollow because it is a trigger of landslide initiation. We can assume that the drainage capacity through pipe-like preferential paths (McDonnell, *Water Resour. Res.* 26, 1990) plays an important role in the suppression.

One hydrological analysis for addressing the assumption is attempted from estimating the expansion of stormflow contribution areas from rainfall-runoff responses in a small catchment. In the wet conditions when most of all the rainfall contributes to the stormflow, a hydraulic continuum under a quasi steady state is created and a single tank model can well simulate rainfall-runoff responses (Tani: *Hydrol. Earth Syst. Sci.*, 17, 2013). This simple characteristic was utilized to estimate the contribution-area expansion with rainfall increases inversely from the runoff responses.

Results show that except a short dry period at the beginning of a storm, the waveform transmission of rainfall to runoff was simulated well by the same model parameters of our tank model though the contribution area only increased. This result suggests the waveform transmission was originated mainly from the vertical water movement instead of the downslope subsurface flow or the overland flow. As suggested from a conceptualized model (Montgomery and Dietrich, *Water Resour. Res.* 38, 2002), rainwater may be confined within the soil layer due to a large drainage capacity of the pipe-like preferential paths. This strongly encourages the soil-layer evolution process against strong erosional forces not only in a nose but also in a hollow.

Runoff and erosional processes are certainly linked, and collecting field evidences is expected. In addition, however, reanalyzing the existing hydrological data may also provide a new interesting finding from the linking point of view.

Keywords: erosion, hillslope hydrology, soil-layer evolution, stormflow, variable contribution area, zero-order basin

Interaction between bedrock groundwater and surface-hydrological and geomorphological processes in mountainous headwater

KOSUGI, Ken'ichirou^{1*} ; FUJIMOTO, Masamitsu² ; YAMAKAWA, Yosuke³ ; MASAOKA, Naoya¹ ; ITOKAZU, Tetsushi¹

¹Kyoto Univ., ²Ritsumeikan Univ., ³Tsukuba Univ.

Enormous landslides with deep slipping surfaces, which are likely to be triggered by the huge storms expected with climate change, can be one of the major geomorphological processes in the temperate climate zone. This study focuses on groundwater in mountainous headwater regions as a potential cause of such landslides. Recent hydrological studies have revealed that large amounts of rainwater infiltrate into bedrock, suggesting the possibility that steep mountains could contain greater amounts of groundwater than previously thought. The decline in groundwater levels due to water harvesting should be effective for the prevention of landslides. At the same time, the exploitation of groundwater resources in mountainous regions may contribute to establish a sustainable supply of safe water; that is, groundwater in mountainous regions is of better quality and less vulnerable to pollution because human activities are limited in the source areas. Thus, the exploitation of groundwater resources in mountainous regions should produce a win-win situation that achieves both disaster mitigation and a sustainable water supply. This study investigates hydrological methods for observing and analyzing quantitative and qualitative signals in mountain streams that can be used for detecting groundwater dynamics in steep mountains. Such hydrological methods are effectively combined with geophysical surveys.

In the steep Rokko mountain range of central Japan, which consists of granite and has been greatly affected by diastrophic activities, discharge hydrographs are characterized by significant amount of baseflow. In order to elucidate contributions of bedrock groundwater to the hydrograph formation, long-term hydrological observations were conducted by using bedrock wells with depths of 7-78 m drilled at 31 points within a 2.1-ha headwater catchment in the Rokko mountain range. Results indicated a fairly regionalized distribution of bedrock groundwater; that is, upper, middle, and lower aquifers were present. We observed large differences in water level among the aquifers, instead of a gradual and continuous decline in water level. Discharge hydrograph from the catchment was notably characterized by gentle and significant variations in base flow and exhibited triple-peak responses. Flashy first peaks occurred just after rainfall peaks, while the second peaks lagged behind the rainfall peaks by a few days. Broad peaks in the base-flow discharge corresponded to the third peaks, which occurred once or twice in each hydrological year. The triple-peak discharge responses were explained by three types of water pathways: the first peak was caused by the peak in soil mantle groundwater around the outlet of the watershed; the second peak was caused by the first peak in the lower aquifer, which was fed by vertical rainwater infiltration; and the third peak was caused by the second peak in the lower aquifer, resulting from an increased lateral water supply from the middle aquifer. The middle aquifer was recharged by vertical infiltration through weathered bedrock and lateral flow from the upper aquifer. Because of its broad regional expanse and large capacity, the middle aquifer had a dominant effect on formation of the discharge hydrograph. Thus, this study has demonstrated how discharge from the steep headwater catchment is dominated by complex flow systems within bedrock groundwater; the spatial expanse of bedrock aquifers and interaction among aquifers are key factors.

Keywords: enormous landslide, geomorphological processes, headwater catchment, bedrock groundwater, water resources

Evaluation of transpiration in a mature stand of Japanese cedar in Kanto region, Japan

IIDA, Shin'ichi^{1*}; SHIMIZU, Takanori¹; TAMAI, Koji¹

¹Department of Soil and Water Conservation, Forestry and Forest Products Research Institute

Forests cover about 70% of land area of Japan, and Japanese cedar (*Cryptomeria japonica*) occupies about 20% of total forested area. To understand the hydrologic cycle in Japan, we need measurements conducted in forested area, especially for the most representative species of Japanese cedar. Recently, the water balance of a stand of Japanese cedar has been made clear quantitatively by using eddy-covariance method and sap flow technique in Kyushu Island, south-western part of Japan (Kumagai et al., 2014; Shimizu et al., submitted). However, although Japanese cedar is most representative species in Japan, very few studies have been carried out in other part of the country. Based on the sap flow technique, we started to evaluate the amount of transpiration of a stand of Japanese cedar located in Kanto region, in the central part of Japan. In this paper, we show the relationship between outermost sap flow (Q_{0-20}) and single-tree transpiration (Q), tree-size parameter affecting Q , and correlation between stand transpiration (TR) and meteorological factors.

We conducted measurements in a mature stand of Japanese cedar, whose age is 61, within Tsukuba Experimental Watershed located in southern part of Mt. Tsukuba, Japan. Tree density is 1115 trees/ha, and annual mean leaf area index measured with LAI-2000 (LI-COR, USA) is 3.6. We set an observation plot in a Japanese cedar stand, and measured sap flux densities for all trees of the plot, 13 trees, with Granier method (Granier, 1985). Based on the wood core sampling with an increment borer, we determined the width of sapwood for 13 trees. Japanese cedar has white zone, in which water movement stops, in the sapwood area. We injected acid fuchsin into stem, and distinguished colored area as sapwood. The length of Granier sensor was 20 mm: in case that the width of sapwood was more than 20 mm, additional sensors were inserted into the sapwood at the depths from 20 to 40 mm and 40 to 60 mm. The sap flow at each depth is calculated as the product between the sapwood area corresponding to the depth and measured sap flux density. Q is finally obtained as total sum of sap flow of all depths. We calculated TR as the sum of Q of 13 trees divided by the area of the plot. On the meteorological tower, air temperature, humidity and net radiation were measured. Analyses are performed in the period from August to November, 2013.

The value of $Q/(Q_{0-20})$ had positive linear relationship with canopy projection area unshaded by other trees (CPA_{TH}). This trend implied that the contribution of Q_{0-20} to Q is small for trees having good light condition. Q had positive linear correlation with diameter at breast height ($R^2=0.62$), however, the higher correlation ($R^2=0.70$) was found between Q and CPA_{TH} . In this stand, CPA_{TH} is probably important factor affecting distribution of sap flow within the stem and tree-to-tree difference in Q . On the other hand, through the analysis period, TR had high positive correlation with equilibrium evaporation ($R^2=0.83$), but had lower correlation ($R^2=0.39$) with vapor pressure deficit (D). Focused on the summer period from August to September, we found higher correlation between TR and D ($R^2=0.74$). Thus, in summer, the driving energy of transpiration is mainly D due to the large aerodynamic conductance at the stand. However, the correlation between TR and D became small in the autumn. This stand is located in the north-facing slope, and has very high contrast in meteorological condition between summer and autumn. The different relationship between TR and D probably implies that plant physiological response of Japanese cedar in summer is different from that in autumn.

Cited paper

Granier 1985. Ann. Sci. For. 42: 193-200.

Kumagai et al. 2014. J. Hydrol. 508: 66-76.

Shimizu et al. Submitted for publication.

Keywords: Japanese cedar, sap flow, transpiration, tree-size parameter, vapor pressure deficit

SURFACE RUNOFF ESTIMATION BASED ON TOTAL RAINFALL-TOTAL LOSS RAINFALL RELATIONSHIP FOR CATCHMENTS IN ISHIKARI RIVER

SUPRABA, Intan^{1*} ; YAMADA, Tomohito J.²

¹Member of JSCE, M.Sc., Doctoral Student, Graduate School of Engineering, Hokkaido University, ²Member of JSCE, PhD., Associate Professor, Faculty of Engineering, Hokkaido University

One of the main objectives of research in hydrology is to improve the accuracy of surface runoff estimation for enhancing flood prediction. Rain water falling to the ground surface will infiltrate into the soil and the excess rainfall will be surface runoff. The infiltrated water is defined as loss rainfall and loss rainfall is subtracted from total rainfall (actual rainfall intensity) to obtain the surface runoff (excess rainfall intensity). The non-linearity of surface runoff phenomena in the mountainous basins based on universal lumped kinematic wave model has been studied. Current study about total rainfall-total loss rainfall relationship by using tanh fitting curve has been conducted for 65 catchments located in 27 prefectures in Japan. Hourly rainfall and hourly runoff observation data for 10 years during summer time is used as required input data. Runoff parameters in the tanh function represented by a and b parameters are utilized to estimate effective rainfall based on water holding capacity theory. The purpose of this study is to estimate surface runoff by using effective rainfall for semi-ungauged river basins at the upper catchments area in Ishikari River Basin, Hokkaido Island, Japan. The obtained results are compared to the observation data for validation purpose.

Keywords: Surface Runoff, Flood Prediction, Total Rainfall-Total Loss Rainfall, Water Holding Capacity Theory

Integrate simulated annealing algorithm and WASH123D to develop an automatic identification system for Chuoshui River in

CHANG, Ya-chi^{1*} ; WANG, Yu-chi¹ ; CHEN, Cheng-hsin²

¹Associate Researcher, Taiwan Typhoon and Flood Research Institute, NARL, Taiwan, ²Assistant Researcher, Taiwan Typhoon and Flood Research Institute, NARL, Taiwan

Taiwan is located in the subtropical areas and often suffers from typhoons and heavy rains. In order to reduce the threat caused by typhoon, it is necessary to accurately estimate the water level of a river for flood disaster prevention and mitigation. Hydraulic analysis of a river is important in river management planning and engineering design. The identification of hydraulic parameter has huge impact on the water level estimation of a river during the hydraulic analysis. Manning's roughness coefficient is usually used to describe a river's surface roughness and sinuosity in hydraulic modeling. This coefficient is usually determined empirically in the past, which is tedious and time-consuming. Therefore, the optimization algorithms become an effective tool for engineers to select the Manning's roughness coefficient.

The concept of simulated annealing algorithm (SA) is based on an analogy to crystallization process of the physical annealing from a high temperature state. Since SA has the Metropolis mechanism to escape local optimum trap, it has been applied to various types of optimization problems. In addition, the hydraulic model plays a crucial role for flood simulation and the WASH123D, an integrated multi-media, multi-processes and physics-based computational model suitable for various spatial-temporal scale, is selected in this study to simulate the water level. The purpose of this study is to integrate SA and WASH123D to develop a system for automatically identifying the optimal Manning's roughness coefficients of the reach according to the given upstream and downstream boundary conditions of the river. Firstly, the cross sections and related hydrological data of the river are collected for flood hydrograph simulation in WASH123D and make sure the model can be executed for the reasonable range of the Manning's roughness coefficient. Then, the system incorporates SA with WASH123D to identify the optimal Manning's roughness coefficient according to the objective function for minimizing the difference between observed and simulated water level. The system is applied to the Chuoshui River in Taiwan. Flood in two typhoon events is simulated and the flood hydrograph is analyzed in this study to find the optimal Manning's roughness coefficient. Results demonstrate that the system proposed in this study has feasibility to automatically identify the Manning's coefficient.

Keywords: Simulated annealing algorithm, WASH123D, Manning's roughness coefficient, Automatic identification system

Groundwater levels and qualities in megacities of Korea

YUN, Sang woong^{1*} ; JEON, Woo-hyun¹ ; LEE, Jin-yong¹

¹Department of Geology, Kangwon National University, Republic of Korea

This study was conducted to evaluate the groundwater levels and groundwater qualities in six metropolitan cities (Seoul, Busan, Daegu, Incheon, Daejeon and Ulsan) of Korea. For this purpose, we collected the groundwater level data of 2001-2011 from the Korean National Groundwater Monitoring Stations in the cities and semi-annual groundwater quality data analyzed by the Korean Ministry of Environment for the same period. Using these collected data, we analyzed the change in the water levels in and outskirt of the cities and in groundwater qualities in the cities. The groundwater levels in the outskirt were generally higher (0.84-15.66 m bgs), compared with those in the central part of the city (3.89-75.16 m bgs), and well responded with the seasonal rainfall (higher in the summer but lower in the winter). However, the groundwater levels in the central part of the city were largely affected by pavement, deep underground building such as subway, and artificial pumping, not by the seasonal effect. The six metropolitan cities showed ranges of 0-507 mg/L and 0-22,000 mg/L for NO₃-N and coliform, respectively. In addition, groundwater contamination with TCE (0.00-4.50 mg/L), PCE (0.00-0.48 mg/L) and 1.1.1 TCA (0.00-0.11 mg/L) was also found. The groundwater contamination with these contaminants was relatively severe especially in Seoul and Busan, which may be attributed to their high densities of populations and industrial facilities. This research was supported by Basic Science Research Program through the National Research Foundation of Korea (NRF) funded by the Ministry of Education (NRF-2011-0007232).

Keywords: groundwater levels, qualities, metropolitan cities, contaminants, Korea

Variation in groundwater-stream water interaction with season: focus on water level, temperature and chemistry

JEON, Woo-hyun^{1*} ; YUN, Sang woong¹ ; LEE, Jin-yong¹

¹Department of Geology, Kangwon National University, Republic of Korea

This study was conducted to reveal seasonal variations of the groundwater and stream water interaction in Gangwon province of Korea using analyses of measured water levels, water temperature and water chemistry from August to November of 2013. For measuring the water levels in the hyporheic zone, four piezometers (IYGW-1~4) were installed at depths of 0.830~1.565 m below stream bed, perpendicular to stream flow direction and the stream level was also measured at IYSW-1. The water level and water temperature were measured every hour using an automatic logger (DIVER). In addition, nearby groundwater, hyporheic water and stream water were collected for ion and stable isotope analyses in the wet (September) and dry seasons (November) along with field measurements of pH, EC, DO and ORP. The water levels of the piezometers generally increased with rainfall, and they were lower than the stream water level in September, indicating a losing stream, but the former was higher than the latter in November, indicating a gaining stream. The reversal of the heads occurred at October 10. The stream water temperature (IYSW-1), directly affected by the surrounding air, was between 0.9~22.9 °C with a large fluctuation. However, the hyporheic water (IYGW-4; 1.565 m depth) showed a small range of 13.2~17.8 °C. The water temperature at IYGW-4 was lower than those of the other piezometers but the reversal of the water temperatures also occurred at October, like the water levels. The groundwater, hyporheic water and stream waters were all classified as Ca-HCO₃ type by Piper diagram, which is indicative of effect of ambient air. The EC of IYGW-4 was the highest (136.7 μS/cm), indicating relatively higher influence of the groundwater. This research was supported by Basic Science Research Program through the National Research Foundation of Korea (NRF) funded by the Ministry of Education (NRF-2011-0007232).

Keywords: hyporheic zone, interaction, groundwater, piezometer, Korea

Change of groundwater condition by operation of geothermal heat pump

PARK, Youngyun¹ ; MOK, Jong-koo² ; PARK, Yu-chul² ; LEE, Jin-yong^{1*}

¹Department of Geology, Kangwon National University, Republic of Korea, ²Department of Geophysics, Kangwon National University, Republic of Korea

This study was conducted to evaluate the influence of open loop geothermal cooling and heating system (OLGCHS) and closed loop geothermal cooling and heating system (CLGCHS) on temperature and water level of local groundwater. For this study, groundwater temperature and level were measured daily using level logger at two sites where OLGCHS and CLGCHS are installed for approximately 30 months. In OLGCHS, fluctuation of groundwater temperature was similar to seasonal variation of ambient air temperature. However, this is not attributed to influence of air temperature. The groundwater temperature was fluctuated according the load of OLGCHS. The groundwater temperature was largely changed by operation of OLGCHS in summer compared to those in winter. These results represent that load of OLGCHS in summer is larger than that in winter. The groundwater levels were mainly controlled by precipitation and were slightly influenced by operation of OLGCHS. In CLGCHS, the groundwater temperature and level did not affected by operation of CLGCHS. The groundwater temperature was changed with 3°C. The groundwater level was mainly influenced by precipitation because groundwater is not used directly in CLGCHS. In addition, response of groundwater level for precipitation was slower than those at OLGCHS because of difference of hydraulic conductivity. These results show that groundwater temperature and level did not significantly changed by OLGCHS and CLGCHS. However, it is necessary that long-term monitoring of groundwater temperature and level at sites, where OLGCHS and CLGCHS are installed, because OLGCHS and CLGCHS can affect the hydrological properties of aquifer with scale and type of use of geothermal energy. This work is supported by the Energy Efficiency and Resources of the Korea Institute of Energy Technology Evaluation and Planning (KETEP) grant funded by the Korea government Ministry of Knowledge Economy (No.20123040110010) and by the Korean Ministry of Environment under "The GAIA project (No. 171-101-011)".

Keywords: open loop geothermal cooling and heating system, closed loop geothermal cooling and heating system, time series analysis, groundwater level, groundwater temperature, Korea

Impact of ground source heat pumps operation on groundwater condition

KIM, Namju^{1*} ; PARK, Youngyun¹ ; JEON, Woo-hyun¹ ; YUN, Sang woong¹ ; LEE, Jin-yong¹

¹1Department of Geology, Kangwon National University, Republic of Korea, ²Geo Engineering Co. Ltd

This study was conducted to summarize status of installation of open loop geothermal cooling and heating system (OLGCHS) and to evaluate impact caused by its operation on groundwater condition. In this study, six facilities where OLGCHS is installed were considered. Groundwater is directly used in OLGCHS. The facilities considered in this study have been operated over two years. Groundwater temperature ranged from 6.0 to 24.2oC. Water temperature of natural groundwater and groundwater used to operating of OLGCHS showed difference of 5 to 9oC. pH and EC ranged from 7.5 to 9.1 and from 138 to 465 uS/cm, respectively. pH and EC of natural groundwater and groundwater used to operating of OLGCHS did not show significant difference. All groundwater meet Korean standard of water quality for domestic purpose In addition, saturation indexes of most major dissolved components except H₄SiO₄ showed lower than 1. These results represent undersaturated condition and that there are no minerals which can be precipitated from groundwater used in OLGCHS. Consequently, impact of ground source heat pumps operation on groundwater condition do not observed. However, these monitoring have been conducted continuously because contamination by ground source heat pumps operation can occur in any time. This work is supported by the Energy Efficiency and Resources of the Korea Institute of Energy Technology Evaluation and Planning (KETEP) grant funded by the Korea government Ministry of Knowledge Economy (No.20123040110010).

Keywords: Heat pump, groundwater, ground source

Change of the stream discharge process affected by the rainstorm magnitude in the small headwater catchment

KUDO, Keishi^{1*} ; SHIMADA, Jun¹ ; TANAKA, Nobuhiro²

¹Kumamoto University, ²Kumamoto prefecture office

Recently, because rainstorm characteristics such as total and peak rainfall is increasing along with global warming, a lot of disaster as flood and landslide has been occurring in many areas worldwide. This change might engender changes in the water resource of a particular area. Therefore, this study was conducted for the two component hydrograph separation using EC value during rainstorm event between July 2012 and November 2013 in two small adjacent forest and grassland catchments at the headwaters of the western foot of Mt. Aso, Kumamoto prefecture, southwestern Japan, aims to understand the relationship between the groundwater discharge ratio and rainstorm magnitude. EC values of the stream water were recorded at 10-min interval at each Parshall flume using EC logger. We compared our results and data which we summarized, with published literature (Onda et al.,2006; Ichianagi and Kato, 1998; Ichianagi et al.,1994; Iwagami et al.,2010; Ohruai et al.,1992; Katsuyama et al.,2000; Katsuyama et al.,2001).

We observed 18 rainstorm events of varied magnitude in which total rainfall range from 9 mm to 727 mm and peak rainfall range from 5 mm/h to 94 mm/h. As a result, we reaffirmed that the groundwater discharge ratio decreased due to increase total rainfall and peak rainfall for small rainstorm event where total and peak rainfall were less than 200 mm and 20 mm/h respectively, and agreed with previous studies. The total discharge also increased in conjunction with an increase of "new water" component. However; increasing of groundwater discharge ratio was observed for large rainstorm event where total and peak rainfall were larger than 200 mm and 20 mm/h, respectively. In this case, the total discharge increased in conjunction with an increase of "old water" component. Therefore, we found that the rainstorm magnitude has an impact on the formation of the peak stream discharge during rainstorm. The peak stream discharge phenomena from catchment can be classified into two stages based on previous literature and our present studies. In the first stage, stream discharge is dominated by the old water before rainstorm, but the old water component of stream discharge decrease gradually with an increase of rainstorm magnitude. As the total rainfall reach 200 mm, most of stream discharge is dominated by the new water. Under larger rainstorm events, additional stream discharge increased in conjunction with an increase of "old water" component (the second stage).

Keywords: Two component hydrograph separation, Stream discharge process, Rainstorm magnitude, Groundwater discharge

General discussion on insight into change and evolution in hydrology

TANI, Makoto^{1*}

¹Graduate School of Agriculture, Kyoto University

Fluctuations in the water and chemical cycles including floods, droughts, and water-quality impacts are influenced by long-term changes and/or evolutions in catchment properties and climate conditions. For example, to predict stormflow responses only from the catchment topography is difficult because the runoff mechanism is strongly controlled by bedrock-weathering and soil-evolution processes.

Such a concept of change and evolution is raised by IAHS, called 'Panta Rhei,' as its decadal initiative from 2013 following PUB (Predictions in ungauged basins), and the international discussions have started.

In parallel with this activity, we are now conducting a project on dependences of rainfall-runoff responses on a temporally-nested structure of topographic, soil, and vegetation developments under the JSPS budget from 2011 to 2015.

In this session, presentations addressing effects of natural changes and their interactions on the water and chemical cycles are encouraged, and changes originated from human influences including the disturbances and managements are also welcomed.

Keywords: general discussion

Radon Concentration around Tachikawa Active Fault

TSUNOMORI, Fumiaki^{1*}

¹Graduate School of Science, University of Tokyo

Characteristics of a radon concentration distribution around the Tachikawa active fault will be focused in this report.

According to the Headquarters for Earthquake Research Promotion, occurrence potentials of earthquake in active faults in Japan were updated after the Tohoku Earthquake (March 11, 2011). The report denotes the potential of the Tachikawa active fault while next 30 years was increased from 0.5-2% to 0.9-2%. In order to monitor a state change of the fault system by groundwater analysis, we have been surveying water qualities of spring water and hot-spring water.

Our survey of shallow spring waters around the fault in 2012 revealed that the radon concentration of shallow groundwater was affected by a cultivation process of groundwater on the ground surface around the northwest area of the Tama district. Therefore the shallow groundwater around the fault is not appropriate to get information on the state change of the fault. Our survey of deep hot-spring water around the fault in 2013 indicated the good relation between the radon concentration distribution and the location of the fault. The nearer the location of the hot-springs to the fault is, the higher the radon concentration becomes. Therefore the deep groundwater around the fault is useful to monitor the state change of the fault.

Keywords: Grounwater, Hot Spring, Radon, Active Fault

Reconstruction of summer precipitation during last two millennia in central Japan by tree-ring oxygen isotope ratios

NAKATSUKA, Takeshi^{1*}; SANO, Masaki¹; XU, Chenxi¹; OHISHI, Kyohei²; SAKAMOTO, Minoru³; NAKAO, Nanae⁴; YOKOYAMA, Misao⁵; HIGAMI, Noboru⁶; MITSUTANI, Takumi⁷

¹Research Institute for Humanity and Nature, ²Grad. Sch. Env. Studies, Nagoya Univ., ³National Museum of Japanese History, ⁴Musashi University, ⁵Grad. Sch. Agriculture, Kyoto Univ., ⁶Aichi Pref. Center for Archaeol. Operations, ⁷Nara Nat. Res. Inst. Cultural Properties

Introduction

To establish long-term plans of flood control by river management and/or water supply by dam construction, it is necessary to predict future change in precipitation due to global warming. Because precipitation can change at various time scales, it is important to understand the statistical probability of giant flood occurring once a century or millennium. However, due to the shortage of hydrological and meteorological records, it has been difficult to understand statistical characteristics of precipitation in very long time scales. Recently, we have found that tree-ring cellulose oxygen isotope ratios (d18O) record summer precipitation in the corresponding years very precisely and started reconstructions of long term summer precipitation changes in annual time resolution all over Asia monsoon area. Here, we present the two millennial data of summer precipitation in central Japan based on the tree-ring d18O of Hinoki cypress samples obtained from various periods and discuss its meanings in historical hydrology.

Fundamental of precipitation reconstruction

Because cellulose is produced from carbohydrate originally photosynthesized in leaf, its d18O records changes in leaf water d18O. Leaf water d18O is controlled by two meteorological factors, precipitation d18O and relative humidity. It is positively correlated with precipitation d18O and negatively correlated with relative humidity due to the transpiration process. Because there are negative correlation between rain amount and precipitation d18O (amount effect) and positive correlation between rain amount and relative humidity, we can finally realize that there is distinct negative correlation between rain amount in growing season and tree-ring cellulose d18O.

Tree ring samples for long d18O time series

Because trees can seldom live more than several hundred years, we must collect many tree-ring samples during various periods to establish reliable time series of tree-ring d18O beyond last two millennia, not only from living trees, but also from old architectures, archaeological remains, tree logs buried by landslides and so on. Tree-ring samples of Japanese cypress were collected from a certain wide area in central Japan, where we can find consistent tree-ring d18O variations among different trees at different sites and combine many d18O time series, according to the consistent d18O patterns, to establish statistically reliable two millennia length of tree-ring d18O time series.

Application to historical hydrology

The time series of tree-ring d18O was first compared with various meteorological, historical and archaeological evidences on summer precipitation in Japanese history, including modern instrumental meteorological records, summer rainfall amounts quantitatively reconstructed from early modern diary weather notes, medieval documentary records on notorious flood and drought, and pit-house number in lowland plains of ancient Japan, and it was demonstrated that the tree-ring d18O coincides those records very well and successfully reconstruct past change in summer precipitation irrespective of reconstructed periods. However, the tree-ring d18O of Japanese cypress has a distinct age effect where it decreases gradually during its all life time, so that we cannot extract real precipitation trends more than 200 years periodicity from the cypress data. By comparing the tree-ring d18O time series with historical flood records in various rivers in central Japan, we found that there are very good coincidences in decadal time scale before 11th century, but the relation becomes diverse in 18th century, so that good coincidence disappeared in highly developed area where artificial flood control and/or excess logging might have influenced river hydrology. The summer precipitation records based on tree-ring d18O are useful to elucidate both of natural variability and human responses on the historical precipitation changes.

Keywords: two millennia, precipitation, central Japan, tree ring d18O

Water vapor origins in all over Japan in winter simulated by the regional isotope circulation model

TANOUE, Masahiro^{1*} ; ICHIYANAGI, Kimpei¹ ; YOSHIMURA, Kei² ; SHIMADA, Jun¹

¹Graduate School of Science and Technology, Kumamoto University, ²Atmosphere and Sea Research Institute and Institute of Industrial Science, University of Tokyo

In this paper, water vapor origins in all over Japan in winter were simulated by using a regional isotope circulation model with stable isotopes in water ($\delta^{18}\text{O}$ and δD). Precipitation and stable isotopes were simulated for the period between December to February in 2001 — 2010, spatial distributions of them were reproduced observations well. Simulated daily sea-level pressure patterns were divided into two types: winter monsoon (WM) type and extratropical cyclone (EC) type. In the WM type, precipitation rate was high and low along the Japan Sea side and the Pacific Ocean side, respectively. Spatial distribution of $\delta^{18}\text{O}$ in precipitation was recognized the latitude effect (values decrease with increasing latitude) on the Pacific Ocean and the Japan Sea. Spatial distributions of d-excess ($=\delta\text{D}-8\times\delta^{18}\text{O}$) in precipitation and evaporation were above 16 ‰ around Japan, those were extreme high (above 22 ‰) especially on the Pacific Ocean and the Japan Sea. Simulated water vapor evaporated from the Japan Sea was predominant in all over Japan in the WM type without southwestern islands of Japan. Interestingly, a portion of this moisture moved eastward to the Pacific Ocean, however, the moisture was not contributed to total amount of precipitation along the Pacific Ocean side because it was little precipitation. In contrast, precipitation rate was high in all over Japan in the EC type. Spatial distribution of $\delta^{18}\text{O}$ in precipitation was recognized the latitude effect on the Pacific Ocean and the Japan Sea and the amount effect (values decrease with increasing precipitation amount) across Japan. Spatial distributions of d-excess in precipitation and evaporation were below 14 ‰ around Japan without the western part of the East China Sea. Simulated water vapor evaporated from the Pacific Ocean was predominant in all over Japan. Comparing $\delta^{18}\text{O}$ and d-excess in precipitation between the WM type and the EC type, those were 2 ‰ and 8 ‰ higher along the Japan Sea side in the WM type than in the EC type, respectively.

Keywords: stable isotopes in precipitation, water vapor origins, regional isotope circulation model, in all over Japan

Preliminary results of the stable isotopes in precipitation throughout Japan observed in 2013

ICHIYANAGI, Kimpei^{1*} ; TANOUE, Masahiro²

¹Isotope Mapping Working Group, JAHS, ²Kumamoto University

Stable isotopes in precipitation are used for a proxy of climate change, which is related with temperature or precipitation amount. By using the atmospheric general circulation model with stable isotopes in water, water vapor origins (where the water vapor evaporated from?) can be estimated to determine the air mass transportation process. There are a lot of studies to observe stable isotopes in precipitation at only one or a few places in Japan. Tanoue et al. (2013) revealed seasonal variation and spatial distribution of stable isotopes in precipitation over Japan from the previous observational data at about 50 stations. However, spatial and temporal variations of stable isotopes in precipitation across Japan are still unknown, because a specific site and an observation period are different among the previous studies. Intensive observation of stable isotopes in precipitation over the whole Japan is required during the same period.

The Isotope Mapping Working Group of Japanese Society of Hydrological Sciences was conducted intensive observation of stable isotopes in precipitation throughout the year in 2013 (IOP2013). More than 2,000 precipitation samples are already collected at about 50 stations, and are analyzing its stable isotopic ratios by the Isotope Ratio Mass Spectrometer (Delta-V, Thermo Scientific) in Kumamoto University. Stable isotopic ratios in precipitation across Japan will be considered the relationships with locations (i.e. latitude, altitude, and distance from the coastline) and meteorological elements (i.e. temperature, precipitation amount, winds, specific humidity). Also, water vapor origins are estimated by using atmospheric general circulation model with stable water isotopes. Finally, the equations to reproduce stable isotopic ratios in precipitation at a specific place in Japan will be determined by its location and/or meteorological elements. It's a useful for the paleo-climate change as a proxy data of temperature and/or precipitation amount in the past.

In this study, we present the preliminary result of the IOP2013.

Keywords: Stable isotopes in precipitation, d-excess, Japan, IOP2013

Tracking phosphorus sources and cycling in freshwater: stable isotope approach

CID, Abigail^{1*}; SONG, Uham¹; TAYASU, Ichiro¹; OKANO, Jun-ichi¹; TOGASHI, Hiroyuki²; ISHIKAWA, Naoto F.⁵; MURAKAMI, Aya¹; HAYASHI, Takuya⁴; IWATA, Tomoya⁴; OSAKA, Ken-ichi³; NAKANO, Shin-ichi¹; OKUDA, Noboru¹

¹Ctr Ecol Res, Kyoto Univ, ²Field Sci Educ Res Ctr, Kyoto Univ, ³Univ Shiga Pref, ⁴Dept Ecol Syst Engineer, Univ Yamanashi, ⁵JAMSTEC

Stable isotope technique is increasingly used to provide ecological information to understand biological cycling and tracking environmental pollutants. The technique used for tracing phosphorus (P) in water is primarily based on the possibility of distinguishing the different P inorganic sources by phosphate oxygen isotopic signatures ($\delta^{18}\text{O}_p$) [1]. To date, there are only few studies to examine P cycling on watershed scales using the phosphate oxygen isotope analysis.

Here we aim to characterize individual $\delta^{18}\text{O}_p$ signatures of water, natural sources and potential anthropogenic sources in the Yasu River, the largest tributary river in the Lake Biwa Watershed. Special attention was paid to identify primary sources of P loadings in the Yasu River, associating with the land use pattern in its each catchment.

Materials & Methods

We collected river waters from 19 sites across the mainstream of Yasu River and its branches, whose catchment areas greatly vary in land use pattern. We also gathered water samples from 8 sewage treatment plants, 2 agricultural waste water plants and one livestock farm as point sources of anthropogenic P. We regarded phosphate fertilizers and sewage treatment plant waste waters as indicators for agricultural and domestic non-point P sources, respectively. We also collected sand from the riverbed of 5 headwaters as natural P sources. The sand samples were acid extracted to desorb dissolved inorganic phosphates [2]. These samples were treated with magnesium-induced coprecipitation (MagIC) method for phosphate extraction and then converted to silver phosphate after purification through the sequence of resin separation and precipitation [1,3]. We determined $\delta^{18}\text{O}_p$ for each of these silver phosphate samples using a thermal conversion elemental analyzer coupled to a continuous flow isotope ratio mass spectrometer via a helium stream.

We constructed an isotopic mixing model to estimate the relative contribution of individual P sources in each catchment.

Results & Discussion

A wide range of $\delta^{18}\text{O}_p$ in river water was detected. This indicates that this technique is a promising tool to trace P sources in the watershed ecosystems.

The isotopic mixing model showed that urban land use accounted for spatial variation in the relative contribution of domestic P loadings though there were some uncertainty in the model simulation.

[1] Young et al. (2009) Environ. Sci. Technol, 43:14, 5190-5196

[2] Tamburini et al. ni et al. (2010) Eur J Soil Sci, 61, 1025-1032

[3] McLaughlin et al. (2004) Limnol. Oceanogr. : Methods 2, 204-212

Keywords: Biological recycling, Eutrophication, Land use, Non-point phosphorus loading, Phosphate oxygen isotope analysis

Stable isotopic map of spring water and surface water in the Shirakami Mountains, Japan

AMITA, Kazuhiro^{1*} ; MIURA, Takuya¹ ; HAYASHI, Takeshi²

¹Department of Earth Science & Technology Faculty of Engineering and Resource Science Akita University, ²Faculty of Education and Human Studies, Akita University

The Shirakami Mountains is the general name given to an extensive mountainous region of 130,000 hectares ranging from the southwest of Aomori to the northwest of Akita prefecture. Within this area are 16,971 hectares of land, enclosing virgin forests of Japanese beech, which were registered as a world heritage region in December 1993. However, environmental impact by acid rain at the Shirakami Mountains is becoming an issue these days. Acid rain deposits nitrates that can lead to increases in nitrogen in forests. So we have studied about the chemical and isotopic compositions of river and spring waters in the Shirakami Mountains area, to clarify origin and geochemical characteristics since 2011.

The result of the investigation was that $\delta\text{-}^{18}\text{O}$ and $\delta\text{-D}$ of water samples showed -8.8 to -11.5 permil and -48.8 to -64.8 permil, respectively. Stable isotope composition of the samples roughly resemble those of meteoric water ($\delta\text{-D} = 8\delta\text{-}^{18}\text{O} + 20$), thereby indicating that these are local meteoric water. The least-squares regression line for all data is: $\delta\text{-D} = 5.7\delta\text{-}^{18}\text{O} + 1.7$ ($R^2 = 0.88$). On the other hand, the regression line calculated with data from NW-part is: $\delta\text{-D} = 6.0\delta\text{-}^{18}\text{O} + 0.5$ ($R^2 = 0.98$). Characteristics of two regression line suggest that these water origin were brought by rain from different air mass, respectively.

Keywords: The Shirakami Mountains, Stable isotope map

Source of spring water and nitrate in northern foot of Mt.Fuji

NAKAMURA, Takashi^{1*} ; HASEGAWA, Tatsuya² ; YAMAMOTO, Shinya² ; UCHIYAMA, Takashi²

¹ICRE, University of Yamanashi, ²Yamanashi institute of environmental Sciences

Water chemistry of spring water in Northern foot of Mt. Fuji is discussed with special reference to its source of water and nitrate. Monthly spring water and river water samples were collected from 8 springs and 7 locations of the 3 rivers, from June 2013 to January 2014. Land use of the study area are urban located about <1000m, forest distributed >1000m and forest limit is about 2500m. The oxygen isotope range of all spring water samples shows temporal variation (>1.0 permil), which suggests the possibility of the water changes of groundwater water recharge elevation. The nitrate-nitrogen concentration ranges from 0.2 to 1.8 mg/L and from 0.1 to 2.2 mg/L in river water and spring water samples respectively. Similarly, nitrate-nitrogen isotope values ranges from 2.7 to 9.9 permil and 1.4 to 10.4 permil in river water samples and spring water samples respectively. Although nitrate concentration was low, nitrogen isotope values overlaps with forest soil nitrogen and sewage or manure nitrogen. This trend suggests that the recharge elevation of the spring water might spread across a wide area. This presentation will discuss about recharge processes of the spring water including temporal variation of the isotopic values and water quality.

Keywords: Mt.Fuji, spring water, oxygen and hydrogen isotopes in water, nitrogen and oxygen isotopes in nitrate

Spatial distribution of vanadium concentrations and water isotopes in lake bottom water from Lake Kawaguchi

YAMAMOTO, Shinya^{1*}; HASEGAWA, Tatsuya¹; YOSHIZAWA, Kazuya²; NAKAMURA, Takashi³; UCHIYAMA, Takashi¹

¹Yamanashi Institute of Environmental Sciences, ²Yamanashi Institute for Public Health, ³International Research Center for River Basin Environment, University of Yamanashi

Spatial distribution of vanadium concentrations was examined in bottom water from Lake Kawaguchi, on the northern foot of Mt. Fuji, in order to test the hypothesis that the water outflow from underwater springs in Lake Kawaguchi could affect the vanadium concentrations of lake water. The samples were collected from the east lake basin and the Funatsu lake basin on July 14-August 2, 2005, and from the west lake basin on November 1 and October 31, 2013. Vanadium concentrations in the bottom water from Lake Kawaguchi range from 0.66 $\mu\text{g/L}$ to 3.18 $\mu\text{g/L}$. Because vanadium concentration in precipitation is generally $<0.1 \mu\text{g/L}$, the variations are most likely attributed to the dilution of the lake water due to precipitation, and/or the input of water masses with high vanadium content. Although the concentrations of vanadium are significantly lower than those in the groundwater of the Mount Fuji, we found a relatively vanadium-enriched water mass along the southern coast of the west lake basin, off coast of Higashiken lava flow from Mount Fuji. The area matches well with the potential location of underwater springs in Lake Kawaguchi, and the lack of any riverine input around the area suggests that a water mass with relatively high vanadium concentration is likely provided from underwater springs that are located in off coast of the basaltic lava flow of Mount Fuji. We also plan to discuss the source of underwater springs based on stable water isotope ratios in the presentation.

Keywords: Kawaguchiko, vanadium, stable water isotopes, Mount Fuji

Contribution of volcanic gas to spring waters in the Mt. Yotei.

KUSANO, Yukiko^{1*}; YASUHARA, Masaya²; ASAI, Kazuyoshi³; INAMURA, Akihiko²; TAKAHASHI, A., Hiroshi²; MORIKAWA, Noritoshi²

¹The University of Tokyo, ²Geological Survey of Japan, AIST, ³Geo science Laboratory Co. Ltd.

The Mt. Yotei is a stratovolcano in southwest Hokkaido with an altitude of 1893 m. There are a lot of springs in the foot of the mountain and most of these are found from the altitude of 200 to 260 m. This elevation is consistent with that of boundary between volcanic rocks of the volcano and basement consists of tuff and pumice. Northern, eastern, and southern slopes of the mountain are covered by pyroclastic fall and reworked deposits of that, while the western slope is covered by lava erupted from summit and parasitic volcanos in western slope (Katsui, 1956).

It is revealed that springs in eastern and southern slopes tend to show larger discharge and lower dissolved components, while those in the western slope tend to show smaller discharge and higher dissolved components (Yamaguchi and Sato, 1971; Yamaguchi, 1972; Tsurumaki, 1989). Because of higher HCO_3^- and free CO_2 gas concentrations and higher temperature of springs in the western slope, addition of volcanic gas to those is estimated (Yamaguchi and Sato, 1971; Tsurumaki, 1989). However, contribution of volcanic gas to groundwater has not been evident. In this study, contribution of volcanic gas to spring waters will be discussed based on dissolved components and isotopic compositions.

Spring water samples were collected on August 2013, and were analyzed for major dissolved components, isotopic compositions (δD , $\delta^{18}\text{O}$, $\delta^{13}\text{C}$, $^3\text{He}/^4\text{He}$), and groundwater-age indices (CFCs and SF_6). Dissolved components of spring waters are Ca- HCO_3 type or Na- HCO_3 type. Spring waters in the western slope tend to show higher HCO_3^- and free CO_2 gas concentrations. These results are consistent with those of previous studies. $\delta^{13}\text{C}$ of dissolved inorganic carbon (DIC) in spring waters in eastern and southern slopes are -21.7 to -17.7 ‰, while those of the western slope are -18.1 to -3.0 ‰. This result suggests that spring waters in western slope contain DIC of which origin is different from that contained in springs in eastern and southern slopes. Dissolution of marine carbonates is unlikely because groundwater flow in volcanic rocks. Relationship between $\delta^{13}\text{C}$ and inverses of concentrations of total carbon are plotted in mixing zone of volcanic CO_2 and soil CO_2 , and spring water showing higher $\delta^{13}\text{C}$ and total carbon concentration were correspond to higher contribution of volcanic CO_2 . These results suggest that spring waters in western slope showed higher $\delta^{13}\text{C}$ and total carbon concentrations because of addition of volcanic CO_2 . δD and $\delta^{18}\text{O}$ of spring waters are plotted along the meteoric water line (GSJ, undisclosed data), suggesting contribution of magmatic water is quite small. Effect of parasitic volcanos in the western slopes is suggested by Yamaguchi and Sato (1971) as a possible factor for higher contribution of volcanic gas to springs in the western slope. Further discussions based on dissolved components, isotopic compositions, and groundwater-age indices will be performed to reveal relationship between contribution of volcanic gas and groundwater flow system.

References

- Katsui, Y., 1956. Explanatory text of geological map of Japan, scale 1: 50,000, Rusutsu, appendix, Geological Survey of Hokkaido, p14.
- Tsurumaki, M., Journal of Groundwater Hydrology, 31, 3, 165-173.
- Yamashita, K. and Sato, I., 1971. Report of of spring water survey in the Mt. Yotei, Geological Survey of Hokkaido, p27.
- Yamashita, K., 1972. Journal of Geography, 81, 5, 4-20.

Estimation of recharge elevation and residence time for springs in Mt. Yotei

ASAI, Kazuyoshi^{1*}; YASUHARA, Masaya²; KUSANO, Yukiko³; INAMURA, Akihiko²; MORIKAWA, Noritoshi²; TAKAHASHI, Hiroshi²

¹Geo science laboratry, ²AIST, ³University of Tokyo

Mt Yotei is a stratovolcano located on southwestern part of the Hokkaido. 17 springs with flow rate over 20 L/s distribute on the foot of the volcano body. We used the multi tracer method to estimate the recharge elevation and the residence time for the springs. Water samples were collected from 14 springs at August 2013, and were measured in stable isotope, Tritium, CFCs and SF₆. In this presentation, we discuss the relationships between the scale of groundwater flow system and the hydrogeology of volcano body, based on the recharge elevation and the residence time for springs.

Keywords: Mt. Yotei, spring, recharge elevation, residence time, transient tracer

Isotope characteristics of groundwater in and around Mt. Sambe, an active volcano in western Japan

YASUHARA, Masaya^{1*} ; SUZUKI, Hidekazu² ; ASAI, Kazuyoshi³ ; INAMURA, Akihiko¹ ; YAMAMOTO, Atsushi⁴ ; MORIKAWA, Noritoshi¹ ; TAKAHASHI, Hiroshi¹ ; TAKAHASHI, Masaaki¹ ; KAZAHAYA, Kohei¹ ; KITAOKA, Koichi⁵

¹Geological Survey of Japan, AIST, ²Komazawa University, ³Geo Science Laboratory, ⁴Kinki University, ⁵Okayama University of Science

A study using a coupled hydrological and geochemical (water chemistry, δD - $\delta^{18}O$, $\delta^{13}C$, and helium isotope) approach is in progress to elucidate the groundwater system in and around Mt. Sambe, a 1126-m high active volcano located in western Japan. Groundwater in its south to east flanks proved to be characterized by high $\delta^{13}C$ values (in the range between -9 - -5 ‰ $\delta^{13}C$) as well as an elevated concentration of total carbon compared to those in other flanks. These observations clearly indicate an admixture of magmatic fluid into shallow groundwater of the south to east flanks, being also in accordance with its water chemistry with an increased chloride ion concentration.

Keywords: active volcano, groundwater, water chemistry, isotopes, volcanic fluid

Origin of the high-chloride groundwater in the central part of the Kanto Plain from the viewpoint of noble gas hydrology

MORIKAWA, Noritoshi^{1*} ; YASUHARA, Masaya¹ ; HAYASHI, Takeshi² ; MIYAKOSHI, Akinobu¹ ; INAMURA, Akihiko¹ ; TAKAKASHI, Masaaki¹ ; NAKAMA, Atsuko¹

¹Geological Survey of Japan, AIST, ²Akita University

There exist three regions in the Kanto plain, central Japan, whose artesian groundwater is characterized by a high Cl⁻ concentration: 1) central parts of the Kanto plain (Saitama Prefecture), 2) south-east parts of Gunma Prefecture), 3) floodplains and deluvial uplands along the lower reaches of Kokai and Tone rivers (Ibaraki and Chiba Prefectures).

As for that in the central parts of the Kanto plain, confined groundwater with a high Cl⁻ concentration of up to 216 mg/l is obtained from the productive boreholes of 200-430 m depth. The area of Cl⁻-rich groundwater, spreading from the northwest to southeast, corresponds with the so-called Motoarakawa tectonic zone (ca. 10 km wide by 35 km long) bounded by the fault on its longer sides. The ³⁶Cl/Cl results of these high chloride groundwaters imply that admixture of meteoric water and sea water in the period of the Shimosueyoshi transgression (peak period at around 125,000 yrs. BP) is likely to account for its elevated Cl⁻ concentration (Yasuhara et al., 2011). Morikawa et al (2006) conducted dissolved noble gas analyses for the groundwaters in the Motoarakawa tectonic zone. The results of helium isotopes are as follows; (1) there is a tendency of high ⁴He concentration in the groundwaters inside the tectonic zone, (2) helium isotopic ratios (³He/⁴He) are relatively homogeneous with an end member of 0.8-1.1 x 10⁻⁶. Helium-4 concentration show clear positive correlation with chloride concentration. Combined with this correlation and characteristics of helium isotopic ratio, it is inferred that the groundwater from the tectonic zone is a mixture of meteoric water and high chloride saline water bearing with high ⁴He or is stagnant old groundwater and that the groundwater flow system is distinct from those from outside of the tectonic zone.

In this study, we investigated the noble gas in the deeper groundwaters (hot springs) around the Motoarakawa tectonic belt and the high-chloride groundwaters from south-east parts of Gunma Prefecture to elucidate the origin of water and chloride component in the central parts of the Kanto plain. Low ³He/⁴He ratios in the hot springs indicate that there is no interconnectivity between the high chloride groundwater and hot spring water around the Motoarakawa tectonic zone. In contrast, both ³He/⁴He ratio and correlative ⁴He and Cl concentration in the high-chloride groundwaters from south-east parts of Gunma Prefecture are similar to those in the groundwaters in the Motoarakawa tectonic zone.

Keywords: Kanto Plain, groundwater, chloride ion, Noble Gas, Helium isotope

Geochemical study of hot spring waters and gases in Jozankei area, Hokkaido, northern Japan

TAKAHASHI, Masaaki^{1*} ; KAZAHAYA, Kohei¹ ; SASAKI, Munetake¹ ; MORIKAWA, Noritoshi¹ ; TAKAHASHI, Hiroshi¹

¹Geological Survey of Japan, AIST

Jozankei hot spring area is located in the western part of Sapporo city, Hokkaido, northern Japan. In this area, hot spring waters >85 degree C. are springing out from the entire Toyohira river valley. Total discharge rate of hot spring waters is about 10 tons/min and the "heat energy index" is rank V (Fukutomi, 1965). Hydrogen and oxygen isotopic study clarified that the major origin of hot spring water is local meteoric water (Matsubaya et al., 1978)

To understand the other origin of Jozankei hot spring, analyses of chemical compositions, hydrogen and oxygen isotope ratios were carried out for hot spring waters from Jozankei area and its adjacent area. From the good correlation among chloride ion content, oxygen and hydrogen isotope ratio of hot spring waters in Jozankei area, it is clarified that one of the end member of hot spring waters of Jozankei area is originated from magmatic fluid and chemical composition of magmatic fluid is 3-5 NaCl wt%.

(References) Fukutomi(1961)J.Fac.Sci.Hokkaido Univ.Ser.VII, 315-330; Matsubaya et al.(1978)Papers of the Institute for Thermal Spring Research, Okayama Univ., 47, 55-67.

Keywords: Jozankei, magmatic fluid, hydrogen and oxygen isotopic ratio

Genesis of Kashio brine: slab-derived fluid

KAZAHAYA, Kohei^{1*} ; TAKAHASHI, Hiroshi¹ ; MORIKAWA, Noritoshi¹ ; OHWADA, Michiko¹ ; INAMURA, Akihiko¹ ; YASUHARA, Masaya¹ ; TAKAHASHI, Masaaki¹

¹Geological survey of Japan, AIST

In this study, we show the results obtained by investigation of a very saline spring named Kashio brine, central Japan and discuss its genesis and cause of chemical and isotopic features. The brine water is spouting out through the cracks of metamorphic rocks close to Median Tectonic Line (MTL) at 700m asl. The Cl concentration of water is greater than that of the seawater with ¹⁸O-shifted isotopic composition. The brine is thought to originate from slab-derived fluid with the chemical and isotopic composition of water like the Arima hot spring, in spite of its low temperature and CO₂-less features. The cause of this chemical character might be explained by a reaction with ultramafic rocks existed close to Kashio area which causes high pH condition to deposit all the CO₂ as CaCO₃. The low temperature may be interpreted by the low upwelling rate because of the low ³He/⁴He ratio (lower than 2Ra) due to the addition of crustal ⁴He. The amount of NaCl is finally supplied to the river and is estimated to be 2000kg/day.

Keywords: Kashio brine, isotopic ratio, flow rate, slab-derived fluid

GC/C/IRMS as a tool to evaluate the degradation of chlorinated organic compounds in groundwater

YONEYAMA, Yuki^{1*} ; ARAI, Yohei² ; NAKAMURA, Takashi¹ ; KAZAMA, Futaba¹

¹ICRE, UNIVERSITY OF YAMANASHI, ²Hitachi Plant Services Co.,Ltd

The in-situ remediation techniques by microbial activity are used for reduction of chlorinated organic compounds in polluted groundwater. However, the evaluation of microbial activity for decomposition of chlorinated organic compounds is not clear by only the concentration analysis. So, we focus on the usage of the stable carbon isotope analysis of chlorinated organic compounds such as trichloroethylene (TCE), and its daughter products; cis-dichloroethylene (cis-DCE) and vinyl chloride (VC).

The stable carbon isotope ratio ($\delta^{13}\text{C}$) of these organic compounds were analyzed by a GC (Agilent : 7890A) coupled to an isotope ratio mass spectrometer (SerCon : 20-22) with combustion interface (SerCon : GC-CP) (GC/C/IRMS). The system was equipped with a purge-and-trap concentrator (GL science : AQUA PT 5000J PLUS) connected to the GC. In the $\delta^{13}\text{C}$ value measurement, the measurement limit was usually 200ng-C, and standard deviation in TCE, cis-DCE and VC were ± 0.08 , ± 0.37 , ± 0.11 permil, respectively.

Groundwater samples were collected at polluted site with and without bioremediation treatment.

In samples from without treatment site, even the concentration decreasing were detected, the $\delta^{13}\text{C}$ values of TCE are almost same as original one. On the other hands, $\delta^{13}\text{C}$ values of not only TCE but also the daughter products increase with a decrease in concentration of TCE. These results show the usefulness of GC/C/IRMS for distinguishing the reason of concentration reduction by in-situ microbial activity of decomposition of these organic pollutants from physical factors such as dilution, diffusion, and adsorption.

Keywords: GC/C/IRMS, chlorinated organic compounds, biodegradation

Isotope characteristic of rain water and atmospheric vapor in Hiratsuka, Japan

TAKAGI, Kenta^{1*}; OOKI, Seigo²; OHBA, Takeshi²

¹Course of Chemistry, Graduate School of Science, Tokai University, ²Course of Chemistry, School of Science, Tokai University

Introduction

The stable isotope ratios of hydrogen and oxygen in meteoric water (δD and $\delta^{18}O$) are affected by geological and climatic conditions. Global meteoric water line (GMWL) describes the average isotopic compositions in the world. According to Craig (1961), the relationship between δD and $\delta^{18}O$ was expressed as

$$\delta D = 8\delta^{18}O + 10 \quad (1)$$

However those intercept are not always 10 in each area. In Japan, the meteoric water originates in both Pacific Ocean and Japan Sea. The effects of two seas vary due seasonally. The isotope ratio of atmospheric vapor is important for study of atmospheric circulation, however, the number of published paper is not so much. In this study, we investigate the d-excess ($d = \delta D - 8\delta^{18}O$) of rain water and atmospheric vapor in Hiratsuka, Japan.

Sampling methods

Samples were collected on the roof of a No.17 building at Shonan campus, Tokai University from May to December 2013. Rain water samples were collected based on a method described by Negrel et al. (2011) and Yoshimura (2002). The collection duration was days or hours in scale. Rain water samples were percolated through 0.2 μm filter, and kept into a 100 ml low-density polyethylene bottle. Atmospheric vapor samples were collected through a trap cooled with ethanol and dry ice mixture. Samples were 42 of rain water and 11 of atmospheric vapor. δD and $\delta^{18}O$ of samples were measured by a Cavity Ring-Down Spectrometer analyzer (model L2120-I from PICARRO). Some data of rain water, which were sampled several times in a day, were processed to be the average value.

Results and discussion

Rain water shows a wide variation in δD and $\delta^{18}O$ from -86.4 to +6.2 ‰ and -12.6 to -2.6 ‰, respectively. Atmospheric vapor shows a variation from -223.5 to -98.6 ‰ and -31.2 to -14.7 ‰, respectively. The δD - $\delta^{18}O$ relationship of rain water gives a regression line: $\delta D = 9.2\delta^{18}O + 24.0$ ($R^2 = 0.95$) and that of atmospheric vapor gives a regression line: $\delta D = 7.3\delta^{18}O + 7.9$ ($R^2 = 0.96$). The d-excess values show a variation from 4.4 ‰ to 33.2 ‰. In Japan, origin of meteoric water affects to d-excess (Waseda and Nakai, 1983). In case of Pacific Ocean, d-excess is low ($10 \geq d$). In case of Japan Sea, d-excess is high ($20 \leq d$). In this study, the d-excess was low in summer when southern winds were blown from Pacific Ocean as the seasonal wind, and that value was high in winter when northern winds were blown from Japan Sea. Samples of atmospheric vapor show also this trend. Suggesting that atmospheric vapor is influenced by the same effect of meteoric water. The meteoric water line of rain samples was affected by d-excess which reflects variations of moisture sources, which is the reason why the slope of this line would be bigger than GMWL.

Keywords: rain water, isotope

Exploring the sources of sulfur ion deposition and runoff in forest watersheds on the northern side of Lake Biwa

NAKAZAWA, Koyomi^{1*} ; HORIE, Seigo¹ ; NAGAFUCHI, Osamu¹ ; OSAKA, Ken'ichi¹ ; NISHIMURA, Takuro¹

¹The University of Shiga Pref.

To clarify the sources of sulfur ions in precipitation and runoff from forest watersheds, bulk deposition and stream water samples were collected within the small Kutsuki and Surumi forest watersheds on the northern side of the Lake Biwa basin, central Japan. Samples were analyzed for major ions and $\delta^{34}\text{S}$. Continuous monitoring from 1990 to 2010 showed that the average SO_4^{2-} concentration in stream water samples was 1.62 ± 0.31 (0.76, 3.58) mg l^{-1} at Kutsuki and 6.59 ± 1.54 (3.68, 16.1) mg l^{-1} at Surumi (t-test, $p < 0.01$). However, the average SO_4^{2-} concentration in bulk deposition samples was similar in both watersheds: 2.15 ± 1.31 (SD) mg l^{-1} (range, 0.202-10.2 mg l^{-1}) at Kutsuki and 2.24 ± 1.29 mg l^{-1} (0.350-6.07 mg l^{-1}) at Surumi (t-test, $p > 0.05$). The $\delta^{34}\text{S}$ values in bulk deposition samples fluctuated from +8.86 to +9.14 ‰ at Kutsuki and from +9.87 to +11.1 ‰ at Surumi, whereas non-sea salt (nss-) $\delta^{34}\text{S}$ in stream water samples varied from +6.89 to +12.0 ‰ and from +4.64 to +5.11 ‰, respectively (t-test, $p < 0.01$). It is said that the $\delta^{34}\text{S}$ values in coal products from northern China varied from -3 to -1 ‰ and Japanese oil varied from +5 to +18 ‰.

Our findings suggest that the difference in the ability of canopies in the watersheds to catch SO_4^{2-} dry deposition is the reason for the significant difference in nss- $\delta^{34}\text{S}$ values in stream water samples. The more open canopy in the Kutsuki watershed consists of young conifers and deciduous broadleaf trees, whereas the canopy in the Surumi watershed consists of mature conifer trees at a high density. Therefore, it appears that the Kutsuki watershed was only affected by SO_4^{2-} deposition from the Asian continent. There were not any domestic air pollution sources on the north side of Kutsuki. In contrast, the dense canopy of the Surumi watershed was affected by local SO_4^{2-} pollution sources of national roads which were located 1 km northwest from Kutsuki, rather than continental sources. Overall, this investigation suggests that the difference in stream water SO_4^{2-} concentrations in both watersheds is caused by the canopy differences.

Geochemical and isotope systematics of Asahi and Yoshii rivers

KAMEI, Takahiro¹ ; YAMASHITA, Katsuyuki^{1*} ; OONISHI, Ayaka² ; KURIHARA, Yoko² ; CHIBA, Hitoshi¹ ; NAKANO, Takanori³

¹Graduate School of Natural Science and Technology, Okayama University, ²Faculty of Science, Okayama University, ³Research Institute for Humanity and Nature

We have undertaken a detailed geochemical and isotopic analysis of water samples collected from the Asahi and Yoshii rivers of the Okayama Prefecture, Japan. More than 300 samples were collected from the rivers and their tributaries during March 2011 to January 2014. In several locations, samples were collected periodically in order to monitor the long-term fluctuation of the geochemical properties. All samples were filtered with 0.2 μm filter prior to the analyses for major dissolved constituents (F, Cl, NO₃, SO₄, Br, PO₄, Ca, Mg, Na, K), trace elements and O-H-Sr-S isotopes.

Based on the results obtained so far, we have constructed a high-resolution geochemical map of the rivers covering central to eastern Okayama Prefecture. The map shows that the concentrations of most major dissolved constituents, as well as the O-H-Sr isotope ratios changes systematically from the upstream towards the downstream. For example, the deuterium excess (DE) is generally high in the upstream (>20) and gradually decreases towards the downstream (<12). This difference in the DE exceeds the seasonal variation observed in locations where the long-term monitoring was conducted. Thus, the regional change in the DE is interpreted to be the result of different air mass contributing to the meteoric water of different locations.

The Ca, Sr, and Ba concentrations are generally low in the upstream and gradually increase towards the downstream. The ⁸⁷Sr/⁸⁶Sr also changes from approximately ~ 0.705 and ~ 0.706 in the headwaters of the Asahi and Yoshii rivers, respectively, to ~ 0.708 in the areas close to the Seto inland sea. The shift in the Sr isotope ratio seems to correlate well with the change in the ages of the rocks exposed in the river basin. This implies that these variations are likely related to the water-rock interactions.

The concentrations of other important dissolved constituents such as the NO₃ and SO₄ tend to increase abruptly in the densely populated regions. This is also accompanied by a shift in the S isotopic composition. These variations may reflect a change in the degree of human influence such as breakdown of fertilizers used for agricultural activities.

Keywords: Geochemical map, Asahi River, Yoshii River

Characteristics of groundwater discharge around western foot of Mt.Chokai

ASAI, Kazumi^{1*} ; ASAI, Kazuyoshi¹ ; HAYASHI, Takeshi² ; KUSANO, Yukiko³ ; MOGI, Katsuro³ ; YASUHARA, Masaya⁴ ; MORIKAWA, Noritoshi⁴ ; TAKAHASHI, Hiroshi⁴

¹GEO-SCIENCE LABORATORY, ²Akita university, ³University of Tokyo, ⁴AIST

To clarify the total discharge rate of the submarine spring from Mt. Chokai, base-flow observation was conducted on 15 streams around western foot of Mt. Chokai at the end of January 2014. In this presentation, based on the distribution of specific discharge rate, we discuss the characteristics of the groundwater discharge and the hydrological balance in this area.

Keywords: Mt.Chokai, submarine spring, base-flow, hydrological balance, groundwater age

Estimation of groundwater recharge area at the south foot of Mt. Bandai using the observation data in 2013

YABUSAKI, Shiho^{1*}

¹Faculty of Symbiotic Systems Science, Fukushima University

The Mt. Bandai (1,816 m a.s.l.) which is an active volcano of the Quaternary period is located at Fukushima prefecture. Because of the geological characteristics in the volcanic area, it is estimated the groundwater recharge is large around Mt. Bandai. The groundwater and spring water around Mt. Bandai is used as the source of the public tap water, so it is important to comprehend the groundwater flow and groundwater recharge ratio at Mt. Bandai. To make clear the groundwater flow systems at Mt. Bandai, the investigation was carried out.

The EC value is under 10 mS/m and water quality indicates the Ca-HCO₃ type at most points in the south slope of Mt. Bandai. The oxygen isotopic ratios ($\delta^{18}\text{O}$) are -11.1 to -10.8 ‰ (Site 1) and -11.2 to -11.1 ‰ (Site 2), and hydrogen isotopic ratios (δD) are -67 to -65 ‰ (Site 1) and -68 to -67 ‰ (Site 2). The altitude effect is recognized in these areas. The average recharge area (altitude) in the south slope at Mt. Bandai is estimated from 1,150 to 1,270 m (Site 1) and from 1,360 to 1,420 m (Site 2). These recharge area (altitude) in the south slope is lower rather than the north and west slopes. In future, the investigation at more low altitude area (about 520 to 550 m) will be carried out, and estimate the groundwater flow in the south slope at Mt. Bandai.

Keywords: Mt. Bandai, recharge area, spring water, water quality, stable isotopes

Future Projection of flow regime and water quality in Arakawa river basin

ISHIDAIRA, Hiroshi^{1*}

¹Interdisciplinary Graduate School of Medicine and Engineering

The research project of Core Research for Evolutional Science and Technology (CREST): "Development of well-balanced urban water use systems adapted for climate change" (PI: Hiroaki FURUMAI, Univ. of Tokyo, Research area: Innovative Technology and System for Sustainable Water Use) have been conducted from 2009.

The objectives of this project are 1) to reexamine the current urban water use system, and 2) to propose a new urban water use system adaptive to the future climate change. In the new system, each water resource is properly allocated to each water use by considering the balance between supply potential of various water resources and demand. The information on available amount and detailed quality of water resources should be evaluated.

For the implementation of the project, 5 sub-groups were organized:

- (1) Watershed Water Resources group
- (2) Urban Rainwater Management and Use group
- (3) Urban Groundwater Management and Use group
- (4) Water Quality Assessment group
- (5) Urban Water Use Design group

In this presentation, activities of Watershed Water Resources group (and collaborative work with Urban Groundwater Management and Use group) will be presented.

Keywords: climate change, water resources

AHW26-02

Room:424

Time:May 1 14:30-14:45

Cl⁻ concentration in pore water beneath Tokyo bay area, Urayasu, Chiba Japan

YOSHIDA, Takeshi^{1*} ; KAZAOKA, Osamu¹

¹Research Institute of Environmental Geology, Chiba

We investigated Chloride concentration of Holocene and latest Pleistocene in Urayasu city, Chiba Japan. As a result of analysis, Chloride concentration of Holocene in this area is affected by flushing of rain and groundwater flow from Pleistocene.

Keywords: Alluvium, Profile of Cl⁻ concentration, basal topography

An isotopic study on the origins of sulfate ion in shallow urban groundwater of the Musashino Plateau, Tokyo, Japan

YASUHARA, Masaya^{1*} ; HAYASHI, Takeshi² ; NAKAMURA, Takashi³ ; INAMURA, Akihiko¹ ; ASAI, Kazuyoshi⁴

¹Geological Survey of Japan, AIST, ²Akita University, ³University of Yamanashi, ⁴Geo Science Laboratory

Shallow groundwater in the highly-urbanized Shakuji-gawa River basin on the Musashino Plateau, Tokyo, Japan shows a remarkable spatial variability of its sulfate ion concentration in the range between 7-135 mg/L. The average sulfate ion concentration is 35mg/L, 36mg/L, 33mg/L, 21mg/L, 19mg/L, and 28mg/L in Kita Ward, Itabashi Ward, Toshima Ward, Nerima Ward, Nishi-Tokyo City, and Kodaira City, respectively, indicating higher concentration in the lower reaches of the river where urbanization has started earlier and progressed more rapidly than its upper reaches. To discuss possible origins of sulfate ion in groundwater, a hydrologic study using stable isotope of sulfur was carried out in 2012 to 2013. Although a limited number of samples, higher sulfur isotope measurements (+10.5 and +10.6 per mil delta-34S for Toshima and Kita Wards, respectively) suggest contribution of leaking sewage from aging, deteriorated sewer pipes, accounting for an elevated sulfate ion concentration in the lower reaches of the river.

Keywords: urban groundwater, central Tokyo, shallow groundwater, sulfate ion, sulfur isotope

PPCPs pollution in an urban watershed in Musashino upland, Tokyo

HAYASHI, Takeshi^{1*} ; YASUHARA, Masaya² ; NAKAMURA, Takashi³

¹Faculty of Education and Human Studies, Akita university, ²Geological Survey of Japan, AIST, ³ICRE, University of Yamanashi

Human activities discharge various chemical substances to water environment in urban area around the world. Some substances are concerned to affect health of human and aquatic organism because these substances are hardly decomposed not only in natural environment but also water treatment plant. We study on shallow groundwater environment in Musashino upland, Tokyo to evaluate sources and recharge processes of groundwater and present state of groundwater pollution by domestic wastewater (e.g. Hayashi et al., 2012; Nakamura et al., 2013; Yasuhara et al., 2013). Based on the result of our previous research, we newly collected water samples of river water and shallow unconfined groundwater in the watershed and measured PPCPs components. Three samples of river water were taken from two rivers: a natural river mainly recharged by groundwater and an artificial river recharged by treated waste water. 15 groundwater samples were collected from private wells that were distributed in the watershed of the natural river. As for PPCPs, 78 substances were measured by semi-quantitative analysis and another six substances (amantadine, caffeine, carbamazepine, crotamiton, ibuprofen, N,N-diethyl-m-toluamide) were measured quantitatively.

As for river water samples, 19 substances from semi-quantitative analysis and six substances from quantitative analysis were detected in the artificial river, and three substances from semi-quantitative analysis and five substances from quantitative analysis were detected in the natural river. On the other hand, only one substance from semi-quantitative analysis and four substances (amantadine, carbamazepine, crotamiton, N,N-diethyl-m-toluamide) from quantitative analysis were detected in groundwater samples in both peri-urban upstream area and urbanized downstream area.

We present present characteristics of PPCPs components and spatial distribution in the study area.

Keywords: Musashino upland, urban river, shallow groundwater, pollution, PPCPs

Title: Household water treatment for the removal of contaminants in groundwaters in Hanoi, Vietnam

DO, Thuan an¹ ; TAKIZAWA, Satoshi^{1*} ; KURODA, Keisuke¹ ; HAYASHI, Takeshi² ; TRAN, Viet nga³

¹The University of Tokyo, ²Akita University, ³University of Civil Engineering, Hanoi

Between 2000 and 2025, the urban population in Vietnam is expected to double from 19 million to 40 million. Therefore, urbanization and increasing water demand is one of the most important challenges in Vietnam, especially in Hanoi. At present, Hanoi city relies on groundwater as a main source of water supply, but it is going to shift to the surface water as the demand increases in the near future. However, variation of rainfall, dam construction in the upstream of the Red River and climate change in the near future make the surface water unreliable water source for water supply in Hanoi City. As the extension of water supply coverage is slow, many households still rely on groundwater as their drinking water sources. However, groundwater is contaminated by ammonia, arsenic, iron, bacteria and others. In order to obtain clean drinking and cooking water many households use point-of-use (POU) treatment devices including sand filters, ceramic filters, reverse-osmosis filters, and UV irradiation.

To identify the impact of POU usage to water consumption and water quality, a survey of POU usage in 170 households in six communes in Hanoi was carried out in 2012 and 2013. Water samples were also taken to investigate the treatment efficiency of those POU. As a result of the household survey, it was found that many households in rural and suburban areas have multiple water sources and use them for different purposes, while the urban households use only piped water supply. The result indicated that between 18% and 76% of the households in these communes used POU water treatment devices, of which RO devices accounted for 58%. Groundwater was contaminated by arsenic (max 0.3 mg/L), ammonia (max. 26 mg/L), and manganese (max. 3 mg/L). Although most of the arsenic was As(III) form in groundwater, it was oxidized to As(V) in the sand filters. Thus, RO filtration was found quite effective in removal of arsenic from groundwaters.

Keywords: ammonia, arsenic, household water treatment, MDGs, reverse osmosis device, safe drinking water

AHW26-06

Room:424

Time:May 1 15:30-15:45

Prevention of heavy metals release from natural soil

SUMIKURA, Mitsuhiro¹ ; ASADA, Motoyuki^{1*} ; TASAKI, Masaharu¹ ; SERIZAWA, Sadayoshi¹

¹Shimizu Corporation

In marine silts of bay areas, or volcanic ash rocks of mountainous areas, heavy metals derived from natural soils or rocks, such as lead or arsenic have become a problem. In this paper, prevention of arsenic release from soils is reported using laboratory tests results.

Recent surface displacement in Bangkok associated with groundwater recovery

ISHITSUKA, Kazuya^{1*} ; FUKUSHIMA, Yo² ; TSUJI, Takeshi³ ; YAMADA, Yasuhiro¹ ; MATSUOKA, Toshifumi¹

¹Graduate School of Engineering, Kyoto University, ²Office of Research Promotion, Tohoku University, ³International Institute for Carbon-Neutral Energy Research (I2CNER), Kyushu University

In many cities in the world, groundwater level decrease and subsequent land subsidence has been observed associated with groundwater pumping. Bangkok, the capital city of Thailand, is also one of the cities that had been suffered from land subsidence due to groundwater extraction. Since 1960s, groundwater has been extracted for commercial and personal use. Subsequently, the cumulative subsidence of about 1 m has been reported. Recently, Thailand government has implemented several measures to regulate groundwater use, and groundwater level recovery has been reported.

In this study, we used persistent scatterer SAR interferometry (PS-InSAR) analysis, which is the method to process a series of SAR data equipped on repeat-pass satellite, to estimate ground displacement in Bangkok from November 2007 to December 2010. Since SAR data is acquired by satellite, PS-InSAR analysis has an advantage for mapping displacement pattern in wide area with high spatial density.

As a result, we estimated ground uplift with the rate of about 1 cm/year. The secular uplift has decayed over time, and can be modeled by exponential function of time. Since the groundwater recovery has been observed in areas where uplift was estimated, this uplift is likely associated with groundwater recovery. Moreover, we also estimated seasonal displacement correlated with the cycle of precipitation in eastside of Bangkok.

Keywords: groundwater recovery, surface displacement, Bangkok, persistent scatterer SAR interferometry

The Use of Isotopic Technique to the Assessment of River Recharge to the Depleted Ground Water Systems in Dhaka, Banglad

NAHAR, Mst. shamsun^{1*} ; ZHANG, Jing¹

¹University of Toyama, Department of Environmental Biology and Chemistry

Surveys of groundwater quality across Dhaka demonstrate the impact of intensive groundwater abstraction, which has led to invasion of the Dupi Tila aquifer by lower quality water in parts of the city. Groundwater chemical/isotopic monitoring is capable of discriminating between the effects of induced recharge from the polluted River Buriganga and of enhanced vertical leakage through the Madhupur Clay in contaminated urban areas. Over-exploitation of the aquifer has led to a progressive decline in water levels. The resulting cone of depression is thought likely to be causing the infiltration of polluted surface water. Stable isotopic techniques were used to characterize the hydrogeology and water sources the Dupi Tila aquifer beneath Dhaka. An interpretation of the linear $\delta^{18}\text{O}$ versus $\delta^2\text{H}$ relationship as a simple two-member mixing series between river water and recent meteoric recharge suggests that all groundwater in the lower Dupi Tila aquifer of Dhaka contains at least 30% river water.

Environmental isotope distributions approaches identify the polluted River Buriganga as the main threat to groundwater quality, indicating priorities for monitoring and aquifer protection.

Keywords: Ground Water, Dupi Tila Aquifer, Isotopic Technique, Dhaka

Groundwater Level and Flow Rate Model and Barometric Response of Water Level of Well at Otomeyama Park in Shinjuku Ward

TAKANO, Yuki^{1*} ; YOSHIMURA, Kei² ; MURAKAMI, Michio³ ; UEMURA, Takeshi⁴

¹Dept. of Earth and Planetary Phys., Univ. Tokyo, ²Atmosphere and Ocean Research Institute, Univ. Tokyo, ³Institute of Industrial Science, Univ. Tokyo, ⁴Kaijo Junior and Senior High school

Spring at Otomeyama Park in Shinjuku Ward is one of the 57 Great Springs of Tokyo, Japan. Recently, decreasing of the spring water quantity at Otomeyama Park has been at issue. In order to figure out long-term variations of the spring water quantity, the flow rate and the groundwater level have been continuously observed by Kaijo Earth Science Club since 2011. In this paper, we report the results of the examination concerning the groundwater level variation and the model, which can express the groundwater level and the flow rate simultaneously.

Otomeyama Park is located at Ochiai escarpment on the eastern part of Musashino plateau. The stratum near Otomeyama park are Kanto loam layer, Shimosueyoshi loam layer (tuffaceous clay layer), Musashino gravel layer, Tokyo layer (sand layer or clay layer) and Tokyo gravel layer from the top. Sato et al. (2013) estimated that the aquifer of the spring water is Musashino gravel layer and the catchment area is about 10-100 ha. The spring water finally joins Kanda River through the water way in the park.

Based on the flow rate observation at Otomeyama Park for more than one year, the arithmetic mean flow rate was about 20 L/min. The flow rate intensely responded to precipitation. The flow rate increased from 4 L/min to 50 L/min in 35 hours at the rainfall event in April 2-3, 2012, whose total amount of rainfall was 118 mm.

The water level of wells were observed at three stations: well No.1 (at Otomeyama park), well No.2 (at Otomeyama park) and Mejiro well (at Shinjuku Ward, 0.5 km to the north from Otomeyama park). The water level of the wells was calculated by subtracting atmospheric pressure from the water pressure in aquifer. The aquifer of well No.1 is Musashino gravel layer and is confined, while the aquifer of well No.2 is Tokyo gravel layer and is confined. The aquifer of Mejiro well is Kanto loam layer and is unconfined.

Semidiurnal fluctuation of water level was observed at well No.1 and No.2. The daily composites of water level of well No.1 in dry periods showed that the atmospheric pressure was at its top at about 9 a.m. and 9 p.m. (JST) in Tokyo by atmospheric tide, while the water level of well fluctuated anti-phase to atmospheric pressure. This barometric response caused by balancing the water level variation of well with atmospheric loading when pore pressure of aquifer is not affected by atmospheric loading (Rojstaczer, 1988). This is attributed to three reasons for the barometric response of water level of well No.1. The mouth of the well is open, so that barometric fluctuation is directly transferred to the water surface in the well. Since the well diameter is 51mm, small water exchange between the well and the aquifer can change the water level in the well. Shimosueyoshi loam layer above the aquifer is difficult to infiltrate atmospheric pressure. In contrast, the water level of Mejiro well was not responded to atmospheric load, since there is no air-barrier layer above Kanto loam layer.

Better performance model is needed to figure out long-term variations of the spring water quantity. Sato et al. (2013) predicted flow rate from precipitation using two-tank model, but the model did not utilize groundwater level. We developed a model, which express both flow rate and groundwater level. Our model was based on three-tank model. The first tank of the model represents intermediate flow. The second tank infiltrates water into the third tank but does not have side outlet. The third tank corresponds to the groundwater level. The model parameters were estimated for the flow rate and the water level of Mejiro well by means of SCE-UA method (Duan et al., 1993). In the simulation, the model accurately reproduced the observed value.

Keywords: spring water, groundwater level, tank model, barometric response, atmospheric tides

The Seasonal variation of the amount of flowing artesian well springwater in the Ashigara Plain, Kanagawa Prefecture.

MIYASHITA, Yuji^{1*}

¹Hot Springs Res. Insti. of Kanagawa Pref.

Introduction

Many of cities are located in the alluvial plain of an area along the shore for our country which is an island country. In the alluvial plain, the confined groundwater cultivated in an upside fan or mountain area is used as the source of industrial water, or a source of tap water with river water. Overuse of groundwater in the city region in period of high economic growth caused groundwater obstacles, such as ground subsidence as one of the seven typical pollution and depleted of springwater.

Also in the flowing artesian well area from which is distributed in the Ashigara plain in the western area of Kanagawa prefecture decline has been reported after the 1960s. Moreover, the investigation in 2011 showed that there were 1,000 or more flowing artesian wells in the whole Ashigara plain. Furthermore, it turned out that about 50,000 tons per day of from the whole artesian wells. However, although relation with the irrigation to a paddy field is pointed out about the seasonal variation of the amount of the springwater from flowing artesian wells, there are many questions about details.

So, in this study, investigation over one year was conducted about the flowing artesian well springwater distributed in the Ashigara plain, and seasonal variation of the amount of springwater which gushes from a flowing artesian well was clarified.

Results of an investigation and consideration

Investigation conducted one investigation per month for 205 flowing artesian wells for June, 2013 to one year, and performed measurement of the amount of natural flows, water temperature, electrical conductivity, pH, and dissolved ion concentration. Since the amount of natural flows measured at 205 points had the large variation in the amount of natural flows for every point, it standard scoreized the amount of natural flows of every month, and grouped by cluster analysis for every point where the change pattern of the amount of natural flows was alike.

As a result, the change pattern of the amount of natural flows was able to be classified into "the type corresponding to an irrigation term" which increases to the irrigation term to a paddy field, and "the type corresponding to un-irrigation term" with which a remarkable changing trend is not seen through every year. Moreover, many flowing artesian wells on the west side of the Sakawa river of "the type corresponding to an irrigation term" classified according to the above-mentioned method were distributed, and "the type corresponding to un-irrigation term" was mostly distributed on the east side of the Sakawa river.

Keywords: flowing artesian well, Ashigara Plain, amount of flowing artesian well springwater, seasonal variation, irrigation to a paddy field

Three-dimensional mapping of geochemical and isotopic characteristics of groundwater beneath the Osaka Plain

SHINTANI, Tsuyoshi^{1*} ; MASUDA, Harue¹ ; FUCHIDA, Shigeshi¹ ; EVEN, Emilie¹ ; MORIKAWA, Noritoshi² ; YASUHARA, Masaya² ; NAKANO, Takanori³

¹Graduate school of science,Osaka city University, ²National Institute of Advanced Industrial Science and Technology, ³Research Institute for Humanity and Nature

Osaka Basin, which is a large Quaternary sedimentary basin beneath the Osaka Plain, is a large reservoir of groundwater resources. The uptake of groundwater has been strictly regulated since 1960 to avoid land subsidence, which actively occurred in the period of rapid economic growth. Although the land subsidence has stopped since 1970s because of the regulation, it became a threat again due to start of uptake of groundwater for private water supplies after 2000's. Excess groundwater uptake from 100 to 300 m depths for those purposes would squeeze porewater from impermeable marine clay layers causing subsidence again.

In this study, groundwaters were mainly sampled from the wells >100 m depths, and stable hydrogen and oxygen isotope ratios and major chemical components were determined to estimate origins of water. Combining the results of our and previous studies, overall picture of three-dimensional mapping of groundwater geochemistry was drawn to discuss the groundwater flow system and the relationship to the land subsidence.

In the coastal region below sea level, seawater invaded into the groundwater aquifers <100 m depth. Stable isotope ratios of the groundwater at >100m of this area($\delta^2\text{H}$:-50‰~ -60‰, $\delta^{18}\text{O}$:-8‰~ -9‰) is smaller than those of groundwater at <100m($\delta^2\text{H}$:-40‰~ -50‰, $\delta^{18}\text{O}$:-6‰~ -7‰). Especially low isotope ratios of the groundwaters, of which chemistry was diluted Na-HCO₃ type, from the lowland west of Uemachi plateau suggest squeezing the pore water from clay layers.

In the same area, high electric conductivity and Na-Cl type chemistry indicates seawater invasion into the groundwater aquifers <100 m depth. Uemachi Fault works as recharging path for the groundwater aquifers <100 m along the western edge of Uemachi plateau. However, the recharge is not enough to fill the aquifer >200 m apart from the fault. These observations indicate that the aquifers in the aquifers beneath western lowland of Osaka Plain have not been recovered by newly recharged groundwater.

Keywords: groundwater, isotope

Source of nitrate in shallow groundwater in the Shakujii river catchment, central Tokyo, Japan

NAKAMURA, Takashi^{1*} ; HAYASHI, Takeshi² ; YASUHARA, Masaya³

¹ICRE, University of Yamanashi, ²Akita University, ³Geological survey of Japan, AIST

Water chemistry of shallow groundwater in the Shakujii river catchment in the downtown Tokyo is discussed with special reference to its nitrate and chloride concentrations. The catchment is divided into the highly urbanized lower reaches (Toshima, Kita and Itabashi Wards) and the upper reaches which have been urbanized to a lesser extent (Nerima Ward, and Nishi-Tokyo and Kodaira Cities). Shallow groundwater samples were collected from 28 wells of less than 10m deep at October 2012 and October 2013. Groundwater aquifer is in the Kanto loam layer and/or underlying stream terrace gravels. The nitrate-nitrogen concentration had wide ranges (from 0.1 to 13.6mg/l). The total coliform was detected from all shallow groundwater samples. The nitrate nitrogen isotope ranges from 5.6 to 12.3 permil, which overlaps fertilized soil and wastewater nitrogen. Moreover, End-member mixing analysis using hydrogen and oxygen isotope values revealed spatial distribution in the contribution ratios of the local precipitation and domestic water (sewage and tap). The concentration of nitrate nitrogen and total coliform was increasing along with contribution ratios of precipitation in shallow groundwater, except some samples that has high nitrogen isotope and chloride concentration. This trend suggests that the nitrate source in this area is not only from sewage leakage. It also needs to consider the loading of the nitrogen fertilizer to shallow groundwater by the precipitation infiltration.

Keywords: tokyo, urban, groundwater, nitrate nitrogen and oxygen isotopes

Underground structure and groundwater flow in Saijo plain

RYOTA, Ochi^{1*} ; TANAKA, Kazuhiro² ; SUZUKI, Koichi³ ; TOKUMASU, Minoru⁴

¹Yamaguchi University, ²Yamaguchi University, ³Central Research Institute of Electric Power Industry, ⁴Saijyo City Hall

Many flowing wells are excavated in the Saijo plain, Saijo-shi, Ehime Prefecture, which have been made use for supplying an industrial and agricultural water.

Objectives of the study is to investigate the underground structure and groundwater flow in the Saijo plain and to discuss about the relationship between geological structure and groundwater flow by CSA-MT geophysical exploration and groundwater geochemistry. The study area is composed of the late Cretaceous Izumi Group and Holocene sediments. CSA-MT method was applied to obtain the two dimensional resistivity distribution about 2 km long and 500 m deep along 3 lines with north-south direction in the Saijo Plain. As a result, the Okamura fault that displaces the Holocene and the Izumi Group with east-west strike was detected in the southern part of the area. The newly named Kita-Saijo fault that displaces the Holocene sediments with west-east strike was detected in north of the area, displacing the Kikai-Akahoya tephra (K-Ah) bed erupted at 6 Ka. River waters are penetrated from the Kamo river to the Holocene sediments in the Saijo Plain and flow on the paleo-seawater with low resistivity. Some of them were penetrated under the impermeable layer composed of silt and clay and interrupted by impermeable layer 2 m thick disturbed by the Saijo-Kita fault. Consequently, penetrated groundwater is pressurized by impermeable layer and fault. Then, pressurized groundwater erupts at the flowing wells named Uchinuki.

Keywords: flowing wells, CSA-MT method, groundwater flow, underground structure

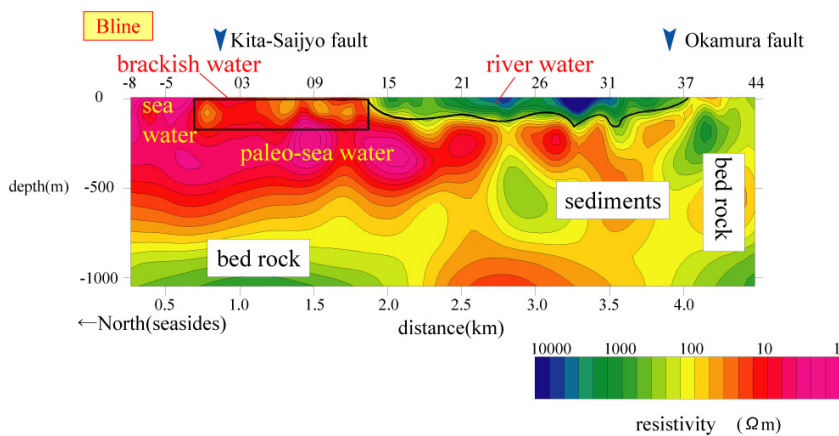


(Fig.1). two dimensional resistivity distribution of Bline

The subsurface distribution of saltwater and freshwater in the Nakano-shima island, by electromagnetic exploration

KUSANO, Yukiko^{1*} ; SUZUKI, Koichi² ; TOKUNAGA, Tomochika¹

¹The University of Tokyo, ²CRIEPI

Groundwater recharged during the last glacial period is revealed to remain in coastal aquifers and sub-seafloor formations, and it has been interpreted that the low-permeability formations have delayed the intrusion of saltwater into sub-seafloor formations (e.g. Groen et al., 2000). Thus, the effects of long-term sea-level change should be taken into account to better understand the groundwater flow system in coastal areas.

The Nakano-shima island, Oki-Dozen, is a volcanic island on a continental shelf. Because the island is situated on the continental shelf, the seafloor around the islands was most likely widely exposed during the last glacial period, and hence the distribution of salt/fresh water in subsurface is estimated to have been affected by the sea-level change after the Last Glacial Maximum. According to a well-drilling report of a hot spring well in the island, groundwater of which Cl concentration corresponds to 20% of sea water was obtained when the well reached to 320 m deep, and groundwater of which Cl concentration corresponds to 5% of sea water was obtained when the construction was completed (screen depth: 560 - 866 m). In addition, the hot spring water taken from the screen depth is suggested to be recharged in colder climate than present based on the stable isotopic ratios of water, dissolved components, and groundwater-age indices (Kusano et al., in press). These results suggest that the groundwater containing higher salinity exists in shallower than 320 m deep, and that the groundwater containing lower salinity and recharged in colder climate exists in deeper formations. In this study, electromagnetic exploration using CSAMT method was conducted to reveal the distribution of salt/fresh water beneath the island.

A 2.5 km-long measurement section for the electromagnetic exploration was set, along which the hot spring well exists, in east-west direction. Measurement points were placed at about 100 m intervals. Measured apparent resistivity data were used to obtain a two dimensional resistivity structure along the measurement line by two-dimensional inversion scheme developed by Uchida and Ogawa (1993). For better interpreting the resistivity structure in the island, volcanic and sedimentary rock samples obtained from the island were used to measure the bulk resistivity as a function of salinity of the pore water.

The result of two-dimensional inversion showed the higher resistivity zone from the surface to about 100 m depth, a continuous lower resistivity zone throughout the section in between 100 and 200 m depth, higher resistivity zone below, and lower resistivity zone further below, i.e., existence of four distinct resistivity zones. Resistivity values in between 100 and 200 m depth and those in the deepest zone were consistent with bulk rock resistivities saturated with higher salinity water. The results are consistent with the fact that groundwater with higher salinity was obtained when the well reached to 320 m depth and that groundwater with lower salinity was obtained after the well reached to 866 m depth. The obtained resistivity structure might suggest that fresh groundwater recharged in the last glacial period remains in the subsurface of the island, and salt water was intruded into the 100-200 m deep zone after transgression.

References

- Groen, J. et al., 2000. *J. Hydrol.* 234, 1-20.
- Kusano, Y. et al., in press, *J. Hydrol.*
- Uchida, T. and Ogawa, Y. 1993. Geological Survey of Japan Open-File Report, 205.

AHW27-02

Room:424

Time:May 1 09:15-09:30

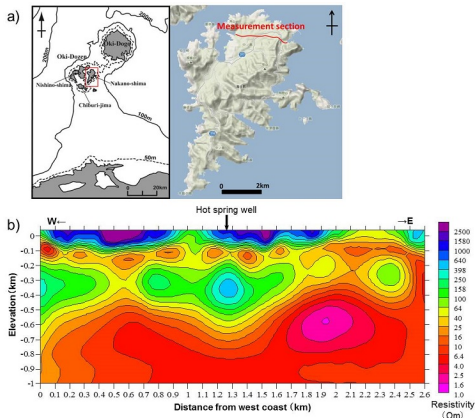


Fig. a) Location of measurement section of CSAMT survey and b) resistivity profile analyzed by 2D inversion of the CSAMT survey in the island.

The method of an estimation of underground parameters of a geyser induced by boiling using the dynamical model

KAGAMI, Hiroyuki^{1*}

¹Nagoya College

We have proposed a static model, a dynamical model and a modified dynamical model of a geyser induced by gas inflow based on observation and model experiments of it and have also proposed a combined model combining above two models. And numerical simulations of the modified dynamical model or the combined model reappear spouting dynamics of a geyser induced by gas inflow and it becomes possible that parameters (volume of the underground space, depth of spouting hole and so on) under a geyser are estimated through comparison between results of numerical simulation and those of observation. Moreover we proposed a dynamical model which assumed more than two underground gas supply sources by extension of above-mentioned usual dynamical model. As a result, irregular spouting dynamics of a geyser induced by gas inflow could also be reappeared by the modified model. As a result, spouting mechanism of all kinds of geysers induced by gas inflow has been clarified.

However, in general, geysers are classified into two types dependent on inducer. That is, one is a geyser induced by inflow of gas and the other is a geyser induced by boiling. The latter is more popular and many ones exist all over the world. Though qualitative spouting models of a geyser induced by boiling have been proposed, its dynamics has not been discussed sufficiently. Therefore, then we derived a dynamical model of a geyser induced by boiling applying the above-mentioned dynamical model of a geyser induced by inflow of gas. Then we tried to estimate time derivation of spouting rate of a geyser induced by boiling through numerical simulations. Using the model we can estimate underground parameters of a geyser induced by boiling by comparison of results of numerical simulation of the model and those of observation of a geyser induced by boiling.

In this presentation, after we review above-mentioned models of a geyser induced by gas inflow and one induced by boiling in outline, we explain the method of an estimation of underground parameters of a geyser induced by boiling using the dynamical model.

Rapid alkalization in Lake Inawashiro: implications for future changes in the carbonate system of terrestrial waters

MANAKA, Takuya^{1*} ; USHIE, Hiroyuki¹ ; ARAOKA, Daisuke¹ ; INAMURA, Akihiko² ; SUZUKI, Atsushi² ; KAWAHATA, Hodaka¹

¹Atmosphere and Ocean Research Institute, The University of Tokyo, ²National Institute of Advanced Industrial Science and Technology

The global carbon cycle, one of the important biogeochemical cycles controlling the surface environment of the Earth, has been greatly affected by human activity. Anthropogenic nutrient loading from urban sewage and agricultural runoff has caused eutrophication of aquatic systems. The impact of this eutrophication and consequent photosynthetic activity on CO₂ exchange between freshwater systems and the atmosphere is unclear. In this study, we focused on how nutrient loading to lakes affects their carbonate system. Here, we report results of surveys of lakes in Japan at different stages of eutrophication. Alkalization due to photosynthetic activity and decreases in *PCO*₂ had occurred in eutrophic lakes (e.g., Lake Kasumigaura), whereas in an acidotrophic lake (Lake Inawashiro) that was impacted by volcanic hot springs, nutrient loading was changing the pH and carbon cycling. When the influence of volcanic activity was stronger in the past in Lake Inawashiro, precipitation of volcanic-derived iron and aluminum had removed nutrients by co-precipitation. During the last three decades, volcanic activity has weakened and the lake water has become alkalized. We inferred that this rapid alkalization did not result just from the reduction in acid inputs but was also strongly affected by increased photosynthetic activity during this period. Human activities affect many lakes in the world. These lakes may play an important part in the global carbon cycle through their influence on CO₂ exchange between freshwater and the atmosphere. Biogeochemical changes and processes in these systems have important implications for future changes in aquatic carbonate systems on land.

Keywords: the global carbon cycle, lake, alkalization, nutrient, *PCO*₂

Variation of $\delta^{13}\text{C}$ carbon isotope signatures of particulate organic matter in the Kuzuryu River system in Japan

NAGAO, Seiya^{1*} ; KANAMORI, Masaki² ; ARAMAKI, Takahumi³ ; OCHIAI, Shinya¹ ; YAMAMOTO, Masayoshi¹

¹LLRL, INET, Kanazawa University, ²Grad. School of NST, Kanazawa University, ³National Institute for Environmental Studies

Radioactive and stable isotopes of carbon (^{14}C and ^{13}C) can serve as powerful tools for identifying sources and estimating turnover times of organic matter in aquatic systems. This study discussed with the transport of particulate organic matter in the rivers from a river system with different watershed condition using carbon isotopic signatures.

The Kuzuryu River system is located in Fukui Prefecture in the central part of Japan and consists of a main river, Kuzuryu River and a main tributary of the Hino River. River research was conducted at a fixed station in the Hino River (Fukatani site) and the Kuzuryu River (Nakatsuno site) during June-October in 2010. Suspended solid samples were collected from 130-140 L of river waters using continuous centrifugation. Prior to analysis, inorganic carbonates were removed by adding 0.1 M HCl solution, rinsing with Milli-Qwater, and drying again. Stable carbon isotopic ratio of a sample and the VPDB standard used for normalization were made by analyzing sub-samples of CO_2 gas generated during graphite production using a triple collector mass spectrometer with precision of ± 0.2 ‰ as the $\delta^{13}\text{C}$ value. Radiocarbons were determined using accelerator mass spectrometry at the Japan Atomic Energy Agency. Radiocarbon values were reported as $\Delta^{14}\text{C}$ corrected for sample $\delta^{13}\text{C}$ with absolute error of less than 10 ‰.

$\delta^{13}\text{C}$ of organic matter in riverine suspended solids has -26.3 to -24.0 ‰ for the Kuzuryu River and -27.0 to -26.1 ‰ for the Hino River. The $\Delta^{14}\text{C}$ vales of the Kuzuryu and Hino samples are -168 to -87 ‰ and -209 to -143 ‰, respectively. The $\Delta^{14}\text{C}$ values of Hino River depleted in $\Delta^{14}\text{C}$ rather than the Kuzuryu River. The averaged TOC/TN ratio is 9.1 ± 1.1 for the Kuzuryu and 8.2 ± 1.1 for the Hino. There is a positive correlation with the $\Delta^{14}\text{C}$ vales and water discharge. These results indicate that the differences in POM character may be explained by the differences in watershed conditions and controlled by water discharge.

Keywords: POC, carbon isotopes, river waters, migration, water discharge

Age dating of spring water, groundwater and stream water in mountainous watersheds using multi-tracer approach

IKEDA, Hayato^{1*} ; TSUJIMURA, Maki² ; KATSUYAMA, Masanori³ ; NAGANO, Ryuhei⁴

¹College of Geoscience, School of Life and Environmental Sciences, University of Tsukuba, ²Faculty of Life and Environmental Sciences, University of Tsukuba, ³Inter-Graduate School Unit for Sustainable Development and Survivable, Kyoto University, ⁴Graduate School of Agriculture, Kyoto University

This study aims at estimation of mean residence time (MRT), to reveal the spatial distribution using multi-tracer approach in mountainous catchment, and to make clear relationship between hydrological characteristics and the variation of the residence time. First, we conducted field survey and sampling in Kiryu Experimental Watershed, in southern Shiga, in June, August and October, 2013 and analyze major dissolved inorganic ions, SiO₂, chlorofluorocarbons (CFCs) and stable isotopes (SI). Second, we estimated MRT using CFCs. We also evaluate MRT using seasonal variation of SI of rainfall, groundwater and stream water that collected monthly from 2008 to 2012.

The MRT of stream water and groundwater were estimated to be ranging from approximately 2.8 to 4.4 years by using SI as tracers. The MRT of spring water and groundwater were estimated to be ranging from 1.5 to 8.5 years and 15 to 23 years, given a water temperature as recharge temperature using CFCs. The relationship between Na⁺ concentration and MRT based on CFCs suggested that short MRT that provided from decrease trend in atmospheric CFCs concentration is appropriate.

The MRT of water by CFCs ranged from 1.5 to 8.5 years, whereas that by SI ranged from 2.8 to 4.4 years in this catchment. This result conforms that of previous studies using SI, however the MRT by CFCs shows larger value range because CFCs represent time resolution information. In addition, the MRT varies in time and space due to mixing of different subsurface flow with different MRT and flow path.

Keywords: multi-tracer approach, mean residence time, stable isotope, chlorofluorocarbons

Sources and recharge process of groundwater in sub-urban area of Hanoi city, Viet Nam

HAYASHI, Takeshi^{1*} ; KURODA, Keisuke² ; AN, Do thuan² ; TAKIZAWA, Satoshi² ; NGA, Tran thi viet³

¹Faculty of Education and Human Studies, Akita university, ²School of Engineering, the University of Tokyo, ³Hanoi University of Civil Engineering

Water demand in Hanoi city, the capital of Viet Nam, has been increased with recent rapid urbanization. Although high concentration of Arsenic is contained, groundwater is one of important water resources in this city. Groundwater abstraction has induced depletion of groundwater levels in major aquifers (Holocene shallower aquifer and Pleistocene deeper aquifer) not only in the central area but also sub-urban areas. On the other hand, urbanization reduces the surface water areas such as ponds, rivers and canals, and paddy fields. We focus on the interaction between surface water and groundwater to clarify water cycle and solute transport process in Hanoi area for sustainable water resource management. We are carrying out regular measurement of geochemical properties of surface water and groundwater, monitoring of groundwater levels in the major aquifers, and evaluation of groundwater age in some sub-urban villages.

The result of our previous study shows the surface water with evaporation process is a major source of groundwater in the study area. From the result of the regular measurement of surface and ground water and monitoring of groundwater levels in the shallower aquifer (unconfined condition), we found seasonal change of groundwater levels and geochemical properties of groundwater related with fluctuation of rainfall between rainy season and dry season. Also, seasonal change of geochemical properties was delayed several months to that of groundwater levels. This difference suggested the relatively slow infiltration of surface water with evaporation process into the shallower aquifer. On the other hand, result of CFCs and SF₆ measurement showed apparent groundwater age in the shallower aquifer of the study area is several decades. These results may suggest groundwater abstractions enhance water cycle in the study area.

Keywords: Hanoi city, groundwater recharge process, fluctuation of groundwater level, isotopes, groundwater age

Long-term trends of climate variability in upper Dong Nai river basin in Vietnam

TRUONG, Nguyen cung que^{1*} ; KONDOH, Akihiko²

¹Department of Earth Sciences, Graduate School of Science, Chiba University, ²Center for Environmental Remote Sensing, Chiba University

According to a report of the Intergovernmental Panel on Climate Change (IPCC) and last studies, Vietnam is considered as one of the most countries affected by climate change. That are in the sea level rises (SLR) 1 m scenarios, about 10-12% of Vietnam's population are directly impacted and the country will lose up to 10% of GDP. With the combination of SLR and an increase in precipitation in the rainy season, there is a possibility of a serious impact on low-lying coastal area and leads to flooding of up to 40,000 km² of the coastal delta and 90% of the Mekong River delta. It is also expected that temperatures will rise more significantly in the plateau region. Dong Nai river basin is located in the Southern Vietnam along with the Mekong River, that have supplied the major water resources of southern. Dong Nai river originates from the plateau of the Southeastern, through the Tri An reservoir, a major power generating dam of southern Vietnam, in the lower area it mixed with the tributaries of the Mekong Delta downstream and after that flows to East sea.

In the state which continues of changes on water resources Mekong river due to climate change, controversy about the potential impact of sediment transport and river flows downstream due to the cascade hydroelectric power plant system or dam construction on the upper Mekong basin, because of Dong Nai river basin is a water resources that can controlled by Vietnam, it is considered that is necessary to analyses change in hydrological regime due to climate variability and adaptation to that changes. The purpose of this study is detecting long-term changes in the climate data and runoff due to climate change in the Dong Nai river basin.

As hydrological information of the target basin, the Dong Nai river basin, last 20 years (form 1992 to 2011) data which observed by National Center for Hydro-Meteorological Forecasting (NCHMF), Department of Natural Resources and Environment (DONRE) of each region, Tri An hydroelectric power plant management office were analyzed by Empirical Mode Decomposition (EMD) to detected a long-term change in rainfall, temperature, potential evapotranspiration and runoff at the basin outlet (inflow of Tri An reservoir). EMD has recently been pioneered by Huang et al. for adaptively representing nonstationary time-series data as sums of zero-mean amplitude modulation frequency modulation components. The components, called intrinsic mode functions (IMFs), allow the calculation of a meaningful multicomponent instantaneous frequency.

The results show that trend of rainfall and temperature slightly increase, but the trend of potential evapotranspiration and runoff decrease in the last two decades within the basin. In the comparison with the results of Mekong River Commission or World Bank research on Climate change in Vietnam, we similarly conclude that rainfall and temperature tend to increase. It is considered change in land cover and land use within the basin is one of the causes of the downward trend of runoff. This is planning on the next study.

Keywords: Dong Nai river basin, climate variability, empirical mode decomposition, EMD

A consideration of sustainable grazing over Mongolia, as point of view of recent climate change and vegetation responses

KAWAKAMI, Satoshi¹ ; HIGUCHI, Atsushi^{2*}

¹HP Japan, ²CEReS Chiba University

We will present two topics. One is winter extreme-cold-events (ECE) detected by JRA-25/JCDAS reanalysis object dataset over Mongolia. Since 2000's ECE frequently occurred rather than 1990's, closely linking with synoptic scale circulation change in mid-high latitude. Such synoptic scale circulation change triggered by changing area of sea-ice over Barents Sea. Second topic is vegetation reaction process revealed by satellites observation. We used MODIS spectral reflectance dataset boarded on Terra/Aqua platform. Also we used two vegetation indices: One is major vegetation index, NDVI, the other is Green-Red ratio Vegetation Index (GRVI). NDVI is applied as proxy index of biomass, GRVI is regarded as proxy of biodiversity index. Based on matrix field of NDVI and GRVI, we define the recover status (2012) from herbaceous degradation in 2009. We found that faster recovered areas were located in the foot-fill. More detailed (e.g. degradation process period) analysis will be show in presentation.

Keywords: Mongolia, grazing, extreme colod events, NDVI, GRVI

Effect of snow depth on hydrology of highland marshes - Analysis of PALSAR/ALOS data at Kiritappu, Sarobetsu and Oze -

IGARASHI, Masatoshi¹ ; HISADA, Yasuhiro¹ ; DEMURA, Hirohide¹ ; OGAWA, Yoshiko^{1*} ; SOBUE, Shinichi¹

¹Univ. of Aizu, ²RESTEC

It is basically very difficult to monitor the hydrological environment of highland marsh with snow in winter. We lastly reported that the most famous highland marshes Oze keeps a largest amount of liquid water body under the thick snow layer (more than 2 m) in midwinter based on our analysis of PALSAR/ALOS data, a kind of L-band radar. We concluded that such liquid water would be squeezed out from peat layers by the load of heavy snow and not the meltwater. In this presentation, we show our new analysis results at Kiritappu and Sarobetsu, both of which are highland marshes locating in Hokkaido, where it snows a lot but not as much as Oze in winter. The PALSAR/ALOS data is used again. This time we find almost no liquid water body in midwinter and recognize the singularity of Oze. We try to evaluate the effect of snow depth, peat depth on hydrology of highland marshes in winter.

Keywords: highland marsh, hydrology, PALSAR, remote sensing, snow, peat

Modeling of hydrological temporal-spatial data by a universal model

KUZUHA, Yasuhisa^{1*} ; ARAKI, Daisuke¹ ; SAITOH, Hanako² ; GOMI, Chieko³ ; SENDA, Makiko⁴

¹Graduate School of Bioresources, Mie University, ²Faculty of Bioresources, Mie University, ³Aichi Prefectural Government, ⁴Kyoto Koka Women's University / Osaka Seikei University / Osaka Seikei College

We propose "the universal model" which generates hydrological temporal or spatial data. First a white noise is generated, then the white noise is filtered by a specific filter and data are generated. If a field is fractal, log-log-linear-filter (ω vs. $P(\omega)$) is used (Lavallée, 2008). If a field is modeled by e-model (Gomi and Kuzuha, 2013), an exponential filter is used. We examined rainfall time series, spatial rainfall fields, time series of ion concentration in river water, and ion concentration in tap water. As a result, those data were modeled by the universal model.

Gomi, C. and Y. Kuzuha(2013), Simulation of a Daily Precipitation Time Series Using a Stochastic Model with Filtering, Open Journal of Modern Hydrology, DOI: 10.4236/ojmh.2013.34025

Lavallée, D.(2008), On the Random Nature of Earthquake Sources and Ground Motions: A United Theory, Advances in Geophysics, Vol. 50, 2008, pp. 427-461.

Keywords: fractal, hydrological temporal-spatial data, filtering, universal model, e-model

Characteristics on groundwater salinization in a downstream area of dam reservoir, a coastal region of NorthEast Tunisia

UCHIDA, Chisato^{1*} ; KAWACHI, Atsushi² ; TSUJIMURA, Maki² ; SHIBAYAMA, Naoyuki¹ ; ZIADI, Amira³ ; TARHOUNI, Jamira³

¹Graduate School of Life and Environmental Sciences, University of Tsukuba, ²Faculty of Life and Environmental Sciences, University of Tsukuba, ³National Institute of Agronomy in Tunisia

This study tried to characterize salinization processes of coastal shallow groundwater in a downstream area of dam reservoir, based on field investigation and chemical water analyses in order to indicate positive effects of dam reservoir on prevention of the groundwater salinization or seawater intrusion. Thus, focusing on two neighboring watersheds: Lebna and Chiba watersheds located in Korba aquifer (North-East Tunisia), the field investigation was carried out at 72 locations in June 2013, then water samples were collected at the 63 locations.

At first groundwater table contour map was drawn using investigated groundwater level data, and the groundwater flow was estimated. From the chemical analyses, spatial distributions of dissolved inorganic ions' concentrations, and stable hydrogen and oxygen isotopic compositions were obtained. Then, the seawater ratio in the groundwater samples were calculated using mass balance equation of chloride concentration under assumption chloride was derived from seawater. Using the seawater ratio, a theoretical concentration of each parameter were estimated, and differences between the analytical and theoretical concentrations were obtained. Additionally saturation indices were calculated based on chemical equilibration theory. Moreover, multivariable analyses: Cluster Analysis (CA) and Principal Component Analysis (PCA), were conducted to classify the groundwater salinization process and to determine the important parameters associated with the process.

As a result, the groundwater level (GWL) in the downstream of Lebna dam reservoir was higher than the sea level, while the GWL in Chiba watershed was lower than the sea level. The lowest point is about -10 m above sea level. According to seawater ratios and stable isotopic compositions, the study area were categorized into the following three types: (i) high seawater ratio, (ii) low seawater ratio and low isotopic compositions, and (iii) low seawater ratio and high isotopic compositions. On the other hand, CA results showed the study area were categorized into 5 clusters, and the PCA showed the following three phenomena were main reasons for the 5 clusters: (a) seawater ratio in groundwater, (b) inverse cation exchange by reaction between seawater and clay minerals, and (c) directly or indirectly groundwater recharge from Lebna dam reservoir. Moreover, considering totally the three types (i), (ii), (iii), three phenomena (a), (b), (c), and groundwater level, the study area could finally be divided into 3 areas A, B, C which have different characteristics on groundwater salinization

Area A is located around Lebna dam reservoir, in which groundwater level is higher than sea level and the stable isotopic compositions are relatively higher. High groundwater level is probably sustained by the direct recharge from the reservoir, or by infiltration of the irrigation water from the reservoir in the farm land. Area B is located near shoreline, in which groundwater level ranges 0 to -4 m above sea level, and high seawater ratio and high concentration of each dissolved ion are observed. The groundwater in this area has high concentrations of sodium and chloride (derived from seawater) and calcium (derived from inverse cation exchange) due to seawater intrusion. Area C is located in inland area of Chiba watershed, in which groundwater level is lower than -4 m above sea level. There should be three groundwater flows: from Area A, and the upstream of Chiba watershed with fresh groundwater derived from precipitation, and from Area B with saline water, especially high concentration of calcium. Therefore, the groundwater in this area probably consists of the three different origin waters.

Keywords: seawater intrusion, dam reservoir, dissolved inorganic ions, stable hydrogen and oxygen isotopic compositions, mass balance, multivariable analyses

Geochemical features of groundwaters around the southern Itoigawa-Shizuoka tectonic line, western Kofu Basin

YAGUCHI, Muga^{1*} ; MURAMATSU, Yoich² ; CHIBA, Hitoshi³ ; OKUMURA, Fumiaki⁴ ; YAMAMURO, Masumi¹

¹Gra.Shc.,The Univ.Tokyo, ²Fac.Sci. and Tech.,Tokyo Univ.Sci., ³Fac.Sci.,Okayama Univ., ⁴Japex R.C.

Over the last few decades, drilling of thermal wells for hot spring bathing purposes were performed extensively on a deep aquifer at the depths more than 1000m in the non-volcanic area of Japan. Around the southern part of Itoigawa-Shizuoka Tectonic Line (ISTL), western Kofu Basin of central Honshu, many numbers of ground waters from drilled wells have been used for hot spring bathing. Some of these waters have high salinity, up to more than sea water salinity level, but their genesis and the formation mechanism of water quality have not been clarified previously. In this study, chemical and isotopic compositions of hydrogen (D/H), oxygen (¹⁸O/¹⁶O) and sulfur (³⁴S/³²S) of several ground water samples from, such as, natural spring and drilled wells around the southern part of ISTL, western Kofu Basin were analyzed in order to discuss the origin of waters and the formation mechanisms of water quality.

Temperature of the samples was up to 48.8 °C, and the pH is between 6.4 and 9.7. The waters were subdivided into a Ca-HCO₃ type, Ca·Mg-HCO₃ type, Na·Ca-HCO₃ type, Na-HCO₃ type, Ca-SO₄ type, Na-Cl·HCO₃ type, and Na-Cl type. Among these, Na-Cl type was the most dominant water quality and maximum Cl concentration of the samples was up to about 23000 mg/L.

Due to plot of Na and Cl concentration of groundwaters were distributed along with mixing line between rain water and sea water, Na-Cl type water, which is dominant water quality type in the study area were appears to be derived from mixing of rain water and sea water end-members. δD and δ¹⁸O plot of the low salinity waters were distributed along with the Global Meteoric Water Line, supporting that the low salinity end-member is originated from rain water. However, δD and δ¹⁸O values of the waters which have high salinity (more than sea water salinity) were low compared with modern seawater values. The Mg/Cl and SO₄/Cl ratio of these high salinity waters were very low compared with modern sea water, whereas the Ca/Cl ratio is higher than modern sea water. These chemical and isotopic characteristics of the sample waters indicate that the high salinity end-member of the study area is altered sea water.

Keywords: Itoigawa-Shizuoka tectonic line, deep fluid, water quality, formation mechanism

A Study on the Origin of a Spring in Tottori Sand Dunes using various geophysical and hydrological methods

SHIOZAKI, Ichiro^{1*} ; KAWAI, Takayuki² ; NOGUCHI, Tatsuya¹ ; SAITO, Tadaomi³

¹Graduate School of Engineering, Tottori University, ²Research Institute for Natural Hazards and Disaster Recovery, Niigata University, ³Faculty of Agriculture, Tottori University

There is an oasis that changes its appearance depending on the season in the depression south of Umanose (horseback), which is a symbol of the undulations of Tottori Sand Dunes. This oasis is not always visible. It disappears during the summer. The influent that constantly flows over the ground surface into the oasis depression forms Shirinashigawa River when oasis is gone, as the inflow water permeates into the sand or evaporates. By what mechanism does this oasis appear and disappear? That is, where does this influent come from and where does it go? This question about the oasis spring has been a scientific interest for a long time. For example, there have been a proposal that the rainwater from rain in the sand dunes became groundwater, some of which formed a spring and appeared on ground surface again(Akagi, 1991), a proposal that the rainwater permeating into the sand dunes with low water-holding property accumulated as groundwater near the impermeable stratum of the bedrock or volcanic ash layer with low water permeability and formed spring (Natural Parks Beautification and Management Foundation, 1995), and a recent study that investigated the relevance of oasis formation and the changes in water level in Tanegaiké which is located south of the sand dunes (Hoshimi, 2009).

To answer this question, that is, to search for the origin of the spring in sand dunes (oasis), this study was conducted on the subsurface structure and circulation of groundwater in Tottori Sand Dunes. We estimated the subsurface structure of Sand Dunes and obtained basic data on groundwater existence, mode of its flow, the base structure of sand dunes using various nondestructive geophysical exploration methods, and tried to elucidate the origin of the oasis spring and the quantitative rise and fall mechanism also incorporating hydrological methods. While the specific methodologies used here will be described in a later section, we applied electrical resistivity imaging method, 1 m-depth geothermal prospecting, self-potential method, tremor probing and gravity probing to estimate the former subsurface structure and introduced continuous water level observation on oasis and analysis of evaporation quantity, groundwater level survey in oasis and its proximity, and analysis on stable isotope ratio of oasis spring water and water sampled from Tanegaiké for the latter. For the former application, we conducted a GPS survey using a differential method so that we could understand the positions of observation points and grasp the overall topography of the sand dune area. For the latter application, we conducted a survey using total station to grasp the microtopography of the oasis area and its proximity.

As a result, we reached a conclusion as described below regarding the subsurface structure of Tottori Sand Dunes and the origin of the spring in sand dunes (oasis). “ Rainwater permeates into the sand dunes and form groundwater. A part of it is lead to the aquifer mainly formed on the volcanic ash layer (as perched water) and flows into the oasis spring. Then, the oasis spring flows into the sea through underground of Umanose. There is no simultaneous or direct relevance between oasis spring and the water in Tanegaiké. We found association between the overall groundwater distribution in Tottori Sand Dunes area (sand dunes for sightseeing) and the undulations of the bedrock structure estimated by the subsurface structure analysis.” It is surmised that this study verified these things from quantitative observation values including subsurface structure, changes in water level, changes in isotopes and so forth of sand dunes had significance of its own. This article will report on the basic scientific background, an outline of the study, the results of multiple surveys and their interpretation, and an overall summary of them.

Keywords: Tottori sand dunes, underground water, geophysical exploration methods

Spatial distribution and transport of phosphorus in a hillslope profile in Ichikawa City, Chiba Prefecture, Japan

PIAO, Jingqiu^{1*}; TANG, Changyuan¹; ZHANG, Han¹; SAKO, Yoko¹

¹Graduate School of Horticulture, Chiba University

Transport of phosphorus (P) in subsoil is presumed to be minor in comparison to transport in topsoil. Three Soil columns that located at upland (agriculture land), hillslope and forest (background) were sampled in Ichikawa City (35.76°N, 139.97°E), Chiba Prefecture, Japan. Contents of the total P (STP), organic P (OP) and inorganic P (IP) were determined to assess the spatial distribution, origin and transport pathways of P in the soil of unsaturated zone. In unsaturated zone soil texture is in a sequence surface layer (SF), Kanto loam layer (LO), Joso clay layer (CY) and Narita sand layer (SA) of the upper part of slope profile and SF, the secondary deposited loam layer (SE), clayey sand layer (MI) and SA of the down part of slope profile. Soil samples were obtained from the slope profile at four sites (A, B, C, D). LO, CY and SA is covered the forest soil profile.

In forest soil, the contents of STP, OP and IP were 30-163 mg/kg, 5-63 mg/kg and 19-103 mg/kg, respectively. There averages in different layers were in the order: LO >CY >SA, respectively. In hillslope, the contents of STP, OP and IP were 42-1723 mg/kg, 20-1229 mg/kg and 18-839 mg/kg, respectively. The average in different layers were in the order: SF (1564 mg/kg) >SE (1349 mg/kg) >LO (494 mg/kg) >MI (492 mg/kg) >SA (91 mg/kg) >CY (69 mg/kg). There were similar changing trends between OP, IP and STP with the average in different layers. And the contents of OP were not higher than IP content in most layers, however, more than twice in SF and SE. Ratios of OP/STP in SF and SE were 63% and 64% which were similar with the ratios in topsoil of upland profile. Therefore, it is supposed that P in topsoil of hillslope was transported from upland by runoff and soil erosion. In addition, the average ratios of OP in LO, CY, MI and SA were 30-52%, lower than the average in SF and SE in hillslope profile.

STP contents of subsoil in hillslope were much higher than forest. It is assumed that there was external phosphorus loading on the subsoil in slope profile. The results indicated that P transported from the surface soil to subsoil. Moreover, there was an accumulation on the soil above CY which the depth is 2.8-3.4m than upper LO of A site. The CY is supposed to block the P transport along the profile. In SE, there was no obvious change of site B and C, showing that the soil of SE may be in saturation status of the P adsorption. And STP contents of MI and SA were lower than SE. It means there was no a great phosphorus accumulation on MI and SA. So P could transport toward to deeper stratum with soil water flow. Finally, P would be likely to enter the groundwater.

The results indicated that the contents of STP, OP and IP varied greatly in different stratum. And this study inferred that two P transport pathways. One was P transports as particulate form by surface runoff, soil erosion in the topsoil. The other one was P transports with the infiltration of soil water as soluble phosphate in the unsaturated zone. And P is likely to enter the groundwater, and would be moved towards wetland with groundwater flow, affect the ecological environment finally.

Keywords: phosphorus, spatial distribution, transport, hillslope profile

Nitrogen budget of a headwater wetland

LI, Xing^{1*}; TANG, Changyuan¹; HAN, Zhiwei¹; CAO, Yingjie¹; PIAO, Jingqiu¹

¹Graduate School of Horticulture, Chiba University

As human activities continue to alter the global nitrogen cycle, understanding of the impact of increased nitrogen loading to freshwater systems is becoming more and more important. The study area is a typical headwater wetland, located at Ichikawa City (35.76°N, 139.97°E), Chiba Prefecture, Japan. The wetland valley is U-shaped with an elevation of about 16 m above sea level. The wetland receives discharge (both groundwater and overland flow) from an adjacent upland (elevation 26-31m) area with vegetation consisting of mostly pear orchard. A stream flowing through the wetland valley is recharged by spring water and groundwater in the wetland. Average flow rate of the stream all around a year is 21.7 L S⁻¹ at the export of the wetland. The wetland is with surface area of 48000 m², corresponding to 4.7% of the watershed. The uplands are covered by pear orchard, whereas the lowland is wetland. The average nitrate load is 501.9 mg S⁻¹ at export of stream and average dissolved N₂O load is 151.9 µg S⁻¹ at export around a year. Ammonia and nitrite were nearly undetectable in the upland groundwater stream water in this study.

For the upland, annual nitrogen inputs refer to the sum of fertilizer application and atmospheric deposition, whereas the outputs refer to root absorption, N₂O emission from soil surface and leaching of nitrogen. Nitrogen fertilizer is 346 kg ha⁻¹yr⁻¹ which is relative high to other studies. Annual average N deposition by precipitation over Japan was from 7 to 10 kg ha⁻¹yr⁻¹ (with a mean value of 8.5 kg ha⁻¹yr⁻¹) during the past few decades (Hara, 1995). The composition in leaching nitrogen is only nitrate and the leached nitrate is 202 kg ha⁻¹ yr⁻¹ in upland. The annual N₂O emission was 5.77 kg ha⁻¹ from the upland area.

For the wetland, annual nitrogen inputs refer to the sum of nitrate leaching from upland and atmospheric deposition of wetland. Annual nitrogen outputs refer to the sum of export by stream, and gas emission. The wetland receives 20652 kg-N yr⁻¹ from atmospheric deposition and groundwater which recharge from agricultural upland. The nitrogen exports by stream were 15359.8 kg yr⁻¹. The measured emission of N₂O was 61.6 kg yr⁻¹ and the calculated emission of N₂ was 5218.6 kg yr⁻¹. As a result, our estimate of N retention for the wetland watershed was 26.5%. Valigura (1996) and Whitall and Paerl (2001) estimated that N retention in urban watersheds ranges from 25% to 95%, with a best estimate of 40%. From the view of literature, the nitrate-nitrogen retention by mass was extremely low in this study. It is assumed that the high loading of nitrogen is a limit factor of nitrogen retention in wetland. The reason that the low percentage of nitrate-nitrogen retention may due to the extremely high load of nitrate input of groundwater (430 g-N m⁻²yr⁻¹ or 4300 kg ha⁻¹ yr⁻¹). However, the nitrate-nitrogen retention was 110 g-N m⁻²yr⁻¹ which is much higher than that (39 g-N m⁻²yr⁻¹ and 46 g-N m⁻²yr⁻¹) in study of William J. Mitsch (2005) and reach the retention level of constructed wetland.

Direct emission factor EF₁ was 0.017 which is higher both than the default values of IPCC 1996 and 2006, but was still in agreement with the range of uncertainty. Indirect emission factor EF_{5-g} was 0.003 which is much lower than the default value of IPCC 1996, whereas it was agreement with the default value of IPCC 2006. EF_{5-g} value in this study was also consistent with the result of (0.0025) another study in Japan (Sawamoto, 2005). Ratio of dissolved N₂O and NO₃⁻ in groundwater ranged from 0.00026 to 0.0157, with an average value of 0.0025. Using 0.0025 as the EF_{5-g} value would revise the estimation of the indirect emission from this wetland, resulting of 51.5 kg yr⁻¹. The measured emission of wetland was 61.5 kg yr⁻¹ which is the same order of magnitude with calculated value, indicating that the method advised by IPCC could reasonable predict the indirect emission of wetland.

Keywords: nitrogen budget, dissolved N₂O, wetland

Influence of the Noboribetsu hydrothermal systems on surrounding water regions

OCHIAI, Yasuhiro^{1*} ; CHIKITA, Kazuhisa¹

¹Division of Earth and Planetary Dynamics, Department of Natural History Sciences, Faculty of Science

A variety of hydrothermal systems exist in the Noboribetsu area, Hokkaido, which produces neutral to acidic hot springs. The high δD and δO^{18} values for the hot springs suggest that they originate from magmatic water (Matsubadani et al., 1977). Also, this area, including Lake Kuttara next to Noboribetsu, exhibits high geothermal gradient of 90 °C/km (Matsubadani et al. 2011). However, a short knowledge of the geological structure makes us difficult to discuss the whole hydrothermal systems. In this research, water and heat budgets of a boiling pond, downstream of the Ohyunuma Pond, were estimated by monitoring water temperature. As a result, the heat fluxes from the bottom of the pond were estimated at 2,482 W/m² and 3,360 W/m² for two periods. Meanwhile, water temperature of Lake Kuttara was measured vertically and continuously at the deepest point. Using the data of a TCTD profiler, the heat flux at the bottom was estimated at 1.01 W/m², suggesting hot water input to the bottom. Henceforth, we will explore the relations between the bottom thermal variations and Noboribetsu geothermal activity.

Keywords: Noboribetsu hot spring, Lake Kuttara, Heat budget, Heat flux, Hydrothermal system

Nitrogen and phosphorus export to watershed from Water-Conservation Forest

KAWABE, Ryosuke^{1*}; TANJI, Kazunori²; OKAMURA, Masato³

¹Faculty of Policy Management Keio University, ²Faculty of Environment and Information Studies Keio University, ³Graduate school of Media and Governance Keio University

The purposes of this study are to estimate and validate water contamination of Total nitrogen(T-N) and Total phosphorus(T-P) from forest as runoff, in order to discuss policy measures for controlling non-point source loads. The study area is Doshi village in Yamanashi Pref. Total population of the area is 1,884, forest area is 7,468ha, 4,594ha of whole region is designated as Water-Conservation Forest for Yokohama City. Rest 2,823ha is private forest area for forestry.

The Water-Conservation Forest has been done thinning by Yokohama Waterworks Bureau, but private forest, especially coniferous plantation area has been hardly done thinning because of the decline of forestry. Therefore it is great concern that decreasing of water supply, declining quality of drinking water by increasing of sediment discharge and non-point source loads from the forest. A mean inflow at Doshi reservoir is 6.7(?/sec), Water transfer to other reservoirs from Doshi reservoir reached 3.0(?/sec), as a result of them water discharge to downstream is 3.7(?/sec). Consequently, increase of non-point source loads of nitrogen and phosphorus influence on water quality of reservoir such as Sagami reservoir and Miyagase reservoir.

Non-point source load of forest depends on surface run-off volume. To take account of this difference InVEST model (P.Kareiva et.al., 2011) is adopted for estimation of non-point source loads. Equations are shown (1)-(3):

$$EXP_x = EAF_x * pol_x * \prod (1 - E_y) \quad (1)$$

$$EAF_x = \log \sum Y_u / \log \sum Y_w \quad (2)$$

$$Y_x = \sum (1 - AET_x / P_x) A_x \quad (3)$$

Where EXP_x is non-point source loading value at pixel x , pol_x is the export coefficient at pixel x , y is a pixel of the upper reaches of pixel x . u means all grids located upstream of x , w means a basin including x and y . We used the export coefficients at the Fuji river basin (S.Shrestha et. al., 2007) as pol_x value. E_y is nutrient retention coefficient. Because of calculating E_y by comparing with result of L-Q equation, E_y is set to be equal zero. EAF_x is the hydrologic sensitivity score at the pixel x which is calculated as (2). Y_x is the water yield at pixel x . P_x is the annual precipitation. AET_x is the annual actual evapotranspiration on pixel x . A_x is the area on pixel x .

In addition, we made two L-Q equations to explain relation of Total Nitrogen and water discharge., Total phosphorus and water discharge based on the observed water discharge from 1956 to 2012, and water quality from 1991 to 2012.

As a result, when nutrient retention coefficient is zero, non-point source loads of nitrogen is 251.5(t/yr) and that of phosphorus is 5.9(t/yr). In these result, artificial load s of nitrogen such as household is 1.8(t/yr) and that of phosphorus is 0.1(t/yr). These results show that non-point source loads come from forest area. Results of L-Q equation are $TN = 0.791 * Q^{0.0616}$, ($R^2: 0.8374$), $TP = 0.00762 * Q^{0.0238} + 0.004$. Using these L-Q equations non-point loads are 192.3(t/yr) in T-N, 2.4(t/yr) in T-P.

In conclusion, the difference of nitrogen between result of InVEST model and L-Q equation is 59.0(t/yr) 23.5%, that of phosphorus is 3.5(t/yr) 59.3%. These difference due to amount of nutrient retention functions of forest area. It is also cleared that discharge of run-off are concentrated in valleys. Therefore, we conclude that it is important and necessary that forests in valleys are managed by appropriate thinning.

Keywords: Water-Conservation Forest, Non-point sources, Nitrogen, Phosphorus, L-Q Equation

Estimation of hourly nitrogen flux in a suburban watershed using SWAT model

SHIMIZU, Yuta^{1*} ; ONODERA, Shin-ichi² ; MATSUMORI, Kenji³

¹NARO/WARC JSPS-PD, ²Graduate School of Integrated Arts and Sciences, Hiroshima University, ³NARO/WARC

The objective of this study is to estimate hourly nitrogen flux from a suburban watershed, using Soil Water Assessment Tool (SWAT). SWAT, which is a model developed by USDA-ARS and Texas A&M University, is a river basin-scale model to simulate the quality and quantity of surface and ground water. The model is widely used in assessing soil erosion prevention and control, non-point source pollution control and regional management in watersheds because one of the reason is that it can estimate reasonable result even if data is limited. However it is not suit for estimation of nitrogen flux in flood condition because the time step of the model is basically calculated in daily. On the other hands, the model has an option for hourly estimation of runoff if sub-daily precipitation data are inputted. So we tried to estimate hourly nitrogen flux in Takaya watershed located on Hiroshima prefecture using the option. Monthly water quality data in ordinary condition and hourly data in flood condition which are observed by authors' group were used for validation. A result show that although the reproductively of hourly runoff was slightly decreased than daily estimation in validation period, estimated runoff peaks were fitted to observed. It was found that improvement of the model for hourly estimation of nitrogen flux, however, the result of the estimation was almost acceptable.

Keywords: Nitrogen flux, Hourly estimation, SWAT model, suburban watershed

Trace elements fluxes and budgets in two forest watersheds

ITOH, Yuko^{1*} ; KOBAYASHI, Masahiro¹ ; SHINOMIYA, Yoshiki²

¹FFPRI, ²FFPRI, Tohoku

Atmospheric deposition supplies some nutrients to forest ecosystem, serving as a source of reactive nitrogen, sulfur and the trace elements.

The objective of this study was to compare the behavior of four trace elements (Rb, Cs, Sr, Ba) in forest soil profiles in two forest sites: the Tsukuba experimental forest watershed and the Katsura experimental forest watershed.

Keywords: forest watershed, Rb, Cs, Sr, Ba

The percolation mechanism in a forested drainage basin: The Oikamanai River basin

MIYAMOTO, Takuto^{1*} ; CHIKITA, Kazuhisa² ; IWASAKA, Wataru¹ ; HOSSAIN, Md motaleb¹

¹Graduate School of Science, Hokkaido University, ²Faculty of Science, Hokkaido University

The rainwater movement in soils of high permeability is important to know how river runoffs are produced, and how sediment and nutrient are additionally loaded. In this study, we focus on runoff processes in the forested Oikamanai river basin, Tokachi Hokkaido. The catchment area is 62.6km², consisting of 88.3% forest and 10.6% farmland (mostly, grassland). Surface geology of the basin is mostly Miocene conglomerate, sandstone and mudstone. These are distributed on the hillslope or in mountainous regions. Farmlands are developed on the Holocene flood plane deposits. The Miocene sedimentary rocks are supposed to be highly permeable. We set a soil moisture profiler (4 channels) at each of forested area and grassland, and calculated the amount (mm) of percolation in the rainfall events (total rainfall of more than 50mm). As a result, the amount of percolation is near to total rainfall amount, and the ratio of the percolation amount to runoff height at a gauging station was low at ca. 12% in the forested area and ca. 19% at grassland. These low values suggest that the groundwater recharge to the deep zone is great because of the high permeability of the bedrock with many faults. Meanwhile, there is a soil layer of low permeability at depths of more than 20cm at grassland. Hence, it is suggested that saturated throughflow is more active than in forested area during the rainfall events. We set one more observation point near the upstream end of farmland. We will quantitatively estimate the farmland's contribution to water discharge and nutrient load by their comparison between the upper and lower observation points.

Keywords: percolation, soil moisture profiler, nutrient, river

The radioactivity of cesium in stream water during base flow from a small watershed in forested headwaters

SHINOMIYA, Yoshiki^{1*} ; KOBAYASHI, Masahiro² ; TAMAI, Koji² ; OHNUKI, Yasuhiro² ; ITOH, Yuko² ; SHIMIZU, Takanori² ; IIDA, Shin'ichi² ; NOBUHIRO, Tatsuhiko³ ; SAWANO, Shinji² ; TSUBOYAMA, Yoshio² ; HIRUTA, Toshihide⁴

¹Tohoku Res. Ctr. For. and For. Prod. Res. Inst., ²For. and For. Prod. Res. Inst., ³Hokkaido Res. Ctr., For. and For. Prod. Res. Inst., ⁴Fukushima Pref. For. Res. Ctr.

The radiocaesium was released by the accident in Fukushima Dai-ichi nuclear power plant. Although the woodland is thought to have strong tendency to maintain radiocaesium within a forest ecosystem, the very small amount of radiocaesium flows downwards through stream water. As stream water was used for agriculture and transported nutrient materials to river and lake. Therefore, radiocaesium discharged from headwaters may influence the ecosystem in river and lake or agriculture, like rice crop. In this time, we report the radioactivity of cesium in stream water during base flow from a small catchment in forested headwaters, Fukushima Prefecture.

The investigation was carried out in a small catchment (drainage area 1.2 ha) in the Tadano experimental forest of the Fukushima Prefecture forestry research center in Koriyama city, Fukushima Prefecture (Annual rainfall 1163 mm and mean air temperature 12.1 °C; the elevation 358 to 409 m, and the relief 0.42). The geology is a sedimentary rock (sandstone and tuff). As for the vegetation, the deciduous broad-leaved species such as *Quercus serratas* exists together with the Japanese red pine woods in the *Cryptomeria japonica* and the *Chamaecyparis obtusa* plantation (about the 48 years old). The runoff was observed by setting up the v-notched weir and the water level gauge in the catchment end. Stream water was collected twice a month (volume; about 10L) near the weir. The radiocaesium was divided to particulate and dissolved fractions by filtration (Glass fiber filter, 0.7µm). Dissolved cesium-137 was measured after concentration by extraction disk(Sumitomo 3M, Empore Raddisk Cesium)

Based on results obtained from June 2012 to March 2013, the radioactivity of cesium-137 tended to be higher in summer and lower in winter. In January and February, the radioactivity of cesium-137 was not detected, but it began increasing in March. There is a possibility that variation in the radioactivity of dissolved cesium-137 has a relation with the decomposition of organic matter according to the temperature elevation. The change in radioactivity of particulate cesium-137 was almost same way as dissolved cesium-137. This is because the discharge of suspended solid was increasing during high flow and because suspended solid concentration kept low while a catchment was covered by snow.

Keywords: radiocaesium, baseflow, streamwater, forest

Contribution of suspended solids to the migration of radiocaesium in forests

KOBAYASHI, Masahiro^{1*} ; SHINOMIYA, Yoshiki² ; OHNUKI, Yasuhiro² ; HIRUTA, Toshihide³

¹Forestry and Forest Products Research Institute, ²Tohoku Research Center, Forestry and Forest Products Research Institute, ³Fukushima Prefectural Forestry Research Centre

A wide area of forested land in eastern Japan was seriously contaminated by radiocaesium after the accident of the Fukushima Daiichi Nuclear Power Plant. In the contaminated forests, radiocaesium first trapped at the canopy and the litter layer has migrated to the mineral soil as throughfall (TF) and litter leachate (LL). TF and LL often contain suspended solids (SS) which are thought to transport the radiocaesium. The objective of this study is to clarify the contribution of the SS to the migration of radiocaesium in forests.

Throughfall (TF) and litter leachate (LL) were collected in forested slopes in Ibaraki and Fukushima prefectures. The concentration of Cs-137 of the water samples were measured by germanium detectors before and after filtration using membrane filters with pore size of 0.45 micrometer.

The concentrations of Cs-137 of the TF collected in the Ibaraki site (evergreen coniferous forest) in March and April 2011 were 14 - 60 Bq/L. In this period, the most of Cs-137 was detected as dissolved. Then the total concentration (dissolved + SS) of Cs-137 decreased and the proportion of Cs-137 in SS increased. The total concentration temporarily exceeded 20 Bq/L in the following summer season and the most of Cs-137 was detected from SS. The temporal increase in the radiocaesium in SS also observed in LL. The similar patterns of the concentration change of Cs-137 in summer observed in TF and LL at the evergreen coniferous forest and the deciduous forest in Fukushima. In winter, the total concentration of Cs-137 decreased and the migration rate also decreased. From these results, it was confirmed that the contribution of SS to the migration of radiocaesium as TF and LL in forests increased during summer.

Keywords: Radiocaesium, Forest, Migration, Suspended solid

Water and radiocesium balance in several paddy fields in Fukushima

YOSHIKAWA, Seiko^{1*} ; EGUCHI, Sadao¹ ; ITAHASHI, Sunao¹ ; IGURA, Masato¹ ; KIHOU, Nobuharu¹ ; FUJIMURA, Shigetō² ; SAITO, Takashi³ ; FUJIHARA, Hideshi¹ ; KOHYAMA, Kazunori¹ ; YAMAGUCHI, Noriko¹ ; OHKOSHI, Satoru³

¹National Institute for Agro-environmental Sciences, ²National Agriculture and Food Research Organization, ³Fukushima Agricultural Technology Centre

1. Introduction

By the released radionuclides from the Fukushima nuclear disaster in March, 2011, brown rice harvested at a 0.2% of paddy fields exceeded the provisional regulation value in 2011 in Fukushima. Water and radiocesium balance was studied in 3 paddy fields at different geographical sites in Fukushima to estimate radionuclides contamination in brown rice and to develop models for predicting radionuclides dynamics at watershed scale.

2. Monitoring and measurements

Field monitoring has been conducted in the following three paddy fields in Fukushima since spring in 2012. ; (1) a reorganized paddy field facing to forest in one side (clayey soil), (2) mountainous terraced paddy field surrounded by forest in three sides (sandy soil), (3) mountainous terraced paddy field surrounded by forest in three sides (organic soil). Water levels and turbidity of irrigation and drainage water in paddy fields and precipitation have been measured continuously. Water infiltration rates were measured several times during rice cultivation period in (2) and (3) fields. Water samples have been collected once a month for atmospheric precipitation, irrigation, surface drainage, subsurface pipe drainage, and seepage water on a ridge between terraced paddy fields. A membrane filter (0.025 μ m) was used to suspended solid (SS) and filtrate samples. The radiocesium concentrations were determined by Ge semiconductor detector after drying the SS and filtrate samples, respectively. Rice which was grown experimentally was harvested and measured its radiocesium concentrations by each part. Based on the relationship between turbidity and radiocesium concentrations, and flow rates of irrigation and drainage water, radiocesium concentration in rice plant, in/out flows of radiocesium in paddy fields were estimated for the monitoring period of one year (23rd May, 2012 ~27th May, 2013). Radiocesium in/out flows induced by heavy rainfalls of 50~150 mm by in July and October in 2013 were also estimated.

3. Results and Discussions

Monitored precipitation was about 800,900 and 1000mm, the estimated flow-in water (irrigation(+flow-in from spring which could be measured)) was about 300, 1300 and 3300 mm, the estimated flow-out water (surface drainage) was about 600mm, 1000mm and 7700mm for the one year in the (1), (2) and (3) field, respectively. Continuous spring-out of water was observed from side slope of the upper field in (2) and (3) fields. Infiltration and spring-out were almost same level in the surface in (2) field, however, averagely about 4 mm/day of spring-out was measured from the surface of (3) field during rice cultivation period. Furthermore, water flow-in and flow-out on the soil surface under snow and/or ice was observed in winter even in the latter part of January. Therefore, larger amount of water in/out flows were gained in the mountainous paddy fields (2) and (3) in comparison with common paddy fields located in flat areas like (1) field. Radiocesium concentrations of water samples, mainly taken at usual meteorological conditions, were 0.1-0.31 Bq/L for irrigation water, 0.02-1.4 Bq/L for surface drainage, 0.2-0.9 Bq/L for atmospheric precipitation, and 0.01-0.03 Bq/L for pype drainage. Most of the radiocesium was existent in the SS. Radiocesium inflow by irrigation, inflow by atmospheric precipitation, outflow by surface drainage, and carryout by rice harvest were 10^2 , 10^2 , and 10^3 , and 10^2 Bq/m² orders in the 3 fields for the one year, respectively. Radiocesium net flow in the 3 fields for the one year was estimated to be outflow of 0.2%, 0.2%, and 0.7% to the amount of radiocesium in soil, respectively. Most of outflows of SS and radiocesium occurred at events such as puddling, transplanting, midsummer drainage, drainage, and heavy rain etc.. The heavy rainfalls in July and October in 2013 induced large amount of SS and radiocesium outflows.

Keywords: radiocesium, water balance, mountainous paddy field, suspended solid

The characteristics of sediment load from a coastal forested drainage basin and their agents (2)

CHIKITA, Kazuhisa^{1*} ; IWASAKA, Wataru² ; HOSSAIN, Md motaleb² ; MIYAMOTO, Takuto²

¹Faculty of Science, Hokkaido University, ²Graduate School of Science, Hokkaido University

Some of the five coastal lagoons in the Tokachi region of southeastern Hokkaido, open a few times per year to the Pacific Ocean. The openings affects water quality and deposits in the marine coastal region by discharging the lagoon water offshore. The Oikamanai River is a main river flowing into the Oikamanai Lagoon. The river basin is almost forested (ca. 88 % in area), from which the discharge and sediment load build up the ecosystem of the lagoon and its back marsh. In order to explore how the suspended sediment discharges into the Oikamanai Lagoon, we obtained hourly time series of discharge, Q (m³/s), and suspended sediment concentration, C (mg/L), in the upper Oikamanai River. As a result, it was found that, following the sediment availability (sediment amount to be eroded), the precedent type (peak C temporally precedes peak Q), synchronous type (two peaks synchronously appear) and antecedent type (peak Q precedes peak C) appear on the Q vs. C diagrams for sequential rain-fall runoffs. The river-suspended sediment often originates from the river channels and/or basin slope. Hence, In order to judge the criterion for sediment erosion in the river channel and basin slope, the extended Shields diagram was applied to lognormal subpopulations separated for cumulative grain size distributions of river-bed sediment and basin soils.

Keywords: forested catchment, sediment load, precedent tyep, antecedent type, land collapse

Changes of mineral composition and load of suspended materials in the Saru River, Hokkaido before and after 2003

IRINO, Tomohisa^{1*} ; NAKADA, Satoshi² ; IKEHARA, Ken³ ; YAMASHITA, Youhei¹ ; SEKI, Osamu¹ ; NAGAO, Seiya⁴

¹Hokkaido University, ²Kyoto University, ³Institute of Geology and Geoinformation, National Institute of Advanced Industrial Science and Techn, ⁴Kanazawa University

Supply of detrital material from river can affect the continuity, sedimentation rate, and composition of marine sediments deposited in front of the river system, which is controlled by the relief, weathering rate, and precipitation of the hinterland. In spite of the small drainage area, the small rapid rivers in the island arc located under warm humid climatic condition supply a huge amount of detrital materials to the surrounding seas. In addition, sediment transports tend to be concentrated during flooding events. In order to understand the depositional history and utilized it for paleo-climate reconstruction, it is necessary to study a mechanism of suspension generation and controlling factor of its composition.

We conducted a field survey during 2005-2011 in the Hidaka area in Hokkaido, Japan, to evaluate the influence of the flooding mud to marine sediments, promoted by the typhoon precipitation in August, 2003. We selected the Saru River as our target, and conducted the river water sampling and turbidity measurements along the main stream and a major branch called Nukabira River. Water samples were taken from the surface of flow center of each stream and stored in plastic bottles. The collected water was filtered through Millipore filter with 0.4 μm opening and the suspended particles were collected and weighed in the laboratory. Mineral composition of the collected suspended materials on the filter was measured using an X-ray diffraction analysis (XRD).

Distribution of the turbidity in the Saru River drainage shows that high turbid water is localized only to the Nukabira River and others are relatively clear. The turbidity seems to be supplied only from one local source. Mineral composition of the suspended material in the Nukabira River does not contain serpentine, while the upper main stream before the junction with the Nukabira River contain serpentine. The suspended material in the lower main stream is also characterized by the lack of serpentine because of higher contribution from the Nukabira River. The surface sediment at the mouth of the Saru River also shows the same character. We also examined the mineral composition of marine surface sediments supplied as flood mud during the typhoon event in August, 2003. The flood mud contains the major amount of serpentine, which was not expected from the mass budget of suspended materials from the upper main stream and the Nukabira River under usual condition.

In order to estimate the suspension loads from the upper main stream and the Nukabira River, we compared the water discharge and suspension loads and established the rating curve for each tributary. Water discharge data for the main stream was available from the Water Information System of the Ministry of Land, Infrastructure and Transport, Japan. However, since the database contains too many missing data for the Nukabira River after 2008, we calculated the water discharge for this branch using the Hydrometeorological and multi-Runoff Utility Model (Nakada et al., 2012). As a result, the rating curve of the upper main stream is steeper than that of the Nukabira River, and the suspension load of the upper main stream could be larger than the Nukabira River at the water discharge of $>300 \text{ m}^3/\text{s}$. Therefore, the Nukabira River transports 5-10 times more suspended materials than the main stream during the usual discharge, which is reversed during the flooding situation.

Keywords: river suspended material, Saru River, Typhoon Etau, mineral composition

Estimation of Sediment discharge with distributed USLE and L-Q Equation in Water-Conservation Forest

NAKASHIMA, Ryoichiro^{2*} ; TANJI, Kazunori² ; OKAMURA, Masato³

¹Faculty of Policy Management Keio University, ²Faculty of Environment and Information Studies Keio University, ³Graduate school of Media and Governance Keio University

The purpose of this study is to estimate and validate sediment discharge from forest area for providing water resources in order to discuss policy measures for controlling sediment discharge. The study area is Doshi village in Yamanashi Pref. Its population is 1,884, forest area is 7,468ha, 4,594ha of whole region is designated as forest area preserved for provision of water resource for Yokohama City. Rest 2,824ha is private forest area for forestry. The forest area preserved for provision of water resource has been done thinning by Yokohama Water Bureau, nowadays the private forests are seldom do because of a decline of forestry. Therefore, it is concerned that the degradation of provision of water resources, the increase of sediment discharges volume.

To estimate the sediment discharge, we adopted USLE (Universal Soil Loss Equation) model. It considers 5 factors, R (the rainfall erosivity index), K (the soil erodibility factor), LS (the slope length-gradient factor), C (the cover-management factor) and P (The support practice factor).

We converted and integrated sets of data such as forest management plan in Doshi village, soil texture map, precipitation data analyzed by radar-AMeDAS and others to the proper dataset for utilizing GIS. The output data shows sediment discharge in 60 sub-watershed (Max:1,000ha) and in distributed 25m² grid. In addition, we tried to estimate more detailed information which is related to the land information, such as slope degree, land use and land cover.

Next, to validate the estimated result, we calculated the annual SS flux derived from L-Q equation, which makes correlation between the water discharge and SS density data. They were observed from 1955 to 2012 at the Doshi reservoir located downstream of Doshi River. Based on the LQ equation, we estimated the annual sediment discharge.

As a result of evaluation with USLE, sediment discharge per year is valued 97,820 (t/yr). On the other hand, SS flux estimated 400(t/yr) [$SS=1.732Q^{0.0238}(R^2=0.3223)$] and sediment deposition in the reservoir is 62,500(t/yr) with LQ equation. It is known that SS load from households are valued 1.8(t /yr). Therefore the anthropogenic loads is not dominant factor in this area.

The result of USLE does not mean exported sedimentation to observation station. This indicates potential of sediment loss in each grid and their summation in total grid. The reason why sediment loss value decay in runoff process is considered to be the function of sediment retention of each grid. On the other hand, there are three dominant factors of sediment runoff from forest area.

First, more sediment runoff come from natural forest area than coniferous area. Second, more sediment runoff come from abandoned coniferous plantation area. Third, Slope factor is main reason of sediment export.

The results suggests that 1st sediment retention of in this area is able to retain 27% of total sediment discharge in this region, 2nd dominant sediment supply come from natural forest and abandoned coniferous plantation area, preservation measures to control sediment discharge are prioritize forest management in steep area.

Keywords: Water Conservation Forest, Sediment Discharge, Universal Soil Loss Equation, LQ equation

Sediment loading processes in a tectonic and forested catchment: field observations and modelling

HOSSAIN, Md motaleb^{1*} ; CHIKITA, Kazuhisa² ; MIYAMOTO, Takuto¹

¹Graduate School of Science, Hokkaido University, ²Faculty of Science, Hokkaido University

Exploring fluvial sedimentary processes on catchment scale is useful for studies on the forest management, material cycle and ecosystem of short time scale and topographic evolution of long scale. The fluvial transportation of sediment is also related to sedimentation, material cycle and ecosystem in coastal regions. A considerable portion of suspended sediment discharging into a costal lagoon, the Oikamani Lagoon, Tokachi, Hokkaido annually is contributed by the forested Oikamanai River catchment with many tectonic faults. It is important to find out the sediment source in such forested catchments. Here, we have tried to find how sediment load occurs by rainfall and snowmelt runoffs in the forested (ca. 90% area) catchment. Grain size and mineralogy of catchment soil and stream sediment, survey techniques, and turbidimeters provide the information that allows us to understand fluvial sedimentary processes and the sediment source and its availability. Here, a semi-distributed model, ArcSWAT2012, was applied to time series of discharge and sediment load, which were obtained in 2011 to 2013. In ArcSWAT2012, the total basin area (62.48 km²) was divided into 3 sub-basins, as subbasin into hydrological response unit (HRU) based on soil type, land use and slope classes that allow a high level of spatial detail simulation. In this study we have used the data of discharge, Q (m³/s), suspended sediment concentration (SSC; C , mg/L) and sediment load, L (kg/s) of April 2011 to October 2013, weather data of 2008 to 2013, and soil data. Discharge and sediment load simulations by SWAT2012 offer reasonable results. The simulations of sediment load time series and hysteresis analysis indicate that most of the sediment input is coming from sub-basin 2, especially, from its basin slope.

Keywords: tectonic, forested, sediment load, SWAT, hysteresis

Interaction properties between river and groundwater with assessment of oxygen isotope ratio and nutrient concentration

MARUYAMA, Yutaka^{1*} ; ONODERA, Shin-ichi¹ ; SAITO, Mitsuyo² ; KITAOKA, Koichi³

¹Graduate School of Integrated Arts and Sciences, Hiroshima University, ²Graduate School of Environmental and Life Science, Okayama University, ³Department of Applied Science, Okayama University of Science

In the alluvial fan, there are many palaeo-channels which are composed of more permeable media like gravel and sand, and many springs and wells on those have been useful for human life as well as ecosystem. These type of the springs have the different waveforms of the seasonal thermal variation from those of the river or air which is the thermal source. In detail, the phase shifting and amplitude declining are confirmed in springs. In this research, we examine to confirm the thermal waveforms in the river and springs and to estimate the horizontal bypass flow velocities in palaeo-channels around the river in the alluvial fan. The study areas are Asahi river springs in Okayama prefecture of western Japan. At the springs of Asahi River, the temperature data was collected 1 week interval. The temperature data of Asahi River springs was analyzed, assuming the subsurface water flow only through the bypath as the one-dimensional advection-diffusion equation and heat flux from the ground surface depends on the temperature gradient between the aquifer and the upper layer. The analytical solution of this equation was verified by parameter fittings with the data.

The Darcy velocity of subsurface flow was estimated about 1.3 m/day. The distribution of one-dimensional subsurface temperature in the alluvial fan was simulated that thermal conductive flux from the river exponentially decreased. The flux was mainly controlled by the advection process. In addition, the heat flux from the ground surface varied spatially from the rivers depends on the variation of the heat gradient. Especially, the flux was about 0 at several sites where heat gradient decreased.

Keywords: Surface water-groundwater interaction, Oxygen-18 isotope, Nutrient concentration, Temperature, Alluvial fan

Surface water ? groundwater interaction and its effect on nutrient transport; the example in Hachiro-gata

ONODERA, Shin-ichi^{1*} ; SAITO, Mitsuyo² ; HAYAKAWA, Atsushi³ ; JIN, Guangzhe¹ ; MARUYAMA, Yutaka¹

¹Hiroshima University, ²Okayama University, ³Akita Prefecture University

We examined to confirm the surface water-groundwater interaction in Hachiro-gata of Akita prefecture and nutrient transport with the water flow. Hachiro-gata have decreased since 1960s. The reclamation land touches mainly at the east and south side to Hachiro-gata. The height of the reclamation land is lower than the lake water level. Water flow in the underground between the lake and land would have the stable direction from the lake to the land. Because the eutrophication often occurs in Hachiro-gata lake, the nutrient would accumulate in sediment. We installed three piezometers at the bankside of the lake and reclamation land, respectively. The water levels were monitored from September to December in 2013 and water samples were collected in September and December in 2013. We confirmed water flow from the lake to the land with the gradient of from 0.05 to 0.1. In addition, DOC and nutrient concentrations of groundwater were higher in the land than in the lake and lake water. The lake water has recently eutrophic condition, and so many organic matter originated from phytoplankton are deposited. The porewater in the lake bottom near the bank had the high nutrient and DOC concentrations. Based on this research, we can make a hypothesis of nutrient conversion from the lake to the land with groundwater flow.

Keywords: surfacewater, groundwater, interaction, nutrient, Hachiro-gata

Identification of flow system, sources and behaviors of major anion in a typical soil water-groundwater continuum hills

CAO, Yingjie^{1*} ; TANG, Changyuan¹ ; LI, Xing¹ ; KANG, Zhiwei¹ ; PIAO, Jingqiu¹

¹Graduate School of Horticulture, Chiba University

1 Introduction

In the hydrological system, headwater catchments are source areas for water, nutrients, sediment, and biota for larger streams (Sidle et al., 2000). Unsaturated zone is an important pathway for nutrition leaching in headwater where baseflow dominates (Costa et al., 2002), and the leach pattern is mainly controlled by soil texture and corresponding hydraulic properties. In this study, an intensive study including soil physics investigation, long-term monitoring about the soil water and groundwater hydrochemistry and sources identification of nitrogen by nitrogen isotope are conducted to describe the conceptual soil water-groundwater flow system and discuss the factors controlling the local groundwater hydrochemistry.

2 Study area

The study area is a typical headwater catchment in Ichikawa City (35.76oN, 139.97oE), Chiba Prefecture, Japan (reference). The annual average precipitation is 1,316mm, with the maximum monthly precipitation of 226.5mm/month in study area. The annual average temperature is 15.6 oC while the highest temperature of 31.2 oC occurring in August.

3 Result

From the surface, there are sandy loam (0-1 m), loam (1-2.5 m), clay loam (2.5-3.2 m) and sandy clay (3.2-4.5 m). The porosity shows slight increases from 0.68 at the surface to 0.78 at depth of 4.3m. Due to the occurrence of the Joso clay underlying the loam, the Ks of layer below 3.2 m in depth about two orders lower than the loam and sandy loam. The vertical profile of θ_r changes little with an average of 0.30.

The average background values for Cl⁻, NO₃⁻ and SO₄²⁻ were 17.64 mg/L, 0.33 mg/L and 1.52 mg/L, respectively. At the pear orchard, Cl⁻, NO₃⁻ and SO₄²⁻ concentrations increased dramatically due to anthropogenic inputs of fertilizers. The average concentrations of Cl⁻, NO₃⁻ and SO₄²⁻ were 32mg/L, 233 mg/L and 85 mg/L, respectively. The concentrations of Cl⁻, NO₃⁻ and SO₄²⁻ in groundwater of the valley in average are 35.17 mg/L, 129.67 mg/L and 2.39 mg/L, respectively.

4 Discussion

Base on the soil texture of the cross section A-A, there are three flows, interflow along the slope (I), local groundwater flow (LG) and regional groundwater flow (RG), and all of them finally discharge to the valley wetland. In average, the groundwater discharging to the valley at S4 is consisted of waters from LG (43%), RG (56%) and I (less than 1%). Mixing ratios also show seasonal variations. In winter, the ratio of RG with an average of 68% is larger than LG (32% in average), which implies that lateral discharge of groundwater is the dominant factor controlling the groundwater flow in the wetland. While in summer, the contribution of LG becomes higher, and the ratio of LG has exceeded that of RG in May and July, showing the strength of recharge from the upland to LG.

5 Conclusion

An intensive study including both hydrochemical monitoring and numerical simulation are applied to discriminate pollutants sources, evaluate pollutants behaviors and predict long-term effect of soil pollution to local groundwater.

Base on the soil texture and physics investigation, three runoff components interflow (I), local groundwater flow (LG) and regional groundwater flow (RG), are discriminated in the hillslope soil water-groundwater flow system. Two anthropogenic pollutants NO₃⁻ and SO₄²⁻, which have been approved keep conservation in both soil groundwater according to isotope and redox analysis, are treated as traces to separate these components. And it is found that in average, about 43% of groundwater comes from local groundwater recharge (LG) and 56% comes from regional groundwater recharge (RG). The ratio of interflow (I) only takes up smaller than 1%.

Reference

Sidle, R.C. et al., 2000. Stormflow generation in steep forested headwaters: a linked hydrogeomorphic paradigm. *Hydrological Processes*, 14(3): 369-385.

Costa, J.L. et al., 2002. Nitrate contamination of a rural aquifer and accumulation in the unsaturated zone. *Agricultural water management*, 57(1): 33-47.

Contrasting vertical phosphorus profiles in sediment of Hachirogata ; considering water flow effect

JIN, Guangzhe^{1*} ; ONODERA, Shin-ichi¹ ; OTA, Yuki¹ ; SATOU, Takaharu¹ ; SAITO, Mitsuyo² ; HAYAKAWA, Atsushi³ ; ARITOMI, Daiki¹

¹Hiroshima University Graduate School of Integrated Arts and Sciences, ²Graduate School of Environmental and Life Science, Okayama University, ³Faculty of Bioresource Sciences, Akita Prefectural University

Coastal shallow lake sediment play an important role in the lake eutrophication process, it should be considered important sinks and sources of phosphorus. The accumulation and regeneration of sediment nutrients would be affected by some hydrological process. Lake Hachirogata is a shallow eutrophic lake located in north of Akita City. It used to be the second largest brackish water lake in Japan before the land reclamation project finished in 1977. A salt water barrier has been constructed at the outlet of the regulating reservoir through which water is discharged intermittently out to the Japan Sea. There probably exists the water flow from lake water into sediment due to the lower altitude of the farmland than lake water level after the land reclamation project. We would like to research on the sediment phosphorus accumulation and its activities base on the sediment phosphorus profiles, in consideration of the water flow effects. In order to better understand the possible change on lake phosphorus cycle by land reclamation.

Two core sediment samples were collected by piston core sampler (7-8 cm diameter), in east and west part of the lake (core HL-1 represents the core samples near river mouth area, core HL-2 represents the core samples which was collected near land reclamation area) during the investigations in September 2013. Samples were sliced at 1cm interval then centrifuged for extracting pore water soon after sampling, pore water nutrient and chlorine ion were determined in the laboratory with a spectrophotometer. The advanced SEDEX methods was used in sediment phosphorus fractionation.

Our results shows different pore water Cl^- and nutrient patterns between two locations. In HL-1 core, it shows an increasing trend of Cl^- from around 50mg/L at surface to around 500mg/L at bottom, however in HL-2 this profile shows relatively a constant range around 40mg/L. Both the DTP and DTN concentrations from the HL-1 core showed an increasing trend towards bottom, and they shows relatively constant and low in the HL-2 core, respectively. In sediment P fractionations, Iron bounded P comprise the main phosphorus species in HL-2 core, which comprises 42-72% of total phosphorus. this value is 15-28% in HL-1. Based on the dating information calculated by ²¹⁰Pb, it shows a larger sediment accumulation rate in HL-2 than HL-1 but with higher phosphorus burial trend in HL-1.

The sediment pore water profile shows significant change after the land reclamation project. Due to the enclosing of the sluice gate decades before, the changing from saline environment to freshwater could reflected by gradually decreasing trend of Cl^- profile towards current in HL-1. The pore water DTN DTP molar ratio shows large variations in HL-1 core. In HL-2, the low Cl^- and DTP in HL-2 provides an evidence that the diluting and transporting pore water phosphorus by water flow from lake into the sediment. On the other hand, it shows high sedimentation accumulation rate and sediment P accumulation rate in HL-2 core site, both at about 3.5 times of the HL-1 core. The supplying of relatively oxic lake water in into pore water may inhibit the iron bounded phosphorus releasing from sediment, decrease and average the mineralization process in sediment, this change in sediment could also be reflected by high phosphorus content, high phosphorus activities in HL-2 core. The increasing in sediment nutrient may be resulted from filtration by water flow into sediment, enhancing the sediment accumulation. Large mobile phosphorus trapped in sediment may increase the phosphorus releasing risk and intensify the algal bloom in Lake Hachirogata. Due to the high sediment phosphorus content and high activities in core HL-2, it would also be a considerable pollutant resources brought by water flow into coastal groundwater. The detailed results on sediment phosphorus property would be described in the presentation.

Keywords: Lake Hachirogata, sediment, pore water, phosphorus fractionation, water flow, land reclamation

Effect of DO fluctuation on the manganese cycle around the sediment water interface in bottom of the Lake Biwa

ITAI, Takaako^{1*} ; HYOBU, Yuika¹ ; CHIKAOKA, Kosuke¹ ; MORISHITA, Yohei¹ ; SHIN, Yoshiki¹ ; KUMAGAI, Michio³ ; NAKANO, Shin-ichi² ; TANABE, Shinsuke¹

¹Center for Marine Environmental Studies (CMES), Ehime University, ²Center for Ecological Research (CER), Kyoto University, ³Ritsumeikan University Research Center for Biwako Sigma

Enrichment of Mn and As in the surface of sediment has been reported from various lakes in the world. This enrichment is generally caused by the precipitation/adsorption of MnO₂ and arsenate after upward diffusion of Mn²⁺ and arsenite. Lake Biwa is a typical example, in which clear enrichments of Mn and As within thin surface enriched layer (<2 cm) of sediment were observed. However, progressive hypoxia recently reported from the lake can induce release of these elements into water column (Yoshimizu et al. 2010, Itai et al. 2012). In order to reveal the dynamics of Mn and As in the lake bottom, we made geochemical survey through determination and speciation of Mn and As in sediment, porewater and lake bottom water. According to our estimation, total Mn and As in the enriched layer of Lake Biwa was roughly 10000 and 240 tons, respectively (Itai et al., 2012). These amounts are ca. 1800 and 12 times respectively higher than the inventory of these elements in Lake water, suggesting that releasing a portion of Mn and As from enriched layer can be a cause of large increase of these in lake water. The speciation of Mn and As in sediment determined by X-ray absorption fine structure (XAFS) indicated that predominant species of Mn from surface to 2 cm depth was MnO₂ while divalent Mn, likely ionic form, was predominant below enriched layer. Similar to Mn, oxidation state of As was gradually changed with depth, i.e., arsenate was predominant in surface, then arsenite and As in sulfide becomes predominant toward deep. These results suggested that Mn and As in enriched layer should be reduced when DO level in lake bottom becomes lower. The flux of Mn and As from the lake sediment to water column estimated by porewater profile were 3400 - 16000 and 400 - 1800 mg m⁻² year⁻¹, respectively. The fluxes were higher in deeper part of the lake in which sediment character was more reducing than shallower part. With progressive hypoxia, this flux should increase. The monthly monitoring of DO and Mn level in lake water suggested that Mn level in water above 1 m of the lake floor increased from August to December with the highest level was ca. 100 times higher than the baseline level. This trend is consistent with the gradual decrease of DO during thermal stratification period. In the bottom water, the threshold DO level where apparent Mn release started was estimated to be 5-6 mgO₂/L. This value is higher compare to the inter-annual DO minimum ever reported (<4 mgO₂/L). If 40% of Mn released from enriched layer then completely mixed in whole lake, the Mn level becomes 0.6 mg/L which corresponds to lethal levels of some crustaceans and insects. Although such an extreme situation is unlikely, continuous monitoring Mn and As levels is important to safeguard the lake ecosystem and food supply.

Keywords: Lake Biwa, dissolved oxygen, manganese, arsenic, pore water, speciation

Current status of the research on the phosphorus dynamics in the coastal groundwater discharge area

SAITO, Mitsuyo^{1*} ; ONODERA, Shin-ichi²

¹Okayama Univ., ²Hiroshima Univ.

A large fraction of phosphorus (P) in groundwater generally exists as the dissolved form which is more efficiently used in nutrient cycle and ecosystem than the suspended form. It suggests phosphorus transport by groundwater discharge (e.g. SGD: Submarine Groundwater Discharge) significantly effects on the coastal ecosystem. In the paper, we aimed to review the previous researches related on phosphorus dynamics in the coastal groundwater discharge area and discuss on the future prospects on it.

Distribution and sources of uranium in Okinawan rivers, Japan

MOCHIZUKI, Akihito^{1*} ; HOSODA, Ko¹ ; SUGIYAMA, Masahito¹

¹Graduate School of Human and Environmental Studies, Kyoto University

We measured natural background concentrations of dissolved U in 194 Japanese rivers and the highest concentrations were observed in two Okinawan rivers in the limestone region, the Hija and Kokuba Rivers (Mochizuki and Sugiyama, 2012). However, the U concentrations in the earth's surface of their drainage areas are relatively low and therefore the mechanisms of U supply to these rivers are of interest. In this study, we determined U concentrations as well as major chemical compositions in 17 Okinawan rivers and estimated the sources of U supplied to these rivers.

The major chemical compositions of the rivers in the northeastern region of the island were the Na-Cl or Na-HCO₃ types, while those in the southwestern region were the Ca-HCO₃ type. The Ca-HCO₃-type composition is derived from the dissolution of limestone, which is widely distributed in the southwestern region. The U concentrations in rivers were much higher in the southwestern region (32 - 3500 ng/L) than in the northeastern region (5.6 - 18 ng/L).

In the 11 rivers with Ca-HCO₃-type compositions, the limestone-derived fraction of U was estimated using the concentration ratio of U/Ca in the limestone and the Ca concentration derived from limestone. The U concentrations were almost explained by the simple dissolution of limestone in 6 rivers, but this mechanism could not account for the concentrations in 5 rivers with higher U levels (710 - 3500 ng/L). These results suggest that the U in these 5 rivers is supplied by other mechanisms, such as selective dissolution of U from rocks in the drainage areas by carbonate ions.

Keywords: Uranium, Okinawan rivers, Limestone

Longtime behavior (<50 yr) of Groundwater Quality with Dissolution of a Ryukyu-limestone Aquifer in Okinawa Island

NAKAYA, Shinji^{1*}; YASUMOTO, Jun²; PHAN MIN, Ha¹; AOKI, Hideto¹; NAKANO, Takuji²

¹Shinshu University, ²The University of Ryukyu

Dissolution of a terrestrial limestone layer by chemical weathering is one of the most important factors affecting the carbon cycle and the transport of calcium from the land to the ocean. Residence times of sulfur hexafluoride (SF₆) and chlorofluorocarbons (CFCs), as well as their chemical composition in the groundwater, were investigated to estimate the longtime behavior of field dissolution of the Ryukyu-limestone aquifer on Okinawa Island, Japan. The Ca, (HCO₃+SO₄) and Pco₂ increase with groundwater residence time. The field dissolution of Ca was estimated to be 0.090 mM(Ca)/L/yr, with groundwater Ca ranging from 1.75 to 4.0 mM/L. The increase observed in groundwater alkalinity and SO₄ over time (0.170 meq(HCO₃+SO₄)/L/yr; 16 to 34 yr) implies that the groundwater acts as a CO₂ sink through chemical weathering of the Ryukyu-limestone aquifer when groundwater CO₂ (gas) concentrations range from 1.0% to 4.5% (logPco₂=-2 ~-1.35 atom). The (Ca + Mg) content of groundwater was also affected by groundwater alkalinity (HCO₃), SO₄ and NO₃ derived from fertilizers used on Okinawa Island. These findings imply that the influence of fertilizer and the high partial pressure of groundwater CO₂ on the dissolution of Ryukyu-limestone aquifer may not be negligible. pH decreases with dissolution of the Ryukyu-limestone aquifer.

Keywords: Groundwater, Limestone, Dissolution, Residence time, Sulfur hexafluoride, Okinawa Island

Rapid procedure for $\delta^{15}\text{N}$ and $\delta^{18}\text{O}$ determination and identifying nitrate sources in agricultural watershed

YADA, Saeko^{1*}; NAKAJIMA, Yasuhiro¹; UNO, Hikaru¹; ITAHASHI, Sunao¹; ASADA, Kei¹; YOSHIKAWA, Seiko¹; EGUCHI, Sadao¹

¹National Institute for Agro-Environmental Sciences

The natural abundance of nitrogen ($\delta^{15}\text{N}$) and oxygen isotopes ($\delta^{18}\text{O}$) of nitrate (NO_3^-) can be a powerful tool to discriminate the source of NO_3^- in agricultural watersheds. This dual isotopic approach has been used successfully to evaluate the denitrification process in an upland vegetable-field dominant watershed. Recently, determination of $\delta^{15}\text{N}$ and $\delta^{18}\text{O}$ of NO_3^- has been updated using an autosampler for automatic analysis. In this study, we developed a further time-saving procedure, which advanced the time-event efficiency by controlling sample traps and 6-port valves. Moreover, the procedure was used to identify sources of riverwater NO_3^- in a rice paddy watershed in Tsukuba, Japan, where the irrigationwater was supplied from out of the watershed.

The $\delta^{15}\text{N}$ and $\delta^{18}\text{O}$ values were determined by isotope-ratio mass spectrometry (IRMS) after converting NO_3^- to N_2O gas using the denitrifier method. We conducted sample purge and determination at the same time. Our developed procedure doubled the sample throughput, saving the amount of He carrier gas and liquid N_2 . It also engaged the versatile utility of IRMS, since changeover of equipment was not required. This rapid procedure can be applied to other trace gas analysis, which require cryofocus e.g. CO_2 , and will contribute for GWG dynamics studies.

Using the developed procedure, we identified principal sources of NO_3^- in mainstream riverwater of the watershed. The $\delta^{15}\text{N} - \delta^{18}\text{O}$ relationship during irrigation period indicated that NO_3^- in mainstream riverwater were mainly provided from mountainstream and irrigationwater, and that significant effects of denitrification on the decrease in NO_3^- concentration were locally limited at some irrigationwaters and drainagewaters in the watershed.

Keywords: agriculture, irrigation, IRMS, nitrate, stable isotope, watershed

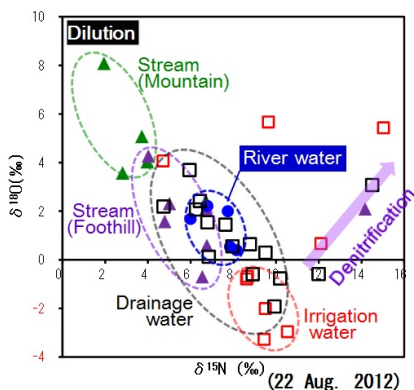


Fig.1 Identifying sources of riverwater nitrate using $\delta^{15}\text{N}$ and $\delta^{18}\text{O}$ values in an irrigated rice paddy watershed.

Study on Effect of Rainfall Distribution and Rainfall Intensity on Discharge at The Concentration Point of The Basin

YOSHIMI, Kazuhiro^{1*} ; WANG, Chao-wen¹ ; YAMADA, Tadashi²

¹Graduate School of Science and Engineering, Chuo University, ²Department of Civil and Environmental Engineering, Chuo University

In recent years, the damage caused by flood comes obvious because of unprecedented record-breaking rainfall event or largest recorded rainfall. Because of this situation, river planning starts to be looked at again in Japan. For example, it has been reported by MLIT (Ministry of Land, Infrastructure, Transport and Tourism) that even if total rainfall is the same when the rainfall distribution differs in a basin, the discharge at a reference point may differ (refer to MLIT). In other words, it is necessary to innovate a new intellection considering the difference of rainfall distribution when creating river planning.

This study aims to clarify the relation between rainfall distribution in a target basin and peak discharge at a reference point. The authors therefore verified how the peak discharge at a basing point responds to rainfall distribution at an intended basin. Moreover, the authors examine the impact on discharge at a reference point if rainfall intensity increases or decreases in a basin.

A target basin of this study is *Tone* upper river basin. In addition, largest recorded flood of this basin is Kathleen typhoon which 3-days accumulated rainfall is about 320mm(refer to document of Japan Society of Civil Engineers) in the basin. First, the authors separated the target basin into 4 parts (refer to document of Science Council of Japan). Then, we did runoff analysis for a number of rainfall distributions using this typhoon event as basic rainfall pattern. The conditions of this calculation are, first, average rainfall of *Tone* upper river basin is the same in every rainfall distribution. Secondly, soil condition and geotechnical condition do not change in every case. After that, we compared every peak discharge at the reference point. Moreover, the authors also did runoff analysis using a number of average-rainfall over watershed 0.8, 0.9, 1.1, 1.2 times as much as basic rainfall event. And then, we compared the peak discharge in the same way.

In consequence, the authors indicated that peak discharge at the point of reference was about from 20800m³/s to 23800m³/s in which case rainfall distribution differs. These range of values is $\pm 7\%$ in contrast with basic design flood of *Tone* river. In particular, the peak discharge of the reference point becomes 22000m³/s or more in which case heavy rainfall intensity occurred in a watershed nearby the point. Furthermore, it was found that the range of values of peak discharge grows wider as average-rainfall over watershed builds in intensity. Therefore, flood exceeding the designed level is necessary to be defined newly and exactly in *Tone* upper river basin.

Keywords: rainfall distribution, runoff analysis, peak discharge, average-rainfall over watershed

Increasing Water Level in the Vietnamese Mekong Delta

FUJIHARA, Yoichi^{1*}; HOSHIKAWA, Keisuke²; FUJII, Hideto³; YOKOYAMA, Shigeki³; NAGANO, Takanori⁴; KOTERA, Akihiko⁴

¹Ishikawa Prefectural University, ²Kyoto University, ³Japan International Research Center for Agricultural Sciences, ⁴Kobe University

The Mekong Delta is highly susceptible to the impacts of flood, sea level rise, and land subsidence. We considered three factors that could have increased the water level: (1) decrease in flood mitigation functions due to dyke constructions, (2) sea level rise, and (3) land subsidence. We used daily maximum water level, daily minimum water level, and daily water level data. We analyzed data of 21 stations from 1987 to 2006. First, we classified the Delta into two groups; one area is dominated by flows from the upstream, while the other is dominated by the tide. Moreover, we obtained the trend of annual maximum and minimum water levels. Regarding land use, we used the NDVI to estimate the area of dyke construction and the area of the flood plain. It is found that (1) the constructed area of the dyke does not coincide with the area of water level increase, (2) the area with the water level increase correlates with the area with the minimum water level increase. The area with the minimum water level increase is located in the tide dominated zone, indicating that the increase in the maximum water level is caused by the relative increase of sea level.

Furthermore, we examined the trend of sea level rise, and detected a 2.4 mm/year sea level rise. The average of the minimum water level increase was 7.3 mm/year, and therefore, 4.9 mm/year must be the subsidence. In addition, we eliminated the trend of the increasing water level and reconstructed the data without sea level rise and subsidence. We estimated the probabilistic value of water level using the reconstructed data set, and estimated the probability of 100-year water level using the current data set. As a result, the 100-year probabilistic water level in the reconstructed data becomes 21.2-year water level in the current.

Keywords: Mekong delta, Increasing water level, Flood, Sea level rise, Land subsidence, Dyke

Applicability of EUROSEM for surface runoff in forested slope plain

IKEDA, Hideshi^{1*} ; WAKAMATSU, Takashi¹ ; NAKAYA, Ko¹ ; ABE, Seiya¹

¹Central Research Institute of Electric Power Industry

Sediment yield in agricultural area has been environmental and economic problems in many countries. In order to restrain sediment yield and to conserve water resource, scientific watershed managements are required in many watersheds. In USDA (United State Department of Agriculture), USLE model (Universal Soil Loss Equation) was developed and applied to many sites. USLE model is empirical model, and requires long term observation data. Then, physical based models, such as WEPP (Water Erosion Prediction Project) and EUROSEM (EUROpean Soil Erosion Model), were developed and applied to watersheds where long-term observation had not been conducted.

In some Japanese forest, forest management, such as thinning, has not been conducted fitly in these years. In poorly managed forest area, sediment yield with surface runoff has occurred and supplied suspended solids into stream, reservoir and coastal area. However, in forested watersheds, application of these models has not been conducted frequently, and it is required to validate and apply these models based on observation of meteorology, forestry, pedology and hydrology.

EUROSEM model is one of the useful tools for evaluation of sediment yield in forested area. In this study, hydrological applicability of EUROSEM is discussed. EUROSEM is a prediction model for sediment yield, which was developed by European Union in 1990s. It consists of hydrological and sediment sub-models, those are physical-based process models in non-steady state. EUROSEM has been applied to agricultural areas in Europe and China, for example in watershed of Three Gorge dam, Yangtze River. On the other hand, it is not applied to Japanese forest area frequently, where sediment yield is reported recently.

In Central Research Institute of Electric Power Industry (CRIEPI), we have been conducting observation for sediment yield since June 2010 in Akagi testing center, located in north Kanto plain. The observation system consists of 3 sites, one open field and two forest stands. For open field, precipitation was observed using Laser Precipitation Monitor (LPM,THEIS, FRG) consequently. For in two forest stands, vegetation, meteorology and hydrology survey were conducted. In vegetation survey, canopy analyzing and forest floor survey were conducted in every months. In meteorology survey, precipitation was observed using LPM consequently. In hydrology survey, surface runoff was observed in experimental area with 2m length and 0.5m width using tipping gauge continuously. Soil moisture and temperature were observed in every 10 minutes in experimental area.

In these two forest stands, EUROSEM hydrological sub - model was applied in 35 storm events, and simulated surface runoff was validated based on observed data. EUROSEM hydrological sub model was applied to 10 storm events in previous study and appeared to simulate surface runoff for storm events with rainfall intensity between 2.0 - 5.0mm / 10min. In this study, surface runoff was simulated well in storm events with rainfall intensity larger than 5.0mm/10min using infiltration rates lower than those in laboratory experiments.

Keywords: Forest, Surface Runoff, Sediment Yoelds, Prediction Method, EUROSEM, Storm - Runoff

Distribution of trace elements in 3 small rivers and the surrounding geology in the North Osaka prefecture, Japan

EVEN, Emilie^{1*} ; NOJIMA, Aki¹ ; MASUDA, Harue¹

¹Department of Geosciences, Osaka City University, Japan

The Rivers Yono, Ibaraki and Minoh, that are tributaries of the River Yodo in the northern part of the Osaka prefecture, Japan, flow across the Paleozoic-Mesozoic sedimentary formations and the Ibaraki granitic complex. Waters from these rivers have been used for domestic purposes and some trace metals have been reported in concentrations above the environmental standard limits. Previous studies have shown that the sedimentary rocks were the sources of trace metals, especially arsenic, whereas the granitic sequence of quartz diorite, granodiorite and adamellite is believed to be the source of rare earth elements (REEs). In addition to track back of the origin of these trace elements, the transportation phases and the geochemical budget of trace metals along the river flow are examined as a first step to set up a simple transportation model. Here are presented first results.

Results showed that the geochemical patterns of riverbed sediments matched the distribution of the source rocks. The geochemistry of trace elements in river water is likely controlled by the weathering of riverbed sediments. River sediments from sandstone and quartz diorite contained high amount of trace elements and yielded high concentrations of trace metals in river water but low concentrations of REEs. Comparatively, river sediments originated from adamellite contain lower amounts of trace elements but river waters flowing across this formation showed to have the highest concentrations of REEs. O/H isotopic ratio in river water pointed at the meteoritic origin of the water in the upper reaches of rivers and the contribution of groundwater in the lower reaches. The fractionation of trace elements regarding the different size pools of total concentration, 0.45 μ m and 0.22 μ m filtration showed that most of the trace elements were transported within the <0.22 μ m phase. Temperature of river water seems to influence the concentrations of elements, as concentrations increased with increasing temperature throughout the year. The role of organic matter (likely as colloidal carriers) is limited since an inverse relationship was observed. Water mixing calculation with major and trace elements yielded accurate geochemical budget model (<5% error), where as redox sensitive species induce large errors of >15%, even on few meters distance along the flow path.

Keywords: Rare Earth Elements, River Water, Source rock, Trace Metals, Transportation

AHW28-P03

Room:Poster

Time:April 30 18:15-19:30

Seasonal variation in oxygen stable isotopic ratio and nitrate concentration in a mountain agricultural watershed

ARITOMI, Daiki^{1*} ; ONODERA, Shin-ichi¹ ; SAITO, Mitsuyo² ; MARUYAMA, Yutaka¹ ; JIN, Guangzhe¹ ; ONISHI, Koki³

¹Hiroshima University, ²Okayama University, ³Fukken Co., Ltd.

We aimed to examine the groundwater flow and seasonal variation of NO₃-N in coastal aquifer of a granite catchment considering the contribution of bedrock groundwater and denitrification processes.

An Overview of Recent Hydrological Models for Estimating Phosphorus flux

SHIMIZU, Yuta^{1*} ; ONODERA, Shin-ichi² ; SAITO, Mitsuyo³

¹NARO/WARC JSPS-PD, ²Graduate School of Integrated Arts and Sciences, Hiroshima University, ³Graduate School of Environmental and Life Science, Okayama University

Phosphorus which derived from forest, agricultural area and urban is discharged to river stream via surface runoff and drainages. There is a time lag from "inflowing to river channel" to "outflowing to coastal area" because most of transported phosphorus is retained in river channel due to physical, chemical and biological processes. Previous studies about material balance in watersheds show that total amount of phosphorus emission is not correspond to total amount of discharged phosphorus. This is because of phosphorus retention in watersheds. So it is necessary to understand about phosphorus retention processes for estimation of phosphorus transportation. In recent years, distributed hydrological models are used to estimate phosphorus transportation. Most of these models are developed in western countries, and have been improved its accuracy of estimation of sediment and water quality. The objective of this study is to review phosphorus retention process in watersheds and model description for understanding model limitation for phosphorus transportation.

Keywords: Hydrological Model, Phosphorus, Material transport, Watershed

Water pollution and arsenic behavior in the Red River, North of Vietnam

INOUE, Ryo^{1*}

¹graduate school of science,Osaka City

Water pollution and arsenic behavior in the Red River, northern Vietnam.

Inoue,R1.Shinntani,T1.Masuda,H1.Yonezawa,G1.Truong Xuanluang2.Hang Do Thi2.
(1 Osaka City University, 2 Hanoi University of Mining Geology)

The Red River, flowing through the northern part of Vietnam, is originated in Yunnan, China and running parallel to the Hoang Lien Son mountain range. Arsenic pollution of groundwater has been a serious problem in rural area located on the Red River delta. The sources of arsenic must be carried to the aquifer through the river, although transportation processes are not well understood. In this study, arsenic transportation process through Red River was studied from the analytical results of river water, suspended particles, river-bed sediments which were collected in the Vietnam territory. In addition, general situation and the cause of the river water pollution was considered.

Total dissolved ions of river water sample is 5.0meq/L in Lao Cai located at the upper most stream in Vietnam, 2.4meq/L in Bao Ha and 2.1meq/L in Yen Bai at middle-stream, and 3.4meq/L in Hanoi at downstream. Low concentration of dissolved solids between Lao Cai and Hanoi is due to the inflow of the surface water from Hoang Lien Son mountain range. Such an inflow is clear from the lower oxygen and hydrogen isotope ratio of river water than those of main channel waters. $\delta^{18}\text{O}$: -9.9~-10.0 ‰ and $\delta^2\text{H}$: -69 ‰ in Lao Cai. $\delta^{18}\text{O}$: -12.9~-13.0 ‰ and $\delta^2\text{H}$: -91~-92 ‰ in the branch channel in Hoang Lien Son mountain range, and $\delta^{18}\text{O}$: -11.6~-11.9 ‰ and $\delta^2\text{H}$: -82~-84 ‰ in Bao Ha and Yen Bai at middle-stream. Branch channel water in Hoang Lien Son mountain range diluted the dissolved salts and pollutants such as As and Pb. Arsenic is transported as dissolved components (~60%) and adsorbed components (~40%) in the river.

Arsenic concentration has clearly positive correlation to the XRD intensity of smectite. Weak positive correlation between arsenic and kaolinite was also found. However, there is no relationships between arsenic and iron, indicating that the arsenic doesn't behave with iron oxyhydroxides in the river. And, smectite found only in suspended particles sample of Red River main channel water, thus, the arsenic is transported with clay minerals in the Red River.

Keywords: arsenic, Red River, Vietnam, Isotope

Estimation of water balance in a coastal agricultural catchment using SWAT and HYDRUS Model.

JIN, Guangzhe^{1*}; SHIMIZU, Yuta²; ONODERA, Shin-ichi¹; SAITO, Mitsuyo³; MATSUMORI, Kenji²

¹Hiroshima University Graduate School of Integrated Arts and Sciences, ²National Agriculture and Food Research Organization, Western Region Agricultural Research Center, ³Graduate School of Environmental and Life Science, Okayama University

Quantify the rate of ground water recharge and clarify the water balance in watersheds is basic and important for efficient ground water resource management. It is particularly important in regions with little rain which face with the risk of water shortage. However, the rate of aquifer recharge is one of the most difficult factors to evaluate. Especially, the former method of groundwater recharge estimation, are normally subject to large uncertainties and easily to cause errors. Recently, there are several attempting for estimation of groundwater recharge using distributed hydrological models in the world.

The Soil and Water Assessment Tool (SWAT) Model is one of a physically based and quasi-distributed continuous time hydrological model used to estimate water budget in previous researches around the world. SWAT Model has been implemented for watershed hydrology related issues such as estimation of surface water flow and groundwater recharge rate. We could more specific testify the groundwater flux combined SWAT Model with HYDRUS Model which is a software package for simulating water, heat, and solute movement in two- and three-dimensional variably saturated media. The objective of this research is to estimate water balance and to clarify the groundwater recharge parameter in an agricultural catchment in the Seto Inland Sea, using the SWAT Model, and to estimate the groundwater flow using the HYDRUS Model.

The study site is located on the southern part of Ikuchi Island, which is one of the islands in central Seto Inland Sea. The orange groves cover approximately 50% of the total catchment area. Due to the small annual precipitation (approx.1000mm/y) with large inter-annual variation, Ikuchi Island is facing a risk of water shortage in the serious dry year.

As input to SWAT Model, topographic data (10 m grid), soil map (1/25000), land use map (1/25000) and weather information were used to build and calculate the SWAT Model. Evaporation was estimated by the Penman-Monteith method. Simulation time periods is 2000-2013, including warm up period of 2000-2003 and calibration period of 2003-2004. The calibration was conducted using the Sequential Uncertainty Fitting (SUFI2). The reproducibility of daily discharge in calibration period by the model was found to be acceptable (NSE=0.69, RSR=0.56, PBIAS%=18, R²=0.75). Amount of groundwater recharge is accounted as the water discharge into aquifer except the flows which are eventually discharged from aquifer, such as return flows into river and amount of water moving into the vadose zone.

The result shows spatial difference in groundwater recharge rate. About 10 times higher groundwater recharge rate was found in middle and downstream areas. While middle and downstream area are indicated the main groundwater recharge area, upstream is small recharge rate due to steep slope. Groundwater recharge shows smaller volume than river discharge, it comprise about 17% of total precipitation in annual average consideration. From the comparison of water balance calculation, it is found that both of river discharge and groundwater recharge fluctuated in high precipitation year of 2011 (1,527mm), low precipitation year of 2005 (781mm) compared to average balance. In high precipitation year, groundwater recharge rate increased about 6 times than in low precipitation year, the increasing of river discharge is at about 2.5 times.

Consequently, it was confirmed that spatial and temporal variation of groundwater recharge rate in long term. And we could estimate the long term water balance base on these information. However, it is noted that this result may include some uncertainty and chance to improve. Seat model could not reflect the groundwater flow, simulated with HYDRUS Model on the groundwater flow could provide us with the groundwater data. In the presentation, more detailed data cover long time periods and results testifying groundwater level variation with HYDRUS Model will be displayed.

Keywords: Ikuchi Island, SWAT Model, HYDRUS Model, groundwater recharge rate, water balance

Seasonal variation in nutrient dynamics in the tidal zone of Yamato river

ONODERA, Shin-ichi^{1*} ; SAITO, Mitsuyo² ; SHIMIZU, Yuta³ ; MARUYAMA, Yutaka¹ ; MIYAOKA, Kunihide⁴ ; JIN, Guangzhe¹ ; ARITOMI, Daiki¹

¹Hiroshima University, ²Okayama University, ³NORO, ⁴Mie University

In coastal megacities, severe groundwater depression and water pollution occurred. These impacts affected to river environment change. Especially, the river mouth area has been deposited the polluted matters. These areas have characteristics of water level fluctuation which causes river water-groundwater interaction and the associated change in dynamics of nutrients. However, these effects on the nutrient transport in tidal reaches and nutrient load to the sea have not been fully evaluated in previous studies. Therefore, we aimed to clarify the nutrient dynamics with the river water-groundwater interaction in the tidal river of Osaka metropolitan city. We conducted the field survey from the river mouth to the 7km upstream area of Yamato River, which has a length of 68km and a watershed area of 1070 km². In addition, model simulations were also conducted. Spatial variations in radon (²²²Rn) concentrations and the difference of hydraulic potential between river waters and the pore waters suggest that the groundwater discharges to the river channel in the upstream area. In contrast, river water seeped into the groundwater in the river mouth area. It may be caused by the lowering of groundwater level associated with the excess abstraction of groundwater in the urban area. The spatial and temporal variations in nutrient concentrations indicate that nitrate-nitrogen (NO₃-N) concentrations changed temporally and it negative correlated with dissolved organic nitrogen (DON) concentrations. Inorganic phosphorous (PO₄-P) concentrations showed the increasing trend with the increase of the river water level. Based on the mass balance, nutrient reproduction from the river bed was suggested in tidal reach during a summer, especially phosphorus was large.

Keywords: seasonal variation, nutrient dynamics, tidal river, pollution, phosphorus

Examination on the classification and ecological index of ponds based on the stability of stratification

OKUBO, Kenji^{1*} ; SAITO, Mitsuyo¹ ; TAKAGI, Shinya¹ ; ONODERA, Shin-ichi² ; MARUYAMA, Yutaka² ; JIN, Guangzhe² ; ARITOMI, Daiki² ; SHIMIZU, Yuta³

¹Okayama Univ., ²Hiroshima Univ., ³JSPS PD, NARO/WARC

We aimed to examine on the classification and ecological index of the small ponds based on the stability of stratification. The seasonal variation of the stratification was examined using the monitoring data of water temperature in multiple depths in the 4 different ponds located on an island which is highly influenced by agricultural activity. DO, fluorescence, nutrients data were used for the evaluation of ecosystem condition.

*This research is supported by the Grants-in-Aid for Scientific Research (A) (No. 25241028, Shin-ichi Onodera).

Rock magnetic profiles of sediment cores in Hachirogata : effect of a land reclamation

OTA, Yuki^{1*} ; SATO, Takaharu¹ ; ONODERA, Shin-ichi¹ ; JIN, Guangzhe¹ ; SAITO, Mitsuyo² ; HAYAKAWA, Atsushi³

¹Graduate School of Integrated and Arts Sciences, Hiroshima University, ²Graduate School of Environmental and Life Science, Okayama University, ³Faculty of Bioresource Sciences, Akita Prefectural University

We examined the influence of land reclamation on rock magnetic profiles in Lake Hachirogata. In this lake, all flowing rivers exist on an east side and a large reclamation land touch at west and north sides. Two sediment core samples were collected at the eastern central (HL-1) and northwestern bankside (HL-2) sites in this lake in September 2013, using the 1m piston core sampler (7-8 cm diameter). HL-1 was 77cm and HL-2 was 78cm.

Keywords: Lake Hachirogata, sediment, rock magnetism, land reclamation

Spatial distribution of radon ($^{222}\text{-Rn}$) and radium ($^{226}\text{-Ra}$, ^{228}Ra) in the coastal seawater of Seto Inland Sea and its con

SAITO, Mitsuyo^{1*} ; ONODERA, Shin-ichi² ; OHTA, Tomoko³ ; GUO, Xinyu⁴ ; TAKEOKA, Hidetaka⁴ ; ONISHI, Hidejiro⁴ ; KUBOTA, Takumi⁵

¹Okayama Univ., ²Hiroshima Univ., ³Hokkaido Univ., ⁴CMES, Ehime Univ., ⁵KURRI, Kyoto Univ.

Previous studies have revealed that submarine groundwater discharge (SGD) is one of the important pathways for nutrients and the other dissolved materials from terrestrial area to the marine environment. For the evaluation of the effect of SGD, the timescale of nutrient transport in the coastal area derived by SGD such as residence time is important as well as nutrient flux by SGD. Radioactive isotopes of radon ($^{222}\text{-Rn}$) and radium ($^{226}\text{-Rn}$, $^{228}\text{-Ra}$) are one of the useful tracers for the evaluation of SGD and residence time of water mass in the coastal area. The objective of the study is to examine the spatial variation of $^{222}\text{-Rn}$ and $^{226}\text{-Rn}$, $^{228}\text{-Ra}$ in the coastal seawater of the central part of Seto Inland Sea and its controlling factors. The study area is southwestern part of the Hiuchi-Nada with the area of approximately $30\text{ km} \times 13\text{ km}$. Relatively high concentrations of $^{222}\text{-Rn}$, $^{226}\text{-Rn}$ and $^{228}\text{-Ra}$ were detected in the southern part of the study area. These results suggest the effect of SGD from seafloor.

*This research was supported by the KWEF research grant program by Kurita Water and Environment Foundation (No. 24254, Mitsuyo Saito) and cooperative research project in KURRI, Kyoto University (No. 2434, Shin-ichi Onodera) in 2012.

Arsenic distribution in porewater and coexisting sediments of Kumano Basin, Nankai Trough

YOSHINISHI, Haruka^{1*}

¹Osaka City University

Arsenic contamination of groundwater is a serious problem in the world, especially in the deltas along large rivers originated from Himalayas such as Bangladesh and West Bengal, India. Sulfide minerals including pyrite in shales is one of the candidates of source minerals causing arsenic contamination. However, the mechanism of arsenic concentration in sedimentary rocks has not been well understood. In this study, arsenic behavior in the porewater and host sediments was determined to understand the fixing process of arsenic during early stage of diagenesis in modern marine sediments.

Porewaters and squeezed cakes were sampled at three sites (C0002, C0021, C0022) in the Nankai trough by IODP, Expedition 338. The sediments from Site C0002 is composed hemipelagic mud of distal turbidites, those from Site C0021 of mass transport deposits (MTDs), Site C0022 is dilled at right above the megasplay fault, and highly fractured zone, likely related to the megasplay faulting was found at 100 mbsf (meters below seafloor).

Arsenic concentration of the porewaters at Site C0002 was constant 0-1.1 μM at 200-300 mbsf, and it increased with depth to 3 μM in 300-400mbsf. The highest concentration (3 μM) was recorded at 400 mbsf, and the concentration decreased below that depth. In C0021, arsenic concentration of the porewaters is 0.2 μM on an average at 0-160 mbsf and give no relationship to the depths. It increased quickly to 1.2 μM down to 200 mbsf. In C0022, arsenic concentration is 0.3 μM on average at 0-100mbsf. The highest concentration (1.5 μM) was observed at 130-160mbsf, and then drastically decreased to 200 mbsf. Arsenic concentration became constant below that depth.

Arsenic concentration of sediments is 40-120 μM at 300-500 mbsf in Site C0002, 40-90 μM at 100-150mbsf in Site C0022. The arsenic concentration is varied without relationship to the depth.

Mineral composition determined by XRD showed that the all sediments analyzed were dominated by quartz, feldspars, micas, calcites, smectite, and chlorite/ kaolinite. Hornblende and pyrite were occasionally observed.

Compared to the major chemical composition determined onboard, arsenic concentration of porewater correlated to pH, Fe, Pb, and Mn. It is suggested that the arsenic was accumulated in the sediments via coprecipitation with iron hydroxides/oxides at the sea floor, similar to many trace heavy metals, and was released into the porewater by desorption under reducing environment, or by decomposition of iron hydroxides/oxides. After that, arsenic may be fixed into pyrite with depth, however, the fixing mechanism of arsenic in the deep is not clear at present.

Keywords: Arcenic, Nankai Trough, IODP

Research on dissolved inorganic phosphorus concentrations forming process in a forested mountainous stream

TAKEDA, Manami^{1*} ; OHTE, Nobuhito¹ ; EGUSA, Tomohiro¹ ; SUZUKI, Masakazu¹

¹Department of Forest Science Graduate School of Agricultural and Life Sciences

Since the ecosystems of river, lake, and ocean are supported by P supply from terrestrial area, it is important to understand the mechanisms behind the P discharge from the catchments through the aquatic system. It has generally been considered that loss of P from a forested area through a headwater stream is small, because it is preserved tightly within forested ecosystem. It has previously been reported that heavy rainfalls lead to a large P loss from forested catchments, and major fractions of exported P is particulate form absorbed onto soil particles. Therefore, many studies have focused on particulate P load during high flow condition. However, it has been still poorly understood about the controlling mechanisms of sources and transport of dissolved inorganic phosphorus (DIP), which is directly available for organisms. In order to explain the controlling mechanisms of DIP discharge, we conducted field investigations on the DIP dynamics through the elemental hydrological processes in the hill slopes of a headwater catchment, and illustrated the spatial distribution of DIP concentrations of the stream network in meso-scale catchment.

The study site was Fukuroyamasawa experimental watershed located in The University of Tokyo Chiba Forest and Inokawa watershed including Fukuroyamasawa. The size of Fukuroyamasawa is 1 ha, and that of the Inokawa watershed is 503 ha. Through fall water, stem flow water, litter layer infiltration water, soil water, groundwater and stream water were sampled once every two weeks from August 2013 to November 2013. Rainwater was collected at the meteorological station located near by Fukuroyamasawa. In Inokawa watershed, flow observation and stream water sampling at the point with various watershed area on low-flow period in September 2013 and December 2013. The samples were filtered by 0.45 micrometer membrane filters immediately after the sampling. Then DIP was analyzed using molybdenum blue (ascorbic acid) absorptiometry.

The average DIP concentration of rainwater was 0.2 micromol / L during the observation period. That of through fall, stem flow and litter layer infiltration water were 0.9, 1.7 and 10.9 micromol / L respectively. DIP concentration felt remarkably with soil layer passage, and the average DIP concentration of soil water, groundwater and stream water was 0.6 micromol /L. DIP concentration in Inokawa stream water ranged from minimum limit of determination, 0.1 micromol /L, or less to 9.2 micromol / L. When we investigated the relation between DIP concentration and a contributory area, DIP concentration differed in about 2 km² or less, and it increased at the larger than 2 km² as the contributory area became large. There was a strong positive correlation between DIP concentration and EC.

In Fukuroyamasawa, it was shown that DIP added during canopy passage was almost absorbed in the soil layer at particles, and was removed from the water, and hardly contributing to the outflow to a mountain stream. EC is an index for underwater dissolved matter concentration, and it turns out that the amount of the dissolved matter concentration of mineral origin is shown at Inokawa watershed. Therefore, the relationship of DIP concentration and EC has suggested that mountain stream underwater DIP mainly originates in bedrock weathering, and that the spatial distribution of DIP concentration is determined with the contribution of a groundwater course which passes bedrock.

Keywords: Dissolved Inorganic Phosphorus (DIP), forested mountainous stream, spatial distribution, catchment area

Mixing of river water as deduced from major component concentration, Sr and S isotopic ratios in Tama River, Akita.

WAKASA, Sachi^{1*} ; ISHIYAMA, Daizo² ; MATSUBAYA, Osamu³ ; SATO, Hinako² ; SHIN, Kicheol⁴ ; NAKANO, Takanori⁴

¹Center for Geo-Environmental Science, Akita Unisity, ²Faculty of International Resource Sciences, Akita University, ³Emeritus professor, Akita University, ⁴Research Institute for Humanity and Nature

The acidic high temperature hot spring discharged from the Tamagawa hot spring (Ohbuki) into the Tama River system through the Shibukuro creek is still acidic downstream. The acidity of the Ohbuki hot spring water is neutralized using limestone before it discharges into the Shibukuro creek. In this study, geochemical signatures of mixing between Tama River and its tributaries were deduced from concentration of major chemical components, Sr and S isotopic ratios. The Ohbuki hot spring water has high concentration of chloride and sulfate. The $\delta^{34}\text{S}$ of sulfate is the highest ($\delta^{34}\text{S} = 31.8 \text{ ‰}$) in the watershed. Due to the neutralization, the concentration of calcium, strontium and strontium isotopic ratio increases ($^{87}\text{Sr}/^{86}\text{Sr} = 0.7068$). The mixing rate of water flowing out from the neutralization facility is about 20% and 8% before and after the confluence of Shibukuro and Tama Rivers, respectively. The concentration of the major chemical components decreases gradually downstream and is almost similar to other tributaries in the Tama and Omono Rivers system. The pH of the water also decreases from 3 to neutral (about 7). The strontium isotopic ratios of 0.7040, 0.7068 and 0.7049-0.7062 for the Ohbuki, the neutralization facility and tributaries of the Tama River respectively, reflect the geology of the catchment area. A two component mixing phenomena is observed in the Tama River and its tributaries based on the major chemical components. However, the two component mixing relationship is not clearly distinct with the Sr isotope ratios. The $\delta^{34}\text{S}$ of sulfate in the Ohbuki thermal water (+31.8 ‰) and Tawa River (+6.6 – +8.8 ‰) near the confluence of the Tama and Omono Rivers supported the two component mixing relationship observed from the major chemical component. The results observed in this study are used to interpret the mixing mechanisms operating between the Tama River and its tributaries.

Keywords: Mixing of river water, Akita, Concentration of major chemical components, Strontium isotopic ratio, Sulfur isotopic ratio

Feature of distribution of radioactive cesium in irrigation canal

KUBOTA, Tomijiro^{1*} ; TARUYA, Hiroyuki¹ ; TANAKA, Yoshikazu¹ ; HAMADA, Koji¹

¹National Institute for Rural Engineering, NARO

The purpose of this study is to clarify distributive characteristics of a radioactive cesium in the irrigation canal by examining the radioactive cesium contained in the bottom sediment along the canal from its intake to the downstream. One of the millrace located in Fukushima Prefecture was selected as a case for investigation, and the distribution of the amount of the sedimentation, the concentration of radioactive cesium in the bottom sediment, and the air dose rate were examined. The sandy deposit was seen in the upstream of the canal, and those concentration of radioactivities Cs were comparatively low with $1-5\text{kBq kg}^{-1}$. On the other hand, relatively high concentration of radioactivity Cs was seen in the downstream of canal, and was within $3-28\text{kBqkg}^{-1}$. The air dose rate in the waterway were relatively low because of the influence of ponding, relatively high air dose rate were seen in the place where the depositional surface had been exposed.

Keywords: radioactive cesium, irrigation canal, sediment, air dose rate

Current status of the groundwater use in an island of the Seto Inland Sea: a case study of Ikuchijima-island

TANIGUCHI, Tomomasa^{1*} ; ONODERA, Shin-ichi² ; TAKAHASHI, Hidehiro³ ; SAITO, Mitsuyo⁴ ; SHIMIZU, Yuta⁵

¹Faculty of Humanities, Law and Economics, Mie University, ²Graduate School of Integrated and Arts Sciences, Hiroshima University, ³NARO Western Region Agricultural Research Center, ⁴Graduate School of Environmental and Life Science, Okayama University, ⁵NARO Western Region Agricultural Research Center, JSPS PD

The study is aimed to examine the current status of the groundwater use in an island of the Seto Inland Sea, southern Japan. This area is characterized by high risk of drought with low annual rainfall and limited water resource. We conducted face-to-face surveys in the form of a multiple-choice questionnaire in two areas (districts of Miyabara and Hayashi) with different main resource of agricultural water in Ikuchijima-island, Onomichi-City. Citrus farms such as orange, lemon etc. are widely cultivated in both areas.

The rate of households having domestic well is about 74% in Miyabara district, and is about 62% in Hayashi district. The main purposes of groundwater use are watering in garden and car wash in both areas. About 20% of respondents answered that groundwater resource is not enough for the agricultural use in the dry season. It indicates the groundwater is regarded as one of the important water resource in the island. Averaged daily domestic use of groundwater per household are estimated to be 361L/day and 271L/day in Miyabara and Hayashi, respectively.

*This research is supported by the Grants-in-Aid for Scientific Research (A) (No. 25241028, Shin-ichi Onodera).

Evaluating the impact of disturbances on the carbon balance of forest ecosystems in Hokkaido by using data and model: fr

HIRATA, Ryuichi^{1*} ; ITO, Akihiko¹ ; TAKAGI, Kentaro² ; HIRANO, Takashi³ ; SAIGUSA, Nobuko¹

¹National Institute for Environmental Studies, ²Field Science Center for Northern Biosphere, Hokkaido University, ³Research Faculty of Agriculture, Hokkaido University

Changes in carbon flux and storage in forest ecosystems are influenced by climate at various temporal and spatial scales, whereas carbon flux and storage are affected instantaneously and heterogeneously by artificial and natural disturbances at the local scale. Disturbance events such as forest fire, damage by insects, and forest harvest drastically change NEP and carbon storage. In this study, we address the effect of disturbance on carbon balance based on two scale; one is site scale and another is local scale.

First, we performed a baseline simulation of carbon dynamics and compared these values with those observed across a wide range of stand ages (old mixed forest and young and middle-aged larch forests). By taking into account seasonal variation in the understory leaf area index, simulated net ecosystem production (NEP), gross primary production, ecosystem respiration, and biomass for the three types of forests were consistent with observed values.

We compared two cases of simulations concerning the carbon balance: one taking account of spatial distribution of disturbance-induced forest age derived from forest inventory data (disturbance case) and another ignoring the disturbance impact (non-disturbance case). NEP was gradually and spatially changed ranging from 0 to 1 t C/ha/y depending on meteorological conditions such as temperature or solar radiation. On the other hand, in the case of disturbance, large NEP ranging from 3 to 5 t C/ha/y were distributed patchwise like hotspots, because forest age of these spots ranging from 20 to 100 years old and then younger than those of the non-disturbance case. In the 1970s, wood harvest and tree planting were intensively conducted in Hokkaido. In the disturbance case during this period, there were many hotspots which show negative NEP.

Keywords: process-based ecosystem model, eddy covariance method

Examining initialization procedures of terrestrial carbon cycle models

ITO, Akihiko^{1*}

¹National Institute for Environmental Studies

It has been realized that long-term trends in model simulation is affected by initialization procedure. In terrestrial carbon cycle models, insufficient stabilization can result in artificial trends (lingering sink or source in CO₂ flux) in the simulated carbon budget, making it difficult to interpret simulation results and make comparison with observational data. Conventionally, an equilibrium state of terrestrial carbon budget has been obtained through iterative calculations using an appropriate forcing data. This spinning-up method requires high computational cost, typically, at over 90% of total computational cost. On the other hand, terrestrial modeling has another problem related to initialization; actual ecosystems are not always at steady state due to disturbance and environmental change. As a result, different model groups adopt different initialization procedures, raising some problems in inter-model comparison. In this study, I examined how an alternative initialization method (semi-analytical solution) works in a terrestrial carbon cycle model and is effective to reduce computational cost in comparison with the conventional spinning-up. I discuss possibility of better initialization procedures, in terms of idealism, realism, and generality, not only with model researchers but also with field researchers.

Keywords: terrestrial ecosystem model, initialization, carbon budget

Interannual variation of carbon allocation in a cool-temperate deciduous forest from 1999 to 2006

KONDO, Masayuki^{1*} ; ICHII, Kazuhito² ; UYAMA, Masahito³

¹Faculty of Symbiotic Systems Science, Fukushima University, ²Japan Agency for Marine-Earth Science and Technology, ³Graduate School of Life and Environmental Sciences, Osaka Prefecture University

Carbon allocation is the key factor controlling the dynamics of carbon cycle. It determines partitioning of assimilated carbohydrate to components of vegetation, leaves, woody organs, and fine roots. To analyze seasonal and annual scale carbon allocation of forest ecosystems, it is conventional to use the mass-balance approach, which combine individual estimations of flux and biometric observations such as gross primary production, ecosystem respiration, soil respiration, net ecosystem production, leaf and tree biomass, litterfall, and soil organic carbon considering appropriate balances with each components. However, it is often the case that an attribution of fine roots was not fully assessed because it is required significant effort to monitor its dynamics in a long term. Pulse labelling technique allows directly measure allocation of assimilated carbon from foliage to belowground in various tree species. This approach provides detailed aspects of allocation dynamics, but assessing labelled carbohydrate allocated to fine roots is still challenging. Absence of allocation to fine roots limits our knowledge about mechanism of carbon allocation because net primary productivity of fine root (frNPP) potentially account for one-third of the annual total NPP. To compensate limited observation, a model-data integration technique would be a useful tool, in which a process-based biosphere model combined with multi-year biometric observations to inversely estimate plausible allocation to fine roots.

This study investigated the interannual variability of carbon allocation of a cool-temperate forest in the Takayama Forest Research Site, Japan. The multi-year biometric observations are available for most of carbon cycle components at the Takayama site (e.g., woody tissue net primary productivity (wNPP), foliage NPP (fNPP), aboveground and belowground woody biomasses, litterfall, recruitment, and mortality) except fine root NPP (frNPP); only one year data of frNPP is available for 2000?2001. To compensate the limited frNPP measurement, we calculated frNPP from 1999-2006 by a model-data integration technique. In the process of calculation, unnecessary freedom in the simulation of a process-based ecosystem model, Biome-BGC, was constrained as much as possible with multiple biometric observations at the Takayama site. With the observed components of allocation (fNPP and wNPP) in conjunction with the modeled frNPP, we characterized the interannual variability of carbon allocation at the Takayama site by focusing two aspects: (1) allocation priority among leaves, woody components, and fine roots, and (2) controlling climate factors for these allocation components.

Acknowledgments

This research was supported by the Environment Research and Technology Development Fund (RFa-1201) of the Ministry of the Environment of Japan.

Keywords: Allocation, ecosystem modelling

Net nitrogen input through the atmospheric deposition and irrigation water at a paddy field in central Japan

HAYASHI, Kentaro^{1*} ; ONO, Keisuke¹ ; TOKIDA, Takeshi¹ ; NAKAMURA, Hirofumi² ; HASEGAWA, Toshihiro¹

¹Natl. Inst. Agro-Environ. Sci., ²Taiyo Keiki

The aim of the present study was to evaluate the net nitrogen input through the atmospheric deposition and irrigation water at a paddy field for single cropping of paddy rice in central Japan, where the wet deposition and exchanges of gases and particles (as the difference between the dry deposition and emissions) were measured for the atmospheric deposition. Target species of reactive nitrogen (Nr) were ammonium (NH_4^+) and nitrate (NO_3^-) for the wet deposition, ammonia (NH_3), nitric acid (HNO_3), and nitrous acid (HNO_2) as gases and particulate ammonium (p NH_4) and nitrate (p NO_3) as particles for the atmosphere-rice paddy exchange, and NH_4^+ , NO_3^- , and organic nitrogen (OrgN) for the irrigation water.

Monitoring of those processes were conducted for three years from September 2010 to September 2013 at a paddy field in central Japan which was devoted for an experimental site of free-air CO_2 enrichment (FACE). Rainwater samples were collected weekly and the wet deposition was calculated using the Nr concentration and the collected volume of water. The air concentrations of Nr were measured using a filter-pack method at two heights of 6 m and 2 m above the ground surface on a weekly mean basis with day/night separation. A filter-pack consisted of five filter holders to collect the target Nr. The diffusion velocity was calculated using the micrometeorological and eddy covariance data in half-hourly basis and then the weekly-mean values in the daytime and nighttime were calculated. The exchange fluxes were expressed as the product of the difference in air concentration between the two heights multiplied by the diffusion velocity. Cumulative exchange fluxes were also calculated based on the weekly mean exchange fluxes. The flow rate and quality of irrigation water was monitored in the cropping seasons in 2011, 2012, and 2013 at a bay in the paddy field. Each of two inlets and one outlet at the bay was equipped with a flow gaging weir and the water flow was measured continuously. Water was sampled at the weirs every week in principle and the concentrations of Nr were measured, where OrgN was calculated as the difference between the total nitrogen and the sum of NH_4^+ and NO_3^- . The inflow and outflow of Nr by irrigation were then calculated using the flow rate and concentration data.

Annual wet deposition of Nr was 9.5, 8.6, and 5.9 $\text{kg N ha}^{-1} \text{ yr}^{-1}$ for the first, second, and third years, respectively, where NH_4^+ and NO_3^- showed similar contributions quantitatively. In addition, the contribution of OrgN was negligible in the wet deposition. Annual exchanges of Nr between the paddy field and the atmosphere were estimated to around 2-3 $\text{kg N ha}^{-1} \text{ yr}^{-1}$, where a certain extent of the dry deposition was counterbalanced by the emissions. Ammonia was the most dominant Nr among the target species in the atmosphere. Ammonia also showed the largest dry deposition among Nr; however, a large part of which was canceled by the emissions of NH_3 from the paddy field. The differences between the inflow and outflow for the irrigation water were 10.7, 8.8, and 6.7 $\text{kg N ha}^{-1} \text{ yr}^{-1}$ for the first, second, and third years, respectively, where OrgN accounted for 30-40% of Nr. In total, the net input of Nr to the paddy field through the atmospheric deposition and irrigation water was estimated to approximately 20 $\text{kg N ha}^{-1} \text{ yr}^{-1}$ which corresponds to approximately 30% of a standard application rate of nitrogen fertilizers in this area. However, it is desired that the following processes are also incorporated to complete the evaluation of the nitrogen balance: the biological nitrogen fixation and the dry deposition of nitrogen oxides (nitrogen monoxide and nitrogen dioxide) as inputs; and the denitrification (nitrogen monoxide, nitrous oxide, and dinitrogen) and the leaching of Nr to the groundwater as outputs.

Keywords: reactive nitrogen, nitrogen balance, atmospheric deposition, emission, irrigation, rice paddy field

The variations of ORP in the paddy soil and effects on the methane emission from a periodically irrigated paddy field.

YAGI, Kenta¹ ; WAKIKUROMARU, Naoki¹ ; IWATA, Toru^{1*}

¹Graduate school of Environmental and Life Science, Okayama University

Oxidation-Reduction Potential (ORP) in the paddy soil was measured during rice cultivated season at a periodically irrigated paddy field, and some effects on the methane flux from the paddy soil was investigated. ORP showed rapid decrease when irrigation water was introduced in the paddy field, and lower ORP was shown under the longer flooded condition. From the seasonal-term point of view, lower ORP was shown in later rice season. ORP was suitably modeled as a function of irrigation time. During an irrigation period for four days, higher methane emissions were shown under lower ORP conditions. From the seasonal-term point of view, however, no significant relationship between ORP and methane fluxes. It is suggested that seasonal change of methane flux is affected by seasonal changes of soil temperature and the growth level of rice plants.

Keywords: Rice Paddy, Methane, soil, Oxidation-Reduction Potential

Carbon emission by open burning from a paddy field and decomposition of the residual biomass in the paddy soil

OKADA, Kazuya¹ ; ONO, Keisuke² ; IWATA, Toru^{1*}

¹Graduate school of Environmental and Life Science, Okayama University, ²National Institute for Agro-Environmental Sciences

Twice sampling surveys of residual biomass above ground surface were conducted before and after the open burning, and carbon contents compared for the estimation of carbon emission by the burning. It is suggested that about 43% of carbon contents of above-ground rice plant was yield out as grain by the harvest, and about 30% of carbon emitted as CO₂ by burning. Coarse Organic Matter (COM) in the paddy soil of a single-crop rice field was sampled on a regular schedule for three years. The carbon emission from the COM decomposition of residual biomass was estimated by analyzing of the variations in carbon content of COM. Decrease in COM was accelerated at the warming season between April and June, but it was resisted during rice cultivated season. It is estimated that 70% of COM was decomposed after a year.

Keywords: Organic Carbon, Rice Paddy, Soil, Decomposition, Carbon Dioxide

Continuous measurement of forest floor CO₂ fluxes in a larch forest on the base of Mount Fuji

TERAMOTO, Munemasa^{1*}; LIANG, Naishen¹; ZENG, Jiye¹; IDE, Reiko¹; SAIGUSA, Nobuko¹; TAKAHASHI, Yoshiyuki¹

¹Center for Global Environmental Research, National Institute for Environmental Studies

Carbon fluxes of forest floor are thought to be important part of forest carbon dynamics. Multi-channel automated chamber system was installed to a larch forest site on the base of Mount Fuji in 2006 for continuous measurement of forest floor CO₂ fluxes. We prepared soil chambers for measuring soil respiration (Rs) and heterotrophic respiration (Rh). Root trenching was applied to separate Rs and Rh. Net ecosystem exchange (NEE) on the forest floor was measured with plant chambers. In 2013, the average efflux of CO₂ was 2.24, 1.81 and 2.11 $\mu\text{mol CO}_2 \text{ m}^{-2} \text{ s}^{-1}$ in Rs, Rh and NEE, respectively. Root respiration was estimated to occupy 80.7% of Rs. Plants of forest floor was suggested to absorb about 5.9% of CO₂ in Rs, and it meant that the amount of carbon fixed by those plants was relatively low. There was little rain in summer time (July-August), and forest floor CO₂ fluxes were decreased due to decreased soil moisture. Q₁₀ was 2.49 and 2.87 in Rs and Rh, respectively. Soil respiration was estimated to be 8.48 tC ha⁻¹ yr⁻¹, and the forest floor was seen as 7.98 tC ha⁻¹ yr⁻¹ carbon source.

Keywords: soil respiration, chamber, forest floor plants, photosynthesis

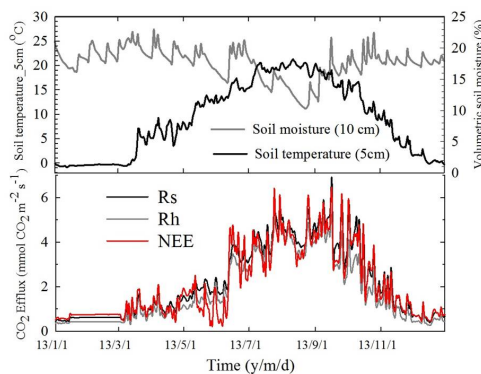


Fig 1. Seasonal variation of soil temperature, soil moisture and CO₂ efflux of each fluxes in 2013.

Change in carbon dioxide absorption by a deciduous broadleaf forest due to the 2004 typhoon disturbance

MIZOGUCHI, Yasuko^{1*} ; YAMANOI, Katsumi¹ ; UTSUGI, Hajime¹ ; TOBITA, Hiroyuki¹

¹Forestry and Forest Products Research Institute

Natural disturbances occur in forests at various scales and frequencies. It has an impact on the amount of carbon dioxide (CO₂) absorption by a forest. In Japan, large-scale disturbance often occurs in forests due to damage caused by strong winds of a typhoon. The 18th typhoon passing in 2004 brought about large-scale damage to forests, mainly in Iburi and Ishikari districts of Hokkaido. The Hitsujigaoka experimental forest (Sapporo forest meteorology research site, SAP) located in the southeastern area of Sapporo also suffered large-scale damage. An investigation related to CO₂ absorption, including flux observation, was conducted before the typhoon disturbance. After a 1-year interruption of the investigation due to facility damage by the typhoon, flux observation was reinitiated. To study the process of regeneration in the forest, the fallen trees were left into site. We report the results of a long-term observation of flux and biomass.

According to flux observation data, the annual carbon budget changed to negative after the disturbance. At present, carbon release is continuing. The supply of a lot of dead trees has caused a large amount of decomposition, which has led to 1.5-fold heavy increases in ecosystem respiration. Meanwhile, average annual GPP from 2007 to 2012 decreased 5% compared with that before the typhoon.

Yearly maximum LAI including both trees and dwarf bamboo estimated by the attenuation rate of photosynthetically active radiation and the biomass survey was approximately 7 before the disturbance. It decreased to 4 in the following year and increased thereafter. It has been approximately 5.5 since 2007. The main source of total LAI recovery is the LAI of dwarf bamboo, which increased 2-fold. The amount of biomass of trees decreased to 70% after the typhoon, while that of dwarf bamboo increased 1.5-fold. However, biomass of bamboo was approximately 10% of that of trees. Therefore, dwarf bamboo did not fill in gaps due to a decrease in biomass of trees.

Photosynthetic increase due to dwarf bamboo partially compensated for photosynthetic decrease due to trees, and ecosystem respiration increased due to the increase in dead trees. As a result, the forest became the carbon source. To change the status of the forest from the carbon source to a carbon sink, it is necessary for carbon release to decrease with the advancing decomposition of dead trees.

Keywords: deciduous broadleaf forest, dwarf bamboo, CO₂ flux, disturbance

Evapotranspiration of tropical peat ecosystems

HIRANO, Takashi^{1*} ; KUSIN, Kitso² ; LIMIN, Suwido² ; OSAKI, Mitsuru¹

¹Research Faculty of Agriculture, Hokkaido University, ²University of Palangkaraya

In Southeast Asia, mainly in Indonesia and Malaysia, peatland is widely distributed, coexisting with swamp forest, over an area of 2.48×10^5 km² and accumulates 11-14% of global peat carbon (Page *et al.*, 2011). The peatland, however, has been rapidly degraded by deforestation and drainage. As a result, the proportion of forest cover in the peatlands of Peninsular Malaysia, Sumatra and Borneo fell from 77% to 36% from 1990 to 2010 (Miettinen *et al.*, 2012). Such human pressures made the huge peat carbon pool vulnerable and raised the risk for the pool to be a large carbon source to the atmosphere chiefly because of peat fires and lowered groundwater level (GWL). The carbon balance of peatland is chiefly controlled by local hydrology, which determines saturation or unsaturation of surface peat. Under unsaturation conditions, peat is aerated, and its soil organic compounds are easily oxidized into carbon dioxide (CO₂). Therefore, drainage to lower GWL necessarily enhances oxidative peat decomposition and its resultant CO₂ emissions. Because tropical peatland is typically ombrotrophic, GWL varies according to residuals (storage change) between precipitation as input and evapotranspiration (ET) and runoff as output. Although precipitation can be also affected by large-scale deforestation, ET and runoff are directly affected by deforestation and drainage, respectively. To predict GWL under human pressures and assess the carbon balance of tropical peatland, therefore, it is crucial to quantify ET and elucidate the effects of disturbances on ET.

We have measured fluxes of sensible heat and latent heat using the eddy covariance technique and determined ET and energy balance at three sites within 15 km on tropical peatlands near Palangkaraya, Central Kalimantan, Indonesia (Hirano *et al.*, 2012). The sites are different in disturbance degree: a relatively intact peat swamp forest with little drainage (UF), a heavily drained swamp forest (DF) and a drained burnt swamp forest (DB). Here we show the results of field measurement for four to six years between 2002 and 2009, including El Nino and La Nina events and discuss the effects of disturbances on the energy balance and ET of tropical peat swamp forest.

Because of energy imbalance (84 to 91% on an annual basis), ET was adjusted to close energy balance on a daily basis. Mean annual ET (± 1 standard deviation) for the four years from 2004 to 2008 was 1636 ± 53 , 1553 ± 117 and 1374 ± 75 mm y⁻¹, respectively, for the UF, DF and DB sites, which account for 67, 64 and 56% of mean annual precipitation of 2435 mm y⁻¹, respectively. Annual ET of the DB site was significantly smaller than those of the other sites, mainly owing to less transpiration due to few trees. This fact indicates that more water is lost by surface and groundwater runoff in the DB site. In addition, annual ET showed a positive linear relationship with annually mean GWL at each site. This significant linearity suggests that annually mean GWL is a robust indicator to assess the annual balances of carbon and water in tropical peat ecosystems (Hirano *et al.*, 2012).

Keywords: disturbance, drainage, eddy flux, energy balance, fire

Withering of Japanese oak by sulfuric acid of an air pollutant. and prevention from withering by charcoal

OMORI, Teiko^{1*} ; YOSHIIKE, Yuzo² ; OKAMURA, Shinobu³ ; IWASAKI, Masato⁴

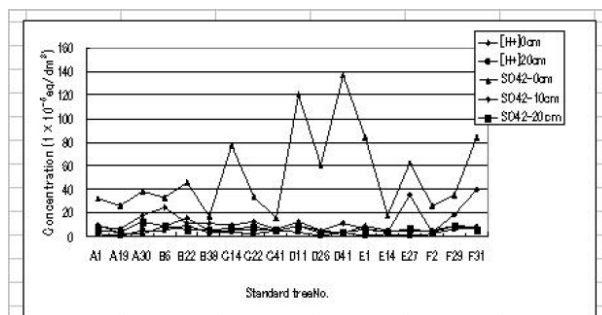
¹Teiko Omori, ²Yuzo Yoshiike, ³Shinobu Okamura, ⁴Masato iwasaki

The sulfuric acid which generates by the combustion of a fossil fuel is carried by wind and adheres to trees and only water evaporates and the sulfuric acid concentrates and accumulates. Sulfuric acid is dropped on the root of a tree by rain and it acidifies

the soil. The metal ingredient in the soil becomes a soluble compound. The eluted metal ion is absorbed by trees and it combines with phosphoric acid. The trees become shortage of phosphoric acid and decay. If the tannin contained in Japanese oak combines

with metal ion it becomes harmless to insect. Withering of trees originates in acidifications of soil. Charcoal can neutralize the acidified soil. The results of an investigation are explained on the basis of consideration from chemical standpoint.

Keywords: air pollutant, charcoal, withering of pine, withering of Japanese oak, tannin, phosphoric acid



sampling: Kanayama, Onuma, Fukushima 10.10.2011
Measuring method: 10g/ dried soil + 25g/water.
Filtration after 60minutes. [H ⁺]/pH meter, SO ₄ ²⁻ /Ion chromatography
The relation of the hydrogen ion and sulfuric acid ion concentration in soil (1 x 10 ⁻⁵ eq/dm ³)

Chemical dynamics of snow in the Japanese Alps region

KURAMOTO, Takayuki^{1*} ; SASAKI, Akihiko¹ ; SUZUKI, Keisuke¹

¹IMS, Shinshu University

The Japanese Alps region is one of the heaviest snowy regions in Japan. In this area, winter precipitation is observed mainly two patterns such as winter monsoon pattern and low pressure pattern. Therefore, the chemical characteristics of the snowpack are different by snowfall types. In this study we aimed to clarify chemical dynamics of snowpack in the Japanese Alps region. We conducted a snow pit studies in the Japanese Alps region. We collected snow samples at the large flat place without obstruct by trees and the impact of human activities. The samples were melted, then pH, electric conductivity and major ions (Na^+ , K^+ , Mg^{2+} , Ca^{2+} , Cl^- , NO_3^- and SO_4^{2-}) were analyzed in clean room. The Na^+ concentration correlates well with Cl^- concentration. These ions are considered to be sea-salt components. On the other hand, SO_4^{2-} concentrations included non-sea-salt components.

Change for chemical component of rime ice in two decades

NAGAFUCHI, Osamu^{1*} ; YOKOTA, Kuriko² ; NAKAZAWA, Koyomi¹ ; HISHIDA, Naoko¹ ; IKEDA, Keisuke¹

¹the University of Shiga Prefecture, ²Toyohashi University of Technology

Rime-ice and snow samples were collected at mountainous sites in Kyushu Island, Japan during from 1991 to 2014, and both soluble and insoluble substances in the melted rime-ice were analyzed by ion chromatography, inductively coupled plasma-mass spectrometry (ICP/MS) and analytical electron microscopy, in order to find the change of composition ratio of atmospheric pollutants cause by East Asian region. Although N/S ratio in rime-ice ranged from 0.1 to 0.3 in 1990's, recent year this ratio increased about 1.0. This phenomenon indicates that the composition of atmospheric pollutants changed during two decades in East Asian Continent.

Variations in chemical composition of surface ice and meltwater on Svalbard glaciers

KONNO, Yudai^{1*}; TAKEUCHI, Nozomu¹

¹Graduate School of Science, Chiba University

Snow and ice on glaciers usually contain small amounts of various soluble substances. These chemical substances were supplied through the atmosphere, rain, and snow. Chemical substances in glacier surface ice and melting water are important to understand atmospheric circulation, material cycle and the ecology of glacial microbes. We analyzed the major soluble ions of surface ice, melt water, and fresh snow for three glaciers (Austre Broggerbreen, Midtre Lovénbreen, and Pedersenbreen) in the northwestern part of Svalbard in the melting season of 2013.

The concentrations of all of the solutes were low generally, but the compositions varied among the samples. Based on the significant correlation on the concentration of each samples, the solutes could be classified into 3 groups: Group A (Cl^- , SO_4^{2-} , Na^+), B (Mg^{2+} , Ca^{2+}), and C (NO_3^- , NH_4^+ , K^+). They are likely to be derived from different sources. Group A solutes are probably sea salt origin, and Group B solutes are terrestrial dust origin, and Group C are anthropogenic or other unknown origin.

The altitudinal distribution of the concentration on Austre Broggerbreen showed that Group A (sea salt) solutes varied significantly although Group B (dust) solutes did not. Group A solutes were particularly higher in the higher area of the glacier. This variation can not be explained by distance from sea. It is probably due to supply from snow area remaining upper part of the glacier.

The chemical composition of the melting water was generally similar to those of the ice at the same site. However, some of the solutes (K^+ and SO_4^{2-}) were more abundant in meltwater than glacier ice at specific locations. This is probably due to supply from upper part of the glacier.

Keywords: Svalbard, glacier, chemical composition, sea salt

Interannual variability of total SWE obtained by snow surveys in the Tuul river basin, Mongolia, from 2002 until 2013

SUGIURA, Konosuke^{1*} ; KADOTA, Tsutomu² ; IJIMA, Yoshihiro² ; KONYA, Keiko² ; ZHANG, Yinsheng³ ; ISHIKAWA, Mamoru⁴ ; YAMAZAKI, Takeshi⁵ ; PUREVDAGVA, Khalzan⁶ ; DAVAA, Gombo⁶ ; OHATA, Tetsuo²

¹University of Toyama/JAMSTEC, ²JAMSTEC, ³Institute of Tibetan Plateau Research, Chinese Academy of Science, ⁴Hokkaido University, ⁵Tohoku University, ⁶Institute of Meteorology, Hydrology, and Environment, Mongolia

It is necessary for the southern limit of snow cover and the semi-arid region to be supplied with sustainable water. Mongolia is located in the southern limit and the semi-arid region. The capital, Ulaanbaatar, lies in a valley on the Tuul River. In order to investigate the actual conditions of snow water equivalent (SWE) in the upper Tuul River as water resources, the snow survey in the upper Tuul River has been carried out from 2002 to 2013. We have observed in each February when it will be the maximum amount of SWE. The snow water equivalent was estimated using a cylindrical snow sampler with 0.005-m² area. The total amount of SWE in the upper Tuul River basin was estimated using a global digital elevation model (DEM) with a horizontal grid spacing of 30 arc seconds (GTOP30) and a relationship between altitude and SWE. The main results obtained are shown below. The amount change of SWE in the upper Tuul River basin fluctuates over multiple years. The range of fluctuation was $0.25 \pm 0.07 \text{ km}^3$. It was not necessarily fluctuating in monotone. The steep rise of the amount of SWE in the upper Tuul River basin coincides with increasing air temperature and snowfall roughly.

Keywords: snow water equivalent, snow cover, water resources, water cycle, Mongolia

Identifying the ice thickness of five perennial snow patches in the Tateyama Mountains based on GPR soundings

FUKUI, Kotaro^{1*} ; IIDA, Hajime¹

¹Tateyama Caldera Sabo Museum

We carried out ground penetrating radar (GPR) soundings in the Kuranosuke, the Hamaguri-yuki, the Tsurugisawa, the Chojiro and the Ikenotan-migimata perennial snow patches in the Tateyama Mountains, the northern Japanese Alps since 2012. The Kuranosuke and the Ikenotan-migimata perennial snow patches had large ice masses (>30 m in thickness). We had measured the surface flows of both ice masses since 2011. The maximum surface flows of the Ikenotan-migimata and the Kuranosuke perennial snow patches were about 2 m a⁻¹ and 0.14 m a⁻¹, respectively. Thus, we regard the both snow patches as active glaciers.

The Hamaguri-yuki, the Tsurugisawa and the Chojiro perennial snow patch had thin ice masses (<20 m in thickness). It is possible that these ice masses are not flowing at the present time. Thus, we guess that these snow patches are glacierets rather than active glaciers.

Keywords: glacier, perennial snow patch, Mt. Tateyama, Mt. Tsurugi, GPR

Studies on internal structure of active glacier in the Tateyama Mountains

IIDA, Hajime^{1*} ; FUKUI, Kotaro¹

¹Tateyama Caldera Sabo Museum

In 2013, we carried out 20 m depth boring in the Sannomado Glacier (2000 m above sea level), in the Tateyama Mountains, the northern Japanese Alps. The 20 m core was analyzed paying attention to the structure of firn and ice. The following observations were carried out;

- (i) stratigraphic observation of snow layer and glacier ice.
- (ii) measurement of density profile.
- (iii) measurement of grain shape and profile of grain size.
- (iv) observation of elongation of air bubbles.

The internal structure of the Sannomado Glacier was characterized by obvious boundary between firn and ice. At the depth of 5m, there was a distinct dirt layer formed in the last autumn. Above this dirt layer, firn transformed into ice abruptly and the density curve showed a discontinuity to 850kg/m^3 . The temperature of the snow and ice measured in the borehole was $0\text{ }^\circ\text{C}$ throughout the layer. Spouting water was found in the borehole, indicating an aquifer in the glacier. From these results, such a rapid transformation process from snow to ice in this glacier will be discussed.

The grain size gradually increased with depth and elongation of air bubbles was shown below 15m which suggests internal flow of the glacier.

Keywords: glacier, perennial snow patch, Mt. Tateyama, Mt. Tsurugi, boring

Contribution ratio of glacier discharge to the river water in Mongolian Altai

KONYA, Keiko^{1*} ; KADOTA, Tsutomu¹ ; DAVAA, Gombo² ; PURVDAGVA, Kalzan²

¹JAMSTEC, ²IMHE, Mongolia

The discharge from glaciers is an important theme for arid regions like Mongolia. The water from glaciers are accounted for the important water resources in Mongolia where little water is supplied from precipitation. It is to be revealed that how much water is available from the glaciers. In this study, we estimate how much water is available in the present states and in the future by analyzing water chemistry and water quantity.

We have measured the discharge, water temperature, electric conductivity (EC), pH, dD, d18O of the river at the beginning, middle and end of the melt season of the glacier. The contribution rate of the melt water to the river water were estimated by the two methods; A) discharge and EC, B) glacier melt rate.

The contribution rate was estimated to be 20-50 % of the flow. The future change of the contribution rate was estimated by method B with the temperature warming rate in the future estimated by the climate models in Mongolia. The results show that the river water is supposed to be increasing in next some decades and decreasing in next century. The snow melt water to the river is also need to be taken into account.

Keywords: glacier, glacier discharge, temperature warming, water resources, Mongolia, climate change

Comparison of surrounding land features on the glacier terminal areas in the Himalayas derived from DEM

SUZUKI, Ryohei^{1*}

¹none

Radiation field on the surface of mountain glaciers is reported to be controlled by the surrounding land features and does not distribute uniformly. Net radiation, which is obtained as a result of radiation budget, has been reported as an important factor to melt the ice surface of glaciers in the Himalayas by the previous studies. On the other hand, the lower areas of many glaciers in the south area of Himalayas are covered with debris that has variety of thermal properties, which corresponds to the one of the factor to cause the spatial variety of ice melt rates fields. Considering the surrounding land form features in the radiation field is probably required for estimating thermal properties on the debris-covered glaciers accurately. However, in-situ observation of those phenomena cannot be conducted mainly due to the difficulties of accessibility to the Himalayas. Thus, application of satellite remote sensing techniques is a powerful tool as an alternate method.

This study focuses on the Lunana region, Bhutan, which corresponds to the target area where in-situ observation has been carried out since 2002, as a case study to estimate the influence of surrounding land features around the lower glacier areas on their radiation field. I calculated a distribution of azimuth and zenith angles from each target point (pixel) on the lower glacier areas to each direction to the skylines with an approximate method to derive surrounding land feature; the value 1 corresponds to the full sky view and it decreases to 0 with the decrease of openness. My first result, which was derived from 8 directions for each pixel with the limit of about 4.5 km far from the point as a line of sight, shows it ranges from 0.7 to 0.9 regarding the three glaciers; Thorthormi, Lugge and Lugge II.

Because these values depend on the method to move the line of sight on the DEM, in other words, the method for processing the raster image as well as the accuracy of both elevations and horizontal positions, I would also like to present the other experimental results that were calculated with some different conditions to discuss the influence of the surrounding land form on the radiation field in the Himalayas.

Keywords: Digital Elevation Model (DEM), image processing, glacier melt rate, radiation budget, mountain glaciers, Himalayas

Glacier lake and glacier lake outburst floods in Tien Shan and Ladakh Range

NARAMA, Chiyuki^{1*} ; KAZEHARE, Saiga¹ ; YAMAMOTO, Minako¹ ; UKITA, Jinro¹ ; IKEDA, Naho² ; TADONO, Takeo³

¹Niigata University, Department of Environmental Science, ²Tohoku University, Institute for Disaster Reconstruction and Re-generation Research, ³JAXA

As a result of recent glacier melting, present glacier lakes develop rapidly at glacier fronts in Tien Shan Mountains, Central Asia and Ladakh Range, Indian Himalayas. Although glacier lakes in the Tien Shan and Ladakh Range are small, compared to those in the eastern Himalayas (Bhutan and eastern Nepal), several GLOFs in the past have caused fatalities and serious damage to infrastructure and crops. With recent changes in the development of glacier lakes in these mountain regions, floods are becoming an increasing threat to local residents. However, the current status of glacier lakes is poorly characterized in this region. In this study, we researched glacier lakes in the Tien Shan Mountains and Ladakh Range using high-resolution ALOS/PRISM-AVNIR-2 images taken in 2007-2010. In addition, we report the characteristic of glacier lake and glacier lake outburst floods (GLOFs) in Tien Shan, using investigation of the appearance of glacier lake and GLOFs in the past.

We examined about 1600 glacier lakes ($>0.001 \text{ km}^2$) in the Tien Shan. Although glacier lakes are distributed throughout the Tien Shan Mountains, regional differences in their number and size are large. Larger glacier lakes are found in the Teskey and Ili-Kungoy regions, whereas most small glacier lakes occupy other mountain ranges (4000-5000 m asl), such as the Pskem, Talas, and Kyrgyz Ala-Too ranges. In seven mountainous regions, many present-day glacier lakes have appeared since the 1980s. Glaciers in these mountain regions are most glacier shrinkage area in Tien Shan over the 30 years, and these glacier lakes appeared after glacier shrinkage area. We report our results in detail in JpGU meeting.

Keywords: glacier lake, glacier lake outburst floods, small-size glacier lake region, Tien Shan, Ladakh Range

Chemical Composition on the surface in the Urumqi No.1 glacier, Tien Shan, China

WAKABAYASHI, Kozue¹ ; TAKEUCHI, Nozomu^{1*} ; TANAKA, Sota¹ ; AMEMIYA, Shun¹

¹Graduate School of Science, Chiba University

Various chemical solutes are deposited in snow and ice on glaciers. Such solutes are usually washed out of glaciers during melting season. However, concentration and composition on snow and ice during melting season are little known. The solutes are important to understand microbes living on the glacier surface since chemical conditions affect their growth. In this study, we analyzed chemical compositions of ice surface in the melting season on Urumqi glacier No.1, Tien Shan Mountains in central Asia. Results showed that calcium ion was dominated more than 60% in all of the area on the glacier. This indicates that the chemical composition on the melting glacial surface is greatly affected by dust from desert in this region. Total concentration of nitrogen solutes (ammonium) was highest in the middle part of the glacier. Measurements of chlorophyll a concentration revealed that it was also maximal in the middle of the glacier. The altitudinal variation of solutes may affect the algal community and biomass on the glacier.

Keywords: chemical composition, glacier

Digital-image processing to analyze grain size variation in ice core from Gregoriev Ice Cap, Kyrgyz Tien Shan

MATSUHASHI, Yuta^{1*} ; FUJITA, Koji¹ ; TAKEUCHI, Nozomu² ; VLADIMIR B, Aizen³

¹Nagoya University, ²Chiba University, ³University of Idaho

It is known that impurities in ice core (etc. dust from continental) prevent grain growth rate at high-latitude regions. On the other hand, the effect of impurities for grain growth is not understood for ice cores retrieved from mid-low latitude glaciers, despite of higher dust concentration. This study aims to reveal relation between dust and grain size in an ice core drilled at Gregoriev Ice Cap, Kyrgyz Tien Siam in 2007.

We made thin sections which are reduced to thickness of 0.4mm. Three different images were taken by changing angle of crossed polarizers (0 deg, 30 deg, 60 deg). Changing controlled contrast and RGB, we converted the images into binary. Grain boundaries are then able to be picked by digital image-processing. This process made efficient extracting boundary and obtain area of grain using binary images.

We will present detailed procedures and preliminary results of comparison with dust concentration along the ice core.

Keywords: ice core, grain size, Grigoriev ice cap

Post-depositional alteration of major ions under different accumulation environment in Antarctica

HOSHINA, Yu^{1*} ; FUJITA, Koji¹ ; IIZUKA, Yoshinori² ; MOTOYAMA, Hideaki³

¹Nagoya University, ²Institute of Low Temperature Science, Hokkaido University, ³National Institute of Polar Research

Major soluble ions and water stable isotopes are important for reconstructing paleo-environment and atmosphere circulation. It is also known that ion and isotope signals are modified after deposition if firn or ice core samples are analyzed at high temporal resolution such as seasonal scale. In inland Antarctica, we revealed that low accumulation rates have resulted in significant post-depositional modification of ions and isotopes due to long time exposure of snow near the surface.

We further investigated relation between major ion concentration and accumulation rate using a several snow pits and firn cores taken from east and west Antarctica. To exclude the geographical factor (east or west), we analyzed correlations with ions against oxygen stable isotope. Correlations of sea salt against oxygen stable isotope are gradually changed from no correlations under higher accumulation sites near coast to more negative correlations under dry environment in inland. On the other hand, correlations of MSA (methanesulfonic acid) against oxygen stable isotope rapidly are changed from positive to negative correlations at $100 \text{ kg m}^{-2} \text{ a}^{-1}$ of accumulation sites. Those different trends suggest different mechanisms of post-depositional modification for these ion species.

Keywords: Antarctica, ice core

Greenland temperature variability over the past 2000 years inferred from NGRIP and GISP2 ice cores

KOBASHI, Takuro^{1*} ; GOTO-AZUMA, Kumiko¹ ; KAWAMURA, Kenji¹ ; VINTHER, Bo² ; BLUNIER, Thomas² ; BOX, Jason³ ; BUIZERT, Christo⁴ ; MUTO, Atsuhiko⁵ ; WHITE, James⁶

¹National Institute of Polar Research, ²Copenhagen University, ³Geological Survey of Denmark and Greenland, ⁴Oregon State University, ⁵Pennsylvania state University, ⁶University of Colorado at Boulder

We reconstructed Greenland temperature change for the past 2000 years using argon and nitrogen isotopes in trapped air in NGRIP and GISP2 ice cores. To identify true variability of temperature, we also applied various methods such as borehole temperature inversion, Monte Carlo inversion of borehole temperature, oxygen isotopes of ice, forward and inverse methods for argon and nitrogen isotopes with borehole temperatures. We will present the results of analyses and implications.

Keywords: Greenland, temperature, ice core, GISP2, NGRIP, 2000 years

Greenland temperature variations in the last millennium climate simulation

YOSHIMORI, Masakazu^{1*} ; ABE-OUCHI, Ayako¹

¹Atmosphere and Ocean Research Institute, The University of Tokyo

A series of climate simulations of the last millennium are conducted using the MIROC climate model. These include a simulation under volcanic-only, solar-only, or total forcings. Sensitivity experiments using different strength of volcanic and solar forcings are also conducted. With these dataset, we analyze the factors that influence Greenland temperature variations during the last millennium. Attention is paid to the effect of different external forcings and changes in the atmosphere and ocean circulations such as the North Atlantic Oscillation and the Atlantic meridional overturning circulation.

The variation of the Arctic cryosphere in the Last Millennium simulation using MIROC and MIROC-ESM

SUEYOSHI, Tetsuo^{1*} ; OHGAITO, Rumi¹ ; YOSHIMORI, Masakazu² ; HAJIMA, Tomohiro¹ ; ABE, Manabu⁴ ; O'ISHI, Ryouta⁴ ; OKAJIMA, Hideki¹ ; SAITO, Fuyuki¹ ; WATANABE, Shingo¹ ; KAWAMIYA, Michio¹ ; ABE-OUCHI, Ayako²

¹Japan Agency for Marine-Earth Science and Technology, ²Atmosphere and Ocean Research Institute, University of Tokyo, ³National Institute for Environmental Studies, ⁴National Institute of Polar Research

In this study, we analyze the result of Last Millennium (LM) Experiment using GCM and ESM, to verify the response of the cryosphere to the hundreds-year-scale climate change. In addition to the sensitivity analysis between the forcing conditions, comparison with existing climate/paleoclimate data. The period of the LM experiment covers the Little Ice Age and Medieval Climate Anomaly, and responses of the cryosphere during those periods are of interest.

The models used in this study are the Atmosphere-Land-Ocean General Circulation Model MIROC and the Earth System Model MIROC-ESM. Resolution of atmosphere/land components are T42 (ca 2.8°) in horizontal, 80 layers in vertical. Ocean component has a resolution of 1.4° (longitude) by variable 0.56°-1.4° (latitude) in the horizontal and 44 levels in the vertical. As an ESM, MIROC-ESM has a carbon-cycle components for the land and ocean ecosystems. Setup of the experiments follow the protocol of model inter-comparison CMIP5/PMIP3.

As preliminary results, temporal variations in surface air temperature, snow amount, and snow/rain ratio for Siberia region was analyzed. Winter warming during 20th century is clear. Signatures are shown in rise of February Temperature, decrease in snow amount, increase in runoff during spring. Ratio of Snow fall / Precipitation is sensitive to the temperature, which may caused the above-mentioned trends in snow.

Keywords: paleoclimate, climate modelling, Last Millennium, cryosphere, climate change

A long-term ^{10}Be record from Dome Fuji ice core and cosmic-ray stratigraphy

HORIUCHI, Kazuho^{1*} ; SUGUCHI, Shota¹ ; SUDA, Kensuke¹ ; UCHIDA, Tomoko² ; AZE, Takahiro³ ; YOKOYAMA, Yusuke⁴ ; MURAMATSU, Yasuyuki⁵ ; MATSUZAKI, Hiroyuki⁶ ; MOTOYAMA, Hideaki⁷

¹Graduate School of Science and Technology, Hirosaki University, ²Institute of Geology and Paleontology, Tohoku University, ³Graduate School of Science and Engineering, Tokyo Institute of Technology, ⁴Atmosphere and Ocean Research Institute, The University of Tokyo, ⁵Faculty of Science, Gakushuin University, ⁶Graduate School of Engineering, The University of Tokyo, ⁷National Institute of Polar Research

Cosmogenic nuclides (^{10}Be , ^{14}C , ^{26}Al , ^{36}Cl) in paleoenvironmental archives serve as a proxy indicator of the paleointensity of cosmic ray, controlled largely by the strength of the solar/geomagnetic fields. Here, we present a millennial record of cosmogenic ^{10}Be covering the past 300 kyr and obtained from ice cores drilled at the Dome Fuji station ($77^{\circ}19'S$, $39^{\circ}42'E$), inland East Antarctica. A number of specific increases in ^{10}Be were observed in this record and were connected semi-quantitatively to those in the cosmic-ray intensity caused by geomagnetic excursions during the last 300 kyr. These features can be used as stratigraphic time-markers for synchronization of not only Antarctic ice cores but also various paleoenvironmental archives such as deep-sea sediments

Age synchronization between an Antarctic ice core and Northern Hemisphere marine cores: with special focus on MIS 11

KAWAMURA, Kenji^{1*} ; AOKI, Shuji² ; NAKAZAWA, Takakiyo² ; ABE-OUCHI, Ayako³ ; SAITO, Fuyuki⁴

¹National Institute of Polar Research, ²Tohoku University, ³University of Tokyo, ⁴JAMSTEC

Investigation of the roles of different forcings (e.g. orbital variations and greenhouse gases) on climate and sea level requires a paleoclimate chronology with high accuracy. Such a chronology for the past 360 ky was constructed through orbital tuning of O₂/N₂ ratio of trapped air in the Dome Fuji and Vostok ice cores with local summer insolation (Kawamura et al., 2007). We extend the O₂/N₂ chronology back to ~500 kyr by analyzing the second Dome Fuji ice core, and find the duration of 11 ka, 5 ka, 9 ka, and 20 ka for MIS 5e, 7e, 9e and 11c interglacial periods in Antarctica, with similar variations in atmospheric CO₂. The termination timings are consistent with the rising phase of Northern Hemisphere summer insolation.

Marine sediment cores from northern North Atlantic contain millennial-scale signatures in various proxy records (e.g. SST, IRD), including abrupt climatic shifts and bipolar seesaw. Based on the bipolar correlation of millennial-scale events, it is possible to transfer our accurate chronology to marine cores from the North Atlantic. As a first attempt, we correlate the planktonic d₁₈O and IRD records from the marine core ODP 980 with the ice-core d₁₈O and CH₄ around MIS 11. We find that the durations of interglacial plateaus of planktonic d₁₈O (proxy for sea surface environments) and benthic d₁₈O (proxy for ice volume and deep-sea temperature) for MIS 11c are 20 and 15 ka, respectively, which are significantly shorter than originally suggested. These durations are similar to that of Antarctic climate and atmospheric CO₂. However, the onsets of interglacial levels in ODP980 for MIS 11 are significantly later than those in Antarctic d₁₈O and atmospheric CO₂ (by as much as ~10 ka), suggesting very long duration (more than one precession cycle) for the complete deglaciation and northern high-latitude warming for Termination V. Atmospheric CO₂ may have been the critical forcing for this termination. The long duration of Termination V is consistent with our new ice sheet simulations (extended from the work of Abe-Ouchi et al., 2013) in which an ice-sheet/climate model is forced by insolation and CO₂ variations. In the presentation, comparisons for other interglacial periods will also be reported.

Keywords: Antarctic ice core, Marine core, Chronology, Glacial-interglacial cycles

What is the major factor which control global climate in the ice age?

KUMON, Fujio^{1*}

¹Faculty of Science, Shinshu University

The author and his co-workers have been analyzed total organic carbon (TOC) and total nitrogen (TN) contents of the various lake and marine sediment cores. The temporal changes of TOC show quasi-periodic fluctuation patterns similar to LR04 marine oxygen isotope curve and delta 18O profile of NGRIP ice core. Among the several long records of TOC in and around the Japanese islands, the TOC record from the Japan Sea is the most excellent one, and can be correlated precisely with the NGRIP record both on the orbital- and millennial time-scale in the ice ages.

This intimate relationship of climate is confirmed between Greenland and the Japanese islands. The good concordance of climate change can be explained by a hypothesis that extension of ice sheets in the Arctic region is major factor to control global climate not only in orbital-time scale but also in millennium-time scale.

Keywords: organic carbon content, climate change, ice sheet, Japan Sea sediment, Milankovich hypothesis, pinge-purge model

The influence of glacial ice sheet on Atlantic Meridional Overturning Circulation through atmospheric circulation change

SHERRIFF-TADANO, Sam^{1*} ; ABE-OUCHI, Ayako¹ ; YOSHIMORI, Masakazu¹ ; CHAN, Wing-le¹

¹Atmosphere and Ocean Research Institute, University of Tokyo

In glacial period, huge ice sheet covered the North America and the Northern Europe. Also, the Antarctica Ice sheet had expanded and increased its altitude. It is well known that these ice sheets (hereafter glacial ice sheets) have large influence on climate, for example atmospheric circulation, surface air temperature, and sea surface temperature. On the other hand, recent studies showed that wind stress changes play a crucial role on the AMOC under glacial climate. Moreover, increasing evidence suggests that glacial ice sheets have large influence on the Atlantic Meridional Overturning Circulation (AMOC). However the process how the ice sheets cause such a large impact on the AMOC is yet fully understood. Thus, in this study, we aim to reveal the detailed process of the ice sheet affecting the AMOC through atmospheric circulation change.

Commonly, the Atmosphere-Ocean General Circulation Model (AOGCM) is used to assess the influence of the ice sheet on the AMOC. However, as the atmospheric general circulation model (AGCM) and ocean general circulation model (OGCM) interacts in this model, the wind change as well as other process affect the AMOC. Therefore, it is difficult to divide each effect. Using the AGCM and the OGCM separately can overcome this problem because in this manner, they do not interact and the wind stress or other process can be treated as a boundary condition for the OGCM. This method consists of 2 steps. First, by using the AGCM, the effect of glacial ice sheets on the surface wind stress are evaluated by adding glacial ice sheets as a boundary condition. Second, by using the wind stress result as a boundary condition for the OGCM, the influence of the wind stress change on AMOC is estimated. In addition, by analyzing the results from each model, the underlying mechanism is explored.

As a result, glacial ice sheets largely intensified the AMOC under glacial climate. It was also found that the wind stress change at North Atlantic was important, thus glacial ice sheets at northern hemisphere were important. On the other hand, the AMOC was hardly influenced by wind stress change at Southern Ocean, which is mainly induced by the change in the Antarctica Ice sheet. Therefore change in the Antarctica Ice sheet had small impact on AMOC through surface wind stress change.

By analyzing the results from the AGCM and OGCM, it revealed that two processes were crucial; first, the strengthening of the northward salt transport, which resulted from enhanced westerly due to the North America Ice sheet. Second, the northward sea ice transport due to the southerly wind at Norwegian Sea forced by the Northern Europe Ice sheet. These two processes were found to drastically intensify the AMOC through affecting the sea ice distribution and shifting the NADW formation region.

Keywords: Ice sheet, Glacial climate, AMOC, wind stress

Reconstruction of paleo-vegetation distribution by using an atmosphere ocean coupled GCM and a DGVM

O'ISHI, Ryouta^{1*} ; CHAN, Wing-le² ; ABE-OUCHI, Ayako²

¹National Institute of Polar Research, ²Atmosphere and Ocean Research Institute, the University of Tokyo, ³JAMSTEC

“ The replacement of Neanderthals by Modern Humans has been considered to have occurred during 60,000-30,000 BP, which is also characterized by millennial scale climate change known as the Dansgaard-Oeschger events. The distribution of Neanderthals and Modern Humans during this period suggests correlation with that of paleo-vegetation and animals. This relation reflects the difference between the adaptabilities of Neanderthals and Modern Humans to environmental changes by way of their ability to hunt animals as food resources. Hence, it is important for the RNMH project to predict distribution of fauna, flora and climate change during this period. When estimating fauna distribution of the past, it is necessary to evaluate the changes in flora and thus changes in climate of the past. This can be directly achieved by examining data from sediment proxies, e.g. pollen records and isotopes. However, the availability of such proxies to reproduce the distribution of flora and climate changes is limited.

In the present study, we tried to reconstruct the vegetation distribution across North Africa, the Mediterranean and Europe during 60,000-30,000 BP from the results of a paleo-climate reconstruction by using a general circulation model as input for a dynamical global vegetation model. GCMs consume huge amounts of computational resources and so experiments are usually run using lower resolution models whose grid sizes are not sufficiently small for anthropological studies. In this study, we developed an “ anomaly procedure ” in order to incorporate features from both a high-resolution model and paleoclimate information. As a result of this new method, we successfully obtained a high-resolution vegetation distribution for a specific period of the past. However, it is not yet clear how these results can be validated against paleovegetation records. We need further discussions on how the appropriate paleoclimate can be reproduced by the GCM and how the vegetation model results can make a robust contribution toward the RNMH project.

Keywords: D-O cycle, Paleoclimate, Paleovegetation, Modeling

Arctic amplification and the Greenland ice sheet at the Last Interglacial: the role of vegetation feedback

ABE-OUCHI, Ayako^{1*} ; O'ISHI, Ryouta¹ ; TAKAHASHI, Kunio² ; SAITO, Fuyuki²

¹University of Tokyo AORI, ²JAMSTEC

We calculated the climatic conditions, mass balance and the transient volume of the Greenland ice sheet in the last interglacial period using the atmosphere slab-ocean vegetation general circulation model ASVGCM MIROC-LPJ and IciES ice sheet model. Taking into account the vegetation feedback, the annual mean temperature anomaly increases from +1 K to +2 K, and of summer temperature anomaly from +4 K to +6 K in central Greenland. This is close to the +5 K at NGRIP and +8 K at NEEM as inferred from ice core isotope data, which takes into account that summer precipitation contributes more to oxygen isotope values{reference}. The vegetation feedback, also increases precipitation by 20% averaged over the entire ice sheet and by 30 % in northwestern Greenland. The combination of the sea ice-temperature feedback and the vegetation feedback amplifies both the temperature and precipitation changes in the Eemian.

The increased ablation caused by high temperatures in central Greenland is partly compensated by the increased precipitation. The ice volume loss of Greenland in the Eemian compares to present day amounts to 1 to 2.5 meters sea level equivalent depending on the inferred present day reference climate and model parameters, such as lapse rate. The spatial pattern of increased temperature and increased precipitation is supported by the fact, that the modeled Eemian Greenland ice sheet covers all locations of ice core sites (GRIP/GISP, NGRIP, NEEM and Dye3), for which the existence of Eemian ice is confirmed. The reconstructed sea level elevations in the Eemian range from 6 to 9 m{references} above present day sea level. Thus, our results imply that the larger part of the difference in sea level between Eemian and present day stems from the Antarctica ice sheet.

Sensitivity of Greenland ice sheet to climatic parameters during the last interglacial

TAKAHASHI, Kunio^{1*} ; ABE-OUCHI, Ayako² ; SAITO, Fuyuki¹ ; O'ISHI, Ryouta³

¹Japan Agency for Marine-Earth Science and Technology, ²Atmosphere Ocean Research Institute, University of Tokyo, ³National Institute of Polar research

In the last interglacial (LIG), sea level was 5 to 9 m above present, including contribution from Antarctica. Whole melting of the Greenland ice sheet (GIS) can contribute to the global sea-level rise of up to 7 m. It is important source of sea-level change. In the previous IPCC report in 2007 (IPCC AR4), estimates the GIS contribution to sea-level change during LIG range between 4 to 6 m. New IPCC AR5 points out that based on ice-sheet model simulations consistent with elevation changes derived from a new Greenland ice core, the Greenland ice sheet *very likely* contributed between 1.4 to 4.3 m sea level equivalent.

In this study, we present numerical experiments of GIS from 140 ka to 110 ka by using anomaly approach (present-day climate + perturbation obtained from MIROC-AGCM simulations including dynamic vegetation). We focus on the influence of the climatic parameters such as AMOC or northern hemisphere ice sheets. Our results are consistent with IPCC AR5. Considering of transient response to transient climate change are important to moderate ice melting. Several uncertainties remain however, such as the reference climate condition (influence melt from south, north or both?). and related the ice sheet model itself, more numerical studies are required.

Keywords: Last interglacial, Greenland, Ice sheet, Sea-level

Sea-level changes and crustal deformations in Greenland based on the loading histories derived from 3D ice sheet model

OKUNO, Jun'ichi^{1*} ; SAITO, Fuyuki² ; ABE-OUCHI, Ayako³ ; TAKAHASHI, Kunio²

¹NIPR, ²JAMSTEC, ³AORI, Univ. Tokyo

We study the implications of a recently published ice sheet history in Northern hemisphere and Greenland ice sheet, derived from the 3D thermo-mechanical ice sheet model (Ice Sheet for Integrated Earth system Studies: IcIES developed by Abe-Ouchi et al. 2013). To characterize the effects of this glaciologically consistent ice sheet history, we examine the time-variations of various geophysical quantities in response to the ice and water mass redistributions. They include vertical uplift and subsidence, global patterns of sea-level change, and regional sea-level variations along the coasts of Greenland. Relative sea-level (RSL) changes in response to past ice and water load variations are obtained solving the sea-level equation, which accounts for the crustal deformation due to glacio-isostatic adjustment (GIA). In this study, we report the predictions of RSL and geodetic signals in Greenland induced by GIA process based on the glaciologically and climatologically consistent ice loading history. And also, we show the temporal and spatial characteristics of predicted geophysical signals in Greenland in comparison with these observations. We expect that using the ice sheet histories derived from IcIES as input in GIA model may put better constraints on postglacial rebound and current rates of crustal deformation.

Keywords: Greenland ice sheet, relative sea-level change, crustal deformation, isostasy

Chemical compositions of non-volatile particles in NEEM (Greenland) ice core over the last 100,000 years

OYABU, Ikumi^{1*}; IIZUKA, Yoshinori²; KARLIN, Torbjorn³; FUKUI, Manabu²; HANSSON, Margareta³

¹Graduate school of Environmental Science, Hokkaido University, ²Institute of Low Temperature Science, ³Department of Physical Geography and Quaternary Geology, Stockholm University, Sweden

The polar ice cores provide us with information of past atmospheric aerosols. Soluble aerosols in polar ice cores are well discussed by using proxies of ion concentration/flux, however, there are few studies about chemical compositions of soluble aerosols in ice cores. Using a sublimation method, we show differences in the compositions of non-volatile aerosols over the last 100,000 years in the NEEM ice core, which was drilled during 2008-2012 on the northwest ridge line of Greenland ice sheet (77° 27' N, 51° 03' W).

A total of 86 samples were distributed from NEEM ice core sections from 220 to 2195 m, which covers from late Holocene to Dansgaard-Oeschger event 24. Non-volatile particles were extracted from the ice by sublimation system [Iizuka et al., 2009]. Constituent elements of each non-volatile particle were measured by a scanning electron microscope and energy dispersive X-ray spectroscopy. We made a classification of non-volatile particles into insoluble dust, soluble sulfate salts and soluble chloride salts as following; if Si found in a particle, we regard the particle as dust (Silicates); if S found, we regard the particle as sulfate; if Cl found, we regard the particle as chloride salt. For the sulfate salt, we did further classification that a particle containing Ca and S are assumed as CaSO₄, Na and S are Na₂SO₄, Mg and S are MgSO₄, K and S are K₂SO₄, the residual sulfate particles are "the other sulfate salt (other-S)". In the same way, for chloride salts, we assumed NaCl, CaCl₂, MgCl₂, KCl and the other chloride salt (other-Cl).

The number ratio of soluble salts to total particles is 9±6 % during Dansgaard-Oeschger (DO) events. In Last Glacial Maximum (LGM), the ratio decreased in 3±2%. In Bolling-Allerod (BA), ratio of soluble salts slightly increased (10±5%). In Younger Dryas (YD), the ratio decreased again (6±3%). After Holocene, the ratio increased (16±10 %). In summary, more than 90 % of particles contain insoluble dust during the cold stages. These ratios suggest that during cold periods, insoluble dust concentration is higher contribution to total non-volatile particles than that in warm periods.

We examined chemical characteristics of non-volatile particles by dividing into 7 climatic stages (Late Holocene; LH, Early Holocene; EH, YD, BA, LGM, DO events-warm; DO-W and DO events-cold; DO-C). The 7 stages can be sorted into 2 types; interglacial-type (LH, EH and BA) and glacial-type (YD, LGM, DO-W and DO-C). For the interglacial-type, number of Na-containing particles is larger than that of Ca-containing particles (Na:Ca = 4:3). On the other hand, for the glacial-type, number of Ca-containing particles is larger than that of Na-containing particles (Na:Ca = 5:9). Ca-containing particles is suggested to mainly come from terrestrial materials and Na-containing particles is mainly from sea-salt [Steffense et al., 1997]. Our results of the ratio of Ca and Na particles may be explained by not only absolute concentration of dust and sea-salt but also relative valance of those concentrations. In the three interglacial-type, the ratio of other-S and other-Cl, those are sulfate and chloride salts without Na, Mg, K, nor Ca, during the LH are relatively higher than the other stages. Since NH₄⁺ concentration increased due to increasing of vegetation area and biological activity by warming in LH [Fuhrer and Legrand, 1997], other-S and Cl might be ammonium sulfate and ammonium chloride, respectively. Focusing on Ca-particles more in detail in the four glacial-type, number of Ca-containing particles without S and Cl is higher in LGM (11%) and DO-C (12%) than that in YD (6%) and DO-W (7%). Since the X-ray spectroscopy cannot detect carbon, the Ca-containing particles may be CaCO₃ in the LGM and DO-C because CaCO₃ was founded during the LGM by single particle measurement in the GRIP (Greenland) ice core [Sakurai et al., 2009].

Keywords: ice core, aerosol, paleo climate, greenland, ice sheet, NEEM

Modelling the climate and the terrestrial carbon cycle for the last millennia

ABE-OUCHI, Ayako^{1*} ; O'ISHI, Ryouta¹ ; YOSHIMORI, Masakazu¹

¹University of Tokyo AORI

Climate-induced changes in the terrestrial biosphere and the ocean modulate the release and uptake of carbon dioxide and this, in turn, alters atmospheric composition and influences the climate. This is known as the climate-carbon cycle feedback. The Coupled Carbon Cycle Climate Model Intercomparison Project (C4MIP), using models of the ?terrestrial and ocean carbon cycles inside ocean-atmosphere general circulation models, has shown that the carbon cycle-climate feedback appears to be positive BUT there is great uncertainty about the magnitude. It is important to know the magnitude of this feedback because it affects the amount of carbon dioxide that can be emitted in the future in order to stabilize the concentration of CO₂ at a given level. There are projects attempting to reduce these uncertainties through systematic evaluation of carbon cycle models against observations of the contemporary carbon cycle. An alternative approach is to use knowledge about past variations in climate and CO₂ to provide additional constraints. Here we therefore work on the last millennium (LM) climate-carbon modeling and examine the factors that contribute to atmospheric CO₂ change. Ice core is the only proxy that provides the CO₂ content in detail for the last millennium and it shows up to 10ppm change around the Little Ice Age and during the LM. Several LM experiments by AOGCM are used to drive the terrestrial carbon cycle model LPJ. We investigate the role of external forcing of climate such as volcano and solar forcing as well as that of internal variability of climate in an unforced experiment of decadal to centennial time scale. We show that the CO₂ changes in the same order of magnitude in the unforced experiment as in the forced experiment.

Concentration and Potential Mobility of Trace Metals in Surface Sediment of the North Pacific Ocean By BCR Sequential

ANDREAS, Roy^{1*} ; ZHANG, Jing¹

¹Graduated school of science and engineering University of Toyama

Metals can accumulated in sediment, sludge and soil may therefore pose an environmental problem concerning possible metal transfer from sediment to the aquatic system and including them in the food chain. European Community Bureau of Reference (BCR) sequential methods commonly used to trace metals in the sediment or soil samples and can be provide information about bio-availability, mobility or toxicity which are basically depend on the chemical bonding between metals and solid phases of the samples.

Geochemical fractionation of Cadmium (Cd), Lead (Pb), Cobalt (Co), Zinc (Zn), Iron (Fe) and Manganese (Mn) in sediment of the North Pacific Ocean were determined using four-stages of modified BCR sequential extraction methods combination with ICP-MS. Also the contamination factors and risk assessment code effects on surface sediment samples are discussed.

The mean contents of the trace metals in surface sediment of the North Pacific Ocean were: Cd: 0.00; Pb: 13.94; Mn: 2732.94; Fe: 29795.10; Co: 22.16; and Zn: 76.75 $\mu\text{g}\cdot\text{g}^{-1}$, allowing to arrange the trace metals concentration from higher to lower were in the following order: Fe > Mn > Zn > Co > Pb > Cd. Pb was distributed in three fractions (acid soluble, reducible, and residual). Mn and Co were found in a group with mainly reducible fraction, while Fe and Zn were mainly in residual fraction. The high contamination factor was obtained for Mn and Co in the sediment samples, while the lowest was found for Fe. The result showed non risk for Fe, Co, Pb and Cd, while low risk is indicated for Mn and Zn at all stations.

Keywords: trace metals, BCR sequential extraction, North Pacific Ocean

Leaching Properties of Naturally Occurring Heavy Metals from the Soils around Abandoned Metal Mines

ZHANG, Ming^{1*} ; HOSHINO, Mihoko¹ ; HARA, Junko¹ ; SUGITA, Hajime¹ ; YOSHIKAWA, Miho² ; IMOTO, Yukari¹

¹AIST, ²Chemical Grouting Co., LTD

The major threats to human health from heavy metals are associated with exposure to lead, cadmium, mercury, chromium, arsenic, as well as selenium, fluorine and boron. The effects of such heavy metals on human health have been extensively studied and officially reviewed by international organizations such as the WHO and heavy metal pollutions have been regulated by national environmental standards and/or laws such as the Soil Contamination Countermeasures Act in Japan.

Leaching of naturally occurring heavy metals from the soils around abandoned metal mines into surrounding water systems, either groundwater or surface water systems, is one of the major pathways of exposure. Therefore, understanding the leaching properties of toxic heavy metals from naturally polluted soils is of fundamental importance for managing abandoned metal mines, excavated rocks discharged from tunneling and/or selecting a pertinent countermeasure against pollution when it is necessary.

In this study, soil samples taken from the surroundings of abandoned metal mines in Tochigi, Miyagi, Yamagata, Akita and Iwate prefectures in Kanto and Tohoku regions were collected and analyzed. The samples contained multiple heavy metals such as lead, arsenic and chromium. Standard leaching test and sequential leaching test considering different forms of contaminants, such as trivalent and pentavalent arsenics, and trivalent and hexavalent chromiums, together with X-ray Fluorescence Analysis (XRF), X-ray diffraction analysis (XRD) and Cation Exchange Capacity (CEC) tests were performed. This presentation illustrates the details of the above experimental study, discusses the relationships among leaching properties, and chemical and mineral compositions, indicates the difficulties associated with remediation of naturally polluted sites, and emphasizes the importance of risk-based countermeasures against naturally occurring heavy metals.

Keywords: Naturally occurring, Heavy metals, Leaching properties, Mineral composition, Bulk concentration

Self-potential inversion for the estimation of hydraulic conductivity in the presence of unsaturated zone

OZAKI, Yusuke^{1*} ; MIKADA, Hitoshi¹ ; GOTO, Tada-nori¹ ; TAKEKAWA, Junichi¹

¹Graduate School of Engineering, Kyoto University

Self-potential (SP) is the electrical potential naturally generated in and on the earth. The positive electrical charge in the diffuse layer of the electrical double layer is conveyed by the groundwater flow. The electrical potential is generated when the groundwater flow through the porous medium. This electrical potential directly reflects on the Darcy velocity in the porous material, and therefore the hydraulic conductivity can be estimated from the SP data. The hydraulic conductivity has non-linear characteristics as functions of the water saturation, and so does SP. These features suggest that the effect of the unsaturated zone should be considered for much quantitative analysis of SP. However, the dependency of the SP on the water saturation makes the development of inversion difficult. We solved this problem with the adjoint state method for the calculation of the sensitivity matrix that could save the calculation time. The characteristic of water saturation in SP based on Van-Genuchten model is adapted to our inversion. We applied our inversion to a synthetic SP profile to test the performance of our inversion scheme to compare the results with and without the consideration to unsaturated zone. When the effects of the unsaturated zone are not considered, the value of estimated hydraulic conductivity is underestimated. On the other hands, more accurate image could be derived from the inversion with the consideration to the unsaturated zone. Therefore, our inversion technique would allow us to obtain the accurate hydraulic conductivity structure from SP data at the ground surface, although the SP is affected by the distribution of saturation.

Keywords: Self potential, Inversion, Hydraulic conductivity, Unsaturated zone

Root Water Uptake and Soil Water Storage in a Karst Savanna on the Edwards Plateau, Texas, USA

TOKUMOTO, Ieyasu^{1*}

¹Arid Land Research Center, Tottori University

Woody plants, especially Ashe juniper (*Juniperus ashei*) and honey mesquite (*Prosopis glandulosa*), are encroaching into a karst savanna on the Edwards Plateau in central Texas. However, their impact on hydrology is unclear because of high variability in soil depth and uncertainties about shallow and deep root contributions to water uptake in rocky soil overlying bedrock or other substrates that limit water storage capacity and root growth, and create high spatial variability in plant available water. This complex below-ground structure, while not uncommon, has not been adequately characterized by most hydrological models. We evaluated root water uptake and water storage in the karst of the Edwards Plateau, at a typical savanna site with ~50% woody cover, mainly Ashe juniper (*Juniperus ashei*) and honey mesquite (*Prosopis glandulosa*). Water content profiles to a depth of 1.6 m were measured by neutron thermalization and time domain reflectometry at 36 locations in a 25-by-25 m grid (5 m node spacing). Bulk density profiles were measured by gamma densitometry. Temporal changes in water storage were compared with eddy covariance measurements of evapotranspiration (ET) to evaluate relative amounts of ET originating from root water uptake at various depths. Water storage capacity in the measurement grid ranged from 185 to 401 mm, and coupled with heterogeneous distribution of trees created high spatial variability in root water uptake. Water uptake was higher beneath trees than beneath grass, in part because tree roots were able to extract water from regions of the root zone with high rock density. On average, 81% of the water uptake occurred from the upper 1 m of the profile with the greatest uptake occurring at depths of 0.4 to 0.8 m. An estimated 10% of the uptake occurred from below the maximum measurement depth of 1.6 m. While this result confirms the hypothesis that trees on rocky substrates take up water from greater depths compared to similar ecosystems on soil, it also refutes the view that trees in karst regions have greater access to groundwater.

Keywords: Root water uptake, Karst, Evapotranspiration, Spatial variability

Estimation of Water Flux in Andisol with a Penta-Needle Heat Pulse Probe

SAKAI, Masaru^{1*}; KONDO, Naho¹; JONES, Scott²

¹Graduate school of Bioresources, Mie University, ²Department of Plants, Soils, and Climate, Utah State University

The potential for using heat pulse probes for estimating soil water flux as well as soil thermal properties has received more attention this past decade. Although many studies were carried out to validate water flux estimation using heat pulse probes in sandy soils, few studies were reported for other soils. The purpose of this study was to estimate water fluxes in an aggregated Andisol using a heat pulse probe, and investigate the applicability with hydrodynamic dispersion in a soil.

The Penta-needle heat pulse probe, which has a central heater needle surrounded by two pairs of orthogonally arranged thermistors, was used to estimate two directional water flux. Steady-state saturated water flow and unit-gradient unsaturated water flow experiments were conducted in Mie Andisol. To achieve saturated conditions, the Andisol was packed in the column with a bulk density of 0.85 g/cm³ and afterward it was saturated by applying water from column bottom. A glass filter was located at the bottom of the column. CaCl₂ solutions were applied from the top of the column at fixed rates using a peristaltic pump, and outflows from the bottom were measured by a scale. The flow rates were decreased stepwise from fast (around 350 cm/day) to slow rates (around 5 cm/day). Using faster flow steps, steady state saturated water flows were developed. Steady state conditions for unit-gradient - unsaturated water flow were developed by controlling suction at the column bottom, in which water contents were uniform and water flowed by gravity. At each flow steps, heat pulse measurements were conducted, and the influent solution concentrations were changed to obtain breakthrough curves (BTCs) by measuring soil electrical conductivities with four-probe salinity sensors. Water fluxes were estimated by applying an analytical solution to temperature rise data. Dispersivities were determined by applying the convection-dispersion equation to BTCs. Each experiment, including packing soil and water flow testing, were repeated a few times.

In saturated conditions, water fluxes estimated by the heat pulse probe agreed well with independently measured water fluxes in one experiment and underestimations were found in two cases. For unsaturated conditions, estimated water fluxes agreed well with actual fluxes even in the experiment with disagreement in saturated conditions. The flux estimation errors were compared with dispersivities which can be interpreted as the scale of water flow spreading from mean displacement position. Large estimation errors were found for experiments with large dispersivities ($\lambda > 1.5$ cm), while errors were relatively small for conditions with smaller dispersivities both in saturated and unsaturated water flows. Generally, dispersivity values in aggregated Andisol is larger in saturated condition than in unsaturated condition. The experimental results in this study indicates that the applicability of heat pulse probe to aggregated soils potentially results in better water flux estimation in unsaturated conditions.

Keywords: soil water flux, heat pulse probe, Andisol, dispersivity

Geostatistical Interpolation of Thermal Properties of Boring Core Samples

MUTO, Hirou^{1*} ; SAITO, Hirotaka¹

¹Tokyo University of Agriculture and Technology, ²CREST, JST

Ground source heat pump systems (GSHP) that use ground or groundwater as a heat source can achieve much higher coefficient of performance (COP) than conventional air source heat pump systems. Although use of GSHP systems has been rapidly increasing worldwide, environmental impacts by GSHP systems have not been fully investigated. To rigorously assess GSHP impact on the subsurface environment, instead of relying on "effective" properties, ground thermal properties including thermal conductivity and heat capacity need to be accurately characterized.

A geostatistical least-square interpolation method, known as kriging, has been used to characterize the spatial distribution of soil (or ground) physical (both hydrological and thermal) properties in one, two, and three dimensional domains. Kriging can estimate not only the values of an attribute at un-sampled locations accounting for spatial correlations between variables but also their uncertainties in terms of an error variance. Ordinary kriging (OK) which estimates unknown value as a linear combination of neighboring observations is one of the most commonly used kriging estimators. A secondary variable which is spatially cross-correlated with the primary variable can be used to reduce the estimation variance for the primary variable. Such method is known as cokriging. Ordinary cokriging (OCK) is one of the most commonly used cokriging estimator. The objective of this study was to compare OK and OCK in terms of estimating soil thermal properties along 50-m boreholes through the cross validation. Water content and sand content, which are relatively easy to measure, were used as the secondary attributes in cokriging.

In this study, undisturbed boring core samples were collected from two 50-m long boreholes at the campus of Tokyo University of Agriculture and Technology in Tokyo. Volumetric heat capacity (HC), thermal conductivity (TC), gravimetric water content (WC) and volumetric sand content (SC) were measured every 10-20 cm along the cores. The impact of sampling intensity on prediction errors were investigated by drawing random subsets of increasing size and using them to predict thermal properties at the remaining locations (jackknife approach). Then, subsets of N data were selected randomly or randomly per 10-m depth from the entire data set. For both sampling approaches, 50 different random subsets were selected to account for sampling fluctuations. Thermal properties at the remaining locations were then predicted.

This study showed that increasing the size of the subset leads to smaller mean absolute error. It was also found that kriging with random subsets per every 10-m depth yields lower mean absolute error than that with random subsets. Prediction errors by OCK were smaller than those by OK when the sampling intensity was the same.

Keywords: thermal conductivity, kriging, cokriging, sampling intensity, prediction error

Evaluation of Tangential Model Parameters with Respect to Various Soil Types

THIAM, Magatt^{1*} ; KOHGO, Yuji² ; SAITO, Hirotaka³

¹PhD Student, United Graduate School of Agriculture, Tokyo University of Agriculture and Technology, ²IEAS, Graduate School of Agriculture, Tokyo University of Agriculture and Technology, ³Department of Ecoregion Science, Tokyo University of Agriculture and Technology

Usage of Tangential model (Kohgo, 1995) for Soil Water Retention Curves (SWRCs) fitting requires knowing its parameters which are the numerical values of the coordinates of 3 tree points that are selected on the SWRC obtained from an experiment. Performing such an operation might be time consuming and may also lead to errors in the parameter estimation. This study aims to estimate these parameters and investigate possible relations between the parameters and some basic soil properties. SWRCs data and their corresponding hydraulic and physical properties were taken from the Unsaturated Soil Hydraulic Properties Database (UNSODA). The selected data consisted of 458 soils; among them: sand, sandy loams, loamy sands, sandy clay loams, silty loams, silty clay loams and silty clays. These SWRCs were fitted to Tangential model using nonlinear regression analysis with solver, the in-built Microsoft Excel tool. The iteration procedure, in solver, was the Generalized Reduced Gradient method. Results showed that the model performed well. The sum of the squared residuals (SSR) varied between 0.00011 and 0.2114 for sand and sandy soils, while it ranged between 0.021 and 0.00017 for all the others. Highest SSR values were noted with coarse sandy soils while the lower SSR values were noted with materials of finer structure. This suggests that this model is more adapted to fine structured soils. An attempt is being made in order to predict the Tangential model parameters, through multiple linear regression analysis, by using the soil bulk density values, saturated volumetric water content and the soil grain size distribution data.

Keywords: soil water retention curves, simulation, UNSODA, parametric model, fitting

Quantification of soil pollution concentration of plating metals by bioassay using luminous bacteria

SUGITA, Hajime^{1*} ; KOMAI, Takeshi² ; HARA, Junko¹ ; IMOTO, Yukari¹ ; ZHANG, Ming¹

¹National Institute of Advanced Industrial Science and Technology (AIST), ²Tohoku University

Cd, Cr(6+), Pb, As and CN are substances which closely related to metal plating. These are regulated as Class II Specified Chemical Substances by Soil Contamination Countermeasures Act. However, many other plating metals have not been subject to this law. Some heavy metals, which are used as plating metals, may be harmful to the human body if taken in excess. They must be also assessed risk in the same way as a Class II Specified Chemical Substances.

On the other hand, there is a bioassay using luminous bacteria as one of the acute toxicity evaluation test on hazardous substances. Since there is normally correlation between the concentration of hazardous substances and the intensity of the acute toxicity, it may be possible to estimate the concentration of harmful substances from the intensity of the acute toxic effects.

Focusing on Fe, Ni, Cu, Zn, Ag and Sn which are widely used as common plating metals, in this study, systematic bioassay tests using luminous bacteria (*Vibrio fischeri*) were performed. Based on the data obtained in the experiments, quantification of the correlation between the concentration of the plating metals and the intensity of the acute toxicity was attempted.

Keywords: Soil contamination, Plating metal, Bioassay, Luminous bacteria, Quantification

Effects of in-situ, long-term thermal loading on groundwater quality in marine sediments of Arakawa Lowland, Japan

SAITO, Takeshi^{1*} ; UEKI, Takashi¹ ; HAMAMOTO, Shoichiro² ; MOLDRUP, Per³ ; OHKUBO, Satoshi¹ ; KAWAMOTO, Ken¹ ; KOMATSU, Toshiko¹

¹Saitama University / CREST, JST, ²The University of Tokyo / CREST, JST, ³Aalborg University / CREST, JST

Subsurface temperature increase ("subsurface warming") has been documented below many large cities worldwide. The observed subsurface temperature increase has shown close relations with surface warming effects due to global warming and urbanization. Recently, ground source heat pump (GSHP) systems have become popular as a renewable energy technology for space cooling and heating. Operation of GSHP systems for space cooling discharges waste heat into the subsurface environment and, thus, induces additional subsurface temperature increase. However, any potentially negative impacts of GSHP-induced temperature increase on the subsurface environment have not been studied in detail. The objective of this study was therefore to investigate the effects of in-situ, long-term thermal loading on groundwater quality.

A GSHP system was installed in a 50-m deep borehole with a corresponding 50-m long U-tube heat exchanger at the campus of Saitama University in the Arakawa Lowland, Japan. Four groundwater monitoring wells were installed in a marine sand sediment aquifer (around 17-m depth) at 1-m (W1), 2-m (W2), 5-m (W5), and 10-m (W10) distance from the U-tube. At each monitoring well, temperature detectors were placed in 10 depths at approximately 5-m interval, and the subsurface temperature was monitored before and during thermal loading. For the thermal loading, approximately 40 °C water was circulated inside the U-tube heat exchanger for 13 months, and groundwater was frequently sampled from all four monitoring wells every 1 to 2 weeks. A wide spectrum of chemical properties (including pH, EC, DO, ORP "oxidation-reduction potential", dissolved gases, dissolved organic carbon, inorganic ions, and trace elements) were measured to characterize groundwater quality.

The subsurface temperature at the nearest monitoring well (W1) increased gradually with approximately 8 °C from 17 °C (baseline) to 25 °C during 13 months of thermal loading. In contrast, at the farthest monitoring well (W10), there was no significant change in subsurface temperature, and W10 was therefore selected as a reference (non-temperature affected) monitoring well. A number of chemical components in the groundwater, including boron and potassium, increased markedly at W1 compared to W10. Since marine sediments typically contain high concentrations of chemical components including boron and potassium, the observed increase in groundwater concentration is likely due to thermally-induced dissolution and/or desorption from the marine sediment. The possible mechanisms behind the observed concentration increases will be discussed.

Keywords: subsurface temperature, thermal pollution, long-term thermal loading, GSHP, marine sediment, groundwater quality

Characterization of water repellency parameters in soil water repellency characteristic curves for JP and NZ soils

WIJewardana, Senani^{1*}; Kawamoto, Ken¹; Muller, Karin²; Clothier, Brent³; Hiradate, Syuntaro⁴; Komatsu, Toshiko¹; Moldrup, Per⁵

¹Graduate School of Science and Engineering, Saitama University, Japan, ²Plant & Food Research Institute, Ruakura Research Centre, New Zealand, ³Plant & Food Research Institute, Palmerston North, New Zealand, ⁴Biodiversity Division, National Institute for Agro-Environmental Sciences (NIAES) Japan, ⁵Department of Civil Engineering, Aalborg University, Denmark

Soil water repellency (SWR) is the phenomenon where soil does not wet when water is applied to its surface. Characterization of water repellency in natural soil is very important to understand the soil hydrological processes, surface flow and infiltration rates. Objectives of this study were (i) to characterize SWR using molarity of ethanol droplet (MED) test, sessile drop method (SDM) and water drop penetration time (WDPT) test, and (ii) to identify the relationships between the determined SWR parameters and soil organic carbon (SOC) contents. Soil samples were collected from different soil depths of representative Andosols and Cambisols in Japan (Nishigo, Hiruzen and Nikko; all sites under forest) and New Zealand (Ngahinapouri, Wahihora and Whatawhata; all sites under pasture). The soil-water contact angle was directly measured using SDM, and indirectly derived from MED and WDPT measurements. All the A horizons of the Japanese soils showed water repellency, and the New Zealand soils were also water repellent at all depths except the Ngahinapouri, B horizon. Then, soil water repellency characteristic curves (SWRCCs) were obtained for water repellent (WR) soils, i.e., soil-water contact angle / degree of WR as a function of the volumetric water content (θ). Three WR parameters were determined from the SWRCCs. They are (i) the integrated areas below a SWRCC, $S_{WR}(\theta)$, (ii) the soil water content at maximum (θ_{WR-Max}) and (iii) minimum (θ_{WR-Min}) WR. Further, WR parameters were studied with soil organic carbon (SOC) contents. These relationships were agreed well with recently published work of Kawamoto *et al.* (2007) and Karunarathna *et al.* (2010). The SOC contents of New Zealand soils varied between 1.4% (WR) to 12.1% (WR), for the Japanese soils they ranged between 2.6% (Non-WR) and 26.3% (WR). Although the Japanese soils had high SOC contents in >10 cm depths, they were not WR (for Nikko >5 cm depth-Not WR). Therefore, further studies are needed to assess SWR as affected by SOC.

Keywords: soil water repellency characteristic curve, water repellency parameters, soil organic carbon

A result of Cs redistribution in a forest soil after FNP-I accident.

NISHIMURA, Taku^{1*}

¹The University of Tokyo

Cesium is a large atom which does not likely to hydrate. Similar to potassium and ammonium cation it prefers to site at siloxane ditrigonal cavity of silica sheet of phyllosilicates. Cesium is strongly, almost irreversibly, captured at frayed edge site of layered clay particles. These facts may make partition coefficient of cesium to be very large. The large partition coefficient may produce larger retardation of cesium transport with percolating water. At the same time large partition coefficient may cause enhance in migration of Cs with moving colloids. A comparison of Cs content distribution of near surface soil of between cleared forestry and a forestry with 5cm litter layer in Iitate village, Fukushima suggested organic colloids could be a transporter of Cs at litter covered forest. Soil total carbon content as well as C/N ratio had relation with soil Cs content. A depth where soil had higher organic carbon and lower C/N ratio tended to show high Cs content.

Keywords: Cs, forest, soil organic matter, colloids

Observation of Pore Structure for Differently Compacted Landfill Final Cover Soils Using Microfocus X-ray CT

BANIYA, Arjun^{1*} ; KOIKE, Takuya¹ ; WATANABE, Kai² ; HAMAMOTO, Shoichiro³ ; KAWAMOTO, Ken¹

¹Graduate School of Science and Engineering, Saitama University, Japan, ²Department of Civil and Environmental Engineering Saitama University, Japan, ³Graduate School of Agricultural and life Sciences, University of Tokyo, Japan, ⁴Institute of Environmental Science and Technology, Saitama university, Japan

The final cover soil on a solid waste landfill consists of many layers of materials and is highly compacted. It is used to prevent rain/surface water infiltration in to the waste layer. On the otherhand, the landfill site has a significant emission source of greenhouse gases. Gas and mass transport in soils occurs through the soil pore network, which is highly affected by soil physical properties including compaction, particle size, moisture content and total porosity. However, there are a limited number of studies on visualization and quantification of soil pore network for highly compacted soil like final cover soil. The objectives of this study were setting of microfocus X-ray Computed tomography (CT) for scanning landfill final cover soils in conjunction with 3-D image analysis techniques and analyzing the soil pore structure parameters. In this study, soil samples were collected from landfill site in Saitama prefecture, Japan. Soil pore structure was analyzed using micro focus X-ray CT (Shimadzu inspeXio SMX-90CT, Shimadzu Corporation) for air dried final cover soil samples of particle size ($d \leq 2\text{mm}$) with different dry densities 1.4, 1.55 and 1.65 g cm^{-3} by a hand compaction. The tested soil texture was silty sand. The scanned images were taken by the micro focus X-ray CT. Then, by the use of software VGStudio MAX, they were reconstructed in 3-D images. Finally, using software of EXFact analysis they were analyzed to obtain pore structure parameters such as pore size distribution, coordination number, specific area and pore-network tortuosity. For determining suitable scanned images for soil pore structure and network, several scanning conditions for the microfocus X-ray CT have been tested i.e. different combinations of voxel size (10, 30 and $50 \mu\text{m}$), scan number, view number, field of view(FOV), region of interest(ROI), and percent of interior pore for pore structure analysis. Base on the results from the tested conditions, we will propose a suitable condition on the microfocus X-ray CT scanning for macropore network (typically, effective pore diameter $>100 \mu\text{m}$) in differently compacted final cover soils.

Keywords: Microfocus X-ray Computed Tomography (CT), Pore network and structure, Final cover soil

Consolidation characteristics of landfilling waste samples in Japan: Effects of waste compositions and various mixing pr

IQBAL, Muhammad rashid^{1*} ; OOHATA, Hiroyuki¹

¹Graduate School of Science and Engineering, Saitama University, Japan, ²Graduate School of Agricultural and Life Sciences, the University of Tokyo, Japan, ³Institute for Environmental Science and Technology, Saitama University, Japan, ⁴Center for Material Cycles and Waste Management Research, NIES, Japan

Solid waste materials are highly heterogeneous depending on various waste compositions, making it difficult to understand their consolidation characteristics. The purpose of study is to find out effects of waste compositions and mixing proportions on the consolidation characteristics of compacted solid waste materials. In this study, totally 6 different waste materials, un-burnable domestic waste, un-burnable industrial waste, incineration ash, crushed concrete, organic sludge and inorganic sludge, were used as tested materials.

By using the standard proctor test, compaction curves and maximum dry bulk densities were determined for each sample. Compaction results showed that maximum dry bulk densities of the Incineration ash (1.65 g/cm³) and crushed concrete (1.45g/cm³) were higher than the inorganic sludge (0.90 g/cm³) and organic sludge (0.742 g/cm³) respectively. The maximum dry bulk densities for mixed sample of inorganic sludge, concrete and incineration ash were larger than each independent waste sample. In especial, the maximum dry bulk density for the mixed sample with ratio 1:1:1 (dry mass basis) was 1.48 times larger than that for inorganic sludge.

Consolidation tests were carried out for selected pre-compacted waste samples with degree of compaction higher than 90 % after the compaction tests. For the consolidation tests, oedometer test apparatus which dimension of 10 cm diameter and 10 cm height was used for the waste materials with particle size larger than 2mm. Results of each independent sample showed that the coefficient of consolidation (C_v) for crushed concrete and incineration ash was higher than organic and inorganic sludge wastes while compressibility of un-burnable industrial waste was higher than the other materials due to a presence of compressible material. As the mixing ratio of crushed concrete in the mixed samples increased, the compression index (C_c) decreased. When the inorganic sludge and crushed concrete are mixed with the ratio 1:3, the C_c value of the mixed sample decreased up to 75% as compared to the one for only inorganic sludge. In addition, by mixing the inorganic sludge with the crushed concrete, the C_v values for mixed samples increased in the order of 10¹~10². Effect of mixed proportion of the various wastes on consolidation parameters will be further investigated.

Keywords: Compaction, Consolidation, Sludge, landfill

Remediation of a Tsunami affected saline and sodic soil by calcium carbonate and rice straw

ISHIBASHI, Sakuya^{1*}; NISHIMURA, Taku¹; HAMAMOTO, Shoichiro¹; IMOTO, Hiromi¹

¹Graduate School of Agricultural and Life Sciences, The University of Tokyo

Japanese government recommends leaching of soluble salts as well as adding calcium amendments for remediating saline and sodic soil after Tsunami by the earthquake on March 11, 2011,. Application of calcium carbonate (CaCO_3) is recommended for soils having pH lower than 6 and calcium sulfate (CaSO_4) is that for pH higher than 6. However, since CaCO_3 has low solubility to water, it has not been often used in reclamation of sodic soils (Shainberg et al, 1989).

Solubility of CaCO_3 is controlled by CO_2 - H_2O - CaCO_3 equilibrium in water. The concentration of calcium ion in CaCO_3 solution is affected by CO_2 concentration (partial pressure) of air phase. The higher partial pressure of CO_2 causes the higher concentration of Ca^{2+} . In general, addition of organic matter may enhance soil respiration and increase partial pressure of CO_2 in soil. This might potentially enhance solubility of CaCO_3 and increase Ca^{2+} concentration in soil solution.

Increase in Ca^{2+} concentration in soil decreases exchangeable sodium percentage (ESP) of the soil. Lower ESP may inhibit soil dispersion and help to keep aggregation. Stability of aggregates has a role on soil permeability, and it affects efficiency of leaching practice.

Objective of this study was to investigate the effect of changes in partial pressure of CO_2 by organic matter decomposition on dissolution of CaCO_3 , and subsequent Na^+ - Ca^{2+} ion exchange of a Tsunami affected soil.

Soil was collected at a former paddy field at Terashima, Miyagi, Japan, where was damaged by Tsunami at the Great East Japan Earthquake. EC (1:5) of the soil was 5.2dS m^{-1} . The soil was mixed with rice straw and/or CaCO_3 , and then packed into plastic columns of an inner diameter of 8.5cm and 20cm-high with the bulk density of 0.95g cm^{-3} . Amount of rice straw and CaCO_3 application was 10t ha^{-1} and 1t ha^{-1} , respectively. The soil columns were incubated for 23 days. During the incubation, 18mm of water was supplied for each three days. The temperature inside and around the columns, and soil water pressure were continuously monitored. The CO_2 concentration in soil air phase was measured at 5-days interval.

After the incubation, the columns were leached by 4 pore volumes of 4mmol L^{-1} KCl solution with. The leachate was collected for further analysis of EC, pH and concentration of cations. After the leaching, the soil columns were separated to 3cm thick layers. Each 3cm thick soil sample was used to measure EC, pH, soluble cations, and exchangeable cations of the soil.

In average, soil CO_2 concentration inside the column was high under the rice straw treatment regardless of CaCO_3 application. The CO_2 concentration rose at the periodical water application, and gradually decreased with time. Rise in CO_2 concentration could be due to the enhanced organic matter decomposition and the restricted CO_2 diffusion by higher soil water content following the water application.

Exchangeable cations of the column soil were measured after the leaching. Exchangeable Ca^{2+} slightly increased at whole layer of the four treatment. Increase in exchangeable K^+ coincided with decrease in exchangeable Na^+ , suggesting ion exchange between Na^+ and K^+ was a dominant reaction during the leaching.

In this experiment, the effect of organic matter and CaCO_3 application on remediation of the Tsunami affected saline and sodic soil was not clear. With fluctuating soil water content, soil CO_2 concentration was not always high during the column incubation experiment. It is expected that depression of soil CO_2 concentration with decrease in soil moisture after water application could not enhance dissolution of applied CaCO_3 .

Keywords: Tsunami affected soil, saline and sodic soil, rice straw, calcium carbonate

Enhancing Radioactive Fallout Removal from the Surface Soils by using artificial macropore transport system

SATO, Naoki^{1*} ; MIYAMOTO, Tamami² ; MORI, Yasushi¹ ; INAO, Eiko³ ; NOBORIO, Kousuke⁴

¹Faculty of Environmental Science and Technology,Okayama University, ²Graduate School of Environmental and Life Science,Okayama University, ³Miyagi Prefectural Institute of Agriculture and Horticulture, ⁴Faculty of Agriculture,Meiji University

Fukushima nuclear power plant damaged by the East Japan Great Earthquake caused radioactive fallout around the Tohokuregion. Because radioactive fallout was positively charged,it was reported to be absorbed to soil surface. Surface soil scraper and deep plowing would be,therefore effective for the removal of radioactive materials. However,these techniques were available for flat and wide area like school yard or farm land.

in many orchards,fruit absorbed radioactive Cesium, which indicated radioactive fallout did not immediately absorb to soil surface but stayed as exchangeable ion for a while and was absorbed by plant root. therefore the technique for sloped land is also needed for better management for radioactive fallout.

we applied artificial macropores to effectively remove radioactive fallout from the surface soil. artificial macropore filled with bamboo fiber was made in soil(Field:d=1 length=50cm,Lab:d=0.6cm,length=20cm). Zeolite was placed at the bottom of the macropores(Field:50cm,Lab:20cm)to absorb transported Cesium.Four treatments were prepared for field experiments,such as macropore with ammonium sulfate,no macropore and no macropore with ammonium sulfate. In the lab experiments, Potassium was used for safety reason and a 400mm artificial rainfall was applied for one month. Results showed artificial macropore effectively transported radioactive Cesium/Potassium to deeper profile. In the lab experiment, artificial ,macropore successfully delivered Potassium to deeper profile while no radioactive Cesium was observed from the drainage water.

Keywords: Macropore, Degraded Soils, Radioactive Substance

A Design of Artificial Macropore for Improving Infiltration Process in Degraded Soils

SAKIKAWA, Kazuki^{1*} ; MORI, Yasushi¹ ; SUETSUGU, Atsushi¹

¹Okayama university

Soil is largest carbon storage body in all terrestrial medium such as vegetation and the atmosphere. However, these days, soils could not show its function as water storage layer or culture medium for plant, because of climate change or rough management. In this study, artificial macropores are introduced in soils for purposing enhancing infiltration without cultivation. Fibrous material was inserted so that it reinforced the macropore structure. Moreover, capillary force caused by fibers drag the surface water into the deeper soil prior to saturation. Capillary force caused by fabric introduced vertical transport, while micropore(matrix) enhanced horizontal flow. It makes it possible effective infiltration than empty macropores. In the experiment, an ideal design of artificial macropore was searched. The density of fibrous material was altered as 0.2 0.3 0.5 g/100cm³-soil. Artificial rainfall of 2 (weak rain) and 20 (stormy rain) mm h⁻¹ were applied on the soil column (D=5cm, H=30cm). Results showed that retention curve has gradually changed as we changed the density of fibrous material. Thus, the capillary force was effectively created according to the densities surface water was effectively collected by dense artificial macropore when weak rainfall was applied, while stormy rain was effectively drained by light artificial macropore.

Keywords: macropore, soil degradation

Artificial Macropore installation effect on organic matter storage at a degraded land.

MORIWAKE, Shuichi^{1*} ; MORI, Yasushi¹ ; SUETSUGU, Atsushi¹

¹Okayama University

At ill-drained lands, heavy rain would cause erosion which enhances degradation process much faster. According to our previous study, artificial macropore successfully enhanced vertical infiltration and increased organic matter contents. However, there was a concern that infiltrated fresh soil water transported nutrient and oxygen at the same time, resulting decomposition of the organic matter.

In this experiment, we prepared sandy soil column (D=50mm, H=300mm) with Cellulose, for which artificial rainfall of 210mL with nutrients (N, P, K) were applied on the surface soils. Then columns were placed at 30 °C constant temperature room to enhance organic matter decomposition. In order to observe structural difference for carbon storage, three treatments were prepared such as, cultivation, artificial macropore and control, respectively.

Results showed that evaporation was significant for cultivation column, which meant traditional agricultural practice had disadvantage for conservation of soil water conservation. On the other hand, artificial macropore column showed similar evaporation rate for control column in spite of their well-drained structure. Affected by water content, vertical profiles for carbon contents were different for three treatments. Standard deviations for vertical profiles were small for control column, and larger for macropore column and cultivation column.

Keywords: Artificial Macropore, degraded land

Modelling of Critical Loads for Heavy Metals in Terrestrial Ecosystem in Slovenia

SVETINA VEDER, Marta^{1*}

¹RCE, marta.svetina@rce.si

In Slovenia a modelling application of As, Cd, Co, Cr, Cu, Hg, Mo, Ni, Pb and Zn critical loads in soil were performed. The calculation in the Salek Valley involved 30 research areas in the town Velenje area on a 500 x 500 m grid, where the chemical analyses of precipitation and soil were made.

The aim was application of theoretical models for determination the maximum critical levels of heavy metals in terrestrial ecosystem with empirical data. The basis for calculation was an effect-based approach, which limits are based on adverse effects on the ecosystem and the heavy metal concentrations should stay below those limits. As receptor was used a human health through the eco toxicological risks with use of ground water for drinking water and/or consume crops that are grown on the soil. The simple model based on dynamic mass balance of heavy metals in soil was used for calculation. It was estimated that the critical time well illustrates the acute danger of soil pollution and is recommended as the draft estimation of actual condition in soil which could be valued with few data.

Two different soil conditions at the actual atmospheric input were used in calculation: unpleasant and average. The unpleasant condition was simulated for the surface soil to depth of 5 cm, and the advanced to soil depth of 20 cm and density of 1.500 kg/m³. The critical time for both conditions is calculated for As, Cd, Co, Cr, Cu, Hg, Mo, Ni, Pb, Zn. The comparison between heavy metals indicates high accumulation of As and Hg, and thus their quit fast approach to the critical loads. In second rang of atmospheric input are Cd, Pb and Zn which are accumulated much slowly, followed by Mo, Ni, and Co, and the slowest progress make Cr. The estimated periods to reach the permitted Slovene limits in surface soil are calculated for As, Hg 100, Cd 140, Pb 230, Zn 350, Cu 830, Mo 1.700, Ni 1.800, Co 1.900, and for Cr 6.000 years.

Keywords: heavy metals, soil, contamination, modelling

Predicting soil moisture in arable land under climate change with soil-profile physical properties database

KATO, Chihiro^{1*} ; NISHIMURA, Taku²

¹Faculty of Agriculture and Life Science, Hirosaki University, ²Graduate school of Agricultural and Life Sciences, the University of Tokyo

Soil is foundation of agriculture and ecosystems. Soil physical condition such as soil moisture and temperature directly and indirectly affects yields and quality of crop production. Therefore predicting soil moisture of arable lands under climate change is important and valuable for yield prediction and adaptation under climate change. For predicting soil moisture condition of agricultural lands in arbitrary areas, use of soil database and datasets of General Circulation Model (GCM) projections should be useful since physical properties of soils and meteorological condition vary with location. Most of available GCM projections have spatial and temporal resolution of 100 km and a month. However, using GCM projections as input data for soil moisture and temperature prediction, temporal and spatial scale of the input data is favorable to be small since effective surface soil layer of agricultural production is generally shallow. In this study we investigated possibility of predicting soil moisture of arable lands in arbitrary areas with local-scale (approximately 20km×20km) daily GCM projection dataset “ ELPIS-JP ” (Iizumi et al., 2012) and the agricultural soil-profile physical properties database, Japan, “ Solphy ” (Eguchi et al., 2010).

In this study, soybean fields of Yoshioka and Ookubo, which are located in neighbors (approximately 2 ~ 3km), in Toyama city were chosen as experimental sites and scenario studies were done for predicting soil moisture condition with HYDRUS model (Simunek et al., 2008) under climate change in the future (2071 ~ 2090). Soil physical properties of each site were determined with water retention data in the SolphyJ database by using RETC program (Yates et al., 1992). Before the scenario studies, validation of HYDRUS model and soil physical properties which are obtained with SolphyJ database was conducted by comparing observed and simulated soil moisture of the Yoshioka field. The projection of MIROC-hires 3.2 A1B scenario was chosen among 26 (10 GCMs × 3 Special Report of Emission Scenario) ELPIS-JP scenario datasets. For preparing input data for numerical simulation of soil water movement, daily ELPIS-JP datasets were temporally downscaled to hourly or minutes scale by using weather generator “ CLIGEN ” (Nicks et al., 1995)

Simulated results suggested that the duration of excess soil moisture condition following heavy rainfall events are more likely at Ookubo than Yoshioka even though they are located in neighbors and have similar soil textures. Increase in surface runoff fluxes is possible to be larger in Ookubo than in Yoshioka as well. These results imply that even in a small watershed it is important to consider soil spatial distribution in predicting effects of climate change on agricultural production. Also, combination of temporally downscaled GCM projection dataset and agricultural soil-profile physical properties database may be useful for predicting soil moisture in arbitrary areas.

References: Eguchi et al., 2011, Proceedings of Annual Meeting of JSDIRE, 302-303; Iizumi et al., 2012, Phil. Trans. R. Soc. A, 370, 1121-1139; Nicks et al., 1995, NSERL Report #10, pp.2.1-2.22.; Simunek et al., 2008, Vadose Zone J. 7, 587-600; Yates et al., 1992, Soil Sci. Soc. Am. J, 56, 347-354

Keywords: Climate change, Soil moisture, Numerical simulation, SolphyJ, ELPIS-JP

A Case Study of Combining Geophysics Prospecting Techniques to a Soil Contaminated Site

WANG, Tzu-pin^{1*} ; CHEN, Chien-chih¹ ; DONG, Tien-hsing⁴ ; CHEN, Yi-chieh³ ; LIU, Hsin-chang² ; LIN, Chih-ping⁵ ; HUNG, Hao-chun⁶ ; HO, Ching-jen⁶

¹Dep. of Earth Sciences and Graduate Institute of Geophysics, National Central University, Taiwan, ²Disaster Reduction Research Center, Chien Hsin University of Science and Technology, Taiwan, ³Geophysical Technology and Engineering Co.,Ltd. R.O.C, ⁴Apollo Technology Co.,Ltd. R.O.C., ⁵D.P.W.E. National Chiao Tung University, Taiwan, ⁶Environmental Protection Administration, Taiwan

This study utilizes a combination methods of Electrical Resistivity Tomography (ERT), Ground Penetrating Radar (GPR), and Horizontal Loop Electromagnetic (HLEM) to examine a heavy-metal contaminated site before and after the remediation. It was a processed sludge tacking site of a smelting plant. The sludge is homogeneous red, and the main pollutants are chromium, arsenic and lead. The plant has been closed for more than twenty years. At the time when it was shut down, instead of removing the stacked sludge and underground structures (tank), the site was leveled directly and planted with lawns. Now, it is difficult to know the distribution of the sludge, the depth of its cover, and the correct location of the underground structures.

The pre-remediation investigation conducted with the application of geophysical prospecting techniques found that the HLEM could efficiently define the distribution of sludge efficiently, and ERT could be used to detect the thickness of the sludge and the location of the underground structures, but GPR results failed to meet expectations which may due to a significant attenuation of electromagnetic energy caused by the nature of the sludge. The post-remediation examination shows obvious different morphologies of the site than it was before the remediation. The results can be used to assess the effectiveness of remediation, and to check if any sludge remains.

Keywords: ERT, GPR, EM, pollution

Cs migration to rice crop from soil after stripping the contaminated top soil at Iitate Village in Fukushima Prefecture.

NISHIWAKI, Junko^{1*} ; ASAGI, Naomi¹ ; KOMATSUZAKI, Masakazu¹ ; MIZOGUCHI, Masaru² ; NOBORIO, Kosuke³

¹College of Agriculture, Ibaraki University, ²Graduate school of Agricultural and Life Sciences, The University of Tokyo, ³School of Agriculture, Meiji University

Iitate Village is at about 40 km northwest from a Fukushima Daiichi nuclear power plant. An agricultural fertile layer in agricultural fields was contaminated by radionuclides, e.g., 134-Cs, 137-Cs, and 90-Sr, just after the accident of the Fukushima Daiichi Nuclear Power Plant in 2011. The decontamination work is an important subject for villagers to return to a village and live there again. Three decontamination methods are proposed by a Ministry of Agriculture, Forestry and Fisheries. They are 1) Stripping the top soil off, 2) Removal of fine particles after soil and water mixing, and 3) Tillage reversal. By the report of the Ministry of Agriculture, Forestry, and Fishery, 90% of radioactive contaminant has been removed by the method of stripping the contaminated top soil off. In this time, we examine the Cs migration to rice crop from soil after stripping the contaminated top soil off.

We used ~4*20 m paddy field at Iitate Village in Fukushima Prefecture. At first we decontaminated the site using the method of stripping 5 cm top soil off. After that potassium chloride (KCl) was put in all area as basal fertilizer on June 8, 2013. We compared the area and made three kinds of treatments such as (1) mixed with rice straw that was harvested last year here, (2) only decontaminated, and (3) mixed with farmyard manure, and transplanted rice crop (rice cultivar is hitomebore) on June 9, 2013. We had sampled top soils at three points from each plot twice a month and the 134-Cs, 137-Cs, and 40-K concentration in soils were analyzed using a Ge semiconductor detector. The concentration of 134-Cs, 137-Cs, and 40-K in rice crop was analyzed by a NaI scintillation counter after harvest.

As a result, 134-Cs is about half of 137-Cs. Since the half-life of 34-Cs is two years, it has become approximately a half. Changes of Cs and K concentrations in soil were not observed during a rice cultivation period. The concentrations of radionuclides in mixed rice crop were 572.93 ± 8.05 Bq/kg-dry / Cs-134, 1089.35 ± 11.41 Bq/kg-dry/ Cs-137, and 127.29 ± 27.59 Bq/kg-dry/ K-40. Although these values were comparatively high, soil did not show the high dose. The reason of that would be the volume of mixed rice straw was small and migration of caesium from the rice straw to the soil was hardly happened. The soil dose mixed with manure had been high through the whole cropping period. It might be the original manure dose was high, but the analysis of the manure has not completed yet. The concentration of radionuclides in rice crop below a detection limit of the NaI scintillation counter and it is below the regulation value defined in our country.

Keywords: stripping top soil off, rice crop, caesium

Nitrogen removal and effect of chemical oxygen demand on removal of nitrogen in Coir Fiber Biofilm Treatment System

DHARMARATHNE, Nirmala kumuduni^{1*} ; SATO, Naofumi³ ; KAWAMOTO, Ken¹ ; TAKAHIRO, Koide² ; SATO, Hiroyasu⁴ ; TANAKA, Norio¹

¹Graduate School of Science and Engineering, Saitama University, Japan, ²Institute of Environmental science and Technology, Saitama University, Japan, ³Kokusai Kogyo Co., Ltd, ⁴Graduate School of Frontier Sciences, University of Tokyo, Japan

Biological treatment is the most useful process to remove nitrogen from water and wastewater. In this process, ammonium is first oxidized to nitrate by aerobic autotrophic nitrifying microorganisms. Nitrate is then reduced to nitrogen gas by heterotrophic denitrifying bacteria under anoxic conditions. Oxygen and organic carbon must be supplied to act as electron acceptor in nitrification and electron donor in denitrification. This study has carried out microcosm experiments in the laboratory for evaluating wastewater treatment mechanism and efficiency in the Coir Fiber Biofilm Treatment System (COTS). Coconut fiber was used to encourage the development of contaminant-degrading biofilms. A string of coconut-fiber (0.2-m length) was used as a biofilm support media and experiments were carried out using synthetic wastewater. The string of coconut-fiber was put inside the treatment container (0.012-m³ volume) with two conditions: low fiber density (LFD; single string per a container) and high fiber density (HFD; two strings per a container). As a control condition, a blank container without a coconut-fiber string was also used in the experiment. The flow rate is about 870 cm³/day (two-weeks retention time)

The inflow ammonium nitrogen concentration was 500 mg/l- 640 mg/l and the average nitrate nitrogen concentration in influent was 5.9 mg/l- 6.5 mg/l (low nitrate nitrogen loading rate). Dissolved Oxygen (DO) value of the treatment tanks were range between 0-0.3 mg/l. DO concentration in LFD and HFD treatment tanks were slightly lower than the inflow and blank tank during the whole experimental period. The maximum ammonium nitrogen removal efficiency was recorded in the 14 days of startup. It was approximately 45% and 30% in HFD and LFD treatment tank respectively. After that, ammonium nitrogen removal efficiency shows the slightly decreasing trend over the time. The maximum nitrate nitrogen removal was observed for 70 days of operation. It was around 90% and 72% in HFD and LFD tank respectively. Over the duration of the experiment, very low concentrations of Nitrite Nitrogen were observed and it was below 1 mg/l. low nitrite nitrogen is evident that the oxygen limited anaerobic nitrification-denitrification process leads to removal of ammonium nitrogen in this system. This process involves two-step as partial nitrification and Anammox. One of the most critical parameters of the nitrification process is the influent chemical oxygen demand (COD), because it directly influences the growth competition between autotrophic and heterotrophic microorganism population. The average inflow COD concentration in influent was 18300 mg/l- 19800 mg/l. Ammonium nitrogen removal efficiency decreased with the increasing of COD removal efficiency in both LFD and HFD treatment tanks. So there is a negative relationship between organic carbon concentration and biological ammonia removal. High organic loading can result in decreased nitrification due to faster growing heterotrophic bacteria dominating the surface of the biofilm, and leads to oxygen limitations for the nitrifying bacteria growing deeper inside the biofilm. As considering the results obtained from the microcosm system it can be conclude that partial nitrification and the subsequent anaerobic ammonium oxidation (Anammox) are the major process associated with the removal of ammonium nitrogen. This process is a shortcut biological nitrogen removal without increasing nitrite and nitrate concentration in the system. At the same time treatment tank with HFD always tend to eliminate significant amount of ammonium nitrogen than the LFD tank. Difference between results in HFD and LFD treatment tank indicating that surface provided for growth of biofilms is a major factor for improving biodegradation rates. COTS has effect on remove nitrate nitrogen effectively at low nitrate loading rate from the wastewater.

Keywords: Coir Fiber, Biofilm, Nitrogen removal, Chemical Oxygen Demand

Estimation of water film thickness in geological media based on electric double layer interactions

NISHIYAMA, Naoki^{1*} ; YOKOYAMA, Tadashi¹

¹Department of Earth and Space Science, Osaka University

Water film plays an important role in mineral-water interactions and mass transport in geological media under water-unsaturated conditions (Nishiyama and Yokoyama, 2013, *Geochim. Cosmochim. Acta*). To quantify such reactive-transport in water film, the understanding of the properties of water film is essential. Water film is retained on grain surfaces due to the action of electric double layer force associated with the compression of diffuse layers developed from mineral-water and water-air interfaces. In this study, we focused on the thickness of water film and developed a model to estimate the thickness taking into consideration the effect of ion concentration, pH, and electric double layers overlapping.

The surface charge density and electric potential at mineral-water and water-air interfaces depend on the amount of adsorption-desorption of proton and ions. When two diffuse layers developed from the opposite interfaces overlap, the concentration of ions in diffuse layers changes and consequently the adsorption-desorption reactions at the interfaces achieve a new equilibrium state. To take into account this process, we used a triple-layer model and a double-layer model to numerically solve the Poisson-Boltzmann equation describing the ion distribution in diffuse layer between the interfaces. We considered water film on quartz grains and calculated water film thickness as a function of pH and ion concentration. The results show that water film thickens with decreasing ion concentration and increasing pH. The model presented in this study allows film thickness to be estimated as a function of mineral type, ion concentration, and pH. Such model would be useful for considering the reactive-transport under unsaturated conditions including the geological storage of carbon dioxide and soil formation.

Keywords: water film, electric double layer, unsaturated zone

Coastline as triple boundary among atmosphere, ocean and earth

YAMANAKA, Manabu D.^{1*}

¹JAMSTEC/Kobe U

Coastline is the boundary between ocean and land (earth beyond the sea level), and the liquid-solid heat contrast there produces monsoon or sea-land breeze circulation responding revolution (annual) and rotation (diurnal) periodicity of solar heating. The coastline is also the intersection between ocean surface and bottom, and its location is determined by water budget and erosion-orogeny balance. Furthermore, the coastline is the most active ecological (and also anthropogenic) zone. Based on these geoscientific meanings of coastline, we discuss climatological characteristics of land-sea coexisting planet such as earth.

Keywords: atmosphere-ocean-land interaction, monsoon and local circulation interaction

Cold surge event observed by the research vessel Hakuho-maru over the Pacific in December 2012

OGINO, Shin-ya^{1*}; WU, Peiming¹; HATTORI, Miki¹; ENDO, Nobuhiko¹; KUBOTA, Hisayuki¹; INOUE, Tomoshige¹; MATSUMOTO, Jun¹

¹JAMSTEC, ²Graduate School of Science, Kobe University, ³Tokyo Metropolitan University

1. Introduction

A cold surge from the Siberian High is the typical phenomenon of the Asian winter-monsoon that sometimes reaches the southeast Asian regions, such as Philippines and the Indochina Peninsula, across the Pacific and resulted in heavy rainfall there. Air mass transformation is one of the key processes for this phenomenon. However, the quantitative evaluation based on the observation has not yet been done so far. We succeeded in observing a cold surge event by radiosondes from the research vessel over the Philippines Sea in the end of December 2012. The preliminary results are reported in this paper.

2. Observation and data

We conducted radiosonde observations on board the research vessel "Hakuho-maru" during December 21, 2012 and January 4, 2013. Figure 1 shows the observation points and the launch time of the radiosondes. We launched radiosondes with 6-hour or 12-hour intervals during 23 to 24 December between 21N and 29N along the cruise from north to south. At the southernmost point (21N, 133E), we further carried out the fixed-point observation of 3-hour intervals for about 1.5 days during 24 to 25 December.

3. Synoptic fields

The cold surge from the Siberian High was intensified during December 20 to 26. Northwesterly winds were intensified around Japan and the northeasterly was strengthened in the Pacific Ocean and the Philippine Sea. Convections were activated over the Philippines, and the precipitation also became strong in the coastal area. The cyclonic disturbance propagated westward near the equatorial region over the western Pacific. The easterly flow at the northern edge of the disturbance and the northeasterly by the cold surge formed convergence zone over the offshore of Philippines.

4. Results

Latitude-height section of potential temperature and water vapor mixing ratio obtained by the moving observation during 23 to 24 December revealed the cold air intrusion was observed in the lower layer from the surface to 2 km height. The stable layer was formed at the top of the cold air intrusion (about 2 km height). The temperature and humidity were higher in the southern area. Time-height section of potential temperature and water vapor mixing ratio obtained by the fixed-point observation during 24 to 25 December showed that the stable layer around 2 km height were gradually intensified and that below the stable layer both the potential temperature and the water vapor mixing ratio had the uniform vertical distributions, which is consistent with the well-mixed layer during the cold surge event. The transition to such a typical mixed-layer structure was captured by high temporal resolution observation.

With the help of the operational radiosonde data at Minami-daitojima and at Chichijima, we performed a thermodynamic energy budget analysis and evaluated the transfer of thermodynamic energy between the atmosphere and the ocean. The result indicates that the amount of the energy transfer from the ocean to the atmosphere was even large over the Pacific remote from the Eurasian continent and compares with the one that observed near-continent area over the East China Sea by the AMTEX project (Ninomiya, 1975, JMSJ). The effect of the energy transfer to the precipitation over the Philippine area will be discussed.

Acknowledgement

We would like to thank Dr. Hodaka Kawahata (The University of Tokyo), Mr. Katsura Kameo (The University of Tokyo), Mr. Ei Hatakeyama (Marine Works Japan LTD) and all the crews of Hakuho-maru for their great help with conducting the radiosonde observation on board the research vessel. We wish to express our gratitude in Drs. Kaoru Sato (The University of Tokyo), Naohiko Hirasawa and Yoshihiro Tomikawa (National Institute of Polar Research) for permitting us to use their launch

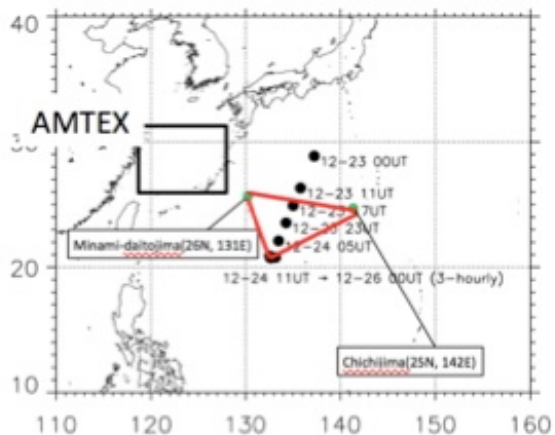
ACG04-02

Room:413

Time:May 1 14:40-14:55

device. Part of this study is supported by The Green Network of Excellence (GRENE) program of the Japanese Ministry of Education, Culture, Sports, Science and Technology.

Keywords: cold surge, air-sea interaction



Lightning climatology around Jakarta, Indonesia, based on 13-years SYNOP observation and GSMaP rainfall data

MORI, Shuichi^{1*}; ARBAIN, Ardhi²; SYAMSUDIN, Fadli²; YAMASHITA, Kozo³; TAKAHASHI, Yukihiko⁴; YAMANAKA, Manabu D.⁵

¹JAMSTEC, ²BPPT, Indonesia, ³Dept.Electrical Engineering, Salesian Polytechnic, ⁴Department of Cosmosciences, Graduate School of Science, Hokkaido University, ⁵JAMSTEC/Graduate School of Science, Kobe University

Operational observation in Indonesia, where has much amount of active convections under the tropical maritime climate with high atmospheric and sea surface temperatures and abundant water vapor supply, showed more than 100-200 days of lightning a year and more than 10 times/km²/year of lightning density. Developed convective systems with lightning (thunderstorms) often generates severe mesoscale phenomena of heavy rainfall, gusty wind, and tornados, as well as lightning strikes at the ground. Indeed, much amount and kinds of serious damages caused by thunderstorms have been reported in Indonesia, e.g., massive blackout and serious damage on electrical devices in urban areas, and forest fires and burn-out of high voltage power lines in rural regions. Although Virts et al. (2013a, 2013b) clearly documented lightning climatology over Indonesia based on TRMM LIS and the World Wide Lightning Location Network (WWLLN) observations, temporal and spatial distributions of lightning activity and their dynamics have not been examined in detail because ground-based radar and lightning locating observations are not well organized and satellite observations have deficiencies in their spatial resolution and sampling frequency.

We started three years (JFY2013-2015) program to study lightning activity mainly over Jakarta, where is the capital megacity in Indonesia and has much risk to be damaged seriously by thunderstorms especially in the social sector, to clarify its characteristics from both the points of precipitation climatological and mesoscale meteorological views based on three approaches as follows: 1) statistical analyses for lightning activity by using operational surface observation and TRMM satellite, 2) case studies on environmental conditions for severe thunderstorms based on a C-band radar and surface observation data already obtained, and 3) campaign observation by using X-band dual-polarimetric radar, VLF receiver network, and hydrometeor video soundings.

We examined 13-years SYNOP data for statistical analysis of lightning activity around Jakarta and its relation to rainfall variation based on GSMaP data as the first step. Seasonal variation of lightning frequency shows two peaks in April and November, which correspond to periods just before and after the peak of the rainy season in February around Jakarta, at most of the stations over the inland region. However, these peaks are not clearly shown at stations close to the coastline of Java Sea and one peak in February is more predominant. Because previous studies (e.g, Hattori et al. 2011, Wu et al 2007) suggested the cross equatorial northerly surge (CENS) intensify local convection around Jakarta in the boreal winter season, the effect of CENS to generate thunderstorms was limited only along the coastal region but not for inland in February. Intraseasonal variation of lightning activity based on MJO index clearly shows a major peak in the MJO phases 3 (eastern Indian Ocean) and minor one in phase 7 (western Pacific). It suggested the lightning activity was intensified at the leading and trailing edges of MJO large scale disturbance which is consistent with previous studies (e.g., Morita et al. 2006). Whereas, GSMaP data show a peak of rainfall around Jakarta in the phase 3 at the same time of lightning peak, though the previous studies showed the rainfall was peaked in the phases 4-5 (maritime continent).

We plan to examine lightning characteristics more focused around Jakarta and its relation to rainfall quantitatively by adapting the rain-yields per flash (RPF) (Williams et al 1992, Takayabu 2006) and the other parameters. More than 15-years TRMM LIS and PR data shall be used in our future study as well as Asia VLF network (AVON) and WWLLN datasets.

Keywords: lightning & thunderstorm, convective diurnal variation, Indonesian maritime continent

Interannual variability of rainy seasons onset over the eastern Indochina Peninsula

NGUYEN-LE, Dzung¹ ; MATSUMOTO, Jun^{1*} ; NGO-DUC, Thanh²

¹Tokyo Metropolitan University, ²Vietnam National University

The onset dates of rainy seasons over eastern Indochina Peninsula (8.5o-23.5oN, 100o-110oE) for individual years from 1958 to 2007 were objectively determined by the principal component of two first dominant empirical orthogonal (EOF) modes of the precipitation data. It is found that onset of summer rainy season (SRS), which is described by the EOF1, is in 6 May on the average, with a standard deviation of 13 days. Meanwhile, the autumn rainy season (ARS) indicated by the EOF2 has the climatological onset and standard deviation is 16 Sep and 12 days, respectively. The SRS starts simultaneously with the eastward shift of the Western North Pacific sub-tropical high (WPSH) and the evolution of summer monsoon westerlies. On the contrary, the retreat of summer monsoon over northern and central Indochina in boreal autumn indeed signifies the onset of ARS. The relationship between the onset and intraseasonal variations (ISVs): the 30?60-day (30?60DV) and the 10?20-day variation (10?20DV), are identified.

The results also insisted that ENSO has considerable influence on the onset of rainy season in the Indochina. In general, La Nina (EL Nino) years with warm (cold) sea surface temperature (SST) anomalies in the western Pacific and cold (warm) SST anomalies in the central?eastern Pacific in the preceding winter-spring have early (late) SRS onset. For an early onset year, the equatorial easterly winds are observed be stronger. Strong convective activities also occur over the southern Indochina Peninsula and the SCS in the preceding winter and spring. Whereas, the early onset of ARS is likely related to El Nino years with weaken equatorial easterly winds. It could be explained by the earlier retreat of westerlies monsoon and farther westward extension of the WPSH. Finally, the differences of ISV between early-late onset years of two rainy seasons are also discussed.

Keywords: monsoon onset, interannual variation, Indochina Peninsula, sub-tropical high, summer monsoon

How did North Atlantic Oscillation (NAO) cause drought in northwestern China at the multi-decadal to centennial scales?

LEE, Harry^{1*}

¹The University of Hong Kong

North Atlantic Oscillation (NAO) plays an important role in the Northern Hemisphere climate system. Although there is growing interest in the connection between NAO and precipitation change in China, there are few studies concerning that connection in northwestern China. Based on fine-grained historical drought disaster records and NAO proxies, we explored quantitatively their possible connection in northwestern China over the past millennium at the multi-decadal to centennial timescales. Statistical results show that NAO and drought disaster were negatively correlated, as positive modes of NAO caused northward-displaced, stronger-than average mid-latitude Westerlies with an enhanced latitudinal water vapor gradient into the central Asian drylands, resulting in reduced drought frequency and intensity in northwestern China. But, their correlation was out-of-phase during the Little Ice Age because of the southward shifting of monsoon, Westerlies, and the East Asian Jet Stream brought by long-term land surface cooling. As it has been indicated that the precipitation in northwestern China is also determined by El Nino-Southern Oscillation and North Atlantic sea surface and air temperature aside from NAO, further studies are needed to evaluate their individual roles and combined impacts upon the drought disaster there.

Keywords: NAO, Precipitation, Drought, Northwestern China

Identifying Precipitation Sources in Northern Mongolia using Back Trajectory Analysis

KOIKE, Yuriko¹ ; ASANUMA, Jun^{2*} ; DAVAA, G.³

¹Graduate school of Life and Environmental Sciences, University of Tsukuba, Japan, ²Center for Research in Isotopes and Environmental Dynamics, University of Tsukuba, Japan, ³National Agency for Monitoring for Environment and Meteorology, Mongolia

Prediction of precipitation variability and understanding of its mechanisms are essential in Northern Asia [Yatagai and Yasunari, 1994]. The objective of this study is to investigate linkages between the interannual variability of precipitation sources and that of precipitation amount in this area.

For this purpose, a back-trajectory model [Merrill et al., 1986] of atmospheric water vapor was developed and applied to the rainfall during the warm season from 2003 to 2009 at semi-arid grassland Kherlenbayan-Ulaan (KBU) in northern Mongolia, where an air parcel is tagged with the ambient potential temperature where it is precipitated, and is tracked adiabatically above the planetary boundary layer (PBL). When a parcel is tracked back into the PBL, its potential temperature is adjusted to the value at the top of PBL. In addition, diffusion process of water vapor evaporated from the ground surface into the atmosphere and the altitude raindrops are formed are calculated using the Monte Carlo simulation [Dirmeyer and Brubaker, 1999]. The model uses JRA-25/JCDAS [Onogi et al., 2007] reanalysis data set with 6hour intervals.

The results show that the major precipitation sources of rainwater at KBU are the local area of Mongolia and the central and the western Asia. Water vapor evaporated from the local area of Mongolia is approximately 20% of the total summer precipitation, and this ratio is particularly higher in Mongolia in compared with the other area on the globe [Dirmeyer et al., 2009]. This result consists with Yatagai and Yasunari, [1995] which suggested that the variability of precipitation in the arid areas in the northeastern Asia has higher correlation with the local atmospheric circulation, and Sato et al., [2007]. Moreover, this paper clearly exhibits that this ratio is fairly constant over the years in spite that the total precipitation varies.

Moreover, it was found that water vapor supply from the central and the western Asia is approximately 30% of the total summer precipitation at the target point, and therefore, the central and the western Asia may explain a major portion of the summer total precipitation.

In addition, the year 2003 and 2004 were found to have an anomalous relation. It is discovered that larger precipitation in the autumn of 2003 [Hirata et al., 2008] was followed by the increased contribution of the local evaporation to the precipitation in the following 2004. Shinoda et al., [2011] claimed that the cold season climate with low evapotranspiration and strong soil freezing acts to prolong the decay time scale of autumn soil moisture anomalies to the next spring over the eastern part of Mongolia. Therefore, it is considered that soil moisture at the local region in the autumn may be preserved during the winter up to the next spring and contribute to precipitation in summer in northern Mongolia.

Philippine summer monsoon onset -Intensive observation PALAU2013 and data rescue for 109 years-

KUBOTA, Hisayuki^{1*} ; SHIROOKA, Ryuichi¹ ; MATSUMOTO, Jun² ; CAYANAN, Esperanza³ ; HILARIO, Flaviana³

¹Japan Agency for Marine-Earth Science and Technology, ²Tokyo Metropolitan University, ³Philippine Atmospheric, Geophysical and Astronomical Services Administration

The Philippines is an archipelago country which is located in the western side of tropical western Pacific. There are distinct summer monsoon in the western side and winter monsoon in the eastern side of the country. This study focuses on the onset of summer monsoon in the western Philippines during May to July. Intensive observation of Pacific Area Long-term Atmospheric observation for Understanding of climate change (PALAU2013) was conducted by launching additional upper-air observation in Cebu, Laoag, and Puerto Princesa during May to August 2013. We captured the onset of summer monsoon in June 10, 2013. Low level strong southwesterly wind associated with moistening air was penetrated in the central Philippines during the onset. We compared the behavior of Philippines summer monsoon onset when there was no continuous upper-air observation in reanalysis data. The recovery of historical station back to 1903 called 'Data rescue' was performed using Monthly Bulletins of Philippine Weather Bureau from 1903 to 1940. We created rainfall dataset in the Philippines from 1903 to 2012 by connecting recovered data and PAGASA station data. Summer monsoon onset was defined by using 8 station rainfall data in the western Philippines. The onset date becomes earlier after 1990s and tends to occur in middle May. Early onsets were also seen in early 20th century.

Keywords: Philippines, monsoon onset, data rescue, Asian summer monsoon

Relationships between heavy rainfall in East/Southeast Asia and track, intensity, duration patterns of tropical cyclones

ISERI, Yoshihiko^{1*} ; KANAE, Shinjiro¹

¹Graduate School of Science and Engineering, Tokyo Institute of Technology

Tropical cyclones (TCs) have considerable impacts to many areas in East/Southeast Asia. For instance, TCs accompanied with heavy precipitation could cause floods, and the strong winds of TC also could induce huge damages on their track and surrounding environment. In addition, Intergovernmental Panel on Climate Change (IPCC) 5th assessment report mentions possible increasing of both global mean tropical cyclone maximum wind speed and rain rates. Thereby, it would be very important to deepen our understanding on the relation between TCs and their impacts to local climate in East/Southeast Asia.

This study aims to extract observed TC patterns by employing a nonlinear classification method, and also examine relations between extracted TC patterns and heavy rainfall in East/Southeast Asian cities. The classification method used in this study is the self-organizing maps (SOM). The SOM has been recently used in climate science and have shown significant performance for analysis of high dimensional climate data.

In this study, we utilized the TC data provided by JTWC (Joint Typhoon Warning Center). The data period used in this study is 62 years from 1951-2012. Then, we extracted longitude, latitude, maximum sustained wind speed, and duration from TC genesis in order to make input for the SOM. Consequently, each TC is represented as 39 dimension vector, and total 1,837 TCs are utilized as input for the clustering by the SOM. We set the map size of the SOM as 3x3 hexagonal grids.

By the SOM algorithm, total 1,837 TCs were classified in nine nodes (i.e. nine patterns). As a result, several distinguishable TC patterns were extracted by the SOM, according to their track, intensity and duration. Then, we extracted the TCs classified in each pattern, and subsequently examined relations between the extracted TC patterns and rainfall at 21 meteorological stations in East/Southeast Asian cities. Our analysis confirmed clustering method is quite useful in identifying TC properties. The result also suggested extracted TC patterns are highly related with heavy rainfall in some of the target cities.

Acknowledgments: This research was supported by the Environment Research and Technology Development Fund (S-10) of the Ministry of the Environment, Japan and the Research Program on Climate Change Adaptation (RECCA) of the Ministry of Education, Culture, Sports, Science and Technology, Japan.

Keywords: typhoon, western North Pacific, heavy rainfall, Self-Organizing Maps

Application of pseudo global warming method and dynamic downscaling for typhoons approaching to Japan

TANIGUCHI, Kenji^{1*} ; HOSOI, Mari²

¹Faculty of Environmental Design, Kanazawa University, ²School of Environmental Design, Kanazawa University

Results of global warming experiments indicate that an intensity of typhoon will be magnified in future climate. In this study, reproductive simulation of typhoons which approach to Japan are made. At the same time, pseudo global warming conditions are composed of a reanalysis product and multiple global warming experiments. Then, numerical simulations using the pseudo global warming conditions were conducted for each actual typhoon and variations of typhoons in future climate were investigated by comparing the reproductive simulation and the runs with pseudo global warming conditions. Results of a typhoon in summer showed significant variations in tracks. When a track deflects eastward, a typhoon goes over the ocean and its center pressure remarkably decreases. In addition, wind speed around the typhoon increases very much. Geopotential height in lower troposphere showed lower anomaly over the Pacific Ocean. Decreasing Pacific high is thought to be a cause of the change in typhoon tracks. In another typhoon in summer, although variations in tracks and center pressure were smaller, total precipitation in the typhoon increased in future. However, another typhoon in summer showed decreasing precipitation with small variation in tracks and center pressure. Results for another typhoon in autumn showed smaller variation in tracks and center pressures, and total precipitation increases in results of future climate. Such characteristics in future variations were found in other typhoons in autumn. On the other hand, hourly precipitations were not necessarily increased in future climate both in summer and autumn. These results indicate that extremely strong rainfall does not necessarily occur in short time, but modestly strong rainfall continues longer time. Even if no significant variation in center pressure, or intensity is similar to current climate, precipitation will increase in future climate.

Keywords: global warming, typhoon, numerical weather prediction, downscaling

Assessment of GSMaP satellite rainfall products in Asian monsoon region

KAMIMERA, Hideyuki^{1*}; NABESAKA, Seishi¹; SYAMSUDIN, Fadli²; NGO-DUC, Thanh³; LE VIET, Xe⁴; HERNANDO, Hilton T.⁵; MATSUMOTO, Jun⁶; USHIO, Tomoo⁷; IWAMI, Yoichi¹

¹International Centre for Water Hazard and Risk Management, Japan, ²Agency for the Assessment and Application of Technology, Indonesia, ³Vietnam National University at Ha Noi, Vietnam, ⁴National Hydro-Meteorological Service, Vietnam, ⁵Philippine Atmospheric, Geophysical and Astronomical Services Administration, the Philippines, ⁶Tokyo Metropolitan University, Japan, also at Japan Agency for Marine-Earth Science and Technology, ⁷Osaka University, Japan

Satellite rainfall products provide the spatial and temporal distribution of rainfall estimates over the ungauged regions where no ground-based measurements with rain gauges and/or meteorological radars are available. For the regions, the satellite products have special importance in, for example, hydrological and agricultural applications such as flood forecasting/warning and water resources management. The Global Satellite Mapping of Precipitation (GSMaP) products have high resolution in space and time (0.1 deg. and 1 h); besides the near-real-time version of GSMaP opens to the public within four hours after measurements. They are thus highly expected to be in operational use in many countries and regions. There are the problems in accuracy and precision of the products due to the limitations on measuring principles, time intervals of sampling and others. However, the above-mentioned strengths of the products are considerable. Therefore, the performance of the GSMaP products needs to be investigated in various areas for the appropriate and effective use; moreover, through the investigation, it can be expected that the knowledge useful for improving the performance will be obtained. The present study investigates the performance of two GSMaP products, GSMaP_MVK and GSMaP_Gauge (a gauge-adjusted GSMaP_MVK), in the four river basins located from the tropics to mid-latitudes in the Asian monsoon region, including: the Solo Basin (16,100 km²) in Jawa, Indonesia; the Thu Bon – Vu Gia Basin (10,350 km²) in central Vietnam; the Pampanga Basin (9,759 km²) in Luzon, the Philippines; and the Tone Basin (16,840 km²), Japan. The study is ongoing and intermediate results mainly for the Solo and Thu Bon – Vu Gia river basins are discussed at this session.

Keywords: Asian monsoon, precipitation, satellite

INTERIOR FLOOD DAMAGE IN JAPAN: PRESENT AND FUTURE

BHATTARAI, Rajan^{1*} ; YOSHIMURA, Kei¹ ; KIGUCHI, Mashasi¹ ; NODA, Keigo¹ ; NAKAMURA, Shinichiro¹ ; OKI, Taikan¹

¹Depart. of Civil Engineering, The University of Tokyo

The assessment of flood risk and its future prediction under anthropogenic climate change are important to policy makers for future preparedness and adaptation planning. Almost all countries in the world including major cities suffer from flood damage every year due to large exposed population and property. The intensity of damage amount varies as per the level of their preparedness. The case of Japan is also similar, having about 100 billion yen annual damage due to interior flood. Flood losses are increasing more rapidly during late 20c and is expected to increase in future too. Another major factor contributes to future climate events like floods and its losses will be anthropogenic climate change. But due to lack of robust analytical framework to estimate future losses and lack of long term damage data; future projections of flood loss still have many uncertainties.

Most studies regarding flood damage assessment have been done for river flood which always excludes interior flood damage usually caused by rainfall inside city area due to poor or insufficient drainage facilities. Also some extreme events corresponding to large return period is usually taken for damage assessment, which always exclude the damages caused by high frequency events, but reported as equal as an extreme event. In this study, we present a robust methodology for interior flood damage assessment exclusively; taking all daily rainfall events into account and its application to future climate.

We use recorded historical daily damage data in Japan that was archived in Ministry of Land, Infrastructure, Transport and Tourism (MLIT) of Government of Japan to produce functions namely damage occurrence probability function and damage cost function. Our statistical approach gives the probability of damage following every daily rainfall event and thereby the annual damage as a function of rainfall, population density, topographical slope, and gross domestic product. Our results for Japan show reasonable agreement with area-averaged annual national damage for period 1993-2002 in calibration and 2003-2009 in validation. The flexibility of this method leads to future projection of interior flood damage in Japan.

Multiple climate models in different resolution with different convective schemes, sea surface temperature (SSTs) and future climate scenarios to predict the future interior flood damage amount in monetary term are being used. For Japan, we use high resolution Meteorological Research Institute (MRI) atmospheric general circulation models (MRI-AGCM) for present and future precipitation. The precipitation parameters are calculated from 1979-2009 in present and 2075-2099 in future using MRI-AGCM with two mesh sizes (20 km and 60 km) and three different convective schemes (Yoshimura Scheme, Arakawa-Schubert scheme & Kain-Fritsch scheme) which give multi-physics ensemble. The future sea surface temperature (SST) is as per the multi-model ensemble mean change of CMIP3 and CMIP5 with A1B and RCP8.5 scenario respectively. Moreover to consider uncertainty of future SST due to geographical SST distribution, three different clusters SST are also taken for future damage assessment.

Initial results for annual average interior flood damage in Japan shows 13.25% increase in average for future [2083- 2099] from the base period [1993-2009] for A1B scenario and 10.08 % increase for RCP8.5 scenario. The range of future estimate of average annual interior flood damage for A1B scenario is 68.17 billion yen to 117.81 billion yen and for RCP8.5 scenario, it is 78.93 billion yen to 119.06 billion yen in 2005 price. Another important notice in the result is future largest annual damage in A1B scenario seems quite same as present largest annual damage, but for RCP8.5, some year shows the largest damage will double than the present.

We will add different models and CMIP5 results and will describe more features of future interior flood damage in our presentation.

Keywords: interior flood damage, damage occurrence probability, damage cost function, preparedness, economic losses, climate change

Application of performance metrics to climate models to project future river discharge in the Chao Phraya River basin

WATANABE, Satoshi^{1*} ; HIRABAYASHI, Yukiko¹ ; KANAE, Shinjiro²

¹the University of Tokyo, ²Tokyo Institute of Technology

Future river discharge in the Chao Phraya River basin was projected, taking into account the performance of multiple General Circulation Models (GCMs). Future hydrological simulations using outputs from multiple GCMs are important for assessing the uncertainty in the projections. In addition, consideration of the spread of GCM projections should be included in the analysis to appropriately evaluate extremes, as there can be significant differences among projections. This study, therefore, developed a bias-corrected dataset for multiple GCMs outputs and a performance metrics to evaluate each GCM in order to project future river discharge more appropriately.

To develop a bias-corrected future climate dataset, an advanced bias correction method is applied, in which the trend of variables from the reference to the projection period is preserved. Then, future river discharge was projected by the H08 hydrological model. The newly developed future climate dataset enabled us to conduct a projection that considered the spread of projection derived from multiple GCMs.

Several metrics to evaluate the performance of each GCM to reproduce monsoon precipitation were proposed to estimate performance-based projection because evaluation of GCM performance in simulating monsoon behavior is important for projecting future discharge in the Chao Phraya River basin. This study was performed to investigate the effects of performance metrics and to estimate the spread of projections derived from the differences in multiple performance metrics.

Multiple future projections using available GCM outputs were conducted in the Chao Phraya River basin and multiple weighted ensemble means were obtained using the proposed multiple metrics related to monsoon precipitation. We compared the projected results obtained and discuss the characteristics of each projection. The performance-based projections indicated that the future river discharge in September is increased by 60%~90% of the retrospective simulation. Our results highlight the importance of appropriate evaluation for the performance of GCMs.

Keywords: Climate Change, River discharge

Variation of the South China Sea Summer Monsoon onset

IMAKAWA, Shin^{1*} ; HIGUCHI, Atsushi²

¹Graduate School of Science, Chiba University, ²CEReS, Chiba University

In this study, we reveal factors of variation of the South China Sea Summer Monsoon(SCSSM) onset. The study area of South China Sea(SCS) is 5-15N, 110-120E. We use the data set of JRA-25/JCDAS, and, calculate the SCSSM onset date for 30 years, 1979-2008, defined as the zonal wind. In Kajikawa and Wang(2012), the authors point out an advance in the SCSSM onset date around 1993/94. Then, we divide the 30 years into 2 groups, before 1993(Prior) and after 1994(Later). Moreover, we pick out the advanced and delayed onset date for 3 years in each groups, after all, classify 30 years into 4 groups(Prior-Advanced, Prior-Delayed, Later-Advanced, Later-Delayed).

Focusing on time-changes of Sea Surface Temperature(SST), it is difference between Prior groups(P-A, P-D) and Later groups(L-A, L-D) for SST over the Philippine Sea(PS: 0-15N, 125-140E). The SST for Prior is higher about 0.5 degrees than that for Later. On the other hand, over the SCS, the SST is higher Advanced groups(P-A, L-A) than Delayed groups(A-D, L-D). This is reason why the strength of meridional surface wind over the SCS before April. Therefore, an effect of the SST to the SCSSM onset date is difference between over the SCS and over the PS. The SST over the SCS affect the annual variation of the SCSSM onset, and, the SST over the PS affect the 93/94 change.

The SCSSM onset is affected by a warming of the Tibetan Plateau(TP: 30-35N, 80-100E) too. In Ueda and Yasunari(1998), they reveal that the onset of summer monsoon over the Bay of Bengal and the SCS coincide with a time of rapidly increase in the thermal contrast the TP and surrounding ocean. We calculate the warming over the TP by a difference of geopotential height between 200hPa and 500hPa. Comparing the time-change of warming in 4 groups, we examine the difference of the period of rapidly warming over the TP in each groups. It is consider a relation between variation of the SCSSM onset and variation of the warming over the TP.

Then, we compare the anomaly of SCSSM onset date defined by the zonal wind, the anomaly of a time of rapidly warming over the TP, and, the anomaly of SST contrast between over the SCS and over the PS in April. As a results, the annual variation of SCSSM onset correlate clearly with the variation of the warming over the TP. Moreover, the low(high) SST difference in over the SCS and over the PS and the advanced(delayed) warming over the TP cause the advanced(delayed) SCSSM onset date.

Keywords: Asia, monsoon

Recent changes in heavy precipitation occurrences along the eastern coast of the Indochina Peninsula

FUKUTOMI, Yoshiki^{1*} ; WU, Peiming¹ ; MATSUMOTO, Jun²

¹JAMSTEC, ²Tokyo Metropolitan University

Long-term changes of the frequency of heavy precipitation occurrence along the eastern coast of the Indochina Peninsula were analyzed using daily data from six Vietnamese meteorological stations for the period September–November of 1961–2010. The heavy precipitation days were defined by the 50 and 100 mm/day threshold values. The frequency of the coastal heavy precipitation days were decomposed into tropical cyclone (TC)-induced heavy precipitation days and non-TC heavy precipitation days, and their contribution to a recent increase in the coastal precipitation was examined. Over the 50-yr period, heavy precipitation occurrence indices show a significant increasing trend that is linked to an increasing trend in seasonal amount of the coastal precipitation. A rapid increase in the coastal heavy precipitation days was found from the mid-1990s through the 2000s. This marked increase is basically due to non-TC heavy precipitation events, suggesting that TC passages do not play a role in the recent increase in the seasonal precipitation amount and the heavy precipitation events. A role of tropical synoptic-scale disturbances (TSDs) as non-developing disturbances for TC formation in the non-TC heavy precipitation events was also explored. About 70% of the non-TC heavy precipitation events are associated with TSDs originated from the western North Pacific–South China Sea region. TSD passages are responsible for the recent increase in non-TC heavy precipitation events.

Keywords: heavy precipitation, synoptic-scale disturbances, Indochina Peninsula

Climatology of explosively developing extratropical cyclones over the Kuroshio Front

NAGAI, Masaki^{1*} ; HIGUCHI, Atsushi²

¹Graduate School of Science, Chiba University, ²CEReS, Chiba University

When the East Asian winter monsoon is strong, the explosive cyclone activity tends to concentrate in the Kuroshio Current (Yoshiike and Kawamura, 2009). It is important to understand the relationship between the heat supply from the Kuroshio extension region and the development process of cyclones. The purpose of this research is to reveal meteorological and oceanic environments that can provide differences of the cyclone path or the rapid development.

Composite analysis for cyclones developed over the westerly (TypeW_P) or easterly (TypeE_P) Kuroshio extension region was conducted. The result suggests the existence of mesoscale circulation over the Sea of Japan is important to the northward path of the TypeW_P cyclone. In addition, before the maximum deepening of the TypeW_P cyclone, latent heat flux clearly increased at the Kuroshio extension region. It was the result of easterly winds, blowing in front of a warm front of the cyclone. The Kuroshio extension region, which was meandering north and south direction, responded to the winds. These results do not appear in composite analysis for the TypeE_P cyclone. The influence on the weather of the Kanto region is also investigated. The results show that TypeW_P cyclones tend to provide heavy rain or snow, and TypeE_P cyclones provide severe winds on that region. These results show the important contribution of water vapor provided from the Kuroshio extension region to the TypeW_P cyclone. We conducted more composite analysis for these cyclones. Composite analysis at the cyclone center revealed some differences in advection of water vapor. The water vapor flux, blowing from the southeast quadrant to the cyclone center, was stronger in the TypeE_P, but the precipitable water that extends to the south of the cyclones was greater in the TypeW_P. As the result of strong water vapor advection, the development of the TypeE_P cyclone was assisted. On the other hand, more humid air masses contributed to the development of the TypeW_P cyclone. These experiments were conducted for cyclones that developed over the westerly or easterly Subarctic frontal zone of the North Atlantic (TypeW_A and TypeE_A, respectively). But no clear difference appeared in the low-level environment associated with the TypeW_A or the TypeE_A cyclone. These results suggest that the differences of low-level fields associated with the difference of the maximum deepening position are a particular phenomenon in the Kuroshio extension region. In addition, the contribution of water vapor advection to the cyclone center was stronger for cyclones developed over the Kuroshio extension region.

Keywords: Explosively developing extratropical cyclone, East Asian winter monsoon

Variability of GPS precipitable water vapor over the northeast Bangladesh

MURATA, Fumie^{1*} ; TABEL, Takao¹ ; TERAOKA, Toru² ; HAYASHI, Taiichi³ ; CHOUDHURY, S. A.⁴

¹Kochi University, ²Kagawa University, ³Kyoto University, ⁴Bangladesh Meteorological Department

Precipitable water vapor (PWV) derived from Global Positioning System (GPS) which were installed in the northeast Bangladesh was analyzed for different seasons. A GPS utilized for the analysis of pre-monsoon (May 2011) was installed at Sylhet. Two GPS utilized for the analysis of monsoon (July 2007) and winter seasons(December 2007) were installed by UNAVCO at Jamalpur and Jaflong. The simultaneous observation with GPS and radiosondes were conducted in May 2011. The PWV derived from GPS was well corresponded with that derived from radiosondes. A sharp PWV increase frequently observed during the passage of severe storms during the pre-monsoon season. The active and break monsoon periods in July 2007 showed average PWV of 67 mm and 62 mm, respectively. Severe flood occurred over Sylhet area during the active period. The PWV in the winter season showed 10-15-day periodicity in PWV between 15 mm in minimum and 25 mm in maximum. The amplitude of diurnal variation was larger in the break monsoon period than the active monsoon period. The nocturnal maximum and early afternoon minimum were remarkable in the diurnal variation of PWV in the monsoon period. The amplitude of diurnal variation was also large in winter. The phase in the diurnal variation was different in the two GPS stations. The PWV was increase on 12-18 LT at Jaflong, but the PWV had minimum on the same period of time at Jamalpur.

Keywords: GPS precipitable water, Bangladesh, Intraseasonal variation, Diurnal variation

Distributed hydrological model simulation on the diurnal-cycle of Ciliwung River basin

SULISTYOWATI, Reni^{1*}; HAPSARI, Ratih indri²; MORI, Shuichi³; SYAMSUDIN, Fadli⁴; OISHI, Satoru¹; YAMANAKA, Manabu D.¹

¹Kobe University, ²State Polytechnic of Malang, ³JAMSTEC, ⁴BPPT

A systematic diurnal-cycle of water level is persistently generated over Ciliwung River basin during the Intensive Observational Period of HARIMAU2010 (15 January to 15 February 2010). It is almost uniquely explained by diurnal-cycle of rainfall observed with weather radar (C-band Doppler Radar) over Jakarta and surrounding area.

In this study, we have shown a simulation of the diurnal cycle of Ciliwung River water level by distributed hydrological model (the CDRMV3 model). Using the CDR rainfall data, river discharge is simulated both for short period and one-month period in two station, i.e. Manggarai (downstream outlet) and Katulampa (upstream outlet), and verified by comparing with the observation discharge from those two station.

Further improvement of the simulation scheme for the diurnal-cycle rainfall is also discussed.

Keywords: Diurnal-cycle, Weather radar, Distributed hydrological model, Rainfall, Runoff

Introduction of the SCOSTEP's VarSITI program - Variability of the Sun and Its Terrestrial Impact

SHIOKAWA, Kazuo^{1*} ; GEORGIEVA, Katya²

¹Solar-Terrestrial Environment Laboratory, Nagoya University, ²Space Research and Technologies Institute, Bulgarian Academy of Sciences

The Scientific Committee on Solar Terrestrial Physics (SCOSTEP) is an interdisciplinary body of the International Council for Science (ICSU) to run international interdisciplinary scientific programs and promotes solar-terrestrial physics research. The last solar minimum in 2008-2009 and the current solar maximum of sunspot cycle 24 show much lower activities compared with the previous two solar cycles 22 and 23. The scientists in the solar-terrestrial physics are watching very low solar activities and their consequences on Earth, which have never been observed since modern scientific measurements become available. The SCOSTEP program "Variability of the Sun and Its Terrestrial Impact (VarSITI)" (2014-2018) will focus on this particular low solar activity and their consequences on Earth, for various times scales from the order of thousands years to milliseconds, and for various locations and their connections from the solar interior to the Earth's atmosphere. In order to elucidate various sun-earth connections, we encourage communication between solar scientists (solar interior, sun, and the heliosphere) and geospace scientists (magnetosphere, ionosphere, and atmosphere). Campaign observations will be promoted for particular interval in collaboration with relevant satellite and ground-based missions as well as modeling efforts. Four scientific projects will be carried out in VarSITI as (1) Solar Evolution and Extrema (SEE), (2) International Study of Earth-Affecting Solar Transients (ISEST/Minimax24), (3) Specification and Prediction of the Coupled Inner-Magnetospheric Environment (SPeCIMEN), and (4) Role Of the Sun and the Middle atmosphere/thermosphere/ionosphere In Climate (ROSMIC). In this presentation we introduce the VarSITI program and its four projects to promote interdisciplinary studies among different fields.

Keywords: VarSITI, solar activity, climate change, atmosphere, magnetosphere and ionosphere, heliosphere

California Nino/Nina in boreal summer

YUAN, Chaoxia^{1*} ; YAMAGATA, Toshio¹

¹APL, JAMSTEC

Anomalous warming/cooling in the coastal ocean off Baja and Alta California has attracted broad attention due to its significant impacts on the coastal marine ecosystem. The anomalous warming/cooling has been attributed, especially in boreal winter, to the remote forcing of the tropical El Nino/Southern Oscillation (ENSO) through both oceanic and atmospheric teleconnections and/or the ENSO-independent basin-wide atmospheric circulation anomalies in mid-latitudes. In the present study, we show for the first time the existence of coastal air-sea coupled phenomenon in the coastal ocean off Baja and Alta California in boreal summer. An initial decrease/increase in the southward alongshore surface winds along the coast weakens/strengthens the coastal upwelling and raises/lowers the coastal sea surface temperatures (SSTs) through oceanic mixed-layer processes. The resultant coastal warming/cooling, in turn, heats/cools the overlying atmosphere anomalously, decreases/increases the atmospheric pressure in the lower troposphere, generates an anomalous cross-shore pressure gradient, and thus reinforces or maintains the alongshore surface wind anomalies. The air-sea coupled phenomenon is analogous to the well-known ENSO in the tropical Pacific but with much smaller time and space scales, and referred to as California Nino/Nina (CAN) after the pioneer work that describe the warming events in the coastal ocean off Baja and Alta California as California El Nino.

Keywords: California Nino/Nina, coastal air-sea interaction

River discharges, ocean circulation and material transport in Japanese coastal waters: simulation with JCOPE ocean model

VARLAMOV, Sergey^{1*} ; MIYAZAWA, Yasumasa¹ ; YAMASHIKI, Yosuke² ; SASAKI, Toshiaki²

¹Japan Agency for Marine-Earth Science and Technology, ²Graduate School of Advanced Integrated Studies in Human Survivability, Kyoto University

The total volume of fresh water discharged by rivers into the world ocean is incompatible with the total mass of ocean waters; however these discharges contribute significantly into formation of fresher coastal waters and details of coastal ocean circulation.

This impact is not local, and supports presence of lower salinity waters in wide coastal areas along Japanese coast. In an absence of rivers in ocean model for appropriate reproducibility of ocean surface salinity it is often required to apply salinity restoration approach. Additionally, rivers could bring to ocean surface-floating, suspended and dissolved substances, some of which are hazardous, like radioactive materials initially dropped on the ground following such disasters as Fukushima Dai-Ichi nuclear power plant accident. These could be washed to rivers by strong rainfalls.

Method of counting inflow of fresh water from rivers as horizontal fluxes to the designated model cells is used. Demonstrated are direct impacts of rivers on formation of fresher waters along the coast of Japan and some cases of induced by discharges local ocean circulation patterns near the river mouth locations. A preliminary experiment when the model utilizes the hourly information on the amount of river discharges demonstrates an importance of such approach for the correct simulation of transport processes in extreme conditions like the typhoon-induced precipitations that often take place in Japan and East Asia. For achieving of this capacity, we are looking for utilization of simple land waters hydrological models for main river basins that could transfer the detailed meteorological precipitation forecast information into the approximate forecasts of river discharges.

Keywords: river discharge, ocean circulation, river-ocean interaction, coastal ocean processes

A spike-like input of perfluoroalkyl substances into the Western North Pacific from the Japanese Coast associated with t

MIYAZAWA, Yasumasa^{1*} ; YAMASHITA, Nobuyoshi² ; TANIYASU, Sachi² ; YAMAZAKI, Eriko² ; GUO, Xinyu³ ; VAR-LAMOV, Sergey¹ ; MIYAMA, Toru¹

¹Japan Agency for Marine-Earth Science and Technology, ²National Institute of Advanced Industrial Science and Technology, ³Ehime University

The recent great earthquake of magnitude 9.0 on 11 March 2011 followed by TSUNAMI and fire in Japan has resulted in serious environmental problems in and around Japan. A huge amount of materials has been discharged into the ocean after the tremendous flood damage by TSUNAMI. A research group of the National Institute of Advanced Industrial Science and Technology has sampled the perfluoroalkyl substances (PFAs), which are chemical materials included in the industrial products, in the Western North Pacific for past a few years. They found some evidences showing an abrupt increase of the PFAs concentration east of Japan in 2011 after the great earthquake. To confirm the anomalous input of two typical PFAs (PFOA and PFOS) from the Japanese coast into the ocean, we conducted a series of chemical tracer simulations using an eddy-resolving ocean reanalysis product, JCOPE2, by assuming the oceanic dispersion of the PFAs dissolved in sea water mainly driven by the ocean current. Comparison of the simulation results with the observation actually indicates a spike-like input of PFOA into the Western North Pacific after the great earthquake; however, the simulations could not well explain the observed distribution of PFOS, suggesting some differences in the oceanic dispersion processes between PFOA and PFOS. We discuss estimates of the total emission amounts of PFOA and PFOS based on a simple process representing the TSUNAMI effect on the emission from the land.

Keywords: perfluoroalkyl substances, the great earthquake 0311, oceanic dispersion, Tsunami, oceanic observation, numerical simulation

Super high resolution experiments of torrential rainfall events with the K super computer

OIZUMI, Tsutao^{1*} ; KURODA, Tohru¹ ; SAITO, Kazuo²

¹Japan Agency for Marine-Earth Science and Technology, ²Meteorological Research Institute / JAMSTEC

In Japan, localized torrential rainfalls sometimes cause severe disasters which impact on the society. (e.g., the urban flash flood disaster at the Toga-gawa River in Kobe in July 2008, and the debris flow disaster in Izu Ohshima Island in 2013). In these events, the precipitation amounts were very different in the small areas, and they were likely strongly affected by geographical features. In the Kobe event case, about 70 % of the initial flow of the flash flood is from the urban area that covers only about 30 % of the entire catchment area (14 square kilo meters). In the Izu Ohoshima case, two meteorological observation stations are in the northern part and the middle part (near the damaged area) in the island, and the distance between the two stations is only 4 km. However, the quantity of observed precipitation in the middle in island was about twice as much as north.

To understand these phenomena, high resolution (several hundred meter scale resolution) numerical weather simulation is necessary. Super high resolution experiments have been made by previous studies such as tornado for limited domains, however, a numerical weather simulation with wide domain is very few due to limitation of the computational resources. We conduct super high resolution numerical weather experiments for Japan area with the K computer and JMA nonhydrostatic model.

Keywords: Numerical weather prediction model, JMA-NHM, Kei super computer

Interannual variability of Kuroshio nitrate flux and transport along western boundary in the North Pacific

SASAI, Yoshikazu^{1*} ; SASAKI, Hideharu¹ ; NONAKA, Masami¹

¹JAMSTEC

An eddy-resolving coupled physical-biological ocean model has been employed to examine the interannual variability of nitrate flux and transport mechanism by the Kuroshio during 1995-2012. The Kuroshio provides an advective flux of nitrate carried in subsurface waters, redistributing nitrate from the tropics to the mid-latitude. Some observed data capture the nitrate flux and transport in the subsurface layers by the Kuroshio. The maximum nitrate flux core appears about 400 m depth in the East China Sea, and the nitrate transport by the Kuroshio had a mean of 170 kmol s⁻¹. The model reproduces the maximum nitrate flux core in the subsurface layer from the Luzon strait to the Kuroshio Extension with the downstream. Along the vertical section of east side of Taiwan (24N), west side of Okinawa (28N), south of Kagoshima (130E), the time series of nitrate flux, volume transport, and nitrate concentration show the interannual variation. The variability of nitrate flux is strongly correlated with the variability of Kuroshio volume transport, but the nitrate concentration shows the increasing trend between 1995 and 2008. This trend may be related to the variability of nitrate concentration in the upstream of Kuroshio.

Keywords: Nitrate transport, Kuroshio, Interannual variability, High-resolution ocean physical-biological model

High Resolution, Terrain Independent Radiation Mapping

SCOTT, Thomas^{1*}

¹Interface Analysis Centre School of Physics University of Bristol

The University of Bristol has developed a terrain-independent, wide area radiation mapping system using an UAV (Unmanned Aerial Vehicle). At the heart of the system is a micro computer, carried by a semi-autonomous multi-rotor copter (drone), combining data from a lightweight gamma spectrometer, laser range finder, and GPS, to geospatially map radioactive anomalies.

Aerial vehicles can be purpose built, according to range/flight time required, payload/sensing strategy and operational environment. For example, an unmanned vehicle could be tailored for mapping over both land and sea areas, where it could land in the sea at different locations to make water based gamma measurements. The system is also adaptable for use on ground vehicles, or handheld, walking surveys.

Information is streamed in real-time, providing high resolution detail on source isotopes, intensity and location of the radiation anomaly. More than just a flying Geiger counter, the system can differentiate between natural and man-made anomalies - such as types of nuclear fuel, radioactive waste or spent munitions.

This is all achieved from a safe distance, keeping people and manned aircraft away from hazardous environments.

Examples of uses include;

*Rapid disaster response monitoring of nuclear events, providing real-time data on spread, source and intensity. This could range from site incidents to terrorist events.

*Routine monitoring of nuclear sites (internally and externally), mining operations and oil and gas facilities.

*Nuclear plants - new build: site survey and characterisation of pre and post construction and monitoring during plant life time.

*Environmental monitoring for site decommissioning.

*Environmental monitoring of war zones for spent depleted uranium munitions.

*Homeland security and nuclear material detection.

The instrument securely transmits the location, identity and intensity of radionuclide contamination to a remote operator or base station. Sub metre resolution is attainable by flying slowly, even to the point of a fixed hover, relatively close to the ground.

It can be operated manually, using traditional radio-controls or semi autonomously via programmed GPS waypoints. Grid lines are used to create survey routes that provide detailed geographical coverage of a designated area. Programming can include automated landing and take-off, such that the device can gather long exposure spectra of the region of interest.

Heat budget analysis on cooling events associated with typhoon passages in Seto Inland Sea, Japan

UCHIYAMA, Yusuke^{1*} ; NISHII, Tatsuya¹

¹Graduate School of Engineering, Kobe University

Typhoons alter coastal oceans significantly through several mechanisms including the enhanced vertical mixing through increased surface wind and waves, resulting in extensive cooling of the upper oceans. In the present study, we investigate impacts of typhoon passages with a detailed ocean modeling in particular on the temperature structure in Seto Inland Sea, the largest semi-enclosed estuary in Japan. We develop a synoptic, double nested downscaling ROMS model (Shchepetkin and McWilliams, 2005; 2008) forced by the assimilative JCOPE2 oceanic reanalysis (Miyazawa *et al.*, 2009) and JMA GPV-MSM atmospheric reanalysis for the surface momentum, heat and radiation fluxes by exploiting a bulk formula developed for COAMPS. The horizontal grid refinement occurs from 1/12 degree (JCOPE2) to 2 km (ROMS-L1) and to 600 m (ROMS-L2), where the L2 model running for about two years (2012-2013) is our test bed for the comprehensive heat budget analysis. The persistent clockwise estuarine circulation and the eastward-flowing Kuroshio are key features that cause the overall circulations of the estuary.

In the fall 2012, SST is found to decrease about two degrees for a two-week period during three consecutive typhoons passing nearby. The first EOF mode of the modeled SST corresponds to the seasonal cooling along with mixed-layer deepening, whereas the effects of the typhoons appear in higher modes. Kuroshio interacts with the topography to form standing cyclonic cold-core eddies as extracted in the second mode, resulting in intermittent eastward cold-water transport beyond the headlands. The third and fourth modes jointly represent cold water formation associated with storm-driven coastal upwelling that propagates with the estuarine circulation. Similar EOF modes are detected in the SST during the fall 2013 when two typhoons attacked the study area.

In the falls in 2012 and 2013 after the mid September when a series of typhoons pass by the estuary, the heat budget analysis exhibits that the net heat flux at surface becomes negative to induce prominent surface cooling and cold-water formation in the upper ocean. Whereas divergence of the horizontal advective heat flux is crucial in the daily-averaged heat budget, the surface net heat flux is essential to long-term temperature variation. Latent heat flux is found to play a primary role in the negative net surface flux as well as decrease of downward shortwave (solar) radiation. Unstable lowest atmospheric planetary boundary layer leads to pronounced changes in the latent heat flux in response to surface wind and abrupt decrease of the near-surface humidity after the typhoon passages.

Keywords: typhoon, estuary, heat budget analysis, EOF analysis, ROMS

Development of a hydro-ocean coupled model

KIDA, Shinichiro^{1*} ; YAMASHIKI, Yosuke²

¹Japan Agency for Marine-Earth Science and Technology, ²Kyoto University

A new hydro-oceanic coupled model is developed for examining the basic dynamics of river-ocean interaction in estuary zones during high water discharge events. These high frequency and vigorous events are not reproduced in climatological river transport data sets that are often used in ocean circulation models. The new hydro-oceanic model is based on an isopycnal layer model. It treats continental and oceanic water with separate layers but allows dynamical interaction between the two. Mixing between the two layers occurs through a Richardson number criterion. When the model is forced with Radar-Rain gauge analyzed precipitation data around eastern Japan, the model simulates the river discharge of Abukuma river basin that is analogous to observations. The abrupt changes in the water mass transport at upstream and downstream locations are well captured, showing its applicability for hydrological basin analysis. Freshwater plumes that hug along the oceanic coasts are also well captured. We find the model, based on single dynamical core, useful for both hydrological catchment and estuary mixing zone and can be used for examining the impact of weather related events.

Keywords: Ocean model, Hydrological model

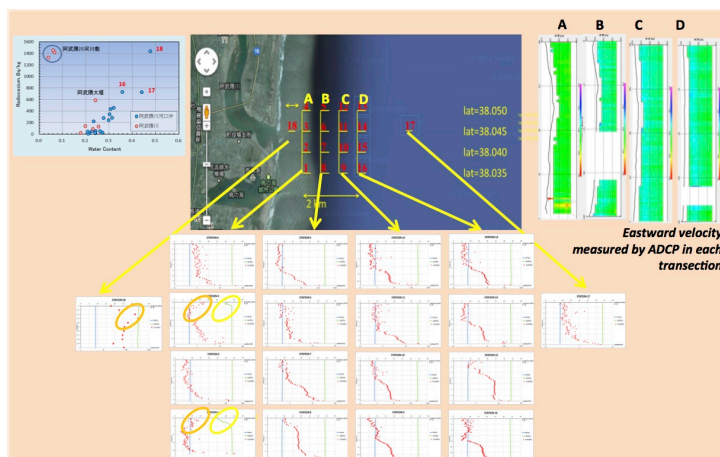
FIELD OBSERVATION ON PHYSICAL CHARACTERISTICS OF ABUKUMA RIVER ESTUARY IN SENDAI BAY

YAMASHIKI, Yosuke^{1*}; PRATAMA, Adhiraga³; VARLAMOV, Sergey⁴; MIYAZAWA, Yasumasa⁴; YAMAZAKI, Hideo⁵; ISHIDA, Masanobu⁵; NIWA, Yoshihiro⁶

¹GSAIS, Kyoto University, ²Application Laboratory, JAMSTEC, ³GSE, Kyoto University, ⁴RCGC, JAMSTEC, ⁵Kinki University, ⁶EPS, The University of Tokyo

Higher amount of radiocaesium transport from Abukuma river into Pacific Ocean, especially during the extreme events, has already estimated. The current study aims to clarify the following: i) to survey estuary mixing processes during freshwater and turbidity intrusion from Abukuma river mouth, largest river basin affected fallout, where annual radiocaesium flux reached 10 Terabecquerel during our observation in 2011-2012; ii) To identify bottom-sediment contamination along the river mouth by sediment sampling. Field observation was conducted both in March 18 and September 2-3 in Sendai Bay. Vertical temperature and turbidity, together with the salinity field are observed using fishing vessel. We analyzed also vertical velocity profile using ADCP to identify the current movement of the bay. The velocity fields in Sendai Bay of the observation date are illustrated using JCOPE2 program. Figures 1 illustrates observation points, vertical salinity, turbidity and temperature field in each points, and vertical velocity profile observed in 18 March 2013. The eastward surface current was observed in each transection line. At near bottom of the sea, westward current was observed, indicating estuary circulation. Southward surface current was observed in most of latitudinal section, weak northward bottom current was also found. Freshwater intrusion was observed on some of the stations in transection A which is located near the mouth of Abukuma River. In most of the station, turbidity peak was observed in near bottom of the sea, except in some station in transection A where the peak of turbidity was found in surface similar to the location of freshwater intrusion. Higher concentration of radiocaesium in the bottom sediment near the Abukuma river mouth is observed where fine argilliferous soil are found, much higher than that in surrounded area, giving important evidence of radiocaesium in particulate form supplied from Abukuma River. Peaks of turbidity near the river mouth were found at slightly lower position than the freshwater-saline boundary at stations 1 and 3 (March 20), implying that the occurrence of coagulation of suspended particulate matter through mixing with saline water, supporting the observed concentration found in (1).

Keywords: Abukuma river, Coastal zone, Estuary circulation, Mixing zone, Radiocaesium



Development of Satellite data manipulator for geography analysis

NAKANO, Fujio^{1*}

¹Japan Aerospace Exploration Agency, ²Kyoto University

Development of Satellite data manipulator for geography analysis

ALOS (Advanced Land Observing Satellite: common name "Daichi") carried the sensor PRISM which can observe earth surface in high accuracy, and enabled acquisition of DSM (Digital Surface Model) data. By utilizing the data acquired by such an advanced sensor, it becomes possible to display high-precision three-dimensional satellite data. Using satellite data as three dimensions means expansion of the utilization range, and it can expect unprecedented multi-functionalization. Furthermore, three-dimensional satellite data was displayed on iPad interlocked with GPS in various satellite data including ALOS data, and "Geo-Sim" which can be used also in area without communication environment was developed. Thereby, the generating situation of a mudflow or the ancient coastline is reproduced by CG, and the matching operation on-site becomes possible.

Keywords: ALOS, AVNIR-2, PRISM/DSM, DEM, Geo-Sim



Fig.1. Manipulation of 3D data on iPad display

Land-Ocean Mutual Interaction: Sediment Transportation Processes in Coastal Zone Induced by Abukuma River Mouth Runoff

TROSELJ, Josko^{1*} ; YAMASHIKI, Yosuke² ; TAKARA, Kaoru³

¹Graduate School of Engineering, Kyoto University, ²Graduate School of Advanced Integrated Studies in Human Survivability, Kyoto University, ³Disaster Prevention Research Institute, Kyoto University

1. Introduction

Modeling of a contact zone between a river coming from potentially contaminated basin and an ocean is especially sensitive case for Land-Ocean coupling interaction due to significant risk of major environmental disaster which can occur in the case of contamination of the coastal zone. Therefore, it is of great importance to study and develop integrated modeling approach to comprehend the complex interaction processes in the contact zone in order to minimize disaster risk potential, which can consequently cause undesirable social and economical costs.

2. Objectives

The focus of this study is to promote relevant numerical simulation on Land-Ocean coupling modeling approach applicable for the bay and estuary zone affected by river inflow and associated sediment transportation from the Abukuma river basin in Japan. By conducting several field observations, we found interesting and unusual temporal and spatial distribution of radionuclides within the coastal zone near the river mouth. Sediment transportation processes which have led to the distribution as well as influence of near-shore bathymetry to sediment dispersion are of close interest for the study. Calculation was conducted by simulating stages and conditions for mechanisms of sediment transport in the coastal zone, from initial deposition onto river bed to final deposition onto ocean floor, with special focus on processes which are occurring during high water periods.

3. Model Description

The modeling approach has been studied by combining river mouth runoff boundary conditions by using Lagrangian particle tracking model for simulating sediment transportation, with coupled atmosphere-ocean-land model (MSSG model, JAMSTEC) which used fine resolution grid, and associated downscaling techniques for oceanic boundary conditions (JCOPE2 model, JAMSTEC) which used coarse resolution grid. We have simulated two different cases, at first circulation of ocean itself in non-equilibrium quasi stationary state, where its dynamics was induced only by its own temperature and salinity data differences among adjacent cells, and at second response of the ocean circulation to inflow from the river outlet, simulated under various boundary conditions and external effects.

ETOPO1, 1 Arc Minute Global Relief Model was chosen as initial database for bathymetry data, while World Ocean Atlas 2005 database was chosen as initial 3D database for temperature, salinity, pressure, and velocity field data. Incompressible Navier-Stokes equation and Yin-Yang grid were used in the calculation of the flow field.

4. Conclusions and follow up

The study is continuous part of the PhD study of the first author, so the results are about to be improved as the course will continue. So far, results neither confirmed nor denied the hypothesis that near-shore bathymetry may have important role in spatial dispersion of radionuclides, so the question still remains open and subject for discussion. Our assumption is that using fine resolution grid within the contact zone between two different fluids should give us better insight into the problem, while simultaneously proper downscaling of outer oceanic boundary conditions and proper coupling with sediment transportation model are needed to be done in order to maintain satisfactory level of simulated physics of processes during the calculation. In follow up of the study, we will try to simulate hydrograph based water wave rather than constant inflow from the river mouth, as well as try to put ocean side into initial dynamic state rather than non-equilibrium quasi stationary state. Also, more focus will be aimed to the physical processes behind mechanisms of radionuclide transportation from the basin towards the river mouth.

Acknowledgements

Dr. Shinichiro Kida, executive supervisor, JAMSTEC
Dr. Keiko Takahashi, MSSG program director, JAMSTEC
Monbukagakusho (MEXT) scholarship, GCOE-HSE program

Keywords: River-ocean interaction, Integrated atmosphere-land-ocean model, Sediment transportation of radionuclides, Lagrangian particle tracking model, Near-shore bathymetry influence

modelling of radiocesium movement in catchment area of abukuma river, japan

PRATAMA, Mochamad adhiraga^{1*} ; YAMASHIKI, Yosuke² ; YONEDA, Minoru¹

¹Department of Environmental Engineering, Kyoto University, ²Graduate School of Advanced Integrated Studies in Human Survivability, Kyoto University

The great earthquake on March of 2011 followed by tsunami caused Fukushima Dai-ichi reactor meltdown which led to explosion and emission of radioactive substances into environment. As a result, Abukuma River, one of the most important rivers in Japan and its catchment area, received up to 2.25×10^6 Bq/m² of radiocesium. Previous study found that 80-90% of radiocesium influx to Abukuma River was in particulate form and it was estimated that 10 TBq of the radionuclide was released into the end point of the river, coastal sea of Sendai Bay. A lot of models of radionuclides movement had been developed, however just few models that account solid wash off process in catchment area. This study tried to simulate the influx of radiocesium into Abukuma River from its catchment area by modifying MOIRA model with addition on solid transport which was calculated with SWAT model. Deposition of the radiocesium was used as an input of the model. Then after, fixation process into surface ground, liquid wash-off by surface run off, and solid wash off by erosion are the mechanisms which govern the dynamic of the radiocesium in this model. The result at the model shows an agreement compared to the observed data. With R² value of 0.8 showed that the model could explain seasonal variability of observed data. However, as several uncertainties were observed such as quantification of storm effect and decontamination activities, further study to optimize and improve the result of the model is deemed necessary

Keywords: model, influx, radiocesium, Abukuma River

A Study of Contribution of "Nanohana Project" and Agricultural restoration in Sukagawa, Fukushima, Japan

KIMURA, Naoko^{1*}

¹GSGES, Kyoto University

This paper explores for what and to what extent "Nanohana Project" contributes to restoration in Sukagawa, Fukushima Prefecture, Japan. Since the huge earthquake and tsunami occurred in March 2011, agricultural fields in these cities have been suffering damages caused by radionuclides classified as nuclear-fission products from the Fukushima No.1 Nuclear Power Plant (Tokyo Electricity Power Company (TEPCO)) due to the accident. Agricultural field restoration, especially decontamination of radionuclides from the soil, is one of the most important issues to be tackled for local farmers. This research reviews literatures regarding and conducted an interview to an agricultural production corporation in Sukagawa in order to grasp what initiatives has been taken to reduce radionuclides in their products as well as to fight to bad rumors among general public. "Nanohana Project" has been implemented with local stakeholders in Sukagawa since 2007. They grow Nanohana (rapeseed flower or colza, Brassica Napus) and produce Biodiesel fuel (BDF) from seeds as well as biogas (BG) out of the pomace (leaves and stems after producing BDF), and they use the BDF and BG in the local area. The Nanohana absorbs some radionuclides in the soil in its growing process, and there was attention to it after disaster, however some scientific researches found that the absorption amount is limited and may not be a remedy itself for decontamination of radionuclides. Nevertheless, "Nanohana Project" has been ongoing and the network is expanding in Sukagawa. This paper discusses contribution of "Nanohana Project" and initiatives by an agricultural production corporation for restoration through qualitative analysis of interview and some key figures in order to speculate the Project's possible roles for future reconstruction in the region.

Keywords: Nanohana, decontamination, restoration, agricultural production corporation, Sukagawa

The relationship between monthly and yearly trend of Ammonia and SS loading at Rhine River and land use change

TERAMOTO, Tomoko¹ ; YAMASHIKI, Yosuke^{2*} ; TAKARA, Kaoru³

¹Department of Environmental Engineering Graduate School of Engineering Kyoto University, ²Graduate School of Advanced Integrated Studies in Human Survivability Kyoto University, ³Disaster Prevention Research Institute, Kyoto University

Rhine River is the international river, which flows through several countries, so it is important to know and maintain the water quality. To estimate the gross loading to the marine environment is necessary for assessment of the current status of the coastal zone, especially for the water quality of Bays and Estuary zone.

In this study, we estimate Ammonia SS loading at Rhine River by using GEMS/Water (Global Environment Monitoring System/ Water) Dataset and GRDC (Global Runoff Data Centre) Dataset.

The procedure of this research is three steps. First, we have used the set of discharge data obtained from GRDC to be used for the loading estimation based on the observed data. Second, the locations of GEMS/Water and GRDC station have been compared to identify appropriate station to set the calculation loading. Finally, we have multiplied concentration and discharge to get the loading.

The characteristics land use of Rhine River basin has been analyzed using the Global Land Cover Characterization dataset prepared by USGS.

For land use change of Rhine River basin has been analyzed by using landsat5 and landsat7 images.

The concentration and loading results show seven things :(1) From December to February, Ammonia concentration was higher than other months. (2) From January to march, Ammonia loading was higher than other months. (3) Ammonia concentration was gradually decreasing except through 1983 to 1987. (4) Ammonia loading was decreasing and the number suddenly dropped at 1989 (5) SS concentration was stable through 1979 to 1994 except 1983, 1984 and 1995. (6) From December to February SS loading was higher than other months. (7) SS loading was gradually decreasing and the number suddenly dropped at 1989.

The Rhine river watershed is mainly forest and grassland by analyzing land use from USGS data. This land use affects water quality

Keywords: Water Quality, loading, land use, Rhine River

NASA Earth Science and Applications

FREILICH, Michael^{1*}

¹Director, Earth Science Div. NASA Headquarters

Earth is a complex, dynamic system we do not yet fully understand. The Earth system, like the human body, comprises diverse components that interact in complex ways. We need to understand the Earth's atmosphere, lithosphere, hydrosphere, cryosphere, and biosphere as a single connected system. Our planet is changing on all spatial and temporal scales. The purpose of NASA's Earth science program is to develop a scientific understanding of Earth's system and its response to natural or human-induced changes, and to improve prediction of climate, weather, and natural hazards. A major component of NASA's Earth Science Division is a coordinated series of satellite and airborne missions for long-term global observations of the land surface, biosphere, solid Earth, atmosphere, and oceans. This coordinated approach enables an improved understanding of the Earth as an integrated system.

Over the coming decades, NASA and the Agency's research partners will continue to pioneer the use of both spaceborne and aircraft measurements to characterize, understand, and predict variability and trends in Earth's system for both research and applications. NASA Earth System Science conducts and sponsors research, collects new observations, develops technologies and extends science and technology education to learners of all ages. We work closely with our global partners in government, industry, and the public to enhance economic security, and environmental stewardship, benefiting society in many tangible ways. We conduct and sponsor research to answer fundamental science questions about the changes we see in climate, weather, and natural hazards, and deliver sound science that helps decision-makers make informed decisions. We inspire the next generation of explorers by providing opportunities for learners of all ages to investigate the Earth system using unique NASA resources, and our Earth System research is strengthening science, technology, engineering and mathematics education nationwide.

JAXA's Earth Observation Missions

NAKAMURA, Kenji^{1*} ; FUKUDA, Toru²

¹Earth Observation Research Center, Japan Aerospace Exploration Agency/Dokkyo University, ²Earth Observation Research Center, Japan Aerospace Exploration Agency

The Japan Aerospace Exploration Agency (JAXA) is promoting the Earth observation from space. JAXA is now operating GOSAT (the Green House Gases Observing Satellite) and GCOM-W1 (the Global Change Observation Mission 1st-Water). The GOSAT mission is a joint effort of JAXA, the National Institute for Environmental Studies (NIES) and the Ministry of the Environment (MOE). GOSAT has been launched in January 2009, and is equipped with the Fourier Transform Spectrometer and the Cloud Aerosol Imager providing global distribution of carbon dioxide and methane with seasonal changes. GCOM-W1 was launched in May 2012 for global water cycle observation and has the AMSR-2 (Advanced Microwave Scanning Radiometer 2). AMSR-2 follows the design of AMSR which was aboard ADEOS-2 satellite, but with improvements in antenna size and onboard calibration, etc. JAXA is also operating the Precipitation Radar (PR) aboard the TRMM (Tropical Rainfall Measuring Mission) satellite and Advanced Microwave Scanning Radiometer (AMSR-E) aboard Aqua satellite of the National Aeronautics and Space Administration (NASA). TRMM is a joint venture of JAXA and NASA. The TRMM satellite was launched in 1997 and is still in operation. The Precipitation Radar (PR) aboard the TRMM satellite is the first spaceborne radar dedicated for precipitation observation developed by JAXA and the National Institute of Information and Communications Technology, Japan (NICT). The data from PR for more than 16 years contributed much for better understanding the precipitation system climatology over tropical and subtropical regions. The Global Precipitation Measurement (GPM) which is led by JAXA and NASA with international collaboration is a multi-satellite system dedicated for the global precipitation observation. The core satellite of GPM will be launched by JAXA at the end of February 2014. JAXA has developed the dual-wavelength radar (DPR) with NICT for the GPM core satellite. DPR will observe rain including solid precipitation with better accuracy than TRMM PR. The ALOS-2 (Advanced Lang Observing Satellite-2) which is equipped with an L-band Synthetic Aperture Radar (PALSAR) is scheduled to launch in 2014. ALOS-2 is a follow-on mission from ALOS contributing to cartography, disaster monitoring, resource survey, etc. EarthCARE for cloud and aerosol observation is a collaboration mission with the European Space Agency (ESA). JAXA has developed a W-band Cloud Profiling Radar (CPR) with NICT for EarthCARE. CPR has high sensitivity to clouds with Doppler function. Using the Doppler function CPR can measure the vertical movement of clouds which is important to understand the cloudy systems. JAXA is also developing GCOM-C1 (the Global Change Observation Mission 1st-Climate) which is for surface and atmospheric measurements related to the carbon cycle and radiation budget. An SGLI (Second Generation Global Imager) will be aboard the satellite. JAXA is also studying future sensors including small sensors for the International Space Station (ISS).

Keywords: Earth observation, satellite, remote sensing

Greenhouse gas observation by GOSAT during its five-year nominal operation period

YOKOTA, Tatsuya^{1*} ; KIKUCHI, Nobuhiro¹ ; YOSHIDA, Yukio¹ ; BRIL, Andrey¹ ; OSHCHEPKOV, Sergey¹ ; INOUE, Makoto¹ ; MORINO, Isamu¹ ; UCHINO, Osamu¹ ; KIM, Heon-sook¹ ; TAKAGI, Hiroshi¹ ; SAITO, Makoto¹ ; MAKSYUTOV, Shamil¹ ; YUKI, Akira¹ ; KANEKON, Sayaka¹ ; KAWAZOE, Fumie¹ ; AJIRO, Masataka¹

¹National Institute for Environmental Studies

The Greenhouse gases Observing SATellite (GOSAT) recently completed its planned nominal operation period of five years on 23 January 2014, and it now entered the phase of extended operation. During the past five years, almost all of the GOSAT standard data products were opened to general users. These data products are publicly available and can be obtained through the GOSAT User Interface Gateway (GUIG, <http://www.data.gosat.nies.go.jp/>). From the spectral data that GOSAT collected, the concentrations of major greenhouse gases (GHGs), namely carbon dioxide (CO₂) and methane (CH₄), were retrieved, and their precisions are now at the level of much less than 1%. These concentration data are used to estimate the monthly surface fluxes of CO₂ and CH₄ on sub-continental and ocean-basin scales. The data are also utilized to monitor GHGs' temporal and spatial changes. Various reports on the results of GOSAT data analysis have appeared in peer-reviewed journals so far. The topics reported include the detection of large GHG point sources and anomalies in the inter-annual trend of CO₂ uptake by terrestrial biosphere.

In this presentation, we will summarize the five-year-long GHG observation by GOSAT and present the global distributions of the GHG concentrations and the surface flux estimates. Also, we will touch on the current status of researches conducted within the framework of the GOSAT Research Announcement.

Keywords: greenhouse gases, carbon dioxide, methane, column concentration, flux, GOSAT

The NASA Orbiting Carbon Observatory - 2 (OCO-2), the next step in CO₂ measurements from space

CRISP, David^{1*}

¹Jet Propulsion Laboratory, Caltech

Global, space-based remote sensing observations of atmospheric carbon dioxide (CO₂) and methane (CH₄) hold substantial promise for future, long-term monitoring of these important greenhouse gases. These measurements will complement those from the existing ground based greenhouse gas monitoring network with increased spatial coverage and sampling resolution. The principle challenge for this approach is the high precision and accuracy needed to resolve the small (<0.3 percent) variations in the background distributions of these gases associated with their emission sources and natural sinks. The European Space Agency (ESA) EnviSat SCIAMACHY and Japanese Greenhouse Gases Observing Satellite (GOSAT) TANSO-FTS were the first two space-based sensors designed to return high resolution spectra of the reflected sunlight in molecular oxygen (O₂), CO₂, and CH₄ bands at near-infrared wavelengths. These spectra are being analyzed to yield spatially resolved estimates of the column-averaged CO₂ and CH₄ dry air mole fractions (X_{CO_2} , X_{CH_4}) over the sunlit hemisphere. The availability of these data has already enabled substantial improvements in instrument calibration techniques, remote sensing retrieval algorithms, and data validation techniques. However, sensors with greater sensitivity, coverage, and resolution are needed to implement the space-based segment of a global greenhouse gas monitoring system.

In July of 2014, these space-based greenhouse gas pathfinders will be joined by the NASA Orbiting Carbon Observatory-2 (OCO-2). This satellite will fly at the front of the 705-km Afternoon Constellation (A-Train), along an orbit track aligned with the ground footprints of the CloudSat radar and CALIPSO lidar. Its 3-channel, imaging, grating spectrometer has been optimized to record high resolution spectra of reflected sunlight in the 765 nm O₂ A-band and in the 1610 and 2060 nm CO₂ bands. Coincident O₂ and CO₂ spectra are combined into soundings that are analyzed with a full-physics retrieval algorithm to yield estimates of X_{CO_2} with accuracies exceeding 0.3 percent over most of the Earth. The OCO-2 spectrometer will collect up to 1 million of these soundings each day along a narrow ground track as it flies over the sunlit hemisphere. Between 20 and 30% of these soundings are expected to be sufficiently cloud free to yield full-column estimates of X_{CO_2} . Even with these assets, OCO-2 is still only a research satellite, designed to validate a space-based CO₂ measurement approach. A coordinated network of satellites with similar capabilities will be needed to discriminate and quantify the CO₂ emissions from fossil fuel combustion, land use practices, and other human activities in the presence of the much larger CO₂ fluxes associated with the natural carbon cycle.

Keywords: Carbon Dioxide, Greenhouse Gases, Remote Sensing, Orbiting Carbon Observatory - 2

ACG06-05

Room:315

Time:April 28 17:30-17:45

NIES GOSAT-2 Project

MATSUNAGA, Tsuneo^{1*} ; MORINO, Isamu¹ ; YOSHIDA, Yukio¹ ; SAITO, Makoto¹

¹National Institute for Environmental Studies

GOSAT-2, a successor of Greenhouse Gases Observation Satellite (GOSAT), is currently being developed by Ministry of the Environment, Japan Aerospace Exploration Agency, and National Institute for Environmental Studies (NIES). Its target launch year is FY2018.

In the presentation, the schedule of NIES GOSAT-2 project will be introduced.

Keywords: GOSAT, GOSAT-2, satellite, greenhouse gas

Development of a 3D solar induced chlorophyll fluorescence simulator for satellite fluorescence observation

KOBAYASHI, Hideki^{1*} ; NAGAI, Shin¹ ; INOUE, Tomoharu¹ ; ICHII, Kazuhito¹

¹Japan Agency for Marine-Earth Science and Technology

Recent studies show that the vegetation canopy scale chlorophyll fluorescence can be observed from satellite, such as GOSAT and OCO-2, using Fraunhofer lines (e.g. Frankenberg et al., 2011). Satellite-based fluorescence can be used to infer the photosynthetic capacity of plant canopy. To understand how the canopy scale bidirectional fluorescence observations are related to three-dimensional fluorescence distribution within a plant canopy, it is necessary to evaluate canopy scale fluorescence emission using a detail plant canopy radiative transfer model. In this study, we developed a three-dimensional plant canopy radiative transfer model that can simulate the bidirectional chlorophyll fluorescence radiance. This modeling was based on the 3D radiative transfer model, forest light environmental simulator (FLiES) (Kobayashi and Iwabuchi, 2008). FLiES is a Monte Carlo ray-tracing model to simulate radiative field in shortwave (solar domain) and long-wave (thermal infrared) radiation in 3D landscape. To realize individual tree crown shapes, the original FLiES model used geometric objects such as cone, cylinder, and spheroid. Recently, FLiES has been extending to utilize voxel-based tree crown datasets, which are favorable to LiDAR based tree crown data sets. In this presentation, we show the current status of the development of the 3D chlorophyll fluorescence simulator.

Keywords: GOSAT, plant canopy radiative transfer model, chlorophyll fluorescence, GPP

Orbital checkout status of the DPR on the GPM core spacecraft

KOJIMA, Masahiro^{1*} ; FURUKAWA, Kinji¹ ; MIURA, Takeshi¹ ; HYAKUSOKU, Yasutoshi¹ ; KAI, Hiroki¹ ; ISHIKIRI, Takayuki¹ ; IGUCHI, Toshio² ; HANADO, Hiroshi² ; NAKAGAWA, Katsuhiko² ; OKUMURA, Minoru³

¹Japan Aerospace Exploration Agency, ²National Institute of Information and Communications Technology, ³NEC TOSHIBA Space systems

The Dual-frequency Precipitation Radar (DPR) on the Global Precipitation Measurement (GPM) core satellite was developed by Japan Aerospace Exploration Agency (JAXA) and National Institute of Information and Communications Technology (NICT). The GPM is a follow-on mission of the Tropical Rainfall Measuring Mission (TRMM). The objectives of the GPM mission are to observe global precipitation more frequently and accurately than TRMM. The frequent precipitation measurement about every three hours will be achieved by some constellation satellites with microwave radiometers (MWRs) or microwave sounders (MWSs), which will be developed by various countries. The accurate measurement of precipitation in mid-high latitudes will be achieved by the DPR. The GPM core satellite is a joint product of National Aeronautics and Space Administration (NASA), JAXA and NICT. NASA developed the satellite bus and the GPM microwave radiometer (GMI), and JAXA and NICT developed the DPR. JAXA and NICT developed the DPR through procurement. The contract for DPR was awarded to NEC TOSHIBA Space Systems, Ltd.

The configuration of precipitation measurement using an active radar and a passive radiometer is similar to TRMM. The major difference is that DPR is used in GPM instead of the precipitation radar (PR) in TRMM. The inclination of the core satellite is 65 degrees, and the flight altitude is about 407 km. The non-sun-synchronous circular orbit is necessary for measuring the diurnal change of rainfall similarly to TRMM. The DPR consists of two radars, which are Ku-band (13.6 GHz) precipitation radar (KuPR) and Ka-band (35.5 GHz) precipitation radar (KaPR). The objectives of the DPR are

- (1) to provide three-dimensional precipitation structure including snowfall over both ocean and land,
- (2) to improve the sensitivity and accuracy of precipitation measurement,
- (3) to calibrate the estimated precipitation amount by MWRs and MWSs on the constellation satellites.

The DPR consists of Ku-band (13.6 GHz) precipitation radar (KuPR) and Ka-band (35.5 GHz) precipitation radar (KaPR). The KuPR unit will measure 2.6m X 2.4m X 0.7m in size. The KaPR unit will measure 1.3m X 1.5m X 0.8m in size. Both KuPR and KaPR have almost the same design as TRMM PR. The DPR system design and performance were verified through the development test and the proto flight test. DPR has handed over to NASA and integration of the DPR to the GPM core spacecraft have completed in May 2012. GPM core spacecraft satellite system test has completed in November 2013. The results of the satellite system test concerning to the DPR satisfied system requirements.

GPM core observatory was shipped to Tanegashima Space Center, JAPAN and Launch Site Operations has started on November 2013 and GPM core observatory will be launched in February 2014. DPR orbital check out will be started in March 2014 and it will be completed in April 2014. The orbital check out status of DPR will be reported .

Keywords: GPM, DPR

Status of the Japanese Global Precipitation Measurement (GPM) Research Project

OKI, Riko^{1*} ; KACHI, Misako¹ ; KUBOTA, Takuji¹ ; MASAKI, Takeshi¹ ; KANEKO, Yuki¹ ; FURUKAWA, Kinji¹ ; TAKAYABU, Yukari³ ; IGUCHI, Toshio² ; NAKAMURA, Kenji⁴

¹JAXA, ²NICT, ³University of Tokyo, ⁴Dokkyo University

The Global Precipitation Measurement (GPM) mission is a satellite program led by Japan and the U.S., to measure the global distribution of precipitation accurately in a sufficient frequency so that the information provided by this program can drastically improve hydrological predictions, climate modeling, and understanding of water cycles. The GPM Core Observatory carries the Dual-frequency Precipitation Radar (DPR) developed by Japan Aerospace Exploration Agency (JAXA) and the National Institute of Information and Communications Technology (NICT), and the GPM Microwave Imager (GMI) developed by the National Aeronautics and Space Administration (NASA). The frequent precipitation measurement about every three hours will be achieved by constellation satellites with microwave radiometers or microwave sounders, which will be developed by international partners. JAXA also provides the Global Change Observation Mission (GCOM) 1st ? Water (GCOM-W1) named "SHIZUKU," launched on May 18, 2012, as one of constellation satellites.

The Japanese GPM research project conducts scientific activities on algorithm development, ground validation, application research including production of research products. In addition to those activities, we promote collaboration studies in Japan and Asian countries, and seek potential users of satellite precipitation products. JAXA develops the DPR Level 1 algorithm, and the NASA-JAXA Joint Algorithm Team develops the DPR Level 2 and DPR-GMI combined Level2 algorithms. JAXA also develops the Global Rainfall Map algorithm, which is a new version of the Global Satellite Mapping of Precipitation (GSMaP), as one of national products to distribute hourly and 0.1-degree horizontal resolution rainfall map. In the GPM era, the GSMaP algorithm will be improved by refining rainfall retrievals over land, considered the orographic rainfall effects, added the rain gauge corrected rainfall product. In the future, information from the Dual-frequency Precipitation Radar (DPR) will be compiled as a database to improve the retrieval accuracy of weak rainfall in mid-to-high latitudes.

The GPM Core Observatory is scheduled to be launched from the JAXA Takengashima Space Center by the H-IIA F23 rocket around 3:07 a.m. thru 5:07 a.m. (JST) on February 28 (Fri.,) 2014. After the initial checkout (about 2-month,) calibration and validation of the DPR, GMI and other products will be implemented toward the public release of all products to general users. Data release date is currently scheduled to be 6-month after the launch.

Keywords: GPM, DPR, GSMaP, ground validation

Initial validation results of Dual-frequency Precipitation Radar on Global Precipitation Measurement Core Observatory

KUBOTA, Takuji^{1*}; IGUCHI, Toshio²; SETO, Shinta³; AWAKA, Jun⁴; URITA, Shinji⁵; YOSHIDA, Naofumi⁵; OKI, Riko¹

¹Japan Aerospace Exploration Agency, ²National Institute of Information and Communications Technology, ³Nagasaki University, ⁴Tokai University, ⁵Remote Sensing Technology Center of Japan

The Global Precipitation Measurement (GPM) Mission consists of a Tropical Rainfall Measuring Mission (TRMM)-like non-sun-synchronous orbiting satellite (GPM Core Observatory) and a constellation of satellites carrying microwave radiometer instruments. The GPM Core Observatory, which will be launched in 28 February 2014, carries the Dual-frequency Precipitation Radar (DPR) developed by the Japan Aerospace Exploration Agency (JAXA) and the National Institute of Information and Communications Technology (NICT). The DPR consists of two radars; Ku-band (13.6 GHz) precipitation radar (KuPR) and Ka-band (35.55 GHz) radar (KaPR). The DPR is expected to advance precipitation science by expanding the coverage of observations to higher latitudes than those obtained by the TRMM Precipitation Radar (PR), by measuring snow and light rain via high-sensitivity observations from the KaPR, and by providing drop size distribution (DSD) information based on the differential scattering properties of the two frequencies. For operational productions of precipitation datasets, it is necessary to develop computationally efficient, fast-processing DPR Level-2 (L2) algorithms that can provide estimated precipitation rates, radar reflectivity factors, and precipitation information, such as the DSD and precipitation type. The L2 algorithms have been developed by the DPR Algorithm Development Team under the NASA-JAXA Joint Algorithm Team.

Before the launch of the GPM Core Observatory, synthetic DPR Level-1 (L1) data are needed as a test bed for the DPR L2 algorithms. In this work, we use data simulated from the TRMM/PR. The primary advantage is that measured Ku-band data from the TRMM/PR, obtained under a wide variety of meteorological conditions, forms the basis of the simulation. As such, the results can be compared directly to the standard TRMM/PR retrievals. Thus, "at-launch" codes of DPR precipitation algorithms, which will be used in GPM ground systems at launch, were evaluated using synthetic data based upon the TRMM/PR data. Results from the codes (Version 4.20131010) of the KuPR-only, KaPR-only, and DPR algorithms were compared with "true values" calculated based upon drop size distributions assumed in the synthetic data and standard results from the TRMM algorithms at an altitude of 2 km over the ocean. The results indicate that the total precipitation amounts during April 2011 from the KuPR and DPR algorithms are similar to the true values, while the estimates from the KaPR data are underestimated. By analysis results, the underestimation of the KaPR can be caused by a problem in the attenuation correction method. This was verified by the improved codes (Version 4.20131129), and so this problem has been resolved in the latest version.

After the launch, calibration and validation of the DPR products will be implemented toward the public release of all products to general users. Data release date is currently scheduled to be 6-month after the launch. In this work, we introduce initial validation results of the DPR-L2 product, mainly based upon comparisons of the TRMM/PR product.

Keywords: Global Precipitation Measurement, Dual-frequency Precipitation Radar, algorithm, validation

Expectations for the Global Precipitation Measurements for Precipitation Sciences

TAKAYABU, Yukari^{1*} ; OKI, Riko² ; IGUCHI, Toshio³ ; AONASHI, Kazumasa⁴ ; KACHI, Misako² ; KUBOTA, Takuji² ; HAMADA, Atsushi¹ ; TAKAHASHI, Nobuhiro³ ; NAKAMURA, Kenji⁵

¹The University of Tokyo, ²Japan Aerospace Exploration Agency, ³National Institute of Information and Communications Technology, ⁴Meteorological Research Institute, Japan Meteorological Agency, ⁵Dokkyo University

Three dimensional precipitation data observed with Ku (13.8GHz) band Precipitation Radar (PR) on board the Tropical Rainfall Measurement Mission (TRMM) satellite have enabled us to discover various precipitation characteristics over the tropics and subtropics between 36N and 36S. Precipitation system regimes are estimated with precipitation characteristics. The multiple instrument observations of TRMM have also made us quantify the discrepancies between TRMM Microwave Imager (TMI) vs. PR estimated rainfall, and provided us with opportunities to investigate various approaches to improve the rainfall retrieval algorithms.

With the launch of the GPM/DPR, scheduled in February 2014, dual band measurements from space with Ku (13.6GHz) and Ka (35.5GHz) band frequencies will be started. Increasing information of the drop size distributions with DPR should improve the accuracy of precipitation profile structures, which are essential to study precipitation characteristics. GPM/DPR will provide excellent cross calibrations for constellation microwave observations to construct better mapping of precipitation from 65N to 65S, which covers 91% of the earth surface. Weak rainfall measurements will enable us better energy budget calculations after all, as well as more precise examinations of rainfall system lifecycles. We can also expect reexamination and further improvements of TRMM PR rainfall products by comparing Ku-band retrievals with DPR retrievals.

Three dimensional satellite measurement of precipitation at mid-to-high latitudes is a completely new scientific experiment. Since the precipitation systems there are very different from those in the tropics and subtropics, we can certainly expect further scientific discoveries to improve our knowledge of precipitation characteristics with thorough observations from the satellite. Using this outcomes, we also expect to provide useful knowledge to improve the numerical models for weather predictions and climate projections.

Keywords: GPM, DPR, Precipitation Science, TRMM, precipitation characteristics, satellite constellation

The Global Precipitation Measurement (GPM) Mission: Advancing precipitation measurement for science and society

KIRSCHBAUM, Dalia^{1*}

¹NASA Goddard Space Flight Center

Too much or too little rain can serve as a tipping point for triggering catastrophic flooding and landslides or widespread drought. Knowing when, where and how much rain is falling globally is vital to understanding how vulnerable areas may be more or less impacted by these disasters. Global Precipitation Measurement (GPM) is an international satellite mission to provide next-generation observations of rain and snow worldwide every three hours. The foundation of the GPM mission is the Core Observatory satellite provided by NASA and JAXA. This satellite, launching in early 2014, carries advanced instruments that will set a new standard for precipitation measurements from space. The Core satellite will measure rain and snow using two science instruments: the GPM Microwave Imager (GMI) and the Dual-frequency Precipitation Radar (DPR). The GMI captures precipitation intensities and horizontal patterns, while the DPR provides insights into the three dimensional structure of precipitating particles. Together these two instruments provide a database of measurements against which other partner satellites' microwave observations can be meaningfully compared and combined to make a global precipitation dataset.

Data collected from the Core satellite serves as a reference standard that will unify precipitation measurements from research and operational satellites launched by a consortium of GPM partners in the United States, Japan, France, India, and Europe. The GPM constellation of satellites can observe precipitation over the entire globe within 3 hours of acquisition. The GPM mission will help advance our understanding of Earth's water and energy cycles, improve the forecasting of extreme events that cause natural disasters, and extend current capabilities of using satellite precipitation information to directly benefit society.

Development of attenuation correction method for GPM/DPR

SETO, Shinta^{1*} ; IGUCHI, Toshio²

¹Graduate School of Engineering, Nagasaki University, ²National Institute for Information and Communications Technology

A new attenuation correction method is developed for the Dual-frequency Precipitation Radar (DPR) on the core satellite of the Global Precipitation Measurement (GPM) mission. Hitschfeld and Bordan's attenuation correction method (HB method) assumes relation between the specific attenuation k and the effective radar reflectivity factor Z_e (k-Ze relation) as $k=aZ_e^b$. The new method is based on HB method, but k-Ze relation is modified as $k=eaZ_e^b$ by using dual-frequency ratio of Z_e (DFR) and surface reference technique (SRT). Therefore, the new method is called HB-DFR-SRT method (H-D-S method in short). While the authors' previous attenuation correction method called HB-DFR method (H-D method in short) results in underestimation of precipitation rates for heavy precipitation, H-D-S method and its improved version try to correct the negative bias by means of SRT. When only single-frequency measurement is available, H-D-S method can be easily switched to HB-SRT method (H-S method in short), which is similar to the attenuation correction method used in the TRMM/PR standard algorithm.

The attenuation correction methods are tested with a simple synthetic dataset of DPR. As long as SRT gives the perfect estimates of path integrated attenuation (PIA) and the parameters of k-Ze relation (a and b) are given properly so that e could be vertically constant, H-S method is much better than the dual-frequency methods. In reality, SRT has error and we cannot give the parameters of k-Ze relation properly so that e should be vertically variable. Tests with SRT error and vertical variation of e show that H-D method is better than H-S method for weak precipitation but H-S method is better than H-D method for heavy precipitation. It is because SRT is unreliable for weak precipitation and DFR is unreliable for heavy precipitation. H-D-S method shows not the best but stable results for both weak and heavy precipitation, and it may work well for medium precipitation. Quantitative evaluation should be done with real measurement dataset of DPR.

Keywords: DPR, GPM, attenuation correction

Analysis of rain characteristics by using CloudSat and TRMM/PR

TAKAHASHI, Nobuhiro^{1*}

¹National Institute of Information and Communications Technology

Spaceborne cloud/precipitation radars are suitable for understanding the global climate (especially precipitation in this study) that means both the average figure of the Earth climate and the local climate in the global climate. In terms of precipitation climatology, major parameters are the precipitation amount and its diurnal/seasonal changes as well as the drop size information that is a kind of proxy of the precipitation processes such as warm/cold rain. The purpose of this study is to develop the climate map of precipitation by using CloudSat that equips W-band (94 GHz) radar and TRMM/PR that equips Ku-band (13.8 GHz) radar; rain amount is estimated by the TRMM/PR level 2 product (2A25) and the drop size information is obtained by combining the CloudSat and TRMM/PR. The basic idea of the analysis method is to compare the histograms of radar reflectivity factor (Z) at near-surface range bin at the overlapping Z range (weak to moderate rain echo). Because the both satellites have different orbit, only the statistical approach is available. Since the different Mie scattering effect appears for the different frequency and drop size, the Z value of rainfall is different between w- and Ku-band radar observations and it reflects the difference in the histograms of w- and Ku-band. Based on these characteristics, drop size information is estimated by comparing the histograms. In this study, median diameter (D_0) is estimated. For the comparison of the estimation, D_0 is estimated by TRMM/PR only.

Climate data are created in 10 x 10 degrees in latitude and longitude boxes and each box consists of the unconditional and conditional rain rate (the former corresponds the rain amount) and D_0 (median diameter) both from the CloudSat-TRMM/PR combined analysis and TRMM/PR-only analysis for every seasons (DJF, MAM, JJA, and SON), diurnal cycle (night time/day time orbit) and over land or ocean.

The results show that the general characteristic of global maps of D_0 through the year and local time is apparent land-ocean contrast; larger D_0 appears over land and smaller D_0 appears over ocean except for relatively small D_0 over southeastern Asia to China. Also, relatively larger D_0 appears in tropical area and mid latitude summer. Diurnal change of D_0 can be seen by comparing the day/night time D_0 ; D_0 is larger in the night time over ocean while day time D_0 is larger over land. Tropical Ocean shows smaller seasonal change, while larger changes are seen over mid-latitude area. Comparison of the two estimates of D_0 between CloudSat-TRMM/PR combined estimation and TRMM/PR-only estimation.

Since the Dual-frequency Precipitation Radar (DPR) onboard Global Precipitation Measurement (GPM) core satellite, which is launched in February 2014, can estimate the drop size distribution (DSD), the approach in this study can be useful of evaluation of the algorithm for DSD estimation.

Keywords: rain, drop size distribution, CloudSat, TRMM

Characteristic differences between the heaviest rainfall and the strongest convection

HAMADA, Atsushi^{1*} ; TAKAYABU, Yukari¹

¹Atmosphere and Ocean Research Institute, The University of Tokyo

Regional and seasonal differences in the rain characteristics between rain-rate and convection extreme events are examined using 11-yr measurements from the Precipitation Radar (PR) onboard the Tropical Rainfall Measuring Mission (TRMM) satellite. After defining a rainfall event as a set of contiguous rainy pixels of TRMM PR measurements, three different types of regional extreme rainfall events are defined, using the maximum values of near-surface rainfall rate (NSR) and 30-dBZ echo top height (ETH30) in rainfall event; Rainfall events of which the maximum NSR is within top 0.1% at a grid but the ETH30 is not are defined as R-only extreme events, those of which the maximum ETH30 is within top 0.1% but the NSR is not are defined as H-only extreme events, and those of which both of the maximum NSR and maximum ETH30 are within top 0.1% are defined as RH extreme events. This is done on a local basis with 2.5 x 2.5 degree horizontal resolution to examine regional extreme events.

It is shown that the fractional occurrence of RH extreme events are less than 30% in most regions, indicating that only a few dozen percent of convection extremes are related to rain rate extremes. There are robust differences in echo profiles, rainfall characteristics, and local environments between R-only and H-only extreme events. These characteristic differences are basically independent on region and season, except for their seasonal occurrence. R-only extreme events exhibit lower echo-top height than H-only extremes, linear downward increase of radar reflectivity (Z_e) below freezing level, and sharp upward decrease of Z_e in 5-7 km, whereas H-only extreme events exhibit slight downward decrease of Z_e below freezing level. R-only extreme events are almost in phase with mean monthly rainfall, while H-only extremes tend to peak slightly out of phase with rainy season. Local environments related to R-only extremes are less convectively unstable, wetter in the low-middle troposphere, and larger moisture flux convergence in the lowermost troposphere, compared with those related to H-only extremes. The features related to R-only extreme events imply a dominance of warm-rain process.

Keywords: precipitation, extreme event, TRMM

The next-generation GSMaP MWI precipitation retrieval algorithm

AONASHI, Kazumasa^{1*}

¹Meteorological Research Institute Japan Meteorological Agency

1. Introduction

The current GSMaP Microwave Imager (MWI) precipitation retrieval algorithm degrades retrieval accuracy for weak precipitation areas where MWI brightness temperatures (TBs) are sensitive to physical variables other than precipitation. In order to address this issue, we have been developing a new algorithm that retrieves the physical variables including precipitation from MWI TBs. The basic idea of this algorithm is to derive the statistically optimal values of the physical variables, based on Bayes's theorem (Elsaessar and Kummerow 2008, Boukabara et.al 2011). We adopted an ensemble-based variational method (EnVA) for deriving the optimal values from MWI TBs that are non-linear functions of the physical variables. The retrieval algorithm consists of the precipitation detection part and the retrieval part for physical variables in precipitation areas. In this presentation, we will report the precipitation detection part.

2. Precipitation detection part

In the precipitation detection part, we chose surface temperature (Ts), sea surface wind speed (SWS), precipitable water content (PWC), and cloud liquid water content (CLWC) as the over-sea control variables, Ts and surface emissivity (Es) as the over-land control variables, assuming no precipitation.

The EnVA employed forecasts of a cloud-resolving model (CRM) as the first guess of the physical variables, and estimated the first guess error covariance from CRM ensemble forecast. The EnVA calculated innovations and post-fit residuals of MWI TBs that were then used for the precipitation detection.

Keywords: GSMaP, MWI, GPM, GCOMW, precipitation retrieval

Gage Adjusted Global Satellite Mapping of Precipitation (GSMaP Gauge)

MEGA, Tomoaki^{1*} ; USHIO, Tomoo¹ ; KUBOTA, Takuji² ; KACHI, Misako² ; AONASHI, Kazumasa² ; SHIGE, Shoichi⁴

¹Graduate School of Engineering, Osaka University, ²Japan Aerospace Exploration Agency, ³Meteorological Research Institute, ⁴Graduate School of Science, Kyoto University

Fresh water is one of the most important resources for human. Precipitation is the main source of fresh water. Precipitation is also heating atmosphere by latent heat and one of important energy transport mechanism of atmosphere. Knowledge of world precipitation activity is important information for not only human activity, but also earth science.

Passive Microwave Radiometer (PMR) is a small and low power consumption sensor, thus many space-borne PMRs observe precipitation from low earth orbit. Space-born PMR provides uniform quality and stable observation data all over the world. PMR have become the precipital sensors for global precipitation retrieval, since these emission and scattering signals have a more direct relationship with precipitation rates than infrared radiometer (IR). The Global Satellite Mapping of Precipitation (GSMaP) project is developing PMR algorithm to provide global precipitation map with space-born PMRs. The GSMaP's goal is to develop the algorithm of high precision and eventually to produce a global precipitation map with high temporal (one hour) and special resolution (0.1 degree). PMR swathes, however, do not cover all surface in one hour. Therefore, it is necessary to utilize a gap-filling technique to generate precipitation maps with high temporal resolution. GSMaP derives Moving Vector (MV) from two successive IR images. GSMaP algorithm interpolates precipitation between gaps when PMRs overpass successive swath with MV by Kalman-filter. GSMaP algorithm now produces 0.1-grid-resolution precipitation map every one hour. Some evaluations, however, show the tendency of underestimation compared to some ground based observations, because PMR precipitation estimation over land has difficulty due to emission variability in surface. Rain gauge provides reliable data, and a rain gauge collects precipitation for certain period at a fixed location. PMR observes signals from precipitation instantaneously. We are developing the GSMaP gauge adjusted product (GSMaP Gauge). The GSMaP Gauge algorithm fits the GSMaP precipitation map to NOAA Climate Prediction Center (CPC) global rain gauge data set. The CPC data set is provided daily with low resolution (0.5-grid-degree). Quality of the CPC data set is not uniform (Quality of gauge-based analysis depends on density of rain gauge). We fill the gap of the precipitation estimation between the satellite and rain gauge attributable to the retrieval difficulty, the spatial and temporal resolution difference. The GSMaP Gauge succeeded to reduce the under estimation of the GSMaP algorithm. In this presentation, we introduce the GSMaP Gauge and its performance.

Keywords: Precipitation, Satellite observations, Microwave observations, Remote sensing

Current Status of the Products of AMSR2 on GCOM-W1 Satellite

OKI, Taikan^{1*} ; KACHI, Misako² ; NAOKI, Kazuhiro² ; HORI, Masahiro² ; MAEDA, Takashi² ; IMAOKA, Keiji²

¹Institute of Industrial Science, The University of Tokyo, ²Earth Observation Research Center, Japan Aerospace Exploration Agency

The Advanced Microwave Scanning Radiometer 2 (AMSR2), on board the first generation satellite of Global Change Observation Mission - Water (GCOM-W1 or "SHIZUKU") satellite, is multi-frequency, total-power microwave radiometer system with dual polarization channels for all frequency bands. The GCOM-W1 satellite was launched on May 18, 2012 (JST), and has started scientific observation since July 3, 2012. After the calibration and validation phase, which confirmed that all the pre-defined release accuracies are satisfied, the AMSR2 bright temperature product (Level 1) and geophysical parameter product (Level 2) were released to public since January 2013 and May 2013, respectively.

Monitoring and validation of the AMSR2 geophysical parameters have been continued for further improvements of the observation accuracy in future algorithms. For example, the precipitation product is validated by comparing with the Precipitation Radar (PR) on board the Tropical Rainfall Measuring Mission (TRMM) satellite, and relative errors were 48% over ocean and 88 % over land for the period from September 1, 2012 to August 31, 2013.

Quality control (QC) of in-situ data is also improved for the better validation. New QC method for buoy data, which is used in the validation of the sea surface temperature (SST) and sea surface wind speed products, is introduced to remove unreliable in-situ observation data from comparisons, including overlap check, movement speed check, comparison with numerical model, and statistical check by Bayes' theorem. Those efforts will contribute to improve the algorithm for future version-up.

The AMSR2 standard products have been distributed through the GCOM-W1 Data Providing Service (<https://gcom-w1.jaxa.jp/>), and quick look of the products, browse images of all AMSR2 brightness temperatures and geophysical parameters are available at the JAXA Satellite Monitoring for Environmental Studies (JASMES) for Water Cycle (<http://kuroshio.eorc.jaxa.jp/JASMES/WC.html>).

Keywords: earth observation, hydrologic cycles, geophysical products, validation, data distribution

Applications of ocean surface wind direction signals in microwave imager observation for atmospheric humidity analysis

KAZUMORI, Masahiro^{1*}

¹Japan Meteorological Agency

An empirical relative wind direction (RWD) model function was developed to represent azimuthal variations of oceanic microwave brightness temperatures of vertical and horizontal polarizations. The RWD model function was based on measurements of observed brightness temperature from the Advanced Microwave Scanning Radiometer and wind vector from SeaWinds, both on board the Advanced Earth Observing Satellite - II, and Special Sensor Microwave Imager Sounder (SSMIS) first guess departure and wind vector data in European Centre for Medium-Range Weather Forecasts (ECMWF) Integrated Forecasting System. The model function was introduced to a microwave ocean emissivity model; a FAST microwave Emissivity Model (FASTEM) in a radiative transfer model for satellite radiance assimilation. Performances of the RWD model function were much more realistic than present azimuthal model functions in FASTEM for low wind speed and high frequency channels.

An assimilation experiment using the RWD model function was performed in the ECMWF system. The experiment demonstrated reductions of first guess departure biases arising from modelling of the azimuthal variations in areas of high wind speed and low variability of wind direction. For example, bias reductions in ascending and descending SSMIS 19 GHz vertical polarized brightness temperature in Somali jet at the Arabian Sea were approximately 0.6 K and 0.7 K. The bias reductions were found for all assimilated microwave imager channels in a wide wind speed range. Moreover, analysis increments of specific humidity in the lower troposphere were reduced (e.g., 0.3 g kg⁻¹ reduction at 1000 hPa in the Somali jet). We found improvements of relative humidity and temperature in short-range forecasts in the lower troposphere. The experiment results clearly showed the importance of modelling the azimuthal variation of emissivity for assimilation of microwave imager observations. The RWD model function should be included in the radiative transfer model used in the microwave radiance assimilation observation operator.

Polar Research using Satellite Microwave Remote Sensing

ENOMOTO, Hiroyuki^{1*} ; ALIMASI, Nuerasimuguli¹ ; SURDYK, Sylviane¹ ; FUJITA, Shuji¹ ; YABUKI, Hironori² ; SUGIMURA, Takeshi¹ ; SUGIYAMA, Shin³ ; HOLMRUND, Per⁴ ; INGVANDER, Susanne⁴

¹National Institute of Polar Research, ²JAMSTEC, ³Hokkaido University ILTS, ⁴Stockholm University

Satellite Microwave remote sensing is the powerful tool to investigate polar regions. The data enables monitoring and surveying ice sheet, sea ice, snow cover conditions for large scale and continuous monitoring in the changing climate, and studying their changing mechanisms. Satellite passive microwave observation has almost 30-years long data set which contribute climatological study. The recent GCOM-W data is useful for more precise investigations.

For the Arctic study, GRENE Arctic climate research project(2011-2016) has started by integrating Japanese scientific activities. satellite microwave data is very important to this project since satellite data expands availability of site data to large area and long term. The Arctic project enhances interdisciplinary study and collaboration between modelling and observation. Multi-disciplinary information and scale-upping by satellite is very important.

Keywords: Polar region, Arctic, Antarctic, Cryosphere, satellite, Microwave

Sea-ice production in Antarctic coastal polynyas estimated using AMSR-E data

NIHASHI, Sohey^{1*}; OHSHIMA, Kay I.²

¹Department of Mechanical Engineering, Tomakomai National College of Technolog, ²Institute of Low Temperature Science, Hokkaido University

Coastal polynyas are newly-forming sea-ice areas formed by divergent ice drift due to prevailing winds and/or ocean currents. In coastal polynyas, huge amounts of heat flux from the ocean to the atmosphere occur because the heat insulation effect of sea-ice is greatly reduced in the case of thin ice, and accordingly sea ice is formed actively. Dense water formed in Antarctic coastal polynyas with the intense sea-ice production is a major source of Antarctic Bottom Water, which is a key player in the global climate system.

In this study, an algorithm for estimating daily thin ice thickness is developed based on a relationship between polarization ratios (PR) of AMSR-E brightness temperatures (TBs) and thermal ice thickness. The TBs at 89 GHz and 36.5 GHz are used. The thermal ice thickness is based on heat flux calculation using ice surface temperatures derived from satellite thermal infrared images. We used cloud-free MODIS images.

In the Antarctic Ocean, landfast sea-ice (fast ice), which is stationary sea ice attached to coastal features such as grounded icebergs, is formed along the coast. Antarctic coastal polynyas tend to be formed adjacent to fast ice. The AMSR-E ice thickness algorithm possibly mis-classifies fast ice as thin ice, because the PR values of thin ice and fast ice are similar. Thus, also the fast ice detection algorithm is developed. Monthly fast ice extent is detected based on microwave characteristics that the horizontally- and vertically-polarized TBs of fast ice tend to be lower than those of thin ice and are similar to those of ice sheet close to the coast.

The spatial resolution of AMSR-E is about 6.25 km, and the pixel density is four times higher than that of SSM/I which has been used in previous studies. This advantage is critical for the coincident detection and monitoring of coastal polynyas and fast ice because their areal extent is fairly small (tens to a hundred kms at most). The accuracy of the created AMSR-E dataset is validated from comparisons with backscatter images acquired by ASAR on Envisat.

Sea-ice production in Antarctic coastal polynyas is estimated based on heat flux calculation using the AMSR-E dataset. For the estimation, it is assumed that heat from the ocean below is negligible and that all of the heat loss to the atmosphere goes towards freezing. The sea-ice production estimated using the AMSR-E data has been improved from the SSM/I ice production because of the finer spatial resolution. First, the AMSR-E data can better resolve the high production area close to the coast. Second, false sea-ice production in the fast ice pixels mis-included by SSM/I is corrected because AMSR-E can detect fast ice that cannot be resolved by SSM/I. In fact, the total sea-ice production in each polynya by AMSR-E does not change much from the SSM/I ice production for many polynyas because these two effects of opposite direction compensate for each other. The AMSR-E dataset presented in this study would give the boundary/validation data of sea-ice production and fast ice for modeling studies.

Keywords: AMSR-E, Antarctic Ocean, Coastal polynyas, Sea-ice production, Antarctic Bottom Water

A proposal of mission combining active and passive microwave sensors and its applications for global water cycle

EBUCHI, Naoto^{1*}

¹Hokkaido University

A mission carrying active and passive microwave sensors is proposed to monitor the global water cycle and air-sea coupling. The passive microwave sensor will be a successor of AMSR2 on GCOM-W2, which was launched by JAXA on 12 May 2012. Channels to observe solid precipitation will also be added to AMSR2. The active sensor will be a scatterometer at operated at Ku- and Ka-bands. The Ka-band scatterometer can measure vector wind fields near the coasts with higher spatial resolution than the Ku-band scatterometer, which is similar to SeaWinds on QuikSCAT and ADEOS-II and OSCAT on Oceansat-2. Merits of the combination of the active and passive microwave sensors will be discussed in aspects of sensor and science synergisms. The microwave radiometer contributes to improve accuracy of vector wind measurements by the scatterometer under rain conditions. The wind direction provided by the scatterometer improves accuracy of the SST, water vapor and precipitation measured by the radiometer. The science synergy includes applications for studies of monsoon, tropical cyclones, air-sea coupling in various scales, global and regional water cycles, sea ice, soil moisture and snow over land.

Keywords: remote sensing, microwave radiometer, microwave scatterometer, water cycle, air-sea interaction

Upwelling events at the western African coast related to atmospheric structures: An analysis with satellite observations

DESBIOLLES, Fabien^{1*} ; BLANKE, Bruno¹ ; BENTAMY, Abderrahim²

¹Laboratoire de Physique des Océans (LPO), UMR 6523 CNRS-Ifremer-IRD-UBO, Brest, France, ²Laboratoire d'Océanographie Spatiale (LOS), IFREMER, centre de Brest, France

Satellite scatterometers provide continuously valuable surface wind speed and direction estimates over the global ocean on a regular grid both in space and time. The Level 3 data derived from the Advanced Scatterometer (ASCAT), available at $1/4^\circ$ spatial resolution (hereafter AS25), and Quick Scatterometer (QuikSCAT), available on $1/2^\circ$ and $1/4^\circ$ horizontal grids (QS50 and QS25 respectively), are studied at regional scales in both the Benguela and Canary upwelling systems. They are compared to the European Center for Medium-Range Weather Forecast surface wind analysis, with insight into their intrinsic and effective spatial resolutions. In the coastal band, the finest spatial patterns are found in the QS25 winds and are $O(75\text{km})$. This demonstrates the sensitivity of the high-resolution satellite-derived winds to coastal processes related to sea surface temperature (SST) perturbations and land-sea transition. More specifically, mesoscale coupling processes between SST and winds play a leading part in structuring the wind stress curl in both the Canary and Benguela upwelling systems. These processes act especially over the upwelling extension zone ($O(100\text{km})$ off the coast). Next, short-lived upwelling episodes (SUEs) calculated from SST anomalies are defined consistently with the QS25 effective resolution. These cold events refer to local, short-lived perturbations that add to seasonal upwelling variability. We characterize concomitant atmospheric synoptic conditions for SUEs identified at chosen latitudes and highlight two subregions in both upwelling systems, with contrasted patterns for the alongshore wind stress component and curl. The complexity of the latter patterns is closely linked to local, short-term SST variability. Closer to the shore, wind stress curl patterns derived from QS25 are only loosely related to SST/wind interactions and, as a working hypothesis, can also be associated with orographic effects that may play an important role in cooling processes. The derivation of a realistic coastal wind drop-off from satellite observations is an almost impossible task, first because a blind zone at the coast, second because the horizontal scales of pure orographic effects (a few tens of kilometers) are finer than the effective resolution of the satellite-derived product ($\sim 75\text{km}$). However, an alternative assessment can be given by evaluating the ocean response to contrasted coastal wind profiles. Numerical sensitivity experiments show that the imbalance between Ekman transport and Ekman pumping has an impact on ocean dynamics: a reduction of the wind in the QS25 forcing, partly induced by orography, contributes to SST cooling.

Keywords: scatterometry, upwelling dynamics, SST/Wind Interactions, orography effects, air-sea coupling

The GNSS Ocean Winds and AIS Mission, An Earth Science and Marine Safety Satellite Constellation

ROSE, Randall^{1*} ; GLEASON, Scott¹ ; RUF, Christopher² ; KITAZAWA, Yukihiro³ ; TANIMOTO, Kazuo⁴

¹Southwest Research Institute, ²University of Michigan, ³IHI Corporation, ⁴Meisei Electric Co., Ltd.

Recent developments in electronics and nano-satellite technologies combined with modeling techniques developed over the past 20 years have enabled a new class of remote wave and wind sensing capabilities that offer markedly improved performance over existing observatories while opening avenues to new applications. Most existing space borne ocean wind observatories operate in the C and Ku-bands which obscures key information about the ocean and the global climate. Using GNSS-based bi-static scatterometry performed by a constellation of nano-satellites, ocean wave and wind data can be provided with unprecedented temporal resolution and spatial coverage across the full dynamic range of ocean wind speeds in all precipitating conditions.

The NASA Cyclone Global Navigation Satellite System (CYGNSS) is a space borne mission being developed to study tropical cyclone inner core processes. CYGNSS consists of 8 GPS bi-static radar receivers to be deployed on separate nano-satellites in October 2016. It is anticipated that numerous additional Earth science applications can also benefit from the cost effective high spatial and temporal sampling capabilities of GNSS remote sensing. These applications include monitoring of rough and dangerous sea states, global observations of sea ice cover and extent, meso-scale ocean circulation studies, and near surface soil moisture observations.

The Automatic Identification System (AIS) is a maritime system used for global identification and tracking of ships. It is proposed as part of the GNSS Ocean Winds and AIS (GOWA) nano-satellite constellation concept to combine and improve upon the GNSS remote sensing capability of CYGNSS with a space based AIS system. GOWA will be capable of monitoring both the ocean roughness and the locations of ship traffic at the same time. This will result in both an increase in maritime safety and valuable Earth science measurements of ocean winds, sea ice and land surfaces.

This presentation will present a summary of the CYGNSS mission and plans for future instrument development to increase the number of science observations. The goal of this development is to enable the GOWA mission being proposed for Japanese science and maritime safety applications.

Keywords: GNSS, Earth Science, Remote Sensing, Satellites, GPS

Development of Cloud Profiling Radar (CPR) for Earth Clouds, Aerosols and Radiation Explorer (EarthCARE) mission

SEKI, Yoshihiro^{1*} ; TOMITA, Eiichi¹ ; KIMURA, Toshiyoshi¹ ; NAKATSUKA, Hirotaka¹ ; AIDA, Yoshihisa¹ ; OKADA, Kazuyuki¹ ; IIDE, Yoshiya¹ ; KADOSAKI, Gaku¹ ; TAKAHASHI, Nobuhiro² ; OHNO, Yuichi² ; HORIE, Hiroaki² ; SATO, Kenji²

¹Japan Aerospace Exploration Agency, ²National Institute of Information and Communications Technology

Earth Clouds, Aerosols and Radiation Explorer (EarthCARE) is a Japanese-European collaborative Earth observation satellite mission aimed to deepen understanding of the interaction process between clouds and aerosols and its effects on the Earth's radiation. The outcome of this mission is expected to improve accuracy of the Global Climate Change prediction.

The EarthCARE spacecraft, which weighs approximately 2,250kg and goes along a Sun-Synchronous 400km-high orbit around the Earth, accommodates four instruments which are to observe the Earth's clouds, aerosols and radiation. The observation data acquired simultaneously by the four sensors will be processed into a variety of synergy products including vertical profiles of clouds and aerosols, microscopic cloud parameters, radiation fluxes and so on. As one of those observatories, the Cloud Profiling Radar (CPR), which has a 2.5m-diameter main reflector and W-band 1.5kW transmitter and receiver, is the world's first space-borne Doppler cloud radar jointly developed by the Japan Aerospace Exploration Agency (JAXA) and the National Institute of Information and Communications Technology (NICT), which provides vertical velocity as well as vertical structure inside clouds. The other payloads on the satellite are the Atmospheric Lidar (ATLID) for vertical structure measurement of clouds and aerosols, the Multi-Spectral Imager (MSI) for horizontal distribution measurement of clouds and aerosols, and the Broad-Band Radiometer (BBR) for measurement of radiation fluxes at top of the atmosphere. ATLID, MSI, BBR and the base-platform of the spacecraft are developed by the European Space Agency (ESA).

In Japan, the critical design review of the CPR has been completed in 2013 and CPR proto-flight model is currently being manufactured, integrated, and tested. After handed-over to ESA, the CPR will be installed onto the EarthCARE satellite together with the other instruments, tested, transported to Guiana Space Center in Kourou, French Guiana and launched by a Soyuz launcher in JFY2016.

Keywords: Cloud, Aerosol, Radiation, EarthCARE, CPR, Cloud Profiling Radar

Shortwave direct aerosol radiative forcing using CALIOP and MODIS measurements

OIKAWA, Eiji^{1*} ; NAKAJIMA, Teruyuki¹ ; WINKER, David²

¹AORI, University of Tokyo, ²NASA Langley Research Center

The aerosol direct effect occurs by direct scattering and absorption of solar and thermal radiation. Shortwave direct aerosol radiative forcing (SWDARF) under clear-sky condition is estimated about 5 Wm^{-2} from satellite retrievals and model simulations [e.g., Yu *et al.*, 2006]. Simultaneous observations of aerosols and clouds are, however, very limited to validate the estimation of SWDARF under cloudy-sky condition. In 2006, the CALIPSO (Cloud-Aerosol Lidar and Infrared Pathfinder Satellite Observations) satellite was launched with the space-borne lidar, CALIOP (Cloud-Aerosol Lidar with Orthogonal Polarization). This enabled us to get data of the vertical distribution of aerosols and clouds all over the world. Oikawa *et al.* [2013] estimated SWDARF under clear-sky, cloudy-sky, and all-sky conditions using CALIOP Version 2 data and MODIS (Moderate resolution Imaging Spectrometer) data. They investigated four scenarios for evaluating the SWDARF: clear-sky, the case that aerosols exist above clouds (above-cloud case), the case that aerosols exist below high-level clouds (below-cloud case), and the case that aerosols are not detected by CALIOP in cloudy-sky condition. The cloudy-sky SWDARF is, then, estimated by the latter three scenarios. The all-sky SWDARF is the combination of clear-sky and cloudy-sky SWDARF weighted by the cloud occurrence.

We calculated SWDARF from 2007 to 2009 using CALIOP Level 2 Cloud and Aerosol Layer Products Version 2 (V2) and Version 3 (V3) with the method of Oikawa *et al.* [2013]. The procedure of daytime calibration, cloud screening, and aerosol-cloud classification are improved in the V3 algorithms [Powell *et al.*, 2010; Vaughan *et al.*, 2010; Liu *et al.*, 2010]; therefore, the distributions of aerosols and clouds are significantly changed from V2 data. Compared V3 data with V2 data, the total cloud fraction and occurrence probability of above-cloud case decrease. In clear-sky condition, marine aerosols increase and single scattering albedo (SSA) of total aerosols increases over the ocean. In cloudy-sky condition, smoke and polluted dust decrease. Annual zonal averages of SWDARF from 60°S to 60°N under clear-sky, cloudy-sky, and all-sky are -2.85, -0.16, and -0.78 Wm^{-2} for V2 data and -3.70, -1.07, and -2.02 Wm^{-2} for V3 data. It indicates that SWDARF largely depends on the retrieval and classification algorithms of aerosols and clouds.

Previous studies reported that the aerosol absorption above clouds cause the underestimation of cloud optical thickness (COT) in the satellite retrievals [Haywood *et al.*, 2004; Coddington *et al.*, 2010]. We, therefore, have a plan to examine the effect on SWDARF from underestimation of COT.

Keywords: aerosol, radiative forcing, DARF, CALIPSO, CALIOP

A new method for estimating biases in multi-spectral cloud parameter retrievals caused by cloud horizontal inhomogeneity

NAGAO, Takashi^{1*} ; NAKAJIMA, Takashi¹

¹Tokai University

Clouds play an important role in terrestrial atmospheric dynamics, thermodynamics, and radiative transfer and are key elements of the water and energy cycles. Modification of cloud properties, lifetime, and amount by indirect aerosol effects has an effect on radiative forcing in the climate. Cloud observations using satellite-borne multispectral imagers (e.g. Aqua/MODIS, GCOM-C/SGLI and EarthCARE/MSI) provide data sets useful for understanding cloud characteristics and their distributions on a global scale. Previous studies, however, pointed out that cloud parameters (e.g. cloud optical thickness, cloud particle effective radius and cloud top temperature) retrieved from multispectral measurements were significantly impacted by vertical and horizontal inhomogeneities of clouds, bimodal particle size distributions in drizzling clouds, and three-dimensional radiative transfer. In this study, we suggest a new method for estimating bias in multi-spectral-retrieved cloud parameters caused by cloud horizontal inhomogeneity. The impact of cloud horizontal inhomogeneity is considered as a key for interpreting discrepancies between cloud parameters from satellite observations and in-situ measurements or numerical cloud models. The estimation method considers the bias as the combination of the following two impacts: One is the impact of clear-contamination in cloud pixel, which is parameterized by cloud-fraction. The other is the impact of subpixel scale variance of cloud properties (but no clear-contamination), which is parameterized by variance of multi-spectral radiances in sub-pixels, and based on error propagation theory. We evaluate the method by using high-spatial resolution measurements of Landsat 8. Additionally, to apply the method to several multi-spectral imagers (e.g. MODIS, GCOM-C/SGLI and EarthCARE/MSI), we also investigate co-variance matrices of adjacent pixels or sub-pixels obtained from different IFOVs because the accuracy of the method depends on the accuracy of the co-variance matrix.

A study of the earth radiation budget using a 3D Monte-Carlo radiative transfer code (2)

OKATA, Megumi^{1*} ; NAKAJIMA, Teruyuki¹

¹University of Tokyo, Atmosphere and Ocean Research Institute

The purpose of this study is to evaluate the earth radiation budget when data are available from satellite-borne active sensors, i.e. cloud profiling radar (CPR) and lidar, and a multi-spectral imager (MSI) in the project of the Earth Explore/EarthCARE mission. The scientific requirement of the evaluation accuracy is less than 10 Wm^{-2} for the upward broadband radiative flux for the instantaneous $10\text{km} \times 10\text{km}$ footprint of CPR (EarthCARE, 2006). For this purpose, we first developed forward and backward 3D Monte Carlo radiative transfer codes called MCsatr that treat a broadband solar flux calculation including thermal infrared emission calculation by k-distribution parameters of Sekiguchi and Nakajima (2008). We have developed Forward and Backward Monte Carlo radiative transfer codes, and we have also developed both of two types for deciding optical mean path by extinction transmittance and scattering transmittance for Forward Monte Carlo radiative transfer code.

In evaluation system, 3D extinction coefficient fields are constructed by two methods: 1) the Minimum Information Deviation Profiling Method (MIDPM) (Barker and Donovan et. al., 2011) and 2) numerical simulation by bin-spectral non-hydrostatic cloud model. In the MIDPM, we first construct a library of pair of observed vertical profiles from active sensors and collocated imager products at the nadir footprint, i.e. spectral imager radiances, cloud optical thickness (COT), effective particle radius (RE) and cloud top temperature (T_c). We select a best matched active sensor-derived vertical profiles from the library for each of off-nadir pixels of the imager where active sensor-derived vertical profile is not available, by minimizing the deviation between library imager parameters and those at the pixel, to construct the 3D cloud field. We applied this method to data of Cloudsat/CPR and AQUA/MODIS for a case of summer stratus cloud of California coast on July 2, 2007.

The second construction of 3D cloud systems is performed by numerical simulation of Californian summer stratus clouds using a non-hydrostatic atmospheric model coupled with a bin-spectral cloud microphysics model based on the NHM+ACBM model (Iguchi et al., 2008; Sato et al., 2009, 2011). Most inner region of a three-fold nesting system is an area of $30\text{km} \times 30\text{km} \times 1.5\text{km}$ with horizontal (vertical) grid spacing of 100m (20m) and 300m (20m). Two different cell systems were simulated for small and large cloud condensation nuclei (CCN) concentration. The area mean cloud optical thickness, $\langle \text{COT} \rangle$, and standard deviation are 3.0 and 4.3 for pristine case and 8.5 and 7.4 for polluted case.

We then re-calculated the solar radiation field by two types of Forward MCstar. We compared flux reflectivities of the 3D atmospheres with those by Plane Parallel Approximation (PPA) and Independent Pixel Approximation (IPA) (Cahalan et al., 1994). As expected, the reflectivity difference between 3D and PPA clouds increases with increasing COT horizontal variability of the 3D clouds. The reflectivity difference between 3D and PPA reaches 0.078 at maximum, which is equivalent to a solar radiative flux error of 70 Wm^{-2} .

On the other hand, the IPA result between the two cases are significantly different. We infer this difference is caused by difference in the spatial characteristic size of inhomogeneity. The mean extinction of the cloud system is of 5 to 8 km^{-1} , so that the kilometer-size clouds in the satellite case are optically dense enough to be approximated by IPA. The difference is less than 0.010 in reflectivity or 10 Wm^{-2} in upward flux. On the other hand, the model simulation case is optically thin to be approximated by IPA. The error reaches 0.07 at maximum by pristine case. A future work is needed to correct this significant error utilizing the 3D structure of the cloud system.

Keywords: 3D radiative transfer, MIDPM, Monte Carlo

Synergistic use of the geostationary and the polar orbit satellites for surveying the cloud evolution process: plan

NAKAJIMA, Takashi^{1*} ; NAGAO, Takashi¹ ; LETU, Husi¹

¹Tokai University

The use of spaceborne radar and imager aboard the CloudSat, Aqua, EarthCARE, GCOM-C1, and the 3rd generation geostationary satellites for investigating cloud evolution process, is suggested. These satellites have been in orbit or will be launched in the middle of 2010-era and contribute for observing aerosols, clouds on the earth system. Since aerosols and clouds exert an important influence on the planet water and energy balances, more understanding of their lifecycle is required. Optical thickness and particle size of clouds are primal information for estimating the cloud evolution process. These parameters are retrieved from multi-spectral imageries obtained from space-borne satellite sensors. Recently, active sensors, such as the CloudSat cloud profiling radar (CPR) and the CALIPSO Lidar present a new epoch of aerosol and cloud observation with the purpose of revealing transition of particles, from cloud condensation nuclei to rain droplets via cloud and drizzle particles. They observe vertical cross section of the cloud system along the satellite footprint. As follow on the CloudSat / CALIPSO, the EarthCARE that has both active and passive sensors is planed by JAXA, NICT, and ESA collaboration. Doppler capability of the EarthCARE CPR will reveals vertical motion of cloud particles. Moreover, the 3rd generation geostationary weather satellite will appear in 2015 and observe aerosol and cloud system in every 10 or 2.5 minutes. Therefore, it is expected that the combined use of polar orbital passive/active sensors and geostationary satellites reveal details of cloud evolution process, statistically and dynamically. In this presentation, we introduce recent progresses of aerosol and cloud observations from satellites, showing the multi-sensor views of cloud growth process obtained from an active radar (CPR) and a passive imager (MODIS).

Keywords: Cloud evolution, Satellite, GCOM, EarthCARE

Retrieval algorithm for aerosols based on GCOM-C1/SGLI

SANO, Itaru^{1*} ; MUKAI, Sonoyo¹ ; NAKATA, Makiko¹ ; HOLBEN, Brent² ; DUBOVIK, Oleg³ ; KOKHANOVSKY, Alexander⁴

¹Kinki University, ²NASA/GSFC, ³Lille University, ⁴EUMETSAT

It is known that atmospheric aerosols have valuable information in many research fields. However estimation of aerosol direct and indirect effects on climate changes in the 5th report of IPCC still involves large uncertainty due to lack of precise aerosol properties.

JAXA (Japanese space agency) is developing the GCOM-C (Global change observing mission?climate) satellite series, which are expected to provide us new aerosol information as well as geo-physical parameters for thirteen years after launch. The first of GCOM-C series will carry the SGLI (second generation global imager) sensor which observes total radiance from near UV to thermal infrared wavelengths including polarization measurements at red and near IR. This work intends to develop an efficient algorithm for aerosol retrieval based on this polarization information to be given by GCOM-C1/SGLI.

Keywords: Aerosol, SGLI, GCOM-C

Ocean primary production algorithm for the GCOM-C1/SGLI

HIRAWAKE, Toru^{1*}; FUTSUKI, Ryosuke¹; SHINMYO, Katuhito¹; TAKAO, Shintaro²; FUJIWARA, Amane³; SAITOH, Sei-ichi¹

¹Faculty/Graduate School of Fisheries Sciences, Hokkaido University, ²Faculty of Environmental Earth Science, Hokkaido University, ³National Institute of Polar Research

One of the objectives of second-generation global imager (SGLI) on the earth observation satellite, Global Change Observation Mission 1st-Climate (GCOM-C1) is to understand the global carbon cycle. Therefore, estimation of column integrated daily net primary production (PP_{eu}) as carbon assimilation by photosynthesis of phytoplankton in the ocean is essential for the objective of SGLI/GCOM-C1 project. Most of the algorithms developed in the past used chlorophyll *a* (chl *a*) concentration. However, estimation of chl *a* concentration from satellite data has uncertainty due to the effect of pigment packaging that leads to underestimation, and the interference of colored dissolved organic matter (CDOM) which leads to overestimation. Another uncertainty is derivation of photosynthetic rate of phytoplankton. Although the vertically generalized productivity model (VGPM) which is one of the frequently used algorithms expressed the maximal photosynthetic rate (P_{opt}^B) as a function of sea surface temperature (SST), the SST derived P_{opt}^B had large error, particularly in the polar waters. Furthermore, discussion on the effect of global warming to primary productivity in the ocean using satellite data is facilitated, if the photosynthetic rate is an independent parameter on the SST.

To reduce these issues, light absorption coefficient of phytoplankton (a_{ph}) was used in the algorithm for SGLI/GCOM-C1; product of P_{opt}^B and chl *a* in the VGPM, which means productivity at the depth with the maximal photosynthetic rate within a water column, was expressed by photosynthetic available radiation (PAR) absorbed in phytoplankton. In situ primary production and optical data to develop the algorithm were measured in the North Pacific, Japan Sea, East China Sea, Southern Ocean, Chukchi Sea (Arctic Ocean), Bering Sea. Additional datasets of the Bermuda Atlantic Time-series Study (BATS), Hawaii Ocean Time-series (HOT) and The California Cooperative Oceanic Fisheries Investigations (CalCOFI) were also obtained for the development and validation of the algorithm. Accuracy in the estimation of product of P_{opt}^B and chl *a* (P_{opt}) and PP_{eu} were fairly well and estimated values from the new algorithms almost satisfied a factor of 2 of the values measured in situ. If accurate value of a_{ph} is derived from SGLI data, global estimation of PP_{eu} without the issues of pigments packaging, CDOM and SST are expected.

Keywords: primary production, phytoplankton, absorption coefficient, GCOM-C, SGLI

Global snow and ice cover observations using GCOM-C1/SGLI for studying climate changes

HORI, Masahiro^{1*} ; AOKI, Teruo² ; STAMNES, Knut³ ; TANIKAWA, Tomonori¹ ; KUCHIKI, Katsuyuki² ; LI, Wei³ ; CHEN, Nan³

¹Japan Aerospace Exploration Agency, ²Meteorological Research Institute, ³Stevens Institute of Technology

The "Global Change Observation Mission-Climate" (GCOM-C) is a project of Japan Aerospace Exploration Agency (JAXA) for the global observation of the Earth environment. The GCOM-C is a part of the JAXA's GCOM mission which consists of two satellite series, GCOM-C and GCOM-W (Water). GCOM-C carries a multi-spectral optical radiometer named Second Generation Global Imager (SGLI), which will have special features of wide spectral coverage from 380 nm to 12 micrometer, a high spatial resolution of 250m, a field of view exceeding 1000km, two-direction simultaneous observation, and polarization observation. The GCOM-C mission aims to improve our knowledge on the global carbon cycle and radiation budget through high-accuracy observation of global vegetation, ocean color, temperature, cloud, aerosol, and snow and ice. As for the cryosphere observation, not only snow and ice cover extent but also snow physical parameters are retrieved from SGLI data such as snow grain sizes at shallow layers, temperature, and mass fraction of impurity mixed in snow layer and so on. These snow physical parameters are important factors that determine spectral albedo and radiation budget at the snow surface. Thus it is essential to monitor those parameters from space in order to better understand snow metamorphosis and melting process and also to study the response of snow and sea-ice cover extent in the Polar Regions to a climate forcing such as global warming. In addition, one of important objectives of the GCOM mission is to monitor long-term trend of the geophysical parameters for understanding the mechanism of earth's climate system. For this purpose, the data from GCOM series satellites are not enough. Thus, JAXA launched a website named "JAXA Satellite Monitoring for Environmental Studies (JASMES)" for semi-near real-time monitoring of earth's environmental variables. Through this website JASMES provides users with not only satellite datasets (flat binary) but also information on the current status of the climate variables such as solar radiation reaching the earth's surface (photosynthetically available radiation: PAR), snow and cloud cover, dryness of vegetation (water stress trend), wild fire and so on. MODIS data since February 2000 are currently processed for this analysis but SGLI data will be used after the launch of GCOM-C. Furthermore, the data from Advanced Very High Resolution Radiometer (AVHRR) onboard polar orbiting satellites operated by the National Oceanic and Atmospheric Administration (NOAA) since 1978 are also under preparation toward establishing a half-century long datasets of remote sensing after the success of the GCOM mission. This presentation will summarize the SGLI cryospheric products and validation plans, and also briefly introduce the JASMES dataset.

Keywords: Snow Cover, Snow Grain Size, Snow Impurity, Surface Temperature, Remote Sensing, Climate

Development of GCOM-C1 land surface reflectance product

MURAKAMI, Hiroshi^{1*}

¹JAXA, Earth Observation Research Center

Land-surface reflectance (RSRF) product is one of the essential products of Global Change Observation Mission-Climate 1/ Global Imager (GCOM-C1/SGLI; to be launched in JFY 2016); it is an input of other land algorithms, such as Leaf Area Index (LAI) and land cover classification (LCC), and will be used for surface albedo in the radiation budget, and used as the background of aerosol and cloud estimation. RSRF is estimated by subtracting scattering and absorption of an atmospheric molecule and aerosol from the top-of-atmosphere (TOA) radiance in cloud-free areas observed by the satellite (i.e., atmospheric correction). However, in order to extract the information on aerosols from the TOA radiation, it is necessary to know the information on land surface used as a background beforehand.

Experiential assumption and a candidate model about the spectral characteristic of aerosol and surface reflectance are often used in the presumption. Since the presumption can influence the output results, it is necessary to accumulate the knowledge of the various spectral characteristics and to perform suitable selection. Change of RSRF by the sun and the satellite geometries (BRDF) should be modeled when we preset the land-surface reflectance, because the satellite observes targets from a specific direction.

Candidate models of aerosol in the atmospheric correction (size distribution and vertical distribution, refractive index, etc.) may be able to be consistent with ones in the traditional aerosol-estimation algorithms which use candidate models as well. Since RSRF is used as a background of aerosol estimation, the consistency will be important for the product evaluation and accuracy improvement. There are groups which study aerosol properties by ground observation network, SKYNET, AERONET, etc., their regional characterization, spectral reflectance of the land surface, and observation and modeling (canopy radiation transfer) of the BRDF in the GCOM-C1 science team. The GCOM-C1 science team held a mini-workshop in summer of 2012, and decided that JAXA develops the land-surface atmospheric correction algorithm step by step by integrating their results. We confirmed importance of the consistency with the algorithms, such as LCC, LAI, albedo, etc., which use the estimated RSRF and BRDF.

We plan to develop the algorithm based on the existing knowledge (i.e., a traditional algorithm) for the at-launch version. Gas absorption of SGLI bands by water vapor, ozone, oxygen, and NO₂ will be considered by using objective analysis data or Climatology. The surface elevation will be corrected by using objective-analysis sea-level pressure data and high-spatial resolution digital elevation data, DEM. Influence of surface slope will be reduced by using surface normal vector calculated by the DEM and solar vector. GCOM-C1/SGLI has a near-ultra violet (NUV) 380nm band, which will be used for the presumption of surface reflectance in the GCOM-C1 atmospheric correction, because reflectance and its directionality is generally small in the NUV and blue wavelengths. The presumption of the NUV band uses vegetation and land-cover information assumed from near infrared (NIR) and short-wave infrared (SWIR) reflectance, which are not so much affected by aerosols, and RSRF in the previous days by assuming temporal change of RSRF is generally smaller than the change of the atmosphere.

For the future algorithm version after the satellite launch, we expect to improve the presumption by knowledge from the canopy radiation transfer, LCC and vegetation phenology, adopt new aerosol estimation schemes, or use results of the aerosol-transport model to find the optimal aerosol models. SGLI has a polarization radiometer which observes the Stokes vector of red and NIR bands with 45-deg along-track slant view. It may be able to improve atmospheric correction accuracy after accumulation of surface BRDF and polarization knowledge in the future.

Keywords: GCOM-C1, SGLI, land surface reflectance, atmospheric correction

Assessing the variations of the Alaskan tundra vegetation using MODIS NDVI 250-m imagery

SETIAWAN, Yudi^{1*} ; KUSHIDA, Keiji¹

¹College of Bioresource Sci., Nihon Univ. Japan

Improving the understanding of Alaskan tundra vegetation using remote sensing data is a challenging task due to a general lack of consistency and coverage from historical and existing platforms. Furthermore, it should be essential for many aspects of global environmental change research.

Vegetation dynamics of the land surface is an integrated reflection of the vegetation and physical and chemical factors that shape the environment of a given land area and determinants for overall biological diversity patterns. In this paper, we demonstrate an approach for displaying detailed information of the Alaskan tundra ecosystem from the vegetation dynamics point of view. We assumed that locations displaying similar temporal vegetation patterns are inferred to have a similar vegetation and/or environment characteristics. Differences among land cover types as reflected in temporal profiles of NDVI are caused by differences in vegetation type composition and/or in their densities, and their responses to local environmental conditions, consequently, the use of long time-series NDVI will capture such different patterns in seasonal growth cycles.

The clustering method yields sets of clusters, which each cluster represents a significant different NDVI pattern at detailed information in the land cover type. However, the complexity and enormous amount of time-series NDVI datasets may lead to the difficulty of obtaining the actual number of clusters in this study. Therefore, to provide maximum effectiveness of the clustering algorithm, we first consider the number of clusters 15 which correspond to the number of dominant physiognomy of Alaska tundra ecosystem (Raynold et al., 2005). The number of clusters was then evaluated based on a statistical measurement of how separate that pattern is to patterns in its own cluster compared to patterns in other clusters. This separability analysis was applied to discriminate among high detailed significant patterns that were theoretically defined to portray the specific characteristics of each land cover type.

Keywords: Vegetation dynamics, Tundra vegetation, Alaska, MODIS

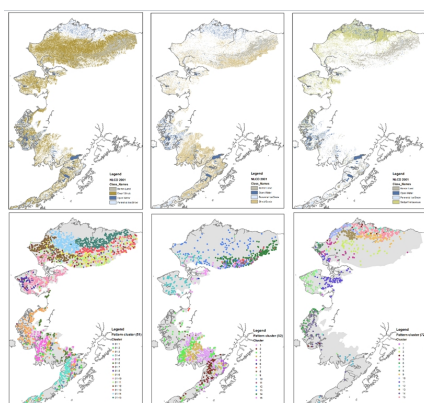


Figure 1. Three-dominant land cover classes of NLCD 2001 in Alaskan tundra: a) dwarf shrub, b) shrub/scrub, and c) sedge/herbaceous. Distribution of the 15-clusters for: d) dwarf shrub, e) shrub/scrub and f) sedge/herbaceous

Detection of regional extent of permafrost thawing and waterlog damage area in boreal forest in eastern Siberia during w

IJJIMA, Yoshihiro^{1*} ; ABE, Konomi² ; ISE, Hajime² ; MASUZAWA, Tadashi²

¹JAMSTEC, ²Regional Environmental Planning Inc.

Wet climate with largely increased in rainfall during summer and snow accumulation during winter had perennially continued since 2004 in eastern Siberia. Soil moisture in the active layer had been rapidly increased corresponding with thawing permafrost near the surface during following years. The perennially water-logged active layer furthermore exacerbated the boreal forest habitat, namely withered and dead forests widely extended in this region. In the present study, we have attempted to extract the region of degraded boreal (larch) forest based on the analysis of satellite data (ALOS-AVNIR2 and PALSAR) in the left and right banks of the central Lena River Basin near Yakutsk, along with expansion of the water-logged forest floor in relation to permafrost degradation.

Keywords: ALOS, permafrost, wet climate, boreal forest, degradation, eastern Siberia

A potential map of precipitation area using the geostationary meteorological satellite for the GSMaP

HIROSE, Hitoshi^{1*}; HIGUCHI, Atsushi¹; USHIO, Tomoo²; MEGA, Tomoaki²; YAMAMOTO, Munehisa³; SHIGE, Shoichi³; SATOMURA, Takehiko³; HAMADA, Atsushi⁴

¹Center for Environmental Remote Sensing, Chiba University., ²Division of Electric and Information Engineering, Osaka University., ³Division of Earth and Planetary Science, Graduate School of Science, Kyoto University., ⁴Atmosphere and Ocean Research Institute, Tokyo University.

The Global Satellite Mapping of Precipitation (GSMaP) produces accurate precipitation data with high time and spatial resolution (per 1hour, 0.1 degree) by utilizing the satellite microwave radiometer. At the time and place which all microwave radiometer satellites are not available, the GSMaP estimates where the precipitation area observed before that time will moves by using a cloud moving vector retrieved from the infrared brightness temperature (IR Tb) observed by the geostationary meteorological satellite (GMS) (GSMaP_MVK, GSMaP_NRT; v5.222.1). However this method has some possibility of missing the convective precipitation which develops quickly (Ushio et al. 2009), and uses only IR1 channel (10.5~11.5 μ m) of the GMS observation to calculate the cloud moving vector. Therefore, this study made more accurate data of estimated precipitation area by using multi-channel GMS observation, called potential map, and then improved the accuracy of GSMaP_MVK and GSMaP_NRT precipitation areas by utilizing the potential map.

As a precipitation area index of the GMS, we used difference of the Tb between IR1 channel and water vapor (WV) channel (6.5~7.0 μ m). This index is based on the assumption which a deep convective cloud with precipitation probably occurs at the area with a small Tb difference of IR1 and WV (Ohsawa et al. 2001). Moreover since almost all of geostationary satellites have the IR1 and WV channel, the index is available globally on a long-term basis. We used near surface rain observed by the precipitation radar of the Tropical Rainfall Measurement Mission (TRMM) (PR; 2A25, V7) and the rainfall intensity retrieved from ground-based precipitation radar of Japan Meteorological Agency (JMA) as the truth of the precipitation area and converted the Tb of the GMS to the probability of precipitation with simultaneous observation between the GMS and the precipitation radar.

At first we compared the precipitation area obtained from the GSMaP and the precipitation radar, and found that the GSMaP_MVK overestimated the precipitation area over the ocean without the microwave observation. And therefore we tried to identify the area which the GSMaP precipitation was less than 1.0 mm per hour and the possibility of precipitation obtained of the potential map was less than 15 % as non-precipitation area. As the result the threat score of the GSMaP_MVK precipitation detection was improved from 0.37 to 0.41 over the ocean without the microwave observation. As it is considered that the threat score of GSMaP_MVK with the microwave observation is 0.45, this improvement is regarded as significant. On the other hand, the GSMaP_NRT underestimated the precipitation area over the land and coast without the microwave observation. And then we identified the area which the potential map was more than 40 % as precipitation area. As the result the threat score of the GSMaP_NRT was much improved from 0.27 to 0.34 over the land and coast without the microwave observation. In these areas and conditions, we can expect that the GSMaP estimates the precipitation area more accurately by utilizing the potential map.

Keywords: microwave radiometer, GSMaP, GMS, precipitation radar, high time resolution, mid-high latitude

A study of multi-pixel and multi-parameter satellite remote sensing for aerosol properties

HASHIMOTO, Makiko^{1*} ; MORIMOTO, Shotaro¹ ; TAKENAKA, Hideaki¹ ; NAKAJIMA, Teruyuki¹

¹AORI, the University of Tokyo

We have developed a new satellite remote sensing algorithm to retrieve the aerosol optical characteristics using multi-pixel information of satellite imagers. In this algorithm, the inversion method is a combination of the MAP method (Maximum a posteriori method, Rodgers, 2000) and the Phillips-Twomey method (Phillips, 1962; Twomey, 1963) as a smoothing constraint for the state vector. Retrieved parameters in our algorithm are aerosol optical properties, such as aerosol optical thickness (AOT) of fine mode, sea salt, and dust particles, a volume soot fraction in fine mode particles, and ground surface albedo of each observed wavelength. We simultaneously retrieve all the parameters that characterize pixels in each of horizontal sub-domains consisting the target area. Then we successively apply the retrieval method to all the sub-domains in the target area.

We conducted numerical tests for the retrieval of aerosol properties and ground surface albedo for GOSAT/CAI imager data to test the algorithm for the land area. The result of the experiment showed that AOTs of fine mode and dust particles, soot fraction and ground surface albedo are successfully retrieved within absolute. We discuss the accuracy of the algorithm for various land surface types. Our future work is to extend the algorithm for analysis of AGEOS-II/GLI and GCOM/C-SGLI data.

Keywords: GCOM/C-SGLI, Aerosol, Satellite remote-sensing

Estimation of Phytoplankton Group-Specific Primary Production in Kuroshio Waters Using Ocean Colour Remote Sensing

HIRATA, Takafumi^{1*} ; SUGIE, Koji¹ ; SUZUKI, Koji¹ ; SAITOH, Hiroaki²

¹Faculty of Environmental Earth Science, Hokkaido University, ²Tohoku National Fisheries Research Institute, Fisheries Research Agency

The ocean is a major sink of carbon dioxide released into the atmosphere. Phytoplankton conducting primary production plays a significant role on temporal and spatial variability in the absorption of the carbon. Also phytoplankton transfers carbon to higher trophic levels in a marine ecosystem, and the carbon pathways to the higher trophic levels affect vulnerability of food web, or the ecosystem, against external forcings. Tremendous efforts to measure primary productivity of the total phytoplankton community in the global oceans have been made historically. On the other hand, measurements of primary productivity of individual phytoplankton groups composing of the total community are relatively sparse. This is partly due to methodological difficulties to differentiate such productivity of individual groups in situ, on top of practical circumstance that in situ observation requiring ship time is usually expensive. Therefore, it is of great interest if satellite remote sensing can overcome these problems, given that a number of earth observation satellites have been and will be launched. Especially, it is a great advantage of satellite observation that one can hindcast primary productivity of individual phytoplankton groups using historical remote sensing data, once a remote sensing methodology/algorithm is developed. In this presentation, we show a primitive result of development of such methodology to estimate primary productivity of diatoms and haptophytes in Kuroshio waters using ocean colour remote sensing.

Keywords: Ocean Colour, Satellite Observation, Phytoplankton, Primary Production

NICT Calibration and Validation experiment for DPR/GPM

NAKAGAWA, Katsuhiro^{1*} ; HANADO, Hiroshi¹ ; KAWAMURA, Seiji¹ ; IWAI, Hironori¹ ; TAKAHASHI, Nobuhiro¹ ; IGUCHI, Toshio¹

¹National Institute of Information and Communications Technology

The GPM core satellite is scheduled to be launched on February 28, 2014. It carries the Dual-Frequency Precipitation Radar (DPR) developed by Japan Aerospace Exploration Agency (JAXA) and National Institute of Information and Communications Technology (NICT), which consists of two radars: Ku-band precipitation radar (KuPR, 13.6 GHz) and Ka-band radar (KaPR, 35.5 GHz). NICT is planning the GPM/DPR onboard calibration experiment at NICT Koganei. The beam matching of two radars will be evaluated. NICT is also planning the post-launch ground validation (product validation) experiment at two locations, NICT Kobe (NICT Advanced ICT Research Institute) and NICT Okinawa (Okinawa Electromagnetic Technology Center). NICT is developing two X-band phased array radars (PANDA: Phased Array radar Network DATA system) and will install at NICT Kobe and Okinawa. PANDA can scan three-dimensionally in thirty seconds. We can compare the radar directly and simultaneously. At NICT Okinawa, the C-band polarimetric Doppler radar (COBRA) is also installed. The differential reflectivity (ZDR) can be used to validate the rain drop size distribution parameter (D_0). The cross-correlation coefficient (ρ_{HV}) can be used to validate the melting layer flag. Using the ground-based rain drop size measurements, the two-dimensional Video disdrometer (2DVD), Joss-type disdrometer, and Laser Optical disdrometer (Parsivel), and so on, the characteristics of DSD itself are analyzed and the $k-Z$ relationship is estimated for evaluation and improvement of the GPM/DPR algorithm.

Keywords: GPM, DPR, Beam matching, Ground Validation, PANDA (Phased Array radar Network DATA system), COBRA

Ground-based Validation of GPM/DPR

KANEKO, Yuki^{1*} ; OKI, Riko¹ ; NAKAGAWA, Katsuhiko² ; NAKAMURA, Kenji³

¹Japan Aerospace Exploration Agency (JAXA), ²National Institute of Information and Communications Technology, ³Faculty of Economics, Dokkyo University

The Global Precipitation Measurement (GPM) mission is an expanded follow-on mission to TRMM (Tropical Rainfall Measuring Mission) and GPM core satellite carries dual frequency precipitation radar (DPR) and GPM Microwave Imager on board. The DPR is expected to advance precipitation science by expanding the coverage of observations to higher latitudes than those of the TRMM/PR, measuring snow and light rain by the KaPR, and providing drop size distribution information based on the differential attenuation of echoes at two frequencies. After launch of GPM core satellite JAXA will perform evaluation of DPR L2 products, for example, precipitation rate, measured radar reflectivity, and drop size distribution. Those physical values will be compared with ground-based observations. This poster presentation will show the preliminary report of DPR evaluation comparison between DPR products and ground-based instruments during the first 2 months after launch, including a ground-based Ka-band radar system.

Keywords: GPM, DPR, validation

Optimal choice of surface reflectance and aerosol types for Multi-Spectral Imager on board EarthCARE

FUKUDA, Satoru^{1*} ; NAKAJIMA, Teruyuki² ; TAKENAKA, Hideaki²

¹Japan Aerospace Exploration Agency, ²Atmosphere and Ocean Research Institute, The University of Tokyo

EarthCARE is a satellite which will be launched in 2016. EarthCARE is a joint mission between Europe and Japan. Four instruments such as CPR, ATLID, MSI and BBR will be equipped. MSI is a multi-spectral imager, and the purpose of it is to get the horizontal structure of aerosol and cloud. We are developing the aerosol retrieval algorithm for MSI. MSI aerosol products are consists of optical thickness over land, optical thickness over ocean, and Angstrom Exponent over ocean. Over ocean we implement two channel method with 0.68 μm and 0.86 μm (Higurashi and Nakajima, 1999) and we retrieve optical thickness and Angstrom Exponent. Over land we estimate the surface reflectance at 0.68 μm from longer wavelength. Kaufman et al (1997) used 2.2 μm to estimate the surface reflectance at 0.68 μm . In this study we tried to use 1.6 μm to estimate the surface reflectance at 0.68 μm . This is because there is a possibility to get better estimation than to use 2.2 μm and we can use this method for sensors which don't equip 2.2 μm such as GOSAT/TANSO-CAI or CAI2. We have made a scatter plot of the reflectance between 0.68 μm and 1.6 μm . As reflectance data set, we used AERONET data of 0.68 μm and GOSAT/TANSO-CAI's reflectance data of 1.6 μm . We found that there are some correlations between these two reflectances when we classified by NDVI. The correlation is larger when the NDVI is large. The error induced by this parameterization is calculated. The standard error is 0.009 when $0.5 < \text{NDVI} < 0.7$, and the standard error is 0.007 when $0.7 < \text{NDVI}$. We also calculated the error as aerosol optical thickness. The error as aerosol optical thickness at 0.5 μm is 0.18 when $0.5 < \text{NDVI} < 0.7$, and that is 0.14 when $0.7 < \text{NDVI}$. We will also develop aerosol models for each area by use of cluster method and linear classifier method.

Keywords: aerosol, remote sensing, EarthCARE

Helicopter-borne observation with portable microwave radiometer in the Southern Ocean and the Sea of Okhotsk

TAMURA, Takeshi^{1*} ; OHSHIMA, Keiichiro² ; LIESER, Jan³ ; TOYOTA, Takenobu² ; TATEYAMA, Kazutaka⁴ ; NOMURA, Daiki² ; NAKATA, Kazuki² ; FRASER, Alex² ; JANSEN, Peter³ ; NEWBERY, Kym³ ; MASSOM, Robert³ ; USHIO, Shuki¹

¹National Institute of Polar Research, ²Institute of Low Temperature Science, ³ACE CRC, ⁴Kitami Institute of Technology

It has been recently recognized that sea ice production in the polar regions is controlled by the thin sea ice area with thickness of less than 0.2 m. Spatial distribution of thin ice area and its variability are important information to better understand the reduction of the sea ice covered region in a changing climate environment. We have developed a thin ice thickness algorithm for satellite passive microwave data of the Advanced Microwave Scanning Radiometer-EOS (AMSR-E) and Special Sensor Microwave Imager (SSM/I). Although the microwave skin depth of bare sea ice is about several cm at most, microwave brightness temperatures correlate with the surface salinity (brine volume fraction), which is sensitive to thin ice thickness. Here, we present in-situ observations using a helicopter-borne portable passive microwave radiometer that has the same specifications as the satellite AMSR-E and AMSR-II sensors (36 GHz-vertical and -horizontal channels), to validate and improve our thin ice thickness algorithm. This study estimates the relationship between the microwave brightness temperatures (both satellite and helicopter-borne portable sensors) and in-situ observations of sea ice thickness.

We present data from two airborne missions, one in early austral spring 2012 during the Sea Ice Physics and Ecosystem experiment (SIPEX-2) of the Australian Antarctic Program in East Antarctica, and one from the Sea of Okhotsk in mid-winter 2009. These microwave data are compared with the satellite AMSR-E and AMSR-II data and ice thickness estimated from Moderate-Resolution Imaging Spectroradiometer (MODIS) data, helicopter-borne IR sensor data, and ship-borne downward looking camera data. High-resolution airborne microwave brightness temperatures show good agreement with low AMSR-E and AMSR-II brightness temperatures, despite the significant resolution mismatch. In the thin ice region, the polarization ratio of 36 GHz vertical and horizontal temperatures (PR-36) is found to be well correlated with ice thickness, supporting the validity of the AMSR-E thin ice algorithm which was developed previously by our group. We also discuss the microwave characteristics of fast versus pack ice, with a view to improving a satellite fast ice detection algorithm.

Keywords: passive microwave, heli-borne portable radiometer, thin ice region, in-situ validation, Southern Ocean, Sea of Okhotsk

Diatom analysis on the late Pleistocene Takano Formation, Nagano, Japan

NAGAYASU, Koichi^{1*} ; OTANI, Hiromi³ ; KUMON, Fujio²

¹Interdisciplinary Graduate School of Science and Technology, Shinshu University, ²Department of Environmental Sciences, Faculty of Science, Shinshu University, ³Faculty of Science, Shinshu University

Diatom analysis has been performed at a 0.5 m interval for a sediment core of 53.88 m length from the late Pleistocene Takano Formation. According to the age-model proposed by Tawara et al. (2006), this core can covers from 170 ka to 40 ka in age and analysis interval correspond to about 1500 years.

From 170 ka to 140 ka, benthic diatoms such as *Achnanthes* spp. and *Staurosira* spp. are dominant, and diatom abundance is very low (lower than 1.0×10^8 valves/g). After 140 ka, planktonic diatoms such as *Cyclotella radiosa*, *Aulacoseira ambigua*, *Cyclotella stelligera*, *Aulacoseira alpigena* are dominant. From 140 ka to 130 ka, *C. radiosa* is dominant, and diatom abundance is low ($1.6 - 6.9 \times 10^8$ valves/g). From 130 ka to 115 ka, *Aul. alpigena* is dominant, and diatom abundance is high (over 10×10^8 valves/g). From 115 ka to 100 ka, *C. stelligera* is dominant, and diatom abundance varies largely ($0.1 - 38.2 \times 10^8$ valves/g). From 100 ka to 70 ka, *C. radiosa* is dominant, and diatom abundance is abundant, between 3.2×10^8 valves/g and 56×10^8 valves/g. From 70 ka to 40 ka, *C. radiosa* and *Aul. alpigena* are dominant, and diatom abundance is low, fluctuating a little between 0.9×10^8 valves/g and 20×10^8 valves/g.

These results are compared with the diatoms analysis of the sediment cores from Lake Biwa. After 140 ka, planktonic diatoms are dominant in the Takano Formation, and the diatom assemblage changes synchronously between Takano Formation and Lake Biwa.

Is small *Abies mariesii* forest in Pseudo-Alpine Zone spreading? :Case study in the Akitakomagatake

KONNO, Asaka^{1*}

¹Miyagi University of Education,MA

Pseudo-Alpine Zone composed of Sasa and shrubs occupies on subalpine zone of mountain along the Sea of Japan in eastern Japan. It is considered that heavy snowfall on those mountains prevents coniferous trees from growing and consequently Pseudo-Alpine Zone exists. But there is Pseudo-Alpine Zone in the part of the Ou Backbone Range which is less snowfall than mountains along the Sea of Japan. On Akitakomagatake, the one of mountains which has Pseudo-Alpine Zone, small *Abies mariesii* forests are scattered.

This landscape has been hitherto considered that spreading *Abies mariesii* forest which finally results in matured coniferous forest on the basis of pollen analysis. Purpose of this study is discussing whether small *Abies mariesii* forest is spreading or not in terms of tree distribution and local environment.

As the result, *Abies mariesii* seeding is distributed only within the small *Abies mariesii* forest, not in surrounding *Sasa kurilensis* and *Fagus crenata*. In addition, soil moisture is higher in the small *Abies mariesii* forest than in the surrounding vegetation. These results suggest that the small *Abies mariesii* forest is not spreading but just being established on appropriate site.

Keywords: *Abies mariesii* forest, Pseudo-Alpine Zone, Spreading range, Soil moisture

The chemical characteristics of spring and river water in Kamikochi at the Japanese Alps

KURAMOTO, Takayuki^{1*} ; SASAKI, Akihiko¹ ; SUZUKI, Keisuke¹

¹IMS, Shinshu University

There are much spring waters in the Azusa River which flows through Kamikochi. These spring waters form the branch of the Azusa River. Spring water shows the characteristics reflecting an underground water flow. Therefore, in order to understand the water cycle of Kamikochi, it is important to understand the formation mechanism of spring water. The purpose of this study is to clarify the chemical characteristics of spring and river water in Kamikochi. We set up the thermometer in five places of a basin for the measuring of spring and river water temperature. The water samples were collected in water temperature measuring site and Azusa River. The pH, electric conductivity, major ions (Na^+ , K^+ , Mg^{2+} , Ca^{2+} , Cl^- , NO_3^- and SO_4^{2-}), and stable isotope of water were analyzed with the pH meter, conductivity meter, ion chromatographs, and isotopic water analyzer, respectively. In addition, HCO_3^- concentration was measured using the sulfuric acid titration method. At almost observation points, the temperatures of spring and river water showed seasonal change. However, only one site did not have change of spring water temperature through a whole year.

Geo-environmental changes after the fire on the alpine slopes of Mount Shirouma-dake, northern Japanese Alps

SASAKI, Akihiko^{1*} ; KARIYA, Yoshihiko² ; IKEDA, Atsushi³ ; SUZUKI, Keisuke¹

¹IMS, Shinshu Univ., ²Senshu Univ., ³Tsukuba Univ

This is the continuous study to clarify the geo-environmental changes on the post-fire alpine slopes of Mount Shirouma-dake in the Northern Japanese Alps. The fire occurred at May 9, 2009 on the alpine slopes of Mount Shirouma-dake, and the fire spread to the *Pinus pumila* communities and grasslands. Although the grass had a little damage by the fire, the *Pinus pumila* received nearly impact of the fire. In the *Pinus pumila* communities where the leaf burnt, forest floor is exposed and become easy to be affected by atmospheric condition such as rain, wind, snow, and etc.

First, we illustrated a map of micro-landforms, based on geomorphological fieldworks. We observed these micro-landforms repeatedly for four years after the fire. As the results of the observation, it is clear that remarkable changes of these micro-landforms have not occurred but some litters on the forest-floor in the *Pinus pumila* communities are flushed out to surroundings. The litter layer on the forest-floor in the *Pinus pumila* communities were 3-4 cm thick in August of 2011, but it became 1-2 cm thick in September of 2013. The *Pinus pumila* communities established on the slopes consists of angular and sub-angular gravel with openwork texture, which are covered by thin soil layer. Therefore, it is necessary to pay attention to soil erosion following the outflow of the litter.

In addition, we observe the ground temperature and soil moisture, under the fired *Pinus pumila* communities and the no fired *Pinus pumila* communities after the fire, to find influence of the fire. The ground temperature sensors were installed into at 1 cm, 10 cm, and 40 cm depth. The soil moisture sensors were installed into at 1 cm and 10 cm depth. The 1 cm depth of the soil on the post-fire slopes, diurnal freeze-thaw cycles occurred in October and November of 2011 and 2012, but it had not occurred in 2009 and 2010. In addition, the period of seasonal frost at 10 cm and 40 cm depth on the post-fire slopes are extended for two weeks. These thermal condition changes are triggered by decrease in the thickness of the litter layer on the fired *Pinus pumila* communities.

Combining time-lapse photography and multisensor data logging to monitor slope dynamics in the southern Japanese Alps

MATSUOKA, Norikazu^{1*}

¹University of Tsukuba

Onsite time-lapse photography (TLP) is applied to visual monitoring of soil movements and rockfalls in an alpine zone (Mt. Ainodake area) of the southern Japanese Alps. The time-series images greatly improve understanding of slope processes in remote, seasonally inaccessible areas. TLP detects the timing of slope movements at a high time resolution. Stereographic view of successive images displays 3D slope dynamics that indicates the location and magnitude of displacement. When combined with sensor-based data logging, TLP allows more reliable evaluation of thresholds (environmental controls) for slope movements. This presentation demonstrates (1) how visual information improves the interpretation of both slow progressive soil movements (frost creep) and rapid temporary movements (rill erosion and rockfalls) and (2) how highly active is slope dynamics in the southern Japanese Alps that experience deep seasonal frost in winter and heavy rain storms in summer.

Continuous monitoring of a painted line drawn on a debris lobe highlights biannual shallow soil movements, mostly derived from diurnal frost heave by needle ice or shallow ice lens formation and approximated by the potential frost creep. The surface velocity shows a small interannual variation mainly reflecting snow conditions, but an extraordinary velocity is recorded once per decade. This is due to episodic rill erosion released when the topmost frozen soil is rapidly thawed and super-saturated by intensive rainfall during seasonal thawing periods.

Year-round TLP images of a rockslide scarp allows evaluation of the timing and magnitude of rockfalls at different scales. Close-up images of color-painted quadrangles (50 cm square) indicates centimeter- to decimeter-scale spalling events. Spalling activity reach a maximum at the beginning of seasonal thawing, when the rockwall experiences both diurnal freeze-thaw alternations within the outermost 20 cm and progressive warming of the still-frozen substrate. Stereographic view of successive images also identifies block-scale rockfalls. Such an event occurred between 16 h on 7 July and 8 h on 8 July 2011, triggered by nocturnal rainfall (total 33 mm).

Keywords: time-lapse photography, field monitoring, rockfalls, solifluction, periglacial, Japanese Alps

Evaluation of long-term variability of rainfall-runoff properties in forested alpine catchment

KOJIMA, Toshiharu^{1*}; ZAINAL, Edwina²; OHASHI, Keisuke³; SHINODA, Seirou⁴

¹River Basin Research Center, Gifu University, ²Graduate School of Engineering, Gifu University, ³Faculty of Engineering, Gifu University, ⁴Information and Multimedia Center, Gifu University

The water conservation function of forest, so-called "Green Dam" in Japan, is recognized as one of the important forest's functions. However it is often miss-understood by general public such as "sponge theory". Water balance in forested catchment is not clear because of its complexity by many hydro processes. The authors investigate the long-term variability of rainfall-runoff properties by forest growth and climate changes in the Gamansawa catchment (3 km²), Nakatsudawa, Gifu, Japan. The study area has long-term hydrological data acquired by Gifu prefecture and Forestry Agency, Japan from 1984 to 2007. Main forest types are cypress(67%), cedar(4%), broad-leaves forest(20%) and so on. The long-term tendency of forest variation is investigated by satellite image analysis with Landsat/MSS, TM and Terra/ASTER images acquired from 1984 to 2010. The mean NDVI over the study area are increasing. Therefore the forest should be growing in the research period. The authors investigate the trend of event based discharge rates f (=total direct discharge at the event / total rainfall at the event). The hydrological data is divided to many rainfall events and event based discharge rates are evaluated. The event based discharge rates are on a slightly decreasing trend with $df/dt = -0.006 [y^{-1}]$. Moreover the long-term hydrological data is divided to four periods and apply to the 4-layer tank model in order to evaluate the variation of hydrological properties in the study area. We assumed that the long-term variation in forest property is mostly surface soil layer such as soil layer thickness and lateral permeability. Vertical permeability depends on bed rock cracks should not so much increase. Based on this assumption, the model parameter of the bottom hole, which is related to infiltration to aquifer, is fixed. The model parameters of the second and lower tanks are also fixed. And the variability of the model parameters of side holes of the first tank, which are related to direct discharge, is investigated. We obtained the results as the model parameters of the side holes have the tendency of decrease as 0.9 to 0.7[d⁻¹], during the research period. Next, using these model parameters, the test rainfall events are simulated and the following results were obtained. 1) The peak discharge volume is decreased. 2) The event based discharge rates f are decreased as 0.6 to 0.5. This trend is the almost same as the mentioned event based discharge rates with long-term hydrological data analysis. These results suggest the flood mitigation function is increased during this period. On the other hand, although the model parameter of the bottom hole is fixed, total infiltration volume to lower tanks and base flow are increased. This result suggests that water conservation to aquifer also increase without increasing of vertical permeability such as bed cracks. It can be explained as follows. Consider a simple tank has one side hole and one bottom hole. The discharge from the side hole q [mm/d] is defined as $q = ah$, where h [mm] is the storage depth of the tank, a [d⁻¹] is the side hole size. The infiltration from the bottom hole i [mm/d] is defined as $i = bh$, where b [d⁻¹] is the bottom hole size. The time variation of h is defined as $dh/dt = q - i$. We obtain the total infiltration volume I as $I = bC/(a+b)$, where C is a constant of integration. By the above equation, when a is decreased with fixed b , total infiltration is increased. Therefore, it is suggested that increasing of water conservation can be explained with lateral permeability depend on forest growth. Moreover, we simulated two cases about evapotranspiration. First case is considered evapotranspiration with Hammon equation, and second is not considered. Hammon equation estimates probability evapotranspiration based on air temperature and daylight time. The results with two cases are the almost same. It is suggested that influence of climate changes have less effect than other factors.

Keywords: water conservation function, climate change, percolation, tank model

Canopy photosynthetic and soil respiratory responses to rising temperature in a cool-temperate deciduous forest

MURAOKA, Hiroyuki^{1*} ; NOH, Namjin¹ ; NAGAO, Ayaka¹ ; SAITOH, Taku M.¹ ; KURIBAYASHI, Masatoshi¹ ; NODA, Hibiki M.² ; ITO, Akihiko² ; NAGAI, Shin³ ; NAKAJI, Tatsuro⁴ ; HIURA, Tsutomu⁴

¹Gifu University, ²National Institute of Environmental Studies, ³JAMSTEC, ⁴Hokkaido University

Prediction of possible influences of global warming on terrestrial ecosystem structure and functions is one of an urgent research tasks in environmental sciences. This paper overviews our challenging research by open-field warming experiments on forest canopy photosynthetic productivity and on soil respiration in a cool-temperate deciduous broadleaf forest at Takayama AsiaFlux and JaLTER site, located on a mountainous landscape in central Japan. Canopy warming experiment is conducted by three open-top canopy chambers (OTCC) on branches of a mature tree of *Quercus crispula*, one of the dominant canopy species in the forest. The OTCC increased mean daytime air temperature by about 2 degree-C, with midday maximum of about 5 degree-C throughout the growing seasons. Soil warming treatment, with 3 degree-C higher than the control area, was made by installing electric heating cables below the soil surface.

Warming treatment at the canopy-top led (1) expansion of canopy photosynthetically active season in about 10 days by 3-5 days earlier leaf budbreak and expansion and about 5 days delay of leaf senescence, and (2) slightly higher chlorophyll content and photosynthetic capacity of oak leaves. Warming treatment of forest soil showed (1) higher soil respiration throughout the seasons, resulting in 15% higher CO₂ efflux from the soil during the growing season, but (2) the temperature response of soil respiration acclimated to the higher temperature condition characterized by lower slope of the response curve. We also examined the possible effects of growing period length on forest canopy and understory vegetation ecosystem CO₂ budget under future climate conditions by using canopy-phenology ecosystem carbon cycling combined model. Our simulation indicated that annual total ecosystem GPP, RE and NEP was greater under the future condition than under the current condition by 9-12 %, 9-13% and 12-17%.

Our study demonstrates that open-field warming experiments provide us with useful and insightful knowledge on the ecophysiological responses of both canopy and soil processes to rising temperature, and their critical roles in predicting future changes of forest carbon cycle processes in cool-temperate region in Japan where ecosystem structure, functions and services are subjected to influence of the climate change.

Keywords: global warming, forest, photosynthesis, soil respiration, phenology

Effects of Open-top Chamber on Soil Oribatid Mites (Acari:Oribatida) at Mt. Kisokomagatake

FUKUYAMA, Kenji^{1*}; NAKAMURA, Hiroshi¹; KOBAYASHI, Hajime¹; TANAKA, Kenta²

¹Faculty of Agriculture, Shinshu University, ²Sugadaira Montane Research Center, University of Tsukuba

INTRODUCTION

Forest limit ecosystem on high mountains was one of the most vulnerable ecosystems against global warming. We investigated effects of artificial warming using an open-top chamber on forest limit ecosystem (2600m in elevation) of Mt. Kiso-komagatake, Chuo-alps, Nagano, central of Japan. Oribatid mites were useful environmental bio-indicator because they distribute most of all terrestrial soil habitats. Therefore, oribatid fauna were compared between artificial warming sites and control site in the study area. We investigate vertical distribution concerned with elevation of oribatid fauna from 2600m to 1250m. On the other hand, Mortality of oribatid species was investigated under different temperature in incubator.

METHOD

Research sites of vertical distribution were established at 1250m, 1700m, 1900m and 2100m above sea level in Nishikoma Station of Shinshu University. We selected two plots (coniferous forest and broad leaved forest) in each elevation site. Five soil samples were randomly corrected using core sampler (100cc) 5cm depth on 26 July 2012. Oribatid mites were corrected using the Tullgren funnel on same day. Additionally, two soil samples (about 400cc) were corrected at 1250m, 1400m, 1700m, 1800m, 1900m, 2000m, 2100m, 2200m and 2600m above sea level on 28 Aug. 2012.

Nine open-top-chambers (1m X 1m, about 2m in height) were established at 2650m above sea level near Mt. Shogigasira. Two soil samples (100cc, 5cm depth) were corrected using core sampler from each open-top-chamber on 20 Sept. 2013. Also two soil samples were corrected from control site close to each open-top-chamber. Two soil samples were set on one Tullgren funnel in laboratory on same day.

Soil samples (about 5000cc) were corrected from 2100m and 1250m above sea level in Nishikoma station of Shinshu University on 17 July 2013 and each soil sample was softly stirred by hand in laboratory and was divided in 15 nonwoven fabric bags (400cc). Each bag was set in unglazed pottery (11cm in diameter). Five potteries were incubated in incubator under 10 degrees centigrade, 20 degrees centigrade and 30 degrees centigrade from 17 July to 12 Aug. 2013.

RESULTS and DISCUSSION

Results of investigation of vertical distribution show that *Cyrtozetes* sp., *Tectocepheus velatus* and *Phthiracarus japonicus* positively increased their population densities correlated with elevation, and especially, *Cyrtozetes* was only found upper from 1900m above sea level.

Results of comparative study using the open-top-chamber show that *Cyrtozetes* and *Phthiracarus* in the open-top-chamber were significantly decreased instead of *Ghilarobizetes* significantly increased.

These results suggest that *Cyrtozetes* and *Phthiracarus* are good indicators for global warming monitoring in high mountain ecosystem.

On the other hand, mortality rate of *Cyrtozetes* and *Phthiracarus* were not affected by temperature from result of incubation one month after. The reason of no affection of temperature on *Cyrtozetes* is probably its long life cycle. More studies will be needed about it.

Keywords: oribatid mites, vertical distribution, global warming, bio-indicator, *Cyrtozetes*

The parametric estimation of the amount of CO₂ to be stored as HWP of the wooden house, based on the each of tree specie

TAKAMURA, Hideki^{1*} ; ASANO, Yoshiharu¹

¹Faculty of Engineering, Shinshu University and Institute of Mountain Science, Shinshu University

In the term of the handling of wood in Kyoto Protocol, it has been considered to release carbon accumulated in growing stage immediately into atmosphere at the time of cutting down from forest in the first commitment period. In the second commitment period, it has been considered to fix carbon while it is used as harvest wood products (HWP), and to release carbon into atmosphere at discarded stage. The main utilization of domestic wood is to build wooden house domestically, and it has an important role as a carbon pool of HWP. However, the rate of utilization of domestic wood has been continued to decrease. In order to take concrete strategy to measure rate of increase in utilization of domestic wood in the future, it is important to estimate present amount of utilization by each of tree species and the amount of prospect for increased use in the future.

Future estimation of carbon pool by HWP for all over the country was studied in the past research. In the estimation for all over the country, national total gross floor space, the number of new constructions per year, the number of households, the amount of average for wood utilization are used as basic date, it has not been estimated by each of tree species. Therefore, in order to estimate target amount of increased utilization for each of tree species, it is urgent issue to make calculation flow based on area characteristic by using the amount of tree species used in each material by region, and the amount of carbon stock (hereinafter called carbon balance) for each of tree species by region.

In this study, it was investigated that estimation method of the amount of utilization by each of tree species and the amount of carbon stock which is applicable to wood statistics and all prefectures. Estimation, which is for Nagano, of the amount of utilization for each of tree species and the amount of carbon stock was conducted by using carbon balance for each of tree species in Nagano which was revealed by Yamagata et al. in the past research, and the rate of utilization for each of tree species which was surveyed by Nagano Prefecture.

As a result of estimation, it revealed that the amount of carbon stock would decrease with a peak of 380,000 [t-C] in 2021 (Heisei 33). From the increase in the total gross floor space in the whole area of Nagano by the increase in the average of gross floor space per house, the amount of carbon stock indicated an upward trend until 2021. However, the amount of carbon stock declined by the decrease in the number of new constructions per year and increase in the number of losses of existing houses in 2022 and later. In this research, we conducted the estimation of the case in which 60% of domestic wood utilization that Forestry Agency advocated as a measure against decrease in the amount of carbon stock was achieved. As a result of having changed the domestic wood utilization up to 60% in 2011 and later, the decrease in the amount of carbon stock was not seen until 2038 (Heisei 50).

The estimation revealed necessity to increase supply of domestic wood approximately 50,000m³ per year to achieve 60% of utilization rate for domestic wood. There is sufficient amount of accumulated forest resources in Nagano, however, it is necessary to secure supply capacity. Ido et al. pointed out that it is difficult to adjust the cut of timber from forest since it is difficult to show demand prospect. For this issue, the estimation of this study is very useful and contributes to increase distribution of domestic wood by feeding back the estimation result to supply side. Since there is a distribution of domestic wood between prefectures, it is necessary to estimate by the method of this study in other prefectures. It is important to create road map which raises rate of utilization of domestic wood by planning and grasping the wood distribution of the whole country by obtaining each demand prospect in the future.

Keywords: Kyoto Protocol, HWP, wooden house, carbon stock, domestic wood

Snow patches of Japanese Alps last until late autumn 2013 and their past variations

ASAHI, Katsuhiko^{1*}

¹Institute of Mountain Science, Shinshu University

Variations in glaciers are visible indicators of climate change, especially in mountain region. In Japan, snow patch can be an alternate indicator since glaciers, long years, were not recognized in the Japanese Alps. One characteristic of the Japanese Alps is their extensive distribution of snow patch last until late autumn. A snow patch inventory for this mountain is urgently required, not only for monitoring snow patch variations but also to evaluate water reservoir in the region. Limited number of studies has attempted to complete snow patch atlas in Japan. As a step in this direction, the author has produced an inventory of snow patch lasts before winter 2013 at the entire area of the Japanese Alps. This study addresses the results of snow patch mapping 2013.

The work of compiling a perennial snow patch inventory for the Japanese Alps initially involved oblique aerial photographs taken from a charter flight throughout the Japanese Alps. These photographs were interpreted using a stereoscope. The photographs were taken on 7th and 10th October 2013. The planimetric outline of each perennial snow patch was manually delimited and drawn on 1:25 000 scale topographical maps and successfully compiled the complete set of snow patch inventory of the Japanese Alps in 2013. Then inventory of 2013 thus compiled reveals 579 snow patches with a total surface area of 3.66 km². The year 2013 distribution was much extensive rather than that of usual years. The lowest snow patch termini appeared at the altitude of 1070 m on Mt. Inu of the northern Japanese Alps and the southernmost was 35° 40' 30.5" at Mt. Kita of the southern Japanese Alps. The largest one was the area of 0.184km² on Mt. Karamatsu of the Northern Japanese Alps. Ca. 80% of them locate east-facing slopes, where leeward side against winter prevailing NW wind. Latitudinal profile of the terminus altitudes of snow patches shows northward gradients. Winter northwesterly blown from the Siberian High, collecting vapor from warm current on the Sea of Japan, bring orographic heavy snowfall to the northern part of the Japanese Alps. Thereafter, peculiar snow patch distribution last before winter is likely to be a ruling by maldistribution of snowfall in winter.

In the same area, the inventory of 1976/77, compiled by the vertical aerial photograph interpretation, counts 264 with the area of 2.48 km². Major distribution concentrated in Mts. Tsurugi and Tateyama, central part of the Northern Japanese Alps. The total area in this mountains were 0.78, 0.77, 0.58, 0.84 km² in 1969, 1977, 2009, and 2013, respectively. Snowfall amount in winter and the snow patch area fluctuate largely year-by-year. However, the area fluctuation limits within a range of 30% the total area.

Keywords: Year 2013, Perennial snow patch, Japanese Alps, Snow patch inventory, Aerial photograph

Effects of forest harvesting on winter microclimate and sediment movements in mountainous area

IMAIZUMI, Fumitoshi^{1*} ; NISHII, Ryoko² ; UENO, Kenichi² ; KUROBE, Kousei³

¹Graduate School of Agriculture, Shizuoka University, ²Faculty of Life and Environmental Sciences, University of Tsukuba, ³Graduate School of Life and Environmental Sciences, University of Tsukuba

Activities of periglacial processes are controlled by the hillslope microclimate (i.e., air and ground temperatures, ground water content) that is highly affected by land cover conditions. Thus, forest harvesting in periglacial areas possibly affects activities of sediment movement (i.e., soil creep, dry ravel) by changing the microclimate of hillslopes. Knowledge on the effect of forest harvesting on sediment movement are needed to protect aquatic ecosystems as well as to develop better mitigation measures for preventing sediment disasters. We also observed difference in the microclimate as well as sediment movement between harvested and non-harvested artificial forests in a periglacial area. The field observation was conducted in Ikawa University Forest, University of Tsukuba, in southern Japanese Alps. In this region, air temperature frequently rises above and falls below 0 degree in winter. Forest harvesting changed both temperature and water condition of hillslopes; diurnal fluctuations in the ground surface temperature in the harvested area (about 15 degree) were much larger than that in the non-harvested area (about 3 degree). In the period without rainfall, water content ratio of soil in the harvested area was lower than that in the non-harvested area. Difference in the freezing and thawing frequency between the harvested and the non-harvested area was also observed by interval cameras. In the period without snow cover, diurnal frost heave was observed almost everyday in the harvested area. In contrast, diurnal frost heave in the non-harvested was observed only several times in one winter. Consequently, forest harvesting changes both microclimate and activities of periglacial processes. Meanwhile, the volume of sediment captured by sediment traps was not clearly different between the harvested and the non-harvested areas. In the harvested area, we found that a large volume of sediment was captured by litters and branches of harvested trees left on the hillslopes. Therefore sediment supply rate from harvested area may be also affected by other factors, such as existence of litters and branches on the ground surface.

Keywords: freeze-thawing, sediment movement, soil creep, frost heave, dry ravel, forest harvesting

Spatial and temporal changes in soil respiration in an old-growth forest on the slope of Mt Hakusan

OHTSUKA, Toshiyuki^{1*} ; SUCHEWABORIPONT, Vilanee¹ ; IIMURA, Yasuo² ; YOSHITAKE, Shinpei¹

¹Gifu University, River basin research center, ²University of Shiga Prefecture, School of Environmental Science

Structure and function of cool-temperate beech forests have been dramatically altered by disturbance. Especially in old-growth forests, canopy disturbance has important influences on the structure and organization of forest communities. As a result, the complexity of forest structure affects the spatial difference in micro-environmental factors such as soil temperature and soil water content. Therefore, the spatial and temporal changes in soil respiration were studied using soda lime in 1-ha study site, and automated open-close chamber using IRGA (AOCC method) in canopy and gap areas in 2013 in an old-growth beech forest, Mt Hakusan. The spatial pattern with the different vegetation and micro-environmental factors showed the high efflux in canopy and the low efflux in gap. All soil effluxes increased from spring (Jun.-Jul.) to summer (Aug.), and then decreased in autumn (Sep.-Nov.). The seasonal pattern showed the hysteresis loop that soil respiration in spring was greater than that at the same temperature in autumn. Diel soil efflux was greatly controlled by soil temperature but a diel lag between soil respiration and soil temperature led to diurnal hysteresis loop in some season.

Keywords: Soil respiration, cool-temperate region, old-growth forests, carbon cycling, beech forests

Spatial distribution of soil microbial characteristics in a cool-temperate deciduous broad-leaved forest in Takayama

YOSHITAKE, Shinpei^{1*} ; YOSHITAKE, Ayako¹ ; IIMURA, Yasuo² ; OHTSUKA, Toshiyuki¹

¹Gifu University, River Basin Research Center, ²The University of Siga Prefecture, School of Environmental Science

1. Introduction

Heterotrophic microorganisms have an important role in nutrients cycling and soil formation through the organic matter decomposition. Therefore, it is important to clarify the spatiotemporal variation in quantitative and qualitative characteristics of soil microbial community and the factor(s) affecting such spatiotemporal variation in considering the matter cycling. Takayama Field Station of Gifu University has studied carbon cycling in a cool-temperate deciduous forest for long term and have clarified that various ecological processes such as soil respiration showed significant spatiotemporal variation. However, the information of soil microbial community is largely limited and especially, the spatial variation of microbial characteristics and factors affecting it still remain unclear. Then, we aimed to describe the spatial distribution of microbial characteristics and clarify the relationships between spatial distribution and environmental factors.

2. Materials and Methods

Our study site was cool-temperate deciduous broad-leaved forest on the northwestern slope of Mt. Norikura, central Japan. The site was dominated by oak (*Quercus crispula*) and birch (*Betula ermanii*, *B. Platyphylla*) and the forest floor is covered with a dense dwarf bamboo (*Sasa senaninsis*) community. A permanent plot of 1 ha was set on a west-facing slope and 100 subplots (each 10 m×10 m) are distributed along five microtopographic type: ridge (30), northern slope (25), valley bottom (19), southern slope (19) and western slope (7) (Fig.1). Litter (L layer) and mineral soil (0-5 cm of A layer) samples were collected from 100 subquadrat on early May 2013. Some soil properties (e.g., water content, pH, NH₄⁺-N, NO₃⁻-N) were determined. Microbial respiration rate from mineral soil sample was determined by open-flow method with infrared gas analyzer in laboratory condition.

3. Results, Discussion and future plan

Average value of microbial respiration rate per gram soil was significantly differed among five topographic types (one-way ANOVA, $P < 0.01$) and that in ridge ($3.6 \pm 0.81 \mu\text{g CO}_2\text{-C g}^{-1} \text{ h}^{-1}$) was significantly higher than that in valley bottom ($2.9 \pm 0.78 \mu\text{g CO}_2\text{-C g}^{-1} \text{ h}^{-1}$) (Tukey-Kramer test, $P < 0.05$). In this poster presentation, the effects of topography on microbial respiration rate will be discussed based on the differences in environmental factors such as soil water content, litter amount, and soil carbon and nitrogen contents. In addition, soil microbial biomass and community structure will be determined for collected mineral soil samples by phospholipid fatty acid (PLFA) analysis in near future and spatial distribution of microbial biomass, community structure, and respiration activity (respiration rate per biomass) will be clarified.

Keywords: a cool-temperate deciduous broad-leaved forest, soil microbial community, microtopography, microbial respiration rate

Global pattern of gene flow in plant species along altitudinal gradients on mountains

HIRAO, Akira^{1*}

¹Sugadaira Montane Research Center, University of Tsukuba

Several studies on mountain plants with wide-altitudinal distributions have found significant genetic differentiation and structuring among populations along altitudinal gradients. In most of the studies, however, the level of genetic differentiation was not highly remarkable. This is somewhat counterintuitive, since one would expect that mountainous species often exhibit heterogeneous environments and phenological differences along altitudinal gradients, which should be forces driving genetic differentiation. Understanding how gene flow corresponds with altitudinal gradients can inform process of the genetic structuring. I reviewed published studies to categorize global patterns of gene flow in mountainous plant species. These outcomes can depend on 1) isolation by distance, 2) mobility within similar altitudes, and 3) mobility among dissimilar altitudes, and imply evolutionary processes of the plant populations on mountains.

Keywords: altitudinal gradients, gene flow, genetic differentiation, plants

Frontier of using stable water isotopic information in studies on land-ecological, hydrological, and atmospheric process

YOSHIMURA, Kei^{1*}

¹Atmosphere and Ocean Research Institute, The University of Tokyo

In this study, it was clearly shown that vapor isotope data retrieved by satellite sensors or in situ monitoring networks have the potential to constrain the atmospheric fields. The results of this study can be applied in two directions. The first direction is a better analysis skill in current weather forecasting systems. Though our understanding of the atmosphere is improving, understanding the hydrological cycles of the mid- to upper troposphere and lower stratosphere in association with convective clouds remains difficult. Because it is apparent that water vapor isotopic information has unique characteristics with regard to the atmospheric hydrological cycle and technical improvements in satellite and in situ instruments are occurring rapidly, this direction is indeed quite promising. The second direction, regarding proxy data assimilation, is even more challenging and is significant in several disciplines. In the past, we lacked direct measurements of the Earth and were forced to rely on proxy data. Interpretation of proxy data is important but can be over-simplified. By using data assimilation for proxy data, an objective analysis of the past (specifically before the nineteenth century) can be achieved without simplifying the empirical relationship between proxy data and climate/environment information. Although there are many technical and theoretical obstacles in both directions, the authors strongly believe that scientific benefits can be achieved.

Keywords: stable water isotope ratio, data assimilation, hydrologic cycle, climate proxy, climate reanalysis, spectroscopic analysis

Significance of hyper spectral solar radiation observation

KUME, Atsushi^{1*} ; AKITSU, Tomoko² ; NASAHARA, Kenlo²

¹Ashoro Research Forest, Kyushu University, ²Faculty of Life and Environmental Sciences, University of Tsukuba

Land plants exhibit relatively weak absorbance of green light at around 550 nm, for reasons which remain elusive. Most research, however, has assumed that the solar radiation spectrum can be averaged without considering the spectral dynamics. The relations between the spectrum of incident radiation and light-harvesting pigments of organisms are crucial to understanding photosynthesis and light use efficiency. Although several light-harvesting pigments exist, most land plants use specific light harvesting chlorophylls, Chl a and Chl b, and carotenoids. Wavelengths longer than 700 nm or shorter than 400 nm are scarcely absorbed by chlorophylls, and cannot be used for photosynthesis. Radiation within the 400 to 700 nm waveband is defined as photosynthetically active radiation (PAR). However, chlorophylls do not absorb photons in the PAR waveband evenly. Only a few per cent of relative absorbance occurs in the green region (500 to 600 nm), nevertheless the photosynthetic quantum yields are equivalent to those from blue and red light.

Incident PAR comprises two main components, direct PAR (PAR_{dir}), which arrives directly from the sun, and diffuse PAR (PAR_{dif}), which is sunlight scattered by sky and clouds. These components are characterized by large differences in light quantity, directional characteristics and spectral quality. PAR_{dir} is highly directional and its energy can be concentrated and localized on a surface. PAR_{dif} is non-directional and its incident energy is well-averaged across a surface, allowing it to penetrate deeper into canopies. Consequently, PAR_{dir} and PAR_{dif} play different roles in the photosynthetic process both at the scale of individual leaves and of canopies. Most research, however, has assumed that the solar radiation spectrum can be averaged without considering the spectral and directional dynamics.

We had developed a precise solar tracking device for detecting direct and diffuse radiation. Direct and diffuse radiations were measured separately by two grating spectroradiometers (MS700, EKO Instruments Co. Ltd., Tokyo, Japan) fixed to sun trackers (STR-22G-S, EKO Instruments Co. Ltd.) equipped with a collimation tube (angle of view 5 degrees) for measurement of PAR_{dir}, and a shadow ball for measurement of PAR_{dif}.

Analyzing the relative absorption spectra of chlorophyll, we found that Chl a does not absorb direct solar radiation, while diffuse solar radiation is efficiently up-taken by Chl b. The spectrum of diffuse solar radiation is almost fixed with a peak wavelength (λ_{max}) around 460 nm. However, that of direct solar radiation shifts from a broad peak with λ_{max} around 700 nm towards a narrower peak around 540 nm, as solar zenith angle decreases. The absorption spectrum of Chl a lies outside the strongest energy regions of direct solar radiation. The λ_{max} of the Chl b absorption spectrum matches that of diffuse solar radiation; therefore, Chl b can absorb the most energetic parts of this radiation. The spectral differences between direct and diffuse solar radiation elucidate the meaning of slight spectral differences in pigments for terrestrial organisms.

Strong light is known to enhance accumulation of carotenoids. We found that β -carotene consistently absorbed more energy per photon than other pigments, indicating that it effectively filters (i.e. accepts) the 350-500 nm waveband, independently of PAR class.

Overall, the spectral differences between PAR_{dir} and PAR_{dif}, as well as the steady λ_{max} of PAR_{dif}, exert multiple effects on terrestrial organisms and may be effective drivers of diversification in pigment distribution and function. Further spectral-directional radiation observation at various sites is needed to reveal the effects of the dynamics of incident solar radiation on the terrestrial ecosystem.

Keywords: spectroradiometer, direct solar radiation, diffuse sky radiation, photosynthesis, spectral light use efficiency, PAR

Simultaneous Estimation of Hydrologic and Ecologic Parameters in an Eco-Hydrological Model Assimilating Microwave Signal

SAWADA, Yohei^{1*} ; KOIKE, Toshio¹

¹School of Engineering, the University of Tokyo

To improve the skill of reproducing land-atmosphere interactions in weather, seasonal, and climate prediction systems, it is necessary to simulate correctly and simultaneously the surface soil moisture (SSM) and terrestrial biomass in land surface models. Despite the performance of hydrological and ecosystem models depends highly on parameter calibration, a method for parameter estimation in ungauged areas has yet to be established. We develop an auto-calibration system that can simultaneously estimate both hydrological and ecological parameters by assimilating a microwave signal that is sensitive to both SSM and terrestrial biomass. This system comprises a hydrological model that has a physically based, sophisticated soil hydrology scheme, a dynamic vegetation model that can estimate vegetation growth and senescence, and a radiative transfer model that can convert land surface condition into brightness temperatures in the microwave region. By assimilating microwave signals from the Advanced Microwave Scanning Radiometer for Earth Observing System, the system simultaneously optimizes the parameters of these models. We test this approach at three in situ observation sites under different hydroclimatic conditions. Estimated SSM and leaf area index (LAI) exhibit good agreement with ground in situ observed SSM and satellite observed LAI, respectively. The root mean square error of SSM and LAI at all sites, estimated by the model with optimized parameters, is much less than that estimated by the model with default parameters. Using microwave satellite brightness temperature data sets, this system offers the potential to calibrate parameters of both hydrological and ecosystem models globally. This global-scale and automated parameter optimization system may contribute to many other research activities related to land surface, hydrological, and ecosystem modelling although the global-scale applicability of this approach should be investigated as a future work.

Keywords: Eco-hydrological model, passive microwave remote sensing, parameter optimization, data assimilation

Changes of permafrost environment and the response to the long term climate change

SUEYOSHI, Tetsuo^{1*} ; SAITO, Kazuyuki¹ ; ISHIKAWA, Mamoru² ; HARADA, Koichiro³ ; IWAHANA, Go⁴

¹Japan Agency for Marine-Earth Science and Technology, ²Hokkaido University, ³Miyagi University, ⁴University of Alaska

Permafrost is soil and sediment that is frozen more than two consecutive years, most of which is located in high latitudes. Ground ice is not always present, as may be in the case of nonporous bedrock, but it frequently occurs and it may be in amounts exceeding the potential hydraulic saturation of the ground material. Permafrost accounts for 0.022% of total water and exists in 24% of exposed land in the Northern Hemisphere.

permafrost contains 1700 billion tons of organic material equaling almost half of all organic material in all soils. This pool was built up over thousands of years and is only slowly degraded under the cold conditions in the Arctic.

Most of the permafrost existing today formed during cold glacial periods, and has persisted through warmer interglacial periods, including the Holocene. The time scale of the thermal process is different depending on the depth (i.e. distance from the ground surface) and the soil thermal properties, while the vegetation processes such as accumulation of organic material have yet different time scales.

In this presentation, we discuss those complex character of permafrost and show the outlook on the future research needs, showing an example study on the relationship between permafrost distribution and long-term climate change.

Keywords: Permafrost, climate change, ground ice, Carbon Cycle

Impacts of representation of stomatal conductance on vegetation distribution and functions under changing climate

SATO, Hisashi^{1*} ; KUMAGAI, Tomo'omi² ; KATUL, Gabriel³

¹RIGC, JAMSTEC, ²HyARC, Nagoya University, ³Duke University

Stomata reponce is under control of light intensity, CO₂ concentration, vapor pressure deficit, leaf water potential. For describing stomatal responses to such environmental factors, several empirical and semi-empirical models have been developed. How these models response to the changing environmental is an important issue, because between 80% and 90% of the total evapotranspiration from the land surface is caused by transpiration, and the process consumes almost half of the solar energy absorbed by the ground (Jasechko et al. 2013).

Here, we examined how representation of stomatal conductance pose impact on the forecast of geographical distribution of vegetation and its functions (i.e. carbon and water fluxes) under the forecasted climatic condition during the 21st century. We studied the African continent, because Africa is a useful target for assessing changes in vegetation due to climate change. The distribution of African vegetation is primarily regulated by soil moisture availability and thus is tightly coupled with climatic variability. For our study, we employed a dynamic vegetation model SEIB-DGVM. Our previous study shows that the model reproduced geographical distributions of the continent's biomes, annual gross primary productivity (GPP), and biomass over the African continent under current climatic conditions (Sato et al. 2012).

References

Jasechko S, Sharp ZD, Gibson JJ, Birks SJ, Yi Y & Fawcett PJ (2013) Terrestrial water fluxes dominated by transpiration. *Nature* 496.

Kumagai, T., Katul, G. G., Porporato, A., Saitoh, T. M., Ohashi, M., Ichie, T. and Suzuki, M. (2004) Carbon and water cycling in a Bornean tropical rainforest under current and future climate scenarios. *Advances in Water Resources*, 27(12), P1135-1150.

Sato H & Ise T (2012) Effect of plant dynamic processes on African vegetation responses to climate change: Analysis using the spatially explicit individual-based dynamic global vegetation model (SEIB-DGVM). *Journal of Geophysical Research-Biogeosciences* 117.

Keywords: Stomatal Conductance, Hydrological Cycle, Carbon Cycle, Dynamic Global Vegetation Models, Global Warming, Africa

Overview for terrestrial model intercomparison project in Arctic

MIYAZAKI, Shin^{1*} ; SAITO, Kazuyuki² ; YAMAZAKI, Takeshi⁴ ; ISE, Takeshi³ ; MORI, Junko¹ ; ARAKIDA, Hazuki⁵ ; HAJIMA, Tomohiro² ; HOSAKA, Masahiro⁶ ; IIJIMA, Yoshihiro² ; ITO, Akihiko⁷ ; MATSUURA, Yojiro⁸ ; NIWANO, Masashi⁶ ; O'ISHI, Ryouta¹ ; OHTA, Takeshi⁹ ; PARK, Hotaek² ; SATO, Atsushi¹⁰ ; SUEYOSHI, Tetsuo² ; SUGIMOTO, Atsuko¹¹ ; SUZUKI, Rikie² ; YAMAGUCHI, Satoru¹⁰ ; YOSHIMURA, Kei¹²

¹National Polar Research Institute, ²Japan Agency for Marine-Earth Science and Technology, ³Tohoku University, ⁴University of Hyogo, ⁵RIKEN, ⁶Metorological Research Institute, ⁷National Institute for Environmental Studies, ⁸Forestry and Forest Products Research Institute, ⁹Nagoya University, ¹⁰National Research Institute for Earth Science and Disaster Prevention, ¹¹Hokkaido University, ¹²The University of Tokyo

1. Introduction

The goals of the modeling group in the terrestrial research project of the GRENE Arctic Climate Change Research Project (GRENE-TEA) are to a) feed to the CGCM research project for the possible improvement of the physical and ecological processes for the Arctic terrestrial modeling (excl. glaciers and ice sheets) in the extant terrestrial schemes in the coupled global climate models (CGCMs), and b) lay the foundations of the future-generation Arctic terrestrial model development. To achieve these goals we are to conduct a model intercomparison project among the participating models, in which we will utilize the GRENE-TEA site observations data (stage 1) and GCM outputs (stage 2) for driving and validating the models. This project (GTMIP) is designated to 1) enhance communications and understanding of the "mind and hands" between the modeling and field scientists, 2) assess the uncertainty and variations stemmed from the model implementation/designation, and the variability due to climatic and historical conditions among the Arctic sites.

2. Data and models for GTMIP

At the stage 1, we will create data for forcing and validating the terrestrial model based on the extant and/or new observation data at GRENE-TEA sites to evaluate the inter-model and inter-site variations. However, the observation data are prone to missing or lack of the necessary variables or parameters to drive the model. Therefore, we create continuous forcing data (Ver. 0) taken from the reanalysis product (i.e. NCEP/NCAR) with the bias correction using the CRU data at the nearest grid to the GRENE-TEA sites. Then, it is merged with the observation data to create site-fit continuous data (Ver. 1) for each GRENE-TEA site (Fairbanks in Alaska, Yakutsk, Tiksi, Tura and Chokurdakh in Russia, Kevo in Finland). These data will be open at Arctic Data Archive System (<https://ads.nipr.ac.jp/index.html>).

The GTMIP participating models include a land surface model (MATSIRO, 2LM, CHANGE, HAL), a material cycle model (VISIT), a terrestrial ecological model (STEM-NOAHbgc), a dynamic vegetation model (SEIB-DGVM), a regional climate model (WRF), physical snow models (SNOWPACK, SMAP), and a permafrost model (FROST). The models enabled to couple with the CGCMs and regional climate model (RCM) consist of the 70% of the all participating models.

3. Results

The Ver. 0 data was compared with site observations near Fairbanks, Alaska, USA, to evaluate its reliability. The daily mean air temperature was well-reconstructed but the diurnal variation was underestimated. The total annual precipitation was close to the observed, but summer (DOY150-250) rain tended clumpy.

The observed ground temperature (T_g) at near surface showed the zero-curtain, while the simulated T_g failed to produce the zero-curtain except for 2LM. The 2LM reproduced the observed snow depth well while the CHANGE and MATSIRO-r showed later start and end of snow cover with lower snow depth than observed. The sensible heat flux was the dominant component of the energy budget in the simulation by 2LM. The daily net ecosystem exchange (NEE) simulated by CHANGE showed the large carbon uptake in summer. The annual gross primary production (GPP) simulated by CHANGE increased during 1988 to 2011. The simulated GPP by SEIB-DGVM using T_g by MATSIRO-r was similar to the GPP using air temperature. The wood biomass and grass biomass simulated by SEIB-DGVM using air temperature and T_g by MATSIRO-r was similar while it was lower when calculated using T_g by MATSIRO-c. The soil organic matter (SOM) simulated by SEIB-DGVM using MATSIRO-r was largest among the SOM using air temperature and T_g by MATSIRO-c.

Keywords: Arctic, Terrestrial model, Snow cover, Permafrost

The assessments of projection uncertainties of global C budget in ISI-MIP study

NISHINA, Kazuya^{1*} ; ITO, Akihiko¹ ; KATO, Etsushi¹ ; YOKOHATA, Tokuta¹ ; ISI-MIP, Team²

¹National Institute for Environmental Studies, ²ISI-MIP team

Global net primary production (NPP), vegetation biomass carbon (VegC), and soil organic carbon (SOC) changes estimated by six global vegetation models (GVMs) obtained from an Inter-Sectoral Impact Model Intercomparison Project study were examined. Simulation results were obtained using five global climate models (GCMs) forced with four Representative Concentration Pathway (RCP) scenarios. To clarify which component (emission scenarios, climate projections, or global vegetation models) contributes the most to uncertainties in projected global terrestrial C cycling by 2100, we applied analysis of variance (ANOVA) and wavelet clustering to 70 projected simulation sets. ANOVA revealed that the main sources of uncertainty are different among variables and depend on the projection period. We determined that in the global SOC and VegC projections, GVMs dominate uncertainties (90% and 60%, respectively) rather than climate driving scenarios, i.e., RCPs and GCMs. The clustering wavelet spectra of VegC and SOC time series data could identify more specific characterization of simulations in each GVM. Our study suggests that the improvement of GVMs is a priority concern for reduction of total uncertainties in projected C cycling for climate impact assessments.

Keywords: Model inter-comparison, Global carbon cycle, Uncertainties, RCP, GCM

An aerosol correction algorithm to improve the GOSAT TANSO-CAI NDVI product

KIKUCHI, Nobuhiro^{1*} ; YOKOTA, Tatsuya¹

¹National Institute for Environmental Studies

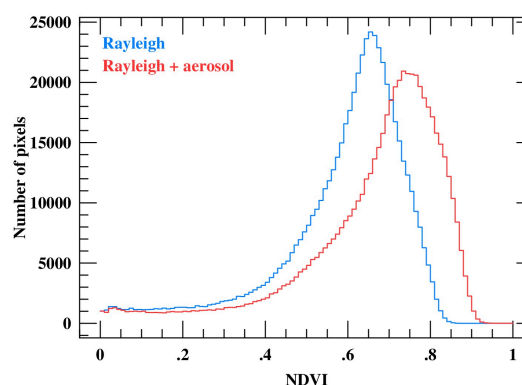
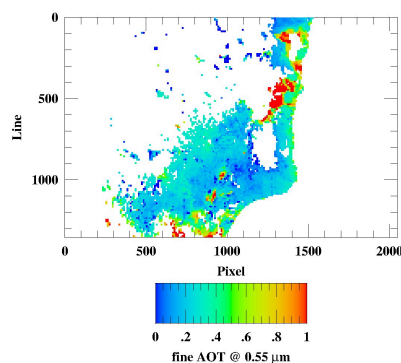
The Cloud and Aerosol Imager TANSO-CAI (CAI), onboard the Greenhouse gases Observing SATellite (GOSAT), is equipped with 4 spectral bands of 380, 674, 86,0 and 1600 nanometers (Band 1-4). The main purpose of CAI is to assist the Fourier Transform Spectrometer TANSO-FTS in retrieving accurately the column amount of carbon dioxide and methane by detecting and characterizing clouds and aerosols in FTS footprints. CAI is also designed to monitor the variation of global vegetation indices, and the CAI Normalized Difference Vegetation Index (NDVI) product has already been released.

Since GOSAT is orbiting with a three-day recurrence, CAI observes the same location from the same direction once in every three days. Unlike the MODIS NDVI product, this makes it difficult to correct the effects of Bidirectional Reflection Distribution Function (BRDF) on the CAI NDVI product, but it has a potential capability to detect changes in vegetation with shorter time scale. In the current version, the CAI NDVI is calculated from 30 days composite of the minimum reflectance to minimize contamination of clouds and aerosols, and the effect of aerosols is not explicitly corrected. The goal of this study is to develop an aerosol correction algorithm that can be applied to the CAI NDVI.

Due to the relatively limited number of spectral bands of CAI, we take an approach slightly different from so-called the Kaufmann method or the minimum reflectance method in developing our aerosol correction algorithm. Since the number of observables is four, which are TOA reflectance at bands 1-4, the maximum number of retrieved parameters is also four. We choose optical thickness of fine mode aerosols and coarse mode aerosols, surface reflectance at band 3 and band 4 as retrieved parameters. We assumed that surface reflectance at band 1 and band 2 is expressed as a function of surface reflectance at band 3 and band 4. The parameterization of band 1 and band 2 surface reflectance is done by utilizing the CAI minimum reflectance product. We do not expect that this parameterization is rigorously valid in pixel-wise. Therefore, we do not determine aerosol optical thickness for every pixel, but for 10x10 pixels (5x5 km in horizontal scale). Moreover, we do not use all TOA reflectance of 10x10=100 pixels, but select the darkest 10 pixels. Then, the number of observables is 40, and the number of retrieved parameters is 22, which can be determined by least-square fitting.

Left panel of the figure shows optical thickness of fine mode aerosol over south-east part of Australia on October 20th, 2013. Currently, aerosol optical thickness is not retrieved for pixels with TOA reflectance greater than 0.2 at band 4. Right panel of the figure demonstrates the effect of aerosols on NDVI by comparing NDVI with and without aerosol correction. We can see that the frequency distribution of NDVI is shifted by about 0.1 as a result of aerosol correction, which is consistent with the result of Vermote et al. (2002).

Keywords: vegetation index, retrieval method, GOSAT



Effects of water stresses due to climate change on production and dynamics of tree community in tropical rain forests

FUJII, Shinjiro^{1*} ; SATO, Hisashi² ; KUMAGAI, Tomo'omi¹

¹Hydrospheric Atmospheric Research Center, Nagoya University, ²Graduate School of Environmental Studies, Nagoya University

Recently, climate changes caused by the El Nino-Southern Oscillation have been reported to result in the widespread death of trees due to droughts in many parts of the world. Strong reductions in tree growth and litterfall production occurred during the record-hot 1997/98 El Nino. Tropical regions receive strong solar radiation, and tropical vegetation shows a strong feedback effect to carbon sequestration, water circulation, and climate formation. In addition, tropical forests are important ecosystems, and they act as a huge carbon sink because they accumulate 40-50% of land vegetation carbon of the Earth. In a biological community such as a tropical forest that consists of various species, response to changes in the physical environment depends on the operating functional group. A dynamic change in a particular functional group that plays a significant role in the biological community may influence the structure and ecosystem functions of the tropical forests. The aim of this study is to predict the impact of drought on matter production and tree community dynamics in tropical rain forests by using a spatially explicit individual-based biogeochemical model developed for predicting vegetation dynamics in response to climate change at the global level, such as global warming (SEIB-DGVM). In the model simulation, applying stochastic rainfall model with the meteorological data, including the 1997/98 El Nino, of the tropical rain forests of Sumatra Island in Malaysia that were measured in 1997-2009, the rainfall experiments were performed by operating some parameters related to daily precipitation and frequency of rainfall events. Based on the experiment results, the turn of production with the amount of tree growth and death, and tree mortality dynamics in the tropical rain forests for 200 years were verified.

Keywords: drought, water stress, El Nino, tropical rain forests, matter production, SEIB-DGVM

Modeling Interactions between Vegetation and Aeolian Processes

BANZRAGCH, Nandintsetseg^{1*} ; SHINODA, Masato¹ ; SHAO, Yaping²

¹Arid Land Research Center, Tottori University, ²Institute for Geophysics and Meteorology

The sustainability of temperate grassland (TGs) ecosystems is determined by the feedbacks between climate, vegetation and human activities, in which Aeolian processes play a key role. Current existing dust models do not have sufficient capability in simulating vegetation growth and decay effects that play a major role in TG aeolian processes. In this study, we purposed to couple the DAYCENT, a vegetation-growth and nutrient-cycle model (the most prominent biogeochemical model), with QF2003, a wind-erosion model. The DAYCENT-QF2003 modeling system enables an examination of the feedbacks between grassland-grazing and aeolian processes. This approach is a completely new approach. First, we assessed the DAYCENT for its capability to provide estimations of vegetation dynamics under different grazing conditions in order to incorporate into the QF2003. DAYCENT was parameterized with the field experiment data (soil physical/chemical properties, vegetation and grazing) at the Bayan-Unjuul (BU) site in 2010-2012. BU is located in north of the most frequent dust outbreak region in Mongolia. Results showed that the DAYCENT could simulate realistically vegetation growth-decay, nutrient-cycle and the effect of grazing on grasslands, which are the factors controlling dust outbreaks in TGs. Then, the DAYCENT model was coupled into the QF2003 wind-erosion scheme. We conducted the numerical test of the coupled DAYCENT-QF2003 model to predict dust flux. With the initial results, we have demonstrated the potential of the DAYCENT-QF2003 coupled model. Therefore, the integrated DAYCENT-QF2003 modeling system will provide a useful tool for an early warning system and the future projection of dust events over dust source areas in TGs region.

Keywords: Temperate grassland, dust, vegetation, model

Effects of water and dissolved material exchanges between land and ocean on coastal ecosystem and fishery resources

TANIGUCHI, Makoto^{1*}

¹Research Institute for Humanity and Nature

There are two pathways of water and dissolved materials from land to the ocean. The first one is river discharge and another is invisible submarine groundwater discharge (SGD). Many studies show the importance of SGD on coastal ecosystem and fishery resources. SGD is evaluated by using seepage meters and piezometers at local point scale, radon and strontium isotopes as tracers in bay scale to identify the origin of the fresh water, which is river water or groundwater. Another method is resistivity measurement which can tell us the salinity of the pore water in the sea bed near the coastal zone.

SGD observed by seepage meter and Rn concentration of the coastal seawater has a positive relationship over the world with different geology, geomorphology, and hydro-meteorological conditions. All SGD studies show that there are two components in SGD, one is fresh SGD and another is recirculated SGD. It is important for understanding coastal ecosystem and fishery resources to evaluate the ratios and processes of fresh SGD which is driven by hydrological condition in land, and recirculated SGD which is driven by oceanographic conditions in the sea.

In this study, SGD studies by using seepage meter and radon measurements over the world are reviewed to evaluate the physical and chemical factors which drive SGD and material transports by SGD, and the effects of SGD on the distribution of the fishery resources such as shell distributions in the coastal zone. River discharge is a main linkage between land and ocean through water and dissolved material transports, however it has huge temporal changes. On the other hands, the amount of SGD itself is not much but continuous contribution by SGD with constant temperature and nutrient discharges make stable physical, chemical, then biological conditions such as sea grass (*Zostera* bed).

Keywords: submarine groundwater discharge, coastal ecosystem, coastal fishery resources, nutrients, seepage, radon

The effect of freshwater input from rivers on the ecosystem in coastal waters

KASAI, Akihide^{1*}

¹Field Science Education and Research Center, Kyoto University

High production in coastal areas is supposed to be supported by large organic and inorganic inputs from rivers. Therefore, excessive reduction of nutrient loads from rivers would decrease nutrient concentrations in coastal areas. This manifests in poor growth of seaweeds, which has been observed in Seto Inland Sea in recent years. However, primary production in coastal areas is not only supported by terrestrial nutrients, but also external nutrients derived from ocean and regenerated nutrients formed in hypoxic water at the bottom. Evaluation of the contribution of each source of dissolved inorganic nitrogen (DIN) to phytoplankton production in Ise Bay revealed that DIN consumption by phytoplankton exceeds the DIN supply from rivers and ocean. This indicates that a large amount of primary production depends on regenerated DIN within the bay rather than on newly supplied DIN, although the ratio of consumption to external supply differs seasonally. We have to pay more attention to the behavior of each source of nutrients for future managements of coastal waters.

The effect of the freshwater input from rivers on coastal areas is not only the nutrient supply, but also the formation of estuarine circulation, which plays an important role in coastal ecosystems. Since the flux of water by the estuarine circulation is considerably larger than the river discharge, it has large effects on the material transport and biological production in estuaries and bays. For example, larvae of temperate seabass do not distribute in the surface, but in the middle layer, and thus the landward flow effectively transports larvae to coastal areas from the spawning grounds in the offshore. Therefore, the year-to-year variation in the amount of juveniles in the coastal area shows that the survival of juveniles improves in the years when the river discharge increases.

Keywords: coastal ecosystem, estuarine circulation, freshwater, nutrients

Possible effects of submarine groundwater on biodiversity and fishery production in coastal ecosystems

SHOJI, Jun^{1*} ; SUGIMOTO, Ryo² ; TOMINAGA, Osamu² ; KOBAYASHI, Shiho³ ; YAMADA, Makoto⁴ ; TANIGUCHI, Makoto⁴

¹Hiroshima University, ²Fukui Prefectural University, ³Kyoto University, ⁴Research Institute for Humanity and Nature

Economic values of the ecosystem services of coastal ecosystems have been evaluated as among the highest of those the world's ecosystems. Recently more attentions have been paid on the mechanisms how the freshwater contribute to the high productivity and species diversity of the coastal ecosystems. In the present paper, previous researches that focused on effects of freshwater input from the land on productivity and species diversity of fishery resources in the coastal ecosystems are reviewed. In addition, results from recent surveys conducted in order to examine the possible effects of river water and submarine groundwater on productivity and species diversity of fishery resources are introduced.

Relationship between river discharge and recruitment of several estuarine-dependent fish species (flatfish, seabass and clupeid) have been reported in the world. Among these fish species, the mechanisms how river discharge promotes survival during the early life stages and recruitment of Morone fishes (striped bass and white perch) have been well studied. Larval survival rate is high and recruitment of 1-year-old fish is successful in years with high precipitation in these species. High freshwater discharge has been reported to increase availability of prey for the larvae, decrease predation through affecting predator species composition and biomass, then increase the growth and survival during the larval stage.

In a previous paper, on the other hand, low salinity zone has been reported to be one of the ecosystems where biodiversity is the lowest among the world's aquatic ecosystems. High fluctuation in salinity and tidal level within a relatively small spatial and temporal scale could be stressful for a variety of animal species. Recently high abundance of juveniles of several flatfish species were observed in low salinity zones nearby an estuary in the coastal waters of Japan. Species diversity of fishes was higher in a seagrass bed where freshwater supply from the land through submarine groundwater was expected compared to the surrounding areas. These observations suggest that low salinity condition does not always decrease diversity of fish species in coastal ecosystems. Future research plan to investigate the mechanism how the freshwater input from the land contributes to the high productivity and species diversity in the coastal ecosystems will be introduced.

Keywords: water-food NEXUS, fishery production, species diversity, submarine groundwater

Evaluation of nitrogen dynamics in the Yodo River estuary using stable isotopes

SUGIMOTO, Ryo^{1*} ; KASAI, Akihide²

¹Faculty of Marine Biosciences, Fukui Prefectural University, ²Field Science Education and Research Center, Kyoto University

The increase in human population in coastal watersheds has increased the delivery of nitrogen from the land to coastal environments. Accelerated nitrogen cycles in coastal environments have led to an increase in hypoxic waters and instances of harmful algal blooms. Physical and biogeochemical processes within estuaries generally regulate nitrogen fluxes from land to sea. The estuaries of major rivers on the continents are thought to be sites of massive nitrogen losses. However, function of estuaries to nitrogen transfer must vary according to each estuarine hydrology and biogeochemistry. A large amount of terrestrial nitrogen empties into Osaka Bay head from the Yodo River. Although the estuary would have a crucial role in modifying nitrogen fluxes, its function to nitrogen transfer is still unclear. In this presentation, we will report the seasonal difference of nitrogen dynamics along the longitudinal section from the estuary to the head of Osaka Bay.

Keywords: nitrogen, stable isotopes, estuarine circulation, eutrophication, regeneration

Factors of the temporal variation of marine phytoplankton at Yodo River estuary

HAYASHI, Mitsuru^{1*} ; KOGA, Ryuraro¹ ; FUJII, Tomoyasu² ; YAMAMOTO, Keigo³

¹Kobe Univ., ²Nara University of Education, ³Marine Fisheries Research Center, Osaka Prefecture

Red tides of *Alexandrium tamarense* have occurred in the estuary of the Yodo River in Japan in 2007, 2011 and 2013. *A. tamarense* is marine phytoplankton and causes shellfish poisoning. We have made in-situ observation in April 2-3 2012, and analyzed the temporal variation of marine phytoplankton by using the numerical ecosystem model. CTD and ADCP observation and water sampling were carried out linked to the tidal change. Nutrient and chl.a concentration and cell density of *A. tamarense* were analyzed. *A. tamarense* was a few in this year. Typical estuary circulation which seawater run up to upstream in the surface layer and fresh water go down to the sea in the bottom layer. Therefore the estuary which have 2800m length was divided to three layers, 0-0.5m, 0.5-1.5m and 1.5m-bottom. The thickness of the bottom layer is changed with the tidal change. Nutrient, phytoplankton, the dissolved organic matter and the particulate matter are in each layer, and the bio-chemical process between the forms, photosynthesis, mortality, decomposition and so on, are formulated. Then the temporal variations of each morphology and *A. tamarense*. Diurnal migration, salt limitation and utilization of organic matter for the photosynthesis and mortality by low salinity were considered in the bio-chemical process of *A. tamarense*. The temporal variations of phytoplankton in each layer were almost reproduced. Marine phytoplankton in the Yodo River estuary were not produced hardly and were supplied from the ocean. Phytoplankton which cannot swim by oneself is almost floated by the horizontal advection, it is the estuary circulation. But only 27% of *A. tamarense* transported from the ocean in the bottom layer go through upstream. 36% of it returned to the ocean in the middle and surface layers, and other 36% die in the surface layer. Weak estuary circulation is effective to limit the transport upstream of *A. tamarense* in Yodo River estuary.

Keywords: Yodo River, Estuary, Numerical ecosystem model, Phytoplankton, *Alexandrium tamarense*

Utilization of terrestrial organic matter by marine benthic polychaetes in estuarine ecosystem

SATO, Takahisa¹ ; SUGIMOTO, Ryo² ; YOKOYAMA, Yoshihiro² ; TOMINAGA, Osamu^{2*}

¹Yamagata prefectural fisheries high school, ²Fukui prefectural university

In semi-enclosed bays, terrestrial plants transported by river have become a major constituent of estuary sediment. Since it is difficult for marine organisms to digest the terrestrial plants which mainly contains the non-living refractory cellulosic matrices, few studies have been taken into account the role played by the terrestrial particulate organic matter (tPOM) in enhancing the productivity of the coastal biotic community. However, the important role of tPOM as the food source for marine benthic organisms has been recognized in estuarine environments. In the present study, we examined the $\delta^{13}\text{C}$, $\delta^{15}\text{N}$ values and cellulase activity of the several species of polychaetes to elucidate the contribution of terrestrial plants to benthic biological production in small semi-enclosed Bay. Polychaete annelids were collected at estuary of the Kita and Minami River in semi-enclosed Obama Bay, the Sea of Japan from August 2007 to June 2010. The carbon and nitrogen stable isotope ratios of polychaetes were analyzed. Cellulase activity analyses were assayed by using carboxymethyl cellulose (CMC) plate assay. The $\delta^{13}\text{C}$ values of deposit or suspension feeding polychaetes were lower than the $\delta^{13}\text{C}$ value of POM but higher than the terrestrial plants. The $\delta^{13}\text{C}$ and $\delta^{15}\text{N}$ values of carnivores-feeding polychaetes were higher than those polychaetes. Cellulase activities was found in many deposit or suspension feeding polychaetes but also carnivorous feeding polychaetes. On the other hand, the polychaete species with lower isotope signature did not show cellulase activities. The polychaetes which showed cellulase activity were abundant through the four seasons in estuary. These results suggest that many polychaetes can decomposition and assimilation the terrestrial plants.

Keywords: terrestrial plants, cellulase,, semi-enclosed bay, polychaetes

The origin of submarine groundwater discharge in the coastal zone of Hiji, Oita prefecture

YAMADA, Makoto^{1*} ; OHSAWA, Shinji² ; MISHIMA, Taketoshi² ; ABE, Yutaka¹ ; TANIGUCHI, Makoto¹

¹Research Institute for Humanity and Nature, ²BGRL, Institute for Geothermal Sciences, Kyoto University

It is said that groundwater discharge from the seabed of the coastal zone of Hiji, Oita prefecture. The marbled sole which lives around this submarine groundwater discharge is called a “Shirosita Karei”, and is loved by the local people. From ancient times, the local people have believed that this Shirosita Karei grows because of submarine groundwater discharge. However, regarding the relevance of the ecology of a marbled sole and submarine groundwater discharge, it is not clear that this is the case. Moreover, although it is clear that there is submarine groundwater discharge, there is almost no information about the origin and dissolved component. Kono and Tagawa (1996) conducted an analysis of the major dissolved components of groundwater of this land area, and a vertical distribution investigation of the electric conductivity of the ocean. As a result, it has suggested the possibility that submarine groundwater discharge is the confined groundwater recharged in the mountain area. However, in that report, they said that they were not able to identify a recharge area clearly by this research. Because of that, we sampled the spring water of the land area, the spring water of a salt water mixture discharged in a seashore area, and a sea water sample, in order to conduct hydrological research using the stable isotope of water in this area and to clarify the flow process of submarine groundwater discharge. The recharge elevation of the spring water of this land area was assumed using the recharge-water line (Ohsawa et al., 2009) made using the data of the Beppu area of the southwest part of this research region. As a result, it became clear that the recharge area of most spring water is at an elevation of 200 m or more. Regarding fresh water and salt water mixture, the mixed rate of sea water and fresh water was calculated using electric conductivity, and the isotopic ratio of the original fresh water was computed using the mixed rate. As a result, it became clear that the recharge elevation of the fresh water mixed in sea water is near 300 m. Moreover, as a result of extracting the terrestrial environment of this area, the area with an elevation of 200 m or more is mainly forest, and there was a boundary between the forest area and plains near an elevation of 200 m. It became clear from these results that the origin of the submarine groundwater discharge in the coastal zone of Hiji is the water recharged in the forest area of the mountain slope, and that the water moves under the plain and is discharged at the sea bed.

Keywords: Submarine groundwater discharge, Stable isotope, recharge area, Hiji

Location estimation of submarine groundwater discharge from Mt. Fuji in Suruga Bay

MURANAKA, Yasuhide^{1*} ; KAMITANI, Takafumi¹ ; WATANABE, Masayuki¹ ; ONO, Masahiko² ; MARUI, Atsunao²

¹Shizuoka Institute of Environment and Hygiene, ²National Institute of Advanced Industrial Science and Technology

Around the foot of Mt. Fuji, the main flow passages of groundwater are thought to be in the Younger Fuji volcano, which consists of the pervious basaltic lavas in new volcanic stage. Especially, the Fujikawa-kako fault zone, which stretches south to north in the southwestern side of Mt. Fuji, has a potentially effect on the local groundwater flow system into Suruga Bay. Therefore, precipitation at Mt. Fuji have been considered to be discharging partly from seabed in Suruga Bay and making a great impact on the biological production at the coastal sea area.

For the purpose of contribution to make sense of the rich coastal ecosystem in Suruga Bay, we conducted a survey for submarine groundwater discharge (SGD) in Oku-Suruga Bay: from the mouth of the Fuji River, at which the fault is found, to Tagonoura, where the lavas of the Younger Fuji volcano are distributed from 100 to 200 m below sea level. We are trying to estimate some locations of SGD from the condition of seabed and geological structure by using the side scan sonar and the sub-bottom profiler. We also use a remotely operated vehicle (ROV) for photographing for the image of the extrapolated spring points. In this presentation, we introduce our works noted above.

Keywords: submarine groundwater discharge (SGD), Mt. Fuji, Suruga Bay, side scan sonar, remotely operated vehicle (ROV)

Evaluation of submarine groundwater discharge in Suruga Bay by using radon 222

ONO, Masahiko^{1*} ; MARUI, Atsunao¹

¹National Institute of Advanced Industrial Science and Technology

Submarine groundwater discharge (SGD) in coastal area has been recognized as an important pathway for material transport from land to ocean. SGD has been widely studied throughout the world and it is expected as ubiquitous phenomenon in coastal zone.

Suruga Bay is adjacent to the southern foot of Mt. Fuji where the permeable lava flow deposits and the active groundwater flow system exist. Therefore, large amount of groundwater input is expected at the coastal area in Suruga Bay. It is also expected that SGD has a significant effect for marine products in this area.

To evaluate submarine groundwater discharge in this area, we applied continuous radon measurement and sampled coastal water for chemical analysis. We will introduce these results in this presentation.

Keywords: Rn-222, Submarine groundwater discharge, Suruga Bay

Estimating submarine groundwater discharge in Obama Bay, Japan, using ^{222}Rn mass balance model

HONDA, Hisami^{1*} ; SUGIMOTO, Ryo¹ ; KOBAYASHI, Shiho² ; TAHARA, Daisuke¹ ; TOMINAGA, Osamu¹ ; TANIGUCHI, Makoto³

¹Fukui Prefectural University, ²Kyoto University, ³Research Institute for Humanity and Nature

Recently, a number of studies have shown that submarine groundwater discharge (SGD) is even more important than surface runoffs in terms of nutrient transport and can drive primary production in coastal seas. Obama Bay is semi-enclosed bay in central Japan. In spring, phytoplankton blooms in the bottom layer around 2 km offshore from the river mouth. Aquifer distribution in the Obama plain and our previous observation of low salinity water around the bottom layer suggests that unconfined groundwater discharges induce this phytoplankton bloom. However, quantitative contribution of groundwater discharge to the coastal ecosystem has not been well evaluated in Obama Bay. In this study, we estimated the input of freshwater and nutrients via SGD into Obama Bay using mass balance model of radon (^{222}Rn) and salinity. As a result, the volume of SGD into the bay was estimated to be $0.05\text{-}0.80 \times 10^6 \text{ m}^3 \text{ d}^{-1}$ during February 2013 to November 2013. Especially, the fraction of SGD in total freshwater flux in summer reached to 44%, because river water discharge decreased drastically. The nutrient fluxes from SGD were approximately 84%, 210% and 28% of riverine fluxes dissolved inorganic nitrogen (DIN), dissolved inorganic phosphorous (DIP) and dissolved inorganic silicate (DSi), respectively.

Keywords: Submarine groundwater discharge, ^{222}Rn mass balance, Obama Bay

A study of primary production in plankton blooms driven by riverine inputs

HOSHIBA, Yasuhiro^{1*} ; YAMANAKA, Yasuhiro¹

¹Faculty of Env. Earth Science, Hokkaido University

Rivers transport nutrients and suspended sediment matter (SSM) as well as fresh water from land to coastal regions, where the biological productivity is high. In the coastal area, the buoyancy of fresh water leads to the formation of horizontal anticyclonic gyres and vertical circulations, which affect the variation of biological production such as plankton blooms. However, the primary production caused by the three-dimensional dynamics have not been quantitatively discussed, and observations can hardly capture the daily temporal variations of phytoplankton blooms. We developed an ocean general circulation model (OGCM) including a simple ecosystem model, to investigate the three-dimensional and temporal changes in phytoplankton blooms caused by riverine input such as flooding.

We first conducted ideal setting-simulations. The distribution patterns of nutrients and phytoplankton differ significantly from that of fresh water. The phytoplankton maxima shift from the downstream (right-hand side of the river mouth) to the upstream regions (left-hand side of the river mouth). The shift from the downstream to the upstream region (D-U Shift) is categorized by the different nitrate origins: (1) river-originated nitrate (RO-nitrate) is dominant in the downstream region; (2) subsurface-originated nitrate (SO-nitrate) is dominant in the upstream region, and is transported by upwelling associated with vertical circulation and horizontal anticyclonic gyre; and (3) regenerated nitrate (R-nitrate) is dominant in the upstream region. The total primary production in phytoplankton blooms is maintained not only by RO-nitrate but also by SO-nitrate that is larger than the river-originated.

Next, we conducted a realistic simulation and a few ideal setting-simulations. The phytoplankton maxima shift toward the left-hand side of the river mouth during the early time, but the shift does not keep going to the left-hand side all the time. This is because much SO-nitrate does not come from the subsurface to the surface layer after the middle simulated time, due to weak upwelling forced by vertical circulation in the left-hand side. The gentle angle of bottom slope weakens the vertical circulation and SO-nitrate supply from the subsurface, and the NPP is small.

It is natural that D-U Shift of phytoplankton maxima often occurs in the real situation like Ishikari Bay when high riverine input such as flooding. The conclusion that the shift is categorized into three stages by the different nitrate origins, RO-, SO- and R- nitrates in turn depends on the bottom slope angle and the way of inputs and the amounts of fresh water and nutrients. Bottom slope angle and the way of fresh water input change the behaviour of plumes, nutrient supply from the subsurface with the change of vertical circulation, and the rate of regeneration.

Keywords: coastal ocean, biogeochemical cycles, 3-D modeling, riverine input, phytoplankton bloom, nutrient supply

Clarification of relationship between nutrient loading and biological productivity in coastal area by ecosystem model

ABE, Masami^{1*} ; TATENO, Satoshi¹ ; NAGAO, Kentaro¹ ; HATA, Kyoko¹

¹IDEA Consultants, Inc.

Recently, the total volume control of COD loading from continental areas to coastal areas that is generally regarded as a barometer of eutrophication produce an effect for water quality improvement. On the other hands, the reduction in biological productivity caused by concentration reduction of nutrient was pointed out. We face the limit of control policies due to build the suitable interaction between continental areas and coastal areas.

Due to understand the interaction between nutrients loading and biological productivity, the investigation how nutrients provide any biological populations and fish catch is effective. The circulation pathway of nutrients is complex web of interactions, for example, relationship between among biological populations (prey-predator relationship, competitive relationship et. al.) or indirect interaction web (extinction of predator caused by anoxic water, et. al.). The ecosystem response to decrease or increase in nutrient loading is complex.

In this report, we apply ecosystem-model which include fishery product (laver culture, clam) to around Kako-river (*Harima-nada*, *Seto-Inland-Sea*, *Japan*). We quantified responses of material circulation to decrease or increase in continental loading by using this model. The biological productivity is responding to decrease or increase in nutrient loading is varying with the structure of material circulation networks.

Keywords: ecosystem model, nutrient loading, material circulation, productivity, Harima-Nada

Construction of the comprehensive aquatic model of the Ise Bay watershed

ONISHI, Takeo^{1*} ; SUGIMOTO, Ryo² ; AOKI, Kazuhiro³ ; SOMURA, Hiroaki⁴ ; YOSHINO, Jun⁵ ; HIRAMATSU, Ken¹

¹Faculty of Applied Biological Sciences, ²Faculty of Marine Bioscience, Fukui Prefectural University, ³National Research Institute of Fisheries Science, ⁴Faculty of Life and Environmental Science, Shimane University, ⁵Faculty of Engineering, Gifu University

Though Integrated Water Resource Management (IWRM) is recognized as an important philosophy for consistent management through terrestrial area to oceans in 1990s', lack of scientific prove and grounds is one of the essential obstacles to implement the philosophy into actual policy making processes. To enhance and enrich scientific basis of IWRM, objective evaluation of change of terrestrial area impacts on oceanic environment is essential. Thus, we are conducting to construct a comprehensive aquatic model which combines water, material, and ecosystem models throughout terrestrial area, rivers, and ocean. The study site is the Ise Bay and its catchment area. Our model is targeting at carbon, nitrogen, and phosphorous for material, and low trophic levels for ecosystems. In addition, model development is based on the philosophy that promotes a model to be opened for public.

The model structure is that combination of hydrological model, river model, oceanic model, and ecosystem model. For about hydrological model, PnET-BGC is used for natural vegetation, SWAT model for agricultural lands, and the tank model for domestic water outflow from urban area. For about river model flow model, one-dimensional open channel model using kinematic wave method is utilized. For ecosystem model, NPZD model was implemented into aquatic systems. And, for ocean model, ROMS was used. In addition, dam operational rules were included to consider the impacts of dams on river discharge regimes. Calibration and validation period was from 2000 to 2010. Simulation time step was 1 day, and spatial resolution of driving force (weather data) of the model was 2km. ASTER-GDEM is utilized for DEM, National Land Numerical Information for vegetation, and Basic Land Classification Survey for soil and geological data. The result showed that while river discharge was relatively good, the level of water quality was not acceptable. One of the possible reasons of this discrepancy was the incomplete implementation of agricultural water use. Moreover, since coupling with ocean model is not yet realized, thus, improvement of terrestrial model, coupling of terrestrial and ocean model, and sensitivity analysis is further required.

Keywords: Integrated Water Resource Management, Landuse change, Eutrophication, Hypoxia, Ise Bay

Spatiotemporal distribution of organic matter buried in estuarine seagrass meadows

WATANABE, Kenta^{1*} ; KUWAE, Tomohiro¹

¹Port and Airport Research Institute

Blue Carbon, captured and sequestered by marine organisms, has attracted attention as one of the major sink of atmospheric carbon dioxide. One of the important process for carbon sequestration is burial of organic carbon into sediments. The burial rate of organic carbon is higher in estuaries and seagrass meadows than open oceans. A large amount of terrestrial carbon flows into shallow coastal systems, consequently being buried in the sediment. Also nutrient inflows elevate autochthonous organic matter production in the systems. Therefore, various organic matter compositions, having different origin and bioavailability, are mixed in shallow waters. In this study, we investigate the quality and quantity of organic matter buried in an estuarine seagrass meadow using elemental and isotopic techniques and ¹⁴C dating.

Our study site, the Furen Lagoon, is located at the high latitude in Japan. The Furen lagoon is eutrophic due to riverine inflows. Seagrass meadows occupy 67 % of the total area of the lagoon. We collected core samples (about 2 m) in the lagoon along the salinity gradient. TOC (total organic carbon) and TN (total nitrogen), as well as carbon and nitrogen isotopic signatures were analyzed along the depth. Also $\Delta^{14}\text{C}$ was analyzed for dating. In the low salinity zone, $\delta^{13}\text{C}$ was low and C/N ratio was high, indicating that terrestrial organic matter was dominant. These signatures were relatively stable with sediment depth, showing that terrestrial organic matter would have been buried for thousands years. Within the seagrass meadow, $\delta^{13}\text{C}$ and $\delta^{15}\text{N}$ were relatively high, indicating that the contribution of autochthonous organic matter (phytoplankton and seagrass) to TOC would increase in the presence of vegetation. $\delta^{13}\text{C}$ fluctuated with sediment depth in the seagrass meadow, showing that the contribution of terrestrial organic matter fluctuated temporally. These results suggest that the lagoon can be the long-term sink of carbon due to autochthonous production and deposition of terrestrial organic carbon.

Keywords: carbon sequestration, blue carbon, estuary, seagrass meadows, stable isotope, ¹⁴C dating

Influences of submarine ground water discharge (SGD) on biogeochemical properties in coastal sea

KOBAYASHI, Shiho^{1*} ; SUGIMOTO, Ryo² ; HONDA, Hisami² ; MIYATA, Yoji¹ ; TOMINAGA, Osamu² ; TAHARA, Daisuke² ; TANIGUCHI, Makoto³

¹Kyoto University, ²Fukui Prefectural University, ³Research Institute for Humanity and Nature

Submarine groundwater discharge (SGD) often influences on biogeochemical properties in coastal seas. We have estimated the flux of SGD using seepage meter and compared it with ²²²Rn, chlorophyll and nutrients concentrations at a fixed point in Obama Bay for a month

Keywords: submarine groundwater discharge, costal ecosystem, land-ocean interaction

Development of simultaneous monitoring method of submarine groundwater discharge and primary production in coastal seas

SUGIMOTO, Ryo^{1*} ; OHKOUCHI, Masaki¹ ; HONDA, Hisami¹ ; SHOJI, Jun² ; OHSAWA, Shinji³ ; TANIGUCHI, Makoto⁴

¹Fukui Prefectural University, ²Hiroshima University, ³Kyoto University, ⁴Research Institute for Humanity and Nature

In recent years, a number of studies have shown that submarine groundwater discharge is an alternative nutrient pathway and can drive primary production in coastal seas. However, very little is known about quantitative relationship between input of groundwater and response of primary production, because both processes are temporally variable. Recent technological advances (i.e., automation) have increased our ability to assess submarine groundwater discharge in coastal ecosystems using natural tracers such as radon-222 (²²²Rn). Simultaneous monitoring of ²²²Rn with indicators of primary production such as pCO₂ and/or chlorophyll-a would allow us to grasp the nexus of both processes. Therefore, automated radon and CO₂ gas analyzer were connected in series and a closed air loop was established with gas equilibration devices to examine the nexus between submarine groundwater discharge and primary production. In this presentation, we will report the results of simultaneous monitoring of ²²²Rn and pCO₂ with other parameters in several coastal environments.

Keywords: simultaneous monitoring, submarine groundwater discharge, primary production, coastal seas

Local scale assessment of submarine groundwater discharge in coastal seas (Beppu, Obama and Otuchi Bay)

HISAMI, Honda^{1*} ; SUGIMOTO, Ryo¹ ; TOMINAGA, Osamu¹ ; KOBAYASHI, Shiho² ; MIYATA, Youji² ; ONO, Masahiko³ ; OHSAWA, Shinji⁴ ; TANIGUCHI, Makoto⁵

¹Faculty of Marine Bioscience, Fukui Prefectural University, ²Field Science Education and Research Center, Kyoto University, ³National Institute of Advanced Science and Technology, ⁴Institute for Geothermal Sciences, Kyoto University, ⁵Research Institute for Humanity and Nature

Submarine groundwater discharge (SGD) is important as a major pathway for freshwater and nutrients loads from land to ocean. Various natural tracers of SGD have been applied to quantify local to regional SGD fluxes. Radon-222 (²²²Rn) is a naturally occurring radioactive gas that is typically 2-3 orders of magnitude higher in groundwater than surface waters. Therefore, it is a powerful tracer of groundwater inputs to oceans. We have applied the continuous ²²²Rn monitoring survey to three local scale coasts (Beppu Bay, Obama Bay and Otsuchi Bay), which have large amounts of groundwater resources in each watershed. As a result, spatial distributions of ²²²Rn and other parameters displayed not only influence of submarine groundwater discharge but also possibility of submarine hot spring discharge.

Keywords: submarine groundwater discharge, ²²²Rn, land-ocean interaction

Stable isotope compositions of dissolved inorganic carbon and water under the seabed of the coastal zone

YAMADA, Makoto^{1*} ; SUGIMOTO, Ryo² ; OKOCHI, Masaki² ; HONDA, Hisami² ; KOBAYASHI, Shiho³ ; ABE, Yutaka¹ ; TANIGUCHI, Makoto¹

¹Research Institute for Humanity and Nature, ²Fukui Prefectural University, ³Kyoto University

Groundwater often discharges from the seabed of the coastal zone. Such groundwater is called “ submarine groundwater discharge (SGD) ” . Mostly, SGD is the water which not fresh water but sea water and fresh water mixed. Although it is assumed that mixture has occurred under the seabed, there is almost no information about the behavior of water and dissolved component under the seabed such as the mixed process, zone of influence of sea water, and the behavior of the dissolved component from the land area. In order to clarify the behavior of water and dissolved component under the seabed of the coastal zone, we conducted the sampling of the water under the seabed of Obama Bay, Fukui prefecture. The stable carbon isotope ratio of dissolved inorganic carbon (DIC) was lower than that of sea water, and higher than that of groundwater which sampled from well near the seashore. The results show that not only mixture of water but mixture of DIC has occurred under the seabed. In the future, in order to comprehend the extent of the impact of sea water, it is necessary to research vertical distribution of the stable isotope composition under the seabed.

Keywords: submarine groundwater discharge, water stable isotope, carbon stable isotope, dissolved inorganic carbon

Catastrophic reduction of sea-ice in the Arctic Ocean - its impact on the marine ecosystems in the polar region-

HARADA, Naomi^{1*} ; KIMOTO, Katsunori¹ ; ONODERA, Jonaotaro¹ ; WATANABE, Eiji¹ ; HONDA, Makio¹ ; KISHI, Michio¹ ; KIKUCHI, Takashi¹ ; TANAKA, Yuichiro² ; SATOH, Manami³ ; ITOH, Fumihiko³ ; SHIRAIWA, Yoshihiro³ ; MATSUNO, Kohei⁴ ; YAMAGUCHI, Atsushi⁵

¹JAMSTEC, ²AIST, ³Univ. of Tsukuba, ⁴NIPR, ⁵Hokkaido Univ.

The sea-ice in the Arctic Ocean has dramatically reduced during the past decade. The drastic sea-ice reduction would cause a complicated and difficulty to understand the perspective on marine ecosystem surrounding the Arctic Ocean, because disadvantage phenomena such as ocean acidification and advantage phenomena such as improving light condition for primary producers, respectively, are simultaneously progressing. We have investigated the response of marine organisms caused by catastrophic sea ice reduction in the Chukchi Sea and Northwind abyssal plain at where the sea ice reduction has progressed most seriously in the Arctic Ocean. The aims of our study are No.1 to understand temporal changes in primary production, No.2 to understand the physiological response of marine phyto and zooplanktons having carbonate tests on warming or freshening associated with sea ice melting, No.3 to develop a new model for marine ecosystems in the Arctic Ocean, to reproduce the primary production by using the model and to understand the response of marine ecosystems on the environmental changes caused by rapid sea-ice reduction. In this presentation, we will show an overview of this project composed of three sub-themes, Observation, Culturing, and Modeling. For the observation, we will show a seasonal change in biogenic components flux obtained at the Northwind abyssal plain by a year round time series sediment trap system and seasonal change in dissolution of pteropod tests due to the seasonal change in the ocean acidification. We will also show the potential mechanism of high biogenic fluxes found in the beginning of the sea-ice season using the original Arctic Ocean ecosystem model. For the culture experiment, the physiological response of *Emiliana huxleyi*, coccolithophorid strain on the environmental changes caused by sea-ice melting will be presented.

Keywords: Arctic Ocean, Biogenic particle, Eddy, Ocean acidification, Coccolithophorid

Hindcast simulation of the ice and circulation in the Arctic Ocean for 1978-2012: An application of AO-FVCOM.

CHEN, Changsheng^{1*}; ZHANG, Yu¹; PROSHUTINSKY, Andrey²; BEARDSLEY, Robert²; LAI, Zhigang³; GAO, Guoping⁴

¹School of Marine Science, University of Massachusetts, USA, ²Department of Physical Oceanography, Woods Hole Oceanographic Institution, USA, ³School of Marine Sciences, Sun Yet-Sen University, China, ⁴International Center for Marine Studies, Shanghai Ocean University, China

A high-resolution, unstructured-grid, finite-volume ice-ocean fully coupled model system, named AO-FVCOM, has been developed for the Arctic Ocean. The governing equations are cast in a generalized terrain-following coordinate system with spatially variable vertical distribution in the vertical and are discretized using flexible non-overlapped triangular grids in the horizontal. This model system includes a) an unstructured grid version of the Los Alamos sea ice model Community Ice CodE (UG-CICE), b) hydrostatic and non-hydrostatic dynamics (NH-FVCOM); c) an unstructured-grid version of the Simulating Wave Nearshore model (SWAN) (named SWAVE), d) 3-D wet/dry point treatment, which can simulate flooding/drainage processes in estuaries and wetlands; e) 4-D nudging, OI and Kalman Filters data assimilation algorithms; f) the mass conservative nesting module to integrate multi-domain FVCOM domains; and g) the MPI parallelized visualization tool ViSiT, which allows users to monitor model performance during the simulation and post-process the model output data. An updated version of AO-FVCOM is capable of simulating the ice imbedded in the ocean.

AO-FVCOM is a regional model nested with Global-FVCOM. Two version of AO-FVCOM were configured with a finest horizontal resolution of 300 m and 2 km for the Arctic Ocean, respectively. The 2-km version has run for a period of 1978-2012. Without data assimilation, the model was capable of reproducing the seasonal and interannual variability of the ice coverage area in the Arctic and also significant drops of the ice coverage in 2007 and 2012. The 35-year simulation results for the circulation and water transport are being validated with comparison to field measurement data. The influence of the model resolution on water transport through the Canadian Archipelago has been also examined over seasonal and interannual scales, and an example of the water transport through Nares Strait will be presented.

Keywords: Arctic Ocean Modeling, Global-FVCOM, Arctic-FVCOM, Multi-domain nesting, 35 year Arctic simulation, Ice-Current Interaction

Changes in the Western Arctic Biogeochemistry over the Last Three Decades: a Modeling Perspective.

SPITZ, Yvette H.^{1*}

¹Oregon State University, CEOAS, Corvallis OR 97331, USA

Over the last three decades, the Western Arctic Ocean (WAO) seasonal and permanent sea ice have experienced significant changes, with the summer sea ice extent still shrinking to record low levels and the permanent ice thickness being greatly reduced. Thus, the WAO circulation (e.g. intensification of the Beaufort Gyre), the oceanic heat content and biogeochemistry are directly impacted. We use the coupled pan-arctic Biology/Ice/Ocean Modeling and Assimilation System (BIOMAS) to investigate changes in the physical system, nutrient fluxes and productivity of the planktonic ecosystem between 1988 and 2011. Model simulations show that an earlier phytoplankton bloom and a slight increase in its biomass in general characterize the WAO. The largest response in the secondary producers is seen as an increase in the magnitude of the microzooplankton biomass as well as in the duration of its growing season. Primary productivity while increasing on average over the WAO shows some decrease in the Beaufort Gyre due to its intensification. Under ice blooms such as the one observed during the ICESCAPE (NASA funded program) in July 2011 are also intensified. This research was done in collaboration with colleagues from University of Washington (Dr M. Steele and Dr. J. Zhang), Woods Hole Oceanographic Institution (Dr. C. Ashjian) and University of Rhode Island (Dr. R. Campbell).

Keywords: Arctic, Modeling, Primary Productivity, Climate Change, Food Web

Relationship of Primary Productivity in Northwind Abyssal Plain with Beaufort Gyre Variation

WATANABE, Eiji^{1*} ; ONODERA, Jonaotaro¹ ; HARADA, Naomi¹ ; TERUI, Takeshi² ; KISHI, Michio³

¹Japan Agency for Marine-Earth Science and Technology, ²National Institute of Polar Research, ³Hokkaido University

The western Arctic marine ecosystem was addressed using a combination year-round mooring observation and multiple numerical models. Our previous studies have revealed eddy-induced biological pump from the Chukchi shelf region to the southern Canada Basin. Whereas this system caused an early-winter peak of sinking flux of Particulate Organic Nitrogen (PON), we then focused on summertime ecological processes. The sediment trap measurements in the Northwind Abyssal Plain (NAP: 75N, 162W) of the western Arctic Ocean captured a maximum diatom flux with dominance of sea ice species in summer 2011. However, the particle fluxes in summer 2012 were considerably suppressed probably due to extension of oligotrophic Beaufort Gyre water to the NAP area. To examine interannual variability in ocean circulation around the target region, the decadal experiment from 1979 to 2012 was performed using the pan-Arctic ice-ocean model COCO. A virtual passive tracer provided inside the Canada Basin certainly suggested that the Beaufort Gyre direction switched southwestward (toward Station NAP) during the early period of 2012. In addition, the three-box lower-trophic model with sea ice species was applied under physical environments at Station NAP to assess an impact of nutrient deficiency on primary production in 2012. Finally, we plan to discuss how to improve existent problems of Arctic marine ecosystem model.

Keywords: Arctic marine ecosystem model, ice algae, oligotrophic water

Estimating potential habitat for chum salmon (*Oncorhynchus keta*) in the Western Arctic using a bioenergetics model coupled

KISHI, Michio^{1*} ; YOON, Seokjin¹ ; WATANABE, Eiji¹

¹Hokkaido University

Chum salmon (*Oncorhynchus keta*) are distributed widely in the Northern Pacific and are an important commercial fisheries resource in North Pacific countries. Chum salmon can be divided into North American and Asian groups, and the Asian groups can be divided further into Japanese and Russian groups, which show different migration routes. Japanese and Russian chum salmon stocks are predominant in the Bering Sea during summer and fall. However, recently, several studies reported different tendency. Higher densities of chum salmon were observed within the vicinity of the Bering Strait and the Chukchi Sea than the eastern Bering Sea on September 2007 and alike Japanese chum salmon migrated to northern areas in the Bering Sea on August 2009. Sea surface temperature in the Arctic marginal seas has increased since the mid-1960s, especially since 2000. We speculated that SST increase affect to salmon northing directly. Therefore, we focused on chum salmon migrating northward to the Western Arctic. We estimated the potential habitat for chum salmon in the Western Arctic using a bioenergetics model coupled with a three-dimensional lower trophic ecosystem model (3-D NEMURO). The model domain contained the entire Chukchi Sea and the southern area of the Canada Basin. The horizontal resolution was about 2.5 km, and there were 25 vertical levels (surface to 4000 m). We assumed chum salmon move to a depth where the growth rate is the maximum within 100 m, because chum salmon migrate vertically to below 100 m depth for controlling their body temperature and searching for prey. The model was run for nine months from March to November 2003, thus representing the entire months chum salmon are distributed in the Bering Sea from June to November. In the bioenergetics model, the growth rate of an individual chum salmon was calculated as a function of water temperature, salinity, and prey density, which were obtained from the 3-D NEMURO model results. We calculated the growth rates of chum salmon of 100 gWW to 4000 gWW and defined 'Potential habitat' as 'an area where chum salmon can grow up (i.e., the growth rate is positive)'. The potential habitat reflected the warm and nutrient-rich Pacific water inflowing from the Bering Strait. That was restricted to the southwestern Alaskan coast on June and expanded to the Chukchi Sea and along the Alaskan northwestern coast from July to September and reduced from October. The main limiting factor was the water temperature on June and November and the prey density on July to October. For global warming scenario, we used the modeled monthly water temperature anomaly between 2005 and 2095 under the IPCC SRES-A1B scenario. Under the global warming scenario, the potential habitat for chum salmon increased during early summer and autumn due to the water temperature increase, whereas during summer the potential habitat for smaller chum salmon increased but that for larger chum salmon decreased because the water temperature exceeded the optimal condition, especially in the southern Chukchi Shelf and near the Bering Strait. The water temperature limitation was relaxed with a water temperature increase on June and November, but regionally the water temperature was the main limiting factor during summer.

Keywords: Arctic, marine ecosystem model, Chum salmon

Seasonal changes in zooplankton swimmer and faecal pellets collected using a sediment trap in the western Arctic Ocean

MATSUNO, Kohei^{1*} ; YAMAGUCHI, Atsushi² ; FUJIWARA, Amane¹ ; ONODERA, Jonaotaro³ ; WATANABE, Eiji³ ; HARADA, Naomi³ ; KIKUCHI, Takashi³

¹National Institute of Polar Research, ²Hokkaido University, Graduate School of Fisheries Sciences, ³Japan Agency for Marine-Earth Science and Technology

Most studies on zooplankton community in the Arctic Ocean have been performed on the basis of net-collected samples. However, seasonal sea ice coverage in this area prevents the accurate evaluation of their seasonal changes. To overcome these challenges, analysis on zooplankton swimmers collected using a moored sediment trap is a powerful tool. In the present study, we analysed the seasonal changes in zooplankton swimmers and faecal pellets collected using a sediment trap moored at the Northwind Abyssal Plain in the western Arctic Ocean.

Samples were collected using a sediment trap moored at 184-260 m at St. NAPt (75N, 162W, bottom depth: 1975 m) in 10-15 day intervals from October 4, 2010 to September 18, 2012. The sample cups were filled with 5% buffered formalin seawater. After the trap was retrieved, a total of 52 samples were gently sieved using a 1-mm mesh, and a fine-size fraction (<1 mm) of each sample was filtered using a membrane filter and subsequently weighed. Next, the total mass flux ($\text{mg DM m}^{-2} \text{ day}^{-1}$) was evaluated. Zooplankton faecal pellets were then quantified in an aliquot of the fine-size fraction, according to four morphological types (oval shape, cylinder shape, spherical shape and brown oval shape). On the basis of both the size fraction samples (<1 mm and ≥ 1 mm), species identification and enumeration of zooplankton were performed under a dissecting microscope. Furthermore, cluster analysis by Bray-Curtis similarity using the connected unweighted pair group method and the arithmetic mean was performed on the zooplankton flux data ($\text{ind. m}^{-2} \text{ day}^{-1}$). To identify the species most responsible for the similarity between zooplankton communities, SIMPER analyses were performed on the flux data.

In addition, satellite data were obtained, which revealed the sea ice coverage period (November-June), open water period (August-October), and high chlorophyll a period (August-October). The total mass flux ranged from 0.1-263.3 $\text{mg DM m}^{-2} \text{ day}^{-1}$, and its peaks occurred in November, which corresponded to the onset of sea ice coverage. In the faecal pellets, oval shaped and spherical shaped morphologies were predominant, and resulted in a total pellet number of 60% and 30%, respectively. With regards to the specific characteristics of the faecal pellets, the brown oval shape occurred only in the open water period (July-August) and their maximum composition during this period reached 80%. The zooplankton flux ranged from 35 to 739 $\text{ind. m}^{-2} \text{ day}^{-1}$ and was significantly higher in September-November compared with other periods ($p < 0.0001$, one-way ANOVA). In addition, poecilostomatoid copepods were numerically the most dominant taxa (annual mean $\pm 1\text{sd}$: $69 \pm 18\%$). For seasonal dominant taxa, bivalve larvae were found in October-November (53%), and barnacle larvae were abundant in August 2011 (33%) but were not present in 2012. Cluster analysis on the zooplankton flux identified five zooplankton community groups. The occurrence of each group clearly showed seasonality, and alterations in their timings corresponded with the timing of the onset or offset of ice coverage or seasonal changes in daylight hours.

On-board experiments demonstrated that the brown-oval-shaped faecal pellets might be egested by amphipods. Furthermore, the high brown-oval-shaped faecal pellets found during the open water period (July-August) might reflect the massive feeding activity of amphipods. For zooplankton swimmers, seasonal abundant bivalve and barnacle larvae may be transported from a shallower region (e.g., the Chukchi Sea). The annual change in occurrence of barnacle larvae (present in 2011, but not in 2012) may be caused by the annual changes in water mass formation in the upper layer of the St. NAPt.

Keywords: western Arctic Ocean, sediment trap, zooplankton community, faecal pellets

Volume, heat and freshwater fluxes of Pacific Water through the Barrow Canyon in the Arctic Ocean

ITOH, Motoyo^{1*} ; KIKUCHI, Takashi¹ ; NISHINO, Shigeto¹

¹JAMSTEC

Interest in Pacific Water flowing from the Bering Strait into the Arctic Ocean has increased markedly in recent years, because of warming and increasing of Pacific Water inflow. Barrow Canyon, in the northeast Chukchi Sea, is a major conduit for Pacific Water to enter the interior Arctic basins. Our study focuses on the quantitative estimate of volume, heat and freshwater fluxes through Barrow Canyon by mooring observations with hydrographic surveys. We conducted year-round mooring observations at one station from 2000 to 2001 and at three stations from 2001 to 2013 in the mouth of Barrow Canyon. The annual mean volume, heat and freshwater fluxes through Barrow Canyon were 0.49 Sv, 2.25 TW and 31 mSv, respectively. Annual averaged volume and freshwater fluxes through Barrow Canyon in recent years from 2010 to 2013 were lower than the 2000-2008 averages, mainly due to strong northerly wind. In contrast, heat flux for the period 2010-2013 was higher than the 2000-2008 average. It tended to be three highest maximum in 2007, 2010 and 2012, when summer sea ice extent extraordinary retreats in the Arctic Ocean, mainly because of the warming of Pacific Summer Water. Heat fluxes observed in these years were 3-4 times larger than that observed in summer 1993. It is sufficient to melt 1-m-thick ice over an area of 360,000 km², which is equivalent to the total land area of Japan. The heat possibly contributes to both sea-ice melt in summer and a decrease in sea-ice formation during winter because this water typically subsides just below the surface mixed layer in the Canada Basin.

Keywords: Arctic Ocean, Pacific Water, Heat flux, Sea ice extent

Water masses transporting process from the Bering Sea to the Arctic Ocean revealed from multiple chemical tracers

JIANG, Kai^{1*} ; ZHANG, Jing²

¹Graduate School of Science and Engineering for Education, University of Toyama, ²Graduate School of Science and Engineering for Research, University of Toyama

The Arctic Ocean is tightly connected to the Pacific Ocean through the only oceanic gateway Bering Strait. Water, heat, nutrients, and other substances inflowing via water masses exchanges affect the marine environment in the Arctic Ocean. In recent decades, the Arctic Ocean has changed dramatically, especially the rapid reduction of sea ice. The changing of water masses through the Bering Strait is thought to be one of the main reasons. Thus, focusing on the process of water masses transporting will contribute to understanding and forecasting the marine environment in the Arctic Ocean. In this research, stable oxygen isotopes, salinity and rare earth elements (REEs) are used to reveal the water masses transporting process from Bering Sea to the Chukchi Sea, which data comes from the Oshoro-Marun C255 cruise during 14 June - 07 August 2013. 182 water samples of $\delta^{18}\text{O}$ from 31 stations were analyzed by IR-MS (Isotope Ratio Mass Spectrometry). The $\delta^{18}\text{O}$ composition and salinity are used to separate the different water sources based that river water is highly depleted in $\delta^{18}\text{O}$ relative to marine waters as well as to sea-ice. Rare earth elements in the sediments from 8 stations were also analyzed by the method of BCR sequential extraction procedure which partitions the elements in sediments among various forms. It aims to trace the material sources, reflecting the water masses transporting process indirectly. The investigations show that in the Bering Sea, $\delta^{18}\text{O}$ value is around -2 ‰ in the surface increasing to -0.8 ‰ in the bottom water, closed to the $\delta^{18}\text{O}$ value of Pacific Ocean water, indicating that the upper layer water is obviously affected by freshwater. In the Bering Strait, $\delta^{18}\text{O}$ value is similar in the whole water column, around -1.3 ‰, consistent with salinity, which means that the water is well mixed in the Bering Strait (East side of Bering Strait). In the Chukchi Sea, $\delta^{18}\text{O}$ value is also affected by sea ice melt water. REEs data shows that different fraction of sediment has different sources, most part of sediments originally come from land, after charged into ocean, they combine with particles or substance under different marine environment.

Keywords: Arctic Ocean, water mass, oxygen isotope, rare earth element

Influence of the Gulf Stream on the Barents Sea ice retreat and Eurasian coldness

SATO, Kazutoshi^{1*} ; INOUE, Jun² ; WATANABE, Masahiro³

¹The Graduate University for Advanced Studies, ²National Institute of Polar Research, ³Atmosphere and Ocean Research Institute, University of Tokyo

Abnormal winter sea-ice retreat over the Barents Sea has been considered as a leading clue to the recent midlatitude severe winters. Barents Sea is considered as a hot spot for the rapid Arctic climate change due to the intense air-sea interaction induced by the sea-ice decrease; however, the underlying mechanisms remain uncertain, in particular causal relation of sea-ice retreat and atmospheric forcing and response. To understand this causality, we selected typical cases, defined as averaged warm and averaged cold years of December using the NCEP Climate Forecast System Reanalysis (CFSR). The composite analysis, revealed that anticyclonic anomaly is obvious over the northwestern Eurasia. The western Barents Sea and Sbarvard locates at the strong pressure gradient zone, prevailing southerly winds. Over the Barents Sea, the difference in daily mean air temperature between warm and cold winters is more than 10°C, suggesting that warm advection prevails during warm years. Therefore, during warm years, decrease in sea-ice cover is induced by southerly warm advection. The positive anomalies of precipitation from the southeast of Greenland to Barents Sea and negative anomalies of them from Nordic Sea to western Eurasia means the poleward shift of cyclone tracks, suggesting that the moisture transport is also changed poleward. Because the cyclones tend to shift poleward in less sea ice year over the Barents Sea, it is natural that the snow depth over the sea ice near the Fram Strait shows a positive anomaly during warm winters. Here we show that the poleward shift of sea surface temperature over the Gulf Stream, where is situated upstream from the Barents Sea, modifies the horizontal distribution of tropospheric condensational heating resulted from change in convection over the warm current, likely acting as a bridge to the Barents Sea by forcing planetary waves. This remote atmospheric response modifies cyclone tracks poleward, resulting in anomalous warm advection over the Barents Sea sector.

Keywords: Gulf Stream, Arctic, Barents Sea, Eurasian coldness

Study of interannual variability of the atmospheric water cycle in the Arctic circumpolar region

ISHIGE, Takaya¹ ; HIYAMA, Tetsuya^{2*} ; FUJINAMI, Hatsuki³

¹Graduate School of Environmental Studies, Nagoya University, ²Research Institute for Humanity and Nature, ³Hydrospheric Atmospheric Research Center, Nagoya University

The thawing depth (active layer depth) in late summer drastically deepened and the soil moisture increased from 2005 to 2008 in the middle of the Lena River Basin. This was partly due to the high rainfall in late summer, as well as the high snowfall in winter. Subsequently, permafrost-forest degradations and waterlogging has been detected in the region. To clarify whether high precipitation occurred in the past in this region, we investigate the atmospheric water cycle and water budget using archived precipitation (PREC/L) and atmospheric re-analysis data (JRA-25, JRA-55). Previous studies revealed a negative correlation in the summer atmospheric circulation pattern between the Lena and Ob River Basins. However, little is known about the atmospheric water cycles in the Arctic circumpolar region, including the Mackenzie River Basin. Hence we analyzed the interannual variability of the atmospheric water cycle in the Arctic circumpolar region, comparing the three large North Eurasian river basins (Lena, Yenisei, and Ob) and the Mackenzie river basin. The analyzed results are as follows.

1) In the highest five-year summer net precipitation in the Lena River basin during the period 1958 to 2012, significant cyclonic deviation was present from the Barents Sea towards the region across from the Yenisei and Lena. The deviation distribution of the height field and the water vapor flux from the west to the Lena river basin were significantly increased, so as to form a positive deviation of net precipitation.

2) A significant enhancement of cyclonic circulation was detected from 2005 to 2008 on the Eurasian side of the Arctic Ocean. However, anticyclones appeared over Mongolia. These probably increased the atmospheric moisture convergence over the Lena River Basin in this period.

3) A significant positive trend in the summer precipitation and the summer net precipitation appeared after 1995 between the Lena and Yenisei River Basins. On the contrary, the negative trends between the Lena and the Ob River Basins became unclear from 1993.

Keywords: summer precipitation, summer net precipitation, Lena River Basin, Arctic cyclone

Evaluation of Large-scale Surface Wetness Variations in Northern High Latitudes During 1980-2010

TAKATA, Kumiko^{1*} ; XU, Jianqing² ; HARA, Masayuki² ; NOZAWA, Toru³

¹NIPR/NIES/JAMSTEC, ²JAMSTEC, ³Okayama University

Large-scale surface wetness is evaluated by a wetness index (WI), calculated from GPCC precipitation divided by potential evaporation (Ep) using ERA interim data during 1980-2010. The climatological distribution of annual WI agrees with that of surface soil moisture (SSM) in ERA interim. Anomalies of annual WI also have strong relation with that of SSM in each region; the correlation coefficient between SSM and WI is higher than that between SSM and precipitation. Therefore WI corresponds to SSM for climatology and year-to-year variations.

The linear trends of WI, Ep and precipitation are calculated, with an attempt to decompose the factors of WI trend into those of Ep and precipitations. In high latitudes of Eurasia and eastern Canada, the increasing precipitation trends are canceled by the increasing Ep trends, resulting in little WI trends. In central Asia, western North America and Alaska, the decreasing precipitation trends and the increasing Ep trends lead to the decreasing WI trends. The precipitation variations dominate the WI variations in most regions. For example in Alaska, the decreasing precipitation trend contributes 72% to the decreasing WI trend and the increasing Ep trend does 27%. On the other hand, there are some regions where the Ep trend is important for the WI trend. For example in monsoon Asia, the precipitation trend is small and contributes only 3% to the decreasing WI trend, while the increasing Ep trend does 99%.

Consequently, it is shown that WI corresponds to surface soil moisture and indicates surface wet/dry conditions, and that the contributions of precipitation and Ep to its trends are quantified. Further analyses will be applied to the outputs of global climate models (GCMs) to evaluate reproducibilities of the surface energy-water balances in those GCMs.

Keywords: surface wetness, large-scale variations, reanalysis data

Multidisciplinary in situ and satellite observations for accurate detection of phenology in sub- and Arctic ecosystems

NAGAI, Shin^{1*} ; TEI, Shunsuke² ; KOBAYASHI, Hideki¹ ; IKAWA, Hiroki⁴ ; NAKAI, Taro³ ; KIM, Yongwon⁴ ; SUZUKI, Rikie¹ ; SUGIMOTO, Atsuko²

¹Research Institute for Global Change, Japan Agency for Marine-Earth Science and Technology, ²Graduate School of Env.Science / Faculty of Env.Earth Science Hokkaido University, ³Hydrospheric Atmospheric Research Center, Nagoya University, ⁴International Arctic Research Center, University of Alaska Fairbanks

To accurately evaluate the spatio-temporal variability of ecosystem functions and service in sub- and Arctic regions under rapid meteorological and climate changes, global, long-term, and comprehensive phenological observations are required. Towards this aim, satellite remote-sensing is useful to detect the spatio-temporal variability of plant phenology such as the timing of start (SGS) and end of growing season (EGS). However, from the in situ ecological research viewpoint, the satellite remote-sensing has not been sufficiently tested and validated by ground-truthing. Here, (1) we performed daily field observations with time-lapse digital cameras in boreal forests in Alaska and Siberia; (2) we examined the relationship between satellite-observed vegetation indices and plant phenology; and (3) we evaluated the spatio-temporal variability of the timing of SGS and EGS in sub- and Arctic regions by using MODIS Terra and Aqua-observed green-red vegetation index (GRVI). We found that (1) satellite-observed vegetation indices (i.e. NDVI, EVI, and GRVI) mainly detected the plant phenology of forest floor in sparse forests; (2) large year-to-year variability of the timing of SGS was detected in eastern Siberia and western Ural Mountains, while that of EGS was not clearly detected; and (3) in contrast, large year-to-year variability of the timing of EGS was detected in western Alaska, which is mainly covered by tundra vegetation, while that of SGS was not clearly detected.

Keywords: phenology, remote sensing, terrestrial ecosystem, Siberia, Alaska, ground-truthing

Estimate of permafrost organic carbon balance in Alaskan boreal and tundra ecosystems using natural radiocarbon tracer

KONDO, Miyuki^{1*}; UCHIDA, Masao¹; UTSUMI, Motoo²; IWAHANA, Go³; YOSHIKAWA, Kenji³; IWATA, Hiroki⁴; HARAZONO, Yoshinobu³; NAKAI, Taro⁵; TANABE, Kiyoshi¹; SHIBATA, Yasuyuki¹

¹National Institute for Environmental Studies, ²University of Tsukuba, ³University of Alaska, Fairbanks, ⁴Kyoto University, ⁵Nagoya University

The high-latitude regions, where a serious warming is expected, currently store large amounts of soil organic carbon in active-layer soils and permafrost, accounting for nearly half of the global belowground organic carbon pool. Despite the importance of these regions in the present carbon cycle, the soil C fluxes and budget are still only poorly known. Here, we use radiocarbon as the tool for quantifying the C balance of the inputs and decomposition in tundra and boreal soil. We evaluated the C inputs (I) and decomposition rates (k , inverse of turnover time) and net C accumulation (CA), using ¹⁴C approaches.

Tundra and boreal soils show different patterns of depth distribution and C storage. Cumulative organic carbon stocks in boreal forest are 5.3 and 19.2 kgCm⁻², in surface organic layer (0-25 cm), and deep organic and mineral layers (25-70 cm), respectively. Large annual C input (0.25 kgCm⁻² yr⁻¹) and relatively slow decomposition (27 years) lead to rapid CA (0.05 kgCm⁻² yr⁻¹) in surface organic layer in boreal forest. Deep organic and mineral layers including near-surface permafrost show slower rate of input (0.03 kgCm⁻² yr⁻¹) and turnover (617 years) and CA about 20 times slower (0.003 kgCm⁻² yr⁻¹) than surface organic layer. Decomposition organic matter (Rh), which in accord with C losses from both surface and subsurface layers, was 0.23 kgCm⁻²yr⁻¹. This value agreed well with Rh (0.23 kgCm⁻² yr⁻¹) simulated by process-based models that simulate the biogeochemical and hydrologic cycle, where Rh averaged 45% of ecosystem respiration and 59% of soil respiration.

In contrast, large amount of SOC (36.4 kg m⁻²) have accumulated over millennia (turnover time: 4540 yrs) below the thin organic layer in tundra. The CA of mineral layer and permafrost is close to zero (0.003 kgCm⁻² yr⁻¹), and Rh is 0.008 kgCm⁻² yr⁻¹. Our radiocarbon data show that the most SOC in tundra soil was mode of stabilizing OC by permafrost and steady-state SOC stocks under current C balance.

Large-Scale Forest Fires in Alaska: Weather Conditions in 2004 and 2005

HAYASAKA, Hiroshi^{1*}

¹Graduate School of Hokkaido University

In Alaska, large-scale forest fires mainly occurred in the boreal forest of the Interior (area roughly around 400 x 800 km) in 2004 and 2005. Number of large-scale forest fires (burnt area more than 500km²) were 17 in 2004 and 12 in 2005. These large-scale forest fires boosted up burnt areas 26,000km² in 2004 and 18,800km² in 2005. Their areas were largest and third largest among the past 58 years from 1956 to 2013.

In order to evaluate large-scale forest fires in both years, statistical analysis for the fire data in the past 58 years was carried out. As a result, annual average burnt area was 3,480 km², and the coefficients of standard deviation (sigma) were +4.25 for 2004 and +2.88 for 2005. In the background of these large standard deviation coefficients, only 11-year could show large burnt area of more than 6,000km², and burnt area of other 47-year were less than 5,000km². In addition to this trend, the occurrence of fire year with burnt area more than 6,000 km² was once per decade from the 1950s to the 1980's. But from the 1990's, fire year tended to occur more frequently. That is, they were 1957 (2nd largest), 1969 (6th), 1977 (7th), 1988 (8th), and these frequencies were once per decade. However, from the 1990s, fire years occurred in 1990 (4th largest), 1997 (9th), and 1991 (11th). From the 2000s, four fire years observed in 2004 (largest), 2005 (3rd largest), 2009 (5th), and 2002 (10th). The frequent occurrence trend of such fire year may be suggesting close relationship with the rapid reduction of sea ice in the Arctic Ocean under a rapid climate change.

From the comprehensive analysis in this paper, largest burnt areas in 2004 happened under the condition made by ridge extended from Canada lasted about three month from June to August. The very severe fires observed in August 2005 occurred along with the movement of the high pressure system from the Gulf of Alaska to the Beaufort Sea.

Keywords: Forest Fire, Hotspot, Climate Change, Lightning, Jet Stream, Sea ice

Detection and attribution of changes in arctic ecosystems and atmospheric CO₂

PATRA, Prabir^{1*} ; KOBAYASHI, Hideki¹ ; SAEKI, Tazu¹

¹RIGC/JAMSTEC

Atmospheric CO₂ responds to terrestrial ecosystem activity widely from sub-hourly to decadal time scales primarily due to photosynthesis, weather and climate variations. The measurements of CO₂ thus consist of source signals from anthropogenic as well as natural ecosystem activities convolved with atmospheric transport. Since the records of CO₂ concentration in ambient air at monthly or finer time resolution began in the late 1950s, the seasonal ecosystem dynamics has enhanced significantly in the recent years (Graven et al., 2013). We further analyse the relative contributions of fossil fuel emissions and atmospheric transport on the CO₂ at a greater number of surface measurement sites since the 1980s using the CCSR/NIES/FRCGC atmospheric general circulation model (AGCM)-based chemistry transport model (ACTM). Our results suggest the trends in fossil fuel emissions and transport have detectable contribution to the CO₂ seasonal cycle changes at the sites in northern tropics to mid-latitudes, and that the seasonal cycle increase in the arctic region is governed mainly by the terrestrial ecosystem.

To attribute causes for the recent changes in carbon cycle dynamics we have chosen the period of 1999-2011, which is covered by high quality process oriented ecosystem parameters from remote sensing and atmospheric CO₂ measurements at the largest network of sites for flux inversion. Our analysis suggests that the early greening by several days in the Alaskan tundra region closely correlated with the amplitude of CO₂ seasonal cycle at Point Barrow, Alaska. But no clear trend in the greening onset is detectable at semi-arid grasslands near Ulaanbaatar, Mongolia, except for the closely coupled interannual variations in greening onset time and CO₂ seasonal cycle amplitude. We estimated CO₂ fluxes from 84-regions of the globe at monthly time intervals using measurements from about 100 sites. The terrestrial CO₂ fluxes are estimated after removing the effects of fossil fuel emissions and oceanic fluxes in measured CO₂ concentrations. We find the carbon exchange of the Alaska region of our inversion is increased both for the seasonal cycle amplitude and net annual uptake over the period of 2002-2011.

Our results have large implications for developing the future and validating the present earth system models for studying climate-carbon-biosphere interactions.

Keywords: CO₂ seasonal cycle, Ecosystem phenology, Arctic environment

Epoch difference of water cycles in eastern and western Siberia

OSHIMA, Kazuhiro^{1*} ; OGATA, Koto² ; PARK, Hotaek¹ ; TACHIBANA, Yoshihiro²

¹Japan Agency for Marine-Earth Science and Technology, ²Mie University

Among all the rivers flowing into the Arctic Ocean, the three great Siberian rivers; Lena, Yenisei and Ob, are the three largest in terms of water discharge (R), and they are a large source of freshwater. We examined the relationship of long-term water cycle variability between eastern and western Siberia on the basis of net precipitation ($P-E$) estimated from an atmospheric reanalysis, and R s from observations at the river mouths and from a reconstruction based on tree rings.

The relationship of summer ($P-E$)s between the Lena and Ob Rivers is different in the first half and the second half of the past three decades. During 1980s to mid-90s, the ($P-E$)s have a strong negative correlation. These variations were affected by the east-west seesaw pattern of moisture flux. These results are consistent with Fukutomi et al. (2003). The decomposition analysis revealed that the stationary component of moisture flux dominates the seesaw pattern during the period. After mid-1990s, the correlation of the ($P-E$)s between the Lena and Ob becomes weak. During mid-1990s to 2000s, the $P-E$ over the Lena was affected by cyclonic moisture flux over the basin. In addition to the stationary component, the transient component of moisture flux also affects the $P-E$ variation in this period.

Long-term records revealed that the R s of the Lena and Ob Rivers have moderate or weak positive correlations and strong negative correlations before the 1980s. Interestingly, the correlations tend to be distributed in the negative side. It implies that the east-west seesaw pattern frequently appear over Siberia. In conclusion, the moisture transport processes over Siberia are different in each era and they result in the different variability of the R s and ($P-E$)s of the Lena and Ob Rivers.

Keywords: Siberian rivers, moisture transport process, net precipitation, river discharge, interannual variation, long-term variability

The Structure Change of Arctic Cyclones on Cyclone Phase Space

AIZAWA, Takuro^{1*} ; TANAKA, Hiroshi²

¹Life and Environmental Sciences, University of Tsukuba, ²Center for Computational Sciences, University of Tsukuba

In this study, we investigated the structure change of the Arctic cyclone's life cycle on a cyclone phase space.

Keywords: Arctic cyclone, Structure change, Cyclone phase space

A negative phase shift of winter AO/NAO due to the recent Arctic sea ice reduction in late autumn

NAKAMURA, Tetsu^{1*}; YAMAZAKI, Koji¹; IWAMOTO, Katsushi¹; HONDA, Meiji²; UKITA, Jinro²; MIYOSHI, Yasunobu³; OGAWA, Yasunobu¹

¹National Institute of Polar Research, ²Niigata University, ³Kyushu University

Attribution of the long-term changes in the wintertime Arctic Oscillation (AO)/North Atlantic Oscillation (NAO) to the recent Arctic sea ice reduction is studied. Observations using ERA interim reanalysis and Merged Hadley/OI-SST show that small (large) sea ice area in summer to autumn leads the negative (positive) phase of AO in early winter and NAO in late winter. Relationship with winter AO/NAO is the strongest with the sea ice variability in November rather than September. To separate influences of sea ice variability and sea surface temperature (SST) anomalies, sensitivity experiments are performed with atmospheric general circulation model (AGCM for Earth Simulator, AFES4.1), in which observed changes (anomalies of 2005-2009 from 1979-1983) of the sea ice and SST are prescribed. The Arctic ice reduction generates the negative AO/NAO pattern that brings cold winter in mid-latitude continental regions. Both SST anomalies in the tropics and mid-/high-latitudes mask the continental cooling. Model-based analysis reveals that stationary Rossby wave response to the ice reduction in Barents Sea induces anomalous meridional circulation corresponding to the negative AO. The ice reduction increases (decreases) a frequency of the large negative (positive) AO occurrence about a twice (half). The anomalous meridional circulation warms the Arctic and cools the mid-latitudes. This provides additional Arctic heating about 25% of heat release due to the ice reduction. As a response to ice reduction, transient eddy activity over northern Eurasia is reduced and the change in the eddy damps the stationary responses.

Keywords: Arctic sea ice loss, Arctic Oscillation, long-term changes

Cross spectral analysis of the AO index using the AOI equation

TANAKA, Hiroshi^{1*}

¹CCS, University of Tsukuba, ²Life and Environmental Science, University of Tsukuba

Arctic Oscillation (AO) is explained as an atmospheric dynamical eigenmode. There is an argument, however, that the AO is a statistical illusion by the EOF analysis. Tanaka and Matsueda (2005) showed AO mode as the most unstable standing mode in the barotropic atmosphere. In addition to the zero frequency of the mode, the growth rate becomes also zero for adequate frictional force and interaction with transient eddies. Such a mode can be amplified resonantly by quasi-situational forcing. This idea of the AO is called singular eigenmode theory. For the problem of missing correlation in surface pressure between the Pacific and Atlantic is explained by Suzuki and Tanaka (2007) by analyzing barotropic height instead of the surface pressure. The barotropic height indicates significant correlation between the two regions. The missing correlation is thus explained by the baroclinic component of the atmosphere. We support the singular eigenmode theory, but a further analysis is required by the data analysis of the AO index. In this study we derived an equation called AOI equation from the definition of the AOI differentiated with respect to time, and substituting the primitive equation. According to the analysis result of the NCEP/NCAR reanalysis for 62 years of data, it is found that the AOI time series is proportional to the linear term of the AOI equation. The nonlinear term and external forcing term indicate inverse correlation with the AOI, which tend to damp the AOI to the normal. The fact that the linear term of the primitive equation is proportional to the AO structure, i.e., $L*x = a*x$ implies that the AO is an eigensolution of the dynamical system. The present study supports the singular eigenmode theory from the data analysis using the AOI equation.

Keywords: Arctic Oscillation, Global warming, Low-frequency variability, Singular eigenmode theory, Normal mode, Barotropic instability

Cryospheric studies using satellite data in the GRENE Arctic Project

ENOMOTO, Hiroyuki^{1*} ; ALIMASI, Nuerasimuguli¹ ; KAMEDA, Takao² ; YABUKI, Hironori³ ; TAKESHI, Sugimura¹

¹National Institute of Polar Research, ²Kitami institute of Technology, ³JAMSTEC

GRENE Arctic Climate Research project aims to establish interdisciplinary collaborations of different scientific area. The GRENE project constructed the Arctic Data archive System (ADS) at NIPR to support this researching frame. ADS stores the field data obtained by the project, satellite data by collaboration with JAXA and modelling output from climate models. This presentation introduces activity of data archiving in GRENE Arctic project and ADS for multiple studies.

This study investigates cryospheric change using satellite data stored in the ADS and other satellite programs.

Keywords: Arctic, Cryosphere, Satellite, data archive

Recent changes of satellite-derived snow grain size and glacial microbial activities in Greenland ice sheet

AOKI, Teruo^{1*} ; KUCHIKI, Katsuyuki¹ ; NIWANO, Masashi¹ ; TANIKAWA, Tomonori² ; HORI, Masahiro² ; SHIMADA, Rigen³ ; TAKEUCHI, Nozomu³ ; STAMNES, Knut⁴ ; LI, Wei⁴

¹Meteorological Research Institute, ²Japan Aerospace Exploration Agency, ³Chiba University, ⁴Steven Institute of Technology

Snow surface albedo strongly depends on snow grain size and mass concentration of light absorbing impurities. These snow parameters are uncertain factors for the recent drastic snow and ice meltings in the Arctic. Particularly, Greenland ice sheet (GrIS) is presently undergoing drastic changes. In 2012 a record melting event of surface snow/ice occurred over the GrIS. When air temperature increases, snow grain size is also increased by accelerating the snow metamorphism and thus the albedo is reduced (positive albedo feedback). This process is mainly dominant in the accumulation areas. On the other hand, the bare ice area is extended by snow melting on ice associate with air temperature raise in ablation areas. It is recently reported that wide bare-ice areas in GrIS are covered with glacial microbes whose albedos are lower than that of blue ice surface. This albedo reduction effect is also another positive albedo feedback effect by glacial microbes. To examin these feedback effects by snow grain growth and glacial microbial activities in conjunction with air temperature increase, we retrieved snow grain size and glacial microbe concentration from Moderate Resolution Imaging Spectroradiometer (MODIS) data. The employed algorithm is based on a look-up table method for bidirectional reflectance distribution function at the top of the atmosphere as functions of snow grain size, snow impurity (soot) concentration, solar and satellite geometry. The employed satellite channels are 0.46, 0.86, 1.24, and 1.64 μm . Since the snow impurity concentrations in accumulation area are the same or lower level of the detection limit of soot concentration in GrIS, we use this retrieval result as an indicator of microbial activities in bear ice areas. The monthly averages of snow grain size and snow impurity concentration from 2000 to 2013 in GrIS derived from Terra/MODIS revealed the following facts. (1) The areas of large grain size changed year by year. (2) There is no constant increasing trend, but the larger values were observed in recent years (2009-2012) and especially for 2012 the remarkable increase in whole Greenland. (3) Larger snow grain size and high impurity concentration, which indicate the areas of high glacial microbial activities, are distributed in coastal regions of GrIS in June (mainly in southern part), July and August. These parameters in colder summer of 2013 than the recent several years, were almost the same as those in 2000.

Keywords: Greenland, snow grain size, glacial microbe, albedo, satellite remote sensing, MODIS

Acceleration and deceleration of ice thickness variations in Greenland from ICESat laser altimetry (2003-2009)

MATSUO, Koji^{1*} ; FUKUDA, Yoichi¹ ; SUZUKI, Kazuyoshi²

¹Graduate school of Science, Kyoto University, ²JAMSTEC

The laser altimeter mission ICESat, launched by NASA in January 2003, measures the Earth's surface elevation with a precision of several cm. ICESat has performed campaign observation of about 90 days a year between September 2003 and October 2009. The spatial resolution of the measurement in Greenland is about 20 km in average. In this study, we analyze acceleration/deceleration of ice thickness variations in Greenland from ICESat elevation data. We employ Plane fitting method (e.g. Zwally et al., 2011) to correct topographic effect coming from gaps of repeat-track paths, and fit the time-series of surface elevation variations with a linear combination of linear and quadratic terms by least-squares method at every 700m interval. The quadratic trend signal thus extracted represents accelerated/decelerated variations.

The obtained linear variation suggests significant ice thinning trend in southeastern and western Greenland. Their thinning rates attain to about 1.5-2 m/yr. On the other hands, inland area shows ice thickening trend with a rate of 0.3 m/yr. Assuming the firn density as 700 kg/m³ in ice thinning area and 300 kg/m³ in ice thickening area, we obtain the total ice loss rate of about -200 Gt/yr, which is equivalent to about 0.55 mm/yr sea level rise. This agrees well with GRACE gravimetric estimate.

Next we focus on the quadratic variation. Western Greenland shows significant negative quadratic variations, suggesting acceleration of ice thinning rate. Such trend is particularly noticeable in Jakobshavn glacier and Qaanaaq area. On the other hands, southern Greenland shows different behaviors: negative quadratic variations (accelerated ice thinning) in Helheim glacier and Kangerdlugssuag glacier, and positive quadratic variations (decelerated ice thinning) in other coastal area. We speculate that accelerated ice thinning in the above outlet glaciers reflects recent global warming, while decelerated ice thinning in other coastal area of southern Greenland does anomalous precipitation of Arctic Oscillation with positive phase during the winter of 2007-2008.

Keywords: Greenland, Ice thickness variation, Climate change, Space geodesy, ICESat, GRACE

Sensitivity of Response of Greenland Ice Sheet to Global Warming on Surface Mass Balance and Initialization methods

SAITO, Fuyuki^{1*} ; ABE-OUCHI, Ayako² ; TAKAHASHI, Kunio¹

¹JAMSTEC, ²AORI, Univ. of Tokyo

We present a series of numerical experiments of Greenland ice sheet under global warming condition using Ice sheet model for Integrated Earth system Studies (IcIES).

In this study, influence on the simulation from the difference in the method to compute the surface mass balance is focused.

Typically, ice sheet simulation is driven by a *reference-anomaly* method, in which the surface temperature and/or the accumulation are decomposed into the reference terms (e.g., observation), the anomaly (e.g., climate scenario from climate models).

Then the surface melting is computed using parameterization such as positive degree-day (PDD) method with the temperature.

These decomposed terms have own uncertainties, which may influence the ice-sheet simulation.

In this study, impact of these properties to the present-day control case, as well as the response under uniform warming condition are discussed, which is thought be a useful and basic information of the property/sensitivity of the Greenland ice sheet.

In addition, several initialization methods (free spin-up, fixed-topography spin-up, etc) are applied to IcIES in order to evaluate the influence of the error in the present-day simulated topography to the short-term response of Greenland ice sheet.

Keywords: Greenland ice sheet, Ice-sheet model

Ice thickness change of Bowdoin Gletscher, northwestern Greenland

TSUTAKI, Shun^{1*} ; SUGIYAMA, Shin² ; SAKAKIBARA, Daiki² ; SAWAGAKI, Takanobu³ ; MARUYAMA, Mihiro²

¹Arctic Environmental Research Center, National Institute of Polar Research, ²Institute of Low Temperature Science, Hokkaido University, ³Faculty of Environmental Earth Science, Hokkaido University

Ice discharge from calving glaciers in the Greenland ice sheet (GrIS) has recently increased through the acceleration of glaciers, and this increase plays an important role in the ice volume change of GrIS and sea level rise. Previous studies have used remote-sensing (RS) data to assess surface lowering of calving glaciers in GrIS. However, because of the remoteness of these glaciers, relatively few field data are available on the surface elevation change. Consequently, RS data have been used without calibration with field data. The accuracy of such studies relies on digital elevation models (DEMs) derived from satellite data.

In this study, surface elevation was measured along longitudinal and three transverse profiles in Bowdoin Gletscher (77°41'18"N, 68°29'47"W) in July 2013. DEMs of Bowdoin Gletscher in August 20, 2007 and September 4, 2010 were generated by Advanced Land Observing Satellite (ALOS) Panchromatic remote-sensing Instrument for Stereo Mapping (PRISM) images with a 50 m grid mesh, and calibrated using field data. Mean surface elevation change along the field survey profiles were -16.3 ± 4.0 m (5.3 m yr^{-1}) in 2007-2010 and -10.8 ± 4.0 m (-3.8 m yr^{-1}) in 2007-2013. Surface elevation change along the lower most transverse profile (800 m from the calving front) was more negative than those along the other profiles in the upper reaches. Surface lowering rate at all profiles has decreased from 2007-2010 to 2010-2013.

Keywords: Calving glacier, Greenland

Estimation of glacier motions at Svalbard, NovayaZemlya with ALOS/PALSAR

KONUMA, Yoshiki^{1*} ; FURUYA, Masato²

¹Department of Natural Sciences History, Hokkaido University, ²Department of Natural Sciences History Hokkaido University

While the Greenland Ice Sheet's mass loss is equivalent to 0.6mm/yr sea level rise, a half of them is attributed to the changes in glacier dynamics (Broeke et al., 2009). Namely, surface velocities of many glaciers in Greenland have increased in the recent decade (Moon et al., 2012). We thus wonder if glacier velocities outside Greenland have also increased or not.

Svalbard and NovayaZemlya are arctic islands located at 78 degrees north and 74 degrees north, respectively, and have many glaciers. Stozzi et al. (2008) estimated glacier motions in these islands with SAR in 1990s. However, there are not any studies with SAR in recent decade.

We examined Duvebreen glacier in Svalbard and Vize Glacier in NovayaZemlya. In this study, we used PALSAR derived by the ALOS satellite launched from Japan. The PALSAR data were acquired 10 times at Duvebreen glacier from July 2007 to October 2010, 13 times at Vize Glacier from February 2007 to December 2010. We compared the result with 1990s velocity in previous study.

Accordingly, two glaciers in Svalbard and NovayaZemlya speeded up from 1990s. This result suggests that velocity of other arctic glaciers increase as Greenland's glaciers.

Keywords: svalbard, novaya zemlya, glacier, alos, duvebreen, vize glacier

Snow impurity concentration and snow grain size measured in Ny-Alesund, Svalbard

KUCHIKI, Katsuyuki^{1*}; AOKI, Teruo¹; NIWANO, Masashi¹; SHIOBARA, Masataka²; GOTO-AZUMA, Kumiko²

¹Meteorological Research Institute, ²National Institute of Polar Research

Mass concentration of light absorbing impurities in snow and snow grain size are important parameters controlling snow albedo. An increase in light absorbing impurities such as black carbon (BC) reduces the visible albedo and that in snow grain size reduces the near-infrared albedo. To monitor these snow physical parameters and evaluate those effects on snow albedo in the Arctic, we have measured the snow parameters using a ground-based spectral radiometer system for albedo and flux (GSAF) in Ny-Alesund, Svalbard (78°55'N, 11°55'E). The BC concentration in snow and snow grain sizes in the topmost and subsurface layers were retrieved from spectral albedos measured using the GSAF from March to June, 2013. Furthermore, the retrieved snow parameters were validated by comparing with in-situ measurements based on snow pit work and snow sampling in April, 2013. The collected snow samples were filtrated, and then elemental carbon (EC), organic carbon (OC) and dust concentrations in snow were measured by filter weighing and thermal optical analysis.

The snow depth gradually increased up to 40 cm during the polar night from late October to late February. It maintained around 40 cm until the middle of May, and then rapidly decreased to 0 cm in early June. The BC concentrations retrieved from the GSAF varied little during March to June with about 110 and 40 ppbw for external and internal mixture models employed in the retrieval algorithm, respectively. The in-situ measured EC, OC and dust concentrations were 8-35, 32-190 and 570-3180, respectively. The BC-equivalent concentrations estimated from the light absorbing effects of both EC and dust were 18-43 ppbw, which agreed with the GSAF-derived BC concentrations using the internal mixture model. The topmost layer snow grain radius retrieved from the GSAF were varied within the range 30-300 μm until the middle of May, then increased more than 1000 μm with the snow melting. The snow grain sizes in the subsurface layer were generally larger than those in the topmost layer, which was consistent with the in-situ measurement. We estimated the possible albedo reduction by snow impurities using a physically based snow albedo model with the GSAF-derived snow parameters. The albedo reduction was enhanced to -0.038 during snow melting period after the mid-May, compared with -0.027 before the mid-May, mainly due to the increase in snow grain size.

Keywords: light absorbing snow impurity, black carbon, dust, snow grain size, Ny-Alesund

New developments of Arctic Data archive System(ADS)

YABUKI, Hironori^{1*} ; SUGIMURA, Takeshi²

¹Japan Agency for Marine-Earth Science and Technology, ²National Institute of Polar Research

Arctic is the region where the global warming is mostly amplified, and the atmosphere/ ocean/ cryosphere/ land system is changing. Active promotion of Arctic environmental research, it is large and responsible for observational data. Promotion of Arctic research in Japan, has not been subjected to independent in their respective fields.

In the National Institute of Polar Research, perform the integration and sharing of data across a multi-disciplinary such as atmosphere, ocean, snow and ice, land, ecosystem, model, for the purpose of cooperation and integration across disciplines, we build a Arctic Data archive System (ADS).

Arctic Data archive System (ADS), to promote the mutual use of the data across a multi-disciplinary to collect and share data sets, such as observational data, satellite data, numerical experiment data. Through these data sets, clarify of actual conditions and processes of climate change on the Arctic region, and further contribute to assessment of the impact of global warming in the Arctic environmental change, to improve the future prediction accuracy.

ADS developed the the online visualization system (VISION) of grid data (a satellite and model simulation), which observational researcher was not good. This VISION which can easily visualize special change can become effective for not only the understanding of the phenomenon but also the design of the observation for an observational researcher.

Keywords: Arctic, Environment, Global Warming, ADS, Visualization, VISION

Recent advance in discussions on the Arctic Environmental Studies

ENOMOTO, Hiroyuki^{1*} ; OHATA, Tetsuo²

¹National Institute of Polar research, ²JAMSTEC

This presentation introduces recent activities of the discussion on Arctic environmental studies. There are many national and international discussions on the Arctic study. Japan Consortium for Arctic Environmental Research (JCAR) has started discussions on the future study plan. IASC and ICARP-III discuss on the enhancement of present and future Arctic research and coordinations.

Keywords: Arctic, Environmental study, planning

Sea ice and ocean primary production and phenology in the Arctic Ocean

JIN, Meibing^{1*}

¹International Arctic Research Center, University of Alaska Fairbanks

In the Arctic Ocean, both phytoplankton and sea ice algae are important contributors to primary production and the arctic food web. We use a coupled ice algal and pelagic ecosystem model embedded in the global physical model POP-CICE (Parallel Ocean Program- Los Alamos Sea Ice Model) to study the ecosystem response to climate changes. The model results showed a mean seasonal cycle of ice algal production from March to May and subsequent ocean production from May to September in the Arctic. The ice algal production, although smaller than that of the ocean, is of ecological importance as a food source for higher trophic levels during the long arctic winter before ice melt. The simulated mean open-ocean upper 100m primary production within the Arctic Circle was 413 Tg C/yr in the years 1998 to 2006, close to the remote sensing derived estimate of 419 Tg C /yr but with higher interannual variations. The mean sea ice algal production in the Northern Hemisphere from 1998 to 2007 was 21.3 Tg C/yr, which is in the range of multi-observational estimations of 9 to 73 Tg C/yr based on in situ measurements. Arctic organisms are adapted to the strong seasonality of environmental forcing. Climate warming causes shrinking ice coverage and earlier ice retreat in the Arctic, which is likely to change the timing of primary production. Using a synthesis of available satellite observation data and the coupled ice-ocean ecosystem model, we found that, over a large portion of the Arctic marginal seas, the timing variability of ice retreat at a specific location has a strong impact on the timing variability of pelagic phytoplankton peaks but weak or no impact on the timing of ice-algae blooms in those regions. The model predicts latitudinal and regional differences in the timing of ice algae biomass peak (varying from April to May) and the time lags between ice algae and pelagic phytoplankton peaks (varying from 45 to 90 days). The correlation between the time lag and ice retreat is significant in areas where ice retreat has no significant impact on ice-algae peak timing, suggesting that changes in pelagic phytoplankton peak timing control the variability of time lags. Phenological variability of primary production is likely to have consequences for higher trophic levels, particularly for the zooplankton grazers, whose main food source is composed of the dually pulsed algae production of the Arctic.

Keywords: Arctic Ocean, primary production, phenology, sea ice algae, phytoplankton

The effect of meteorological condition on energy and carbon budget on taiga-tundra boundary in North-eastern Siberia

MIYAZAKI, Shin^{1*} ; TEI, Shunsuke¹ ; BRAGIN, Ivan⁴ ; SUZUKI, Rikie² ; TAKANO, Shinya³ ; SHINGUBARA, Ryo³ ; MOROZUMI, Tomoki³ ; SUGIMOTO, Atsuko³ ; MAXIMOV, Trofim⁵

¹National Institute of Polar Research,, ²Japan Agency for Marine-Earth Science and Technology, ³Hokkaido University, ⁴FarEast Geological Institute, FE RAS, ⁵nstitute for Biological Problems of Cryolithozone SD RAS

1. Introduction

In Arctic, temperature has increased almost twice the global average rate in the past 100 years. We aim to clarify the land-atmosphere interaction over the boundary between taiga and tundra in northeastern Siberia, where the climate change effect might be remarkable. We have started the energy, water and carbon fluxes observation as well as hydro-meteorological observation in northeastern Siberia, Sakha Republic, Russia in June 2013.

2. Material and methods

Our observation site is located at Kodack site (70.564 N, 148.267E, altitude 7m) about 100km south from East Siberian Sea in Arctic Ocean near Chokurdakh city in the North-Eastern Siberia, Sakha Republic, Russia. The Kodack site is belong to Indigirka river basin (drainage area: 324,244km²) which flow to the East Siberian Sea. The annual air temperature and precipitation are -13.4 deg. C and 200mm respectively (1979-2008, Baseline Meteorological Data in Siberia (BMDS) Ver.5.0, Yabuki et al., 2011). The surface is covered by snow except July and August and the maximum snow depth is 40cm in April. In this region, the permafrost exits and the active layer depth ranges from 25cm to 40cm (van der Molen et al., 2007). The topography at the site consists of higher mounds and lower wet lands, where the difference of the height are about 50cm. At the higher mound, the shrubs and larches are dominant, while the sphagnum are prevailing at the lower wet land. The meteorological and flux observation has been carried out over the mound area.

The air temperature, relative humidity, wind speed and direction, air pressure, precipitation were observed at 1.5m height. The incoming and outgoing shortwave and longwave radiation were observed by 4-component radiometer at 1.37m height. The soil heat flux was observed by heat flux plate at 0.05m depth. The soil temperature was observed by platinum sensor at depths of 0.025, 0.05, 0.225, 0.425, and 0.625 m. The soil moisture was observed by capacitance sensor and frequency domain reflectometry sensor at depths of 0.035, 0.145, 0.335, and 0.535 m. The energy and carbon fluxes were calculated by the eddy covariance method from the observed values of the sonic anemo-thermometer at 2.55m height.

3. Results

The analysis results from 23 June to 27 October 2013 will be shown. The daily mean air temperature and relative humidity varied from 0.5 to 21.9 deg. C and from 53.9 to 90.0%, respectively. The total precipitation was 29.5 mm, and the maximum daily precipitation was 9 mm?day⁻¹. The daily mean wind speed varied from 1.3 to 6.1 m s⁻¹. There was clear relationship between the daily mean air temperature and wind direction. When the wind direction was northerly (southerly), the air temperature was low (high). The soil temperature (Ts) at surface varied from 2.8 to 10.8 deg. C while Ts at deeper than 0.425 m kept below 0 deg. C, which implies the frozen soil. The Ts at depth of 0.225m increased from -0.4 to 1.8 deg. C. The soil water content (SWC) was higher than 50% in surface layer of wet land while SWC at dry mound was lower than 11%. The net radiation varied from 50 to 200 W m⁻² and soil heat flux varied from 11 to 40 W m⁻². The daily mean latent heat flux (average during analysis period: 39 W m⁻² was little higher than the daily mean sensible heat flux (26 W m⁻²). The daily mean net ecosystem exchange (NEE) on 24 and 26 June was 0.32 and 0.41 g C m⁻² day⁻¹, respectively, which implies the carbon was released from the surface to the atmosphere while the NEE of the other days was negative value which implies the carbon was uptaken from the atmosphere. The accumulated NEE during analysis period was about -64 g C m⁻² day⁻¹, which was smaller uptake than the value observed at tundra (-92g C m⁻² day⁻¹; van der Molen et al., 2007). As our observation was started about half month after the start of growing season (late May), further analysis using the next year observation is necessary.

Keywords: Taiga-Tundra boundary, Siberia, Energy and carbon budget

Year to year variations in larch growth and their controlling factors in taiga-tundra boundary ecosystem, NE Siberia

LIANG, Maochang^{1*} ; TEI, Shunsuke¹ ; SUGIMOTO, Atsuko² ; MAXIMOV, Trofim C.³ ; KIYASHKO, Sergey⁴ ; VELIVETSKAYA, Tatiana A.⁵ ; IGNATIEV, Alexander V.⁵

¹Graduate School of Environmental Sci. Hokkaido Univ., ²Faculty of Environmental Earth Sci. Hokkaido Univ., ³Inst. Biological Problems of Cryolithozone, SBRAS, Yakutsk, Russia, ⁴Far East Inst. of Marine Biology, FEB RAS, Vladivostok, Russia, ⁵Far East Inst. of Geological, FEB RAS, Vladivostok, Russia

Eastern Eurasia is covered by permafrost which is the largest and the deepest in the world. In its arctic region of lowland of Indigirka River, taiga-tundra boundary ecosystem covers the area. For better understanding of this boundary ecosystem, it is important to understand controlling factors on the growth of larch trees which is the dominate tree species of taiga. Larch growth can vary spatially and temporally. In spatial variation, we found that high soil moisture influences mortality of the larch trees and N availability explains differences in trees ability of C assimilation among the sites. To know the controlling factors on temporal variation of larch growth, we conducted field measurements on photosynthesis, needle nitrogen (N) content, needle mass and isotopic ratios in larch needle and stem in every summer from 2009 to 2013 at four sites in the Indigirka River Basin, near Chokurdakh (70°37'N, 147°53'E), northeastern Siberia.

There was no seasonal variation in needle mass during the growing season after needles were fully open, while needle N content showed seasonality. Needle N content in the year positively correlated with July air temperature and stem $\delta^{13}\text{C}$ and following year needle $\delta^{13}\text{C}$. These results indicate that, in the year with higher July air temperature, more N was allocated to needle and larch trees exhibited higher photosynthetic rate and photosynthetic C used for needle production was one year delayed. Higher air temperature in the year possibly indicates higher solar radiation based on positive correlation between July temperature and sun hours. Therefore, it can be said that larch growth shows strong dependence on solar radiation. In terms of temperature itself, we found higher temperature could limit photosynthetic rate. In addition, wet event, occurred at some sites in 2011 and 2012, caused low photosynthetic rate and low needle N content in 2012, and higher needle $\delta^{13}\text{C}$ in 2012 and 2013. These results indicate that high soil moisture could limit larch photosynthesis and reduce N uptake and cause stomata closure as well.

Our observational results indicate that solar radiation is one of the most important controlling factors on larch growth, and high soil moisture and high temperature can limit larch growth.

Keywords: Carbon and nitrogen isotopes, Needle N content, Photosynthesis, Air temperature and solar radiation, Soil moisture, Vegetation change

Spacial distribution of vegetation at taiga-tundra boundary ecosystem in eastern Siberia

MOROZUMI, Tomoki^{1*}; BRAGIN, Ivan⁵; STAROSTIN, Egor⁶; SHINGUBARA, Ryo¹; TEI, Shunsuke²; TAKANO, Shinya¹; MIYAZAKI, Shin²; MAXIMOV, Trofim C.⁷; SUGIMOTO, Atsuko³

¹Hokkaido University Graduate School of Environmental Science, ²National Institute of Polar Research, Arctic Environment Research Center, ³Hokkaido University Faculty of Environment Earth Science, ⁴Japan Agency for Marine-Earth Science and Technology, Research Institute for Global Change, ⁵Far East Geological Institute, Far Eastern Branch Russian Academy of Science, ⁶North-Eastern Federal University, ⁷Institute for Biological Problems of Cryolithozone, Siberian Branch of Russian Academy of Sciences

Vegetation types, species compositions were observed with physical environment such as micro topography and soil moisture at taiga-tundra boundary ecosystem in lowland of Indigirka river in north eastern Siberia near Chokurdahk village(70°N,148°E)in July 2012 and 2013. There are 4 types of plant communities: driest Tree mound(*Larix gmelinii* etc.), Shrub(*Betula nana* etc.), Sphagnum(*Sphagnum* sp. etc.), wettest Hollow(*Eriophorum angustifolium* etc.). Large area is also covered by Willow(*Salix udensis* etc.) along the river. Soil moisture is the most important factor controlling vegetation and other biogeochemical cycles, such as methane emission. Thus, it is necessary to make a vegetation map with a classification as a key for estimating methane emission.

The objective of this study is classify land cover vegetation using remote sensing approach on satellite images and photographs. In remote sensing approach we used high resolution satellite multispectral image(GeoEye-1, WorldView-2) and aerial photo by radio-control helicopter. Supervised classification was conducted for spacial distribution of vegetation based on aerial photos. This vegetation map will be used for upscaling of biogeochemical cycle process such as greenhouse gases.

Keywords: Taiga-Tundra boundary, vegetation map, remote sensing, Siberia

Satellite observation of cryospheric change using Arctic Data archive System (ADS)

ALIMASI, Nuerasimuguli^{1*} ; ENOMOTO, Hiroyuki¹ ; YABUKI, Hironori³ ; SUGIMURA, Takeshi¹ ; KAMEDA, Takao²

¹National Institute of Polar Research, ²Kitami Institute of Technology, ³JAMSTEC

Arctic Data archive System (ADS) has been constructed in the GRENE Arctic Climate Research project. ADS is useful for quick look of data and visualizing satellite data in the Arctic. The decline of sea ice area in the Arctic influences on the environment and industrial activities in the coastal region and people's life. Satellite microwave data since 1978 was archived in ADS. They are SMMR, SSM/I, AMSR, AMSR-E and AMSR2. These data sets enable to analyze more than 35-years time series of snow conditions, sea ice conditions in the Arctic.

The data is available for all-weather, even during the polar night season. The data enables climatological analysis for more than 30-years time span. This study demonstrates ADS capabilities for long-time monitoring and snow and ice conditions.

Keywords: Arctic, Cryosphere, Satellite, Data archive

Age of the Pacific Winter Water in the Canada Basin estimated from SF₆

OGIWARA, Yusuke^{1*} ; KAWAI, Michiyo²

¹Tokyo University of Marine Science and Technology, ²Tokyo University of Marine Science and Technology

In the Pacific sector of the Arctic Ocean, Pacific Winter Water (PWW) distributes between 100m and 200m depths. Because the PWW has high nutrient concentrations and low pH, its spreading pathway has implications on primary production and ocean acidification in the Arctic Ocean. In this study, we have observed distribution of SF₆, a transient tracer alternative to CFCs, in order to trace newly formed PWW into the Canada Basin.

Sampling was carried out in summer of 2013 on the CCGS Louis S. St-Laurent. Seawater at the core of PWW (salinity = 33.1) were collected in Niskin bottles and then transferred into custom-made glass bottles. Samples were kept at low temperature and brought back to Japan. Concentrations of SF₆ in seawater samples were determined by an ECD-GC following the method described in Bullister and Wisegarver (2008).

Results show that younger PWW distributes at the periphery of the Beaufort Gyre, a major anticyclonic circulation in Canada Basin. The age of PWW estimated from SF₆ was 13~15 years in the center of the gyre, whereas age was 6~9 years around the gyre. From the distributions of SF₆ age, dissolved oxygen and nutrients, it is suggested that there is a pathway of PWW from the Siberian shelves or slopes into the northeastern Canada Basin.

Keywords: arctic ocean, time transit tracer, SF₆, ocean circulation

Mineralization Rate of Soil Organic Carbon at the Lowland of Indigirka River in North-eastern Siberia

SHINGUBARA, Ryo^{1*} ; TANABE, Shinichi² ; TAKANO, Shinya¹ ; BRAGIN, Ivan³ ; MURASE, Jun⁴ ; TEI, Shunsuke⁵ ; MAXIMOV, Trofim C.⁶ ; SUGIMOTO, Atsuko⁷

¹Grad. School of Env. Sci., Hokkaido Univ., ²School of Sci., Hokkaido Univ., ³Far East Geological Inst. FEB RAS, Vladivostok, Russia, ⁴Grad. School of Bioagr. Sci., Nagoya Univ., ⁵National Inst. of Polar Research, ⁶Inst. for Biol. Problems of Cryolithozone SB RAS, Yakutsk, Russia, ⁷Faculty of Earth Env. Sci., Hokkaido Univ.

The Arctic has a large amount of organic carbon accumulated in the soil. If the enhanced warming under the Arctic amplification leads to higher soil temperature or deepening of the active layer, emission of greenhouse gases, i.e. CO₂ and CH₄ can increase. The decomposition rate of organic matter, which is an important factor of CO₂ and CH₄ emission, depends not only on the quantity of organic matter, but also on that quality. In this work, surface soils from the lowland of Indigirka river in Northeastern Siberia were incubated at constant temperatures (5, 10 °C) to evaluate the production rates of CH₄ and CO₂ and to know the degradability of the soil organic matter.

The study site is around Chokurdakh (70.62 N, 147.90 E) located in the continuous permafrost of Eastern Siberia and situated in the boundary of tundra and taiga. Surface soil layers (ca. 10-60 cm deep) were sampled at 7 points of a drier mound with larch trees and of wetter areas with sedges and *Sphagnum spp.*. Besides thawed layers (10, 20, 30 cm deep) sampled in July were incubated at Chokurdakh for 8 days anaerobically, frozen soil layers sampled in the early summer of June (13-62 cm) were incubated in Japan for 34-42 days both anaerobically and aerobically. These soils include the active layer (ca. 20-50 cm) and the top of the permafrost of this region.

CH₄ production was not detected in the mound soils while CO₂ production was, suggesting areas with dry condition have few methanogens and will not produce CH₄ even if they turn into anaerobic condition. On the other hand, soils from wet areas produced CH₄ (0-0.88 μmol (g dry soil)⁻¹ day⁻¹) and the production as well as that of CO₂ was more active at the shallower layers, representing larger amount of labile organic matter. The rate of CH₄ production at 10 °C were found to be 0.9-1.1 times of that at 5 °C in the shallower layers (ca. 10-40 cm), while 1.9-3.3 times in the deeper layers (32-45 cm). It indicates that the temperature dependency of CH₄ production is higher in the middle to the bottom of the active layer than in the top layer.

Keywords: methane, carbon dioxide, incubation experiment, Eastern Siberia, taiga-tundra boundary, stable isotope ratio

Accurate snowfall measurement at Yakutsk, Russia

HIRASAWA, Naohiko^{1*} ; SUGIURA, Konosuke² ; HOSAKA, Masahiro³ ; MAXIMOV, Trofim⁴

¹National Institute of Polar Research, ²Center for Far Eastern Studies, University of Toyama, ³Meteorological Research Institute, ⁴Institute for Biological Problems of Chryolithozone

In association with global warming, the water cycle in the atmosphere also changes for every climatic region on the globe. In polar regions, change in snowfall turns in change in distribution of snow surface and snow cover period, which will drive the ice-albedo feedback process. In order to know the present condition of the water cycle of polar regions and to study the trajectory of the polar climate systems in future, we have to observe not only air property such as temperature but also hydrological property such as snowfall amount, snow depth and so.

In spite of the development in accurate measurements for air temperature, pressure, wind speed and direction, the accuracy of snowfall measurement is not sufficiently high. While heated raingauge is currently generally deployed all over the world, the capture rate of snow particles falls together with wind speed, e.g., around 0.5 of the rate at 5 m/s. It means we measure only a half of the true value of snowfall amount at 5 m/s. This effect has been known for long time as wind loss. Evaporation loss also is more important in the polar regions than the other regions because many snowfall events have the smaller amounts in the total and lower snowfall rates according to the lower-temperature condition in the polar regions. Now, the accurate measurement of snowfall amount is one of the top issues in polar climate science.

The purpose of this study is to measure the accurate snowfall amount in the Arctic region. Moreover, based upon the results, we intend to correct other data which are measured in other region and in past years and also contribute to improve climate model by provideing accurate snowfall data. This study deploys a disdrometer, which measures diameter and fall velocity for each particle and out put the statistics minutely. It is not affected by wind loss and evaporation loss. This presentation shows a snowfall event observed at Yakutsk in early winter of 2013/14.

Keywords: Yakutsk, Snowfall, Disdrometer

Continuous measurements of the atmospheric O₂/N₂ ratio at Ny-Ålesund, Svalbard

GOTO, Daisuke^{1*}; MORIMOTO, Shinji²; AOKI, Shuji²; NAKAZAWA, Takakiyo²; MURAYAMA, Shohei³

¹National Institute of Polar Research, ²Graduate School of Science, Tohoku University, ³National Institute of Advanced Industrial Science and Technology

Simultaneous observations of atmospheric O₂ (defined as O₂/N₂ ratio) and CO₂ concentrations provide valuable information about the global carbon cycle. For a better understanding of the global carbon cycle, several laboratories have developed precise measurement systems for the O₂/N₂ ratio and carried out systematic observations since the early 1990s. To elucidate the variations of the atmospheric O₂/N₂ ratio in detail and to contribute to a better understanding of the role of Arctic region on the regional and global carbon cycle, we developed a continuous measurement system using a differential fuel-cell O₂ analyzer, and then initiated systematic observation at Ny-Ålesund, Svalbard in November 2012, which is the first continuous observation in the Arctic region. The system is equipped with NDIR analyzer to measure CO₂ concentration simultaneously. The analytical precisions of O₂/N₂ ratio and CO₂ are estimated to be ±1.4 per meg and ±0.03 ppmv, respectively. Here, we will present observational results of the first year.

The O₂/N₂ ratio observed at Ny-Ålesund shows a clear seasonal cycle with peak-to-peak amplitude of about 120 per meg, which reaches a minimum in late March to early April and a maximum in August. On the other hand, the CO₂ concentration varies seasonally in opposite phase with the O₂/N₂ ratio, showing the amplitude of 16 ppm. Short-term variations on time scales of several hours to several days are also clearly seen. In winter, it is often observed that the O₂/N₂ ratio sharply declines in a short time, accompanied by an increase in the CO₂ concentration, and the low values last for several hours or days. The O₂:CO₂ exchange ratio defined as the slope of a linear regression line between the measured values of O₂/N₂ ratio and CO₂ range between -1.6 and -1.5 ppm/ppm, which are close to the average O₂:CO₂ exchange ratio expected from fossil fuel burning in Europe. The results of backward trajectory analysis indicated that the air masses arrived at Ny-Ålesund during the periods when such short-term variations were observed passed near or over Scandinavian Peninsula. Therefore, such a decline in the O₂/N₂ ratio is ascribed to transport of urban air influenced by human activities in Europe. In spring to summer, irregular fluctuations of O₂/N₂ ratio are often observed. The amplitude of such fluctuations reaches 50-60 per meg (corresponding to about 10-13 ppm). Similar fluctuations of CO₂ are also found in opposite phase with O₂/N₂ ratio. However, their amplitudes are 5 ppmv at most. The comparison of backward trajectories of air parcels with the distributions of marine biotic net primary production suggests that such fluctuations of O₂/N₂ ratio are closely related to O₂ emission due to marine biological activity near Norwegian Sea.

Keywords: atmospheric O₂, carbon cycle, O₂:CO₂ exchange ratio, air-sea O₂ flux

Geographical variations in formation process of cryoconite granules on Arctic glaciers

FUJISAWA, Yuta^{1*} ; TAKEUCHI, Nozomu¹ ; NAGATSUKA, Naoko² ; UETAKE, Jun² ; MIYAIRI, Masaya¹

¹Graduate School of Science, Chiba University, ²National Institute of Polar Research

The dark colored impurities deposited on the glacier ice are called cryoconite. Cryoconite is consisted of mineral particles, organic matter and microbes, including snow algae, cyanobacteria and bacteria. They usually form small spherical aggregates known as cryoconite granules. The spherical shape is maintained by filamentous cyanobacteria. The satellite images of Greenland ice sheet revealed that the dark colored bare ice surface has expanded recently and may have a big impact on the melting of ice. The darkening may be due to increase of cryoconite on the surface. Therefore, the understanding of the structure and formation process of the cryoconite granules is important for studies of the influence on the glacier ecosystem and mass balance of glaciers. In this study, we analyzed the structure and characteristics of cryoconite granules on Arctic glaciers and we clarified the differences in the formation process with the glaciers.

We analyzed the cryoconite samples collected on the northwestern part of the Greenland ice sheet, the Longyearbreen glacier of the Svalbard, the Suntar-Khayata glacier of the Siberia, the Gulkana glacier of the Alaska. We observed the cryoconite granules using a microscope in order to clarify the characteristic of the composition, the granule size. Furthermore, to observe inner structures, thin sections of cryoconite granules were made.

Microscopy of cryoconite granules revealed that their size and coloration differed among the glaciers. The size of granules was the largest for Svalbard followed by Siberia, Alaska, and Greenland. The coloration of cryoconite granules was brown for Svalbard, black for Siberia, gray for Alaska, and black to brown for Greenland. Cross section of the granules also showed the distinct features. The granules from Greenland had mostly subgranules inside. The granules from Svalbard had some concentric layers of dense organic matter. The granules from Siberia had a large mineral particle inside. The granules from Alaska had no specific inner structure. These differences of cryoconite granules may reflect physical and/or chemical conditions of each glacier.

Development of a Palsa along the Denali Highway, Alaska

IWAHANA, Go^{1*} ; UCHIDA, Masao² ; KONDO, Miyuki² ; YOSHIKAWA, Kenji¹ ; LARRY, Hinzman¹

¹University of Alaska Fairbanks, ²National Institute for Environmental Studies

Palsa is a peaty permafrost mound distributing in continuous and discontinuous permafrost zones. Main mechanism of the development the mounds is frost heave by ice segregation of peat or mineral soil material. Upper part of palsa usually consists of peat and lower part of a core of alternating layer of segregated ice and mineral soil material. History of paleo-environment around the period of last glacial retrieve in surrounding area can be inferred from analysis of palsa cores and stratigraphy. Our target palsa was located along the Denali Highway, Alaska, and the mound was truncated during highway construction in 1957. The outcrop of palsa have been eroded away from the highway line about 20m partly exposing the internal structure. This permafrost mound was firstly introduced as palsa by Pewe in 1983, and from dating of basal peat, deglaciation of this area occurred at least about 10500 year BP. History of palsa development and environment change was reconstructed from results of analysis from 6.5m core and ground temperature.

Keywords: Alaska, Denali Highway, Palsa

Sr-Nd isotopic ratios of mineral dust in Arctic snow

NAGATSUKA, Naoko^{1*} ; OGAWA, Yoshimi¹ ; GOTO-AZUMA, Kumiko¹ ; SUGIURA, Konosuke² ; ENOMOTO, Hiroyuki¹ ; YAMADA, Hironobu¹ ; NAKANO, Takanori³

¹NIPR, ²Toyama University, ³RIHN

Snow and ice on glaciers contain various atmospheric depositions, such as soot and mineral dusts. These light-absorbing impurities can reduce surface albedo and affect melting of glaciers. Thus, it is important to understand how these impurities were supplied on glaciers.

Stable isotopic ratios of Sr and Nd provide a means of identifying sources of substances and can use for the dusts in snow because it requires low samples for analysis. In this study, we analyzed Sr and Nd isotopic ratio of the mineral dusts collected from snow in several Arctic regions (Mongol, Alaska, and Greenland).

The Sr and Nd isotopic ratios of mineral dusts in Arctic snow showed geographical variations among the sampling sites. The ratios of dust collected from snow in Mongol showed higher Sr and lower Nd values, while those of Greenland were higher Sr and lower Nd values, and were close to the ratios that have been reported in loess, desert sand, soil, or moraine around each region. This result indicates that mineral dusts in snow on the two sampling sites were mainly derived from surrounding regions. On the other hand, the isotopic ratios of dust in snow of Alaska were close to those of deserts in Kazakhstan and Taklamakan Desert, suggesting that the mineral dusts originated from such further deserts were likely to be long-range transported to Alaska.

Keywords: Sr-Nd isotopic ratio, mineral dust in snow, Arctic region

Intercomparison of Arctic atmospheric reanalysis data: Deriving observation-based forcing data for terrestrial models

MORI, Junko^{1*} ; SAITO, Kazuyuki² ; MIYAZAKI, Shin¹ ; SUEYOSHI, Tetsuo² ; IJIMA, Yoshihiro² ; HAJIMA, Tomohiro²

¹National Institute of Polar Research, ²Japan Agency for Marine-Earth Science and Technology

The goals of the modeling group in the terrestrial research project of the GRENE Arctic Climate Change Research Project (GRENE-TEA) are to a) feed to the CGCM research project for the possible improvement of the physical and ecological processes for the Arctic terrestrial modeling (excl. glaciers and ice sheets) in the extant terrestrial schemes in the coupled global climate models (CGCMs), and b) lay the foundations of the future-generation Arctic terrestrial model development.

In GTMIP (GRENE-TEA Model Intercomparison Project), we utilize the GRENE-TEA site observations to drive and validate the participating models. However, the observation data are prone to missing or lack of the necessary variables or parameters to drive the model. Therefore, we create continuous forcing data in the following manner: First, we create 30-year hourly time series (version 0; v0) of 7 meteorological components from the closest point data of the reanalysis products (a model-based dataset for the sub-monthly variations, and the observation-based CRU for the monthly). Then, v0 is merged with the observation data to create site-fit continuous data (v1) for each GRENE-TEA site. Use of this v1 expects to reduce the systematic biases in the input data in comparing the model outputs with the site observations, to delineate the variations among the models.

So far several atmospheric reanalysis datasets, for example NCEP-NCAR or JRA-55 are available as model input data. In this study, six atmospheric reanalysis datasets are compared in terms of the climatic reproducibility in the region north of 60°N to select the one to be used for constructing the v0 data. The compared datasets are ERA Interim, JRA-55, MERRA, NCEP/NCAR Reanalysis 1, NCEP-DOE Reanalysis 2, and NCEP-CFSR. The CRU dataset is used as a representative of the ground-level observations. We take air temperature at 2m high and precipitation as the key parameters representing the climate condition.

Keywords: Arctic region, Terrestrial model, Reanalysis dataset

Automatic measurement of gas emission/uptake of Alaskan permafrost soils

YONEMURA, Seiichiro¹ ; UCHIDA, Masao² ; KONDO, Miyuki^{2*}

¹NIAES, ²NIES

The release of carbon from the decomposition of organic matters in permafrost soils are very important for the acceleration of global warming. We applied our dynamic system to Alaskan soils and measured temperature dependence of gas (CO₂, CH₄, N₂O, NO, H₂, CO) emission/uptake. The Four core samples were placed on petri-dishes which were put into chambers where temperature was controlled. CO₂ emission from soils showed variations different from sample to sample. Even at -5C, CO₂ emissions were observed. From the time series of CO₂ emission rates, we estimated Q₁₀ values. Q₁₀ values were similar between 5-15C and 15 and 25C. Some soils also temperature-dependently emit NO, CO and N₂O.

Keywords: permafrost soil, Alaska, CO₂, NO, laboratory experiment

Simulating effects of natural fire disturbance on soil carbon storage of boreal forest and tundra ecosystems in Alaska

WANG, Xin^{1*} ; YOKOZAWA, Masayuki² ; ARAKIDA, Hazuki³ ; MORI, Kensuke⁴ ; ISE, Takeshi⁵ ; KONDO, Miyuki⁶ ; UCHIDA, Masao⁶ ; KUSHIDA, Keiji⁷ ; TODA, Motomu¹

¹Department of Environmental Dynamics and Management, Graduate School of Biosphere Science, Hiroshima, ²Department of Mathematical and Systems Engineering, Graduate School of Engineering, Shizuoka University, ³Riken Kobe Branch, Kobe, ⁴Department of Geomatics Engineering, University of Calgary, ⁵Graduate School of Simulation Studies, University of Hyogo, ⁶Center for Environment Measurement and Analysis, National Institute for Environmental Studies, ⁷College of Bioresource Sciences, Nihon University

Boreal forest and tundra are the major ecosystems in the northern high latitudes and represent one of the largest reservoirs of carbon over terrestrial ecosystems in the world. Most of the carbon is stored in permafrost where frozen organic matter is protected from decomposition due to biotic activity in the underlying soil. The surface humus layers that should work as the protective layers insulate the permafrost soil far away from the effect of climate warming. Hence, the removal of protective layers by natural fire episodes increases the vulnerability of permafrost to thaw, and the carbon stored in permafrost to decomposition under climate warming in the near future. To elucidate effects of fire severity and temperature sensitivity on the soil carbon storage of boreal forest and tundra ecosystems in Alaska, we conducted simulations using the Physical and Biogeochemical Soil organic carbon Dynamics Model (PB-SDM), which consists of meteorologically-relevant land surface model and soil organic carbon dynamics model. The PB-SDM model of fire severity, designed from the analysis of the field observations, describes the effects of fire characteristics in frequency and size on the reduction of the soil organic layer. The simulation captured realistic annual variations in soil organic carbon storage and thickness in boreal forest and tundra ecosystems individually by finding optimal model parameters in terms of the frequency and size of fire events and temperature sensitivity. The result reveals that our model can be used for predicting soil carbon storage in boreal forest and tundra ecosystems at regional scales where fire regimes play a key role in the soil organic carbon storage as affected by climate warming.

Keywords: High-latitude soil, fire severity, Soil organic carbon, boreal forest, tundra

Methane Oxidation Potential of Arctic Wetland Soil of a Taiga-Tundra Ecotone in North-eastern Siberia

MURASE, Jun^{1*} ; SUGIMOTO, Atsuko² ; SHINGUBARA, Ryo³ ; MAXIMOV, Trofim C.⁴

¹Grad. Sch. Bioagr. Sci., Nagoya Univ., ²Fac. Earth Environ. Sci., Hokkaido Univ., ³Grad. Sch. Environ. Sci., Hokkaido Univ.,
⁴Inst. Biol. Problems of Cryolithozone

Arctic wetlands are significant sources of atmospheric methane and the observed accelerated warming of the arctic causes increased methane formation in water-saturated tundra soil with deepened permafrost thawing. Methane oxidation is regarded as the key process to regulate methane emission from wetlands. In this study we determined the potential methane oxidation rate of the wetland soils of a Taiga-Tundra transition zone in Northeastern Siberia with special reference of the spatial heterogeneity and response to environmental parameters. The surface peat soil samples (0-10 cm) were collected in the summer of 2012 and 2013 from depressions that were covered with tussocks of sedges and Sphagnum spp. and mounds vegetated with moss and larch trees. The potential methane oxidation rate was estimated by a bottle incubation experiment in which homogenized soil samples were incubated with methane at the initial concentration of 0.5-0.8 %v/v. Soil samples from the mounds showed no detectable methane oxidation, whilst the soils collected from depressions exhibited active methane oxidation with no lag. The potential methane oxidation rates at 15 oC were of 270 and 190 nmol h⁻¹ g⁻¹ dw in the moss- and sedge-dominated zones, respectively. Methane oxidation was active over the depths including the water-saturated anoxic layers, suggesting the resilience of methane oxidizing bacteria. The maximum methane oxidation rate was recorded in the layer above the water-saturated layer: the surface (0-2cm) layer in the sedge-dominated zone and in the middle (4-6 cm) layer in the moss-dominated zone. Temperature-dependent methane oxidation was observed at the range of temperature from 0 to 15 oC. The estimated threshold temperature of methane oxidation was -4 to -11 oC, which suggested methane oxidation at subzero temperatures. Treatment with inorganic nutrients and black carbon did not affect the potential methane oxidation rate.

Keywords: Methane oxidation, tundra, peat

Online visualization tool "VISION" on Arctic Data archive System (ADS)

SUGIMURA, Takeshi^{1*} ; YABUKI, Hironori²

¹National Institute of Polar Research, ²Japan Agency for Marine-Earth Science and Technology

We are constructing an online archive system of data about Arctic research that many researchers and institutes have collected, which is named ADS (Arctic Data archive System). We aim at that the many researchers specializing in the various fields of the Arctic research - such as atmosphere, ocean, land, physical and chemical analysis and computer simulation, etc - can become to mutually use their data across their own fields through our data archive. For this purpose, it is necessary for us not only to manage data systematically, but to build the system where researchers can easily grasp the contents of the data archive.

However, it is difficult to exactly understand contents of the data that others made. The researchers try to understand the contents of the data of their own fields and succeed in many cases. But it is not easy for them even to judge the contents of the data out of their fields. Therefore, we developed GUI-based online data visualization application named " VISION " , which all the researchers engaged in the Arctic research can easily operate. It can be expected that " VISION " facilitates an understanding the data of the various fields of the Arctic research among the researchers, then the researchers become also use the data out of their own fields.

We will introduce a structure and function of " VISION " and demonstrate an operation of this system.

Keywords: online visualization, satellite data, SSMI, AMSR

Shrinking glaciers in Suntar Khayata, east Siberia

KADOTA, Tsutomu^{1*}; SHIRAKAWA, Tatsuo²; KUSAKA, Ryo²; TAKAHASHI, Shuhei²; GALANIN, Andrey³; FEDOROV, Alexander³; ENOMOTO, Hiroyuki⁴; OHATA, Tetsuo¹; YABUKI, Hironori¹

¹Japan Agency for Marine-Earth Science and Technology, ²Kitami Institute of Technology, ³Melnikov Permafrost Institute, ⁴National Institute of Polar Research

Introduction

Since Northern Hemisphere high latitude regions are noticeable trend of global warming and climate change, appearance of its impact is interest. Northeastern Eurasia is area of blank of observational research. One of a few regions studied in the past is Suntar Khayata in east Siberia, where Russian scientists carried out wide range of study during IGY (1957-1959).

Study area

Suntar Khayata region, located in the latitudes between 62 and 63 degree north and in the longitudes between 140.7 and 142 degree east, forms a divide between the Arctic Sea and the Sea of Okhotsk. Oymyakon depression, known as the cold pole in the Northern Hemisphere, is located to the northeast. Glacier inventory of this region was prepared based on the aerial photographs taken in 1944-1947 (Koreisha, 1963). Total number and area of glaciers were 205 and 206.28 km². Three glacierized region are recognized, namely Northern massif, Central massif and Southern massif. The highest elevation of each massif is 2959 m, 2933 m and 2944 m.

Glaciers observed are No. 29 to 33 in Northern massif including No. 31 which was intensively studied during IGY.

Observation

We carried out glaciological observations such as mass balance (stake method), ice thickness measurement (radio-echo soundings), and topographic survey (DGPS) in July/August in 2012 and 2013. Automatic weather stations were also set on/around the glaciers.

Results

Glacier-wide mass balance in 2012/2013 was -1.04 m w.e. for a glacier complex (Glaciers No. 29, 30 and 31). This value shows more negative state than those in 1957-1959.

We generated DEMs of surface and bed of the Glacier No. 31 using ice thicknesses obtained by radio-echo soundings and surface elevations by GPS survey, then we estimated the volume of the glacier to be 0.20 km³ (area: 3.02 km², mean thickness: 62 m). Ice thicknesses in its tongue reduced by 110-60 m (terminus to upstream) since 1957.

Based on multi-temporal aerial and satellite imagery, 18 investigated glaciers reduced in area by approximately 36% from 1945 to 2011.

Concluding remark

Summer (July-August) air temperature observed on the glacier in 2012 and 2013 were higher than those in 1957-1959, which brought about more negative mass balance than those in 1957-1959. Superimposed ice formation was also very limited in 2012/2013. This resulted in disappearance of accumulation area. Reconstruction of long-term mass balance history is present target.

Acknowledgement

This study has been jointly carried out by JAMSTEC (Northern Cryosphere Research Program) and GRENE Arctic Climate Change Research Project (The role of arctic cryosphere in global change).

Keywords: glacier, Siberia, Suntar Khayata, shrink

Effect of snow depth on pan-Arctic permafrost thermal regimes

PARK, Hotaek^{1*} ; FEDOROV, Alexander² ; WALSH, John³

¹JAMSTEC, ²Melnikov Permafrost Institute, Yakutsk, Russia, ³International Arctic Research Center, University of Alaska Fairbanks

This study quantitatively evaluated how insulation by snow depth (SND) affected the soil thermal regime and permafrost degradation in the pan-Arctic area, and more generally defined the characteristics of soil temperature (T_{SOIL}) and SND from 1901-2009. This was achieved through experiments performed with the land surface model CHANGE, to assess sensitivity to winter precipitation as well as air temperature. Simulated T_{SOIL} , active layer thickness (ALT), and SND were generally comparable with in-situ or satellite observations at large scales and over long periods. Northernmost regions had snow that remained relatively stable and in a thicker state during the past four decades, generating greater increases in the T_{SOIL} . Changes in SND have led to changes in the thermal state of the underlying soil, which is strongly dependent on both the magnitude and the timing of changes in snowfall. Simulations of the period 2001-2009 revealed significant differences in the extent of near-surface permafrost, ranging from 15.6 to 18.7 million km². This spread was the result of differences in the model's treatment of meteorology. Permafrost loss was greater when SND increased in the autumn rather than in the winter, due to insulation of the soil from the early cooling. Simulations revealed that T_{SOIL} tended to increase over most of the pan-Arctic from 1901-2009, and this increase was significant in northern regions, especially in northeastern Siberia where SND is responsible for 50% or more of the changes in T_{SOIL} at a depth of 3.6 m. In the same region, ALT also increased at a rate of approximately 2.3 cm per decade. The most sensitive response of ALT to changes in SND appeared in the southern boundary regions of permafrost, in contrast to permafrost temperatures within the 60°-80°N region, which were more sensitive to changes in the SND. Finally, the modeling performed in this study suggests that snow cover contributes to the warming of permafrost in northern regions and could play a more important role under conditions of future Arctic warming.

Keywords: active layer thickness, land surface model, permafrost, snow depth, soil temperature

Fixed-point observation of diatom biocoenosis and water mass condition in the northern Chukchi Sea during September 2013

ONODERA, Jonaotaro^{1*} ; NISHINO, Shigeto¹

¹JAMSTEC-RIGC

In order to estimate the relationship between diatom flora and water mass condition in the northern Chukchi Sea, fixed-point ocean observation was conducted at Station 41 (72.45N, 168.24W, 56 m water depth) by R/V Mirai (Cruise MR13-06) in 10-25 September 2013. The optical equipment named "Multi-wave length excitation fluorescence photometer (Multi-Exciter)" was applied with CTD observation for the estimation of chlorophyll concentration in each major phytoplankton groups (diatom, green algae, and blue algae). Chlorophyll concentration gradually increased with the weakening of summer stratification by intensified sea-surface wind. The Multi-Exciter showed the clear increase of diatom in upper water column, which were also suggested by size-fractionated analysis of chlorophyll concentration and microscopic observation by scanning electron microscope and light microscope. However, the increase of diatom cell abundance was minor compared to the increase of total chlorophyll concentration. The dominance of large diatom genus *Proboscia* and the increased chlorophyll concentration in one diatom cell were the main causes on the increase of total chlorophyll concentration. The 3-6 fold increase of chlorophyll concentration within 6 hours was rarely observed around chlorophyll maximum layer during the middle observation period, which is probably explained by not only improved habitat environment for diatom but also movement of water masses such as lateral input of high chlorophyll waters.

Keywords: Arctic Ocean, Chukchi Sea, diatom, excitation fluorescence, chlorophyll concentration

Reconstruction of paleoenvironmental changes in the Chukchi Borderland over the last 15.5kyr

UCHIDA, Masao¹ ; KUMATA, Hidetoshi² ; KONDO, Miyuki^{1*} ; RELLA, Stephan¹ ; SHIBAHARA, Akihiko³ ; AMANO, Chie⁴ ; UTSUMI, Motoo⁵

¹National Institute for Environmental Studies, ²Tokyo University of Pharmacy and Life Sciences, ³National Institute of Advanced Industrial Science and Technology, ⁴Toyo University, ⁵University of Tsukuba

Knowledge on past variability of sedimentary organic carbon in the Arctic Ocean is important to assess natural carbon cycling and transport processes related to global climate changes. However, the late Pleistocene oceanographic history of the Arctic is still poorly understood. In the present study we show sedimentary records of organic carbon(TOC, $\delta^{13}\text{C}$), CaCO_3 , benthic and planktonic foraminiferal $\delta^{18}\text{O}$, BIT index for terrestrial organic carbon input, IP25 for sea ice condition, and the coarse grain size fraction. The 8m length sediment core was retrieved in the northern Northwind Ridge in the far western Arctic Ocean, during the MR08-05 cruise by R/V Mirai. An age model based on oxygen isotope stratigraphy, radiocarbon dating and lithological constraints suggests that the core records paleoenvironmental changes of the last 155 kyr. In this conference, we discuss presented millennial scales records of glacial erosion, intermediate water and/or surface water and sea ice variabilities during cold/warm episodes of the last two glacial interglacial cycles in the light of ice sheet and ocean-atmosphere dynamics.

What the recent international field campaign in and around the Indian Ocean has advanced our knowledge of the MJO?

YONEYAMA, Kunio^{1*}

¹JAMSTEC

A coordinated international field experiment with special focus on the convective initiation mechanism study of the Madden-Julian Oscillation (MJO) took place in and around the central equatorial Indian Ocean from October 2011 through January 2012. This campaign consisted of several projects including CINDY2011 (Cooperative Indian Ocean experiment on intraseasonal variability in the Year 2011), DYNAMO (Dynamics of the MJO), AMIE (Atmospheric Radiation Measurement program - MJO Investigating Experiment), and LASP (Littoral Air-Sea Process). More than 70 institutes/universities from 16 countries joined the campaign. During a four-month intensive observing period from October through January, three MJO events were observed. It is worth noting that while it is clear to identify three events (late October, late November, and late December) from the time-longitude cross section of outgoing long-wave radiation data along the equator, the most popular MJO identification method - Real-time multivariate MJO Index introduced by Wheeler and Hendon (2004) - could not capture the December event.

While the vertical stepwise moistening which was trapped around trade inversion and 0degC level were confirmed from the equatorial sounding data as previously reported, it was emphasized that lateral transport of moisture and dry air from the Southern Hemisphere as well as westward-propagating disturbances from the Indonesian Maritime Continent were also keys. Several topics from published works during past 2 years after the campaign will also be introduced to indicate what we expected and what are not.

Keywords: Madden-Julian Oscillation, CINDY2011

Mesoscale Convective Complex Activities over Indian Ocean and Their Effects on Convections Over Sumatera Island

-, Trismidianto^{1*}; HADI, Tri wahyu²; KODAMA, Yasu-masa¹

¹Meteorological Laboratory, Graduate School of Science and Technology, Hirosaki University, ²Departement of Earth Sciences, Faculty of Earth Sciences and Technology, Institut Teknologi Bandung

Effects of Mesoscale Convective Complexes (MCC) over Indian Ocean on convections over Sumatera Island have been investigated using Multi-functional Transport SATellite (MTSAT) infrared (IR1) imageries, Tropical Rainfall Measuring Mission (TRMM) rainfall data and Cross-Calibrated Multi-Platform (CCMP) surface wind data of 10-year period (2000-2009). Occurrences of MCC were identified using an algorithm that combines criteria of cloud coverage, eccentricity, and cloud lifetime. This study begins with a case study on 16 to 17 August 2005 and 27 to 28 October 2007 to show the evolution of MCC, we found the development phase of MCC was accompanied by surface wind convergence, while wind divergence was clearly seen below decaying MCC. Following the decay of MCC, convective activities were observed in the surrounding regions by the presence of a new convective cell around the MCC, indicating the role of cold pool mechanism. The new convective cell was generated from cold pool affect convective clouds in the surrounding area and propagate to over Sumatera Island so causing extreme rainfall over Sumatra.

The correlation between MCC and convection over Sumatera was further investigated by performing composite analysis using more samples of MCC events. During the 10-year period, about a number of 553 MCC events have been identified over Indian Ocean. However, it is of interest to that MCC events tend to occur with significantly higher frequency during the monsoon transition season of March- April-May (MAM) period. Available data suggest that the life cycle of MCC over Indian Ocean is about 12 to 15 hours. Results of composite analyses confirmed that the MCC have significant influence on the development of cloud convection over Sumatera Island by means of cold pool propagation mechanism. This seems to imply that weather observations over the western Indian Ocean are crucial for rainfall prediction in Sumatera regions.

Keywords: Cold Pool, MCC, Convection, Rainfall

Observed moisture variations associated with shallow convection

BELLENGER, Hugo^{1*} ; KATSUMATA, Masaki¹ ; YONEYAMA, Kunio¹ ; NISHIZAWA, Tomoaki² ; YASUNAGA, Kazuaki³ ; SHIROOKA, Ryuichi¹

¹JAMSTEC, ²NIES, ³University of Toyama

The variability of tropospheric moisture is a key feature of tropical climate. In particular, the importance of moisture variations due to convective transport is still to be quantified on a variety of spatial and temporal scales. For instance, there is a debate on the importance of moisture convective transport in preconditioning the atmosphere prior to deep convection development associated with the Madden–Julian Oscillation (MJO). We use here high frequency observations of humidity and convection in the Indian Ocean by lidars and radars on board the R/V Mirai during the CINDY/DYNAMO campaign. Significant moisture variations on the scale of few hours are observed within the first first kilometers of the atmosphere in association with shallow convective and congestus clouds. We then compare these local tendencies with large–scale ones and discuss the potential importance of convective transport by convection in the moisture budget during the transition from convectively suppressed to convectively active periods.

Keywords: Convection, moisture, MJO, CINDY/DYNAMO, preconditioning, observation

In-situ observed detailed temperature profile in surface 10-meter layer over the tropical western Pacific

KATSUMATA, Masaki^{1*} ; BELLENGER, Hugo¹ ; YONEYAMA, Kunio¹

¹JAMSTEC

The oceanic thermal stratification in the first meters impacts significantly the energy exchanges between the atmosphere and the ocean by modulating the skin Sea Surface Temperature (SST). A thermistor chain was deployed from a research vessel to continuously measure the temperature profile in the ocean first 10 meters during 17 days in June 2013 in the tropical western Pacific (12N-135E). A clear diurnal cycle was captured with daytime warming in the first meters of the ocean that gradually decrease and deepened during the evening. In addition, a 0.5K-cooling event of the first meter with duration of about 3 hours was also captured during the passage of precipitating cloud system. By utilizing meteorological data from on-board instruments, we asses the relative importance of precipitation and accompanying cold pool in this cooling event.

Abrupt cooling associated with the oceanic Rossby wave and lateral advection during CINDY2011

SEIKI, Ayako^{1*} ; KATSUMATA, Masaki¹ ; HORII, Takanori¹ ; HASEGAWA, Takuya¹ ; RICHARDS, Kelvin J.² ; YONEYAMA, Kunio¹ ; SHIROOKA, Ryuichi¹

¹Japan Agency for Marine-Earth Science and Technology, ²University of Hawaii

The cooperative Indian Ocean experiment on intraseasonal variability in the Year 2011 (CINDY2011) was conducted to capture atmospheric and oceanic characteristics of the Madden-Julian Oscillation (MJO) in the central Indian Ocean from late 2011 to early 2012. During CINDY2011, the research vessel (R/V) MIRAI stayed at 8° S, 80.5° E for two months during the special observing period (SOP). Intraseasonal convection associated with the MJO was organized in the central Indian Ocean in late October and late November during the SOP. In the middle of November, both sea surface temperature (SST) and mixed layer temperature decreased suddenly when cold low salinity water intruded into the upper layer around the R/V MIRAI. This intrusion was accompanied by a surface current change from southwestward to westward/west-northwestward associated with the passage of the annual oceanic downwelling Rossby wave. The mixed layer heat budget analysis shows that horizontal advection plays an important role in the abrupt cooling whereas the net surface heat flux cannot account for the cooling. This is an interesting result because the associated downwelling Rossby wave is usually considered to increase SST through a reduction of entrainment cooling. In addition, for the second MJO event convection was activated around 20 November over the central north and equatorial Indian Ocean but not in the south. It is suggested that the cooler surface waters (as seen at the location of the R/V MIRAI) tended to suppress the initial atmospheric convection, resulting in the lagged convective onset in the end of November over the central south Indian Ocean.

Keywords: CINDY2011, abrupt cooling, Indian Ocean

Modulation of Equatorial Turbulence by Tropical Instability Waves

INOUE, Ryuichiro^{1*} ; LIEN, Ren-chieh² ; MOUM, James³ ; PEREZ, Renellys⁴ ; GREGG, Mike²

¹JAMSTEC, ²University of Washington, ³Oregon State University, ⁴University of Miami

Strong modulation of turbulent mixing by a westward propagating Tropical Instability Wave (TIW) was observed during October and November 2008 on the equator at 140°W in the stratified shear layer between the equatorial undercurrent (EUC) and the surface mixed layer. At these depths, the unique deep diurnal-cycle mixing in the stratified layer under the equatorial cold tongue was observed with nighttime turbulent mixing a factor of 10 greater than during daytime. The turbulent kinetic energy dissipation rate, ϵ , was $O(10^{-6})\text{Wkg}^{-1}$, and the turbulent heat flux was $\sim 500\text{Wm}^{-2}$, at least 5-10 times greater than previously observed at the central equatorial Pacific. Turbulence mixing varied significantly during the four distinct phases of the meridional flow associated with the TIW: steady northward ($\sim 0.6\text{ms}^{-1}$), northward-to-southward transition, steady southward ($\sim 0.6\text{ms}^{-1}$), and southward-to-northward transition. During the northward-to-southward transition, we observed the largest values of reduced shear squared ($Sh^2 \gg 4N^2$), where Sh^2 is the total shear squared and N^2 the buoyancy frequency squared, the thickest nighttime surface mixed layer, the deepest penetration of the deep-cycle turbulence, and the largest turbulent heat flux and largest integrated ϵ in the deep-cycle layer. During steady southward flow, the depth of the bases of the nighttime surface mixed layer and of the deep-cycle layer were shallowest. For the first time, a 50-m-thick layer of strong turbulence was observed immediately above the EUC core during the northward-to-southward and steady southward phases. The average ϵ exceeded 10^{-6}Wkg^{-1} , the eddy diffusivity was $\sim 10^{-3}\text{m}^2\text{s}^{-1}$, and the turbulent heat flux was $\sim 500\text{Wm}^{-2}$. It is likely that to accurately parameterize mixing in the central equatorial Pacific, numerical models must properly simulate not only the enhancement of mixing associated with TIWs but also the variability of mixing within individual TIWs. In this talk, some results from the extensive (from November 2008 to February 2009) mooring data set, comparisons with a general circulation model, and details of mixing events will also be shown.

ACG37-07

Room:423

Time:April 28 14:30-14:45

Air-sea interaction over the northern edge of the Pacific warm pool

HASEGAWA, Takuya^{1*} ; NAGANO, Akira¹ ; HATTORI, Miki¹ ; INOUE, Tomoshige¹ ; KUBOTA, Hisayuki¹

¹JAMSTEC

Abstract is written in Japanese.

Keywords: northern edge of the Pacific warm pool, air-sea interaction, multi-scale temporal-spatial variability

Why is initialization of heat content anomalies in the tropical Indian Ocean difficult in a CGCM with SST-nudging?

KOHYAMA, Tsubasa¹ ; TOZUKA, Tomoki^{2*}

¹University of Washington, ²The University of Tokyo

We have evaluated oceanic initial conditions in the tropical Indian and Pacific Oceans prepared by a coupled general circulation model (CGCM) with a sea surface temperature (SST)-nudging scheme. It is shown that the heat content anomalies in the upper 150 m are generated extremely well in the Pacific even though only the SST data is incorporated. In contrast, the upper ocean heat content anomalies produced by the model have negative correlation coefficients over vast areas of the tropical Indian Ocean. We propose that this is due to a difference in the SST-outgoing longwave radiation (OLR) relationship between the Indian and Pacific Oceans; the use of SST-nudging generally assumes that correlation coefficients between SST and OLR are negative, but this is not necessarily true. The correlation coefficients between SST and OLR anomalies are negative in the central to eastern equatorial Pacific, and this feature is well reproduced in the model. As a result, equatorial zonal wind anomalies are well captured by the model, and forced equatorial Kelvin and Rossby waves are accurately reproduced. On the other hand, the model cannot capture the observed positive correlation coefficients in the eastern equatorial Indian Ocean, particularly from January to April. As a result, equatorial zonal wind anomalies tend to have an opposite sign and induce equatorial Kelvin and Rossby waves with a wrong sign. The positive correlation between SST and OLR is an outcome of remote influence, but this is more difficult to simulate in an atmospheric general circulation model (AGCM) and a CGCM with strong SST nudging, in which local air-sea interaction is not explicitly allowed. Since the results presented in this study is based on a single model, it will be interesting to check skills of other models in initializing the upper ocean heat content with an SST-nudging scheme.

Keywords: Tropical Indian Ocean, Ocean-atmosphere coupled model, SST-OLR relationship, Upper ocean heat content, SST-nudging

Two flavors of the Indian Ocean Dipole

ENDO, Satoru^{1*} ; TOZUKA, Tomoki¹

¹Graduate School of Science, The University of Tokyo

The Indian Ocean Dipole (IOD) is known as a climate mode in the tropical Indian Ocean accompanied by negative (positive) sea surface temperature (SST) anomalies over the eastern (western) pole and easterly wind anomalies along the equator during its positive phase. However, the western pole of the IOD is not always covered by positive SST anomalies throughout the region. For this reason, the IOD is further classified into two types in this study based on SST anomalies in the western pole. The first type is close to the canonical IOD with negative (positive) SST anomalies in the eastern (central to western) tropical Indian Ocean. The second type, on the other hand, is associated with negative SST anomalies in the eastern and western tropical Indian Ocean and positive SST anomalies in the central tropical Indian Ocean. Based on a composite analysis, it is found that easterly wind anomalies reach the east coast of Africa in the first type, and as a result, positive rainfall anomalies are observed over East Africa. Also, due to the basin-wide easterly wind anomalies, the first type is accompanied by strong sea surface height (SSH) and thermocline depth anomalies. In contrast, zonal wind anomalies converge in the central tropical Indian Ocean in the second type, and no significant precipitation anomalies are found over East Africa. Also, only weak SSH and thermocline depth anomalies are seen during the second type, because equatorial downwelling anomalies induced by westerly wind anomalies in the west are counteracted by equatorial upwelling anomalies caused by easterly wind anomalies in the east. Due to the above difference in oceanic anomalies, the first type is stronger and lasts longer than the second type.

Evolution and mechanism of the positive Indian Ocean Dipole event in 2012

TANIZAKI, Chiho^{1*} ; TOZUKA, Tomoki¹

¹Graduate School of Science, The University of Tokyo

Evolution and mechanism of a peculiar positive Indian Ocean Dipole (IOD) event that occurred in 2012 are examined. In contrast to the normal IOD event, which starts to develop in late boreal spring, peaks in fall, and decays in winter, the 2012 IOD event was initiated in July, peaked in August, and decayed quickly in fall. Although the normal IOD event is associated with shallower thermocline in the eastern equatorial Indian Ocean, it was deeper than normal in 2012 and this may have delayed the onset of the IOD in this year. For quantitative discussions, mixed layer temperature balance of the eastern pole of the IOD is calculated using outputs from an ocean general circulation model. In agreement with past studies, negative sea surface temperature anomalies in the eastern pole are generated mainly owing to anomalous cooling by the vertical terms (i.e. entrainment and turbulent vertical diffusion) during the normal IOD. However, anomalous cooling by the surface heat flux term played the dominant role in the development of the eastern pole in 2012, and the vertical terms opposed the anomalous cooling. The anomalous cooling by the surface heat flux term is due to stronger cooling by latent heat flux. Also, warming of the surface mixed layer by the climatological shortwave radiation was suppressed owing to deeper mixed layer.

Interannual Variability in SST off Bangladesh

NAGURA, Motoki^{1*} ; TERAO, Toru² ; HASHIZUME, Masahiro³

¹JAMSTEC, ²Kagawa University, ³Nagasaki University

Oceanic variability off Bangladesh is one of the environmental factors which can impact on the local community. For example, Hashizume et al. (2011) pointed out that the number of cholera patients increases in Dhaka, which is populated by 15 million people and the largest city in Bangladesh, when sea surface temperature (SST) off Bangladesh rises. This study examines interannual SST variability in the coastal regions off Bangladesh, which has not attracted much attention in climate sciences so far. We detect a significant interannual SST variability off Bangladesh in two different satellite datasets (NOAA OI SST and TMI SST) and a high-resolution ocean general circulation model driven by a reanalysis dataset. The SST variability is trapped near the coast, amounts to 0.5 to 1.0 degrees Celsius in magnitude, and peaks in the boreal winter. The two observational datasets and the model results show consistency in the spatial and temporal patterns of SST variability, which gives credibility to the detected phenomenon. A statistical analysis shows that SST off Bangladesh tends to be high in the year next to El Nino and in the year of negative Indian Ocean Dipole events, suggesting those climate modes as possible drivers. We are conducting a mixed layer heat budget analysis using the model output, a preliminary result of which shows that a thick barrier layer caused by the freshwater supply from the Ganges plays a role in the generation of the SST variability. Details of the mixed layer heat budget analysis will be reported in the meeting.

A drastic change in predictability of precipitation off the west coast of Australia after late 1990s

DOI, Takeshi^{1*} ; BEHERA, Swadhin¹ ; YAMAGATA, Toshio¹

¹JAMSTEC APL

Global warming and natural decadal variability after late 1990s strongly warm the coastal ocean off West Australia, which drastically changed climate dynamics there. The warm ocean drives precipitation locally there after the late 1990s, while the local atmospheric variability or the remotely forced atmospheric bridges mainly controlled the local precipitation variability before that. By virtue of that, precipitation predictability off West Australia on a seasonal time scale is also drastically changed after late 1990s; austral summer precipitation off West Australia is significantly predictable 5 months ahead after late 1990s, while there is no predictability of that in 1980s and early 1990s. Although the high prediction skill of precipitation off West Australia is useful for its early warning to extreme events and reducing their damages, the extreme event itself might increase due to global warming and decadal climate variability through a local air-sea feedback.

Keywords: Seasonal prediction, Precipitation, Ningaloo Nino

Interdecadal Amplitude Modulation of ENSO and its Impacts on TPDV

OGATA, Tomomichi^{1*}

¹Faculty of Life and Environmental Sciences, University of Tsukuba

ENSO is a major climate mode in the tropical Pacific, and its interdecadal variabilities in ENSO characteristics (e.g. amplitude, propagation, period) are investigated as responses to background mean state change. On the other hand, tropical Pacific decadal variability (TPDV) is known as a major decadal-interdecadal variability, and coupled-GCM has revealed that ENSO also acts to TPDV. This study shows that the GFDL coupled-GCM (GFDL-CM2.1) also captures significant relationship between ENSO amplitude modulation and TPDV in interdecadal timescale. Furthermore, importance of ENSO rectification on TPDV is investigated by OGCM sensitivity experiments.

Keywords: air-sea interaction, tropical ocean, ENSO

The role of interaction between the Pacific and the north Atlantic Oceans in the prediction of ENSO

YAMAZAKI, Kuniko¹ ; IMADA, Yukiko^{1*} ; WATANABE, Masahiro¹

¹Atmosphere and Ocean Research Institute, the University of Tokyo

Observational and climate modelling studies indicate a close link between the north tropical Atlantic (NTA) sea surface temperature anomalies (SSTA) and the El Nino-Southern Oscillation (ENSO). An El Nino peak in boreal winter is followed by a warming of the NTA SSTA in the subsequent spring, which in turn leads to a La Nina in the following autumn/winter. Using the seasonal prediction system based on the atmosphere and ocean general circulation model (AOGCM) MIROC5, we conducted an ensemble of hindcast experiments from 1979 to present, in which the transition from El Nino to La Nina in 1997-1998 was successfully predicted. We also conducted a series of accompanying sensitivity experiments targeted at the transition event in 1997-1998, in which the NTA or equatorial Pacific air-sea interactions were decoupled. We found that NTA SSTA plays an important role in increasing the skill in predicting the following La Nina event. We also found that the preceding particularly-large El Nino SSTA and the associated atmospheric bridge are essential for the generation of NTA SSTA of the observed magnitude.

References

Ham, Y.-G., J.-S. Kug, J.-Y. Park, and F.-F. Jin, 2013: Sea surface temperature in the north tropical Atlantic as a trigger for El Nino/Southern Oscillation events, *Nature Geoscience*, 6, 112-116.

Keywords: ENSO, the north tropical Atlantic climate variability, seasonal prediction, atmosphere and ocean general circulation model

Important factors for long-term change in ENSO transitivity

OHBA, Masamichi^{1*}

¹CRIEPI

El Nino and La Nina exhibit significant asymmetry in their duration. El Nino tends to turn rapidly into La Nina after the mature, while La Nina tends to persist for up to 2 years. Reconstructed historical sea surface temperatures (SST) show a significantly increase in the intensity of El Nino-Southern Oscillation (ENSO) asymmetry, particularly El Nino transitivity, during the last six decades. Atmospheric observational data have shown that the relationship between El Nino and surface zonal wind anomalies over the equatorial Western Pacific (WP) has strengthened, and anomalous WP easterlies have appeared after the 1970s climate regime shift. To investigate the dependency of ENSO transitivity on its amplitude, a suite of idealized experiments using an atmospheric general circulation model (AGCM) is performed by imposing historical SST and 12 different ENSO-related SST anomalies exhibiting equal spatiotemporal distribution but different amplitude. Our AGCM experiments show strong nonlinearity in the WP zonal wind against the amplitude of the warm phase.

Keywords: Sea surface temperature, Pacific Ocean, El Nino/Southern Oscillation, Indian Ocean

Temporal variations of Mascarene High in austral summer and their causes, and influences on the SST field

OHISHI, Shun^{1*} ; SUGIMOTO, Shusaku¹ ; HANAWA, Kimio¹

¹Department of Geophysics, Graduate School of Science, Tohoku University

Changes in intensity and longitudinal/latitudinal position of Mascarene High (MH) in austral summer (November-January) from 1951 to 2012 are investigated using NCEP-NCAR reanalysis dataset. We define the MH intensity and longitudinal/latitudinal position as sea level pressure (SLP) maximum within a region of [40E-120E, 50S-10S]. The intensity has an interannual variation on a dominant timescale of 3-4 years. The pressure variations associated with the intensity show annular and equivalent barotropic structures throughout the troposphere, which are similar to Southern Annular Mode (SAM). The intensity time series shows a significant correlation with the SAM index. Therefore, it is suggested that the MH intensity variation results from the SAM. The MH longitudinal position also shows an interannual variation on a dominant timescale of 5-6 years and the time series has no significant correlation with the intensity time series. The SLP anomalies associated with the longitudinal variation represent a dipole pattern, whose centers of action are located off the western Australia (WA) and off the south-eastern Madagascar Island (SEMI). The geopotential height anomalies in these regions have different vertical structures; those off the WA are confined from the sea surface to the middle troposphere, while those off the SEMI are distributed throughout the troposphere. In addition, the SLP anomalies averaged within these regions show no significant correlation. It is indicated that the SLP variations off WA are associated with El Nino Southern Oscillation (ENSO). On the other hand, the SLP changes off the SEMI have no relationship with the large-scale atmospheric variations such as SAM and ENSO.

The MH intensity variation forms southwest-northeast dipole pattern of sea surface temperature (SST) field, which resembles the Indian Ocean Subtropical Dipole (IOSD) pattern. In addition, the MH longitudinal changes also show the dipole pattern, which is shifted westward by 10 degrees in longitude compared to the SST pattern associated with the intensity variation. The correlations between the MH variations and IOSD index show significant values (0.39 for intensity and -0.57 for longitudinal position). Therefore, it is suggested that both the changes in the intensity and the longitudinal position cause the IOSD.

Keywords: Mascarene High, Indian Ocean Subtropical Dipole, El Nino Southern Oscillation, Southern Annular Mode

Role of tropical SST variability in the generation of subtropical dipoles

MORIOKA, Yushi^{1*} ; MASSON, Sebastien² ; TERRAY, Pascal² ; PRODHOMME, Chloe² ; BEHERA, Swadhin³ ; MA-SUMOTO, Yukio⁴

¹JAMSTEC / RIGC, ²LOCEAN-IPSL, Universite Pierre et Marie Curie, ³JAMSTEC / APL, ⁴Graduate School of Science, The University of Tokyo

Interannual variations of Sea Surface Temperature (SST) in the midlatitudes of the Southern Hemisphere play an important role in the rainfall variability over the surrounding countries by modulating synoptic-scale atmospheric disturbances. These are frequently associated with a northeast-southwest oriented dipole of positive and negative SST anomalies in each oceanic basin, referred to as a subtropical dipole. This study investigates the role of tropical SST variability on the generation of subtropical dipoles by conducting SST-nudging experiments using a coupled general circulation model. In the experiments where the simulated SST in each tropical basin is nudged to the climatology of the observed SST, the subtropical dipoles tend to occur as frequently as the case in which the simulated SST is allowed to freely interact with the atmosphere. It is found that without the tropical SST variability, the zonally elongated atmospheric mode in the mid-high latitudes, called the Antarctic Oscillation (AAO), becomes dominant and the stationary Rossby waves related to the AAO induce the SLP anomalies in the midlatitudes, which, in turn, generate the subtropical dipoles. These results suggest that the tropical SST variability may not be necessary for generating the subtropical dipoles, and hence provide a useful insight into the important role of the AAO in the midlatitude climate variability.

Mechanism of long-term change in the Indian Ocean subtropical dipole mode

YAMAGAMI, Yoko^{1*} ; TOZUKA, Tomoki¹

¹Department of Earth and Planetary Science, Graduate School of Science, The University of Tokyo

The Indian Ocean subtropical dipole (IOSD) is a climate mode in the Southern Indian Ocean associated with negative sea surface temperature (SST) anomalies in the southeastern tropical Indian Ocean and positive SST anomalies in the southwestern part of the southern Indian Ocean during its positive phase. In this study, the long-term change in the IOSD is investigated for the first time using observational data and outputs from an ocean general circulation model. It is found that the frequency of the IOSD has become higher in the recent decade because of a decreasing trend in the mixed layer depth (MLD) over the southwestern pole in January and February. Positive (Negative) SST anomalies associated with the IOSD are generated when the mixed layer becomes anomalously shallow (deep) and the warming of the mixed layer by the climatological shortwave radiation is enhanced (suppressed). The thinner mixed layer in the recent decade amplifies this effect and even weak atmospheric forcing may trigger the IOSD. Based on a diagnosis of the Monin-Obukhov depth, we show that an increasing trend of surface heat flux is the cause of the decreasing trend in the MLD. On the other hand, it is found that the amplitude of the IOSD has become smaller. This is because the IOSD generally starts to develop in December, but the thicker mixed layer in December in the recent decade is unfavorable for its development. Also, the thinner mixed layer in January and February amplifies the negative feedback processes that damp the SST anomalies, as well as the positive effect on generating the SST anomalies. Since no long-term change in atmospheric forcing corresponding to that in the IOSD is observed, the long-term change in the MLD is essential in that of the IOSD.

Multiscale Interactions In The Genesis Of Tropical Cyclone Observed In PALAU2013

YOSHIOKA, Hiroaki^{1*} ; FUDEYASU, Hironori¹ ; KATSUMATA, Masaki² ; YOKOI, Satoru² ; TSUJINO, Satoki³ ; MASUDA, Ayumi¹

¹Yokohama National University Graduate School, ²Japan Agency for Marine-Earth Science and Technology, ³Hydrospheric Atmospheric Research Center, Nagoya University

To understand the formation of a tropical cyclone (TC), has long been a captivating subject at the frontier of science and remains challenging because of the complex multi-scale interactions involved. During the genesis stage, sustained convective activities, which may stem from a variety of processes in a favorable environment, develop into a surface mesoscale or synoptic vortex. The mesoscale processes in the genesis stage have been the least understood aspect of the lifecycle of a TC. Although the climatological large-scale conditions favorable for TC genesis have been well known since Gray (1968, 1979), the interactions between the large-scale conditions and mesoscale processes have been poorly understood. The main purpose of this study is to conduct a detailed analysis on the multiscale interactions involved in the cyclogenesis based on observational data and numerical simulations.

The Japan Agency for Marine-Earth Science and Technology (JAMSTEC) conducted a field project named the Pacific Area Long-Term Atmospheric Observation for Understanding of Climate Change (PALAU2013) over the northwest Pacific Ocean. In this project, a sounding and radar network was deployed over the ocean during the early summer of 2013. During PALAU2013, the four initial disturbances growing tropical depression (TD) or tropical storm (TS) were observed. This study focused on the disturbances, growing TS (T1304) in association with the temporal changes in large-scale environment. We analyzed re-analysis data (JMA-GSM data), observational data during PALAU2013, and simulation results using WRF-ARW. The radiosondes were launched every 3h on the R/V Mirai and every 6h at Koror and Yap. The Doppler radar was installed on this ship, collected volume-scan every 10 and 7.5 min.

Initial disturbances which occurred at (3N, 175W) in 03UTC June 10, 2013, passed through the observation point R/V MIRAI MR13-03 at (12N, 135E), grew T1304 in 00UTC June 18. The disturbance was developing along the convergence region between the trade easterlies and monsoonal westerlies. Results of radiosonde show that potential temperature was higher in the middle and upper troposphere and CAPE increased as disturbances approached. Moreover, the zonal wind component of the lower troposphere changed to the strong easterly, corresponding to the meridional wind component of the troposphere also changed to the south from the north. The temporal variation of the radar-echo area during the convections showed the organization of convective clouds to form the intense cyclones.

Keywords: Tropical storm, Tropical depression, Tropics, Doppler radar, WRF

Seasonality of boreal winter MJO and its relation to SST variability

SUEMATSU, Tamaki^{1*} ; MIURA, Hiroaki¹

¹Graduate School of Science University of Tokyo

Madden-Julian Oscillation (MJO) is a prominent intraseasonal variability in the tropics, which is characterized by eastward moving large-scale convective system along the equator. Overall seasonality of MJO paths has been recognized to be eastward during boreal winter and north-eastward during boreal summer. However, analysis of satellite data of NOAA Interpolated Outgoing Longwave Radiation (OLR) from 1982-2012 suggests that there is a notable variability in MJO paths just within boreal winter season. The paths of MJOs were observed to make a notable shift southward from about 10° N to 10° S from September to April, often with an event passing over the equator during November to December. Structural differences were also recognized between MJOs taking northern paths (northern MJO) and southern paths (southern MJO), with northern MJOs consisting of smaller convective components and being accompanied by more westward propagating components. Using weekly NOAA Optimum Interpolated Sea Surface Temperature (SST) data of the same time period, this shift in the paths of MJOs is further analyzed in relation to variability in SST distribution. Temporal changes in zonal SST gradient of MJO occurring regions, and equatorial asymmetry of SST distribution were evaluated. The result was suggestive of effective influence of positive zonal SST gradient from equatorial Indian Ocean to equatorial Western Pacific on the existence of MJO, and that equatorial asymmetry of SST distribution may be playing a part in the shift of the MJO paths.

Keywords: MJO, SST variability, intraseasonal variability

Seasonal Variations of the Mascarene High and Related Changes in Jetstreams and a Stormtrack

MIYAMOTO, Ayumu^{1*} ; NAKAMURA, Hisashi¹ ; MIYASAKA, Takafumi¹

¹RCAST, University of Tokyo

The subtropical high in the Southern Indian Ocean, called the Mascarene high, is an integral part of the climate system there, influencing not only weather conditions in the surrounding regions but also the oceanic state. The present study examines the mechanisms for the seasonal variations of the Mascarene high. The high resides over the eastern portion of the basin in summer, while it shifts westward in winter toward the Agulhas storm-track core in strengthening. This large seasonal displacement is a distinct feature of the Mascarene High from other subtropical highs. Our analysis reveals that, while low-level thermal contrasts between the Australian continent and southeastern Indian Ocean is important for the formation of the high in summer, its wintertime formation is owing primarily to eddy-feedback forcing due to the seasonally-enhanced storm-track activity that is maintained in the presence of pronounced SST gradient along the Agulhas Return Current. In winter, the mid-tropospheric subsidence over the surface high is associated with upper-tropospheric convergence of the cross-equatorial divergent flow, indicative of a connection between the high and the Asian summer monsoon. From the viewpoint of vorticity budget, the cyclonic tendency by the upper-level convergence is balanced with the westerly advection of the anti-cyclonic vorticity. While the converging upper-tropospheric flux of Rossby wave activity from lower and higher latitudes acts to reinforce the high in winter, the high itself acts as a source of the climatological-mean planetary waves with the net local divergence of the flux, which is suggestive of the importance of the high even on the hemispheric scale.

Keywords: subtropical high, Indian Ocean, Agulhas Return Current, SST front, jetstream, stormtrack

Decadal variabilities in the Pacific and Atlantic Oceans and frequency of hot summers over the Northern Hemisphere

KAMAE, Youichi^{1*} ; SHIOGAMA, Hideo¹ ; WATANABE, Masahiro² ; KIMOTO, Masahide²

¹National Institute for Environmental Studies, ²Atmosphere and Ocean Research Institute, the University of Tokyo

Mean temperature increase over the Northern Hemisphere (NH) land areas during warm seasons enhances frequency of extreme warm events (e.g. Russian heat wave in 2010; 1). Human influences on Earth's climate have been detected in observational records since the late 20th century. During the past 15 years, the increase in global surface air temperature (SAT) has slowed (called hiatus; 2) whereas observations show a continuous increase in summertime (June-July-August, JJA) land-mean SAT and the frequency of hot summers over the NH land areas. This discrepancy represents that some other factors except global sea surface temperature (SST) can influence on the increasing frequency of hot summers. The recent phase shifts of the decadal and multidecadal SST variabilities in the Pacific and Atlantic Oceans could have influenced the mean SAT and extreme events over the land.

For attributing the recent increase in NH hot summers, we performed three sets of ensemble simulations for 1949-2011 using an atmospheric general circulation model (AGCM). An ensemble driven by prescribed observed SST, sea-ice concentration, and radiative forcing agents, reproduces well the observed SAT time series over the NH land. Simulated anomalies can be decomposed into three components: anthropogenic influence via SST increase (ASST); direct effect of anthropogenic forcing including GHG radiative forcing (ADIR); and natural climate forcing and internal SST variability (NAT). The decomposition is made by conducting two additional ensemble, one with prescribed GHGs at the pre-industrial level and the other similar to the SST run but without human induced components in SST and sea ice have been removed.

The model simulates well 1) the long-term increase of the frequency of hot summers and 2) the recent increase during the hiatus period. Both ASST and ADIR contribute to 1). Particularly, the ADIR effect is the dominant factor for the middle and high latitude land areas, consistent with earlier studies presenting the ADIR effects for increase in mean land SAT during warm seasons (3, 4). In contrast, the NAT effect is essential for 2). The recent SST variabilities in the Pacific and Atlantic Oceans are characterized by the negative phase of PDO and the positive phase of AMO. Atmospheric teleconnection patterns associated with these SST variabilities result in low SAT over the Canada and high SAT over the United State middle latitude. In addition, the warm SST in the North Atlantic Ocean and the Mediterranean Sea contribute to high SAT over the Europe.

The recent decadal and multidecadal variabilities in the Pacific and Atlantic Oceans contribute to the increase in land SAT and frequency of hot summers over the NH middle latitude despite the recent climate hiatus. In the recent future, global and regional frequencies of hot summers can be influenced largely by phase shifts of decadal and multidecadal SST variabilities in the Pacific and Atlantic Oceans.

References

- [1] Watanabe, M., H. Shioyama, Y. Imada, M. Mori, M. Ishii, and M. Kimoto, 2013: Event attribution of the August 2010 Russian heat wave. *SOLA*, 9, 64-67, doi:10.2151/sola.2013-015.
- [2] Watanabe, M., Y. Kamae, M. Yoshimori, A. Oka, M. Sato, M. Ishii, T. Mochizuki, and M. Kimoto, 2013: Strengthening of ocean heat uptake efficiency associated with the recent climate hiatus. *Geophys. Res. Lett.*, 40, 3175-3179.
- [3] Kamae, Y., and M. Watanabe, 2013: Tropospheric adjustment to increasing CO₂: its timescale and the role of land-sea contrast. *Clim. Dyn.*, 41, 3007-3024.
- [4] Kamae, Y., M. Watanabe, M. Kimoto, and H. Shioyama: Summertime land-sea thermal contrast and atmospheric circulation over East Asia in a warming climate. Part II: Importance of CO₂-induced continental warming. *Clim. Dyn.*, in revision.

Keywords: global warming, hot summer, heat wave, PDO, AMO

Zonal Momentum Budget Along the Equator in the Indian Ocean from a High Resolution Ocean General Circulation Model

NAGURA, Motoki^{1*} ; MCPHADEN, Michael j²

¹JAMSTEC, ²NOAA

This study examines the zonal momentum budget along the equator in the Indian Ocean, with emphasis on the Wyrтки Jets in a high-resolution ocean general circulation model. The Wyrтки Jets are wind-driven eastward flows in the upper 100 m of the equatorial Indian Ocean that appear typically twice per year during the monsoon transitions in boreal spring and fall. Our results indicate significant contributions from zonal, meridional and vertical advection of zonal momentum, with the dominant contribution coming from zonal momentum advection. These results contrast with those from previous idealized wind-forced model experiments that emphasized the importance of vertical momentum advection. The extra eastward force caused by zonal momentum advection reinforces eastward wind stress, resulting in swifter jets in the eastern basin than in the western basin. Another consequence of these nonlinearities is that, annually averaged, zonal currents in the upper thermocline flow against the zonal pressure gradient rather than down gradient. Thus, there is no mean subsurface undercurrent flowing against the surface winds in the Indian Ocean as there is in the Pacific and Atlantic Oceans. These results indicate that proper simulation of the mean and the semi-annual zonal flows along the equator in the Indian Ocean, including their climatically relevant impacts on the mass and heat balance of the region, requires accurate representation of nonlinearities that derive from a broad range of interacting time and space scales.

Development of a visualization and download system for dataset of ocean state estimation

FUKUDA, Kazuyo^{1*} ; SAITO, Hideaki¹ ; ISHIKAWA, Yoichi¹ ; MASUDA, Shuhei¹ ; SUGIURA, Nozomi¹ ; ISHIGURO, Shun¹ ; SONODA, Akira¹

¹JAMSTEC

In order to promote the use of a dataset of ocean state estimation useful for climate research, a data visualization and download system called "Estimated State of Global Ocean for Climate Research (ESTOC) ^[1]" has been developed. The dataset contains 3- or 2-dimensional grid data of eight physical parameters such as potential temperature and salinity, and five geochemical parameters such as nitrate and phytoplankton. It covers the 53-year period from 1957 to 2009, and consists of 6996 NetCDF files of 55 gigabytes. We have considered the functions required for the system based on the assumption that the main users of the dataset are researchers not only in climatology but also in ocean ecosystem science and fisheries science.

Quick look of the data can be carried out under the conditions specified by users in the visualization page. Contour lines or vector arrows are drawn on a base map. Users can zoom in an area of the map that they are interested in, and change display color with color tables. Animations of the estimated ocean state can also be played easily. The data at users' specified location on the map can be displayed as a graph of time series, vertical profile, latitude-depth or longitude-depth sections. Furthermore, the displayed map and graph can be downloaded as png or jpeg image files.

Logged-in users are able to download a data file of the map being displayed in the visualization page, and also able to download multiple files in the download page. The following two download methods are available. One is the normal download via web browser. The other is the sending an e-mail describing a download URL to user's registered e-mail address to use the wget command. The download state of data files is recorded in the log files for the system administrator. It will be used for improvement of data dissemination service in this system in the future.

URL

[1] <http://www.godac.jamstec.go.jp/estoc/e/>

Development of Wide-area Observation Monitoring System and Data Crawling System for Global Earth Observation

MURATA, Ken T.^{1*} ; NAGATSUMA, Tsutomu¹ ; YAMAMOTO, Kazunori¹ ; WATANABE, Hidenobu¹ ; UKAWA, Kentaro² ; MURANAGA, Kazuya² ; YUTAKA, Suzuki²

¹NICT, ²Systems Engineering Consultants Co., LTD.

This paper is to propose a cloud system for data-intensive science, which has been developed at NICT (National Institute of Information and Communications Technology), Japan. The NICT science cloud is one of the cloud systems for scientists who are going to carry out their research works.

The science cloud is not for simple uses. Many functions are expected to the science cloud; such as data standardization, data collection and crawling, large and distributed data storage system, security and reliability, database and meta-database, data stewardship, long-term data preservation, data rescue and preservation, data mining, parallel processing, data publication and provision, semantic web, 3D and 4D visualization, out-reach and in-reach, and capacity buildings.

In the present talk, we introduce two types of tools for global data collection (crawling) and data transfer. The former is to collect observation data files from a variety of data server public on the Internet. The latter is to manage observation systems at observatories over the world. Data file transfer, monitoring servers and networks and system recovery are easily carried out using this system.

WCRP/AMY data archive and data release on the DIAS

TAMAGAWA, Katsunori^{1*}; OHTA, Tetsu¹; IKOMA, Eiji¹; KINUTANI, Hiroko¹; OYANAGI, Misa¹; MATSUMOTO, Jun²; KITSUREGAWA, Masaru³; KOIKE, Toshio⁴

¹EDITORIA, The University of Tokyo, ²Dept. of Geography, Tokyo Metropolitan University, ³IIS, The University of Tokyo, ⁴Dept.Civil Eng., The University of Tokyo

The purpose of this presentation is to introduce World Climate Research Programme (WCRP)/Asian Monsoon Years (AMY) data archiving and opening status along with its data uploading, data quality control, and metadata registration systems on the Data Integration and Analysis System (DIAS).

DIAS was launched in 2006 as a part of the Earth Observation and ocean Exploration System that provides cooperative opportunities for constructing data archives, and developing data integration and analysis functions (<http://www.editoria.u-tokyo.ac.jp/projects/dias/>).

The goal of WCRP/AMY is to improve Asian monsoon prediction for societal benefits through coordinated efforts and to promote a better understanding on Asian monsoon variability and predictability. Under the framework of the WCRP/AMY the various kinds of in-situ data have been archived among 21 different international projects. (<http://www.wcrp-amy.org/>). The basic for the WCRP/AMY collaborative framework is the mutual consensus among the participating countries, international organizations, individual participants, and their partner projects. It that defines the data sharing and exchange policies and is responsible for the data management.

Keywords: DIAS, WCRP/AMY, in-situ data, Water Cycle, Asian Monsoon

VDVGE: Volume Data Visualizer for Google Earth

KAWAHARA, Shintaro^{1*} ; SUGIYAMA, Tooru¹ ; ARAKI, Fumiaki¹ ; TAKAHASHI, Keiko¹

¹JAMSTEC

Software to visualize volume data that is called VDVGE (Volume Data Visualizer for Google Earth) has been developed. VDVGE visualizes a four-dimensional scalar data, and exports it to KML and COLLADA which are suitable format to Google Earth. Currently, VDVGE are used not only visualization of simulation data, also visualization of observed data, such as meteorological radar and meteorological satellites. In the presentation, the development status of VDVGE is introduced. Application examples of the recent will be also introduced.

Keywords: Google Earth, Volume visualization, Software development

ACG38-05

Room:213

Time:April 28 10:00-10:15

Introduction of the UnderwayCTD observation: A new instrument of oceanography

HASEGAWA, Takuya^{1*}; YOKOI, Satoru¹; MOTEGI, Qoosaku¹; KATSUMATA, Masaki¹; UEKI, Iwao¹; ANDO, Kentaro¹; YONEYAMA, Kunio¹

¹JAMSTEC

Abstract is written in Japanese.

Keywords: In-situ observation in the upper-ocean, UnderwayCTD

Development of a satellite land and cloud data assimilation system coupled with WRF, and its application to Kanto area

SETO, Rie^{1*} ; RASMY, Mohamed¹ ; KOIKE, Toshio¹

¹Department of Civil Engineering, the University of Tokyo

For flood prediction and optimized dam control, it is crucial to predict whether a rain area will be over the river basin or not after few hours, and this needs very fine prediction of time and space distribution. For system development focusing on the 'location' of rain areas, it is effective to introduce the information of cloud distribution from the observations into the model as initial conditions. Clouds can be observed by microwave remote sensing by satellite. But it is not easy to observe the cloud over the land from the satellite because emissivity of clouds is so weak compared to that of land surface.

In order to observe cloud over the land, we at first have to adequately represent the heterogeneity of land state, especially soil moisture distribution, which has large effect on emissivity of the land, and estimate the surface emissivity, then remove it as background information for cloud observation. Therefore, we developed a satellite-based land and cloud data assimilation system coupled with the Weather Research and Forecasting Model (CALDAS-WRF) and applied it to the Kanto area.

The CALDAS-WRF includes Simple Biosphere model version 2 (SiB2) as a land surface driver, radiative transfer models for soil and atmosphere as observation operators, and Ensemble Kalman Filter (EnKF) and 1DVAR as assimilation algorithms for land and cloud, respectively.

The CALDAS-WRF first initializes the whole system, integrates the WRF and the SiB2 repeatedly until observations are available, and then assimilates the soil moisture heterogeneity, using passive microwave brightness temperature (T_b) at lower frequency, which has a high sensitivity to soil moisture. Then the CALDAS-WRF assimilates cloud over the land, using T_b at higher frequency, which is sensitive to cloud, and optimized emissivity of land as a background information.

We applied the CALDAS-WRF to the Kanto area, and the system effectively assimilated information of clouds and largely improved the representation of cloud distribution. Precipitation areas were also reproduced in the correct locations and consistent atmospheric fields were generated around the cloud areas through dynamical and physical processes in the atmospheric model. However the precipitation amount and duration were not enough, which will be the next target of our development.

Keywords: cloud, soil moisture, satellite microwave data assimilation, Kanto area, heavy rain prediction

Atmosphere-Ocean coupled regional modeling for dynamical downscaling of current and future climates

YOSHIMURA, Kei^{1*} ; HAM, Suryun¹ ; LI, Haiqin²

¹Atmosphere and Ocean Research Institute, The University of Tokyo, ²Center for Ocean-Atmospheric Prediction Studies, Florida State University

We have developed regional downscaling system of the Regional Spectral Model for the atmosphere and the Regional Ocean Modeling System (RSM-ROMS) to improve the downscaling simulation accuracy of particularly coastal area, and we have achieved a dynamical downscale of the climate model simulation for 20th and 21st century forced by SST and atmospheric state from the global Community Climate System Model version 3.0 (CCSM3) for California area. The results indicate that the surface air temperature rise was decreased over San Francisco Bay area due to the effect of uplifting current at the Pacific coast. The projected change of extreme warm events is quite different between the coupled and uncoupled downscaling experiments, with the former projecting a more moderate change. The projected future change in precipitation is not significantly different between coupled and uncoupled downscaling. Both the coupled and uncoupled downscaling integrations predict increased onshore sea breeze change in summer daytime and reduced offshore land breeze change in summer nighttime along the coast from the Bay area to Point Conception. Compared to the simulation of present climate, the coupled and uncoupled downscaling experiments predict 17.5 % and 27.5 % fewer Catalina eddy hours in future climate respectively. Similar framework was applied for East Asian region, and preliminary results show quite significant change in surface temperature and precipitation field due to having dynamically predicted fine scale ocean currents. Particularly in summer to fall, when Kuroshio Current direction and prevailing surface wind direction are about opposite, coastal subsidence occurs so that it warms the coastal air temperature. This feature is opposite from the California's case, and potentially indicating the possible underestimation of warming. We will further investigate the detail of the influence of regional atmosphere-ocean coupling in the presentation, as well as the impact of fresh water input from the terrestrial runoff.

Keywords: Atmosphere-Ocean coupled regional model, coastal uplifting current, regional climate projection, dynamical downscaling

ACG38-08

Room:213

Time:April 28 11:00-11:15

What can we find with the ensemble atmospheric reanalysis: ALERA2? -New aspect of the MJO-

MOTEKI, Qoosaku^{1*}

¹JAMSTEC

An ensemble atmospheric reanalysis ALERA2 is now open to public for the period of 2003-2013. New aspect of the MJO with the ensemble spread of the ALERA2 will be introduced.

Keywords: ALERA, ensemble, reanalysis, MJO

Climate Change Signal Represented in Reanalyses

KAMAHORI, Hirotaka^{1*}

¹Meteorological Research Institute

Since NOAA/NCEP completed the first atmospheric reanalysis NCEP/NCAR, 20 years are passed. During these 20 years, many reanalyses NCEP/DOE, ERA-15, ERA-40, JRA-25 MERRA, CFSR, and ERA-Interim were released. Last year, JRA-55 was completed as the third generation reanalysis.

Now a day, the atmospheric reanalyses are widely utilized as fundamental database of pseudo observations in meteorology as well as in various research fields. However, their adaptation to the climate change studies have not been advanced very much, because of less temporal S/N ratio in reanalyses products. That is, present available reanalyses include large artificial variations compared with natural variations in real atmosphere. Since the first reanalysis NCEP/NCAR, all reanalysis assumes the frozen data assimilation system in order to avoid artificial variations accompanying with changes of the system. We expected the homogeneous products with the frozen systems, but there are many artificial changes in the products different from the change of the real atmosphere, due to the change of the observation systems. As the largest artificial change, it should be noted that the large gaps in the products characteristics were introduced due to introduction of geosynchronous satellites around 1979. These artificial variations in the products make difficult to adapt them to climate change studies. On the other hand, continuous efforts have been made to reduce the artificial variation and make the products applicable to the climate change studies. For examples, bias correction techniques for satellite and upper air observations that are input data in the data assimilation system, are developed and adapted in recent reanalyses. As a result, homogeneity of reanalysis products is largely improved, and we become to be able to extract the signals of climate change from the products. Of course, degrees of availability of the climate change signals in the products largely depend on the variables. Here, I introduce specific examples of the application possibilities of the products for the climate change studies.

Keywords: Climate Change, Reanalysis, Data Assimilation, Observation

The data release of Earth observation project data products considering data provider's policies by DIAS

KINUTANI, Hiroko^{1*} ; SHIMIZU, Toshiyuki² ; LI, Jiyi² ; NAKAHARA, Yoko² ; YOSHIKAWA, Masatoshi² ; KITSUREGAWA, Masaru³ ; KOIKE, Toshio¹

¹The University of Tokyo, ²Kyoto University, ³The University of Tokyo, National Institute of Informatics

Our project, DIAS (Data Integration and Analysis System) started in 2006, has a purpose of constructing data infrastructure that can integrate earth observation data, numerical model outputs, and socio-economic data effectively. DIAS also has a purpose to create knowledge enabling us to solve earth environment problems and to generate socio-economic benefits. From October 2010, we have released data of DIAS with Document-metadata, describing about dataset in English and Japanese. Anyone can use the DIAS data discovery system by accessing <http://dias-dss.tkl.iis.u-tokyo.ac.jp/ddc/>, and can download data files of 195 datasets through the system.

The data in DIAS is classified into 4 categories:

- 1) Numerical simulation outputs for the purpose of research,
- 2) Satellite data for the purpose of research,
- 3) Datasets created by DIAS researchers,
- 4) Datasets created at related projects supported by DIAS.

Newly released datasets are **NIES CGER Ochiishi Monitoring Station Greenhouse Gases Data, NIES CGER Tomakomai Energy, Water, CO2 Flux, Spectral Radiation, Vegetational Index Data, Atmosphere and ocean carbon dioxide monitoring using volunteer observing ship (Pyxis) servicing between Japan and West Coast, The Japanese 55-year Reanalysis (JRA-55), GRENE-City Tsunami archive, AGURAM Ground Information Database** and Asian Monsoon Year projects data products.

Data provider to release datasets from DIAS should create the document metadata (both in English and Japanese) that describes the dataset. Data provider should write a policy concerning the data in order to notify to data user in it. In addition to data policy of data provider, project policy of a project that became the background of the data creation, and DIAS data policy are included in the document metadata. If conflicting terms are written among the data policies, we have determined the priority of data policy; the order is data provider, project and DIAS.

The data policy of DIAS is as follows:

1. With regard to Data policy, if there is any data policy indicated by the data provider, that policy always has priority over this DIAS data policy.
2. DIAS data sets are to be used only for scientific research or educational purposes. Commercial use and exploitation of DIAS data sets are prohibited
3. Any modification or change of the original DIAS data sets is prohibited.
4. Any Re-export or transfer of the original data sets to a third party is prohibited.
5. The origin of DIAS data being used for any publication of scientific results must be acknowledged and referenced in the publication, with the *quotation* given below as an acknowledgement.
6. Whenever DIAS data sets are used for publication of scientific results, the author(s) shall send a copy of the respective publication, preferably in an electronic form or in a separate printed version, to the DIAS CONTACTS as indicated

Data policy of DIAS may use as the basis for data providers to create their own data policy.

In addition, the data download system developed by DIAS has 4 level access controls to the data for users' data downloading.

- 1) Registered users are able to download.
- 2) In addition to 1), after agreement of data policy, users are able to download.
- 3) In addition to 2), after sending a use application through the system to the data provider and approval is obtained, users are able to download.
- 4) In addition to 2), after users have negotiated individually with the data provider and approval is obtained, users are able to download.

By considering the data policy of data provider in this way, we are trying to improve the reliability of DIAS data repositories and DIAS data release.

Keywords: DIAS, Earth Observation data, Satellite data, Model output data, In-situ data, data policy

Development of a basic common library (SCALE) for future HPC and datasets created by the library

SATO, Yousuke^{1*} ; NISHIZAWA, Seiya¹ ; YASHIRO, Hisashi¹ ; MIYAMOTO, Yoshiaki¹ ; TOMITA, Hirofumi¹

¹RIKEN Advanced Institute for Computational Science

A basic Common library named Scalable Computing for Advanced library and Environment (SCALE) is now being developed at RIKEN, Advanced Institute for Computational Science (AICS). The library is developed to solve the problems that come from the sophistication of numerical models and the recent trend of high performance computing (HPC). The library is downloadable from the web site of RIKEN, AICS (<http://scale.aics.riken.jp/>). The license of the SCALE is based on BSD 2 license.

SCALE-Large Eddy Simulation (LES) is now available as a component of the SCALE library. The SCALE-LES is based on fully compressible system, and it uses vertically explicit and horizontally explicit (HE-VE) scheme. Even ordered central differential schemes (2nd ordered central differential scheme for the terms relating to the density, 4th ordered central differential scheme for the other terms) are applied for spatial discretization. The 3rd ordered Runge-Kutta scheme is applied for the temporal discretization. Physical components implemented in the SCALE-LES are turbulent scheme, a radiation scheme, cloud microphysical schemes (1-moment bulk, 2-moment bulk, and spectral bin scheme), and surface flux model. The aerosol model, chemical transport model, urban canopy model will be implemented near future.

In future, the SCALE library will be extended to regional model with nesting system, global model. As well as the atmospheric component, the SCALE will be extended to the entire targets for numerical simulation (e.g. ocean, biosphere, molecular dynamics, or so).

We will introduce some examples of the results obtained from the SCALE-LES and some datasets. We aim to share and discuss about not only the model results but also the problem when we treat the big data (e.g. data handling, visualization or so) with the participants regardless of their background.

Japan mosaic land-cover 0.01 degrees raster dataset

HIGUCHI, Atsushi^{1*} ; KAWAKAMI, Satoshi² ; MURAKAMI, Akinobu³ ; MASUTOMI, Yuji⁴ ; TAKAMI, Akinori⁵

¹CEReS, Chiba University, ²HP Japan, ³University of Tsukuba, ⁴Center for Environmental Science in Saitama, ⁵NIES

As one of basic information for numerical weather simulation, land-cover and land-use dataset is essential for initial condition. In Japan, MILT published land-cover information as tile and vector files. We mosaicked tile vector files into one raster (gridded) file dataset over Japan. Such mosaicked raster files are available for 1976, 1987, 1991, 1997 and 2009. We also made convert programs from original land-cover flag (number) into typical land surface model (SiB and SiB2) land-cover flag. We also try to explain how to utilize these dataset for the assessment of urban-green to reduce heat island without use of urban canopy model within the poster session core-time. To make the dataset, SALSA project under RECCA/MEXT supports our activity.

Keywords: land use, land numerical mesh, Japan mosaic, raster data

Meteorological observations for the purpose of educational use in Nagata ward, Kobe

FUKUSHIMA, Azusa^{1*}; OTSUKA, Shigeaki¹

¹Faculty of Humanities and Sciences, Kobe Gakuin University

Weather and climate are the units in science or geography classes in elementary and junior high school. Recently, many data have archived on the Internet by the individuals or scientific groups other than JMA with the spread of the meteorological instruments. However, if a teacher who is working at a public school hopes to do constructive class with some practical works using the meteorological data, he has to spend for hours and hours preparing. For example, he has to choose a case day to learn the unit in effective way, and he has to prepare the data that it can be used in his students easily. Therefore we considered that if a provider prepares some support measures for using the data, the teacher might be easy to introduce the meteorological dataset into his class as a course material. In this study, we report an approach to the educational use of a meteorological dataset observed at the Nagata center of the Center for Area Research and Development, Kobe Gakuin University from 2011.

The Nagata center of the Center for Area Research and Development was established in 2010. It is located in the former buildings of the Futaba elementary school in Nagata ward, Kobe-shi. The instruments for the observation of the meteorology and seismology were installed on summer of 2011. The elements of meteorological observation are air temperature, wind speed and direction, relative humidity, rainfall, net solar radiation, ultraviolet A and B, and pressure. The elements for the seismology are seismic intensity, seismic wave, groundwater level, and underground water temperature. The observation data is automatically saved as daily reports, monthly reports, and annual reports. The daily reports are available on our website to the registered users. The data can be used only for the educational and research purposes.

Observation site is located in the urban area between Shin-Nagata station (JR line) and the port of Nagata. It is at a distance of about 7km southwest of Kobe Local Meteorological Observatory. JMA Akashi AMeDAS station is in Futami coastal area of Harima-Nada. Nagata is the side of Osaka Bay and is located in the south of Rokko-Awaji fault zone. If the observation data used in conjunction with the data of Kobe Local Meteorological Observatory, it can be carried out a research of urban heat island and sea and land breezes at the regional scale. A practical training of the meteorological observation or the tour of equipment at the Nagata center is also possible.

The data that observed in near at hand can be used to understand local scale weather and climate as a course material in the school. Furthermore, it is possible to feed the geographic and the temporal sense of the weather phenomenon by comparing the data of several weather stations including Nagata.

Keywords: Meteorological and Seismological Data, Earth Science Education, Nagata ward, Kobe

Study of tropospheric tomography for water vapor distribution with Neural Network

HIROKI, Akimitsu^{1*} ; HATTORI, Katsumi¹ ; HIROOKA, Shinji¹

¹Graduate School of Science, Chiba University

Many meteorological disasters such as landslides with torrential rain have been reported. Monitoring and a prediction of the precipitation activity are very important to mitigate these disasters. However, in the developing countries such as Indonesia and the Philippines, the observation with the radars is difficult in the present conditions due to the cost and the maintenance. The water vapor tomography using a GPS and/or broadband satellite is considered to be effective for the precipitation monitoring system instead of the radars in the above countries.

When the rain cloud bringing the damage of a heavy rain and the thunderstorm is developing, there is an apparent flow of the water vapor from the neighborhood. It is possible that the GPS can detect the flow and distribution of water vapor. Therefore, in this study, we develop a water vapor tomography from GPS and AMeDAS data using algorithm of residual minimization learning neural network (RMTNN). The numerical simulation demonstrates a capacity of the developed method, that is, the reconstructed image can show the transient changes and the inverse layer in given water vapor distributions. The details will be shown at our presentation.

Keywords: tomography, water vapor, GPS